

SIGNAL PROCESSING FOR SARSAT

To my parents

DIGITAL SIGNAL PROCESSING OF SARSAT SIGNALS  
USING THE MEM AND FFT

By

Kwai-Sum Thomas Chung, B. Eng.

A Thesis

Submitted to the School of Graduate Studies  
in Partial Fulfilment of the Requirements  
for the Degree  
Master of Engineering

McMaster University

July 1982

MASTER OF ENGINEERING (1982)

(Electrical Engineering)

McMASTER UNIVERSITY

Hamilton, Ontario

TITLE: Digital Signal Processing of SARSAT Signals  
Using the MEM and FFT

AUTHOR: Kwai-Sum Thomas Chung, B. Eng. (McMaster University)

SUPERVISOR: Dr. C. R. Carter

NUMBER OF PAGES: xxx, 277

## ABSTRACT

This thesis investigates the processing of emergency locator transmitter (ELT) signals which are used in search and rescue satellite-aided tracking (SARSAT) systems. Essentially, the system relies on the transmission of ELT signals from a distressed platform being relayed through an orbiting satellite to an earth station where signal processing can be performed.

The methods of signal processing investigated here include both linear and nonlinear. The linear methods include the window function, the autocorrelation function, the digital filtering and the Fast Fourier Transform (FFT). The nonlinear processing is based on the Maximum Entropy Method (MEM). In addition, additive white Gaussian noise has been added to simulate the performance under different carrier-to-noise density ratio conditions.

For a single ELT signal, it is shown in the thesis that the MEM processor gives good spectral performance as compared to the FFT when applied to all types of modulation. When multiple ELT signals are present, the MEM also provides certain benefits in improving the spectral performance as compared to the FFT.

## ACKNOWLEDGEMENTS

The author gratefully acknowledges the advice, guidance and encouragement given by his supervisor, Dr. C. R. Carter, throughout the preparation of the thesis.

The author would like to express his appreciation from a number of useful discussions with Dr. S. B. Kesler and Mr. A. Premji.

Finally, the author would also like to thank the SARSAT Group of Communications Research Centre, Ottawa and the SARSAT Group at Canadian Astronautics Limited, Ottawa for many helpful suggestions.

## TABLE OF CONTENTS

	Page
ABSTRACT	iii
ACKNOWLEDGEMENTS	iv
CHAPTER 1 - INTRODUCTION	1
1.1 SARSAT PROGRAM	4
1.2 ELT SIGNALS	6
1.2.1 Sine-Wave Modulation	6
1.2.2 Pulse-Shaped Modulation (Continuous Phase)	7
1.2.3 Pulse-Shaped Modulation (Random Phase)	11
1.3 THE DOPPLER CURVE	11
1.4 SCOPE OF THESIS	19
CHAPTER 2 - SIGNAL PROCESSING METHODS	21
2.1 INTRODUCTORY REMARKS	21
2.2 THE FAST FOURIER TRANSFORM ALGORITHM	21
2.3 THE WINDOWING TECHNIQUES	27
2.4 THE MAXIMUM ENTROPY METHOD SPECTRAL ANALYSIS	31
2.5 USE OF THE AUTOCORRELATION FUNCTION AS A PREPROCESSOR	36
2.6 PREPROCESSING VIA THE AUTOCORRELATION FUNCTION	40
2.7 DESIGN OF NONRECURSIVE DIGITAL FILTER	40
2.8 NOISE CONSIDERATIONS	43
2.9 SUMMARY	47
CHAPTER 3 - PROCESSING OF ONE ELT SIGNAL	48
3.1 DISCUSSION ON THE SIMULATION PROCESS	48
3.2 PROCESSING RESULTS USING THE FAST FOURIER TRANSFORM TECHNIQUE	52
3.2.1 Pulse-Modulated, Continuous Phase	53
3.2.2 Pulse-Modulated, Random Phase	61
3.2.3 Sinusoidal-Modulated	61

Table of contents continued

	Page
3.3 PROCESSING RESULTS USING THE MAXIMUM ENTROPY SPECTRAL ANALYSIS	69
3.3.1 Pulse-Modulated, Continuous Phase	71
3.3.2 Pulse-Modulated, Random Phase	78
3.3.3 Sinusoidal-Modulation	80
3.4 ACCURACY OF FREQUENCY RESOLUTION FOR THE MAXIMUM ENTROPY METHOD	85
3.4.1 Pulse-Modulated, Continuous Phase	89
3.4.2 Pulse-Modulated, Random Phase	93
3.4.3 Sinusoidal-Modulated	103
3.4.4 Overall Performance	103
3.5 THE SPECTRAL PERFORMANCE WITH VARIATIONS IN CARRIER-TO- NOISE DENSITY RATIO	103
3.5.1 Pulse-Modulated, Continuous Phase	107
3.5.2 Pulse-Modulated, Random Phase	114
3.5.3 Sinusoidal-Modulated	125
3.6 SUMMARY	125
CHAPTER 4 - PROCESSING OF MULTIPLE ELT SIGNALS	139
4.1 INTRODUCTORY REMARKS	139
4.2 PROCESSING MULTIPLE ELT SIGNALS EMPLOYING THE FFT ALGORITHM	140
4.2.1 Two ELT Signals	140
4.2.2 Five ELT Signals	141
4.2.3 Ten ELT Signals	147
4.3 PROCESSING MULTIPLE ELT SIGNALS EMPLOYING THE MEM	147
4.3.1 Two ELT Signals	154
4.3.2 Five ELT Signals	156
4.3.3 Ten ELT Signals	166
4.3.4 General Remarks	172
4.4 PREPROCESSING WITH A BANK OF BANDPASS FILTERS	176
4.4.1 Two ELT Signals	177
4.4.2 Five ELT Signals	181
4.4.3 Ten ELT Signals	188
4.4.4 General Remarks	192

Table of contents continued

	Page
4.5 THE SPECTRAL PERFORMANCE OF MULTIPLE ELT SIGNALS WITH VARIATIONS IN CARRIER-TO-NOISE DENSITY RATIO	192
4.6 SUMMARY	197
CHAPTER 5 - CONCLUSIONS AND SUGGESTIONS FOR FURTHER RESEARCH	212
5.1 CONCLUSIONS	212
5.2 SUGGESTIONS FOR FURTHER RESEARCH	214
REFERENCES	216
APPENDIX A - EQUATIONS FOR THE VALUES OF $t_i$ AND $p_i$ OF A PULSE-MODULATED ELT SIGNAL	220
APPENDIX B - PREDICTION ERROR FILTER	223
APPENDIX C - DESIGN OF A BANDPASS FILTER	230
APPENDIX D - LISTINGS OF THE PROGRAM ELTAP, WFIR, PROAP SPMAP AND CURVE	238
APPENDIX E - CALCULATING THE MEM SPECTRA OF A PULSE-MODULATED RANDOM PHASE SIGNAL BASED ON THE AVERAGING TECHNIQUE	266
APPENDIX F - PROCESSING RESULTS FOR ELT SIGNALS WITH MIXED MODULATION	271

## LIST OF ILLUSTRATIONS

		Page
Fig. 1.1	SARSAT System Diagram.	3
Fig. 1.2	Sinusoidal-modulated ELT signal with linear frequency sweep.	8
Fig. 1.3	Sinusoidal-modulated ELT signal with quadratic frequency sweep.	9
Fig. 1.4	The modulating signal, $m(t)$ , for a pulse-modulated ELT signal.	10
Fig. 1.5	Pulse-modulated ELT signal with linear frequency sweep.	12
Fig. 1.6	Pulse-modulated ELT signal with quadratic frequency sweep.	13
Fig. 1.7(a)	A schematic diagram for generating pulse-modulated continuous phase ELT signal.	14
Fig. 1.7(b)	A schematic diagram for generating pulse-modulated random phase ELT signal.	14
Fig. 1.8	Carrier frequency versus time for an ELT signal.	16
Fig. 1.9	Flat-earth model of the SARSAT geometry.	17
Fig. 2.1	The number of operations required for computing the discrete Fourier transform using the FFT algorithm compared with the number of operations required for direct calculation of the discrete Fourier transform.	25
Fig. 2.2	The FFT power of a 512-point pulse-modulated (linear frequency sweep) ELT signal at 9500 Hz.	26
Fig. 2.3	Window functions.	29

List of illustrations continued

	Page
Fig. 2.4	The FFT spectrum of a 512-point pulse-modulated (linear frequency sweep) ELT signal at 9500 Hz windowed by a Kaiser window for $\beta=8.0$ . 32
Fig. 2.5	The MEM power spectrum of a 512-point pulse-modulated (linear frequency sweep) ELT signal at 9500 Hz. The MEM filter order is 2. 37
Fig. 2.6	The autocorrelation function (256-lag) of the signal described in Fig. 1.5. 41
Fig. 2.7	The ACFMEM spectrum of the signal (Fig. 2.6). The MEM filter order is 2. 42
Fig. 2.8	The frequency response of an FIR bandpass filter. The cutoff frequencies are at 7000 Hz and 18000 Hz. The impulse response is 171 points. 44
Fig. 3.1	Pulse-modulated ELT signal (512-point) with continuous phase, linear frequency sweep and 36% duty cycle. Carrier frequency is 12832 Hz. 54
Fig. 3.2	The FFT spectrum of the signal shown in Fig. 3.1. 54
Fig. 3.3	The FFT spectrum of the signal (shown in Fig. 3.1) with quadratic frequency sweep. 55
Fig. 3.4	The signal shown in Fig. 3.1 windowed by a Kaiser window with $\beta=8.0$ . 57
Fig. 3.5	The FFT spectrum of the windowed signal shown in Fig. 3.4. 57
Fig. 3.6	The FFT spectrum of the signal (shown in Fig. 3.1) windowed by a Kaiser window ( $\beta=4.0$ ). 58
Fig. 3.7	The FFT spectrum of the signal (shown in Fig. 3.1) windowed by a Kaiser window ( $\beta=10.0$ ). 58
Fig. 3.8	The FFT spectrum of the signal (shown in Fig. 3.1) windowed by a Hamming window. 59

List of illustrations continued

	Page
Fig. 3.9	The FFT spectrum of the signal (shown in Fig. 3.1) windowed by a Blackman window. 59
Fig. 3.10	The FFT spectrum of the signal (shown in Fig. 3.1) filtered by a bandpass filter. 60
Fig. 3.11	The FFT spectrum of the signal (shown in Fig. 3.1) with duty cycle equal to 40%. 62
Fig. 3.12	The FFT spectrum of the signal (shown in Fig. 3.1) with duty cycle 50%. 62
Fig. 3.13	A pulse-modulated random phase ELT signal with linear frequency sweep and 36% duty cycle. Carrier frequency is 12832 Hz. 63
Fig. 3.14	The FFT spectrum of the random phase signal shown in Fig. 3.13. 63
Fig. 3.15	The FFT spectrum of the random phase signal (shown in Fig. 3.13) with quadratic frequency sweep. 64
Fig. 3.16	The signal shown in Fig. 3.13 windowed by a Kaiser window ( $\beta = 8.0$ ). 65
Fig. 3.17	The FFT spectrum of the random phase signal shown in Fig. 3.16. 65
Fig. 3.18	The FFT spectrum of the random phase signal shown in Fig. 3.13 filtered by a bandpass filter. 66
Fig. 3.19	A sinusoidal-modulated ELT signal with linear frequency sweep. Carrier frequency is 12832 Hz. 67
Fig. 3.20	The FFT spectrum of the signal shown in Fig. 3.19. 67
Fig. 3.21	The FFT spectrum of the signal shown in Fig. 3.19 with quadratic frequency sweep. 68

List of illustrations continued

	Page	
Fig. 3.22	The signal shown in Fig. 3.19 windowed by a Kaiser window ( $\beta = 8.0$ ).	70
Fig. 3.23	The FFT spectrum of the signal shown in Fig. 3.22.	70
Fig. 3.24	The MEM spectra at filter order 2 of a pulse-modulated signal (linear frequency sweep, continuous phase and 36% duty cycle). Carrier frequency is 12832 Hz.	72
Fig. 3.25	The MEM spectra at filter order 3 (continuous phase signal).	72
Fig. 3.26	The MEM spectra at filter order 4 (continuous phase signal).	74
Fig. 3.27	The MEM spectra at filter order 6 (continuous phase signal).	74
Fig. 3.28	The MEM spectra at filter order 8 (continuous phase signal).	75
Fig. 3.29	The MEM spectra at filter order 10 (continuous phase signal).	75
Fig. 3.30	The MEM spectra at filter order 20 (continuous phase signal).	76
Fig. 3.31	The MEM spectra at filter order 2 of the signal described in Fig. 3.24 with quadratic frequency sweep.	77
Fig. 3.32	The MEM spectra at filter order 10 of the signal described in Fig. 3.31.	77
Fig. 3.33	The MEM spectra at filter order 2 of a pulse-modulated random phase ELT signal (linear frequency sweep and 36% duty cycle). Carrier frequency is 12832 Hz.	79

List of illustrations continued

	Page	
Fig. 3.34	The MEM spectra at filter order 3 of the signal described in Fig. 3.33.	79
Fig. 3.35	The MEM spectra at filter order 4 (random phase signal).	81
Fig. 3.36	The MEM spectra at filter order 6 (random phase signal).	81
Fig. 3.37	The MEM spectra at filter order 8 (random phase signal).	82
Fig. 3.38	The MEM spectra at filter order 10 (random phase signal).	82
Fig. 3.39	The MEM spectra at filter order 20 (random phase signal).	83
Fig. 3.40	The MEM spectra at filter order 2 of a sinusoidal-modulated signal with linear frequency sweep. Carrier frequency is 12832 Hz.	84
Fig. 3.41	The MEM spectra at filter order 3 (sinusoidal-modulated signal).	84
Fig. 3.42	The MEM spectra at filter order 4 (sinusoidal-modulated signal).	86
Fig. 3.43	The MEM spectra at filter order 6 (sinusoidal-modulated signal).	86
Fig. 3.44	The MEM spectra at filter order 8 (sinusoidal-modulated signal).	87
Fig. 3.45	The MEM spectra at filter order 10 (sinusoidal-modulated signal).	87
Fig. 3.46	The MEM spectra at filter order 20 (sinusoidal-modulated signal).	88

List of illustrations continued

		Page
Fig. 3.47(a)	The error curve of pulse-modulated ELT signal (continuous phase, linear frequency sweep and 36% duty cycle) using MEM at filter order 2.	90
Fig. 3.47(b)	An expanded view of the curve in Fig. 3.47(a)	90
Fig. 3.48(a)	The error curve of the signal described in Fig. 3.47(a) using the ACFMEM at filter order 2.	91
Fig. 3.48(b)	An expanded view of the curve in Fig. 3.48(a).	91
Fig. 3.49	The error curve of the signal described in Fig. 3.47(a) with quadratic frequency sweep and at MEM filter order 2.	92
Fig. 3.50	The error curve of the signal described in Fig. 3.49 using ACFMEM at filter order 2.	92
Fig. 3.51	The MEM spectra of the signal described in Fig. 3.47(a) with carrier frequency at 1500 Hz and filter order 2.	94
Fig. 3.52(a)	The FFT spectrum of the signal described in Fig. 3.47(a). Carrier frequency is at 1500 Hz.	95
Fig. 3.52(b)	The FFT spectrum of the signal (at carrier frequency 1500 Hz) described in Fig. 3.47(a) and windowed by a Kaiser window ( $\beta = 8.0$ ).	95
Fig. 3.53	The MEM spectra of the signal (at 3250 Hz) using MEM at filter order 2.	96
Fig. 3.54(a)	The FFT spectrum of the signal (at 3250 Hz) described in Fig. 3.47(a).	97
Fig. 3.54(b)	The FFT spectrum of the signal (at 3250 Hz) windowed by a Kaiser window ( $\beta = 8.0$ ).	97
Fig. 3.55	The MEM spectra of the signal (at 7500 Hz) using MEM at filter order 2.	98

List of illustrations continued

	Page
Fig. 3.56	The FFT spectrum of the signal at 7500 Hz. 98
Fig. 3.57(a)	The error curve of a pulse-modulated random phase signal (linear frequency sweep and 36% duty cycle) using MEM at filter order 2. 99
Fig. 3.57(b)	An expanded view of the curve in Fig. 3.57(a) 99
Fig. 3.58(a)	The error curve of the signal described in Fig. 3.57(a) using ACFMEM at filter order 2. 100
Fig. 3.58(b)	An expanded view of the curve in Fig. 3.58(a) 100
Fig. 3.59	The error curve of the signal described in Fig. 3.57(a) with quadratic frequency sweep and MEM order 2. 101
Fig. 3.60	The error curve of the signal described in Fig. 3.59 with ACFMEM at filter order 2. 101
Fig. 3.61	The MEM spectra at filter order 2 of the signal (at 3250 Hz) described in Fig. 3.57(a). 102
Fig. 3.62	The FFT spectrum of the signal (at 3250 Hz) described in Fig. 3.57(a). 102
Fig. 3.63(a)	The error curve of sinusoidal-modulated signal with linear frequency sweep and MEM at filter order 2. 104
Fig. 3.63(b)	An expanded view of the curve in Fig. 3.63(a) 104
Fig. 3.64(a)	The error curve of the signal described in Fig. 3.63(a) with the ACFMEM at filter order 2. 105
Fig. 3.64(b)	An expanded view of the curve in Fig. 3.64(a) 105

List of illustrations continued

		Page
Fig. 3.65	The error curve of the signal described in Fig. 3.63(a) with quadratic frequency sweep and MEM at filter order 2.	106
Fig. 3.66	The error curve of the signal described in Fig. 3.65 with the ACFMEM at filter order 2.	106
Fig. 3.67	The FFT spectrum when only noise is present.	108
Fig. 3.68	The FFT spectrum of a continuous phase signal with carrier frequency = 12832 Hz and CNDR = 34 dB-Hz.	109
Fig. 3.69	The FFT spectrum of a continuous phase signal with carrier frequency = 12832 Hz and CNDR = 39 dB-Hz.	109
Fig. 3.70	The FFT spectrum of a continuous phase signal with carrier frequency = 12832 Hz and CNDR = 44 dB-Hz.	110
Fig. 3.71	The FFT spectrum of a continuous phase signal with carrier frequency = 12832 Hz and CNDR = 54 dB-Hz.	110
Fig. 3.72	The FFT spectrum of a continuous phase signal with carrier frequency = 9237 Hz and CNDR = 34 dB-Hz.	111
Fig. 3.73	The FFT spectrum of a continuous phase signal with carrier frequency = 9237 Hz and CNDR = 29 dB-Hz.	111
Fig. 3.74	The FFT spectrum of a windowed continuous phase signal with carrier frequency = 12832 Hz and CNDR = 34 dB-Hz.	112
Fig. 3.75	The FFT spectrum of a windowed continuous phase signal with carrier frequency = 12832 Hz and CNDR = 39 dB-Hz.	112

List of illustrations continued

		Page
Fig. 3.76	The FFT spectrum of a windowed continuous phase signal with carrier frequency = 12832 Hz and CNDR = 44 dB-Hz.	113
Fig. 3.77	The FFT spectrum of a windowed continuous phase signal with carrier frequency = 12832 Hz and CNDR = 54 dB-Hz.	113
Fig. 3.78	The MEM spectra (filter order 2) when only noise is present.	115
Fig. 3.79	The FFT spectrum when noise is filtered by a bandpass filter.	115
Fig. 3.80	The MEM spectra (filter order 2) of a continuous phase signal with carrier frequency = 12832 Hz and CNDR = 34 dB-Hz.	116
Fig. 3.81	The MEM spectra (filter order 2) of a continuous phase signal with carrier frequency = 12832 Hz and CNDR = 39 dB-Hz.	116
Fig. 3.82	The MEM spectra (filter order 2) of a continuous phase signal with carrier frequency = 12832 Hz and CNDR = 44 dB-Hz.	117
Fig. 3.83	The MEM spectra (filter order 2) of a continuous phase signal with carrier frequency = 12832 Hz and CNDR = 54 dB-Hz.	117
Fig. 3.84	The MEM spectra (filter order 2) of a continuous phase signal with carrier frequency = 9237 Hz and CNDR = 29 dB-Hz.	118
Fig. 3.85	The MEM spectra (filter order 2) of a continuous phase signal with carrier frequency = 9237 Hz and CNDR = 34 dB-Hz.	119
Fig. 3.86	The MEM spectra (filter order 2) of a continuous phase signal with carrier frequency = 9237 Hz and CNDR = 39 dB-Hz.	119

List of illustrations continued

		Page
Fig. 3.87	The MEM spectra (filter order 2) of a continuous phase signal with carrier frequency = 9237 Hz and CNDR = 44 dB-Hz.	120
Fig. 3.88	The MEM spectra (filter order 2) of a continuous phase signal with carrier frequency = 9237 Hz and CNDR = 54 dB-Hz.	120
Fig. 3.89	The MEM spectra (filter order 10) of a continuous phase signal with carrier frequency = 9237 Hz and CNDR = 34 dB-Hz.	121
Fig. 3.90	The MEM spectra (filter order 10) of a continuous phase signal with carrier frequency = 9237 Hz and CNDR = 54 dB-Hz.	121
Fig. 3.91	The FFT spectrum of a random phase signal with carrier frequency = 12832 Hz and CNDR = 34 dB-Hz.	122
Fig. 3.92	The FFT spectrum of a random phase signal with carrier frequency = 12832 Hz and CNDR = 39 dB-Hz.	122
Fig. 3.93	The FFT spectrum of a random phase signal with carrier frequency = 12832 Hz and CNDR = 44 dB-Hz.	123
Fig. 3.94	The FFT spectrum of a random phase signal with carrier frequency = 12832 Hz and CNDR = 54 dB-Hz.	123
Fig. 3.95	The FFT spectrum of a random phase signal with carrier frequency = 9237 Hz and CNDR = 34 dB-Hz.	124
Fig. 3.96	The FFT spectrum of a random phase signal with carrier frequency = 9237 Hz and CNDR = 29 dB-Hz.	124
Fig. 3.97	The MEM spectra (filter order 2) of a random phase signal with carrier frequency = 12832 Hz and CNDR = 34 dB-Hz.	126
Fig. 3.98	The MEM spectra (filter order 2) of a random phase signal with carrier frequency = 12832 Hz and CNDR = 39 dB-Hz.	126

List of illustrations continued

		Page
Fig. 3.99	The MEM spectra (filter order 2) of a random phase signal with carrier frequency = 12832 Hz and CNDR = 44 dB-Hz.	127
Fig. 3.100	The MEM spectra (filter order 2) of a random phase signal with carrier frequency = 12832 Hz and CNDR = 54 dB-Hz.	127
Fig. 3.101	The MEM spectra (filter order 2) of a random phase signal with carrier frequency = 9237 Hz and CNDR = 29 dB-Hz.	128
Fig. 3.102	The MEM spectra (filter order 2) of a random phase signal with carrier frequency = 9237 Hz and CNDR = 34 dB-Hz.	129
Fig. 3.103	The MEM spectra (filter order 2) of a random phase signal with carrier frequency = 9237 Hz and CNDR = 39 dB-Hz.	129
Fig. 3.104	The MEM spectra (filter order 2) of a random phase signal with carrier frequency = 9237 Hz and CNDR = 44 dB-Hz.	130
Fig. 3.105	The MEM spectra (filter order 2) of a random phase signal with carrier frequency = 9237 Hz and CNDR = 54 dB-Hz.	130
Fig. 3.106	The FFT spectrum of a sinusoidal-modulated signal with carrier frequency = 12832 Hz and CNDR = 34 dB-Hz.	131
Fig. 3.107	The FFT spectrum of a sinusoidal-modulated signal with carrier frequency = 12832 Hz and CNDR = 39 dB-Hz.	131
Fig. 3.108	The FFT spectrum of a sinusoidal-modulated signal with carrier frequency = 12832 Hz and CNDR = 44 dB-Hz.	132

List of illustrations continued

	Page	
Fig. 3.109	The FFT spectrum of a sinusoidal-modulated signal with carrier frequency = 12832 Hz and CNDR = 54 dB-Hz.	132
Fig. 3.110	The FFT spectrum of a sinusoidal-modulated signal with carrier frequency = 9237 Hz and CNDR = 34 dB-Hz.	133
Fig. 3.111	The MEM spectra (filter order 2) of a sinusoidal-modulated signal with carrier frequency = 12832 Hz and CNDR = 34 dB-Hz.	134
Fig. 3.112	The MEM spectra (filter order 2) of a sinusoidal-modulated signal with carrier frequency = 12832 Hz and CNDR = 39 dB-Hz.	134
Fig. 3.113	The MEM spectra (filter order 2) of a sinusoidal-modulated signal with carrier frequency = 12832 Hz and CNDR = 44 dB-Hz.	135
Fig. 3.114	The MEM spectra (filter order 2) of a sinusoidal-modulated signal with carrier frequency = 12832 Hz and CNDR = 54 dB-Hz.	135
Fig. 3.115	The MEM spectra (filter order 2) of a sinusoidal-modulated signal with carrier frequency = 9237 Hz and CNDR = 34 dB-Hz.	136
Fig. 3.116	The MEM spectra (filter order 2) of a sinusoidal-modulated signal with carrier frequency = 9237 Hz and CNDR = 39 dB-Hz.	136
Fig. 3.117	The MEM spectra (filter order 2) of a sinusoidal-modulated signal with carrier frequency = 9237 Hz and CNDR = 44 dB-Hz.	137
Fig. 3.118	The MEM spectra (filter order 2) of a sinusoidal-modulated signal with carrier frequency = 9237 Hz and CNDR = 54 dB-Hz.	137

List of illustrations continued

	Page
Fig. 4.1	The FFT spectrum of two continuous phase, pulse-modulated signals with carrier frequencies 9448 Hz and 15039 Hz. 142
Fig. 4.2	The FFT spectrum of two windowed continuous phase, pulse-modulated signals with carrier frequencies 9448 Hz and 15039 Hz. 142
Fig. 4.3	The FFT spectrum of two random phase, pulse-modulated signals with carrier frequencies 9448 Hz and 15039 Hz. 143
Fig. 4.4	The FFT spectrum of two windowed random phase, pulse-modulated signals with carrier frequencies 9448 Hz and 15039 Hz. 143
Fig. 4.5	The FFT spectrum of two continuous phase, pulse-modulated signals with carrier frequencies 9448 Hz and 15039 Hz filtered by a bandpass filter. 144
Fig. 4.6	The FFT spectrum of two random phase, pulse-modulated signals with carrier frequencies 9448 Hz and 15039 Hz filtered by a bandpass filter. 144
Fig. 4.7	The FFT spectrum of two sinusoidal-modulated signals with carrier frequencies 9448 Hz and 15039 Hz. 145
Fig. 4.8	The FFT spectrum of five continuous phase, pulse-modulated signals with carrier frequencies 7588 Hz, 9000 Hz, 11924 Hz, 13527 Hz and 15425 Hz. 146
Fig. 4.9	The FFT spectrum of five windowed continuous phase signals with carrier frequencies 7588 Hz, 9000 Hz, 11924 Hz, 13527 Hz and 15425 Hz. 146
Fig. 4.10	The FFT spectrum of five random phase signals with carrier frequencies 7588 Hz, 9000 Hz, 11924 Hz, 13527 Hz and 15425 Hz. 148

List of illustrations continued

	Page
Fig. 4.11	The FFT spectrum of five continuous phase signals filtered by a bandpass filter. 149
Fig. 4.12	The FFT spectrum of five random phase signals filtered by a bandpass filter. 149
Fig. 4.13	The FFT spectrum of five sinusoidal-modulated signals with carrier frequencies 7588 Hz, 9000 Hz, 11924 Hz, 13527 Hz and 15425 Hz. 150
Fig. 4.14	The FFT spectrum of ten continuous phase signals with carrier frequencies 7441 Hz, 8504 Hz, 9640 Hz, 10483 Hz, 11876 Hz, 12683 Hz, 13636 Hz, 14846 Hz, 16165 Hz and 17595 Hz. 151
Fig. 4.15	The FFT spectrum of ten windowed continuous phase signals. 151
Fig. 4.16	The FFT spectrum of ten random phase signals with carrier frequencies 7441 Hz, 8504 Hz, 9640 Hz, 10483 Hz, 11876 Hz, 12683 Hz, 13636 Hz, 14846 Hz, 16165 Hz and 17595 Hz. 152
Fig. 4.17	The FFT spectrum of ten continuous phase signals filtered by a bandpass filter. 153
Fig. 4.18	The FFT spectrum of ten random phase signals filtered by a bandpass filter. 153
Fig. 4.19	The MEM spectra (filter order 2) of two continuous phase signals with carrier frequencies 9448 Hz and 15039 Hz. 155
Fig. 4.20	The MEM spectra (filter order 4) of two continuous phase signals. 155
Fig. 4.21	The MEM spectra (filter order 6) of two continuous phase signals 157
Fig. 4.22	The MEM spectra (filter order 8) of two continuous phase signals. 157

List of illustrations continued

	Page
Fig. 4.23	The MEM spectra (filter order 10) of two continuous phase signals. 158
Fig. 4.24	The MEM spectra (filter order 20) of two continuous phase signals. 158
Fig. 4.25	The MEM spectra (filter order 2) of two random phase signals with carrier frequencies 9448 Hz and 15039 Hz. 159
Fig. 4.26	The MEM spectra (filter order 4) of two random phase signals. 159
Fig. 4.27	The MEM spectra (filter order 6) of two random phase signals. 160
Fig. 4.28	The MEM spectra (filter order 8) of two random phase signals. 160
Fig. 4.29	The MEM spectra (filter order 10) of two random phase signals. 161
Fig. 4.30	The MEM spectra (filter order 20) of two random phase signals. 161
Fig. 4.31	The MEM spectra (filter order 4) of two sinusoidal-modulated signals with carrier frequencies 9448 Hz and 15039 Hz. 162
Fig. 4.32	The MEM spectra (filter order 20) of two sinusoidal-modulated signals. 162
Fig. 4.33	The MEM spectra (filter order 4) of five continuous phase signals with carrier frequencies 7588 Hz, 9000 Hz, 11924 Hz, 13527 Hz and 15425 Hz. 163
Fig. 4.34	The MEM spectra (filter order 6) of five continuous phase signals. 163

List of illustrations continued

		Page
Fig. 4.35	The MEM spectra (filter order 8) of five continuous phase signals.	164
Fig. 4.36	The MEM spectra (filter order 10) of five continuous phase signals.	164
Fig. 4.37	The MEM spectra (filter order 20) of five continuous phase signals.	165
Fig. 4.38(a)	The 'ELT+MEM' and 'ELT+ACFMEM' spectra (filter order 50) of five continuous phase signals.	167
Fig. 4.38(b)	The 'ELT+FIRMEM' and 'ELT+ACF+FIRMEM' spectra (filter order 50) of five continuous phase signals.	167
Fig. 4.38(c)	An expanded view of the 'ELT+ACF+FIRMEM' spectrum in Fig. 4.38(b)	168
Fig. 4.39	The MEM spectra (filter order 20) of five random phase signals with carrier frequencies 7588 Hz, 9000 Hz, 11924 Hz, 13527 Hz and 15425 Hz.	169
Fig. 4.40(a)	The 'ELT+MEM' and 'ELT+ACFMEM' spectra (filter order 50) of five random phase signals.	170
Fig. 4.40(b)	The 'ELT+FIRMEM' and 'ELT+ACF+FIRMEM' spectra (filter order 50) of five random phase signals.	170
Fig. 4.41(a)	The 'ELT+MEM' and 'ELT+ACFMEM' spectra (filter order 50) of five sinusoidal-modulated signals.	171
Fig. 4.41(b)	The 'ELT+FIRMEM' and 'ELT+ACF+FIRMEM' spectra (filter order 50) of five sinusoidal-modulated signals.	171

List of illustrations continued

	Page	
Fig. 4.42	The MEM spectra (filter order 20) of ten continuous phase signals with carrier frequencies 7441 Hz, 8504 Hz, 9640 Hz, 10483 Hz, 11876 Hz, 12683 Hz, 13636 Hz, 14846 Hz, 16165 Hz and 17595 Hz.	173
Fig. 4.43(a)	The 'ELT+MEM' and 'ELT+ACFMEM' spectra (filter order 100) of ten continuous phase signals.	174
Fig. 4.43(b)	The 'ELT+FIRMEM' and 'ELT+ACF+FIRMEM' spectra (filter order 100) of ten continuous phase signals.	174
Fig. 4.44	The 'ELT+ACF+FIRMEM' spectrum (filter order 100) of ten random phase signals.	175
Fig. 4.45	The 'ELT+ACF+FIRMEM' configuration modified with a bank of bandpass filters as an alternate preprocessor.	178
Fig. 4.46	The 'ELT+ACF+FIRMEM' spectra (filter order 4, using a bank of bandpass filters) of two continuous phases signals with carrier frequencies 9448 Hz and 15039 Hz.	179
Fig. 4.47	The 'ELT+ACF+FIRMEM' spectra (filter order 8) of two continuous phase signals.	179
Fig. 4.48	The 'ELT+ACF+FIRMEM' spectra (filter order 10) of two continuous phase signals.	180
Fig. 4.49	The 'ELT+ACF+FIRMEM' spectra (filter order 4) of two random phase signals with carrier frequencies 9448 Hz and 15039 Hz.	182
Fig. 4.50	The 'ELT+ACF+FIRMEM' spectra (filter order 8) of two random phase signals.	182

List of illustrations continued

		Page
Fig. 4.51	The 'ELT+ACF+FIRMEM' spectra (filter order 10) of two random phase signals.	183
Fig. 4.52	The 'ELT+AVF+FIRMEM' spectra (filter order 4) of two sinusoidal-modulated signals with carrier frequencies 9448 Hz and 15039 Hz.	184
Fig. 4.53	The 'ELT+ACF+FIRMEM' spectra (filter order 8) of two sinusoidal-modulated signals.	184
Fig. 4.54	The 'ELT+ACF+FIRMEM' spectra (filter order 10) of two sinusoidal-modulated signals.	185
Fig. 4.55	The 'ELT+ACF+FIRMEM' spectra (filter order 8) of five continuous phase signals with carrier frequencies 7588 Hz, 9000 Hz, 11924 Hz, 13527 Hz and 15425 Hz.	186
Fig. 4.56	The 'ELT+ACF+FIRMEM' spectra (filter order 10) of five continuous phase signals.	186
Fig. 4.57	The 'ELT+ACF+FIRMEM' spectra (filter order 8) of five random phase signals with carrier frequencies 7588 Hz, 9000 Hz, 11924 Hz, 13527 Hz and 15425 Hz.	187
Fig. 4.58	The 'ELT+ACF+FIRMEM' spectra (filter order 10) of five random phases signals.	187
Fig. 4.59	The 'ELT+ACF+FIRMEM' spectra (filter order 8) of five sinusoidal-modulated signals with carrier frequencies 7588 Hz, 9000 Hz, 11924 Hz, 13527 Hz and 15425 Hz.	189
Fig. 4.60	The 'ELT+ACF+FIRMEM' spectra (filter order 10) of five sinusoidal-modulated signals.	189
Fig. 4.61	The 'ELT+ACF+FIRMEM' spectra (filter order 8) of ten continuous phase signals with carrier frequencies 7441 Hz, 8504 Hz, 9640 Hz, 10483 Hz, 11876 Hz, 12683 Hz, 13636 Hz, 14846 Hz, 16165 Hz, and 17595 Hz.	190

List of illustrations continued

		Page
Fig. 4.62	The 'ELT+ACF+FIRMEM' spectra (filter order 10) of ten continuous phase signals.	190
Fig. 4.63	The 'ELT+ACF+FIRMEM' spectra (filter order 10) of ten random phase signals with carrier frequencies 7441 Hz, 8504 Hz, 9640 Hz, 10483 Hz, 11876 Hz, 12683 Hz, 13636 Hz, 14846 Hz, 16165 Hz and 17595 Hz.	191
Fig. 4.64	The FFT spectrum of two continuous phase signals with carrier frequencies 9448 Hz and 15039 Hz. The CNDR is 34 dB-Hz.	193
Fig. 4.65	The FFT spectrum of two continuous phase signals with CNDR= 39 dB-Hz.	193
Fig. 4.66	The FFT spectrum of two continuous phase signals with CNDR = 44 dB-Hz.	194
Fig. 4.67	The FFT spectrum of two continuous phase signals with CNDR = 54 dB-Hz.	194
Fig. 4.68	The MEM spectra (filter order 20) of two continuous phase signals with CNDR = 34 dB-Hz.	195
Fig. 4.69	The MEM spectra (filter order 20) of two continuous phase signals with CNDR = 39 dB-Hz.	195
Fig. 4.70	The MEM spectra (filter order 20) of two continuous phase signals with CNDR = 44 dB-Hz.	196
Fig. 4.71	The MEM spectra (filter order 20) of two continuous phase signals with CNDR = 54 dB-Hz.	196
Fig. 4.72	The 'ELT+ACF+FIRMEM' spectra (filter order 8) of two continuous phase signals with CNDR = 34 dB-Hz.	198

List of illustrations continued

		Page
Fig. 4.73	The 'ELT+ACF+FIRMEM' spectra (filter order 8) of two continuous phase signals with CNDR = 39 dB-Hz.	198
Fig. 4.74	The 'ELT+ACF+FIRMEM' spectra (filter order 8) of two continuous phase signals with CNDR = 44 dB-Hz.	199
Fig. 4.75	The 'ELT+ACF+FIRMEM' spectra (filter order 8) of two continuous phase signals with CNDR = 54 dB-Hz.	199
Fig. 4.76	The FFT spectrum of two random phase signals with carrier frequencies 9448 Hz and 15039 Hz. The CNDR is 34 dB-Hz.	200
Fig. 4.77	The FFT spectrum of two random phase signals with CNDR = 39 dB-Hz.	200
Fig. 4.78	The FFT spectrum of two random phase signals with CNDR = 44 dB-Hz.	201
Fig. 4.79	The FFT spectrum of two random phase signals with CNDR = 54 dB-Hz.	201
Fig. 4.80	The 'ELT+ACF+FIRMEM' spectra (filter order 20) of two random phase signals with CNDR equals to 34 dB-Hz, 39 dB-Hz, 44 dB-Hz and 54 dB-Hz.	202
Fig. 4.81	The 'ELT+ACF+FIRMEM' spectra (filter order 8) of two random phase signals with CNDR= 34 dB-Hz.	203
Fig. 4.82	The 'ELT+ACF+FIRMEM' spectra (filter order 8) of two random phase signals with CNDR=39 dB-Hz.	203
Fig. 4.83	The 'ELT+ACF+FIRMEM' spectra (filter order 8) of two random phase signals with CNDR=44 dB-Hz.	204
Fig. 4.84	The 'ELT+ACF+FIRMEM' spectra (filter order 8) of two random phase signals with CNDR=54 dB-Hz.	204

List of illustrations continued

		Page
Fig. 4.85	The FFT spectrum of five continuous phase signals with carrier frequencies 7588 Hz, 9000 Hz, 11924 Hz, 13527 Hz and 15425 Hz. The CNDR is 34 dB-Hz.	205
Fig. 4.86	The FFT spectrum of five continuous phase signals with CNDR = 39 dB-Hz.	205
Fig. 4.87	The FFT spectrum of five continuous phase signals with CNDR = 44 dB-Hz.	206
Fig. 4.88	The FFT spectrum of five continuous phase signals with CNDR = 54 dB-Hz.	206
Fig. 4.89	The MEM spectra (filter order 50) of five continuous phase signals with CNDR = 34 dB-Hz.	207
Fig. 4.90	The MEM spectra (filter order 50) of five continuous phase signals with CNDR = 39 dB-Hz.	207
Fig. 4.91	The MEM spectra (filter order 50) of five continuous phase signals with CNDR = 44 dB-Hz.	208
Fig. 4.92	The MEM spectra (filter order 50) of five continuous phase signals with CNDR = 54 dB-Hz.	208
Fig. 4.93	The 'ELT+ACF+FIRMEM' spectra (filter order 8) of five continuous phase signals with CNDR = 34 dB-Hz.	209
Fig. 4.94	The 'ELT+ACF+FIRMEM' spectra (filter order 8) of five continuous phase signals with CNDR = 39 dB-Hz.	209
Fig. 4.95	The 'ELT+ACF+FIRMEM' spectra (filter order 8) of five continuous phase signals with CNDR = 44 dB-Hz.	210
Fig. 4.96	The 'ELT+ACF+FIRMEM' spectra (filter order 8) of five continuous phase signals with CNDR = 54 dB-Hz.	210

List of illustrations continued

	Page	
Fig. B.1	Prediction error filter	228
Fig. C.1	A direct form realization of an FIR system.	231
Fig. C.2	Bandpass filter specifications.	236
Fig. E.1	The MEM spectra (filter order 2) of random phase, pulse-modulated signal using averaging technique. Carrier frequency is 12832 Hz.	267
Fig. E.2	The 'ELT+ACFMEM' spectra (filter order 2) of random phase, pulse-modulated signal.	267
Fig. E.3	The 'ELT+ACF+FIRMEM' spectra (filter order 2) of random phase, pulse-modulated signal.	268
Fig. E.4	The MEM spectra (filter order 10) of random phase, pulse-modulated signal.	268
Fig. E.5	The 'ELT+ACFMEM' spectra (filter order 10) of random phase, pulse-modulated signal.	270
Fig. E.6	The 'ELT+ACF+FIRMEM' spectra (filter order 10) of a random phase signal.	270
Fig. F.1	The FFT spectrum of three pulse-modulated signals with carrier frequencies 8504 Hz (continuous phase), 12683 Hz (continuous phase) and 13796 Hz (random phase). The CNDR is 34 dB-Hz.	272
Fig. F.2	The MEM spectra (filter order 30) of the three pulse-modulated signals with 34 dB-Hz CNDR.	272
Fig. F.3	The FFT spectrum of the three pulse-modulated signals with 39 dB-Hz.	273
Fig. F.4	The MEM spectra (filter order 30) of the three pulse-modulated signals with 39 dB-Hz CNDR.	273

List of illustrations continued

		Page
Fig. F.5	The FFT spectrum of the three pulse-modulated signals with 44 dB-Hz CNDR.	274
Fig. F.6	The MEM spectra (filter order 30) of the three pulse-modulated signals with 44 dB-Hz CNDR.	274
Fig. F.7	The FFT spectrum of the three pulse-modulated signals with 54 dB-Hz CNDR.	275
Fig. F.8	The MEM spectra (filter order 30) of the three pulse-modulated signals with 54 dB-Hz CNDR.	275
Fig. F.9	The 'ELT+ACF+FIRMEM' spectra (filter order 8) of the three pulse-modulated signals with 34 dB-Hz CNDR.	276
Fig. F.10	The 'ELT+ACF+FIRMEM' spectra (filter order 8) of the three pulse-modulated signals with 39 dB-Hz.	276
Fig. F.11	The 'ELT+ACF+FIRMEM' spectra (filter order 8) of the three pulse-modulated signals with 44 dB-Hz.	277
Fig. F.12	The 'ELT+ACF+FIRMEM' spectra (filter order 8) of the three pulse-modulated signals with 54 dB-Hz.	277

CHAPTER 1  
INTRODUCTION

In the past decade, the number of private and commercial aircraft has greatly increased. During this time, the problem of search and rescue for aircraft in distress has also become a significant concern. In the year 1977 alone, statistics [1] show that in the United States there were 4,286 aircraft crashes and of these 1,440 required a search to locate the crash site. The main difficulty facing a distressed aircraft is survival. The United States Department of Transportation studies [1] have shown that survival probability is less than a 10% chance when the rescue extends beyond two days after an aircraft crash. In contrast, if the rescue can be accomplished within eight hours, the survival rate is over 50%. Thus, rapid detection and location of an aircraft crash is of paramount importance in terms of survival.

Search and Rescue (SAR) operations in remote areas can be costly and time consuming since location of a distressed platform may take a month or more. In a country such as Canada with large areas in the north which are sparsely populated, the SAR problem becomes even more significant. Also, the harsh environment in these areas makes SAR operation particularly difficult in winter. A blanket of snow can easily hide a crash site. This leads to a reduction in the probability of survival.

The use of emergency locator transmitter (ELT) sets became

mandatory for all general aviation aircraft in the United States and Canada in the mid 1970's [1] - [4]. The ELT is a low-power radio transmitter (100mW) which emits an amplitude modulated carrier signal having a frequency of either 121.5 or 243 MHz. (A new band of frequency at 406 MHz is in the experimental stages. This will not be discussed here.) These signals can provide both an immediate alert and a homing signal to assist rescue forces in locating the site of distress. Originally, it was thought that this electronic device could solve the problems of rescuing distressed aircraft. However, it was soon evident that, due to the line-of-sight restriction, difficulties still remained which caused long delays in SAR operation and sometimes the aircraft would never be found. Also, the ELT battery has a life time of only several days. Therefore for large areas, a search procedure using aircraft is not practical.

The time and potential cost required for a search and rescue operation can be reduced by the use of a Search and Rescue Satellite-Aided Tracking (SARSAT) system [1] - [4]. It was proposed that use of a satellite in low-polar orbit, might greatly enhance the performance of SAR facilities. The main advantage of this system is that the satellite has a wide field of view and one pass covers many thousands of square kilometers. Thus, rescue procedures can be promptly underway when an ELT signal is detected. In concept, the system operates as shown in Fig. 1.1. When an aircraft is in distress, the ELT unit can be activated either on impact with the ground or by manually setting a switch. It is required that both the ELT and earth station be within

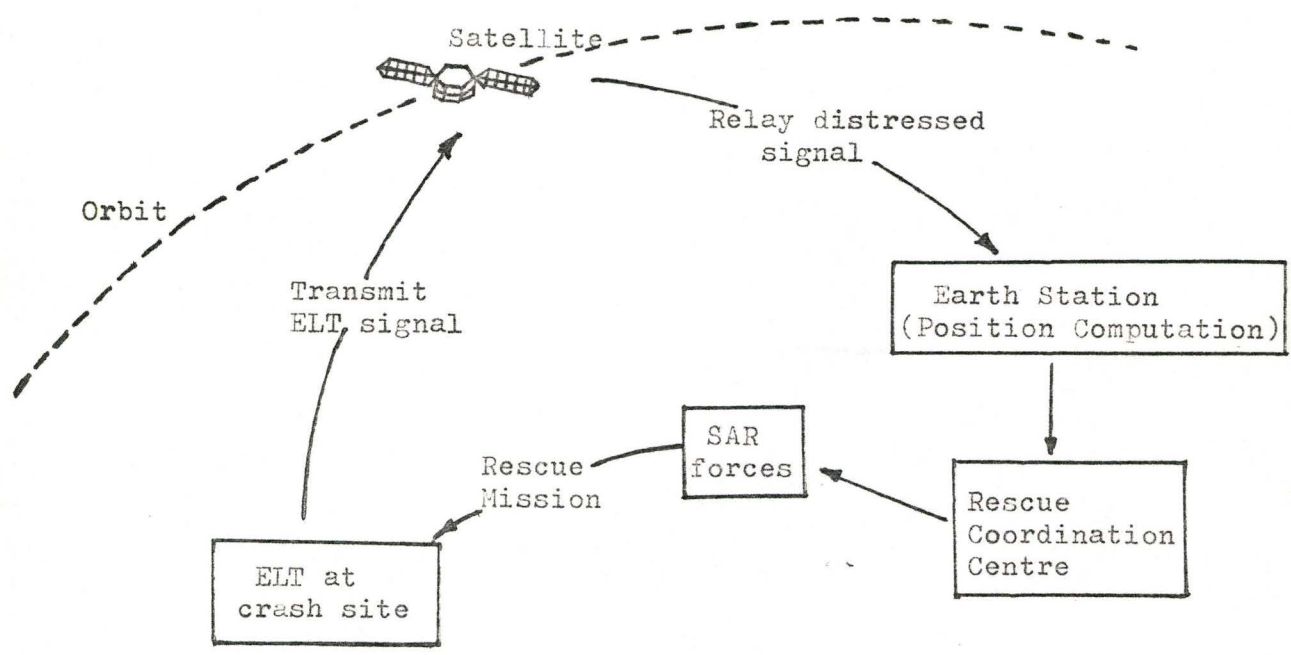


Fig. 1.1: SARSAT System Diagram.

sight of the satellite simultaneously. The ELT signal is detected by an orbiting satellite as it sweeps out a path over the SAR region of interest. Because of the relative motion between the satellite and ELT unit, the signal received at the spacecraft is Doppler shifted. A repeater on board the satellite relays the signal to an earth station where the received signal is analysed to extract an ELT position. The zero Doppler or point of closest approach of satellite to ELT must be determined with as much accuracy as possible. The slope of the Doppler curve at this point is used to calculate the range from satellite to ELT source. This estimate is passed to a Rescue Coordination Centre (RCC) which speedily dispatches search aircraft to the emergency site.

### 1.1 SARSAT PROGRAM

During 1975 and 1976, experiments [3] were carried out by the Communications Research Centre (CRC) in Ottawa, Ontario, Canada, using the AMSAT OSCAR satellite to test the validity of the SARSAT system. Encouraging results were obtained which led to the formation of an international joint venture to fulfill the SARSAT project. The key participants, hitherto, involve Department of Communications (DOC) for Canada, the Centre National d'Etudes Spatiales (CNES) for France and National Aeronautics and Space Administration (NASA) of the United States. The Ministry of Merchant Marine (MORFLOT) of the Soviet Union has also developed a parallel system called COSPAS, which is interoperable with the SARSAT [1],[5]. It is anticipated that, in the near future, other nations will participate in this project.

The National Oceanic and Atmospheric Administration (NOAA) of the United States will provide three weather satellites to perform the satellite-aided SAR missions. The first two spacecraft are scheduled to be launched by mid 1982. These satellites are capable of receiving emergency signals from distressed aircraft. The processing of these signals will permit an estimate of the location of ELT sources.

In the event of emergency, the ELT transmits the distress signal to an orbiting NOAA satellite, which relays the signal to the Local User Terminal (LUT). For a system employing two spacecraft, average waiting time for the United States and Canada is less than six hours. At any one time, the SRSAT system must have the ability to handle a multiple of emergency signals which emit from several different types of ELT units in different locations. Therefore, at an LUT, the Doppler processor is required to process up to ten simultaneously received ELT signals on any one satellite pass and determine the origin of these sources. Data from two such orbital paths and knowledge of the orbit of the spacecraft itself enable an estimate of the position of the ELT to be made. The accuracy of the estimated position is largely dependent on the method employed for processing the ELT signals.

At present, a detailed study of methods of spectral estimation is underway. To date, signal processing methods are based on the Fast Fourier Transform (FFT) and the use of windowing. The main weakness of Fourier analysis is the appearance of sidelobes in the spectrum. The effect of windowing, however, is to broaden the main lobe, which is also undesirable since this increases the ambiguity in the location of the

peak. A new program in operation for approximately two years has considered the use of a non-linear processing method based on the Maximum Entropy Method (MEM) with preprocessing provided by autocorrelation function (ACF) and finite impulse response (FIR) filtering. These techniques of signal processing methods as applied to SARSAT operation are discussed in the subsequent chapters.

## 1.2 ELT SIGNALS

The received ELT signal is an amplitude modulated carrier signal having a frequency of either 121.5 or 243 MHz. A mathematical representation of an amplitude modulated signal can be described as a function of time  $t$  in the form

$$S(t) = A_c [1+m(t)] \sin(2\pi f_c t + \phi) \quad (1.1)$$

where  $A_c$  is the carrier amplitude,  $f_c$  is the carrier frequency,  $\phi$  is the carrier phase angle, and  $m(t)$  defines the modulating signal. The modulating term can be classified as either sine-wave or pulse-shaped.

### 1.2.1 Sine-Wave Modulation

To formulate a sinusoidal-modulated ELT signal, we define

$$m(t) = \mu \sin(\theta_i(t)) \quad (1.2)$$

where  $\mu$  is the modulation factor which can be varied from 85% to 100% and  $\theta_i(t)$  is given by

$$\theta_i(t) = 2\pi \int f_{in}(t) dt \quad (1.3)$$

The instantaneous frequency,  $f_{in}(t)$ , is approximated in the least square sense by a linear function and also by a quadratic function [7],[8].

The linear fit of instantaneous frequency is given by

$$f_{in}(t) = 1400.0 - 700.0 \frac{t}{T_r} \quad (1.4)$$

and the quadratic representation is

$$f_{in}(t) = 1930.8 - 1784.8 \frac{t}{T_r} + 870.82 \frac{t^2}{T_r^2} \quad (1.5)$$

where  $T_r$  is the repetition period (0.25 s) of the signal. Solving these equations, the linear sweep sinusoidal-modulated ELT signal,  $s_L(t)$ , is given by

$$s_L(t) = A_c [1 + \mu \sin(2\pi(1400t - 1400t^2 + 0.75))] \sin(2\pi f_c t + \phi) \quad (1.6)$$

and the quadratic sweep sinusoidal-modulated signal,  $s_Q(t)$ , is given by

$$s_Q(t) = A_c [1 + \mu \sin(2\pi(4644.3t^3 - 3569.6t^2 + 1930.8t + 0.75))] \sin(2\pi f_c t + \phi) \quad (1.7)$$

Examples of these two waveforms, having 512 sample points, are given in Figs. 1.2 and 1.3 with the parameters  $A_c$  and  $\mu$  equal to one. The carrier frequency equals 9500 Hz and the sampling rate is fifty thousand samples per second.

### 1.2.2 Pulse-Shaped Modulation (Continuous Phase)

The modulating signal,  $m(t)$ , for a pulse-shaped ELT signal is depicted in Fig. 1.4 [7],[8]. The duration of these pulses is varied with time. It is, therefore, necessary to specify the rising and falling edges of each pulse. These are denoted by  $t_i$  and  $p_i$  respectively where  $i$  indicates the  $i$ -th pulse. The equations [7] to

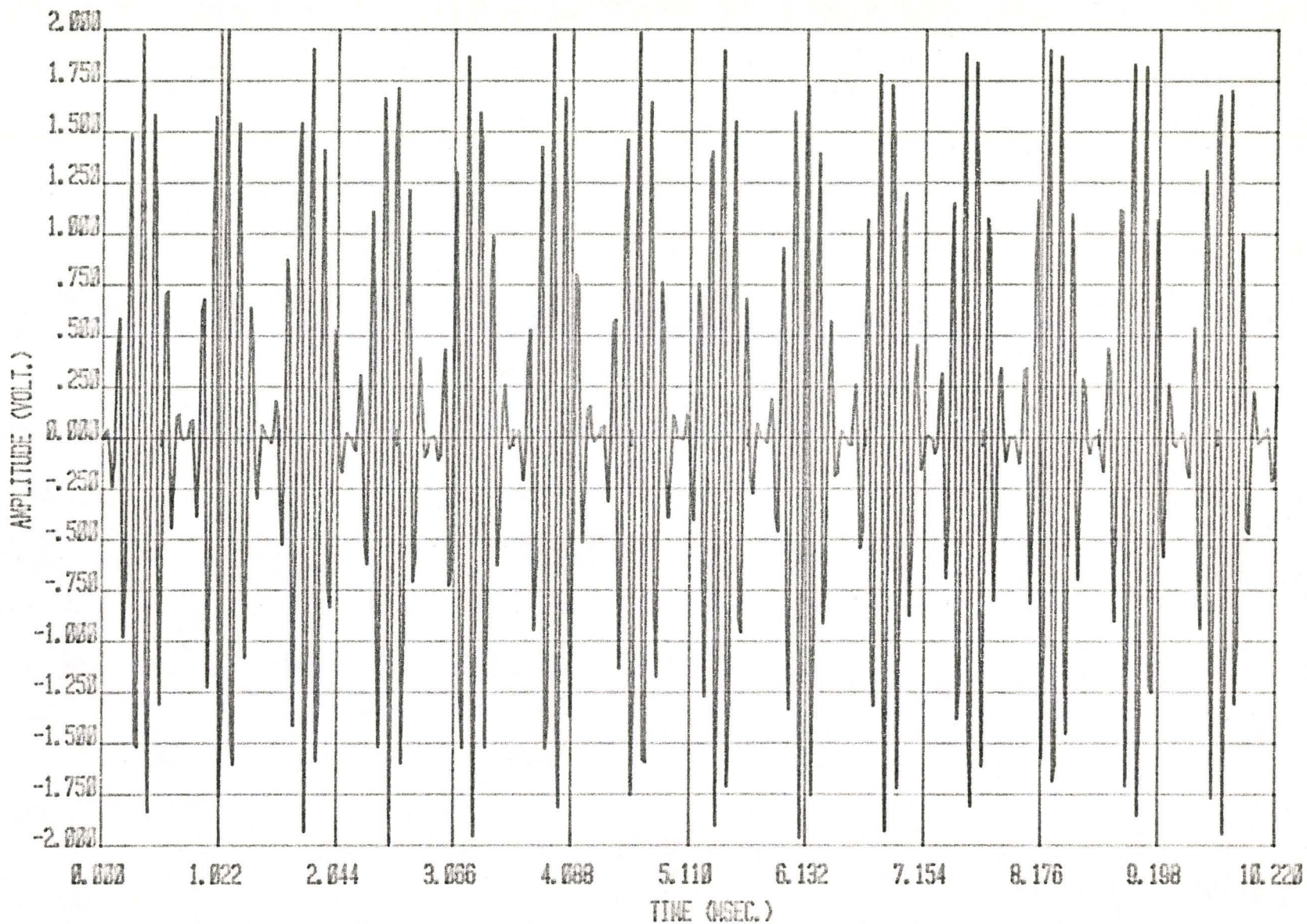


Fig. 1.2: Sinusoidal-modulated ELT signal with linear frequency sweep.

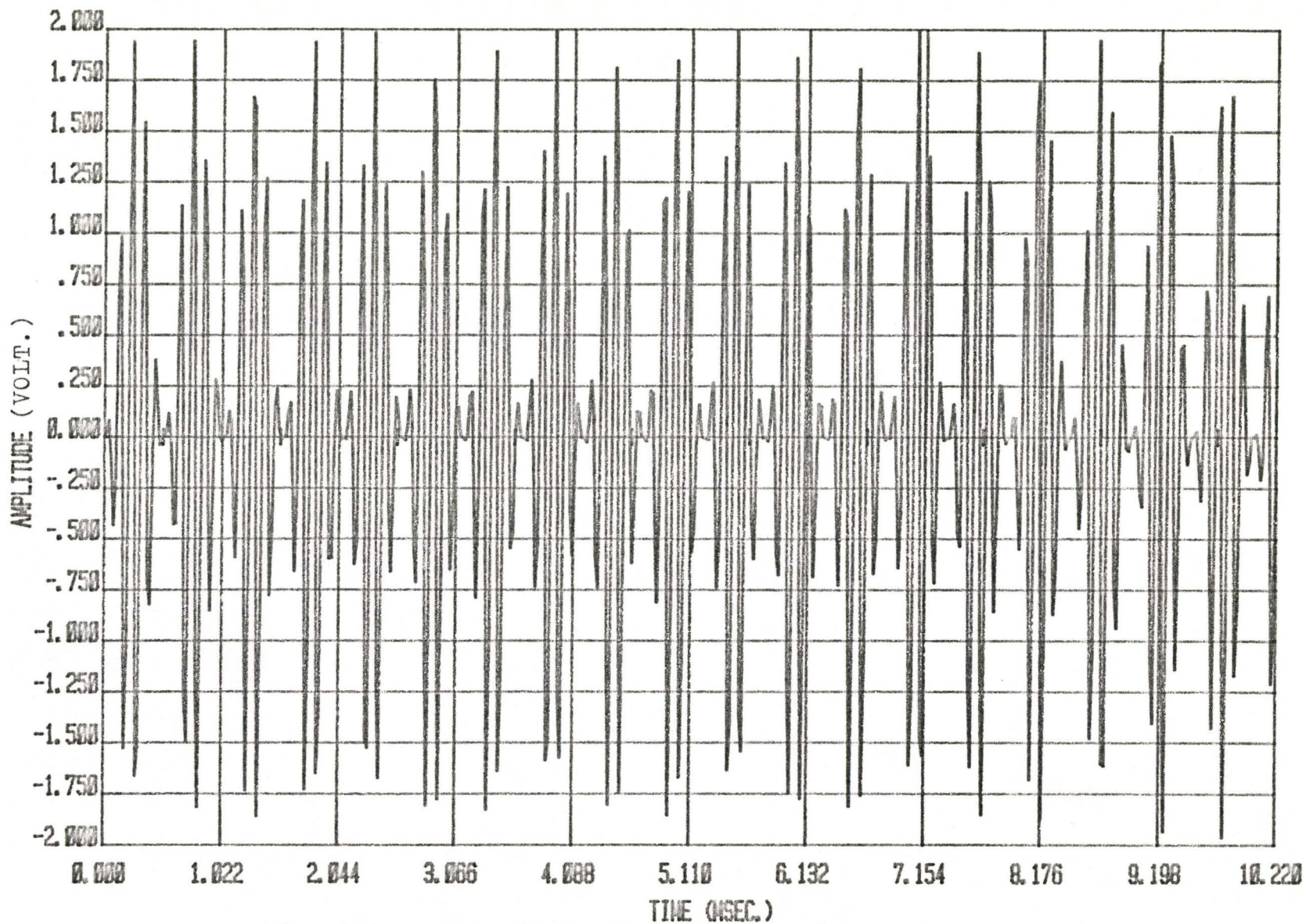


Fig. 1.3: Sinusoidal-modulated ELT signal with quadratic frequency sweep.

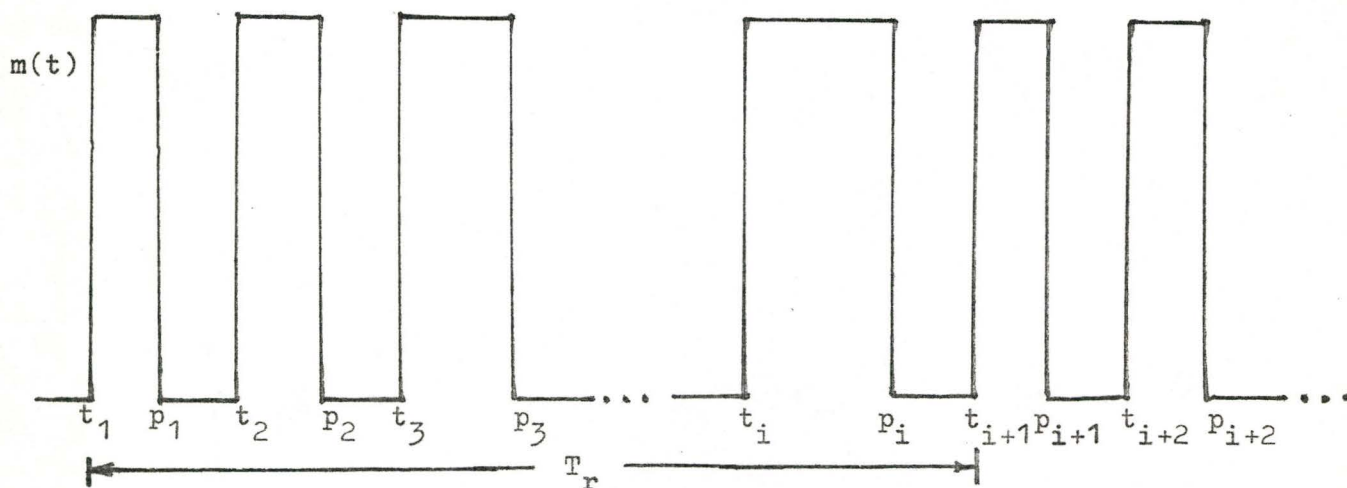


Fig. 1.4: The modulating signal,  $m(t)$ , for a pulse-modulated ELT signal.

solve for these time-indexes are

$$\int_0^{t_i} f_{in}(t) dt = i-1 \quad (1.8)$$

$$\int_0^{p_i} f_{in}(t) dt = i-1+d \quad (1.9)$$

where  $f_{in}(t)$  is defined by Eq. (1.4) or (1.5). The duty cycle,  $d$ , is within the 30% to 50% range. The values  $t_i$  and  $p_i$ , of the  $i$ -th pulse, as applied to the choice of frequency sweeps are computed and formulated in Appendix A. The waveforms of a 512 sample point linear sweep and quadratic sweep pulse-modulated ELT signal are illustrated in Figs. 1.5 and 1.6. Both signals have carrier frequency 9500 Hz and a 36% duty cycle. The length of these signals is 10.22 ms. Fig. 1.7(a) [5] shows a schematic diagram for generating this type of ELT signal.

### 1.2.3 Pulse-shaped Modulation (Random Phase)

Another form of existing ELT signal is a slight variation of the pulse-modulated continuous phase signal. Instead of having the oscillator (Fig. 1.7(a)) always on, the switching pulses are used to control the oscillator on and off. Therefore, the pulses at the output of the oscillator will take on some arbitrary phase at each time  $t_i$  (Fig. 1.4) [8]. This is shown in Fig. 1.7(b).

## 1.3 THE DOPPLER CURVE

When a satellite in low polar orbit receives a distress signal from an ELT source, a Doppler frequency drift occurs due to the relative

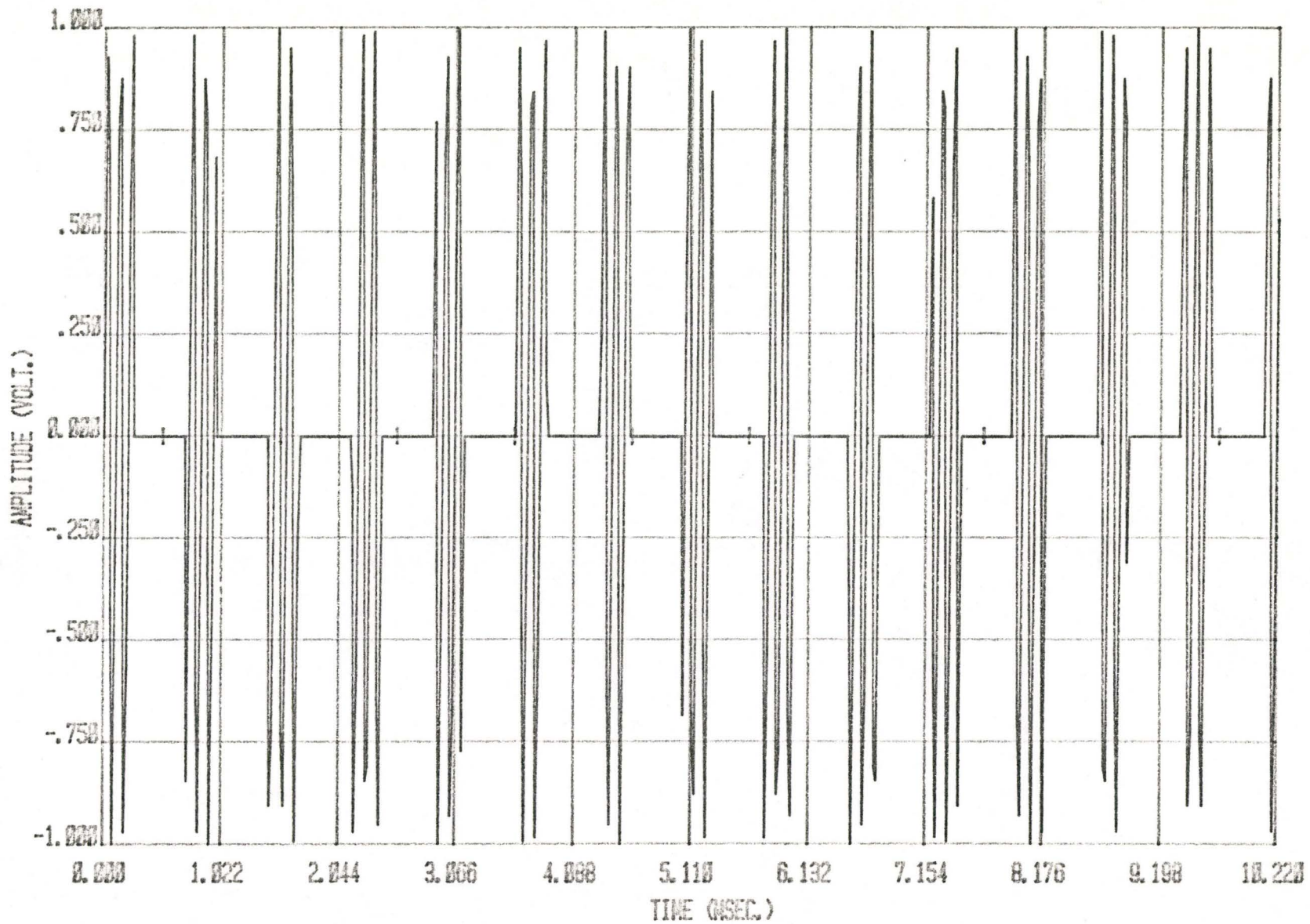


Fig. 1.5: Pulse-modulated ELT signal with linear frequency sweep.

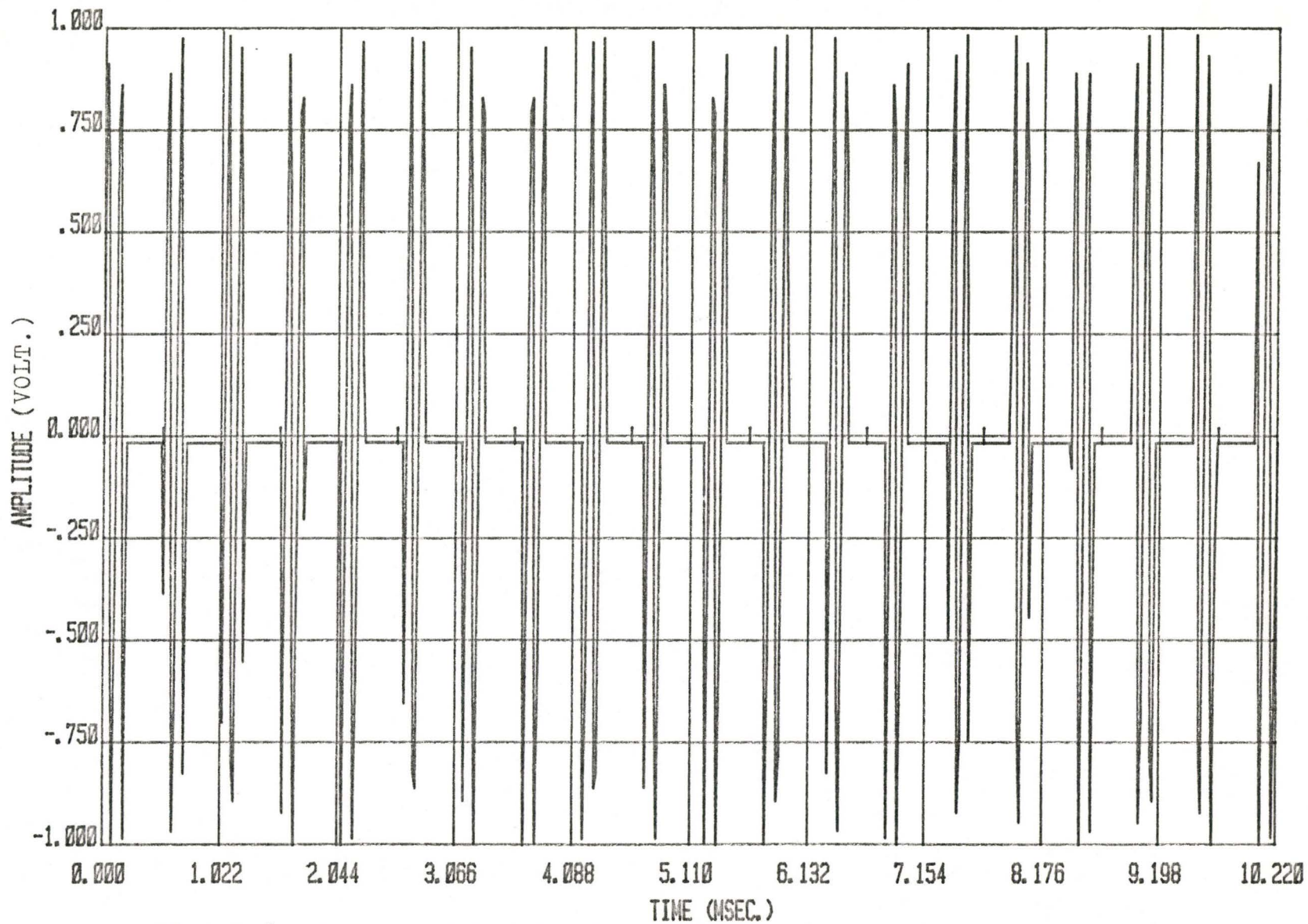


Fig. 1.6: Pulse-modulated ELT signal with quadratic frequency sweep.

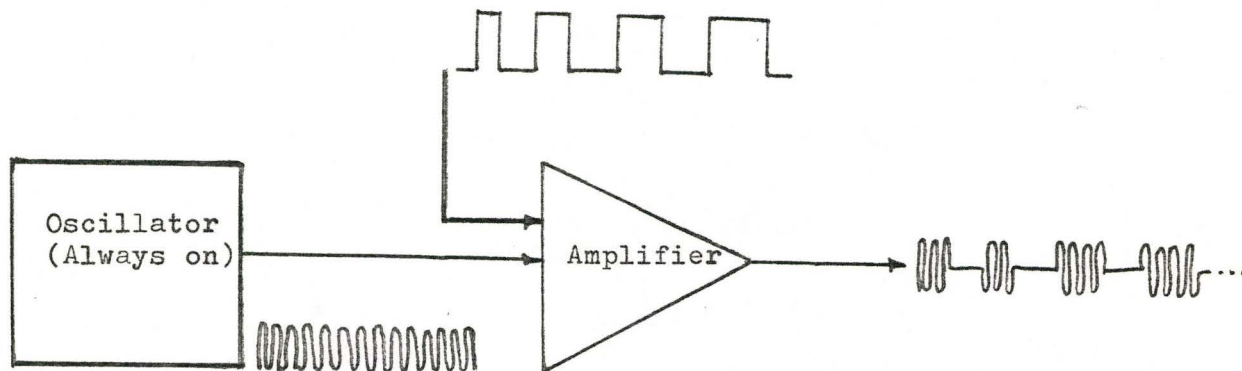


Fig. 1.7(a): A schematic diagram for generating pulse-modulated continuous phase ELT signal.

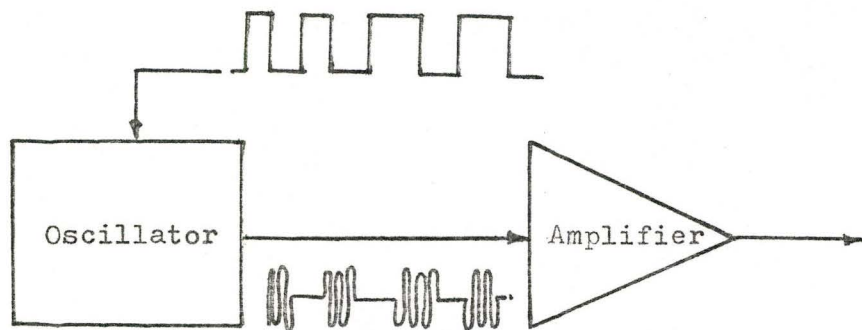


Fig. 1.7(b): A schematic diagram for generating pulse-modulated random phase ELT signal.

motion of the spacecraft with respect to the transmitter. As the satellite approaches the emergency site, the Doppler shift becomes less until the minimum distance is reached where the Doppler shift is zero. Beyond this point, a negative Doppler shift occurs and a plot of frequency versus time produces the S-shaped curve of Fig. 1.8. This curve leads to a measure of ELT position with respect to the known position of the satellite. The measurement is carried out at an earth station where the received ELT signal is processed and information is extracted from the Doppler-time curve. The point of inflection represents the zero Doppler shift and a calculation based on the slope of the curve at this point yields a measure of the range to the crash site.

Using a flat-earth model of Fig. 1.9, as an example, equations are developed to derive a Doppler-time curve. The carrier frequency of the ELT signal received at the satellite is given by

$$f = f_0 + f_d \frac{x}{\sqrt{x^2 + h^2 + z_0^2}} \quad (1.10)$$

where  $f$  = received frequency at the satellite

$f_0$  = carrier frequency of ELT unit

$f_d$  = Doppler shift of the signal along the flight path

$x$  = distance along the flight path

$h$  = altitude of the satellite

$z_0$  = displacement of unknown magnitude.

A plot of the carrier frequency as function of time results in a graph similar to Fig. 1.8. From Fig. 1.9,  $z_0$  can be written as

$$z_0 = h \cot \alpha$$

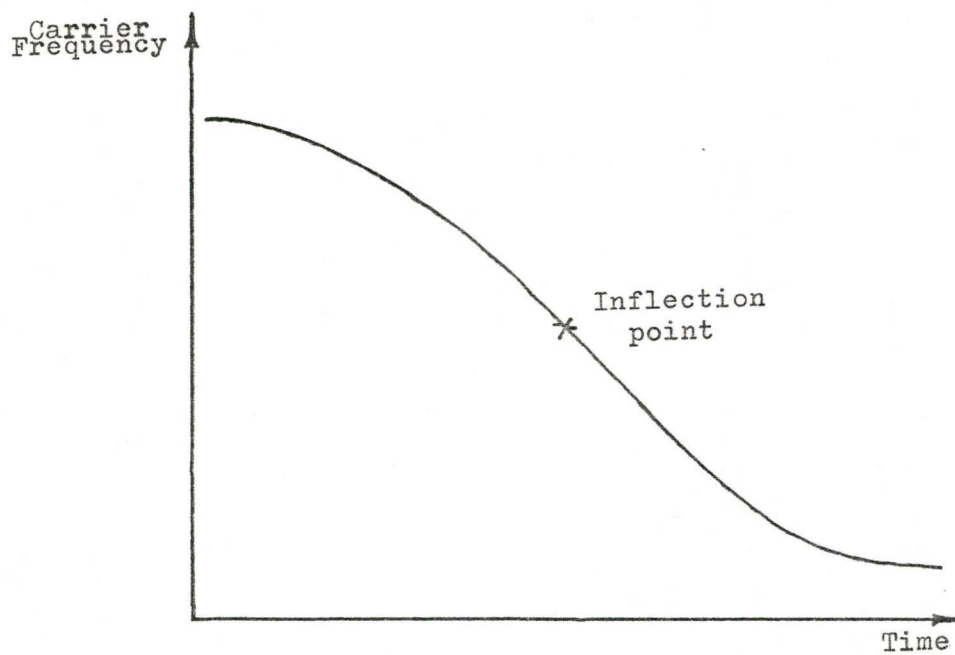


Fig. 1.8: Carrier frequency versus time for an ELT signal.

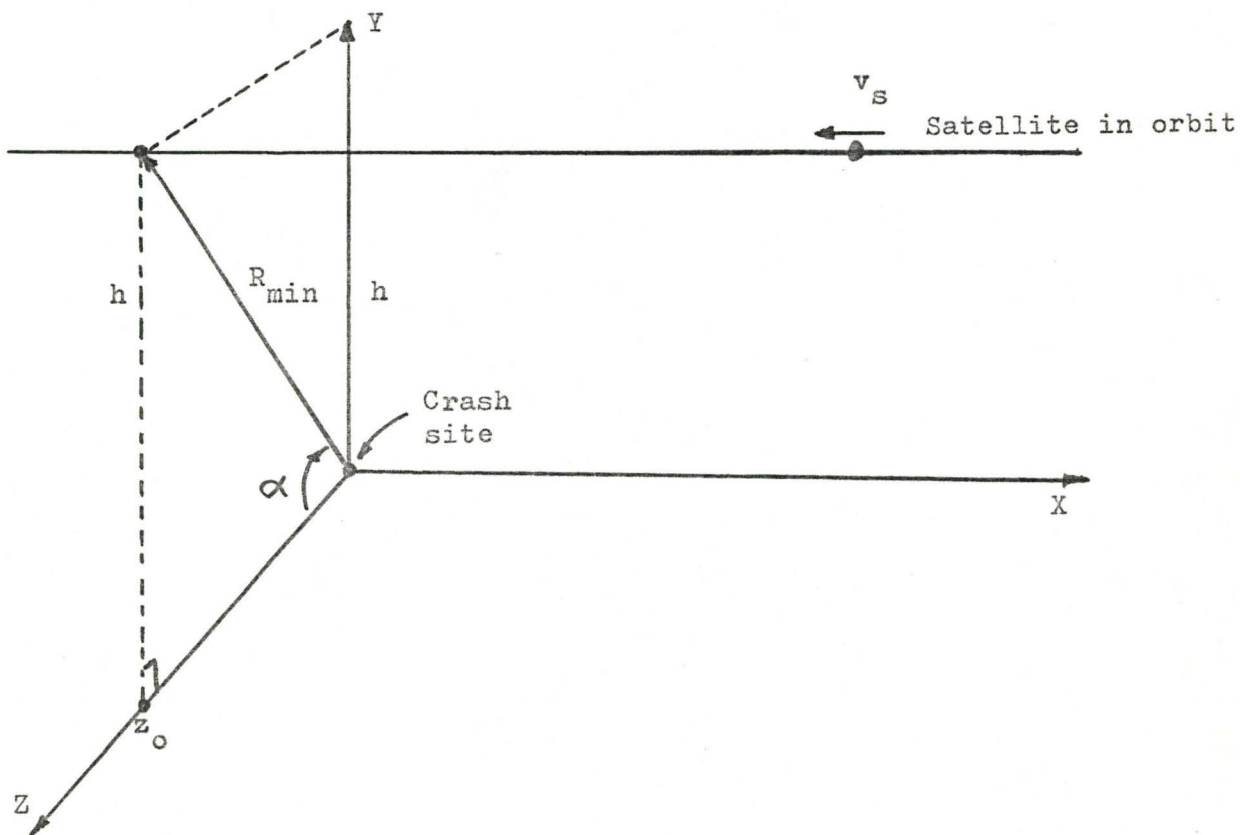


Fig. 1.9: Flat-earth model of the SRSAT geometry.

By substituting this relation into Eq. (1.10) and calculating the first derivative with respect to time, we have

$$\frac{df}{dt} = f_d \left[ \frac{1}{(x^2 + h^2 + h^2 \cot^2 \alpha)^{1/2}} - \frac{x^2}{(x^2 + h^2 + h^2 \cot^2 \alpha)^{3/2}} \right] \frac{dx}{dt} \quad (1.11)$$

But since the satellite travels at a velocity of  $v_s = -\frac{dx}{dt}$ , this yields

$$\begin{aligned} \frac{df}{dt} &= -v_s f_d \left[ \frac{1}{(x^2 + h^2 + h^2 \cot^2 \alpha)^{1/2}} - \frac{x^2}{(x^2 + h^2 + h^2 \cot^2 \alpha)^{3/2}} \right] \\ &= -v_s f_d \left[ \frac{h^2 + h^2 \cot^2 \alpha}{(x^2 + h^2 + h^2 \cot^2 \alpha)^{3/2}} \right] \end{aligned} \quad (1.12)$$

The satellite is closest to the crash site when  $x=0$ , this gives

$$\frac{df}{dt} = \frac{-v_s f_d}{h \sqrt{1 + \cot^2 \alpha}} \Bigg|_{x=0} \quad (1.13)$$

By simple trigonometry identities,  $1 + \cot^2 \alpha$  can be reduced to  $1/\sin^2 \alpha$ , and Eq. (1.13) becomes

$$\frac{df}{dt} = \frac{-v_s f_d}{h} \sin \alpha$$

But  $\sin \alpha = \frac{h}{R_{\min}}$ , thus

$$R_{\min} = \frac{-v_s f_d}{\frac{df}{dt} \Big|_{R_{\min}}} \quad (1.14)$$

where  $R_{\min}$  is the shortest distance between the spacecraft and the ELT source. The inflection point is determined by evaluating  $df/dt$  at  $R_{\min}$ . The parameters  $v_s$  and  $f_d$  are known for any satellite orbit. In order to

have an accurate estimation of the crash site, it is important to measure the Doppler shift information on the ELT carrier frequency. This measurement is strongly dependent on the efficiency of signal processing methods.

#### 1.4 SCOPE OF THESIS

This dissertation investigates advanced signal processing methods as applied to SARSAT system. Fourier analysis in the form of Fast Fourier Transform (FFT) and windowing techniques have been used to determine the frequency spectral characteristics of ELT signals. The frequency resolution, in the presence of multiple ELT signals, reveals that these methods give results which are difficult to interpret. A non-linear spectral analysis method called Maximum Entropy Method (MEM), which is based on the concept of prediction error filtering (PEF), is then employed in the thesis. Significant improvement, by using the MEM, in the resolution is evident. It is found that with preprocessing provided by autocorrelation function (ACF) and finite impulse response (FIR) filtering, the spectral characteristics of these signals have superior resolution.

The next chapter is devoted to review the theories of the mentioned signal processing methods. ELT signals in the presence of white Gaussian noise together with the definition of signal-to-noise density ratio (db-Hz) are also discussed in the same chapter.

Chapter 3 begins with a discussion on the computer simulation package of the ELT signals, digital filter and energy spectrum. This

follows by a presentation of the results of single emergency signals and the accuracy of the MEM resolutions across the frequency band.

Multiple signals are involved in Chapter 4. The final chapter gives conclusions of the investigation and suggestions for further research in SARSAT project.

CHAPTER 2  
SIGNAL PROCESSING METHODS

2.1 INTRODUCTORY REMARKS

The existing ELT units have several confining characteristics which impede the detection of distressed signals. It has been mentioned that the ELT signals can take on various forms of sweep frequency modulations and the signal length varies considerably. Moreover, the transmitters built by different manufacturers not only have a low radiating power and poor spectral characteristics, but also many equipments suffer frequency drift associated with the oscillators. Thus, the carrier frequency is not constant across the signal. The aim of this chapter is to discuss the theories of several signal processing methods in estimating the spectral density of the ELT signals. The power spectra of each spectral estimation method are also given for comparison, but the discussion on the simulation process is given in the next chapter.

2.2 THE FAST FOURIER TRANSFORM ALGORITHM

A paper on the fast method of computing the discrete Fourier transform (DFT) of a series of data samples was published by Cooley-Tukey [10] in 1965. This technique is known as the Fast Fourier Transform (FFT) algorithm [10]-[17]. The advantage of FFT is that the spectral density spectrum (or power spectrum) is obtained by performing

the squared magnitude of the FFT of the given time series. This is usually called the periodogram (or Cooley-Tukey) method. Since the FFT is an efficient method for computing the DFT, it is appropriate to begin by discussing the mathematical representation of the DFT. When a waveform is sampled on a digital computer, the finite version of the Fourier transform is used. This finite duration sequence  $\{x(n)\}$  ( $0 \leq n \leq N-1$ ), has a DFT of the form

$$X(k) = \sum_{n=0}^{N-1} x(n) \exp \left[ (-j \frac{2\pi}{N}) nk \right] \quad k=0, 1, \dots, N-1 \quad (2.1)$$

By putting  $W_N = \exp(-j \frac{2\pi}{N})$ , Eq. (2.1) can be written as

$$X(k) = \sum_{n=0}^{N-1} x(n) W_N^{nk} \quad k=0, 1, \dots, N-1 \quad (2.2)$$

If  $x(n)$  is a complex sequence, a direct evaluation using Eq. (2.2) of an  $N$ -point DFT requires  $(N-1)^2$  complex multiplications and  $N(N-1)$  complex additions [11]. Thus, for reasonably large values of  $N$ , a tremendous amount of computation is needed.

However, the computing speed can be drastically accelerated if we consider an  $N$ -point sequence  $\{x(n)\}$ , where  $N$  is assumed to be a power of 2. Furthermore,  $x(n)$  in Eq. (2.2) is decomposed into two  $\frac{N}{2}$ -point sequences

$$\begin{aligned} x_1(n) &= x(2n) \\ x_2(n) &= x(2n+1) \end{aligned} \quad n=0, 1, \dots, \frac{N}{2}-1 \quad (2.3)$$

where  $x_1(n)$  and  $x_2(n)$  are the even and odd members of  $x(n)$  respectively. The  $N$ -point DFT of  $\{x(n)\}$  is

$$\begin{aligned}
X(k) &= \sum_{n=0}^{N-1} x(n)W_N^{nk} + \sum_{n=0}^{N-1} x(n)W_N^{nk} \\
&\quad (n \text{ even}) \quad (n \text{ odd}) \\
&= \sum_{n=0}^{\frac{N}{2}-1} x(2n)W_N^{2nK} + \sum_{n=0}^{\frac{N}{2}-1} x(2n+1)W_N^{(2n+1)K} \tag{2.4}
\end{aligned}$$

Using the relationship [11]

$$W_N^2 = \exp[-j(\frac{2\pi}{N})2] = \exp[-j\frac{2\pi}{N/2}] = W_{N/2}$$

Eq. (2.4) becomes

$$X(k) = X_1(k) + W_N^K X_2(k) \tag{2.5}$$

$$\text{where } X_1(k) = \sum_{n=0}^{\frac{N}{2}-1} x_1(n)W_{N/2}^{nK}$$

$$X_2(k) = \sum_{n=0}^{\frac{N}{2}-1} x_2(n)W_{N/2}^{nK}$$

Since  $X(k)$  is defined for  $0 \leq k \leq N-1$  and  $X_1(k)$  and  $X_2(k)$  are defined for  $0 \leq k \leq \frac{N}{2}-1$ , [11] shows that for  $k \geq \frac{N}{2}$ ,  $X(k)$  can be represented in terms of  $X_1(k)$  and  $X_2(k)$  as

$$X(k) = \begin{cases} X_1(k) + W_N^K X_2(k) & 0 \leq k \leq \frac{N}{2} - 1 \\ X_1(k - \frac{N}{2}) + W_N^K X_2(k - \frac{N}{2}) & \frac{N}{2} \leq k \leq N-1 \end{cases} \tag{2.6}$$

In a manner similar to the above scheme, the  $\frac{N}{2}$ -point DFT's can be further decomposed as a combination of two  $\frac{N}{4}$ -point DFT's. For  $X_1(k)$

( $0 \leq k \leq \frac{N}{2}-1$ ), this can be expressed as

$$X_1(k) = A(k) + W_{N/2}^k B(k)$$

where  $A(k)$  and  $B(k)$  are the two  $\frac{N}{4}$ -point DFT's of the even and odd members of  $X_1(k)$ . This process can be continued until two points DFT's are left to evaluate.

Algorithm in which the decomposition is based on successively halving the size of the sequence  $x(n)$  is called Radix 2 decimation-in-time FFT algorithm. (Another algorithm is called decimation-in-frequency which is not discussed in this chapter can be referred to [11], [12] and [15]). The mechanics of the FFT algorithm requires only  $\frac{N}{2} \log_2 N$  complex multiplications as compared with the  $(N-1)^2$  computations needed for direct evaluation of Eq. (2.2). Fig. 2.1 [16] compares the number of operations required for FFT and direct evaluation of DFT.

Very often the input sequence  $\{x(n)\}$  is very long. Therefore, in order to achieve a finite duration sequence for Fourier analysis, a finite portion of  $\{x(n)\}$  is obtained by multiplying the very long series by a unity amplitude data window. This rectangular data window has a continuous Fourier transform, which is the form of  $\frac{\sin x}{x}$  function. The multiplication by the data window in the time domain is equivalent to performing a convolution in the frequency domain. This results in a function with an amplitude of the  $\frac{\sin x}{x}$  form. An abrupt change caused by truncation at the endpoints of the data sequence introduces sidelobes in the Fourier spectrum. These sidelobes are hazardous elements in the detection operation. Fig. 2.2 shows the FFT power spectrum of the ELT signal in Fig. 1.2. False alarms are likely to happen if the sidebands

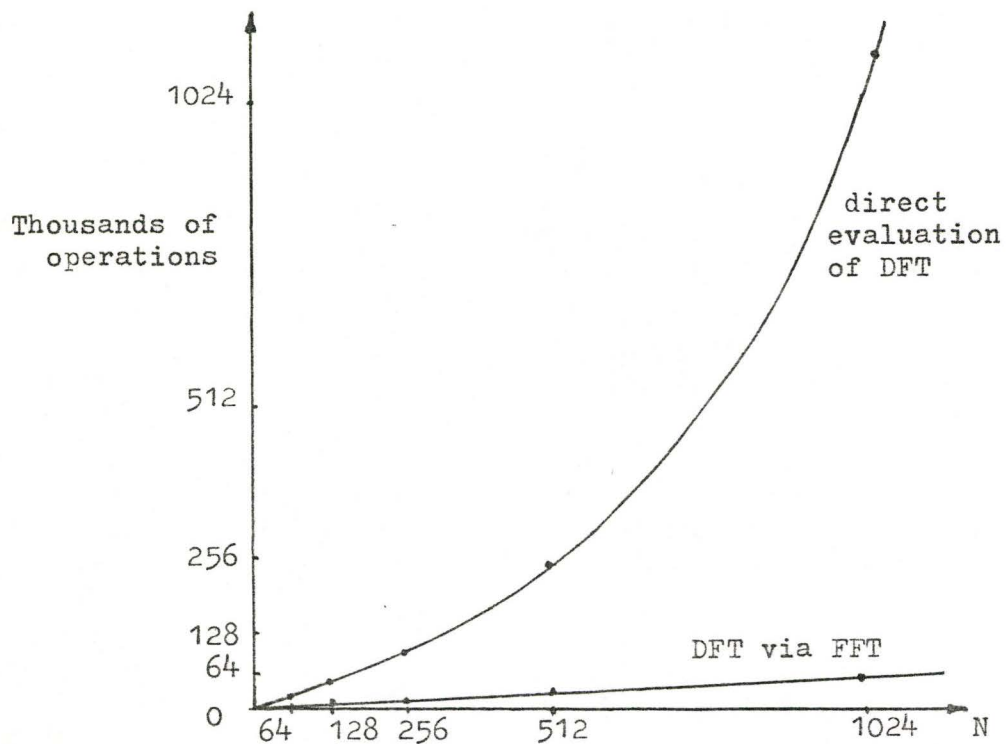


Fig. 2.1: The number of operations required for computing the discrete Fourier transform using the FFT algorithm compared with the number of operations required for direct calculation of the discrete Fourier transform.

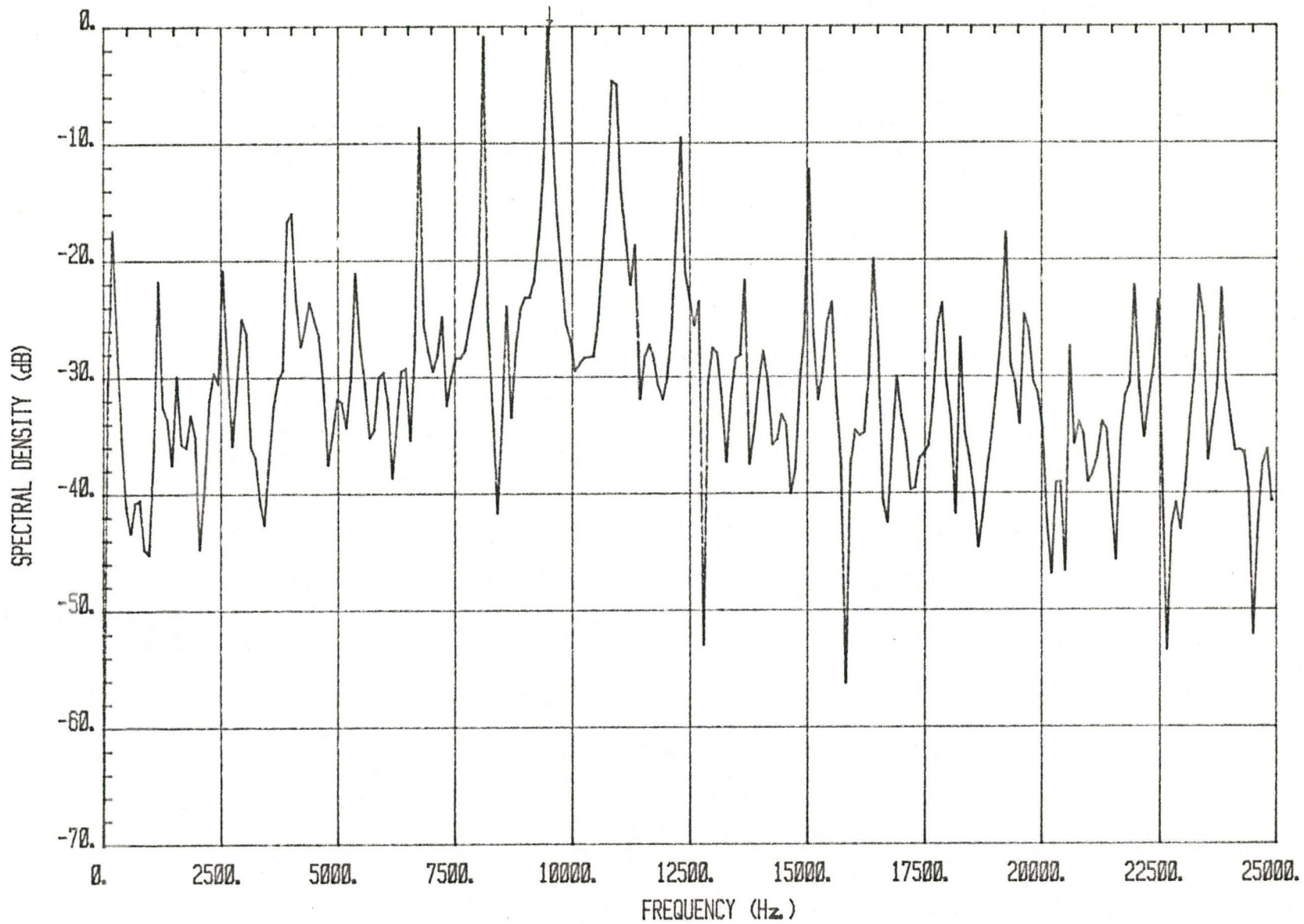


Fig. 2.2: The FFT power spectrum of a 512-point pulse-modulated (linear frequency sweep) ELT signal at 9500 Hz. Arrow indicates carrier frequency.

(and sidelobes) are of sufficient magnitude as compared to the main peak. In this situation, the Doppler processor may give a wrong estimate of distressed platform location. Moreover, in the case of multiple distressed platforms, there is a possibility that these sidelobes may contaminate the power spectrum of the different emergency signals. Failure in detection is not surprising under this situation. A tapered window function may be used to partially alleviate the problem of high sidelobes. This results in a gradual reduction of amplitude at the endpoints of the data samples rather than an abrupt transition. Several window functions are discussed in the next section.

### 2.3 THE WINDOWING TECHNIQUES

This technique is often encountered in performing the FFT spectral analysis and in designing digital filters. One way to convert a very long sequence  $\{s(n)\}$  into a shorter sequence is to simply truncate  $\{s(n)\}$ . This corresponds to multiplying the input time series by a finite rectangular waveform,  $w(n)$  ( $0 \leq n \leq N-1$ ), whose amplitude is unity

$$x(n) = \begin{cases} s(n)w(n) & 0 \leq n \leq N-1 \\ 0 & \text{otherwise} \end{cases} \quad (2.7)$$

where

$$w(n) = \begin{cases} 1 & 0 \leq n \leq N-1 \\ 0 & \text{otherwise} \end{cases}$$

This operation is called the windowing technique. The finite waveform  $w(n)$  is called a data window.

Direct truncation, in the above form, unfortunately leads to the well known Gibbs phenomenon in the frequency domain with an unwanted overshoot at the sharp transition of the input sequence [13]. This is due to the fact that multiplication in the time domain is equivalent to convolving the original frequency characteristics of  $S[\exp(j\omega)]$  with the Fourier transform of the window  $W[\exp(j\omega)]$

$$X[\exp(j\omega)] = S[\exp(j\omega)] * W[\exp(j\omega)] \quad (2.8)$$

where  $*$  denotes convolution operation. The Fourier transform of  $W[\exp(j\omega)]$  is a function with amplitude  $\frac{\sin x}{x}$  (this is usually written as  $\text{sinc}(x)$ ) form. A design criterion for windows is to find a finite window whose Fourier transform can smooth out the sharp transition or discontinuities at the endpoints of the input time series. In other words, we want a finite window with most of its energy in the main lobe of its Fourier transform [19], [20]. The most frequently used windowing functions are shown in Fig. 2.3 [12]. These windows are specified by the following equations [12], [13], [22].

i) Rectangular window:

$$w(n) = 1.0$$

ii) Hamming window:

$$w(n) = 0.54 + 0.46 \cos \left( \frac{2\pi n}{N-1} \right)$$

iii) Hanning window:

$$w(n) = 0.5 + 0.5 \cos \left( \frac{2\pi n}{N-1} \right)$$

iv) Blackman window:

$$w(n) = 0.42 + 0.5 \cos \left( \frac{2\pi n}{N-1} \right) + 0.08 \cos \left( \frac{4\pi n}{N-1} \right)$$

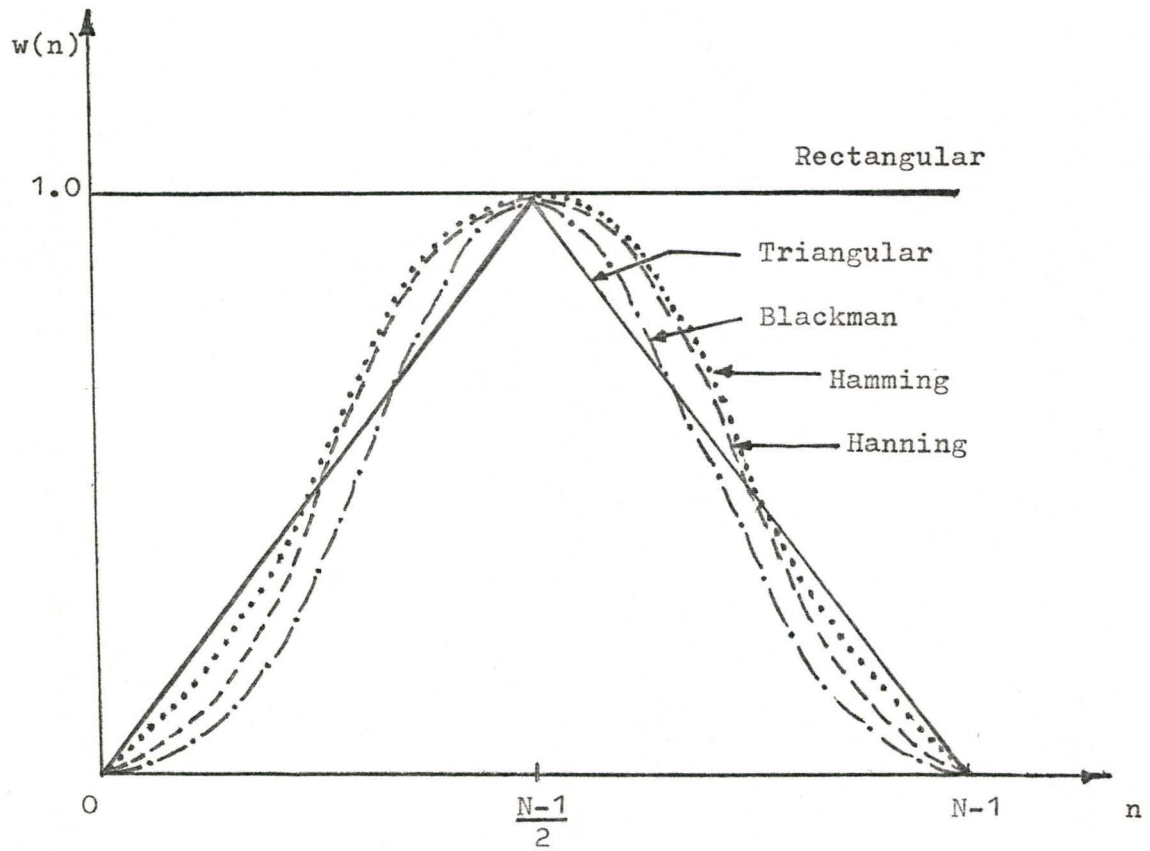


Fig. 2.3: Window functions.

v) Triangular window:

$$w(n) = 1 - \frac{|2n|}{N-1}$$

where  $n$  is defined in the interval  $-\frac{N-1}{2} \leq n \leq \frac{N-1}{2}$ .

Kaiser [18], [20] has proposed a nearly optimum window with characteristics which essentially satisfy the said design criterion. This window function is called the Kaiser window. It is an approximation to the prolate spheroidal wave functions. The equation of the Kaiser window is [11]

$$w(n) = \frac{I_0\left(\beta \sqrt{1 - \left(\frac{2n}{N-1}\right)^2}\right)}{I_0(\beta)} \quad (2.9)$$

where the parameter  $\beta$  is a constant which can be adjusted so as to trade off the main lobe width for sidelobe amplitude.  $I_0(\cdot)$  is the modified Bessel function of the first kind and order zero. This can be evaluated to any desired degree of accuracy by using the rapidly converging series [22]

$$I_0(x) = 1 + \sum_{K=1}^{\infty} \left[ \frac{1}{K!} \left(\frac{x}{2}\right)^K \right]^2 \quad (2.10)$$

Description of the above window functions and their characteristics have been mentioned in the references [11], [12], [13], [18], [19], [21], [22]. By tapering the window smoothly to zero at each end of the input time series, the height of the sidelobes can be reduced. This is achieved at the expense of a wider main lobe. In the view of the SARSAT system, this operation is undesirable because this increases the

ambiguity in the location of the peak in detecting distress signals. The signal used in the FFT power spectrum of Fig. 2.2 is windowed by a Kaiser window with  $\beta=8.0$ . The power spectrum, using the FFT technique, of the windowed ELT signal is given in Fig. 2.4.

#### 2.4 THE MAXIMUM ENTROPY METHOD SPECTRAL ANALYSIS

Spectral density estimation based on the Fourier transform techniques are said to be linear. The shortcomings of these linear estimators are well recognized. These involve the use of window function which is independent of the data being analysed and the assumption of a periodic extension of the data or that the data outside of the available record length is zero [11], [24]. A non-linear spectral estimation method which earns the merits of data-dependent and 'window-free' is called the Maximum Entropy Method (MEM). The principle of the MEM is detailed extensively in the literature [23], [24], [25], [26]. The primary aim of this section is concentrated on solving the prediction error filter (PEF) equation which is the essence of the MEM spectral analysis.

Suppose we are given a weakly stationary zero mean time series  $\{x(n)\}$  ( $0 \leq n \leq N-1$ ). For such a signal, the spectral estimate,  $S(f)$ , by employing the MEM is defined by [24]

$$S(f) = \frac{P(M)}{\left| 1 + \sum_{n=1}^M a(n) \exp(-j2\pi n f \Delta t) \right|^2} \quad (2.11)$$

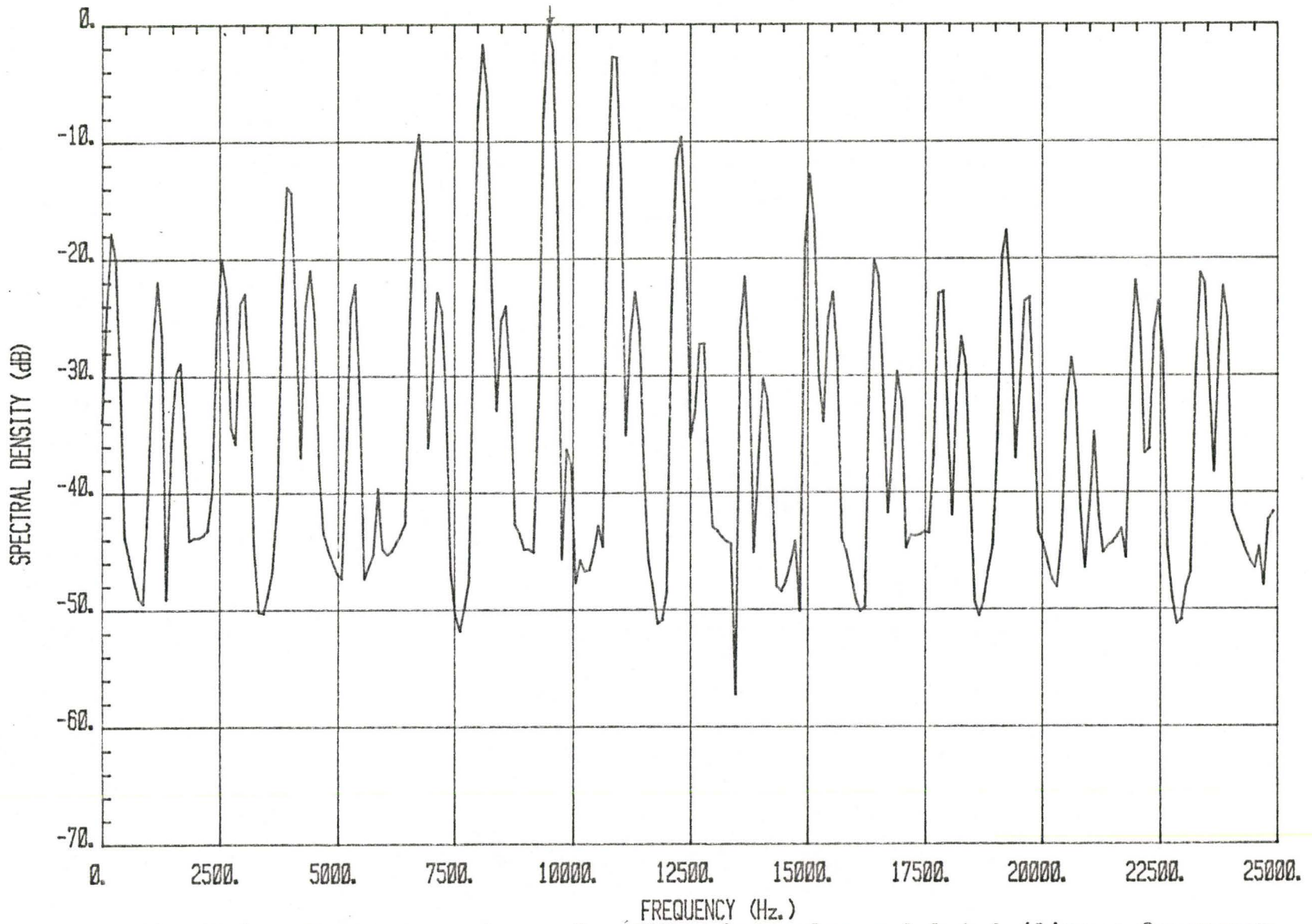


Fig. 2.4: The FFT spectrum of a 512-point pulse-modulated (linear frequency sweep) ELT signal at 9500 Hz windowed by a Kaiser window for  $\beta=8.0$ .

where  $P(M)$  = prediction error power obtained with a prediction error filter of order  $M$ .

$a(n)$  = prediction error filter coefficients ( $n=1,2,\dots,M$ ).

$\Delta t$  = sampling time.

In order to calculate the spectrum of the input data from Eq. (2.11), we obviously need to know the output power  $P(M)$  of the prediction error filter and also the corresponding values of filter coefficients  $a(n)$ . These parameters are determined by the equation [24]

$$\sum_{k=0}^M a(k)R_x(m-k) = \begin{cases} P(M) & m=0 \\ 0 & m=1,2,\dots,M. \end{cases} \quad (2.12)$$

where  $R_x(\cdot)$  is the autocorrelation values of the time series  $\{x(n)\}$  with lag  $(m-k)$ . This equation represents a prediction error filter equation of a PEF of order  $M$ . Appendix B discusses the design of a one step ahead predictive filter which ultimately formulates Eq. (2.12). It is convenient to expand Eq. (2.12) in matrix form

$$\begin{bmatrix} R_x(0) & R_x(-1) & \dots & R_x(-M) \\ R_x(1) & R_x(0) & \dots & R_x(1-M) \\ \cdot & \cdot & \cdot & \cdot \\ \cdot & \cdot & \cdot & \cdot \\ R_x(M-1) & R_x(M-2) & \dots & R_x(-1) \\ R_x(M) & R_x(M-1) & \dots & R_x(0) \end{bmatrix} \begin{bmatrix} a(0) \\ a(1) \\ \cdot \\ \cdot \\ a(M-1) \\ a(M) \end{bmatrix} = \begin{bmatrix} P(M) \\ 0 \\ \cdot \\ \cdot \\ 0 \\ 0 \end{bmatrix} \quad (2.13)$$

where the coefficient  $a(0)$  is equal to unity.

If the autocorrelation matrix can be estimated reliably from the input data, then the solution to Eq. (2.13) will give us the parameter values needed. However, this direct approach requires the assumption of data extensions and the solving of  $M+1$  simultaneous linear equations.

An efficient algorithm for solving Eq. (2.13) recursively is outlined by Burg [23]. This computational technique is referred to as Burg's algorithm.

We begin to discuss the algorithm by assuming we have obtained the coefficients of a prediction error filter of order  $M-1$  and the corresponding prediction error power  $P(M-1)$ . In order to calculate the parameters for the next higher filter order (that is order  $M$ ), the output power  $P(M)$  is expressed as the average power resulting from forward and backward filtering over the entire time interval [24], [31]. This is shown by [27], [29]

$$\begin{aligned}
 P(M) &= \frac{1}{2} (P_f(M) + P_b(M)) \\
 &= \frac{1}{2(N-M)} \sum_{n=1}^{N-M} \left[ \left| \sum_{k=0}^M a(M,k)x(n+k) \right|^2 + \left| \sum_{k=0}^M a(M,k)x(n+M-k) \right|^2 \right]
 \end{aligned} \tag{2.14}$$

where the subscripts  $f$  and  $b$  denote the forward and backward direction. The parameter  $a(M,k)$  is interpreted as the  $k$ th coefficient for the PEF of order  $M$ . The values of these coefficients can be determined by employing the Levinson's recursion [24]

$$a(M,k) = a(M-1,k) + a(M,M) a^*(M-1,M-k) \tag{2.15}$$

The asterisk signifies a complex conjugate and  $k=0,1,\dots,M$ . Note that the set of equations which are represented by Eq. (2.15) have the following properties

$$a(M,k) = \begin{cases} 1.0 & k=0 \\ 0.0 & k>M \end{cases}$$

$a(M,M)$  is an unknown quantity yet to be calculated. Putting Eq. (2.15)

in Eq. (2.14) and minimizing the equation with respect to  $a(M,M)$

$$\frac{\partial P(M)}{\partial a(M,M)} = 0$$

The optimum value of  $a(M,M)$  (for which  $P(M)$  is a minimum) is [27], [28], [29]

$$a(M,M) = \frac{-2 \sum_{n=1}^{N-M} \left[ \left( \sum_{k=0}^M a(M-1,k)x(n+M-k) \right) \left( \sum_{k=0}^M a^*(M-1,k)x(n+k) \right)^* \right]}{\sum_{n=1}^{N-M} \left[ \left| \sum_{k=0}^M a(M-1,k)x(n+M-k) \right|^2 + \left| \sum_{k=0}^M a^*(M-1,k)x(n+k) \right|^2 \right]} \quad (2.16)$$

The output power can readily be determined by solving Eq. (2.16), (2.15) and (2.14). However, as shown in [24], [27],  $P(M)$  is given by a simple expression (rather than the form in Eq. (2.14))

$$P(M) = P(M-1) (1 - |a(M,M)|^2) \quad (2.17)$$

Making use of Eq. (2.16), (2.17) and (2.15) we have now calculated all the quantities necessary for evaluating the Maximum Entropy power spectral estimate given by Eq. (2.11). To initiate the Burg's algorithm, we start with the PEF of zero-order ( $M=0$ ). For this value of  $M$ , we know that  $a(0)$  is equal to unity and  $R_x(0)$  is the zero-lag value of the autocorrelation function of the input time series  $\{x(n)\}$ . Eq. (2.12) becomes

$$\begin{aligned} P(0) &= R_x(0) \\ &= \frac{1}{N} \sum_{n=1}^N x(n)x^*(n) \end{aligned}$$

N. Anderson [29] discusses this algorithm for calculating the filter coefficients for Maximum Entropy Spectral Analysis. Other papers [28],

[30], [32], [33], [34] have been written describing algorithms for MEM spectral estimation.

The signal in Fig. 1.5 is processed using the MEM of order 2 ( $M=2$ ). The power spectrum is shown in Fig. 2.5. Comparing the FFT spectrum (Fig. 2.2) and the MEM spectrum, it is evident that the latter method yields a superior resolution [8], [35]. The advantage of employing low order MEM spectral estimates in detecting emergency signals is the complete lack of sidelobes in the power spectrum. This feature is significant in the event of multiple distressed platforms. We will discuss multiple ELT signals in Chapter 4.

## 2.5 USE OF THE AUTOCORRELATION FUNCTION AS A PREPROCESSOR

Two approaches of spectral estimation techniques are discussed in the preceding sections. It has been demonstrated that the adverse effects, which arise from employing the FFT algorithm to estimate the spectral density of a given signal, are reduced substantially by the Maximum Entropy Method. Since the MEM is described as a 'data-adaptive' method [25], it is beneficial to have some knowledge of the statistical behaviour of the input time series used.

In dealing with power spectra, it has long been known that the correlation function of the signal is an extremely useful tool [11]. Assuming we are given a real-valued time series,  $x(t)$ , over the entire interval  $(-\infty < t < \infty)$ . The autocorrelation function (ACF) is said to reflect one aspect of the behaviour of a given input signal from which the ACF provides a time-domain description of the second-order

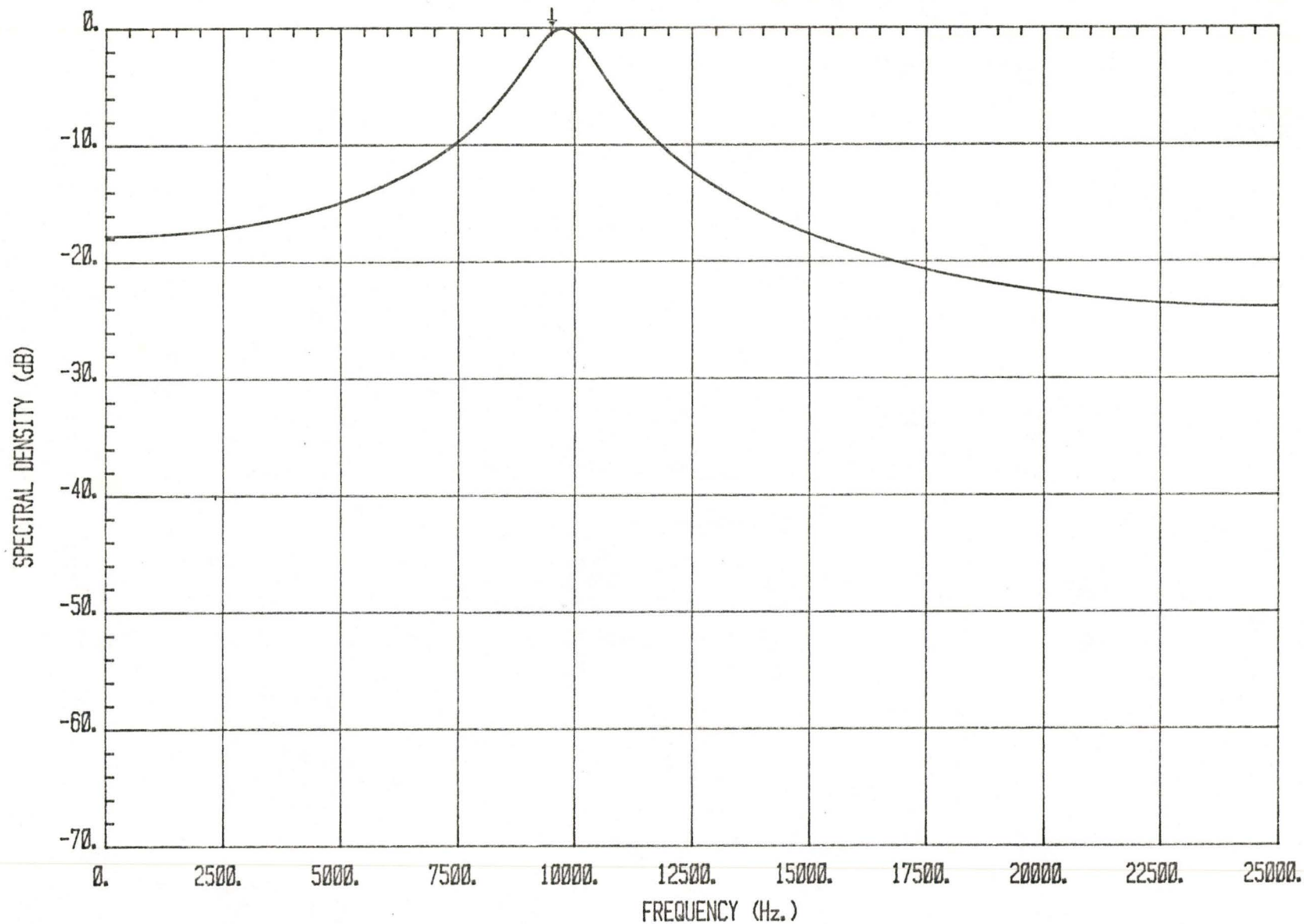


Fig. 2.5: The MEM power spectrum of a 512-point pulse-modulated (linear frequency sweep) ELT signal at 9500 Hz. The MEM filter order is 2.

statistics [24], [40]. If the given time series is a finite energy signal, the ACF is defined by [6]

$$R_x(\tau) = \int_{-\infty}^{\infty} x(t+\tau)x(t)dt \quad (2.18)$$

where  $\tau$  is the value of maximum time delay (or lag). Thus the ACF,  $R_x(\tau)$ , reveals the similarity between a given signal and its own time-shifted version. The properties of ACF are discussed extensively in literature [39], [40]. An important property is that the ACF and energy-density spectrum,  $|S_x(f)|^2$ , form a Fourier transform pair. This is given as [6]

$$|S_x(f)|^2 = \int_{-\infty}^{\infty} R_x(\tau)\exp(-j2\pi f\tau)d\tau \quad (2.19)$$

and

$$R_x(\tau) = \int_{-\infty}^{\infty} |S_x(f)|^2 \exp(j2\pi f\tau)df \quad (2.20)$$

We can interpret Eq. (2.19) in this way: the available time series,  $x(t)$ , is first used to estimate the sample autocorrelation function for a number of lags; next, the Fourier transform of this is determined to obtain an estimate of the spectral density. However, windowing the ACF is required in this method of spectral estimation. This is often referred to as the Blackman-Tukey method [10], [11]. By taking the inverse Fourier transform of a given spectral density spectrum, we obtain the ACF of the input time series. This is exhibited in Eq. (2.20).

The ACF not only reveals the second-order statistics of a given signal, but it also has a significant role in detecting a periodic signal buried in additive noise. The definition of Eq. (2.18) applies to a signal of finite energy. If the signal  $x(t)$  is periodic with period  $T$ , we define the ACF as [39]

$$R_x(\tau) = \frac{1}{2T} \int_{-T}^T x(t+\tau)x(t)dt \quad (2.21)$$

It is evident that for a periodic signal, the ACF is also periodic with the same period [6]. If the additive noise and signal are uncorrelated, the autocorrelation of signal in the presence of noise is the individual sum of the ACF of the signal and the ACF of the noise [6], [38]. For a white noise process,  $w(t)$ , the ACF is defined by [6]

$$R_w(\tau) = \frac{N_0}{2} \delta(\tau)$$

where  $\delta(\tau)$  is a delta function weighted by the factor  $\frac{N_0}{2}$  at  $\tau=0$ ; otherwise,  $R_w(\tau)$  is zero for  $\tau \neq 0$ . This equation indicates that the ACF tends to averaging out (or cancel) the noise component. This is useful information in the analysis of signal corrupted by white noise.

We wish to investigate the statistics of a given ELT signal so as to improve its spectral estimation characteristics. The Blackman-Tukey method, (that is Eq. (2.19)), has a spectrum which is nearly identical to the periodogram method (which is the squared magnitude of the FFT). Thus, ACF does not improve the performance of linear spectral estimation. However, we are interested in investigating the effect of ACF on the non-linear spectral analysis. We are going to discuss this modified Maximum Entropy Method in the following section.

## 2.6 PREPROCESSING VIA THE AUTOCORRELATION FUNCTION

It is suggested in [8] that in estimating the power spectrum of a given time series, by means of the Maximum Entropy Method, the frequency resolution is improved significantly if the autocorrelation function is used as a preprocessor. However, it is a difficult task to give an explicit analysis of why the autocorrelation function favours the performance of the MEM. We can postulate that the second-order statistics (as given by the ACF) of a signal extracts useful information from the original signal such that the ACF improves the data adaptive method which, in this case, is the Maximum Entropy Method. We refer to this operation as ACFMEM technique.

The definition of ACF given in Eq. (2.18) is in continuous form. For a finite duration sequence,  $\{x(n)\}$  ( $0 \leq n \leq N-1$ ), the ACF is estimated by [11]

$$R(m) = \frac{1}{N} \sum_{n=0}^{N-1-m} x(n)x(m+n) \quad \text{for } 0 \leq m \leq N-1 \quad (2.22)$$

This is called a biased estimate [8], [27]. The ACF of the signal (Fig. 1.5) is shown in Fig. 2.6. This is a 256-lag ACF. The ACFMEM spectrum of MEM order 2 is given in Fig. 2.7. Comparing this result with the one in Fig. 2.5, we observe that there is a dramatic improvement in the frequency resolution.

## 2.7 DESIGN OF NONRECURSIVE DIGITAL FILTER

The objective of this section is to discuss the procedure which leads to the design of a bandpass filter. Filtering is desirable since

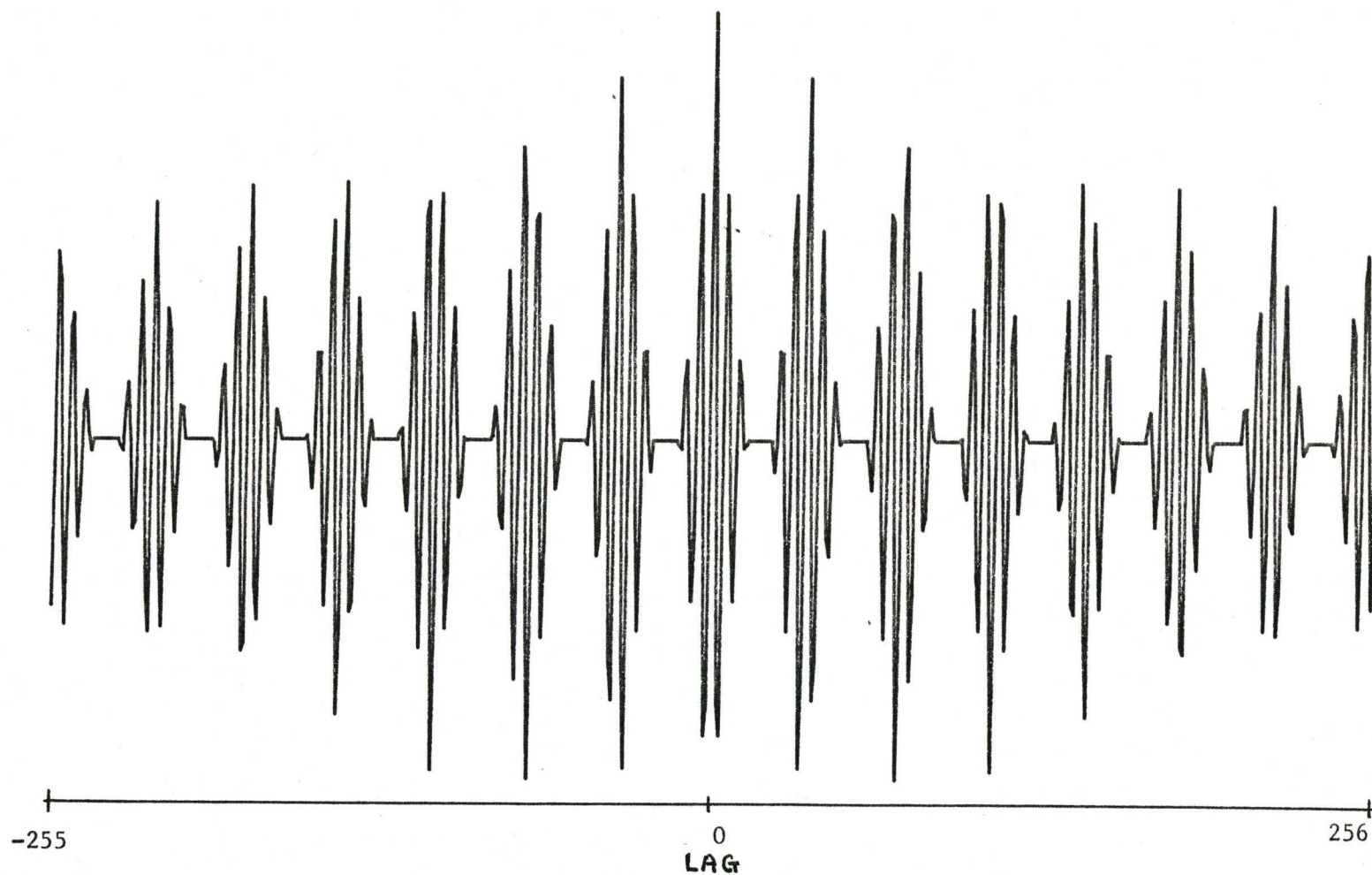


Fig. 2.6: The autocorrelation function (256 lag) of the signal described in Fig. 1.5.

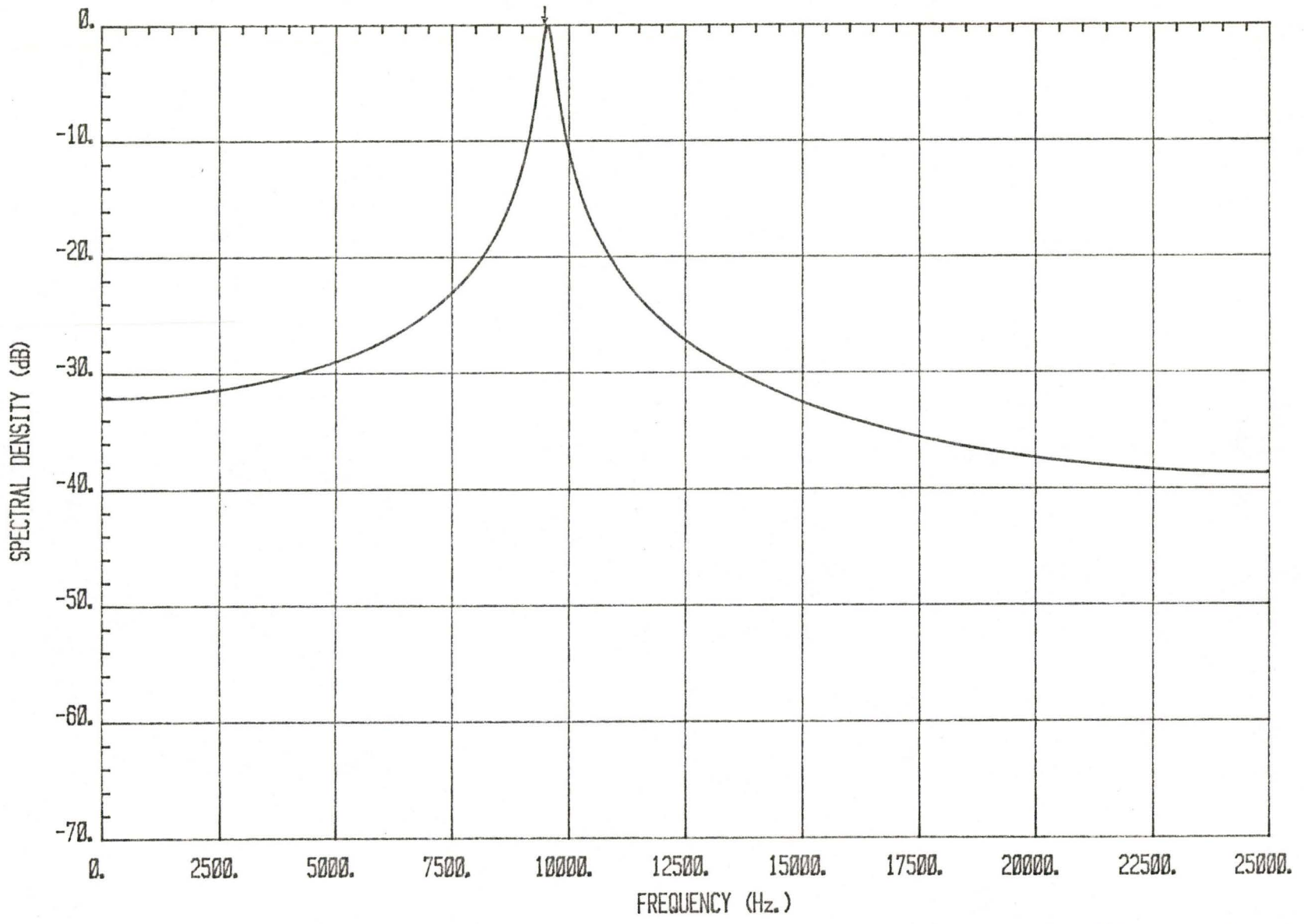


Fig. 2.7: The ACFMEM spectrum of the signal in Fig. 2.6. The MEM filter order is 2.

we wish to examine the power spectrum of the distressed signals limited to certain specified band of frequencies. The bandpass filter is a suitable choice because the ELT signal is a bandpass signal. Appendix C gives the theoretical details of the design.

Based on this theory, we have designed a bandpass filter which has the following specifications:

Number of samples is 171

Minimum stopband attenuation for  $0 \text{ Hz} \leq f < 7000 \text{ Hz}$  is 60 dB

Passband ripple for  $7000 \text{ Hz} \leq f \leq 18000 \text{ Hz}$  is 0.2 dB

Minimum stopband attenuation for  $18000 \text{ Hz} < f \leq 25000 \text{ Hz}$  is 60 dB

Sampling rate is 50000 samples per second.

Figure 2.8 gives the frequency response characteristic. This filter will be used widely, in the subsequent chapters, as a preprocessor to study the power spectrum of the MEM and the ACFMEM of ELT signals.

## 2.8 NOISE CONSIDERATIONS

In this section, we present a brief account on the performance of ELT signals in the presence of noise. A detailed discussion of this subject is given in [8].

In a physical system, the received ELT signal ( $s(t)$ ) at the earth station is a composition of the Doppler shifted ELT signal ( $s_d(t)$ ) and the noise component ( $n(t)$ )

$$s(t) = s_d(t) + n(t) \quad (2.23)$$

The origin of  $n(t)$  comes from several sources. The most typical examples are the uplink and downlink noise effects, the ionospheric

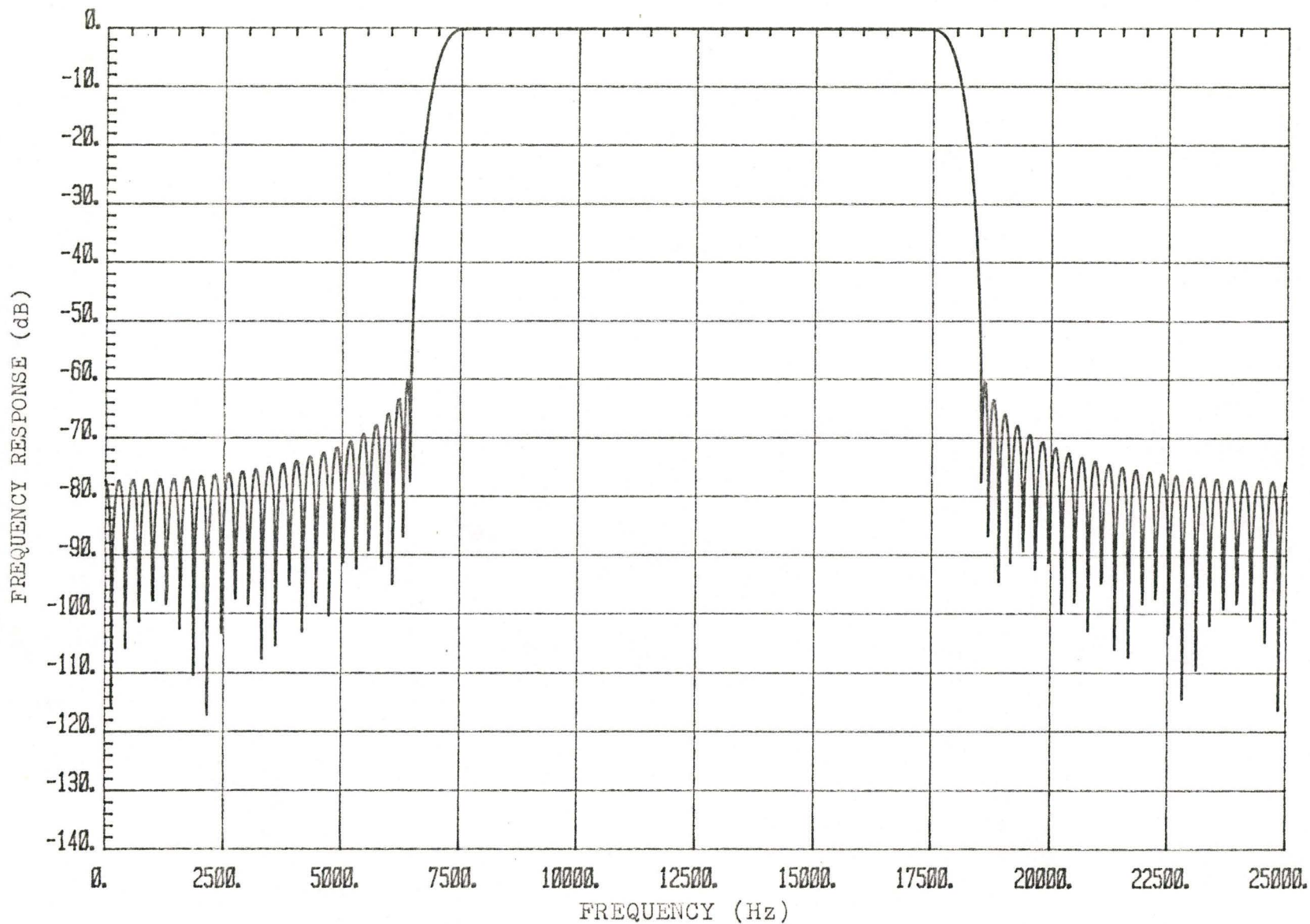


Fig. 2.8: The frequency response of an FIR bandpass filter. The cutoff frequencies are at 7000 Hz and 18000 Hz. The impulse response is 171 points.

effects and the receiver noise. In order to simulate  $s(t)$ , we have to know the statistical behaviour of  $n(t)$ . The Gaussian random variable (with zero mean) is a good approximation for  $n(t)$  used in this analysis. The ratio of signal power to noise power (SNR) is

$$\text{SNR} = \frac{P_S}{P_N} \quad (2.24)$$

where  $P_S$  is the power of ELT signal and  $P_N$  is the noise power. Usually SNR is expressed in terms of the decibel (dB) unit

$$10 \log_{10} (\text{SNR}) = \text{SNR}_{\text{dB}} \quad (2.25)$$

By taking the anti-logarithm of Eq. (2.25), we can express Eq. (2.24) as

$$\text{SNR} = 10^{(0.1 \text{ SNR}_{\text{dB}})} \left( \frac{P_S}{P_N} \right) \quad (2.26)$$

Since  $n(t)$  is a random variable,  $P_N$  can be estimated as the mean square value of the noise component. Eq. (2.24) becomes

$$\text{SNR} = \frac{P_S}{E[N^2(t)]} \quad (2.27)$$

In [8], the power of different forms of ELT signals are estimated. For square modulation the  $P_S$  of both linear and quadratic frequency sweep is approximated by

$$P_S \approx 0.5 A_c^2 d \quad (2.28)$$

where  $A_c$  is the signal amplitude and  $d$  is the duty cycle. The signal power estimation for sinusoidal modulation with linear frequency sweep is

$$P_S \approx 0.5 A_c^2 + 0.25 \mu^2 A_c^2 + 4 \mu A_c^2 (4.3056801 \times 10^{-7}) + \mu^2 A_c^2 (5.8011508 \times 10^{-8}) \quad (2.29)$$

and the quadratic frequency sweep is

$$P_s \approx 0.5A_c^2 + 0.25\mu^2 A_c^2 \quad (2.30)$$

where  $\mu$  is the modulation factor. For a given noise level (that is  $SNR_{dB}$ ) we can measure the performance of the received signal by using the above equations.

The required noise level is, sometimes, given in terms of the noise density unit (dB-Hz) rather than the decibel unit. We can relate  $SNR_{dB}$  and the noise density unit according to Eq. (2.27)

$$P_s = SNR \cdot E[N^2(t)] \quad (2.31)$$

For narrow band noise  $n(t)$ ,  $E[N^2(t)]$  can be estimated as  $N_o B$  [6] where  $B$  is the bandwidth of the signal. Thus, Eq. (2.3.1) gives

$$\frac{P_s}{N_o} = SNR \cdot B \quad (2.32)$$

Multiplying both sides of Eq. (2.32) by  $10\log_{10}$  yields

$$10\log_{10}\left(\frac{P_s}{N_o}\right) = 10\log_{10}(SNR) + 10\log_{10}(B) \quad (2.33)$$

It is evident that this equation has dB-Hz units. Let the right-hand side of Eq. (2.33) be

$$10\log_{10}\left(\frac{P_s}{N_o}\right) = X_{dB-Hz}$$

and substitute Eq. (2.25) into Eq. (2.33). We have

$$SNR_{dB} = X_{dB-Hz} - 10\log_{10}(B) \quad (2.34)$$

The power spectra of the received ELT signals (Eq. (2.33)), using the signal processing techniques that have been described, are given in the next chapter.

## 2.9 SUMMARY

Chapter 2 deals with a detailed description of the signal processing techniques which are used in this thesis for spectral analysis of the ELT signals. These techniques involve:

- i) the Fast Fourier Transform algorithm (FFT).
- ii) the windowed FFT technique.
- iii) the Maximum Entropy Method (MEM).
- iv) the autocorrelation function with MEM (ACFMEM).
- v) the finite impulse response bandpass filtering (FIR).

The FFT highlights two different undesirable features. First, the sidebands due to the modulation of the signal are quite prominent and can easily have amplitude approaching that of the carrier. Second, the FFT generates its own sidelobe structure even when no modulation of the signal is present. This can be controlled by using the 'windowing' technique, however. The overall result of these two effects is that a spectrum is created which combines the desired response at the carrier frequency with an undesired structure which may be a combination of signal sidebands and FFT sidelobes. This combination of sidebands and sidelobes will henceforth be referred to as 'sidelobes'.

Reduction of the sidelobes is desirable when many ELT signals are present since mutual interference can occur. Chapter 3 gives a detailed account of this sidelobe reduction for one ELT signal.

## CHAPTER 3

### PROCESSING OF ONE ELT SIGNAL

The Fast Fourier Transform algorithm and the Maximum Entropy Spectral Analysis are employed to study the spectral characteristics of the emergency locator transmitter signals in this chapter. In addition to these spectral estimation methods, we also introduce the auto-correlation function (ACF) and the finite impulse response (FIR) band-pass filtering as the preprocessing techniques. The theories of these signal processing methods have been discussed in the previous chapter.

We begin, in this chapter, a discussion of the simulation of ELT signals and the implementation of the above signal processing methods on a digital computer. The spectra of different forms of single ELT signals are used to examine and compare the performances of each spectral estimation technique. In the analysis, signals with different values of carrier-to-noise density ratio are also considered.

#### 3.1 DISCUSSION ON THE SIMULATION PROCESS

It is assumed that the distress signal received at the earth station has been converted to a frequency band between 0 and 25 KHz. The expected value of any ELT signal is 121.5 MHz or 243 MHz and this is mixed to fall at the bandcenter frequency of 12.5 KHz. In order to satisfy the Nyquist criterion, the signal is sampled at fifty-thousand samples per second. For a complete modulation sweep (a quarter of a

second), 12500 samples are required. Due to satellite motion, there is a Doppler frequency shift in the signal of up to about  $\pm 3$  KHz for the ELT signals and a further  $\pm 3$  KHz spread due to differences in crystal operation between ELT units. Thus, the total band of interest lies between about 6.5 KHz and 18.5 KHz, although there may be signals outside this band.

A package of computer simulation programs has been developed to study the spectral performances of ELT signals. The package includes five separate programs which are discussed in the following paragraphs. Listings of these programs are given in Appendix D. All simulations are done on the HP-1000 computer system in conjunction with the array processor (FPS-AP 120B). The main advantage of using the array processor is the much faster program execution speed in performing the algorithm repetitively on long sequences of data.

Different formats of a 512-point ELT signal are simulated from the program ELTAP. The simulation includes computer-generated ELT signals which can be processed assuming additive white Gaussian noise thus allowing performance to be measured at different frequencies and at different carrier-to-noise density ratio. Method of implementation is based on sampling the signal at a rate of fifty-thousand samples per second. The signal (512-point) has a record length of 10.22 ms, with the first sample occurring at time equal to zero. A sinusoidal-modulated ELT signal is simulated according to Eq. (1.6) and (1.7). For a pulse-modulated signal, the implementation employs the equations developed in Appendix A. The phase components of a pulse-modulated

random phase signal can be constructed by multiplying a set of uniformly distributed random variables (between 0 and 1) by  $2\pi$ . These random variables are generated by the array processor. Using Eq. (2.26), (2.28), (2.29), (2.30) and (2.34), we can include noise components with the signal. However, we need to generate a set of Gaussian random variables. This can be achieved by converting a pair of uniformly distributed random variables ( $x(n)$  and  $x(n+1)$ ) between 0 and 1 to a pair of Gaussian random variables ( $w(n)$  and  $w(n+1)$ ) with zero mean and unit variance ( $\sigma^2$ ) according to the equations [11], [38]

$$w(n) = y(n)\cos(2\pi x(n+1)) \quad (3.1)$$

$$w(n+1) = y(n)\sin(2\pi x(n+1)) \quad (3.2)$$

$$y(n) = \sqrt{2\sigma^2 \ln \frac{1}{x(n)}} \quad (3.3)$$

A maximum of ten different ELT signals can be generated simultaneously if multiple distress signals are necessary for the analysis.

The program WFIR implements a finite impulse response bandpass filter which has been discussed in Section 2.7. The simulation is based on the Eq. (C.14) to construct the frequency response and Eq. (C.20) to generate the windowed impulse responses.

Windowing, autocorrelation function (ACF) and convolution (due to bandpass filtering) are implemented in the program PROAP. Five different configurations can be selected as preprocessor. These are

- (i) signal + windowing
- (ii) signal + ACF + windowing
- (iii) signal + ACF

(iv) signal + FIR

(v) signal + ACF + FIR

An ELT signal can be windowed by any of the window functions (512-point) described in Section 2.3. The ACF (Eq. (2.22)) is implemented by using the array processor library subroutine. It is more efficient to perform the digital filtering in the frequency domain (fast convolution technique) than by the direct form of convolution sum in Eq. (C.1). The fast convolution technique makes use of the Fast Fourier Transform algorithm. Assume we have a signal  $\{s(n)\}$  of length  $M$  which has to be filtered by an FIR filter whose impulse response is  $\{h(n)\}$  of length  $N$ . We extend the signal and impulse response to a length of  $L$ , which is the maximum power of 2 greater than the sum  $M+N-1$ , such that

$$\begin{aligned}\hat{s}(n) &= s(n) & n=0, \dots, M-1 \\ \hat{s}(n) &= 0 & n=M, \dots, L-1\end{aligned}\tag{3.4}$$

and

$$\begin{aligned}\hat{h}(n) &= h(n) & n=0, \dots, N-1 \\ \hat{h}(n) &= 0 & n=N, \dots, L-1\end{aligned}\tag{3.5}$$

Next, we compute the forward FFT of these equations and obtain the complex product of the two sequences. The operation is completed by performing an inverse FFT on the complex products.

The program SPMAP uses array processor to calculate the spectral estimations of the ELT signals (and the preprocessed signals) by means of the Fast Fourier Transform algorithm and the Maximum Entropy Method. The degree of complexity which involves in the computation of the prediction error filter coefficients of the MEM can be reduced. Both

the numerator and denominator, in Eq. (2.16), contain the forward and backward direction filtering term. A point worthy of note is that the forward filtering and the backward filtering terms have a structure which combines the input signal sequence convolved with the previous values of coefficient  $a(M-1,k)$ . Taking the dot product operation of these two arrays, we obtain the numerator. The denominator is simply the addition of the square of a vector sum of the two operations. This method is conveniently programmed by using the library subroutines of the array processor. For high filter order of MEM, for instance an order of twenty, the computational time using this method is drastically decreased. Employing Eq. (2.11), (2.15), (2.16) and (2.17), the MEM spectrum is determined. The power spectra of the two spectral estimation methods are normalized with respect to their maximum value and are presented in decibel scale.

Simulated results obtained from these programs can be plotted by utilizing the HP-1000 computer graphic package. The program CURVE is able to plot the ELT signal, preprocessed signal and power spectrum of each processing technique. In the following sections, we examine the processing results of one ELT signal.

### 3.2 PROCESSING RESULTS USING THE FAST FOURIER TRANSFORM TECHNIQUE

At present, signal processing methods applied to the ELT signals are based on the Fast Fourier Transform and the use of windowing technique. The theories related to these topics have been discussed in Sections 2.2 and 2.3. This section is devoted to an examination of the

results of one ELT signal, in the absence of additive noise, processed by the FFT and FFT with windowing technique. Results of signal with different modulations and frequency sweeps are detailed. The simulated signal (512-point) is at a carrier frequency of 12832 Hz. First, we discuss the pulse-modulated signal and then the sinusoidal-modulated signal.

### 3.2.1 Pulse-Modulated, Continuous Phase

A pulse-modulated signal (12832 Hz) with continuous phase and linear frequency sweep is shown in Fig. 3.1. The duty cycle of the modulation is 36%. A 512-point Fast Fourier Transform is performed on the signal. The spectral density is given in Fig. 3.2. Five peaks are detected at a threshold level of -10 dB. In the diagram, an arrow indicates the position of the carrier frequency. The main peak is at 12793 Hz. This introduces a frequency error of 39 Hz which is defined by the equation

$$\text{frequency error} = \text{carrier frequency} - \text{frequency resolution} \quad (3.6)$$

at 0 dB amplitude

The two major sidelobes are at 11426 Hz and 14260 Hz. These sidelobes are likely to increase the possibility of false alarm in detecting multiple signals. The same situation arises in the spectrum of the ELT signal with quadratic frequency sweep. Fig. 3.3 shows that the two major sidelobes, in this case, are at 10937 Hz and 14760 Hz with the main peak at 12793 Hz.

In order to reduce the sidelobe amplitude, the signal is windowed by an appropriate window function. A Kaiser window with parameter  $\beta=8.0$  is used to window the signal depicted in Fig. 3.1. This is illustrated

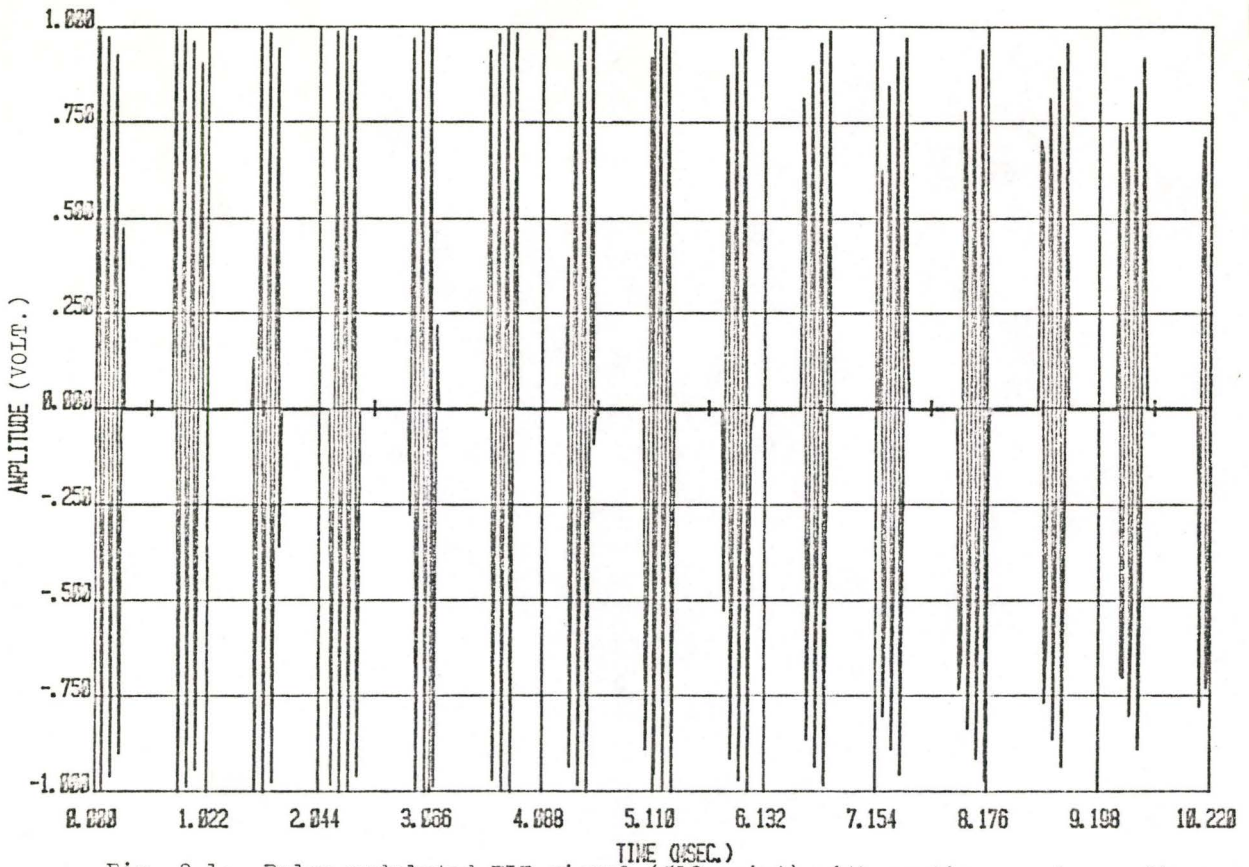


Fig. 3.1: Pulse-modulated ELT signal (512-point) with continuous phase, linear frequency sweep and 36% duty cycle. Carrier frequency is 12832 Hz.

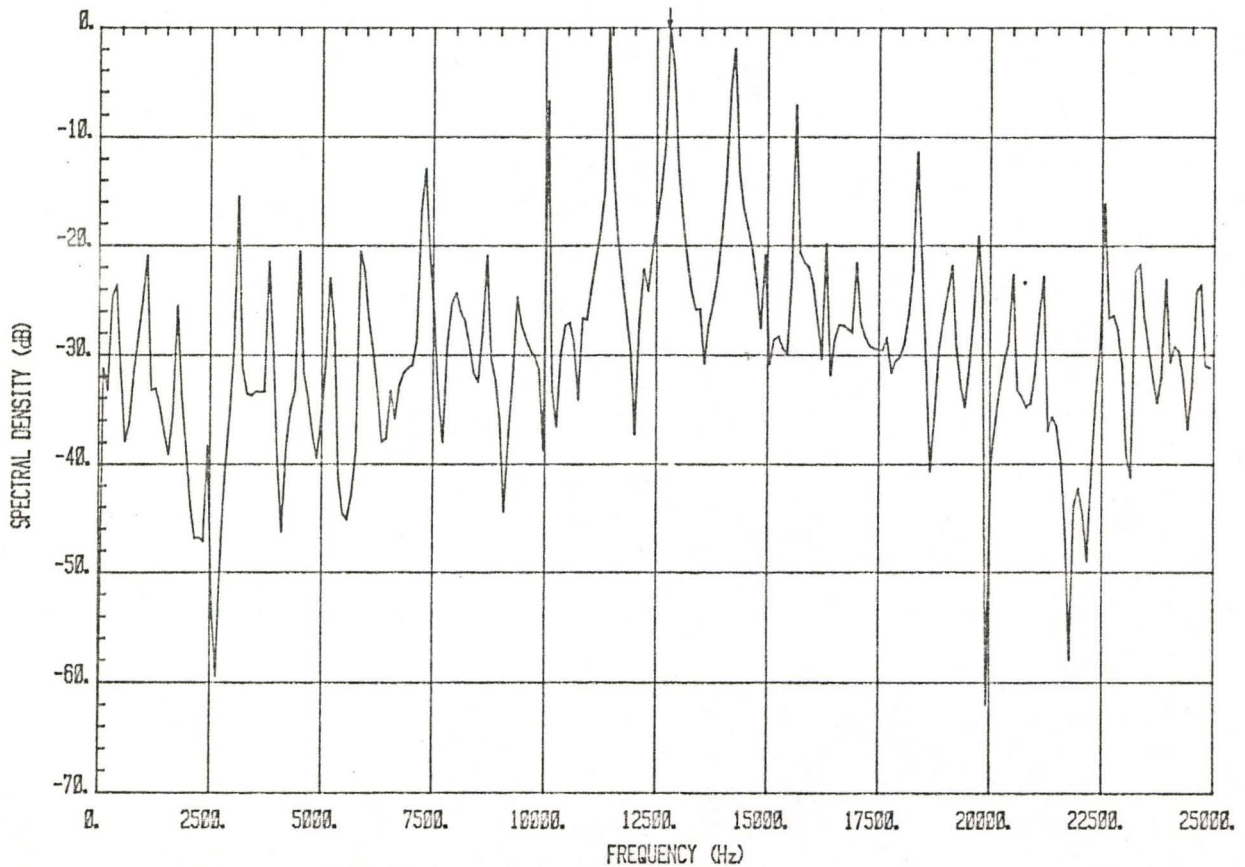


Fig. 3.2: The FFT spectrum of the signal shown in Fig. 3.1.

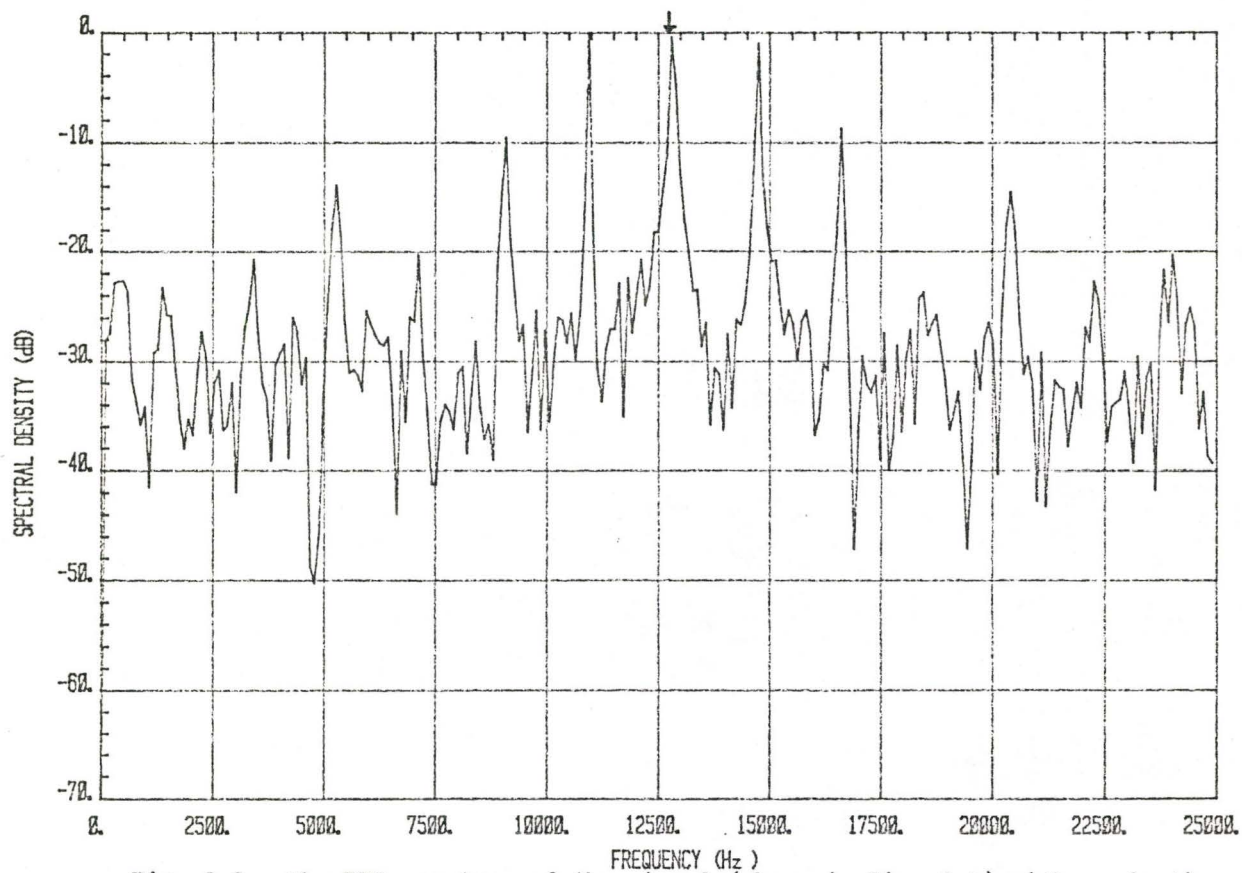


Fig. 3.3: The FFT spectrum of the signal (shown in Fig. 3.1) with quadratic frequency sweep.

in Fig. 3.4. The spectrum of this signal, in Fig. 3.5, indicates that at about -10 dB the minor sidelobes are decreased by 2 dB and the major sidelobe at 11426 Hz is reduced by 1 dB in amplitude. There is no significant improvement for the sidelobe at 14260 Hz. One drawback of using the windowing technique is the relatively broad main peak. Kaiser window has the ability to trade-off the main lobe width for sidelobe amplitude by adjusting the parameter  $\beta$ . This property is illustrated in Fig. 3.6 and Fig. 3.7 which are the power spectra of the same signal windowed by Kaiser window with  $\beta=4.0$  and  $\beta=10.0$  respectively. The minor sidelobes in Fig. 3.6 are reduced by only 1 dB and the major sidelobe (11426 Hz) is down by less than 1 dB. However, the main peak is narrower than the one used  $\beta=8.0$ . For  $\beta=10.0$  there is no conspicuous changes in comparing with Fig. 3.5. Hamming window and Blackman window are also employed. The results are shown in Fig. 3.8 and Fig. 3.9. For the rest of windowing technique, in the analysis, we choose the Kaiser window with  $\beta=8.0$ .

A great improvement in frequency resolution of the FFT spectrum is obtained when the signal (Fig. 3.1) is passed through a finite impulse response filter. The filter characteristics were discussed in Section 2.7 and its frequency response was depicted in Fig. 2.8. Fig. 3.10 shows the FFT spectrum of this processing method. The sidelobes are reduced by 2 dB and the main peak (12793 Hz) is distinctive. The bandpass filter discards unnecessary information outside the frequency band between 7 KHz and 18 KHz. This filter is an appropriate choice since, at earth stations, the received ELT signals are likely to fall

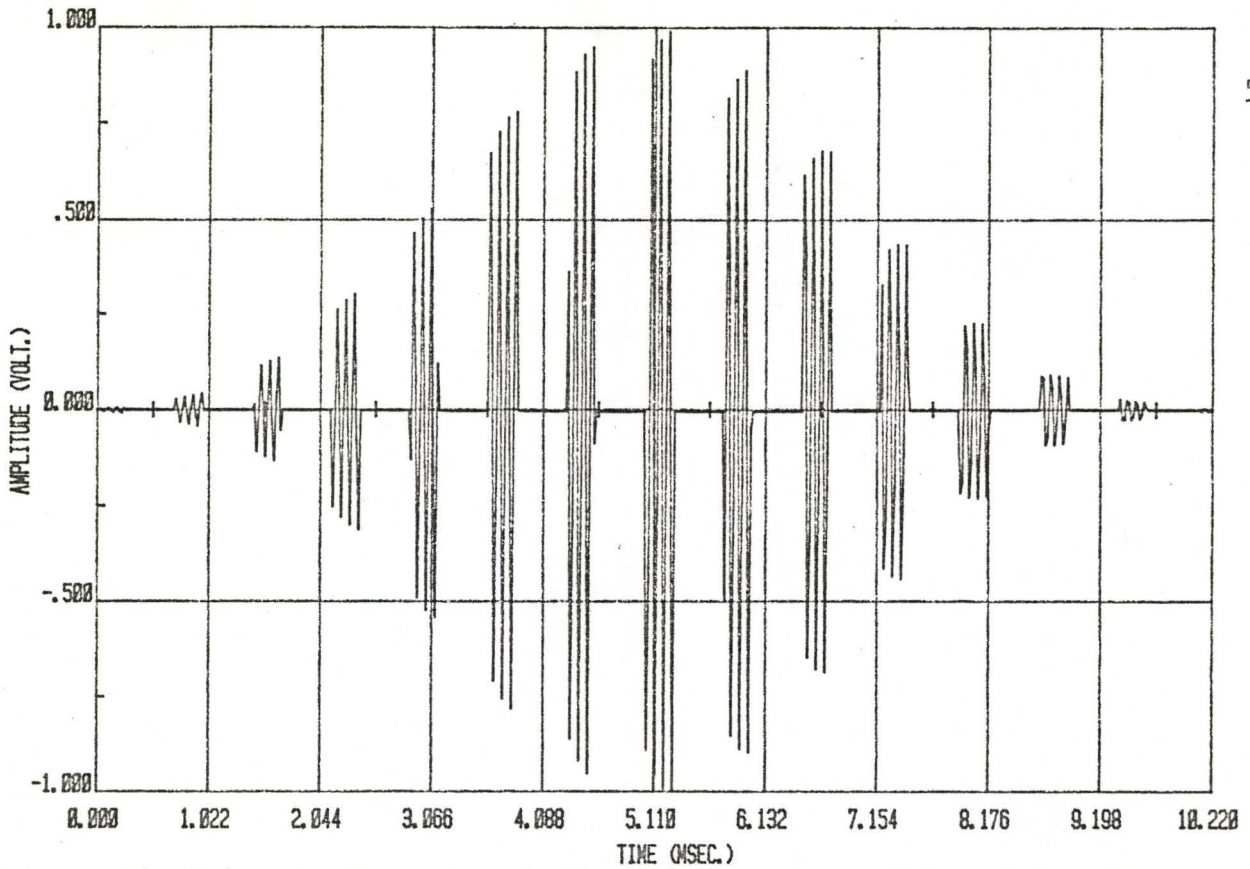


Fig. 3.4: The signal shown in Fig. 3.1 windowed by a Kaiser window with  $\beta = 8.0$ .

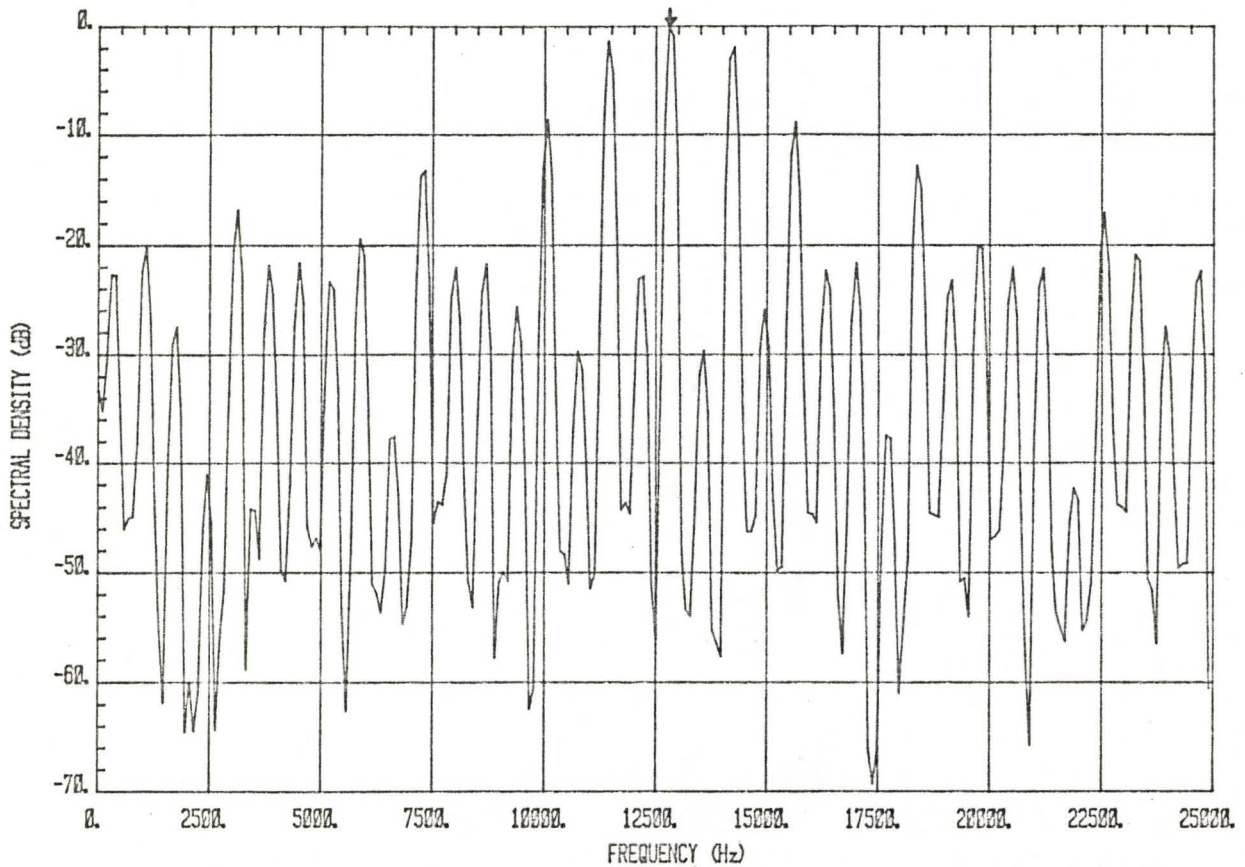


Fig. 3.5: The FFT spectrum of the windowed signal shown in Fig. 3.4.

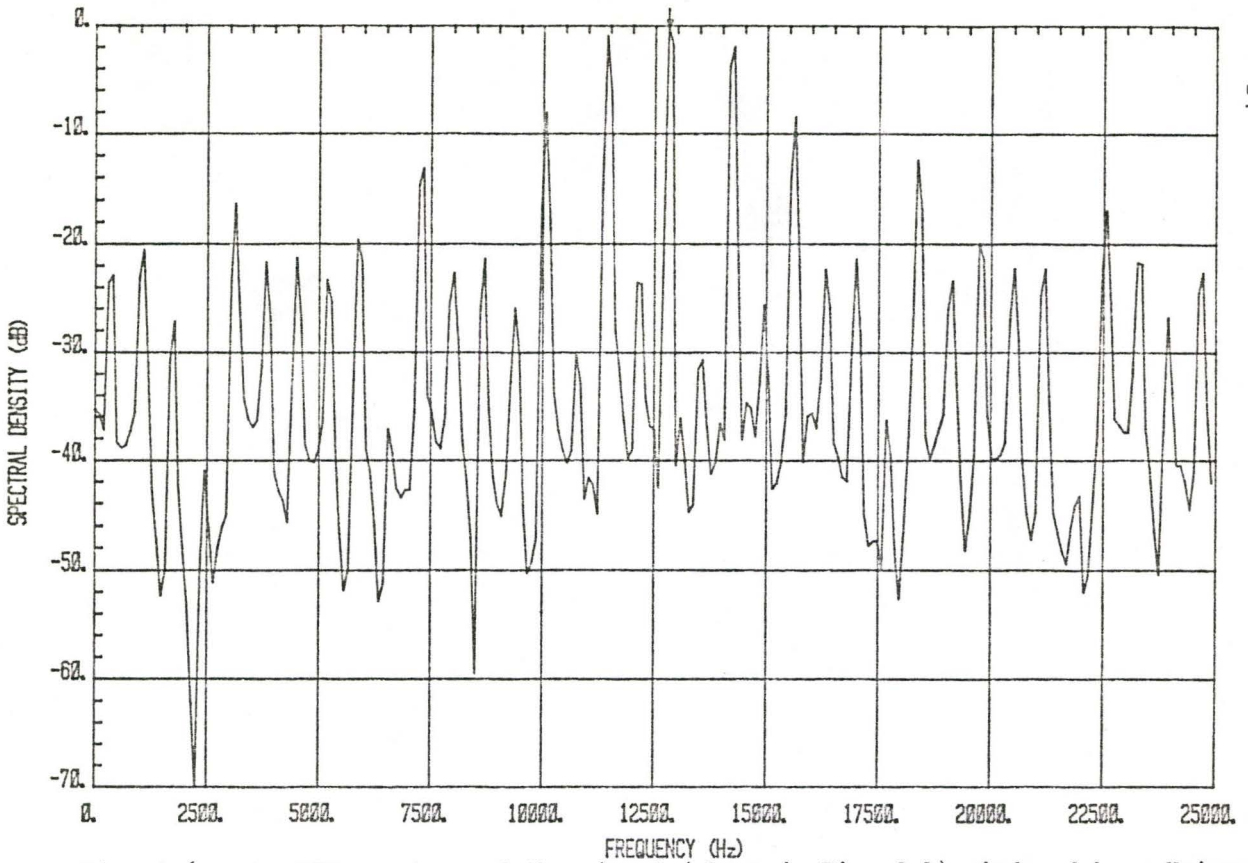


Fig. 3.6: The FFT spectrum of the signal (shown in Fig. 3.1) windowed by a Kaiser window ( $\beta=4.0$ ).

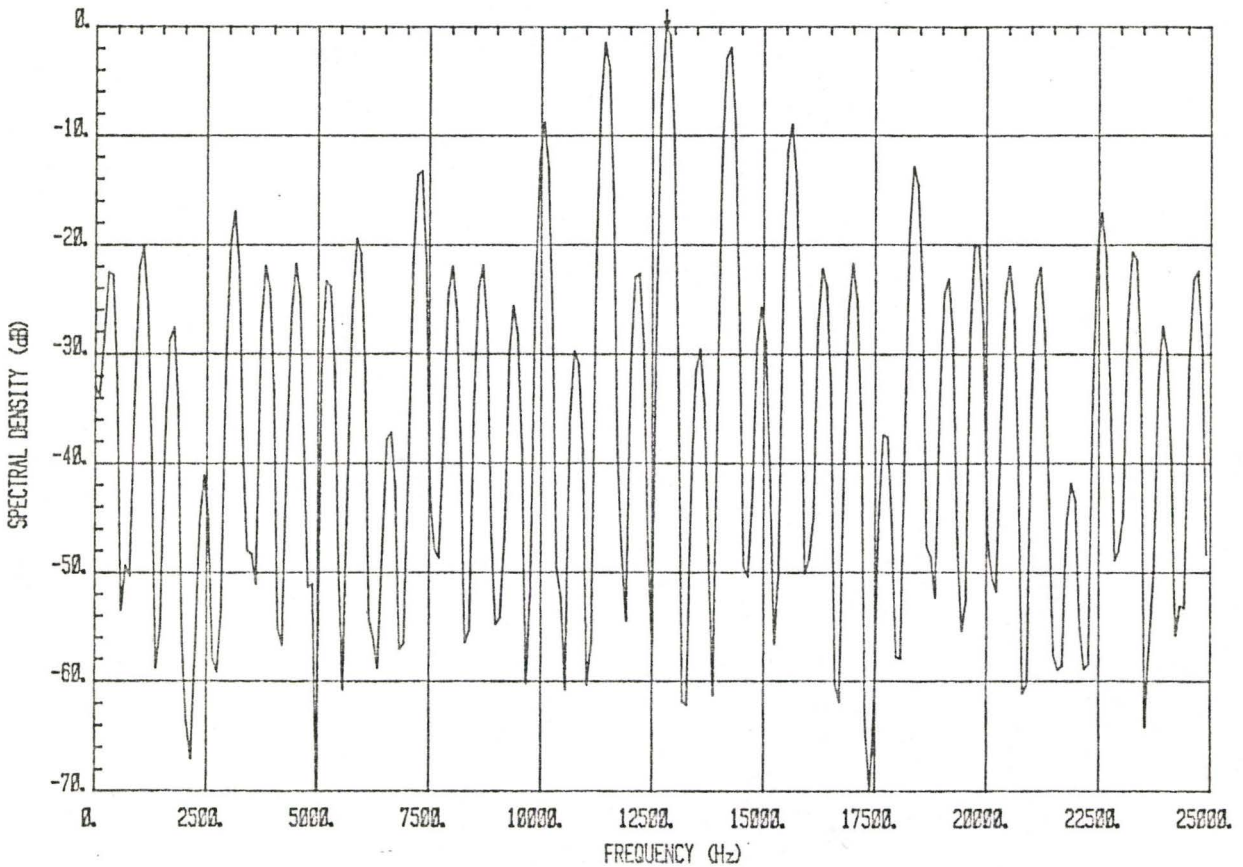


Fig. 3.7: The FFT spectrum of the signal (shown in Fig. 3.1) windowed by a Kaiser window ( $\beta=10.0$ ).

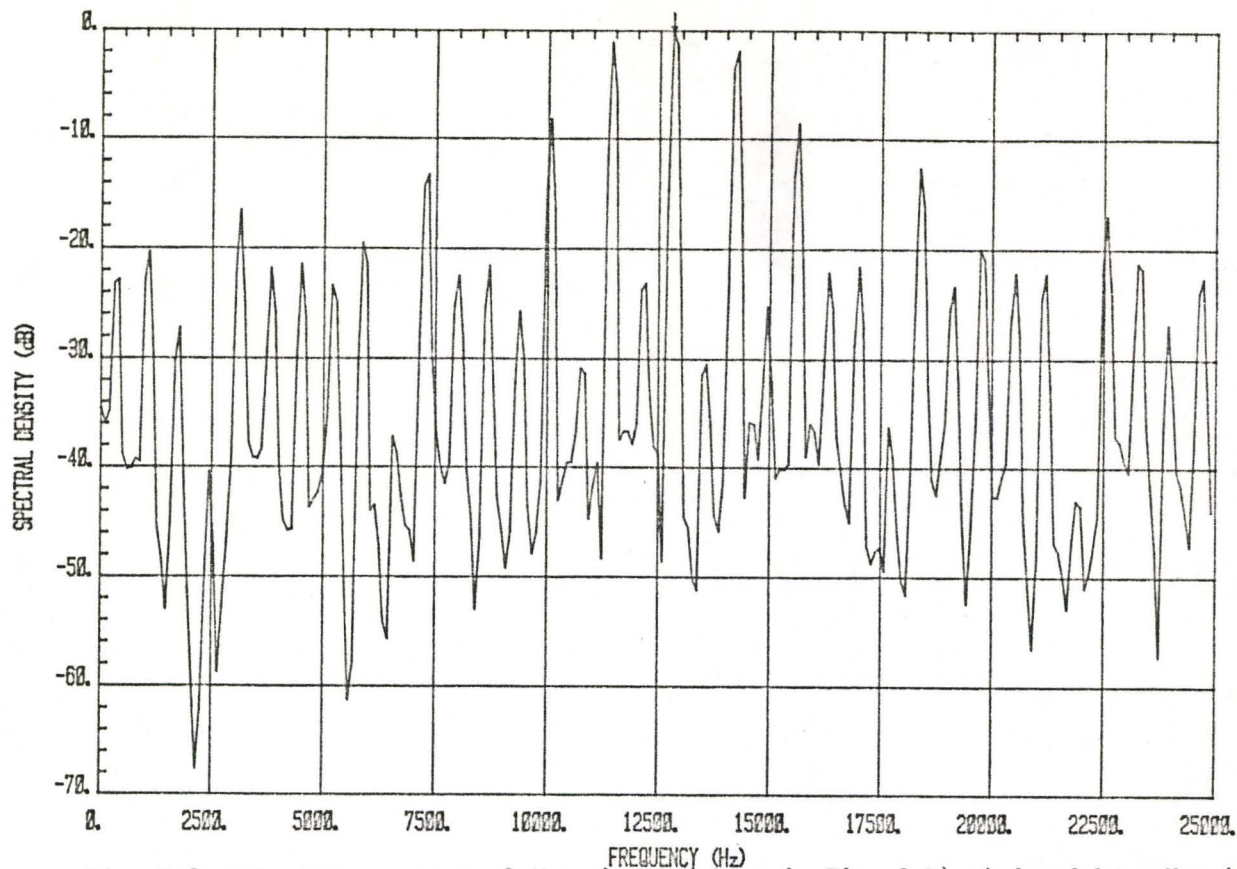


Fig. 3.8: The FFT spectrum of the signal (shown in Fig. 3.1) windowed by a Hamming window.

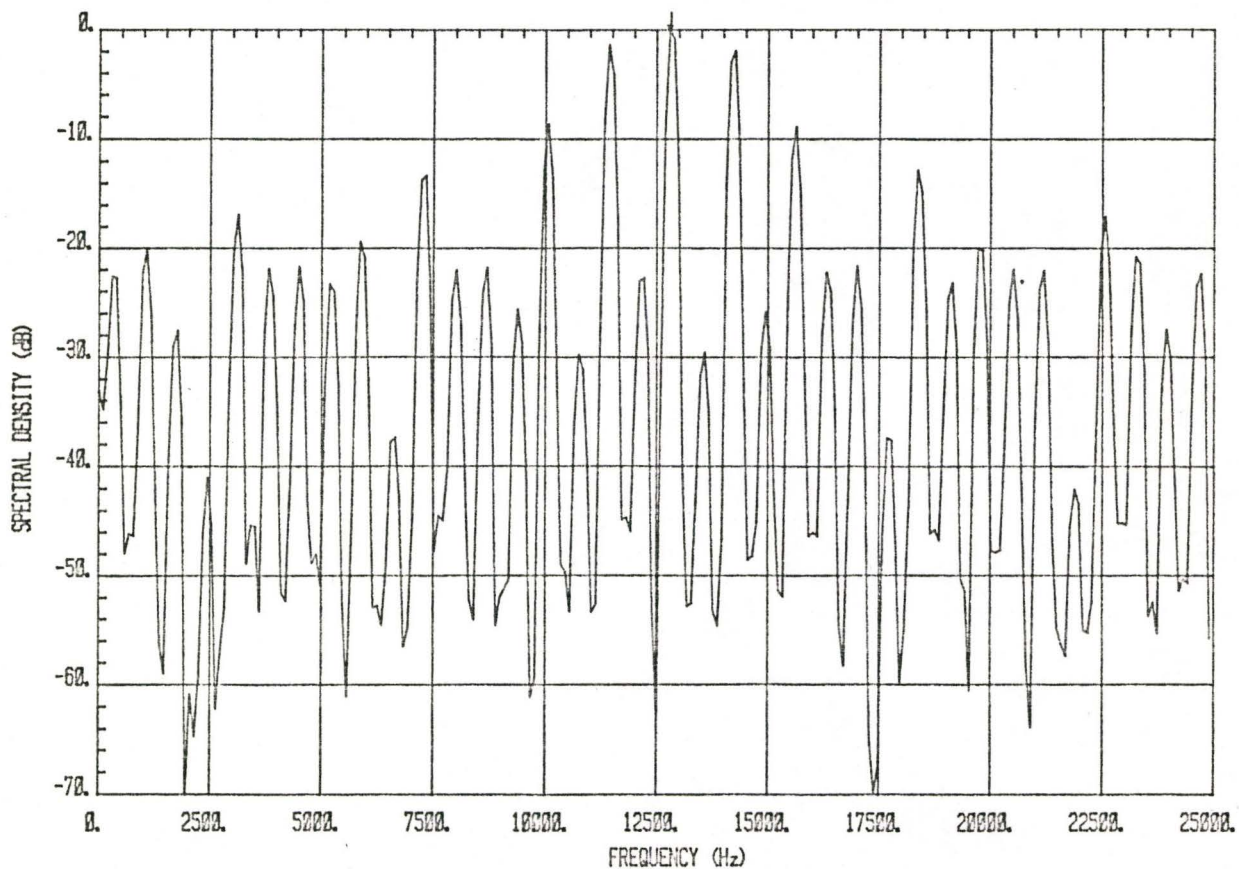


Fig. 3.9: The FFT spectrum of the signal (shown in Fig. 3.1) windowed by a Blackman window.

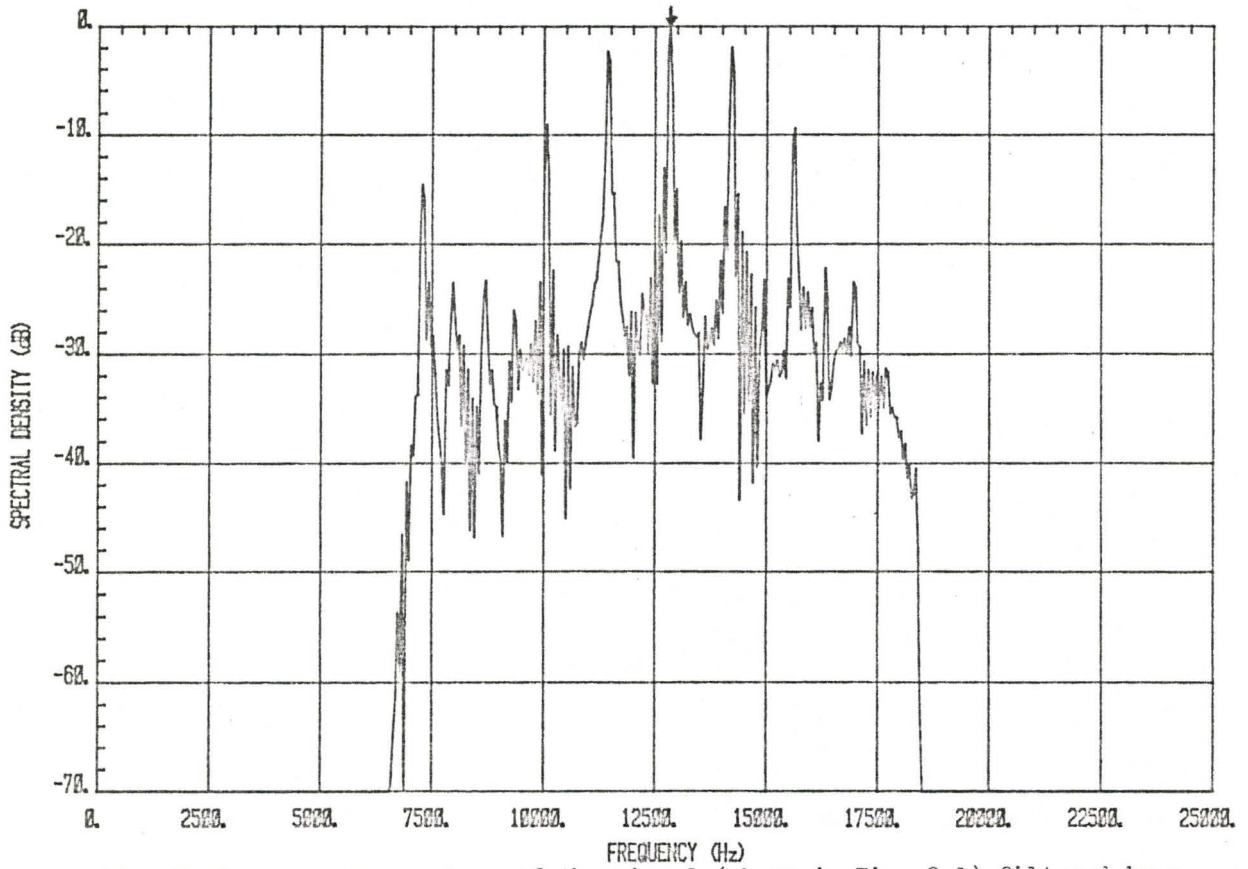


Fig. 3.10: The FFT spectrum of the signal (shown in Fig. 3.1) filtered by a bandpass filter.

within 6.5 KHz and 18.5 KHz range.

The duration of the pulses in the pulse-modulated signal are varied with time. The effect of this parameter on the spectral analysis is examined. We process the pulse-modulated signal (linear frequency sweep) with duty cycles 40% and 50%. The power spectra are shown in Fig. 3.11 and 3.12. We observe that a higher value of duty cycle achieves better performance. This indicates that if an ELT signal (at a complete modulation sweep) is processed on a per block basis, we expect the frequency resolution to be more ~~spectacular~~ as the pulse duration gradually increases with time [8].

### 3.2.2 Pulse-Modulated, Random Phase

A pulse-modulated random phase signal with linear frequency sweep and 36% duty cycle is shown in Fig. 3.13. Fig. 3.14 illustrates the spectrum of this signal and Fig. 3.15 is the spectrum of the signal with quadratic frequency sweep. The numbers of sidelobes at above -10 dB level make detection difficult if not impossible. The windowed signal of Fig. 3.13 is depicted in Fig. 3.16. The spectrum, in Fig. 3.17 shows that line-splitting occurs on the main peak and the peak is lower in amplitude than the adjacent sidelobes. The situation is unchanged when digital filtering is employed. Fig. 3.18 shows this result. It is obvious that phase randomization disrupts the FFT spectra considerably.

### 3.2.3 Sinusoidal-Modulated

The sinusoidal-modulated signal with linear frequency sweep is given in Fig. 3.19. Fig. 3.20 and Fig. 3.21 show the spectra of the signal with linear and quadratic frequency sweeps. A sharp contrast

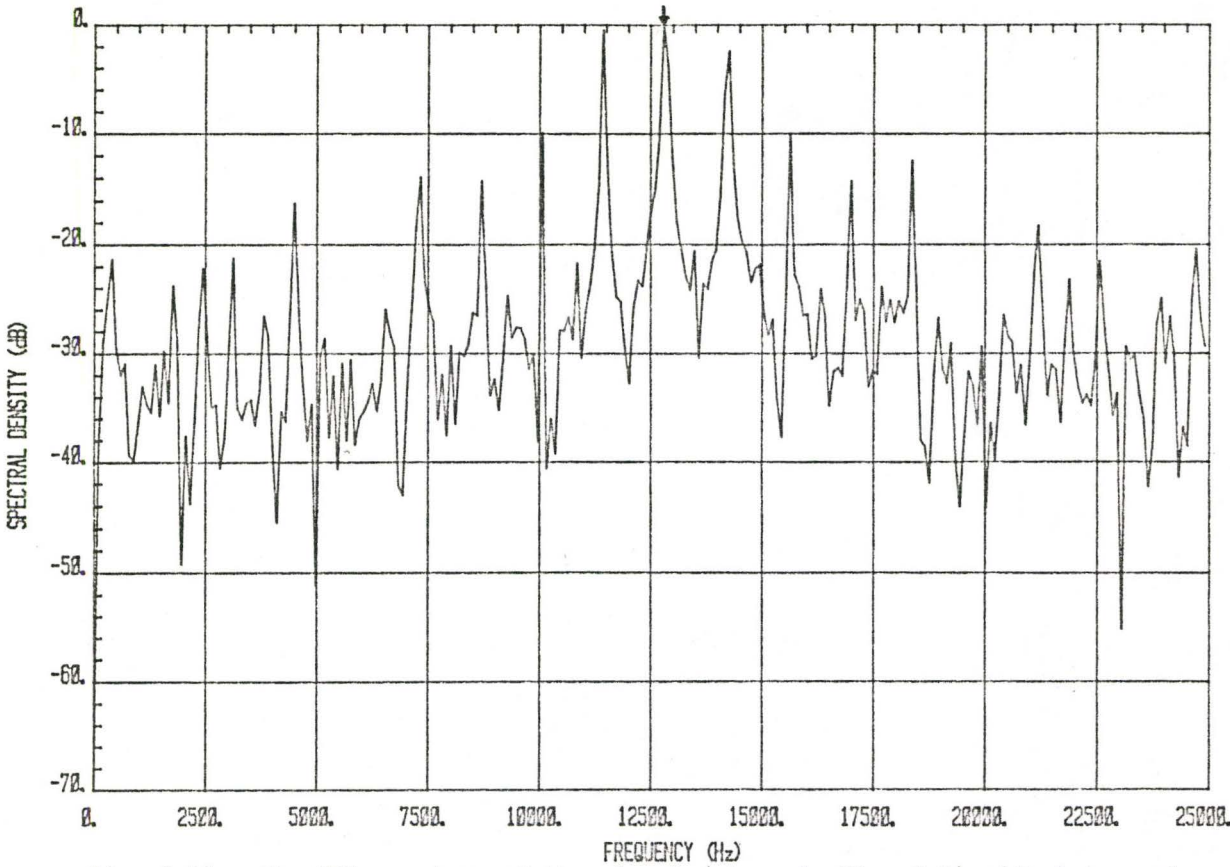


Fig. 3.11: The FFT spectrum of the signal (shown in Fig. 3.1) with duty cycle equal to 40%.

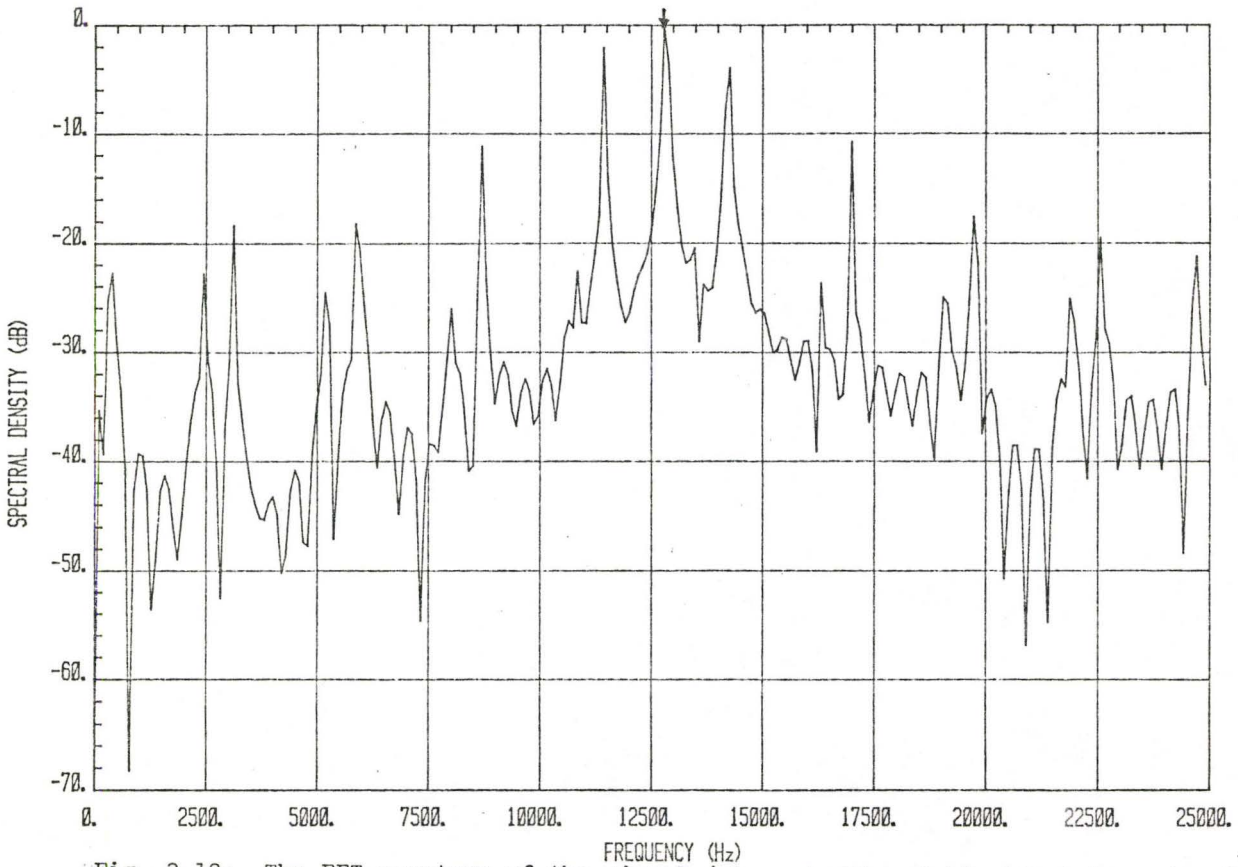


Fig. 3.12: The FFT spectrum of the signal (shown in Fig. 3.1) with duty cycle 50%.

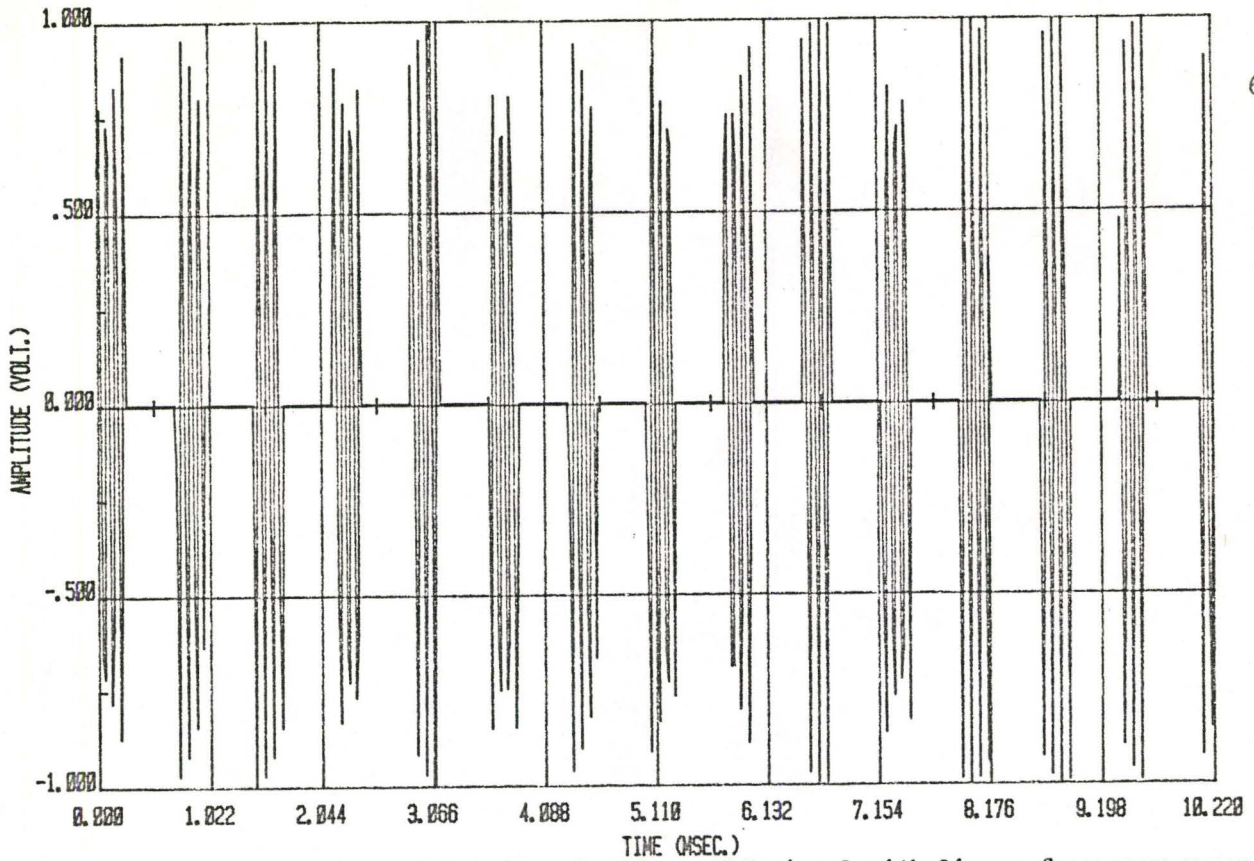


Fig. 3.13: A pulse-modulated random phase ELT signal with linear frequency sweep and 36% duty cycle. Carrier frequency is 12832 Hz.

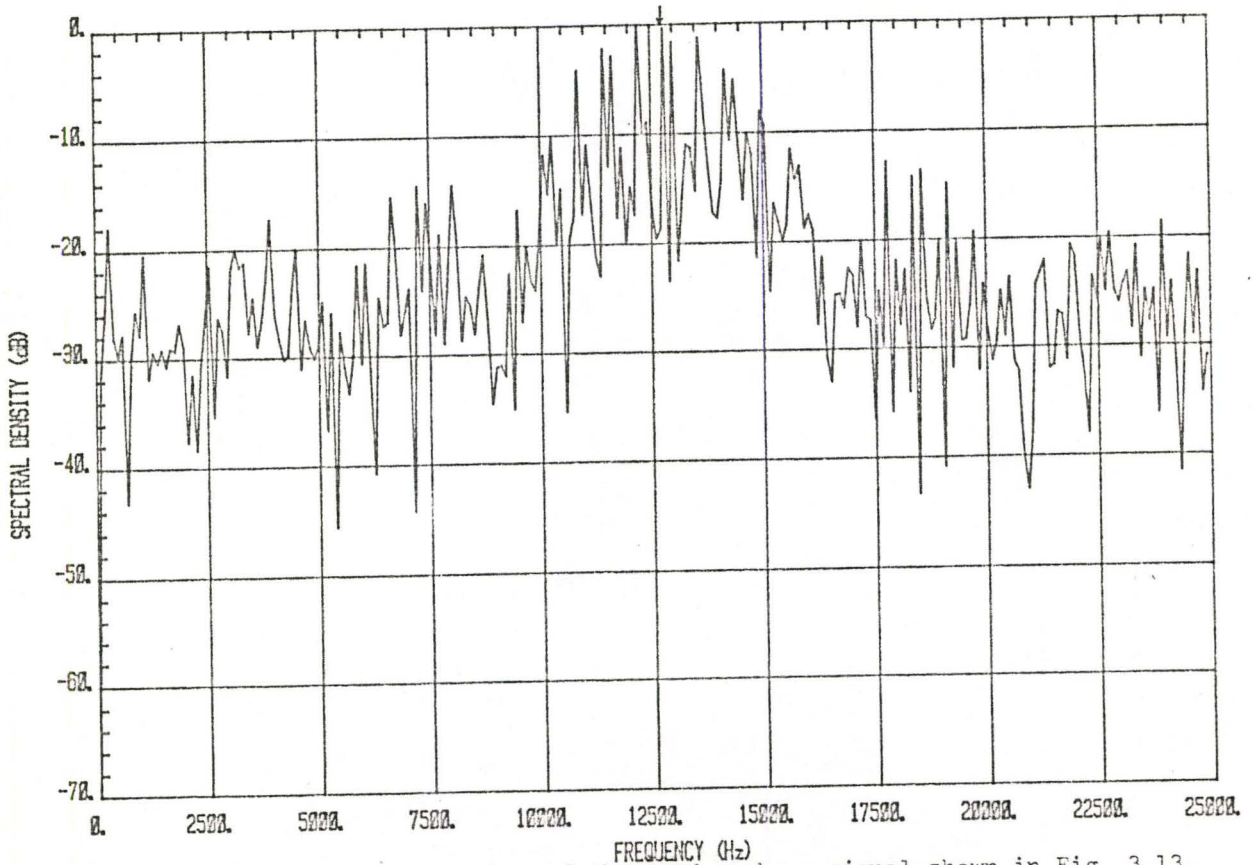


Fig. 3.14: The FFT spectrum of the random phase signal shown in Fig. 3.13.

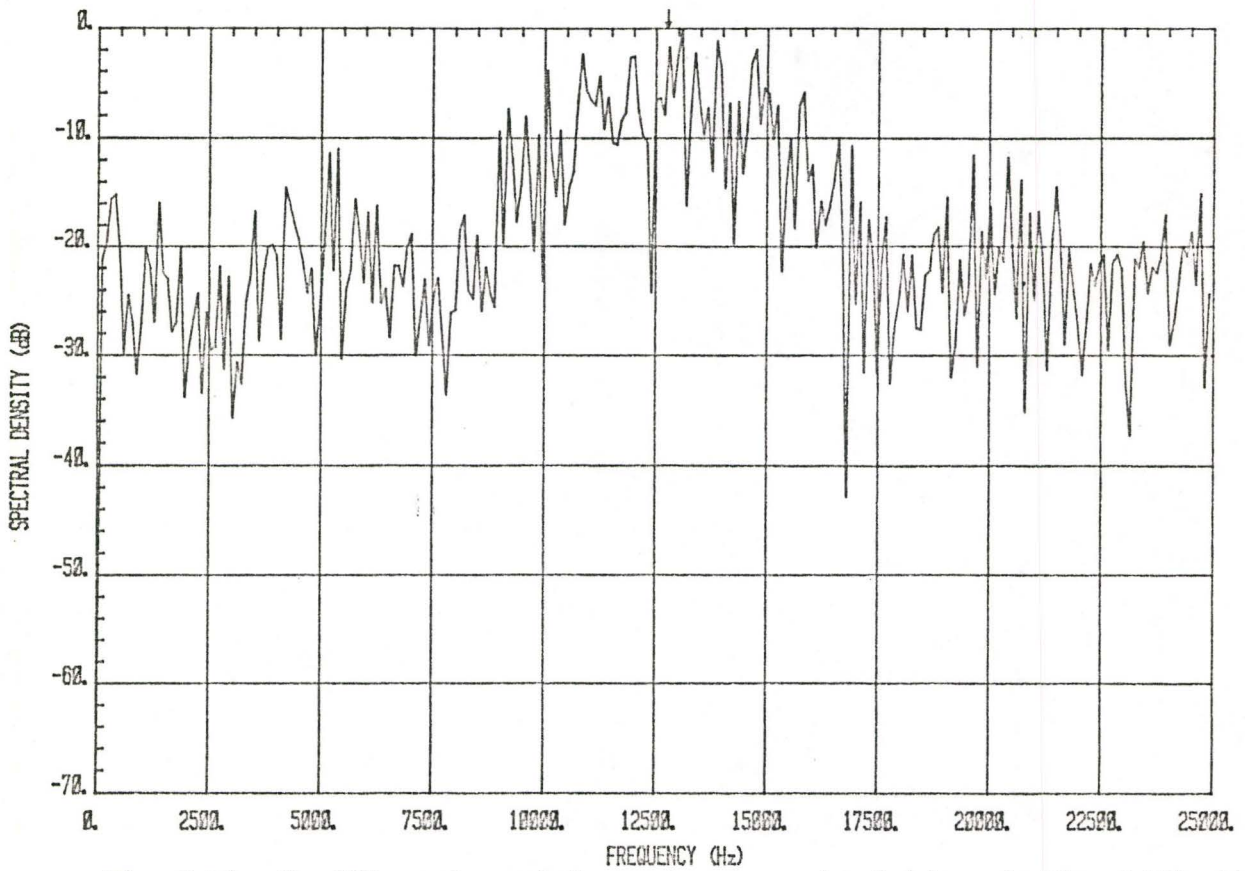


Fig. 3.15: The FFT spectrum of the random phase signal (shown in Fig. 3.13) with quadratic frequency sweep.

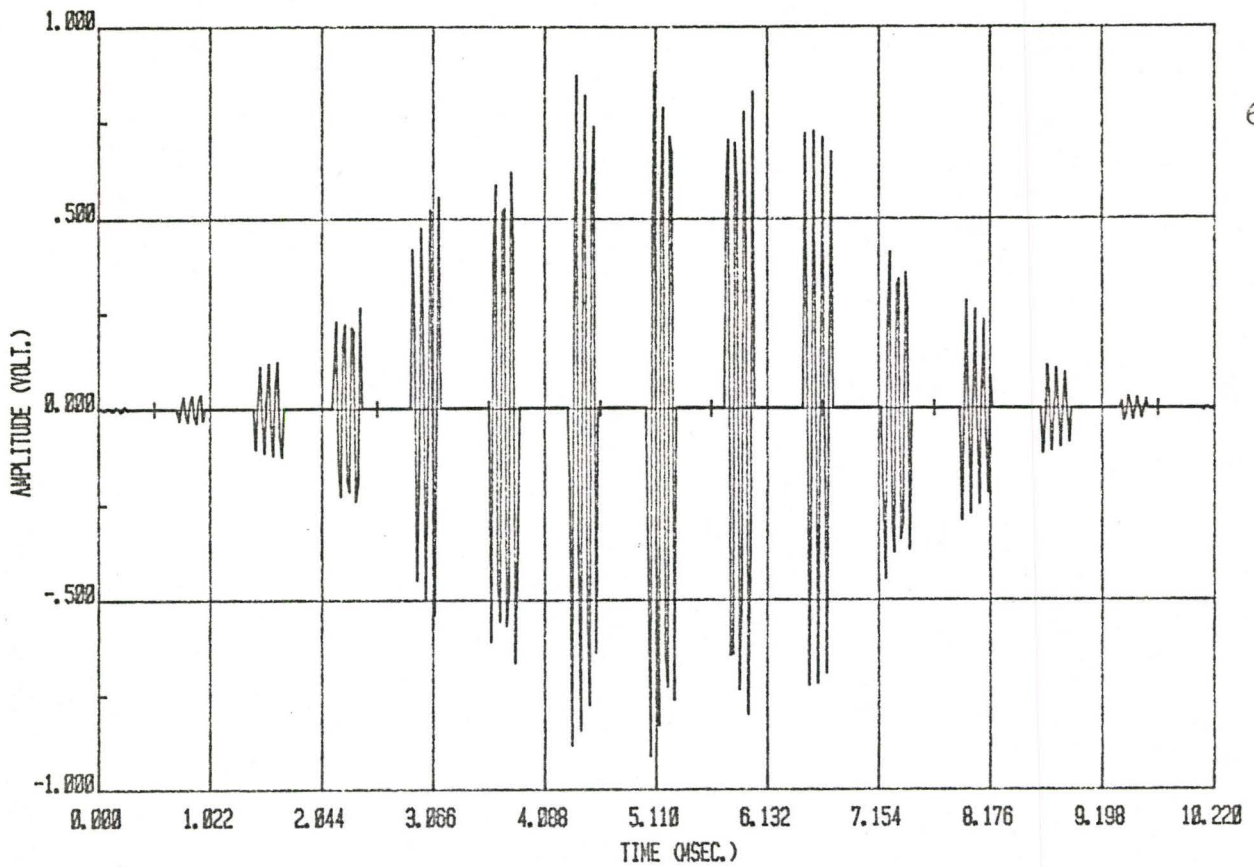


Fig. 3.16: The signal shown in Fig. 3.13 windowed by a Kaiser window ( $\beta=8.0$ ).

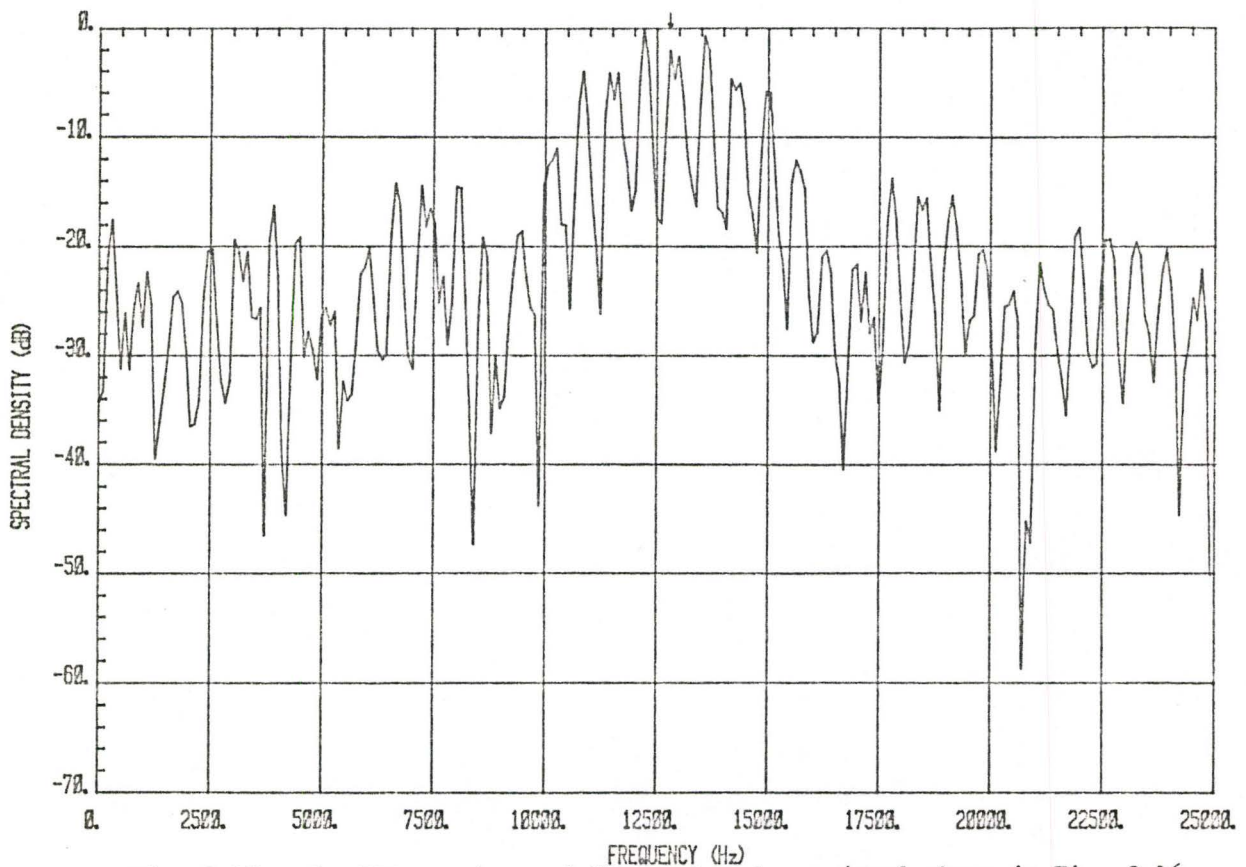


Fig. 3.17: The FFT spectrum of the random phase signal shown in Fig. 3.16.

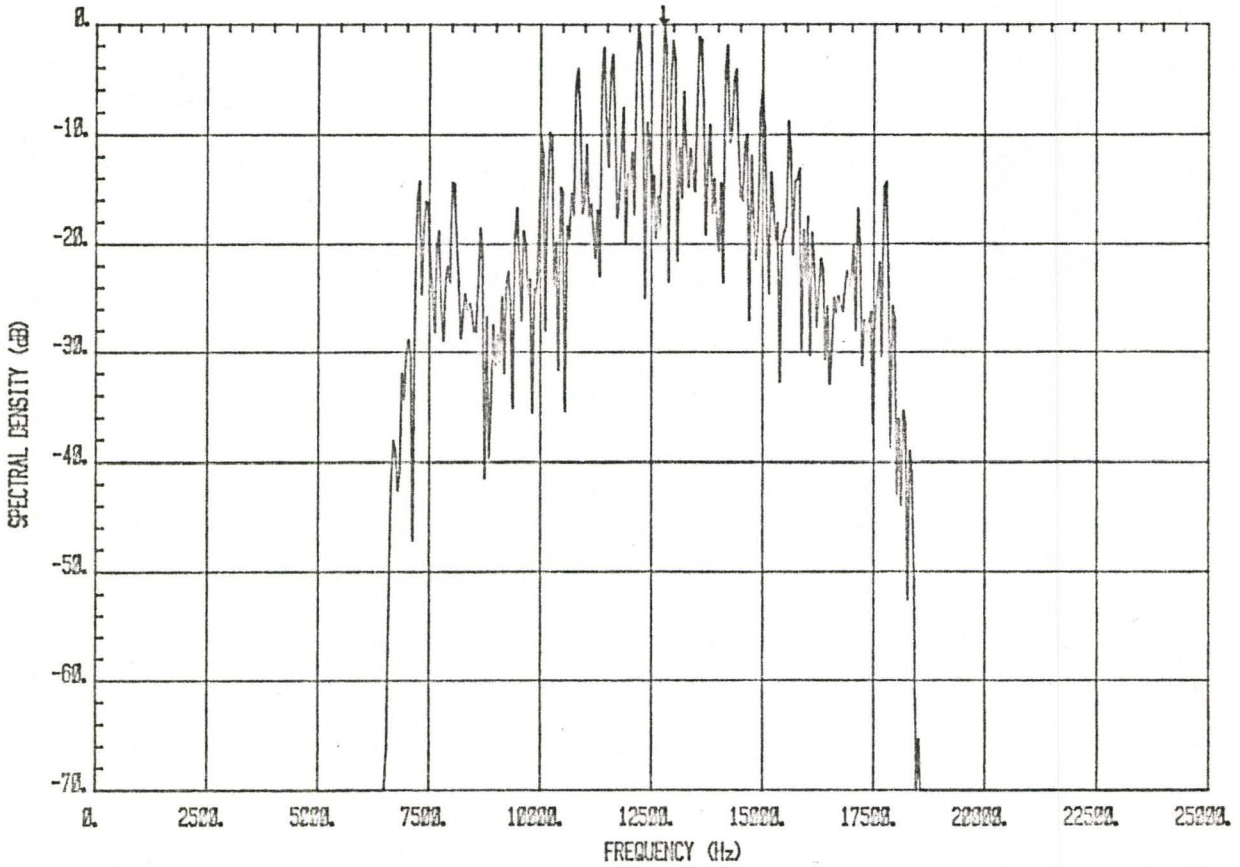


Fig. 3.18: The FFT spectrum of the random phase signal shown in Fig. 3.13 filtered by a bandpass filter.

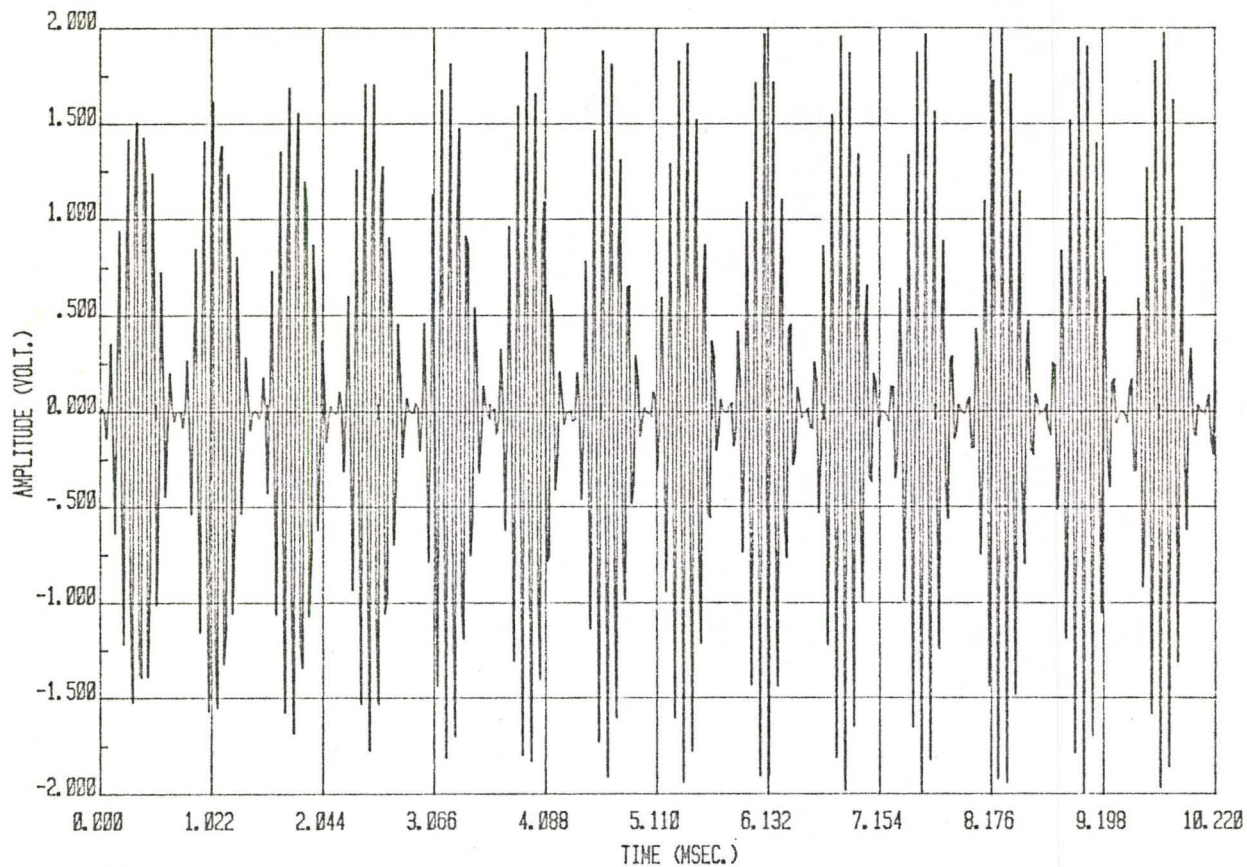


Fig. 3.19: A sinusoidal-modulated ELT signal with linear frequency sweep.  
Carrier frequency is 12832 Hz.

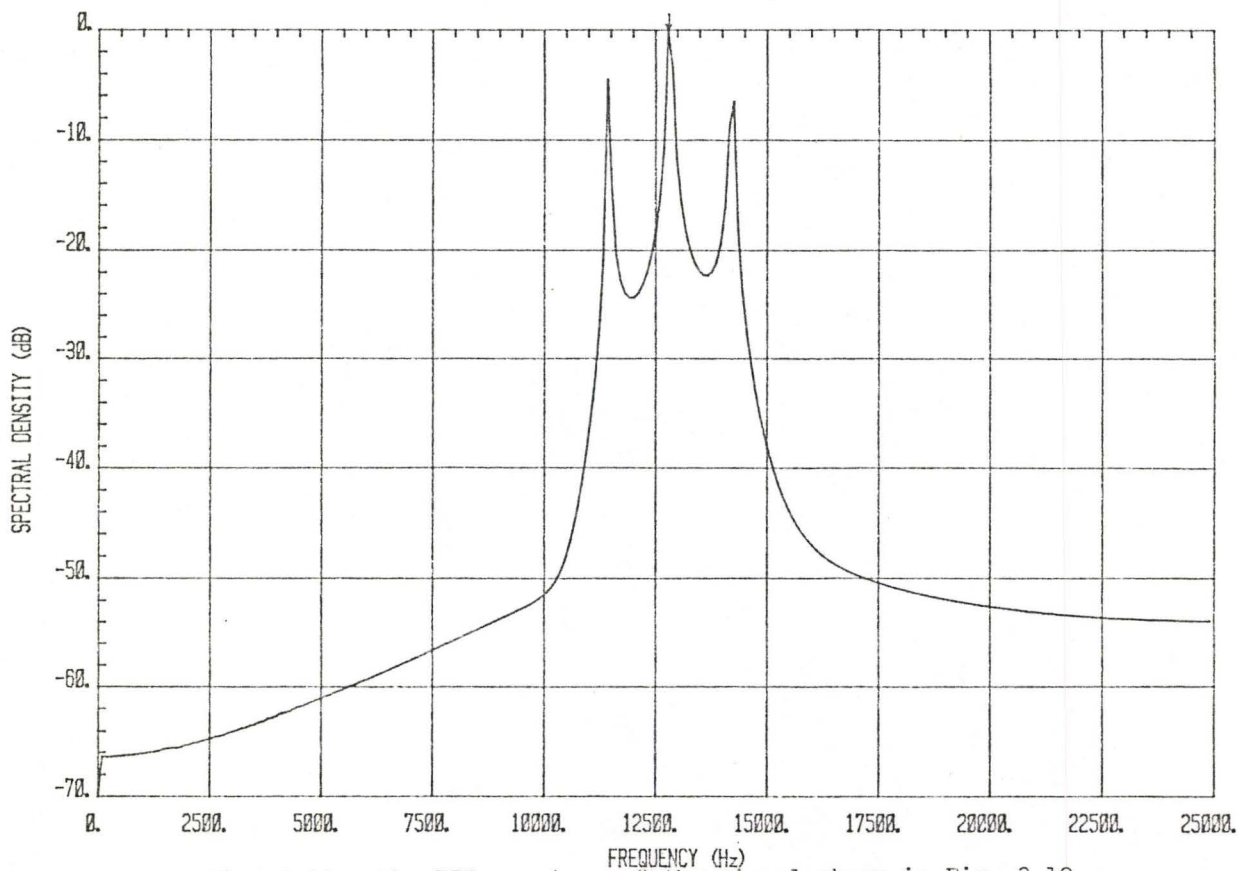


Fig. 3.20: The FFT spectrum of the signal shown in Fig. 3.19.

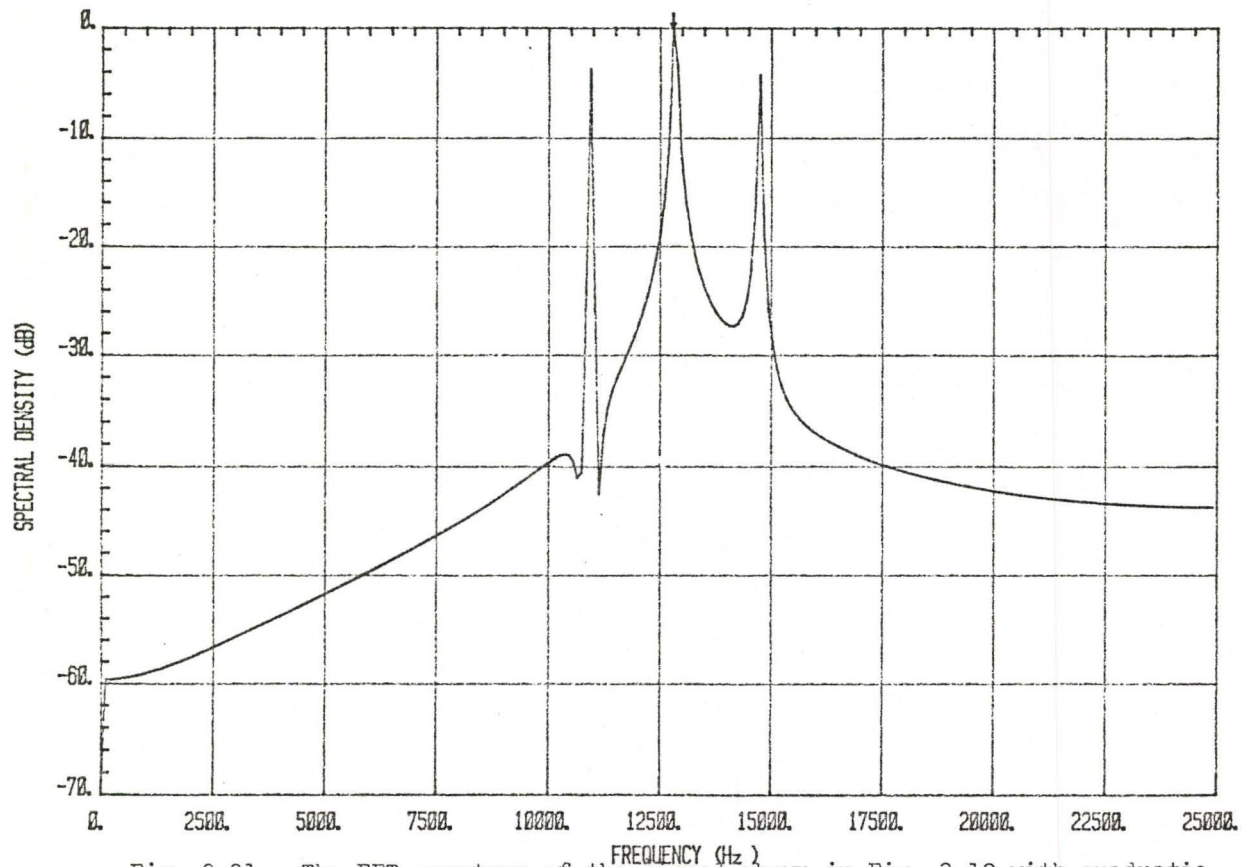


Fig. 3.21: The FFT spectrum of the signal shown in Fig. 3.19 with quadratic frequency sweep.

with the pulse-modulated signal is the reduced number of sidelobes. This is due to the absence of nulls between pulses of the signal. Unfortunately, this type of signal is not popular in the market. The windowed signal (linear frequency sweep) is shown in Fig. 3.22 and the spectrum is given in Fig. 3.23.

In the next section, a non-linear spectral estimation method is employed to compare the spectral performances with the Fast Fourier Transform technique which is a linear operation.

### 3.3 PROCESSING RESULTS USING THE MAXIMUM ENTROPY SPECTRAL ANALYSIS

We mentioned, in Chapter 2, that spectral estimation employing the Maximum Entropy Method yields superior resolution. Four configurations are chosen to explore the spectral performance of the MEM technique. First, we operate the MEM analysis directly on a received ELT signal. This is represented by 'ELT + MEM'. Second, we perform an  $N/2$  - lag autocorrelation function of the signal prior to the MEM (ELT + ACFMEM). Third, the signal is passed through a finite impulse response bandpass filter (shown in Fig. 2.8) and the MEM is applied (ELT + FIRMEM). Lastly, we process the ACF of the signal to this filter before doing the MEM (ELT + ACF + FIRMEM). Since the autocorrelation function and the convolution are linear processes, interchanging the operation of these two preprocessors does not bring any significant differences.

One problem to be solved in evaluating a reasonable MEM spectrum is to determine an optimum number of prediction error filter coefficients. This number corresponds to the filter order of the MEM.

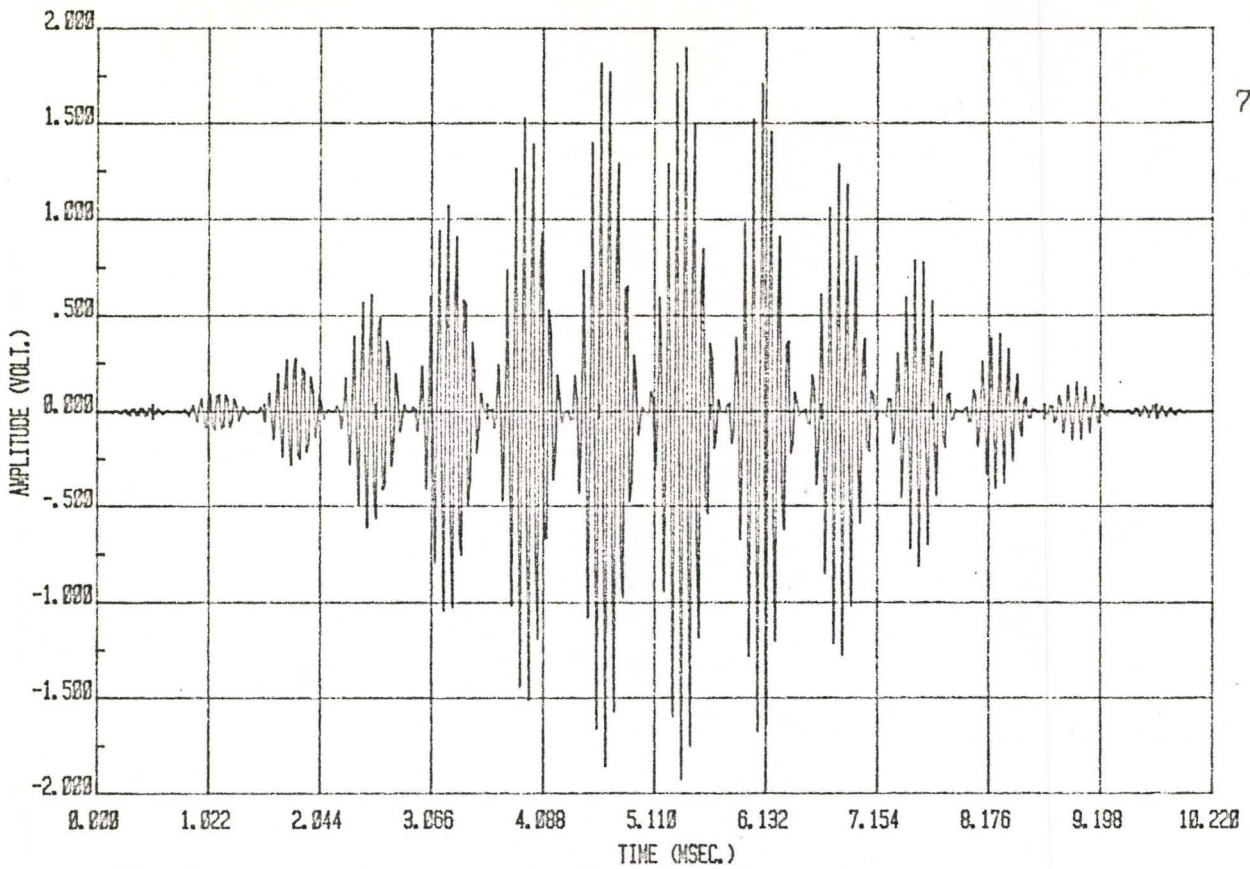


Fig. 3.22: The signal shown in Fig. 3.19 windowed by a Kaiser window ( $\beta=8.0$ ).

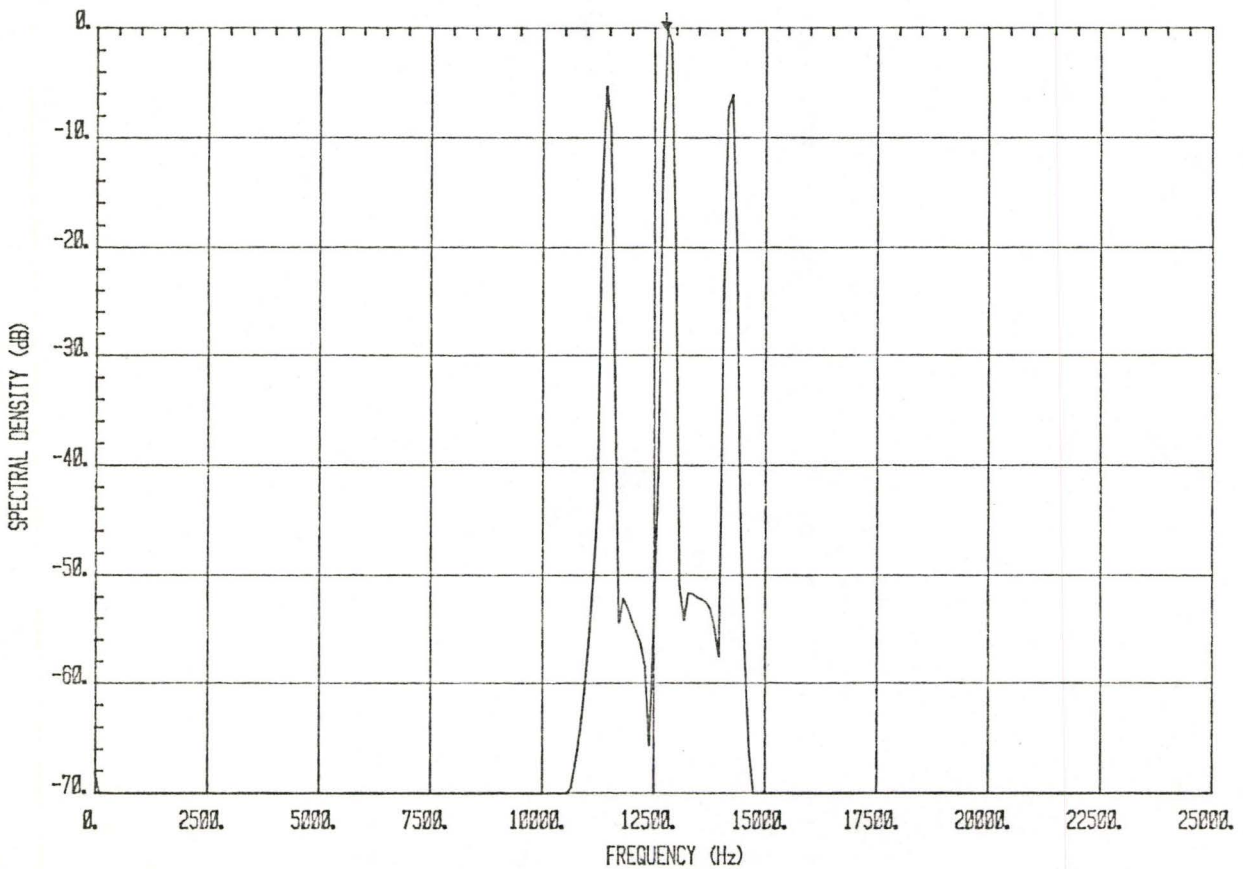


Fig. 3.23: The FFT spectrum of the signal shown in Fig. 3.22.

Three different objective criteria are suggested for selecting the filter order,  $M$  [24]. These are the final prediction error criterion (FPE), the information theoretic criterion (AIC) and the autoregressive transfer function criterion (CAT). However, these criteria are based on the assumption that the input signal is an autoregressive process. Unfortunately, it does not apply to the ELT signal which we have modelled. In order to determine a most suitable MEM filter order, for each of the above configurations, we use different values of  $M$ .

### 3.3.1 Pulse-Modulated, Continuous Phase

The signal depicted in Fig. 3.1 is utilized to study the MEM spectral performances which are compared with the results obtained from the FFT technique. Filter orders of 2,3,4,6,8,10 and 20 are tested individually in the analysis. The four curves on each graph represent the MEM spectra of the different configurations described above.

Fig. 3.24 gives the MEM spectra at filter order 2. Results indicate that both the 'ELT + MEM' and the 'ELT + ACFMEM' lie at 12842 Hz. This is 10 Hz away from the carrier frequency. The 'ELT + FIRMEM' has a relatively broad peak at 12756 Hz. This introduces a displacement of 76 Hz. According to Eq. (3.6), a frequency error of only 2 Hz is measured by the 'ELT + ACF + FIRMEM' (peak at 12830 Hz). The most noticeable feature is the sharpening of the spectra when the ACF is employed. A third order MEM is applied to the same signal, the MEM, ACFMEM and ACF + FIRMEM processes all have resolutions located at the same frequencies as MEM order 2. This is shown in Fig. 3.25. In the 'ELT + FIRMEM' case, the error is reduced to 39 Hz. Comparing these

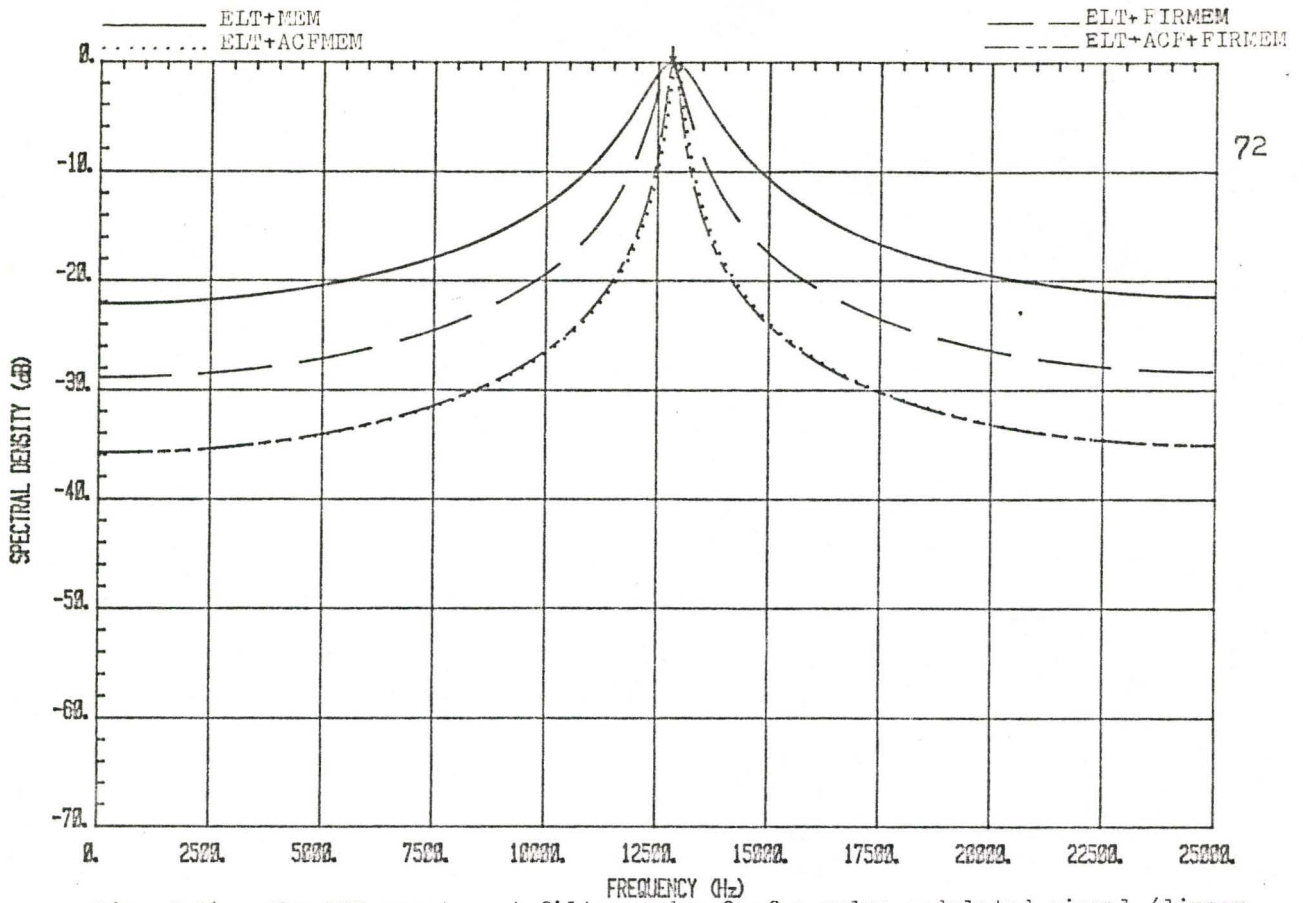


Fig. 3.24: The MEM spectra at filter order 2 of a pulse-modulated signal (linear frequency sweep, continuous phase and 36% duty cycle). Carrier frequency is 12832 Hz.

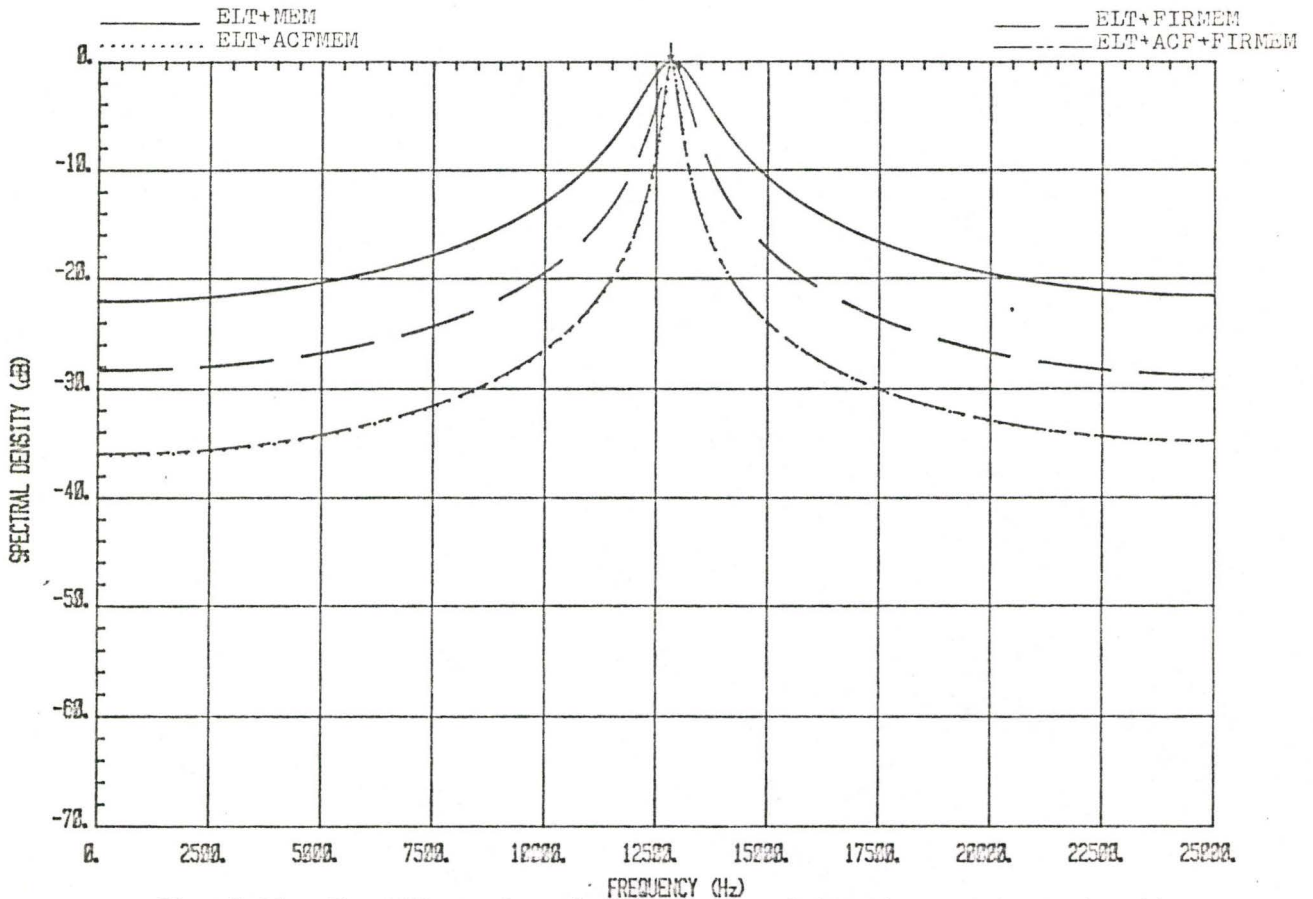


Fig. 3.25: The MEM spectra at filter order 3 (continuous phase signal).

two diagrams with Fig. 3.2 and Fig. 3.5, we observe a remarkable difference. The sidelobe problem does not exist in the second and third order MEM.

We now attempt to use higher MEM filter orders in order to investigate how the MEM spectra evolves. Fig. 3.26 to 3.28 show that only the 'ELT + MEM' configuration yields reasonable resolution when filter orders of 4, 6 and 8 are used. For a tenth order MEM, the spectra are shown in Fig. 3.29. The 'ELT + MEM' and the 'ELT + ACFMEM' give poor resolution. Although the 'ELT + FIRMEM' has discernible peaks, it has an error of more than 200 Hz. The main peak of 'ELT + ACF + FIRMEM' is located at 12830 Hz. This corresponds to an error of 2 Hz. The major sidelobes are at -4 dB level. The spectra of a filter of order 20 are illustrated in Fig. 3.30. A direct application of MEM analysis gives a very wide peak at 12891 Hz. This is a difference of 59 Hz from the carrier frequency. The signal with preprocessor functions, at this filter order, gives good results. In the 'ELT + ACFMEM' cases, it has an error of 39 Hz. Both the 'ELT + FIRMEM' and the 'ELT + ACF + FIRMEM' indicate a peak at 12830 Hz for an error of 2 Hz. The major sidelobes for the latter case are at -3 dB and -6 dB levels. Results are also obtained for the same signal with quadratic frequency sweep. These are shown in Fig. 3.31 (filter order 2) and Fig. 3.32 (filter order 10).

From the above results, we need to elaborate four critical points. First, the choice of the MEM filter order does have an influence on the spectral performances. At a low filter order of the

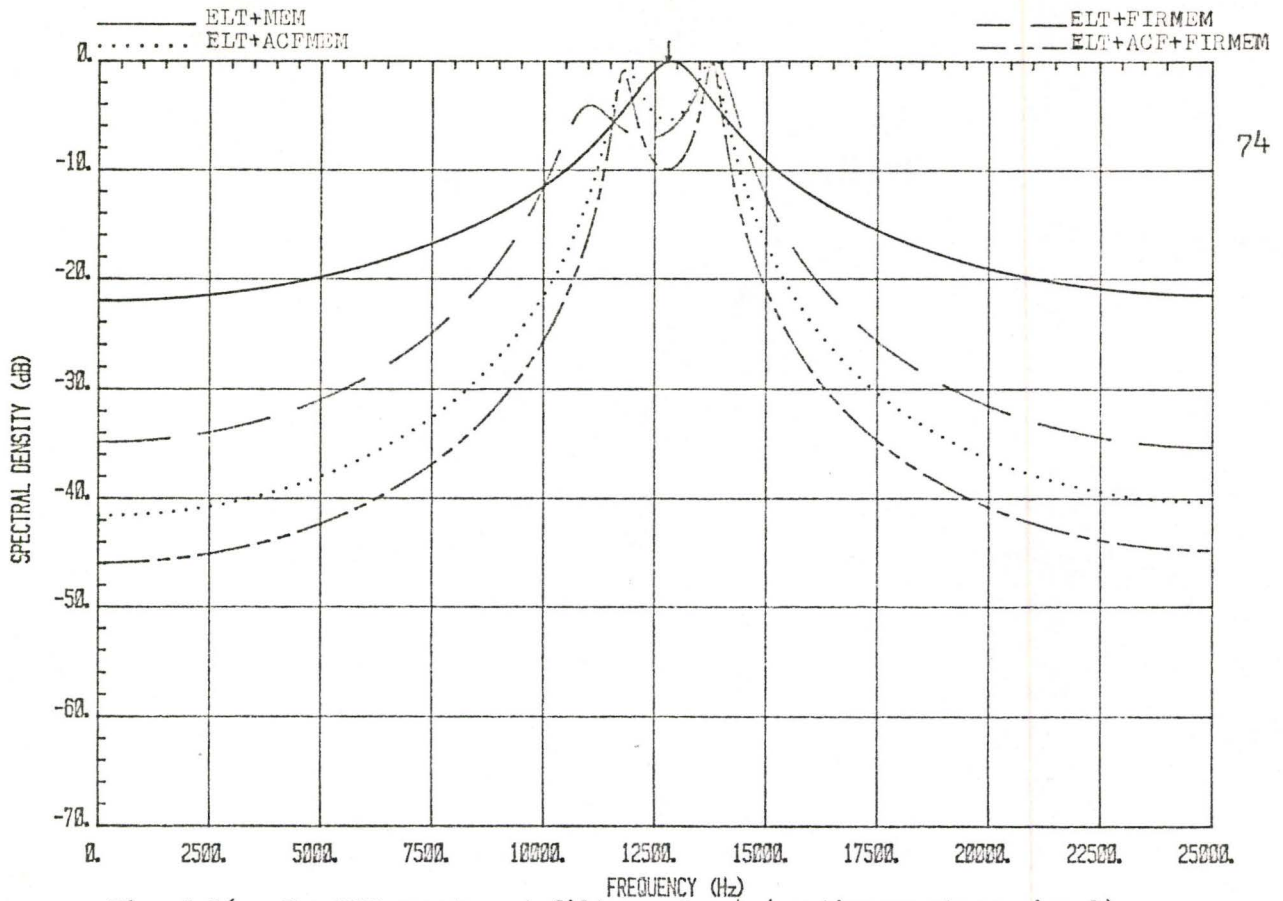


Fig. 3.26: The MEM spectra at filter order 4 (continuous phase signal).

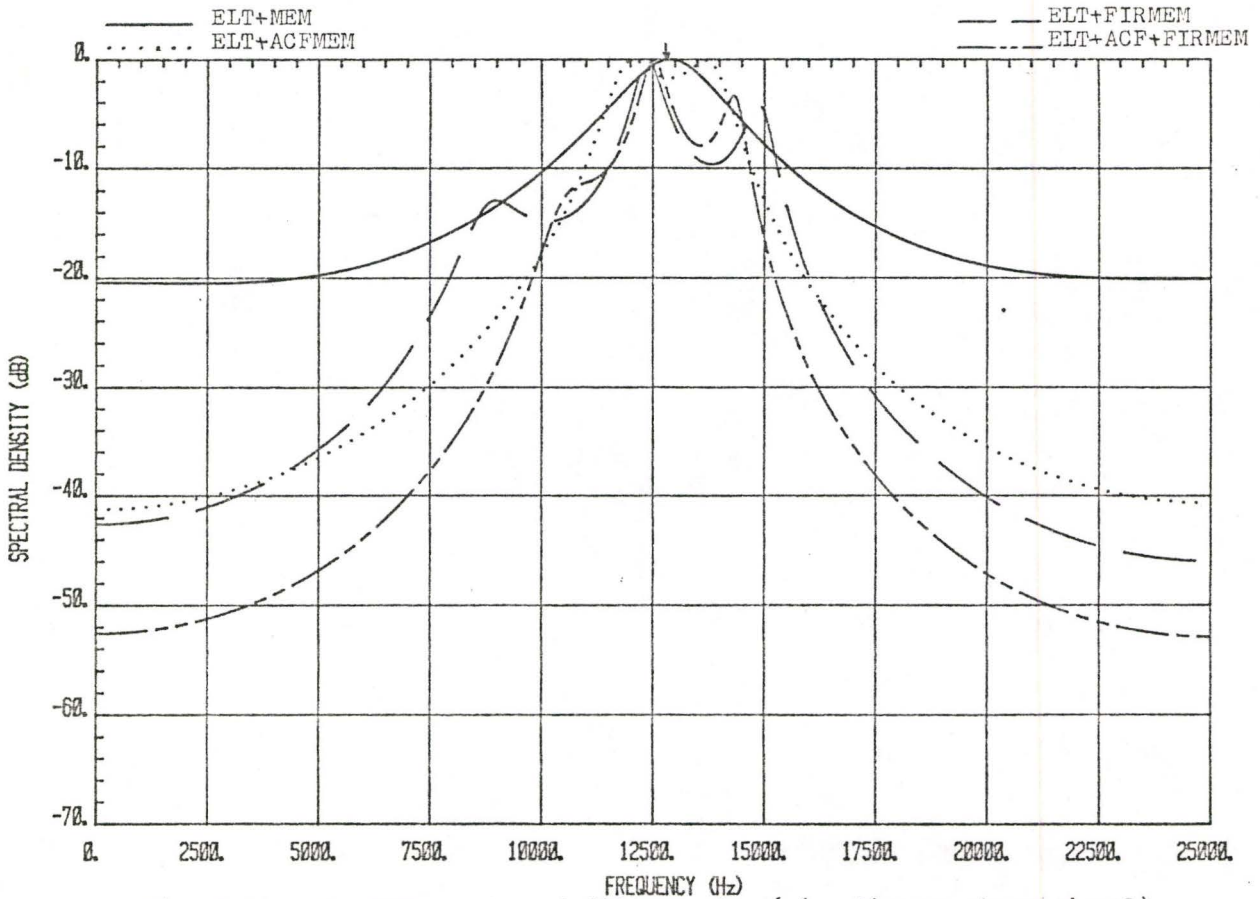
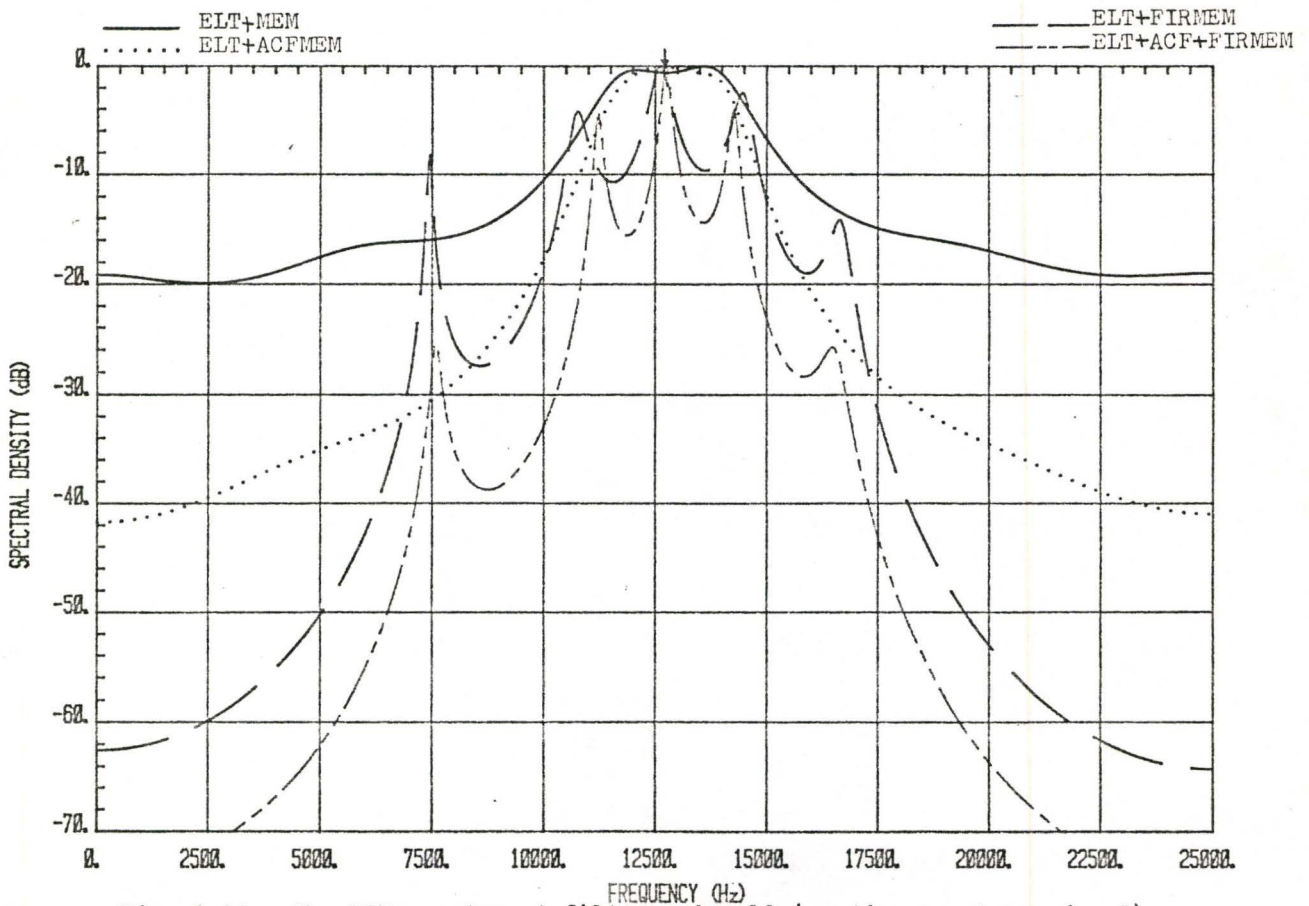
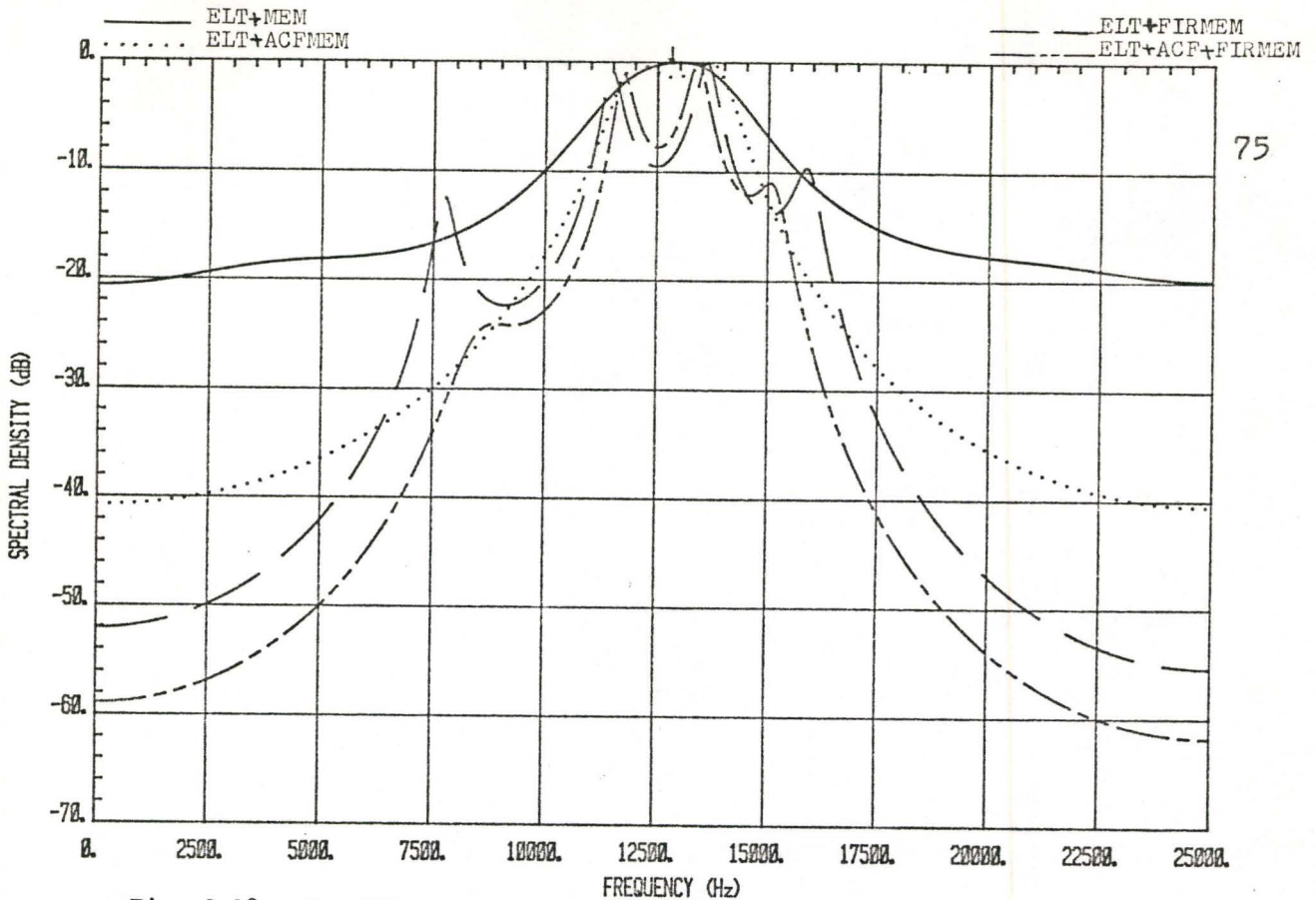


Fig. 3.27: The MEM spectra at filter order 6 (continuous phase signal).



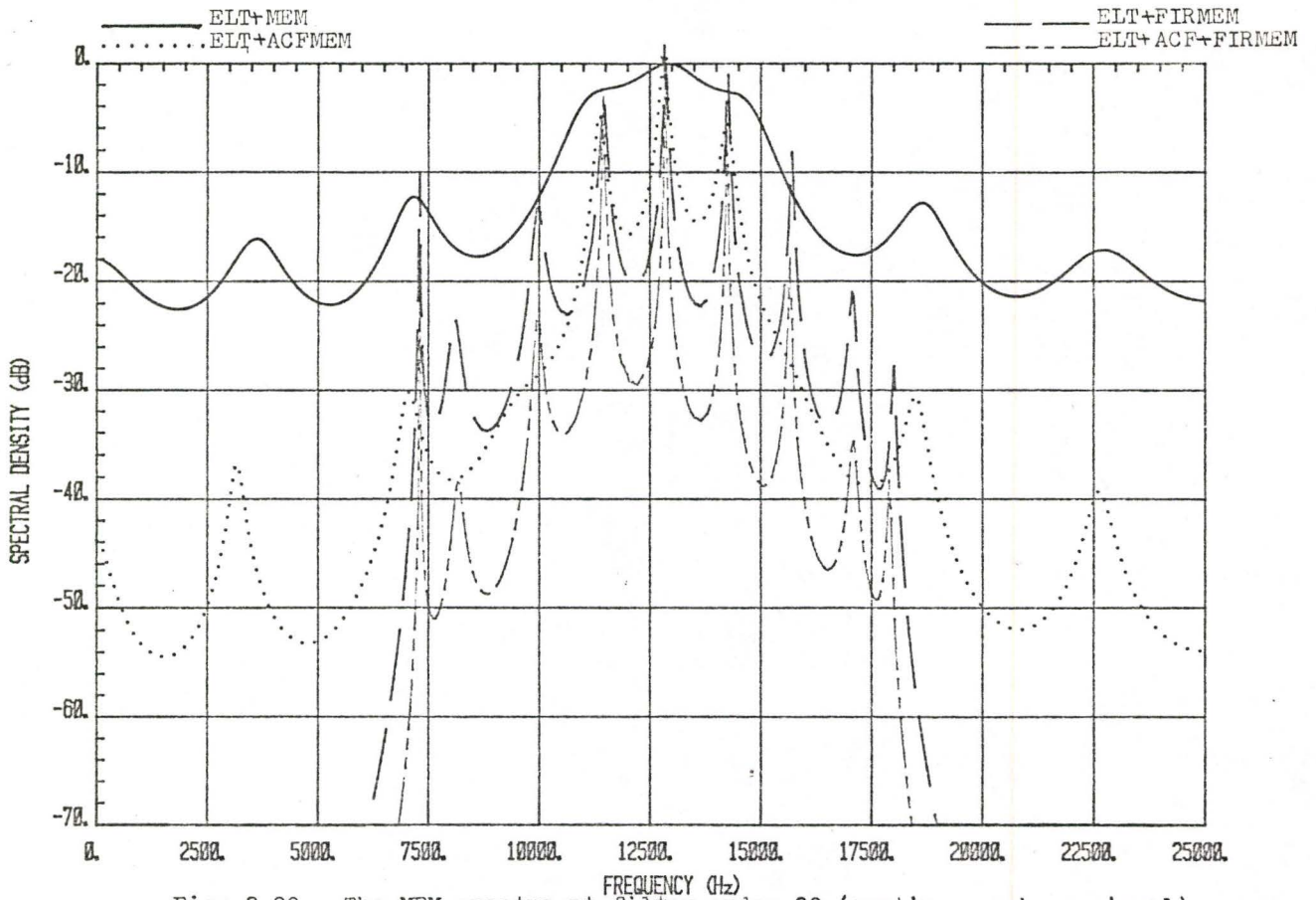


Fig. 3.30: The MEM spectra at filter order 20 (continuous phase signal).

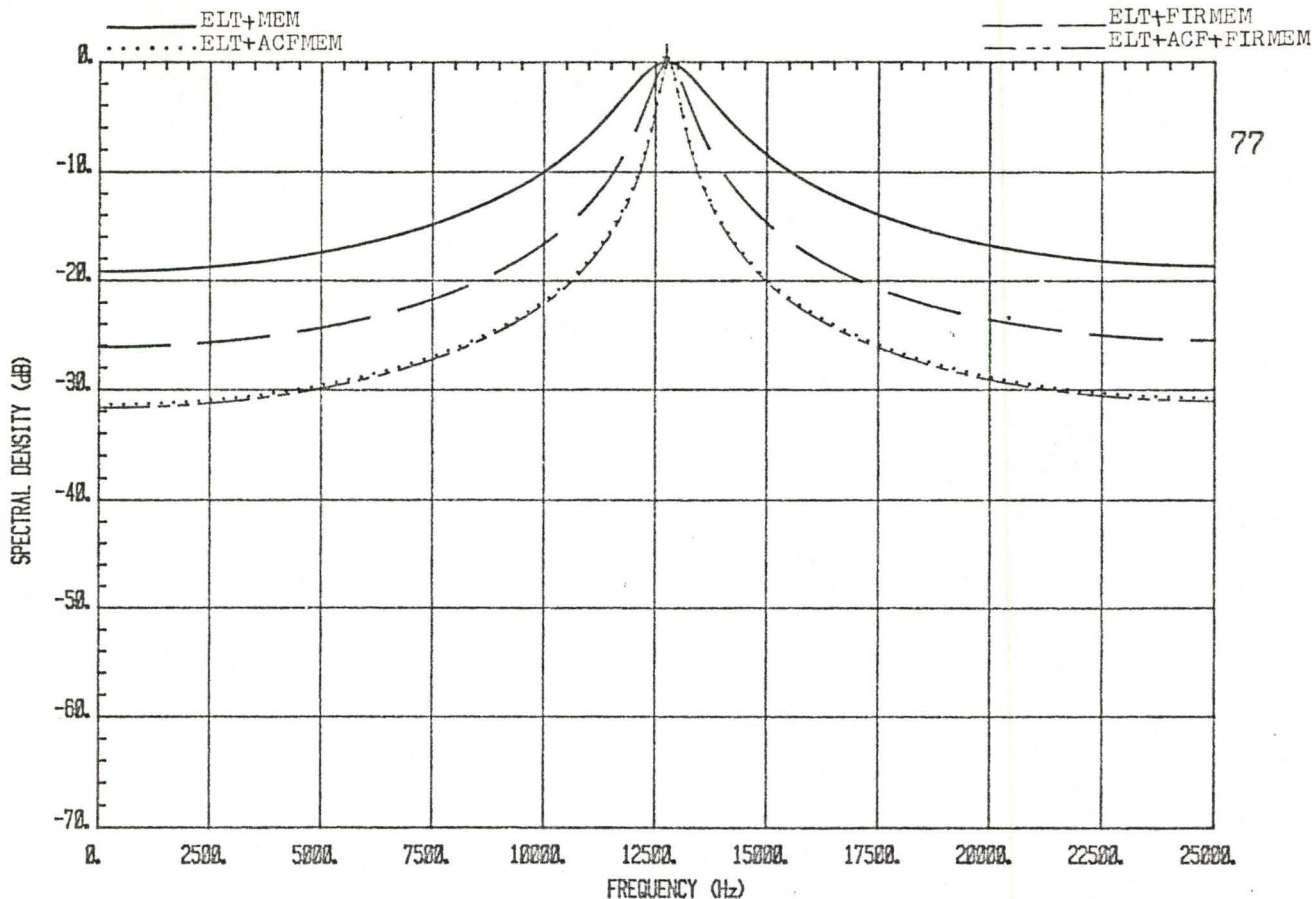


Fig. 3.31: The MEM spectra at filter order 2 of the signal described in Fig. 3.24 with quadratic frequency sweep.

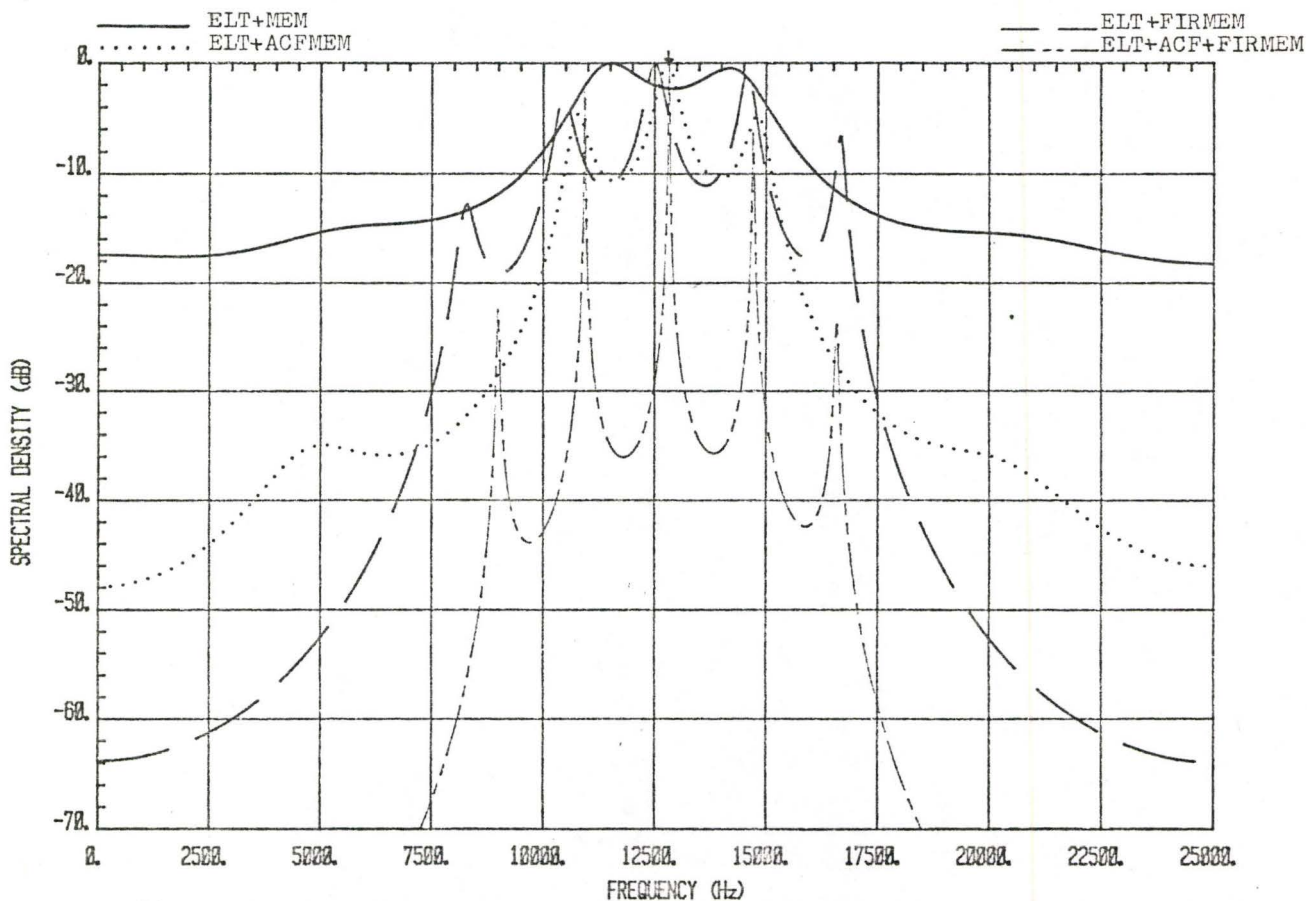


Fig. 3.32: The MEM spectra at filter order 10 of the signal described in Fig. 3.31.

MEM, we can avoid the sidelobe problem. By using a higher filter order, the width of the main peak can be reduced considerably (by the 'ELT + ACF + FIRMEM') but at the expense of giving rise to spurious peaks. However, these interferences are less severe than the FFT spectra. Second, the merit of employing autocorrelation function as a preprocessor is that it averages the information of the received signal over a large interval. As a result, it reduces the duration of nulls between pulses in the pulse-modulated signal [8]. This benefits the adaptive feature of the MEM spectral estimation. Third, digital filtering helps to improve the performances by rejecting unnecessary information outside the filter bandwidth. Fourth, in examining the curves of Fig. 3.24 to Fig. 3.28, we note that the curve depicting the MEM process indicates only one peak even though the order is increased from 2 to 8. This is a valuable indicator of how many signals are present and this result will be further exploited in Section 4, which deals with multiple signals.

### 3.3.2 Pulse-Modulated, Random Phase

We proceed with our discussion to a pulse-modulated random phase signal (Fig. 3.13). The MEM spectra at filter orders 2 and 3 are plotted in Fig. 3.33 and Fig. 3.34. In both diagrams, the 'ELT + MEM' and the 'ELT + ACFMEM' have identical resolution at 12842 Hz. Whereas, the configurations with digital filtering are found to peak at 12793 Hz. The frequency error is calculated to be -10 Hz and 39 Hz respectively. In this case, digital filtering does not offer any advantages. Nevertheless, these results contrast greatly with the FFT spectra which

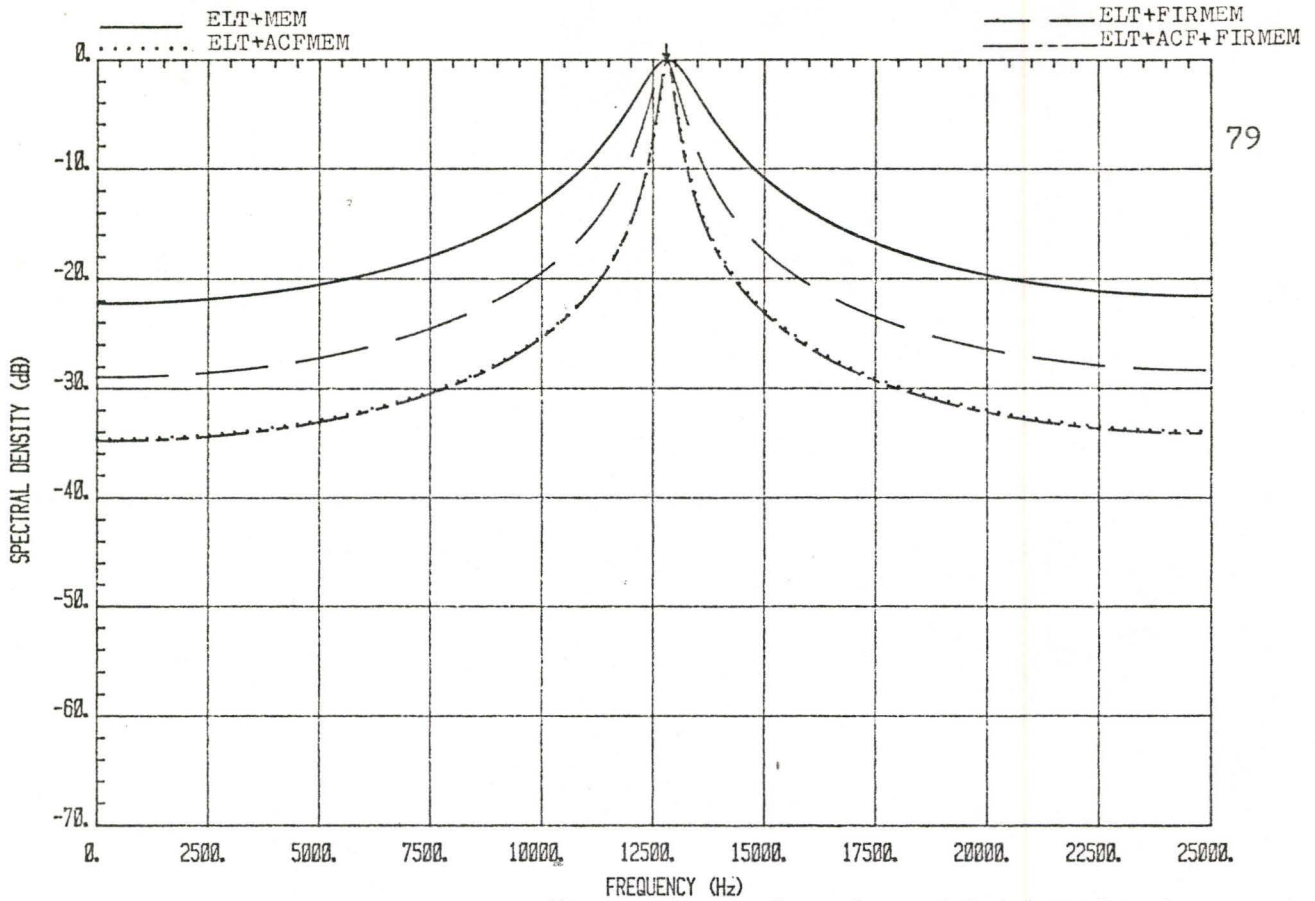


Fig. 3.33: The MEM spectra at filter order 2 of a pulse-modulated random phase ELT signal (linear frequency sweep and 36% duty cycle). Carrier frequency is 12832 Hz.

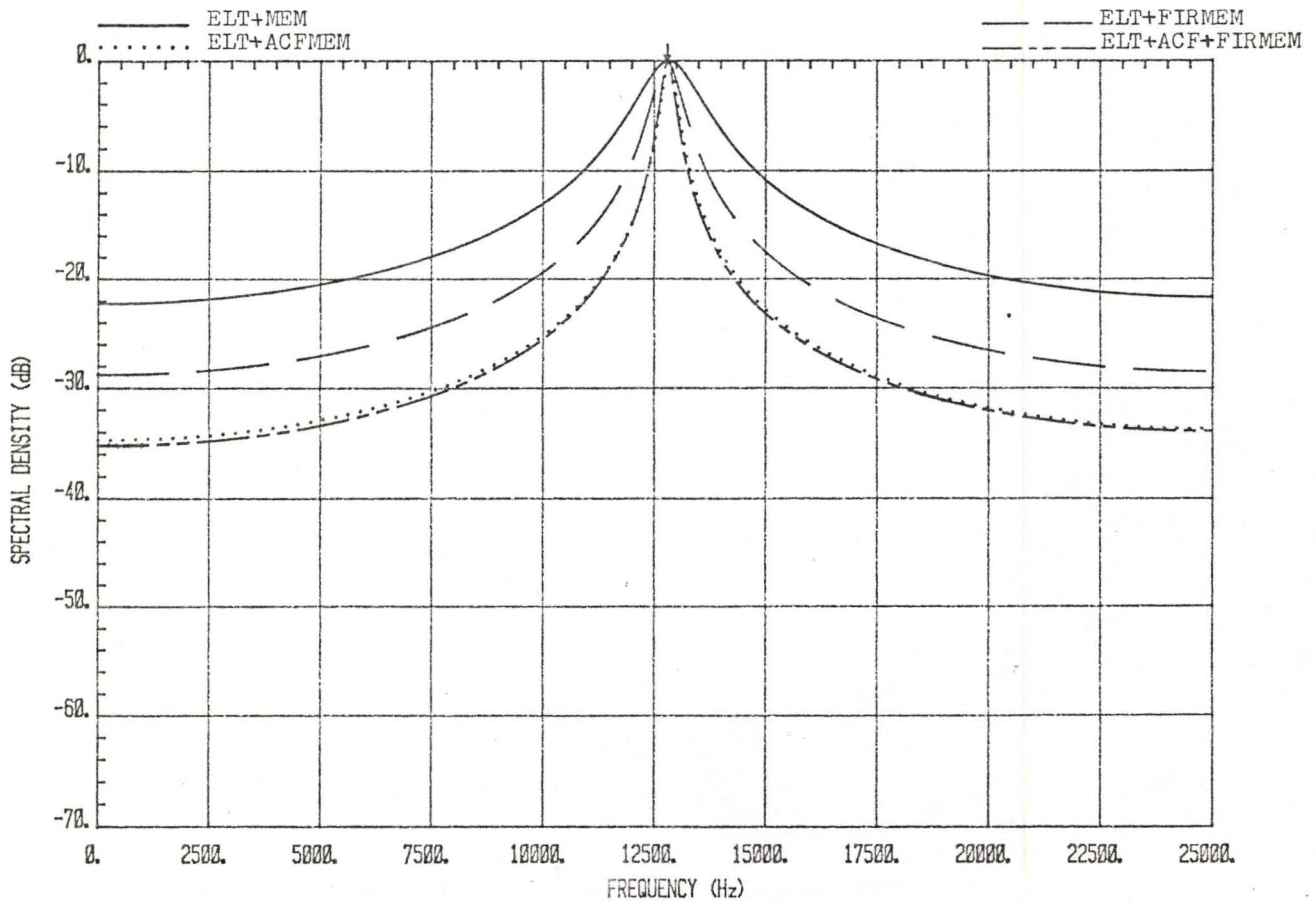


Fig. 3.34: The MEM spectra at filter order 3 of the signal described in Fig. 3.33.

were shown in Fig. 3.14 and 3.17. Phase randomization using the MEM technique achieves better resolution than the FFT approach. Detection is possible only for the 'ELT + MEM' configuration as the filter orders are raised to 4,6 and 8. These are illustrated in Fig. 3.35 to 3.37. At a filter order of 10, Fig. 3.38 indicates that only the preprocessor with digital filtering is capable of giving accurate resolution. The main peaks are relatively wider than those in Fig. 3.29. The 'ELT + FIRMEM' has a peak at 12683 Hz which is 149 Hz in error. The frequency resolution of 'ELT + ACF + FIRMEM' is 12720 Hz. This is 112 Hz less than the carrier frequency. Fig. 3.39 is the spectra of a twentieth order MEM. The resolutions for both digital filtering configurations are shifted by 255 Hz from the carrier frequency. Therefore, a low filter order of the MEM is preferred to combat the pulse-modulated random phase ELT signal. Note that once again, the peak structure of the MEM spectra gives an indication of the number of signals present.

We recall that processing the ELT signal on a per block basis enhances the frequency resolution. In Appendix E we examine this technique by using a modified Maximum Entropy Method which is based on averaging the prediction error power and prediction error filter coefficients.

### 3.3.3 Sinusoidal-Modulation

At filter orders of 2 and 3, the MEM spectra of a sinusoidal-modulated signal shown in Fig. 3.19 gives excellent results. These are illustrated in Fig. 3.40 and Fig. 3.41. The 'ELT + MEM' and the 'ELT + FIRMEM' appear to have the same resolution, but the former lies at

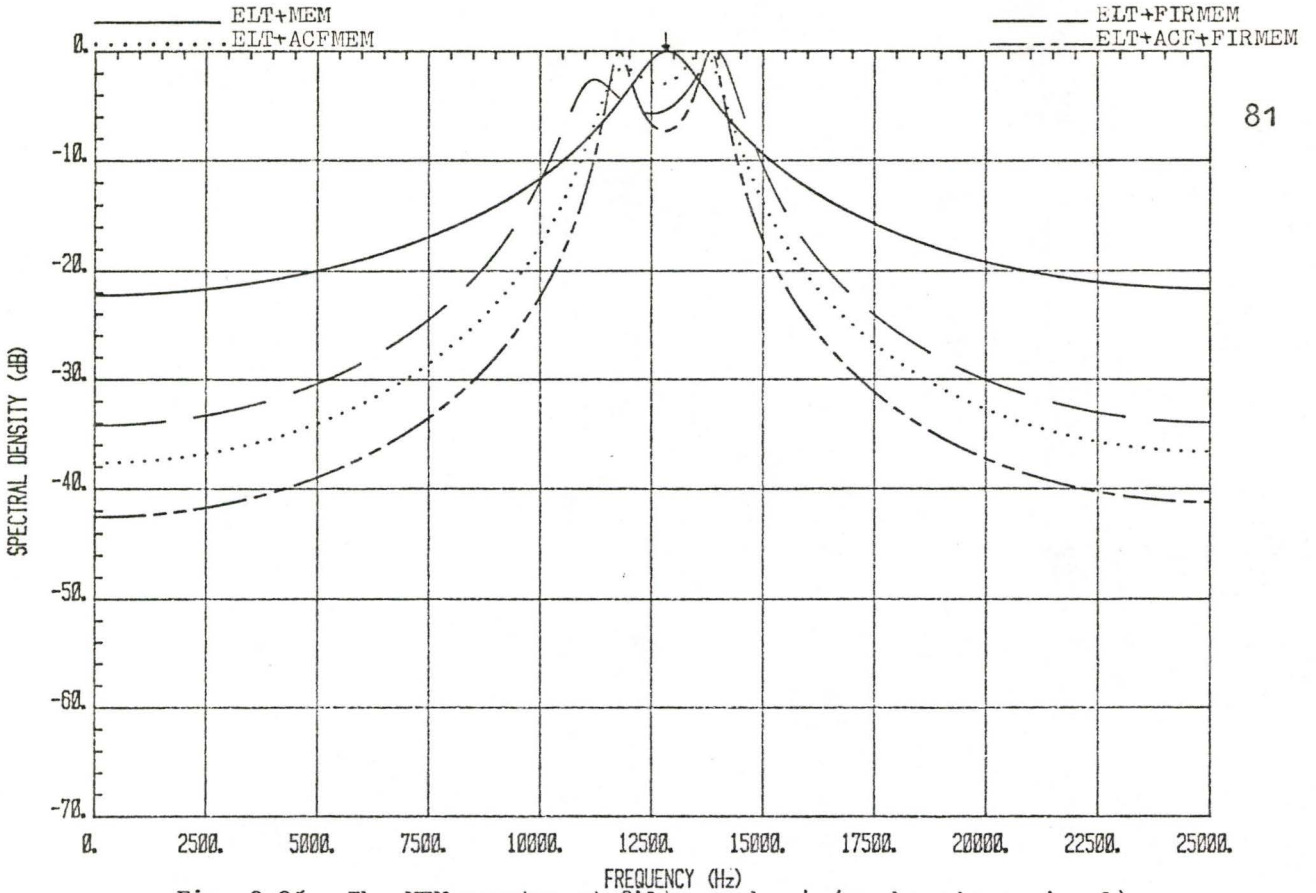


Fig. 3.35: The MEM spectra at filter order 4 (random phase signal).

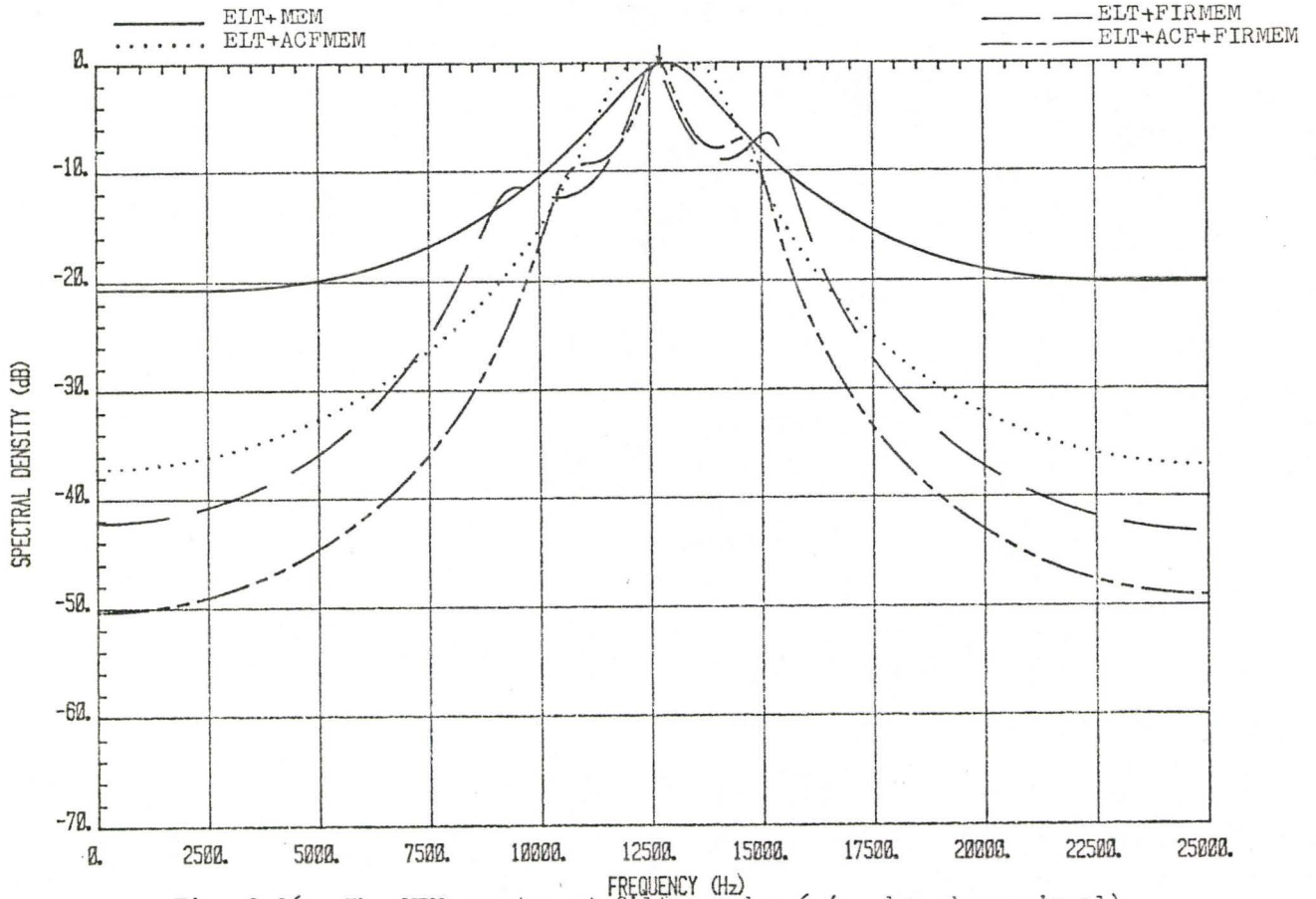


Fig. 3.36: The MEM spectra at filter order 6 (random phase signal).

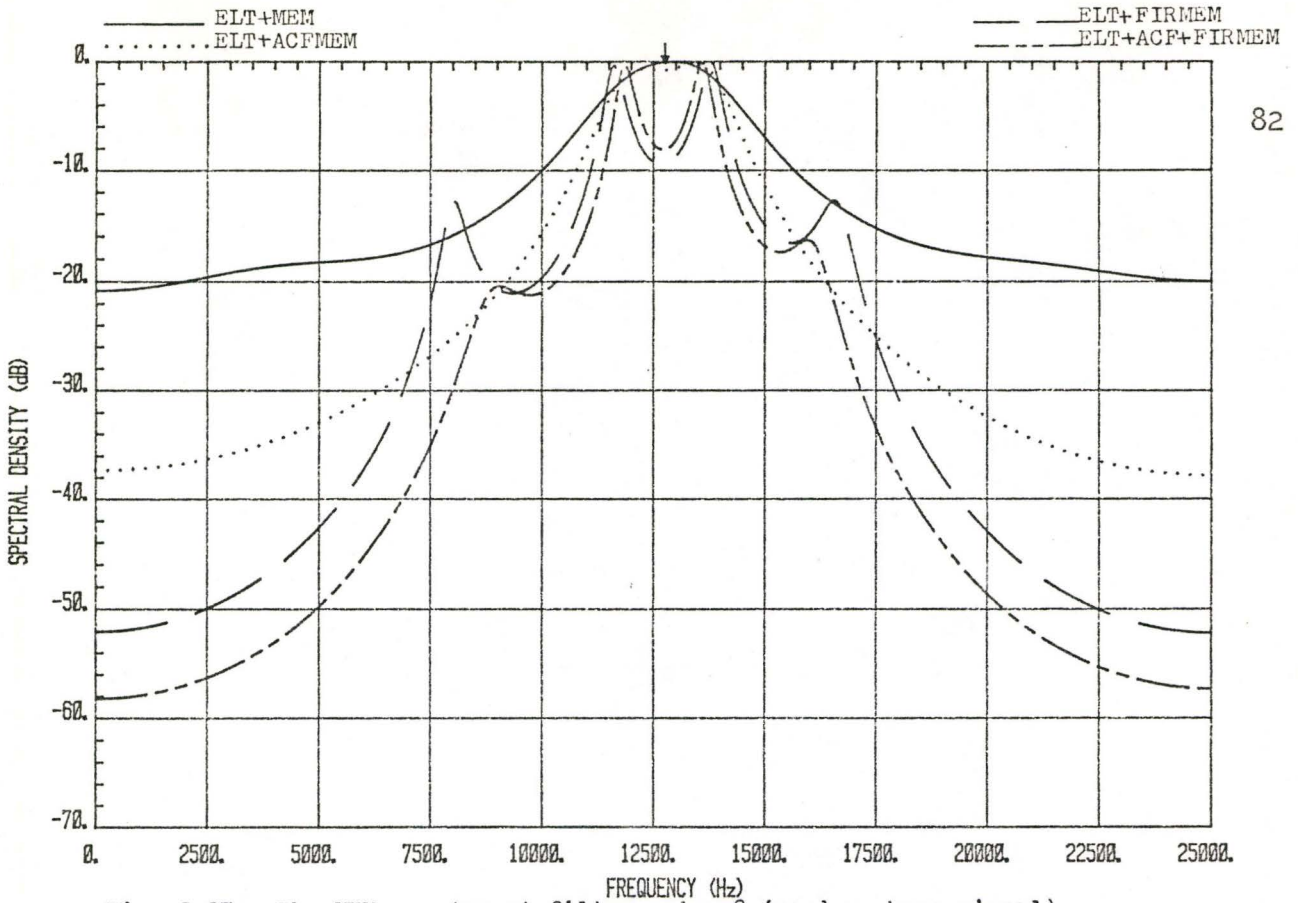


Fig. 3.37: The MEM spectra at filter order 8 (random phase signal).

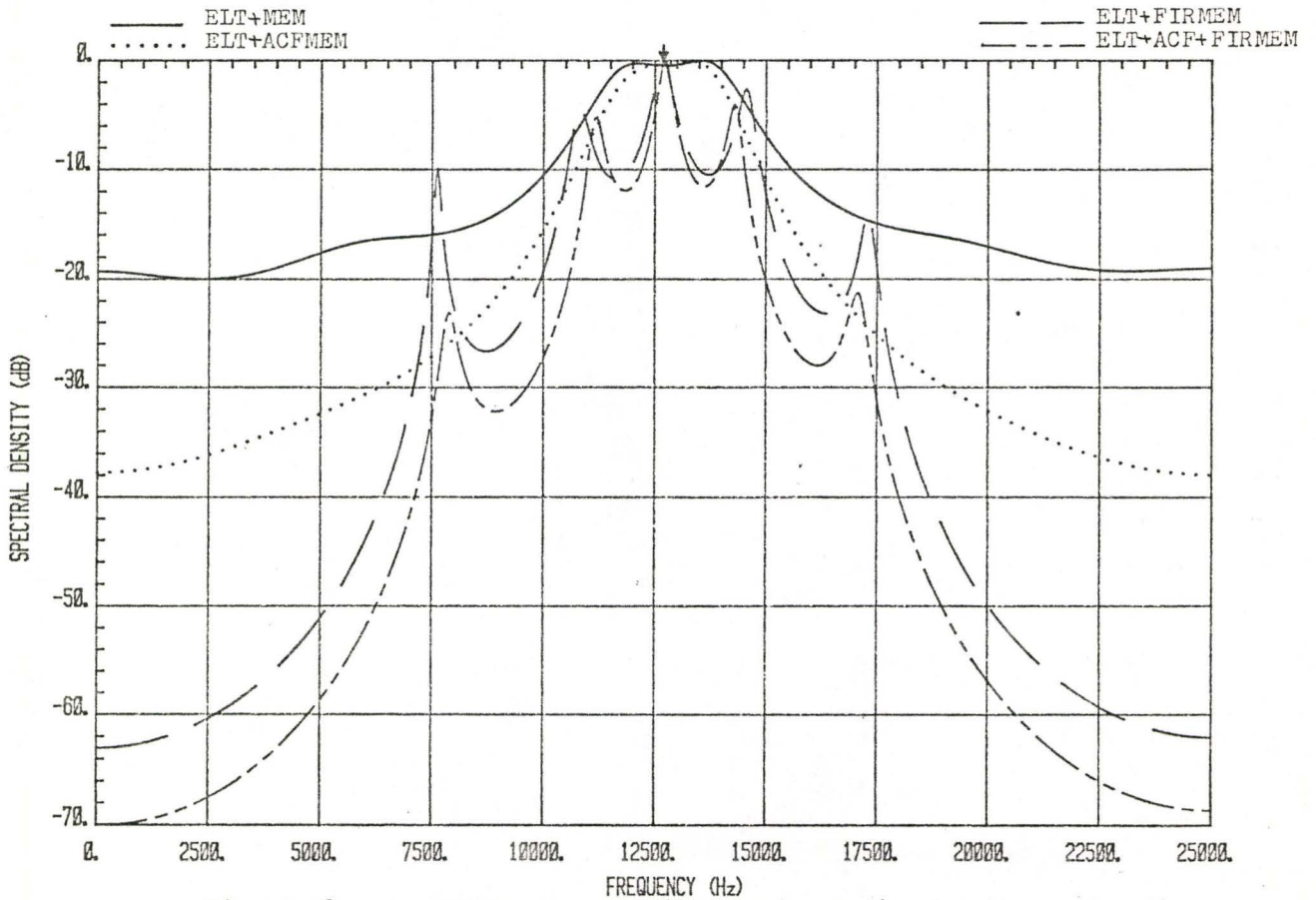


Fig. 3.38: The MEM spectra at filter order 10 (random phase signal).

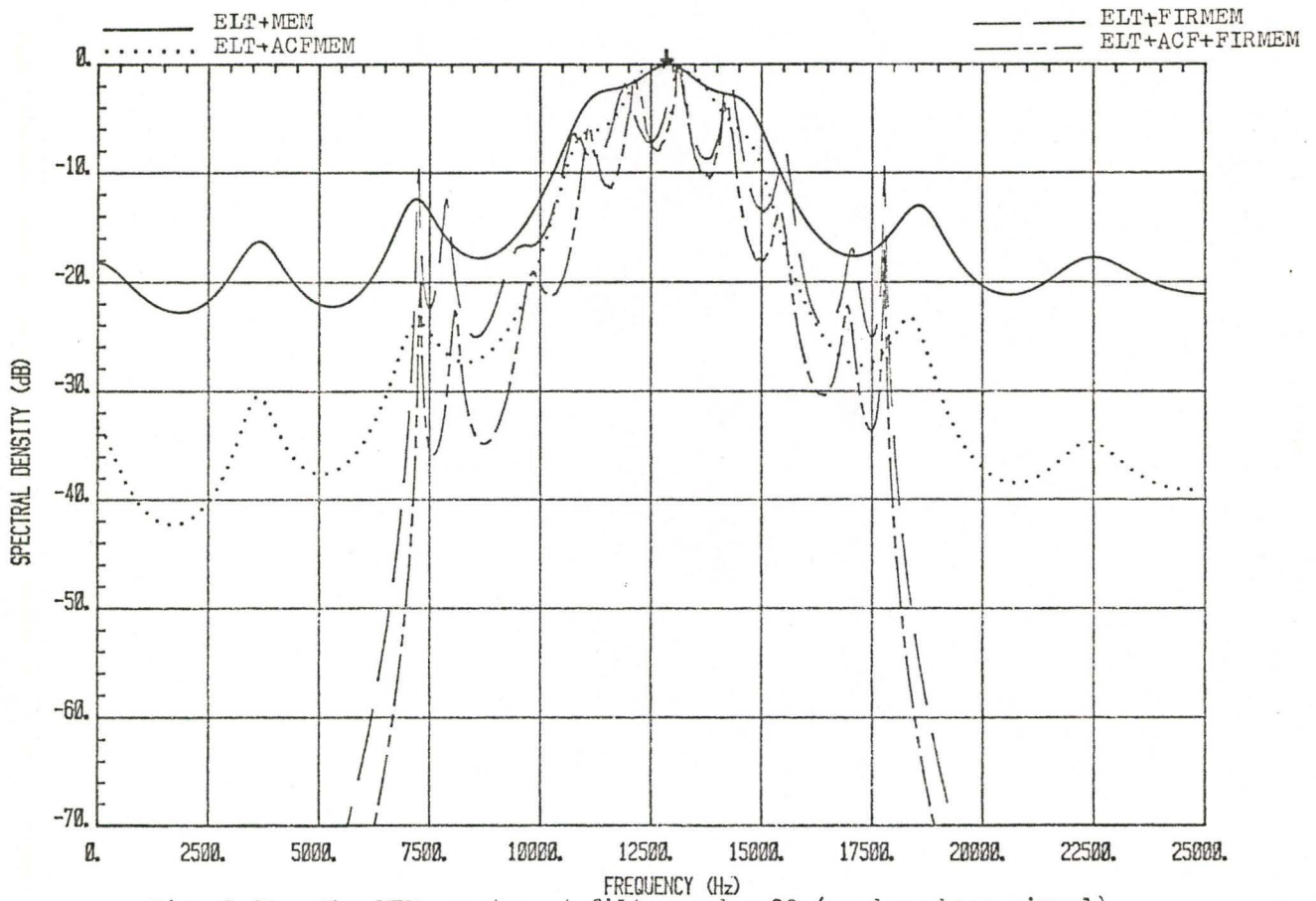


Fig. 3.39: The MEM spectra at filter order 20 (random phase signal).

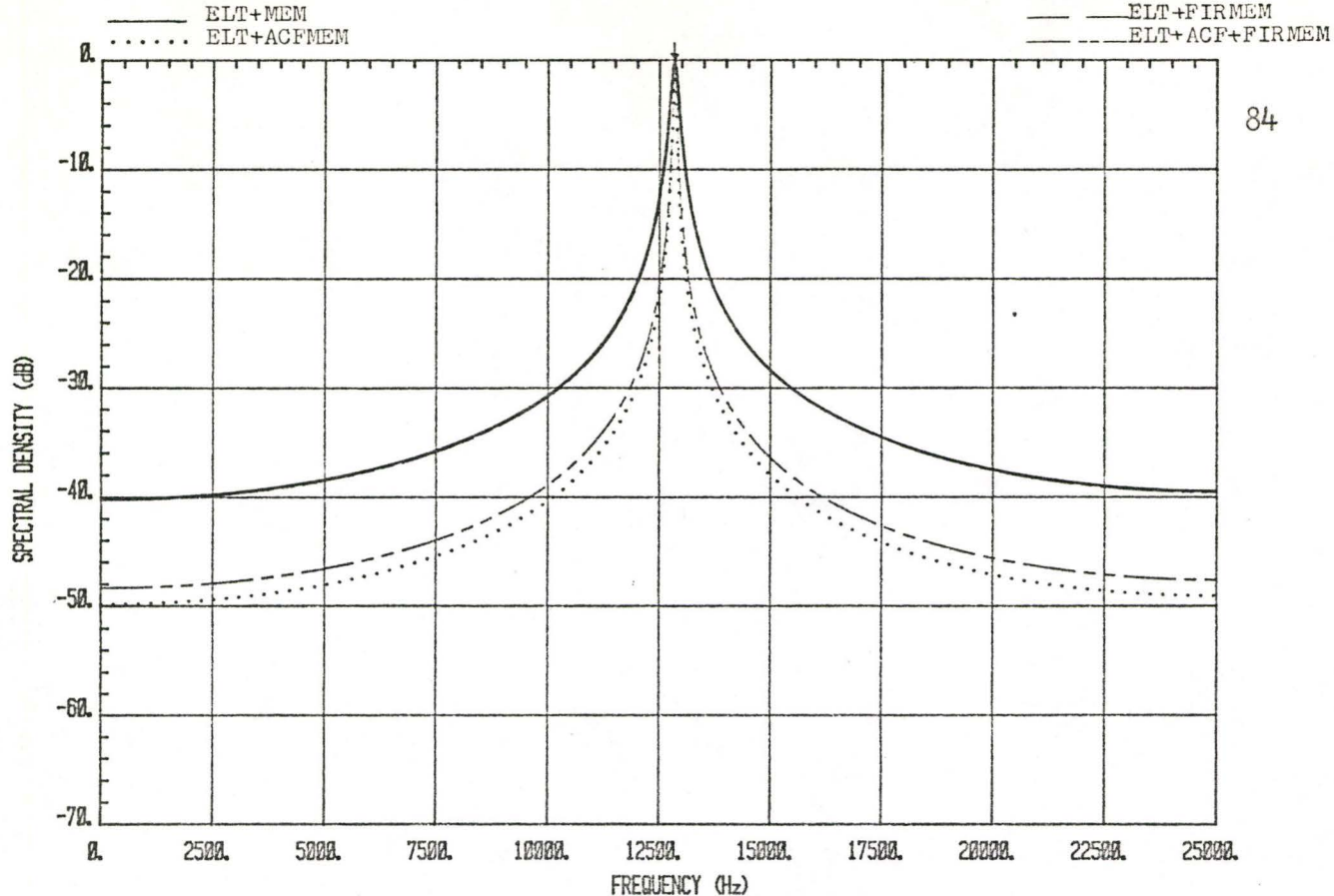


Fig. 3.40: The MEM spectra at filter order 2 of a sinusoidal-modulated signal with linear frequency sweep. Carrier frequency is 12832 Hz.

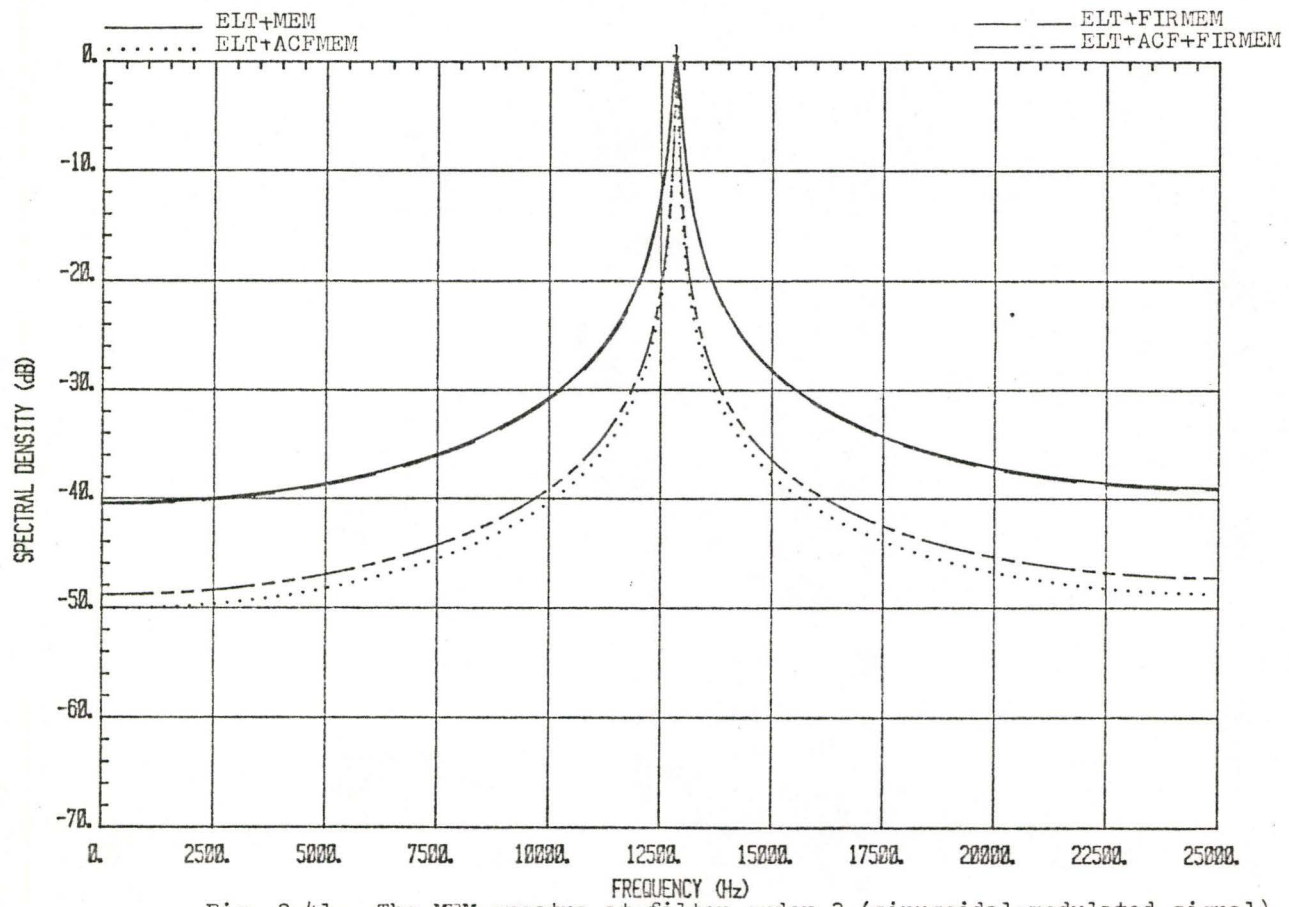


Fig. 3.41: The MEM spectra at filter order 3 (sinusoidal-modulated signal).

12842 Hz and the latter is at 12830 Hz. The sharp distinct peaks given by the 'ELT + ACFMEM' and the 'ELT + ACF + FIRMEM' are located at 12842 Hz and 12830 Hz respectively. Figure 3.42 is the spectra of a fourth order MEM. A direct MEM analysis can produce fine resolution (12842 Hz) at filter orders of 6, 8, 10 and 20. Fig. 3.43 to 3.46 depict these results. This signal does not create any difficulties for both spectral estimation techniques.

In processing a single ELT signal, preprocessing provided by the autocorrelation function and a low filter order of the MEM has an immense effect on the non-linear spectral analysis. It is in the next section that we explore the accuracy of frequency error which is measured by the MEM and the ACFMEM approaches at filter order 2.

### 3.4 ACCURACY OF FREQUENCY RESOLUTION FOR THE MAXIMUM ENTROPY METHOD

This section concentrates on investigating the accuracy of frequency resolution for the MEM spectral estimation. In this analysis, we are concerned with studying the behaviour of frequency resolution error generated by the MEM and the ACFMEM processors. We process ELT signals in 25 Hz steps starting at carrier frequencies of 25 Hz and proceed until 25 KHz is reached. The signal (512-point) is 10.22 ms in length. At each of these frequencies, the MEM and the ACFMEM spectra are evaluated at MEM filter order 2. The resolution errors are measured according to Eq. (3.6). The relationship of resolution error as a function of carrier frequency across the spectrum is plotted to identify the accuracy of the processors.

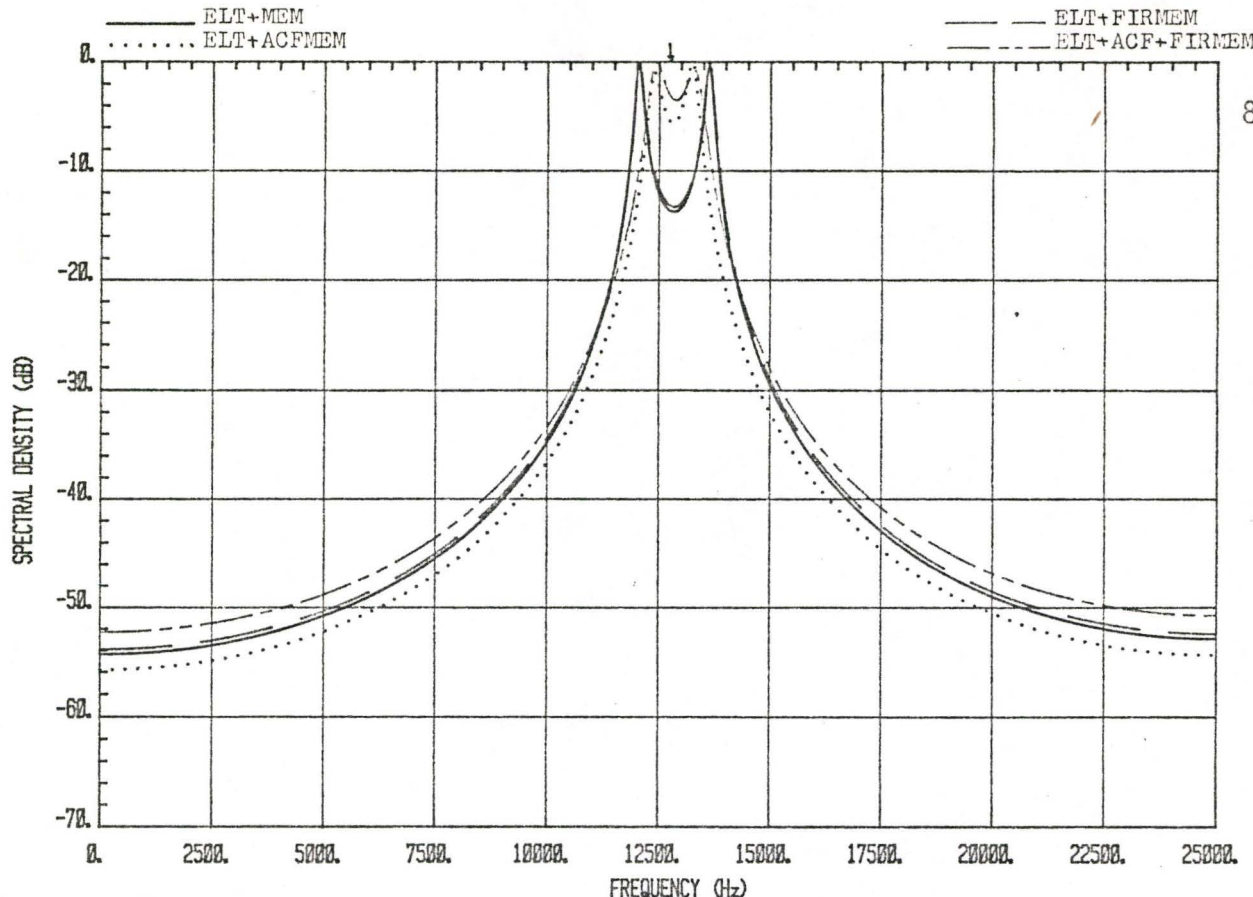


Fig. 3.42: The MEM spectra at filter order 4 (sinusoidal-modulated signal).

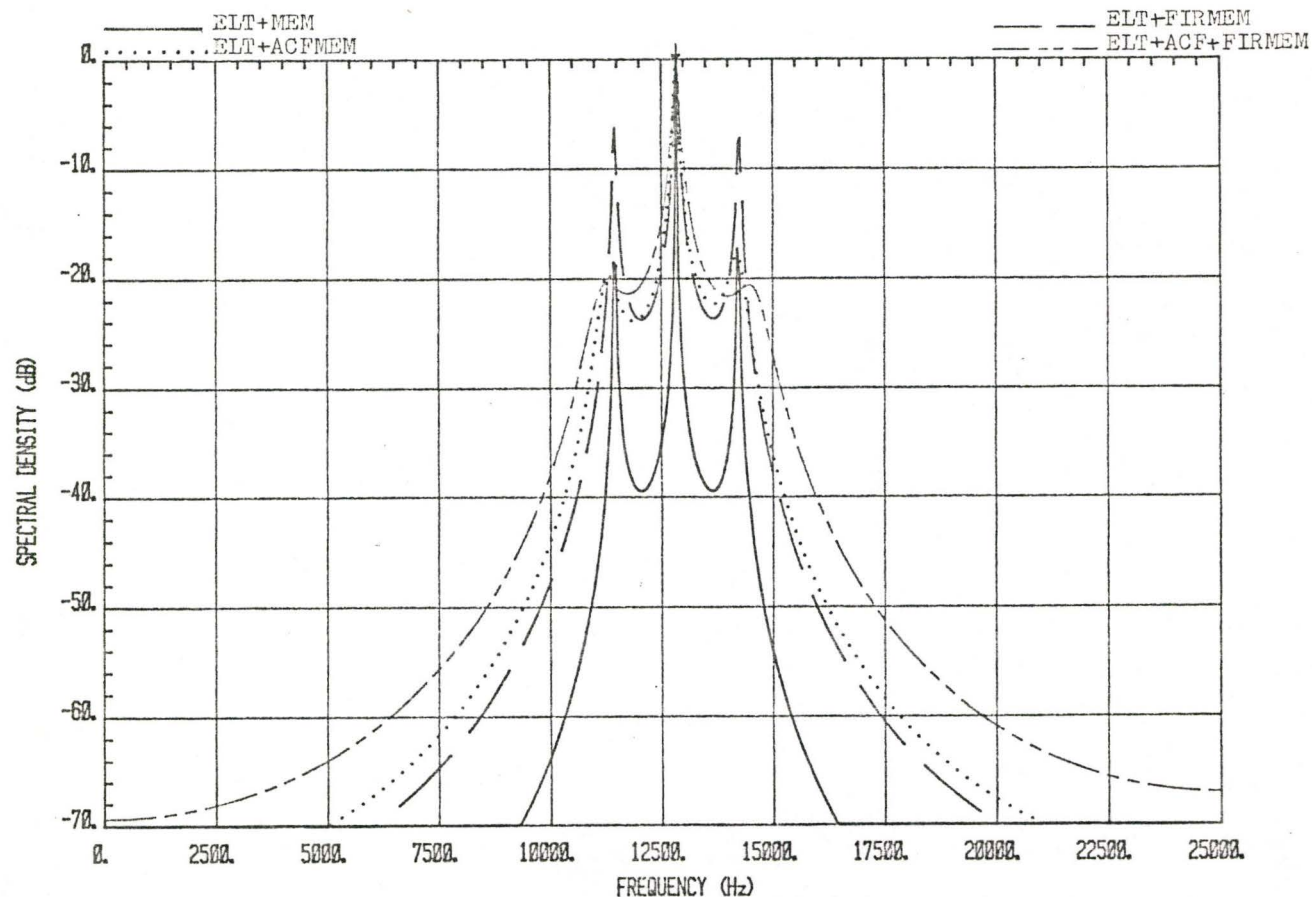


Fig. 3.43: The MEM spectra at filter order 6 (sinusoidal-modulated signal).

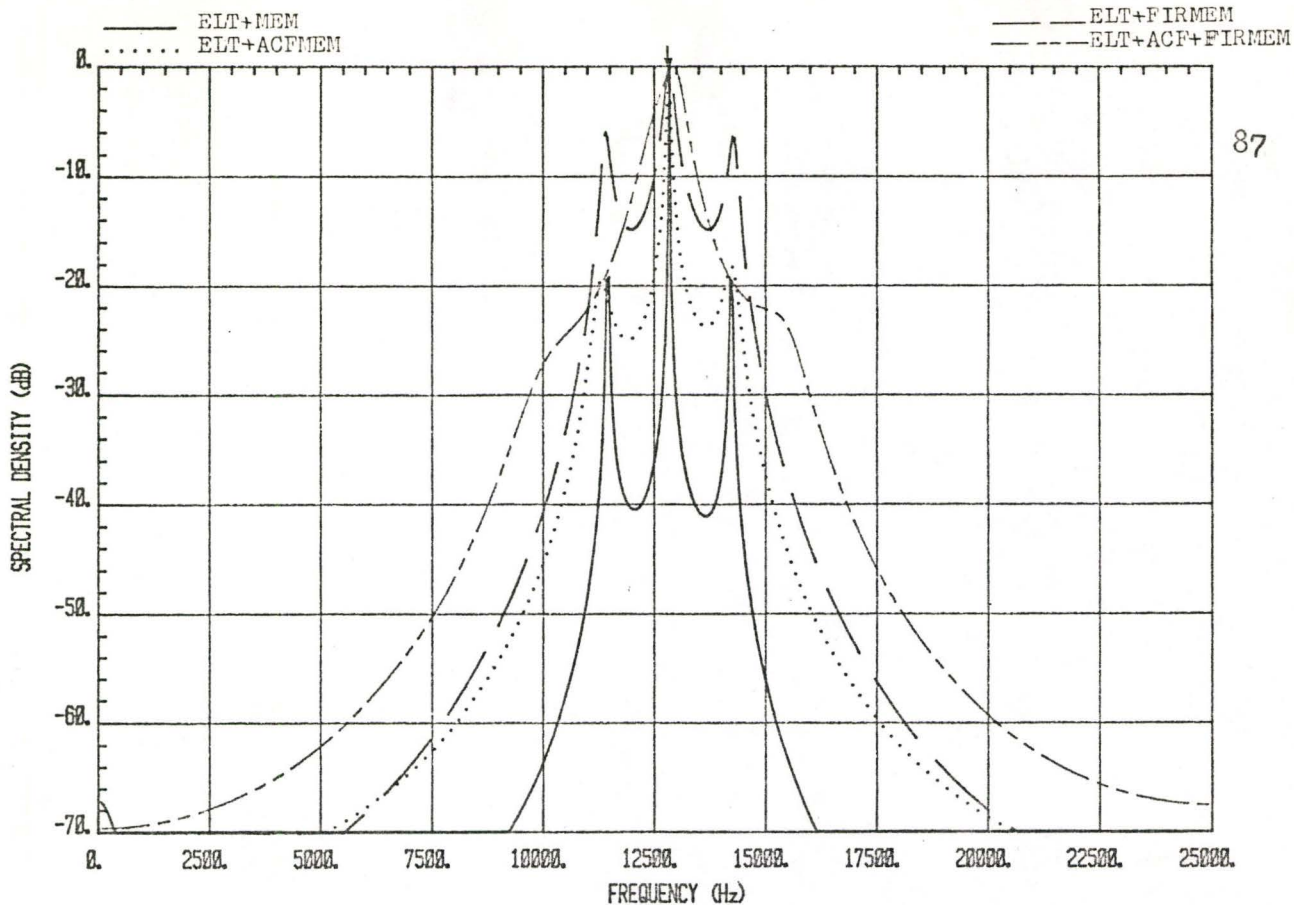


Fig. 3.44: The MEM spectra at filter order 8 (sinusoidal-modulated signal).

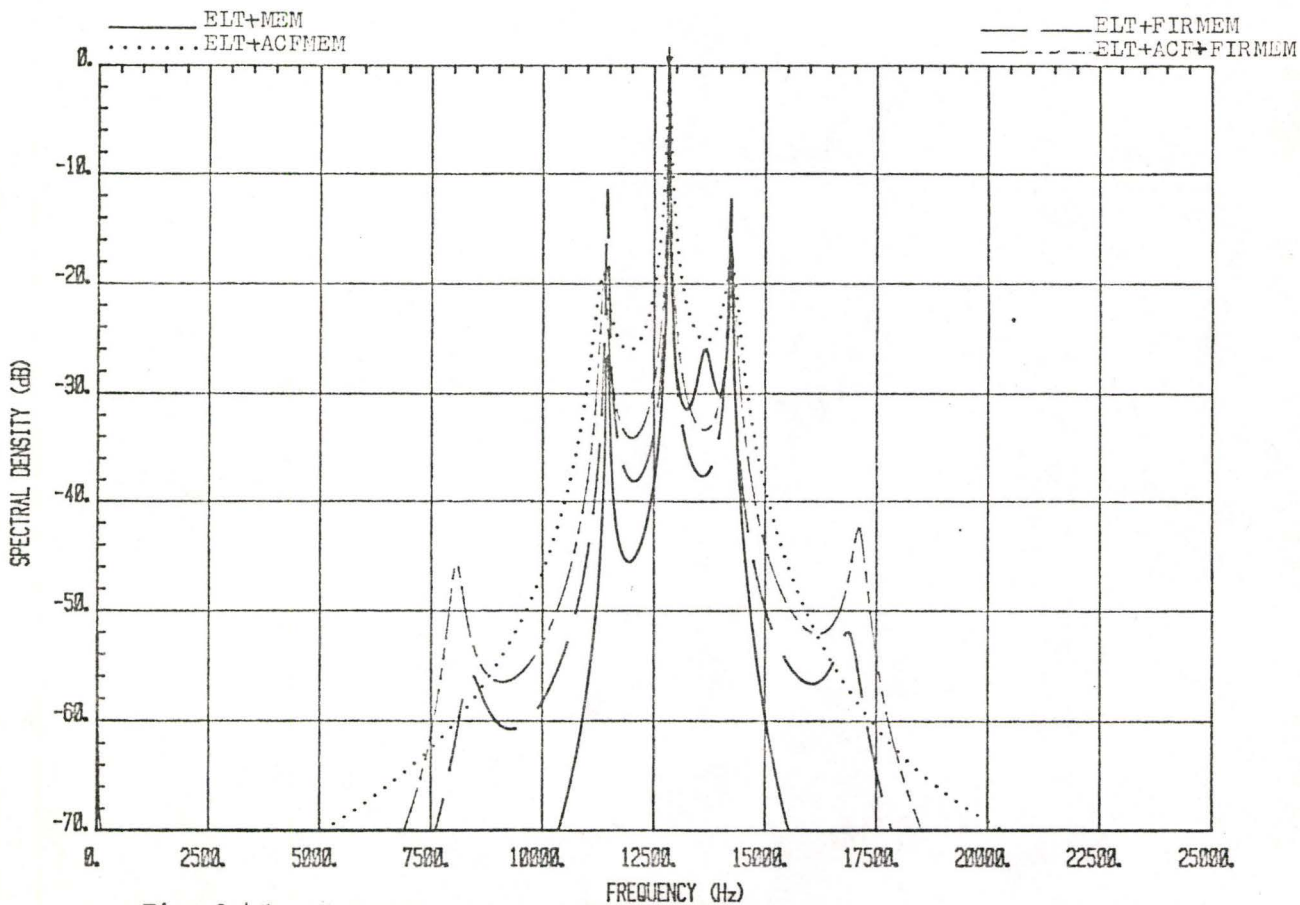


Fig. 3.45: The MEM spectra at filter order 10 (sinusoidal-modulated signal).

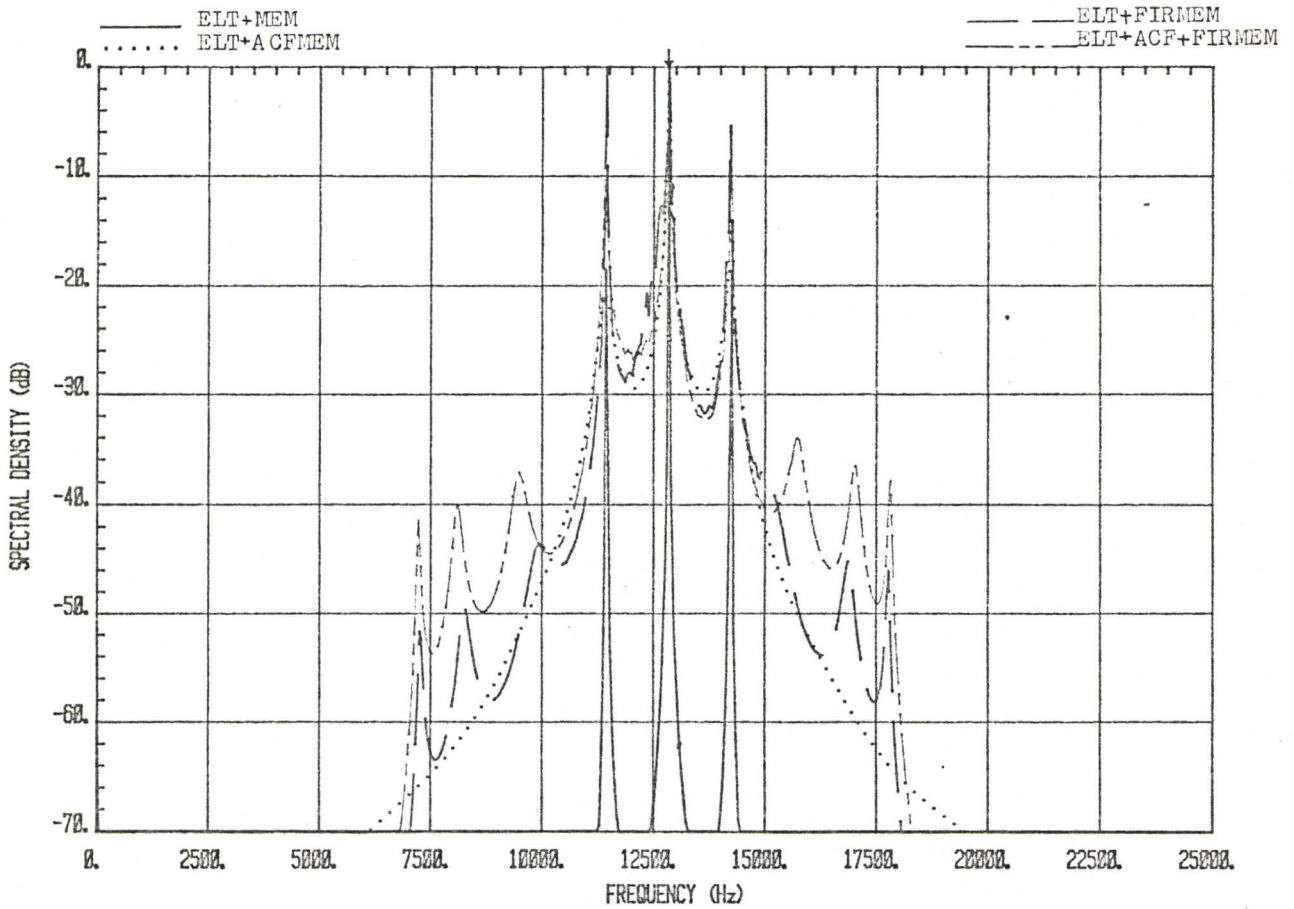


Fig. 3.46: The MEM spectra at filter order 20 (sinusoidal-modulated signal).

### 3.4.1 Pulse-Modulated, Continuous Phase

In Fig. 3.47(a) the error curve of pulse-modulated signals (with continuous phase, linear frequency sweep and 36% duty cycle) is given. The MEM analysis performs poorly from 0 Hz to 3500 Hz and from 21500 to 25000 Hz. An expanded plot from 5 KHz to 20 KHz of the curve is plotted in Fig. 3.47(b). The frequency error varies from approximately -500 Hz to +500 Hz as the carrier varies from 5000 Hz to 20000 Hz. There are large fluctuations along the curve; however, it is expected that spectral averaging will significantly reduce these. ELT signals with frequencies near the bandcenter value suffer less variation in frequency error.

An ACFMEM error curve is illustrated in Fig. 3.48(a). We notice that this processor achieves an outstanding improvement in spectral performance. The frequency error is significantly lower across the entire frequency band. Fig. 3.48(b) shows an expanded plot of the curve for the 5 KHz to 20 KHz range.

For the same ELT signals which carry quadratic frequency sweep, we observe that the error curves produced by the MEM and the ACFMEM in Fig. 3.49 and 3.50 have almost identical patterns as the previous cases. The sole difference is the degree of increased variation along these curves.

Several low values of carrier frequency are selected from Fig. 3.47(a) and 3.48(a) in order to inspect the actual MEM and ACFMEM spectra. At 1500 Hz, the MEM yields an error of 1500 Hz and the ACFMEM measures 215 Hz difference. The spectra, at this frequency, are plotted

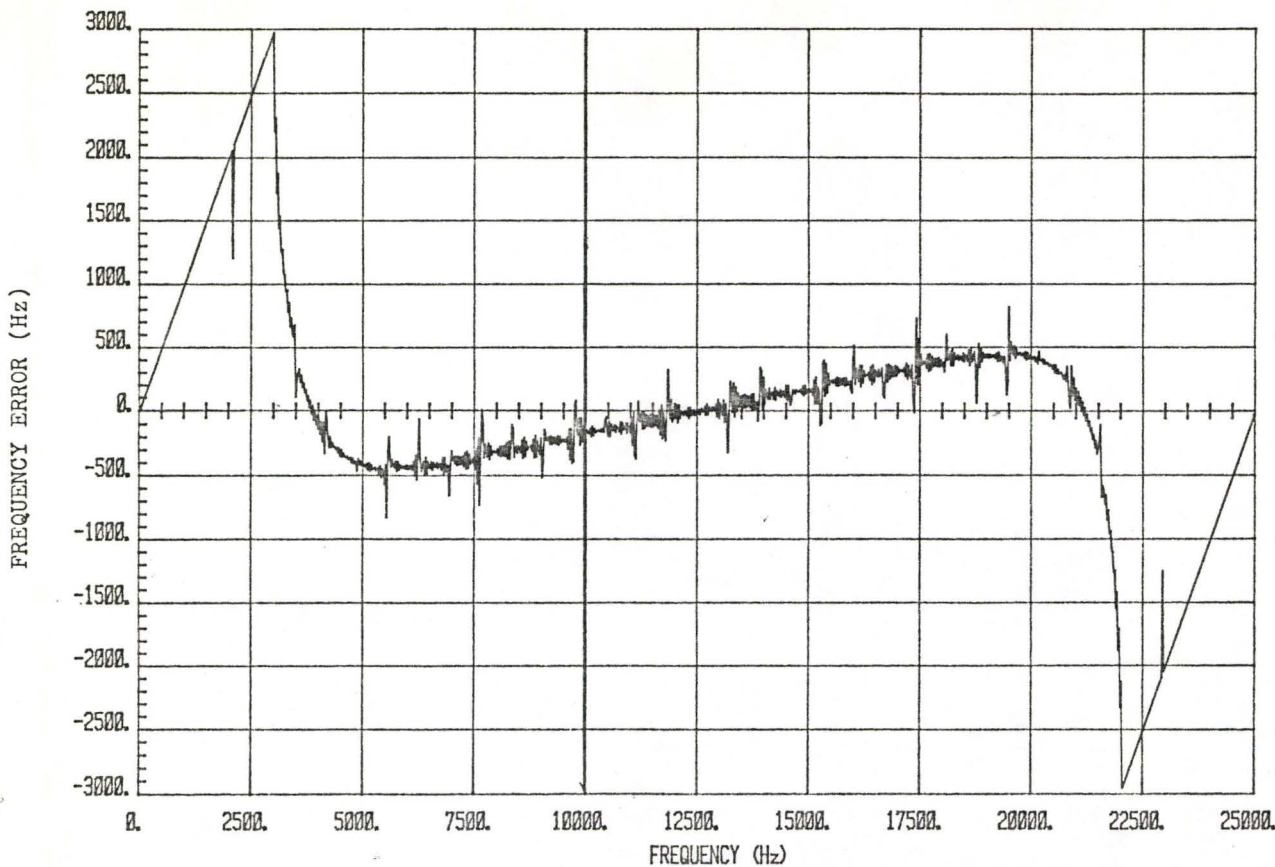


Fig. 3.47(a): The error curve of pulse-modulated ELT signal (continuous phase, linear frequency sweep and 36% duty cycle) using MEM at filter order 2.

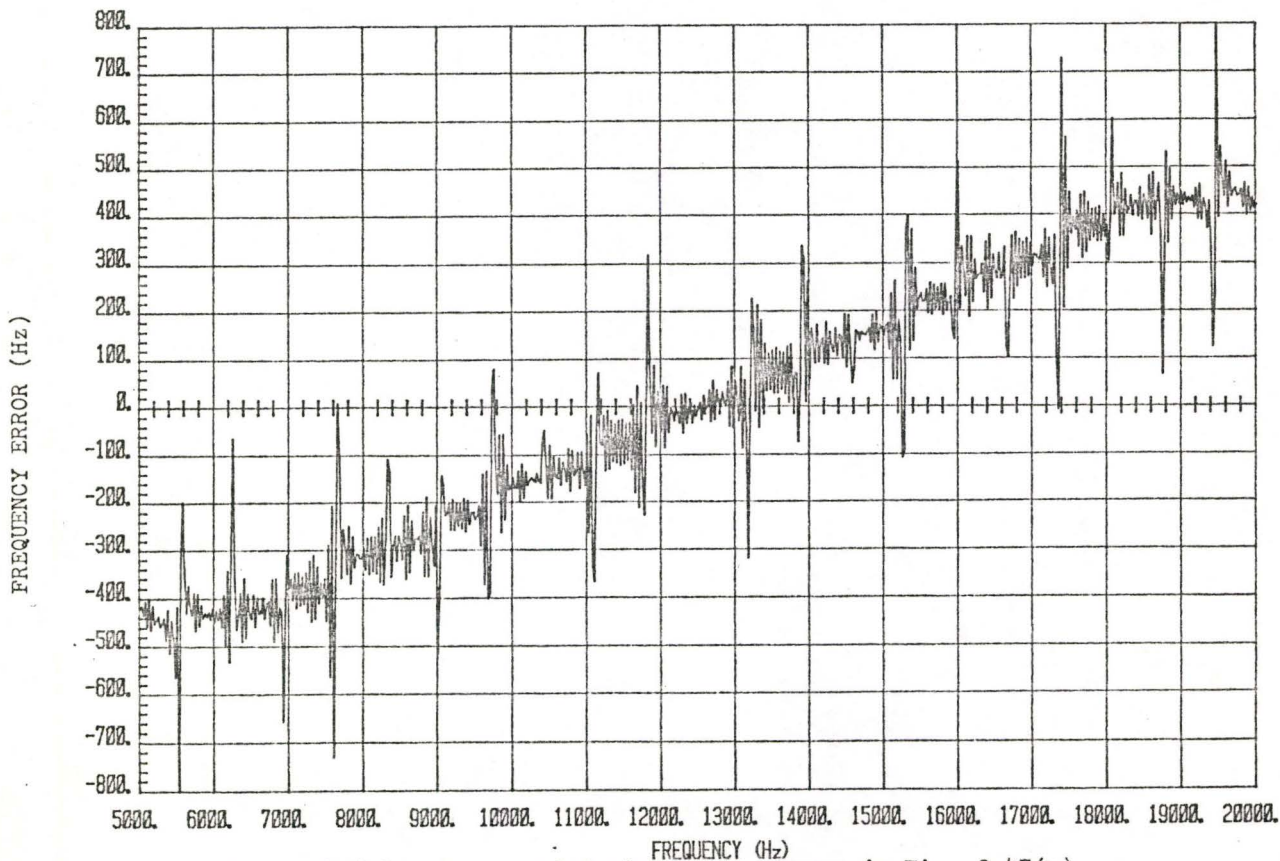


Fig. 3.47(b): An expanded view of the curve in Fig. 3.47(a).

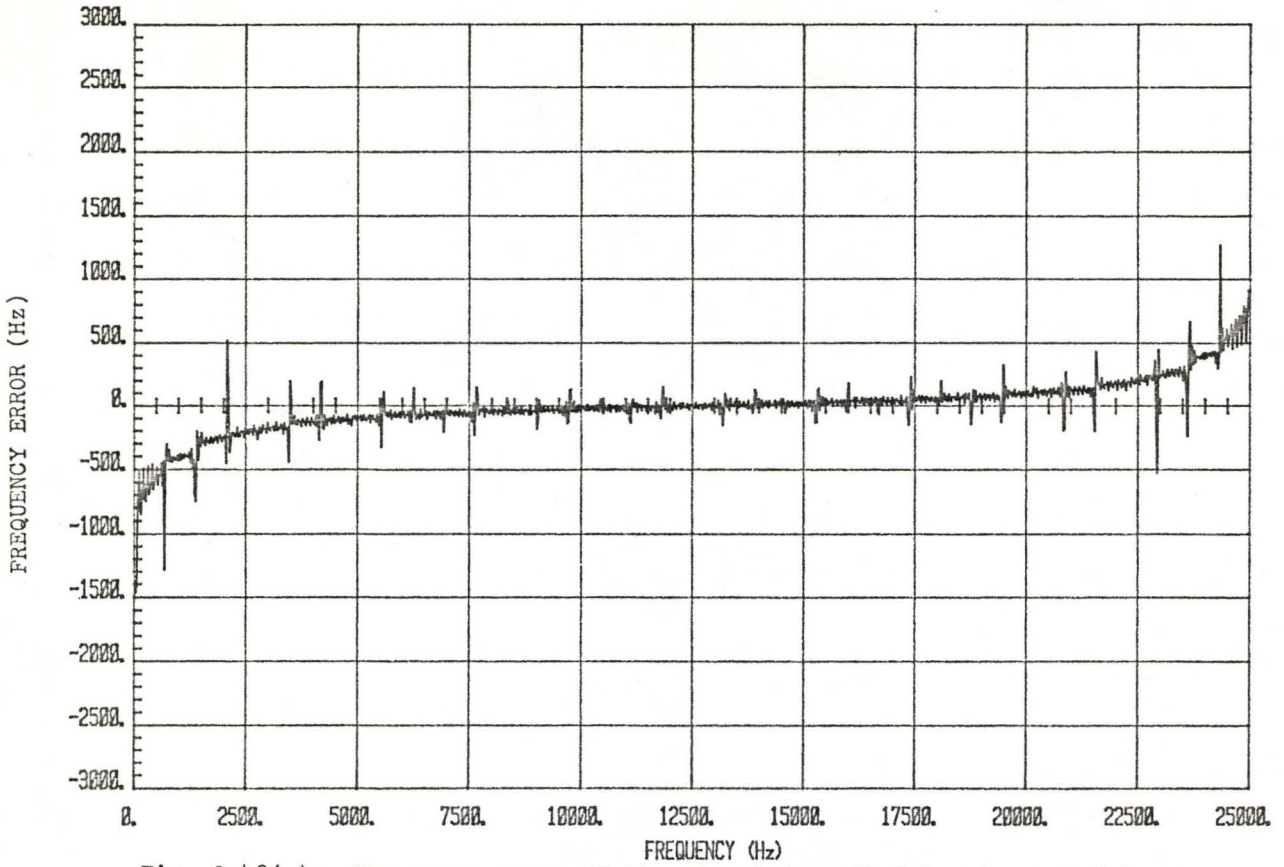


Fig. 3.48(a): The error curve of the signal described in Fig. 3.47(a) using the ACFMEM at filter order 2.

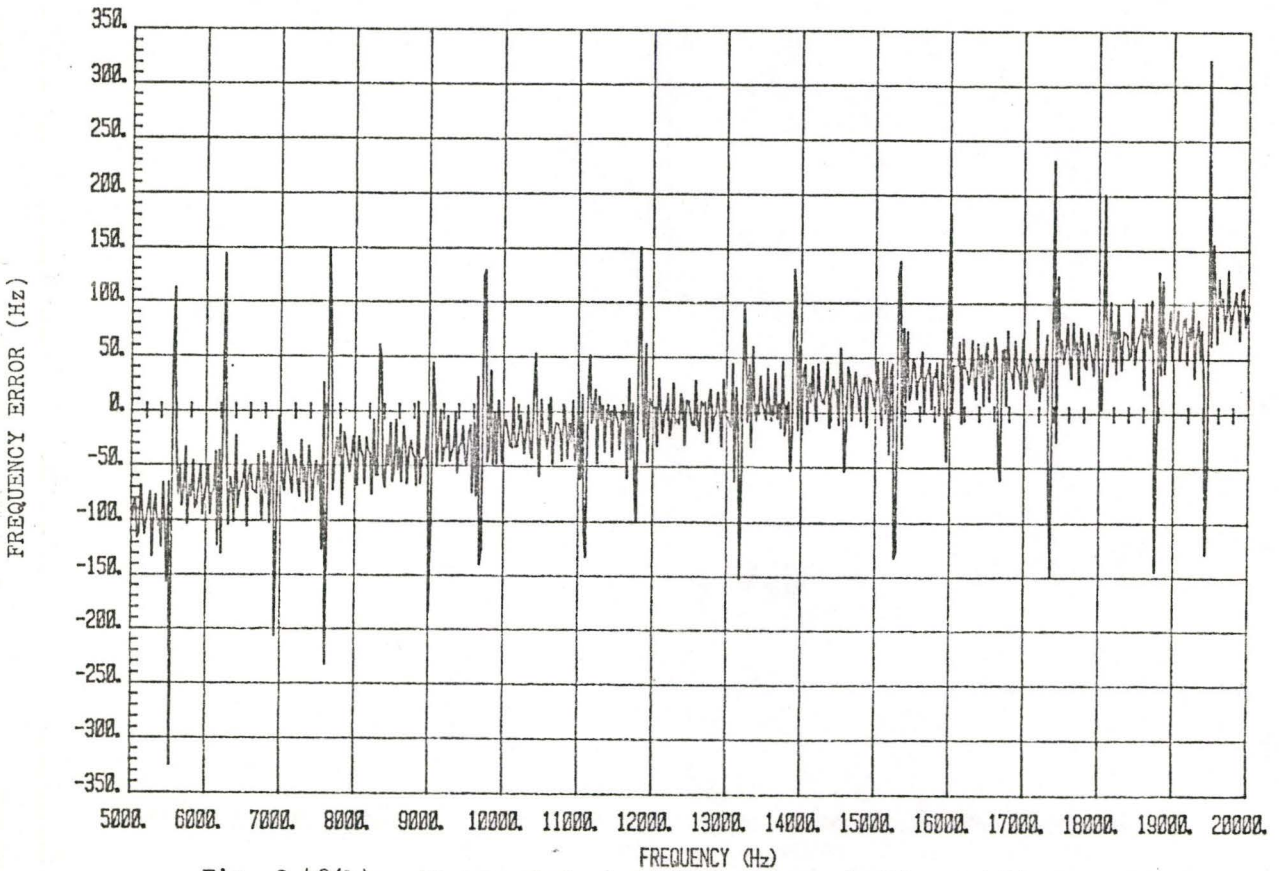


Fig. 3.48(b): An expanded view of the curve in Fig. 3.48(a).

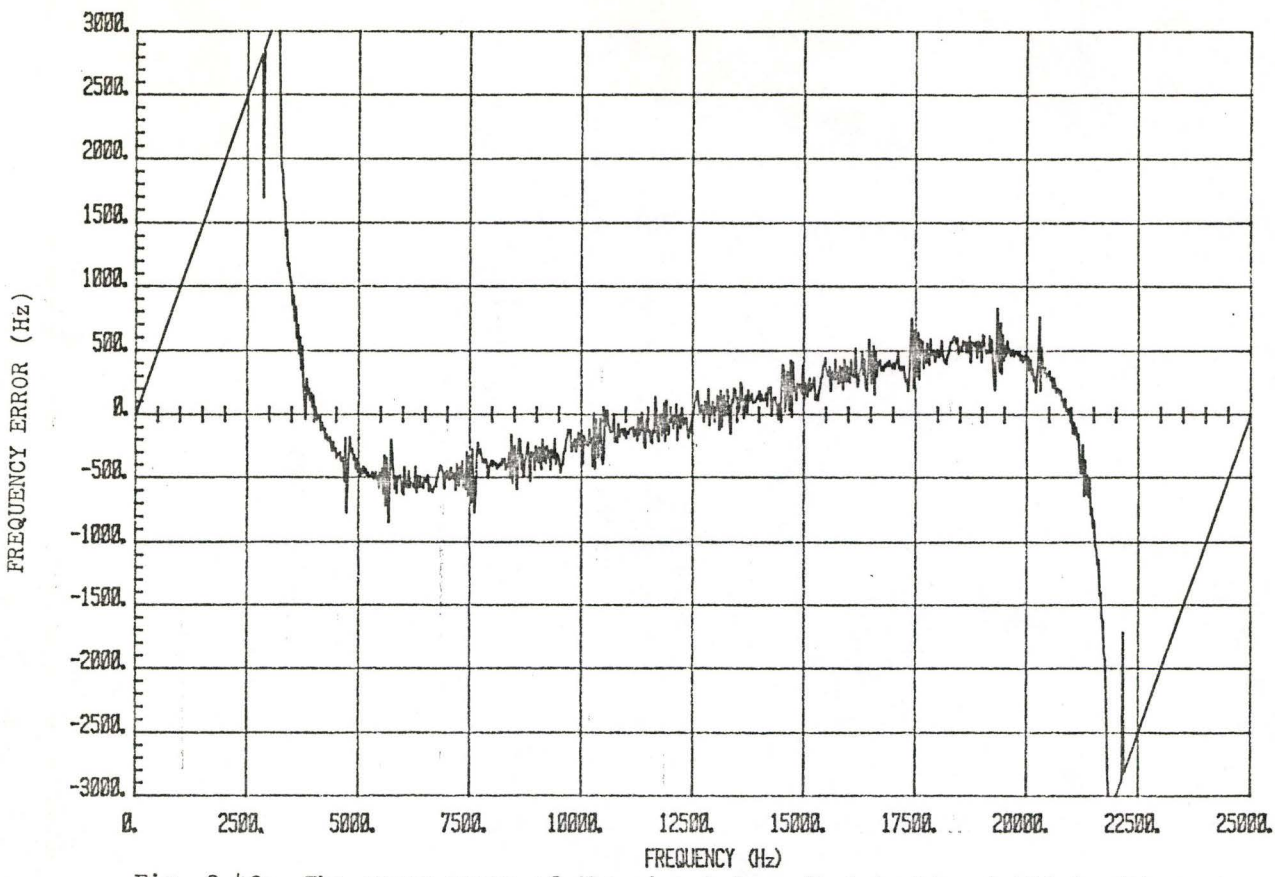


Fig. 3.49: The error curve of the signal described in Fig. 3.47(a) with quadratic frequency sweep and at MEM filter order 2.

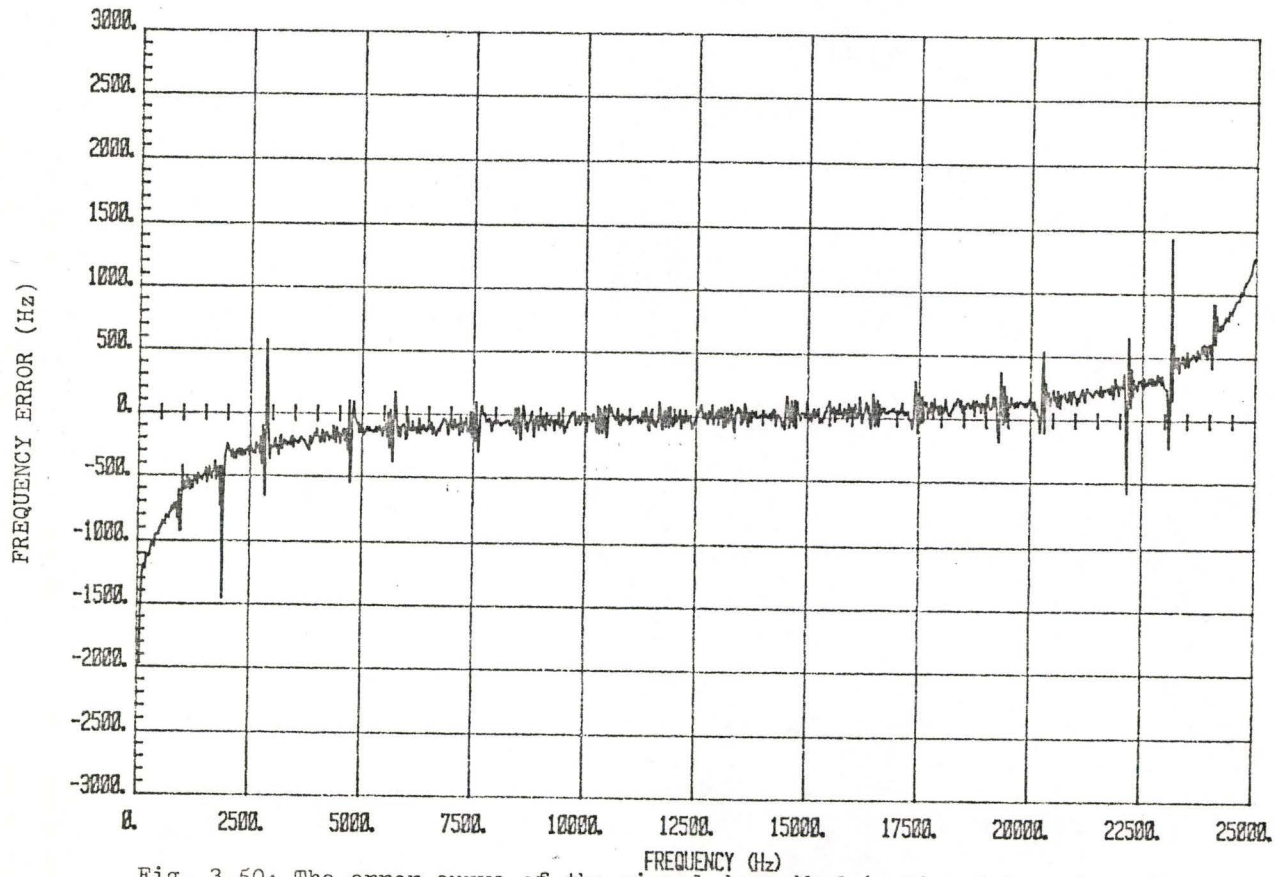


Fig. 3.50: The error curve of the signal described in Fig. 3.49 using ACFMEM at filter order 2.

in Fig. 3.51. The MEM analysis fails absolutely whereas the ACFMEM provides peak at 1715 Hz. These results are used to compare with the FFT spectrum which is shown in Fig. 3.52(a). The sidelobe problem, again, dominates the analysis. Although one of the peaks is located at 1465 Hz (this is very close to the carrier frequency), the other one is calculated at 98 Hz. Thus, a false alarm is likely to occur. Windowing technique (using Kaiser window with  $\beta=8.0$ ) cannot overcome the ambiguity. This is shown in Fig. 3.52(b). At carrier frequency 3250 Hz the MEM and the ACFMEM spectra are given in Fig. 3.53. Again, the MEM performs poorly. The peak measured by the ACFMEM is at 3428 Hz. The FFT spectrum, in Fig. 3.54(a), gives resolutions at 1855 Hz and 3223 Hz. Fig. 3.54(b) illustrates the effect of windowing. Fig. 3.55 and Fig. 3.56 compare the spectra of the non-linear and linear processors at frequency 7500 Hz. The MEM yields a broad peak at 7946 Hz. The error is reduced to 68 Hz when the ACFMEM produces a well defined peak at 7568 Hz. Nevertheless, the FFT analysis gives peaks at 7520 Hz and 8887 Hz.

#### 3.4.2 Pulse-Modulated, Random Phase

Random phase signals (linear and quadratic frequency sweeps) have error curves very similar to those produced by the continuous phase signals. These results are presented in Fig. 3.57 to Fig. 3.60 for the MEM and the ACFMEM. At frequency 3250 Hz, the spectra of MEM, ACFMEM and FFT are compared. Amongst the analyses, Fig. 3.61 and Fig. 3.62 prove that the ACFMEM has the greatest capability of resolving phase randomized signals.

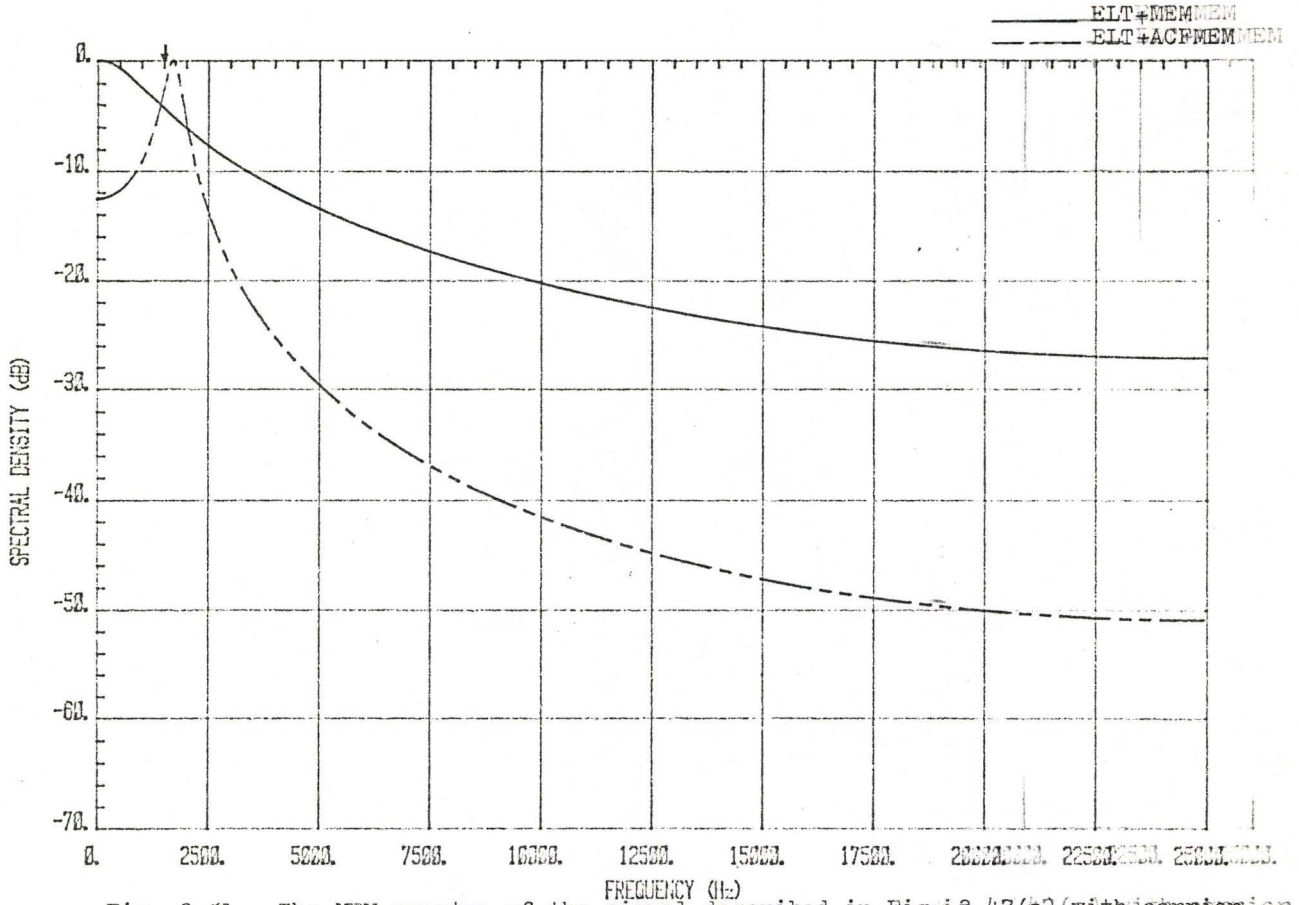


Fig. 3.51: The MEM spectra of the signal described in Fig. 3.47(a) (with carrier frequency at 1500 Hz and filter order 2).

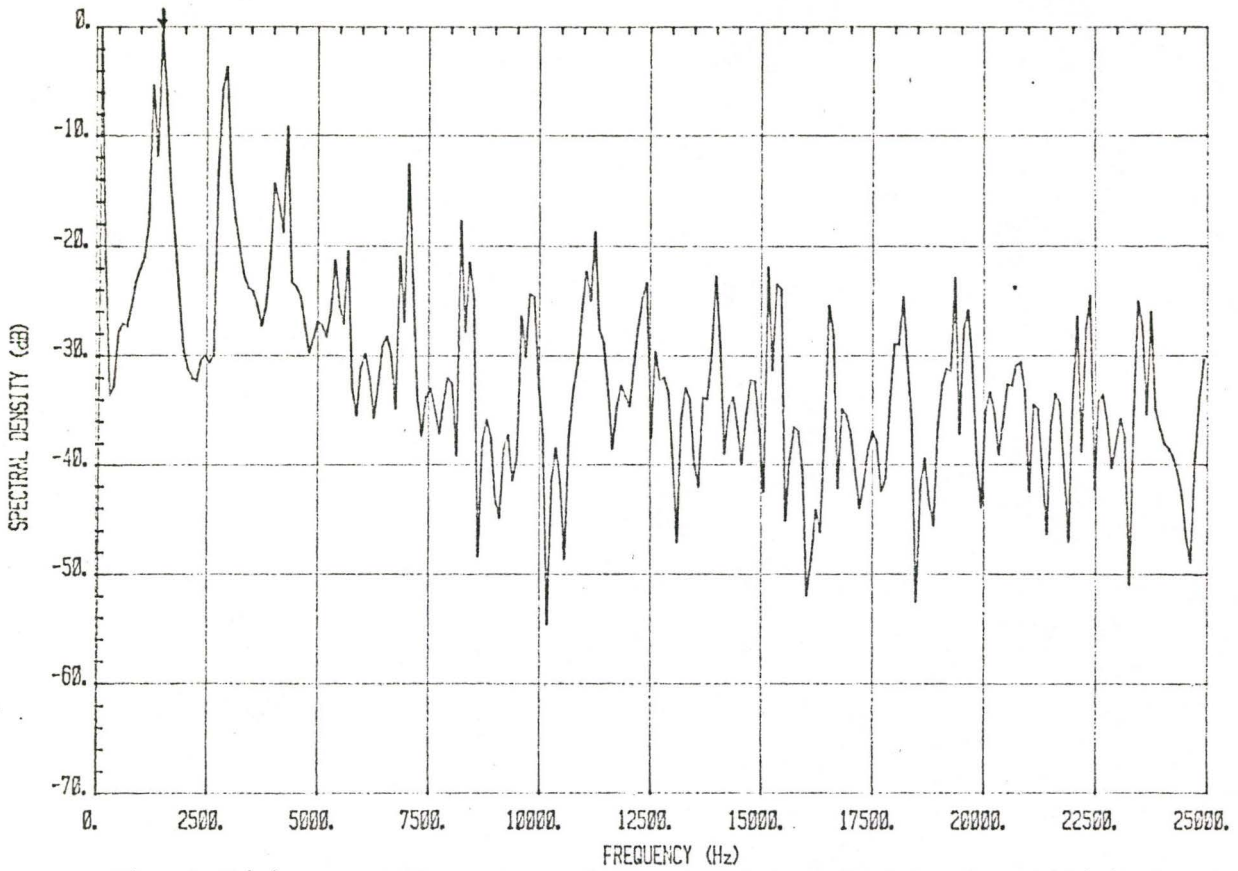


Fig. 3.52(a): The FFT spectrum of the signal described in Fig. 3.47(a). Carrier frequency is at 1500 Hz.

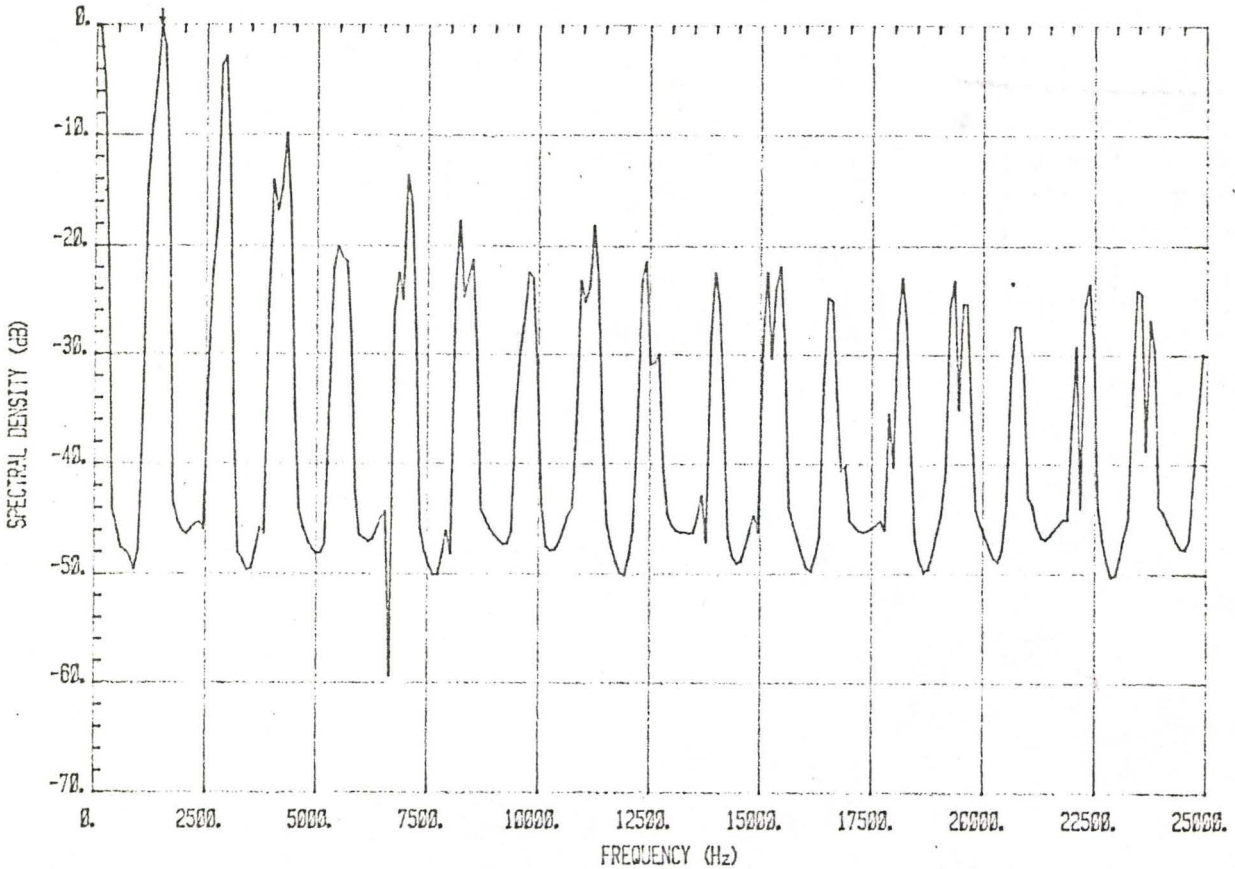


Fig. 3.52(b): The FFT spectrum of the signal (at carrier frequency 1500 Hz) described in Fig. 3.47(a) and windowed by a Kaiser window ( $\beta=8.0$ ).

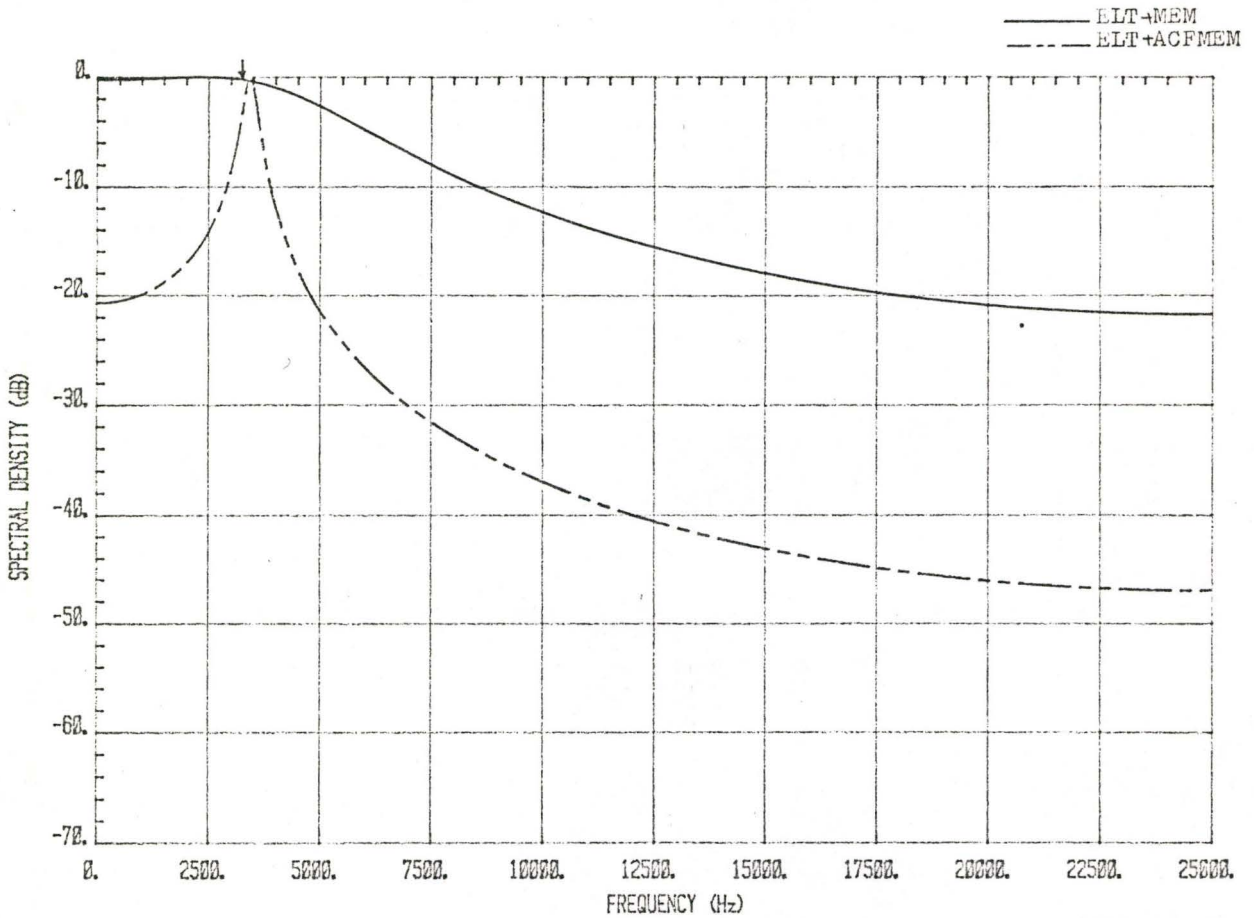


Fig. 3.53: The MEM spectra of the signal (at 3250 Hz) using MEM at filter order 2.

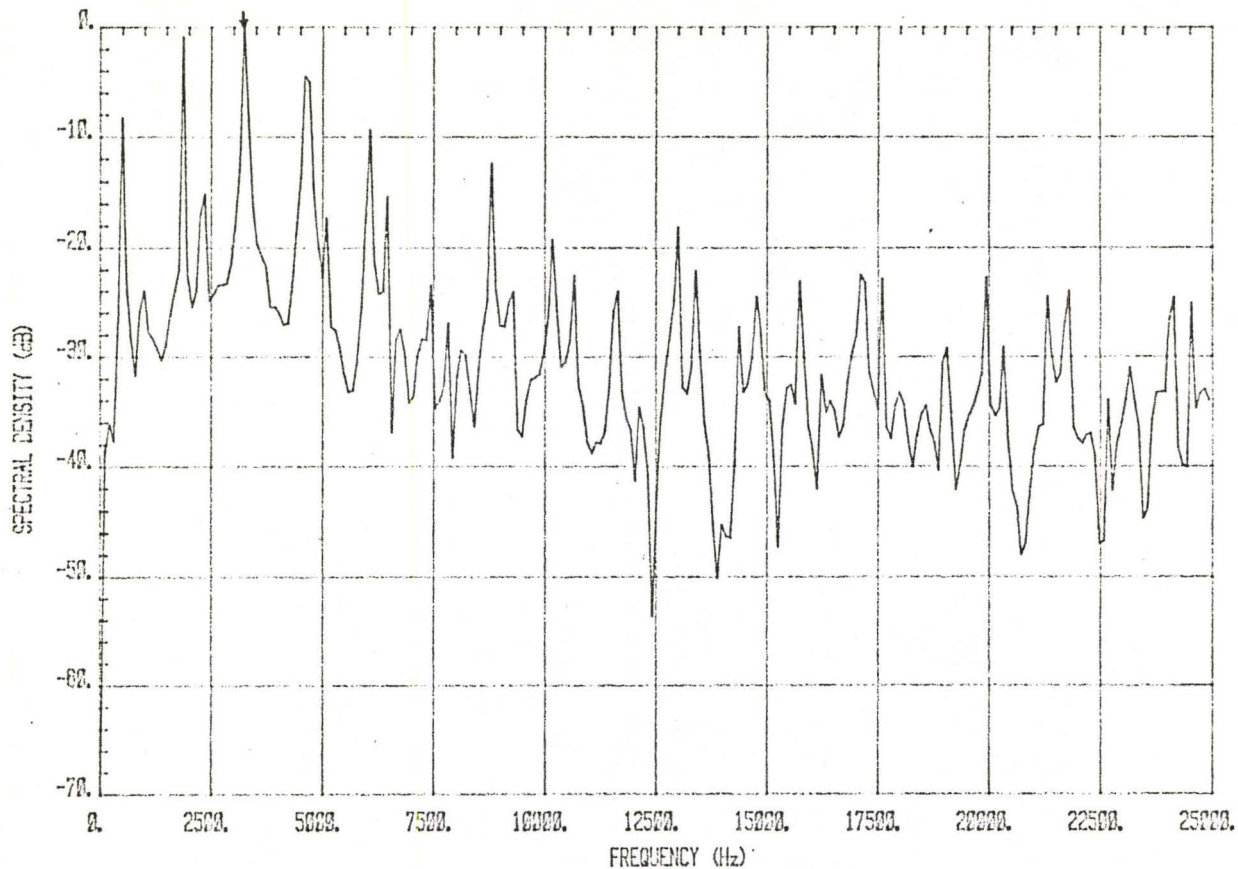


Fig. 3.54(a): The FFT spectrum of the signal (at 3250 Hz) described in Fig. 3.47(a).

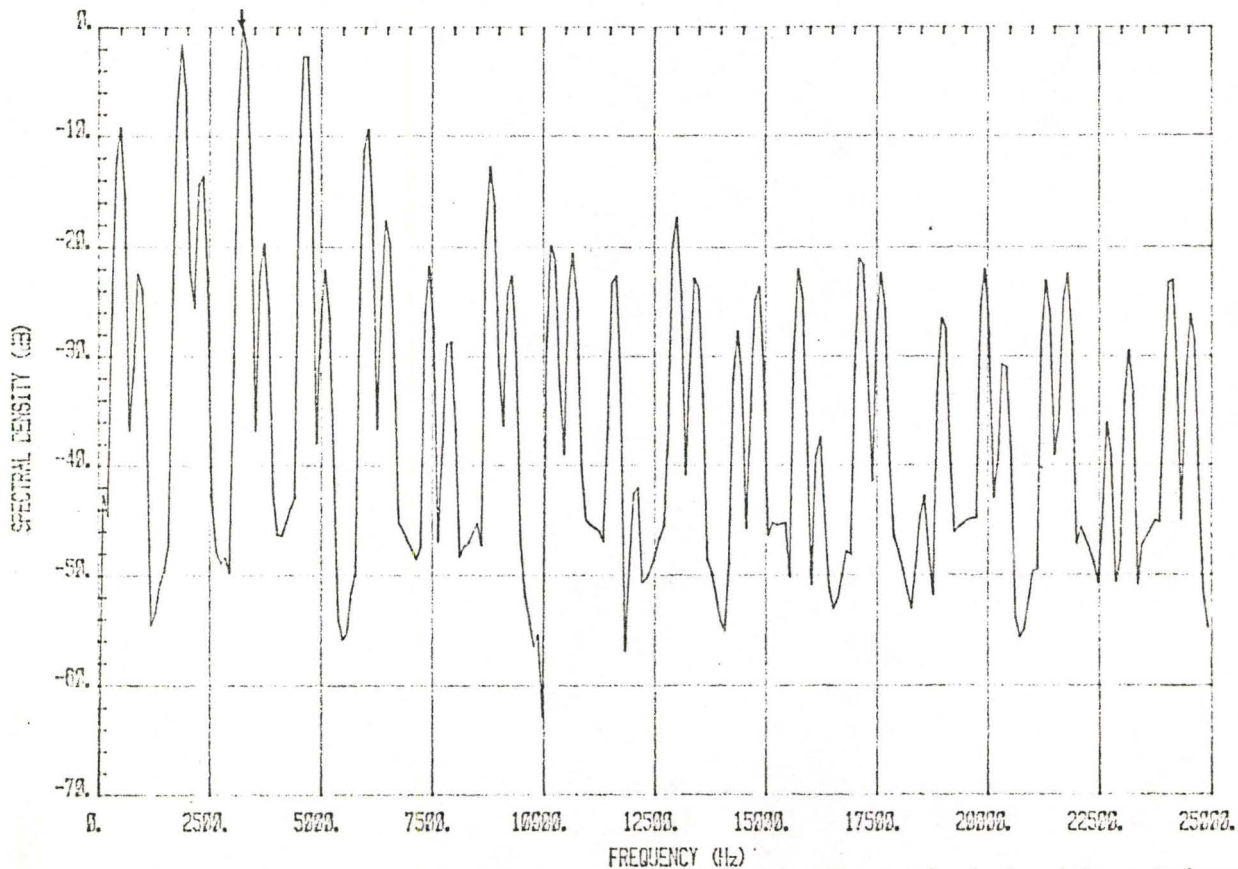


Fig. 3.54(b): The FFT spectrum of the signal (at 3250 Hz) windowed by a Kaiser window ( $\beta=8.0$ )

— ELT+MEM  
- - - ELT+ACFMEM

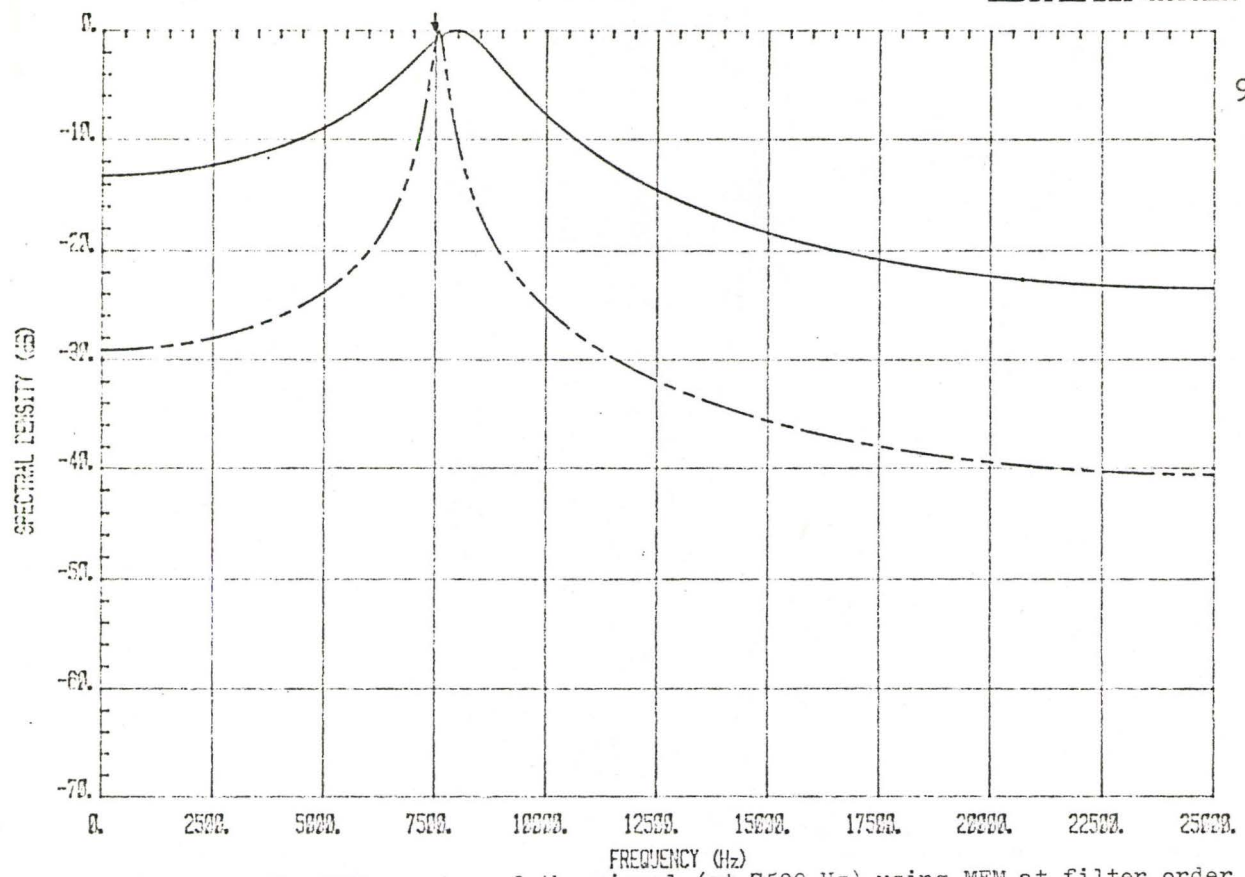


Fig. 3.55: The MEM spectra of the signal (at 7500 Hz) using MEM at filter order 2.

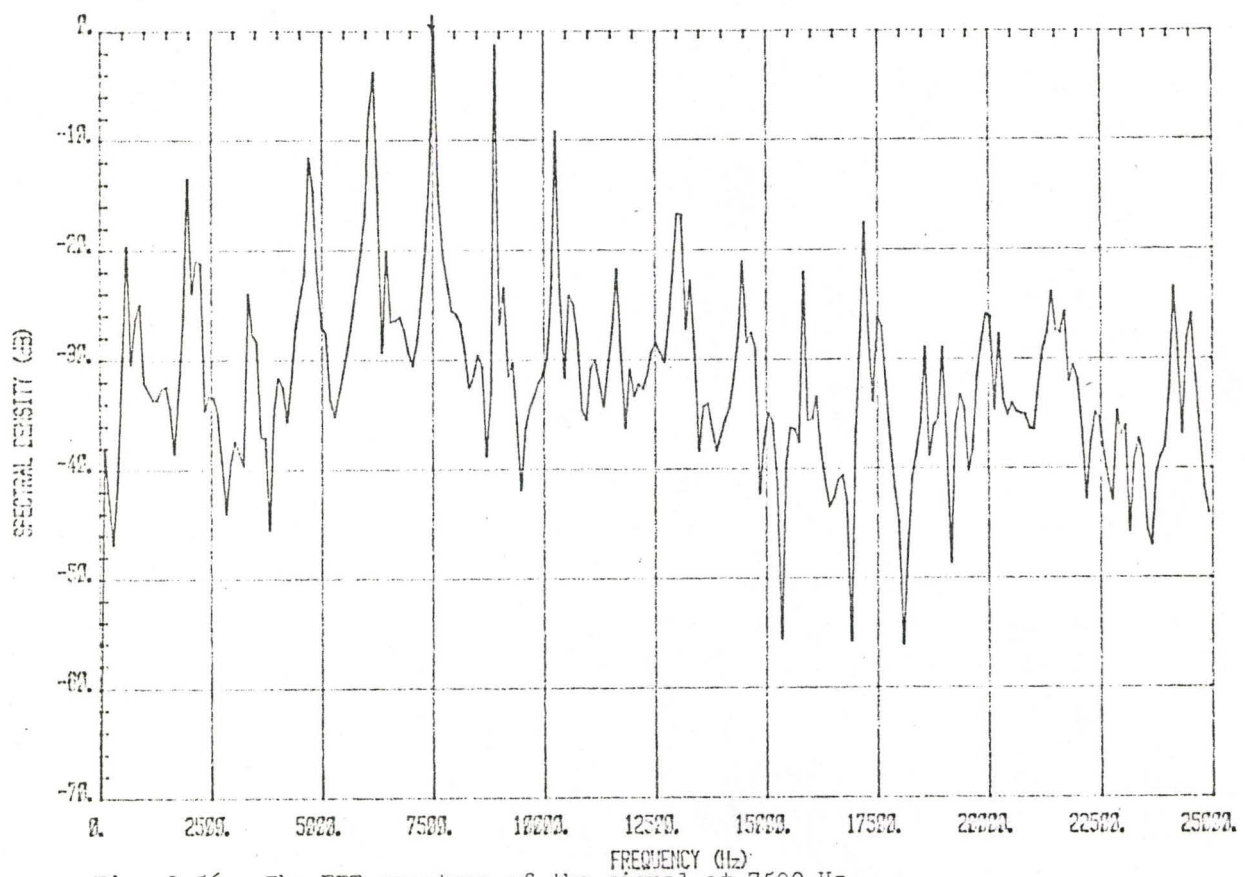


Fig. 3.56: The FFT spectrum of the signal at 7500 Hz

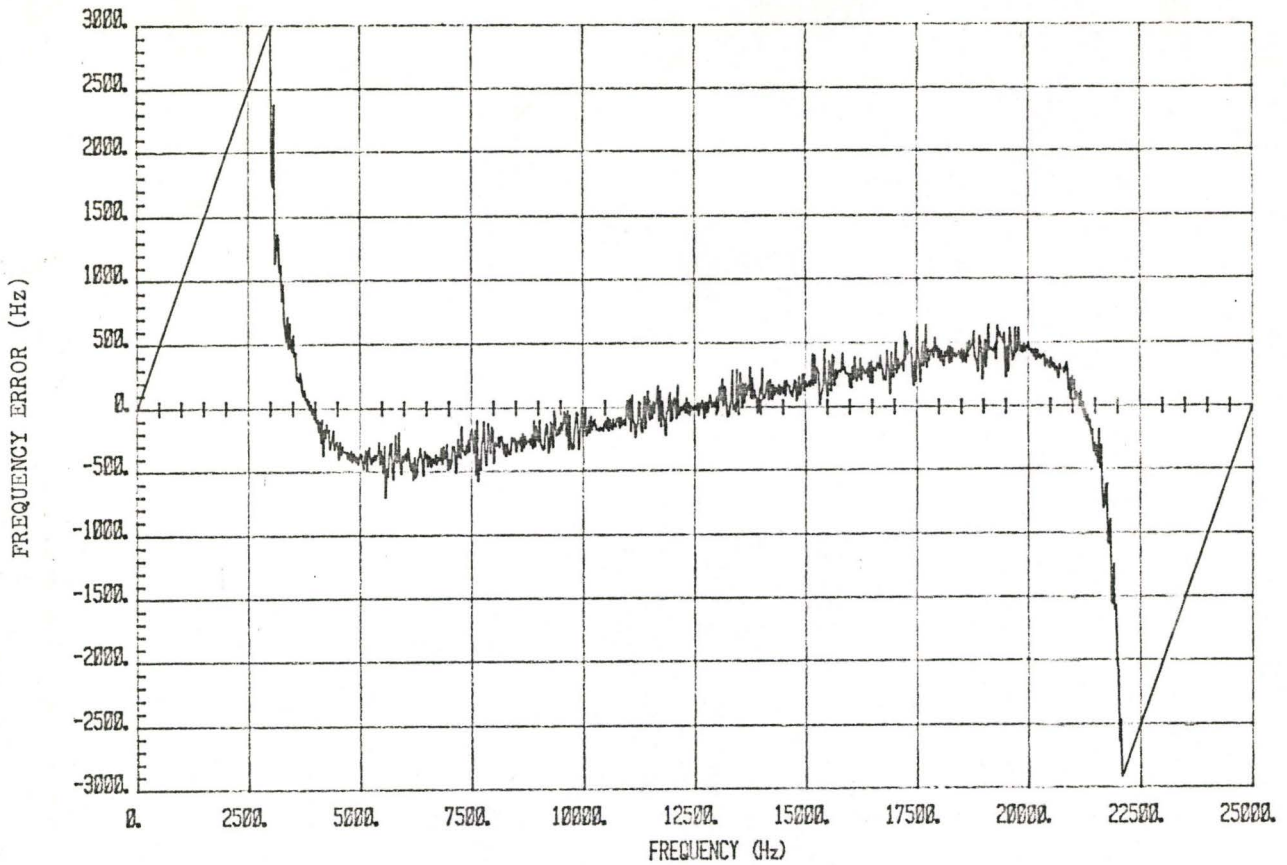


Fig. 3.57(a): The error curve of a pulse-modulated random phase signal (linear frequency sweep and 36% duty cycle) using MEM at filter order 2.

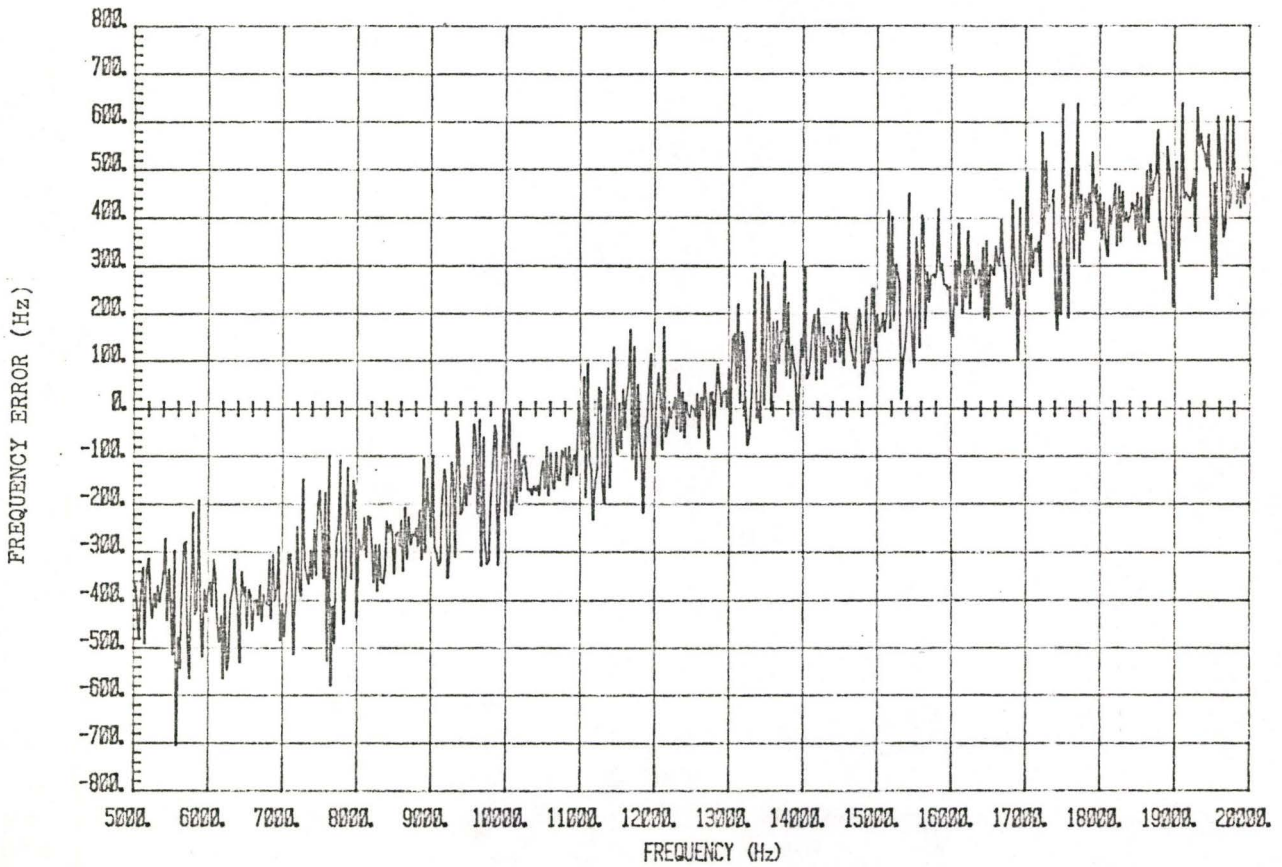


Fig. 3.57(b): An expanded view of the curve in Fig. 3.57(a).

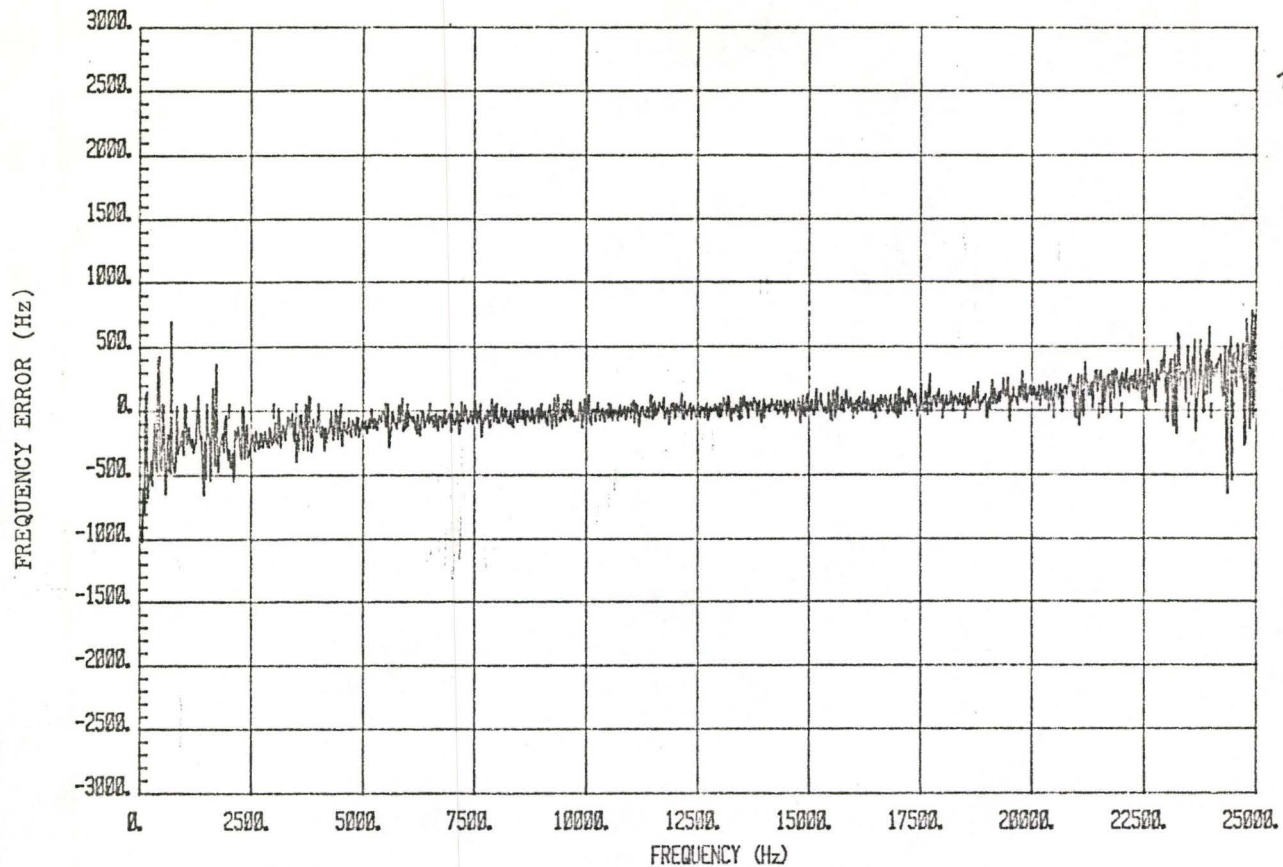


Fig. 3.58(a): The error curve of the signal described in Fig. 3.57(a) using ACFMEM at filter order 2.

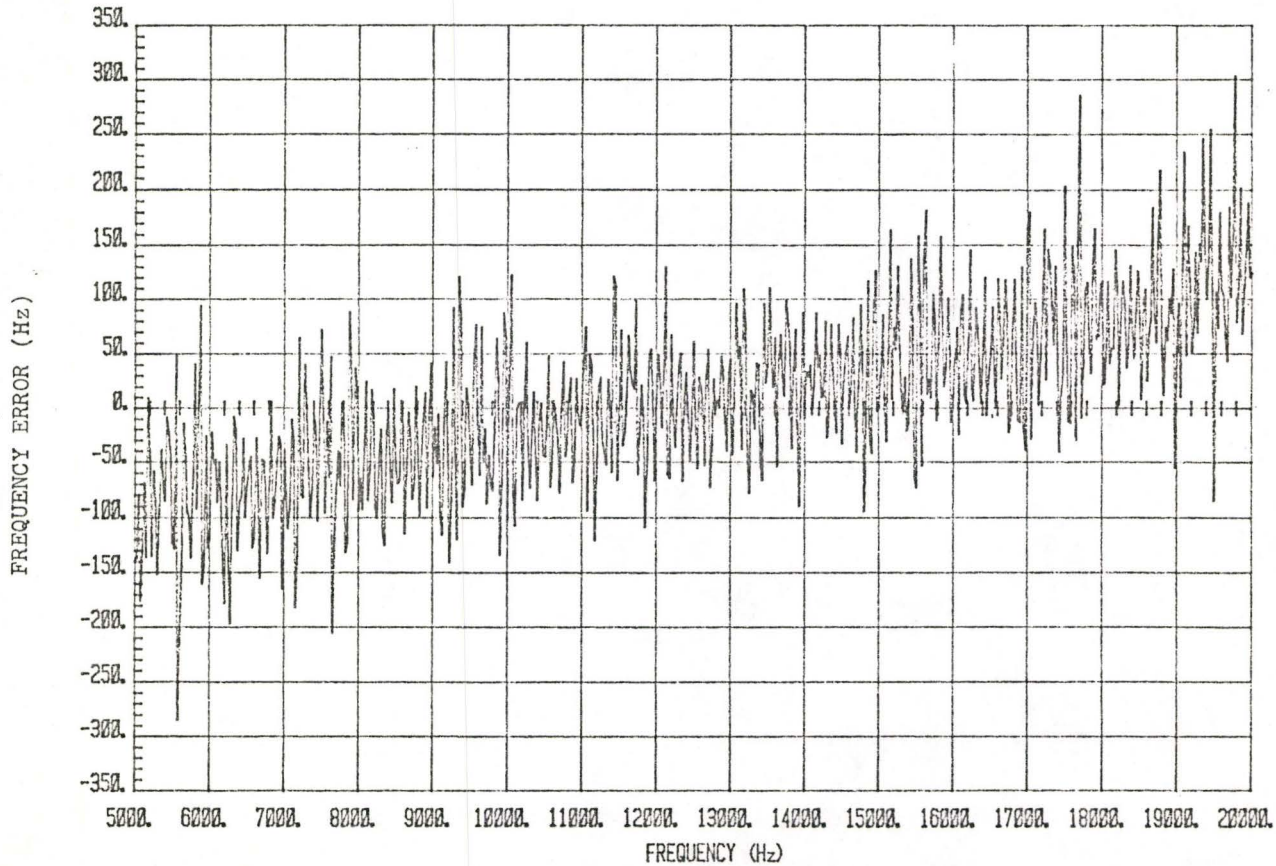


Fig. 3.58(b): An expanded view of the curve in Fig. 3.58(a).

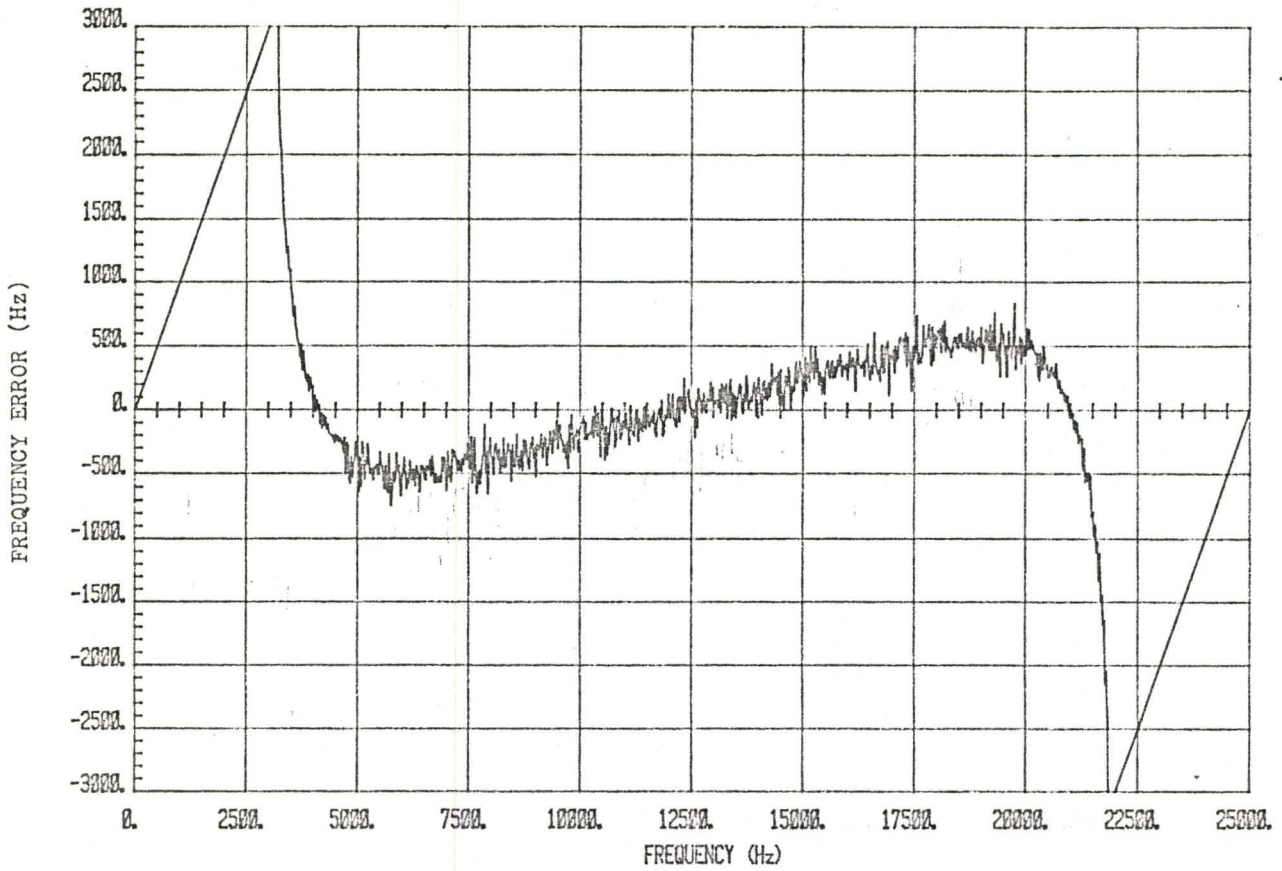


Fig. 3.59: The error curve of the signal described in Fig. 3.57(a) with quadratic frequency sweep and MEM order 2.

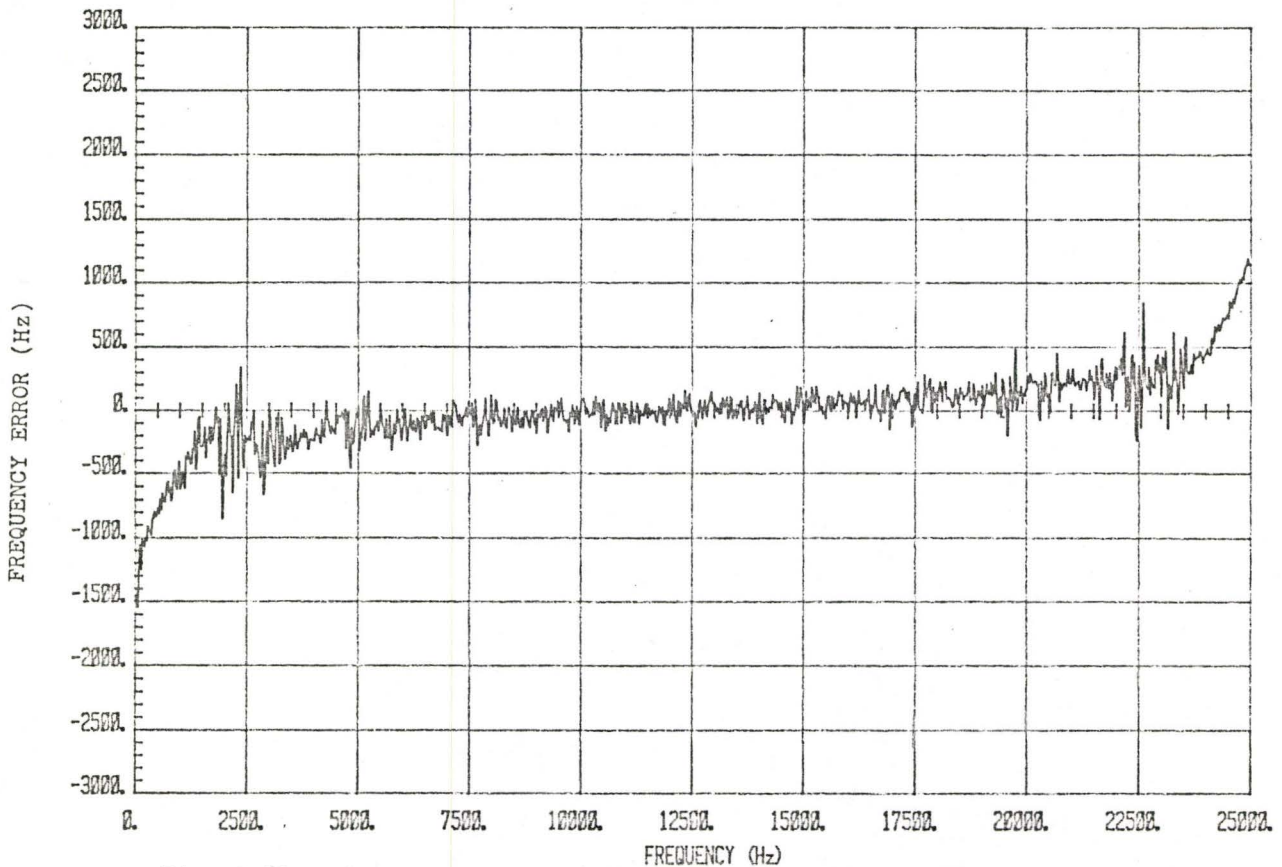


Fig. 3.60: The error curve of the signal described in Fig. 3.59 with ACFMEM at filter order 2.

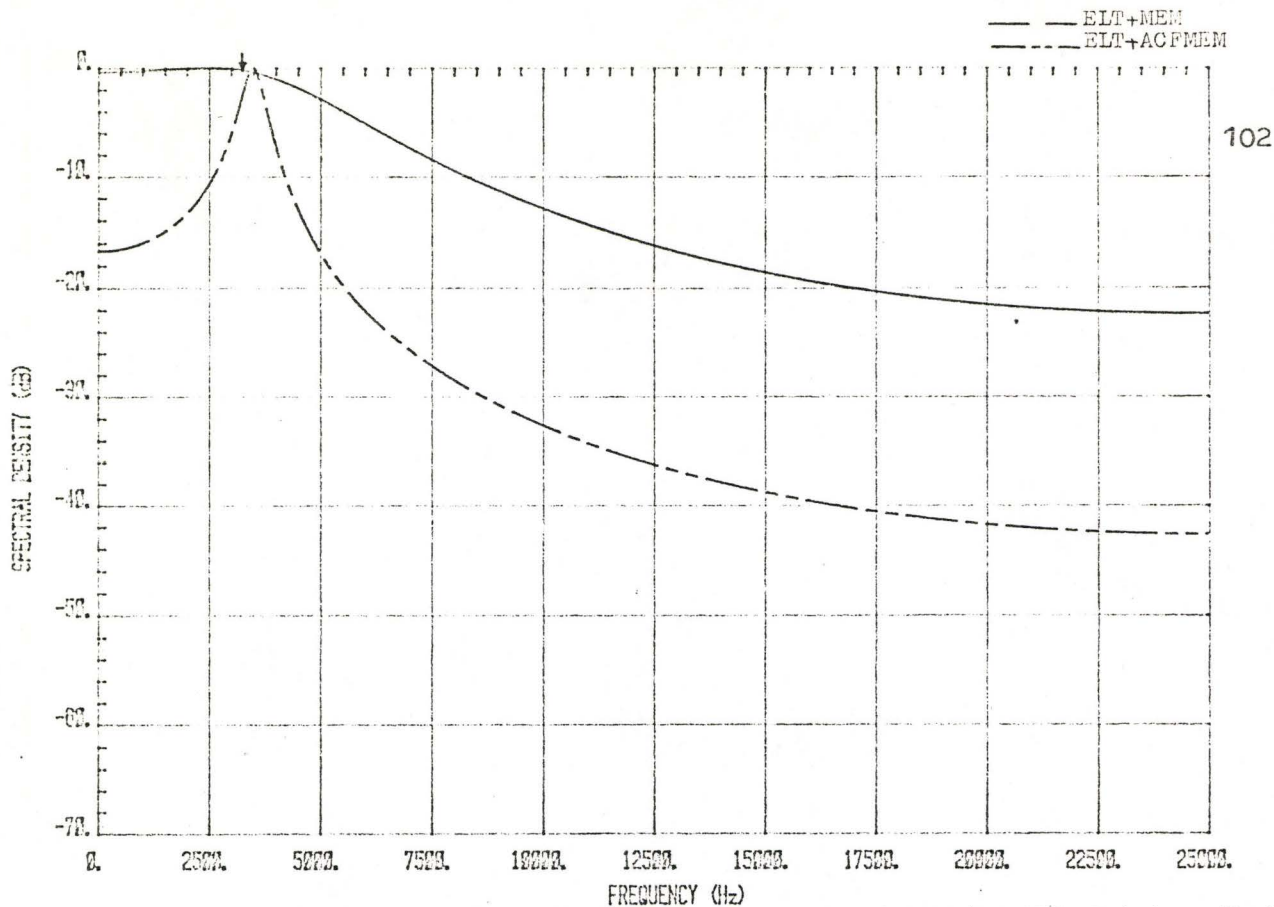


Fig. 3.61: The MEM spectra at filter order 2 of the signal (at 3250 Hz) described in Fig. 3.57(a).

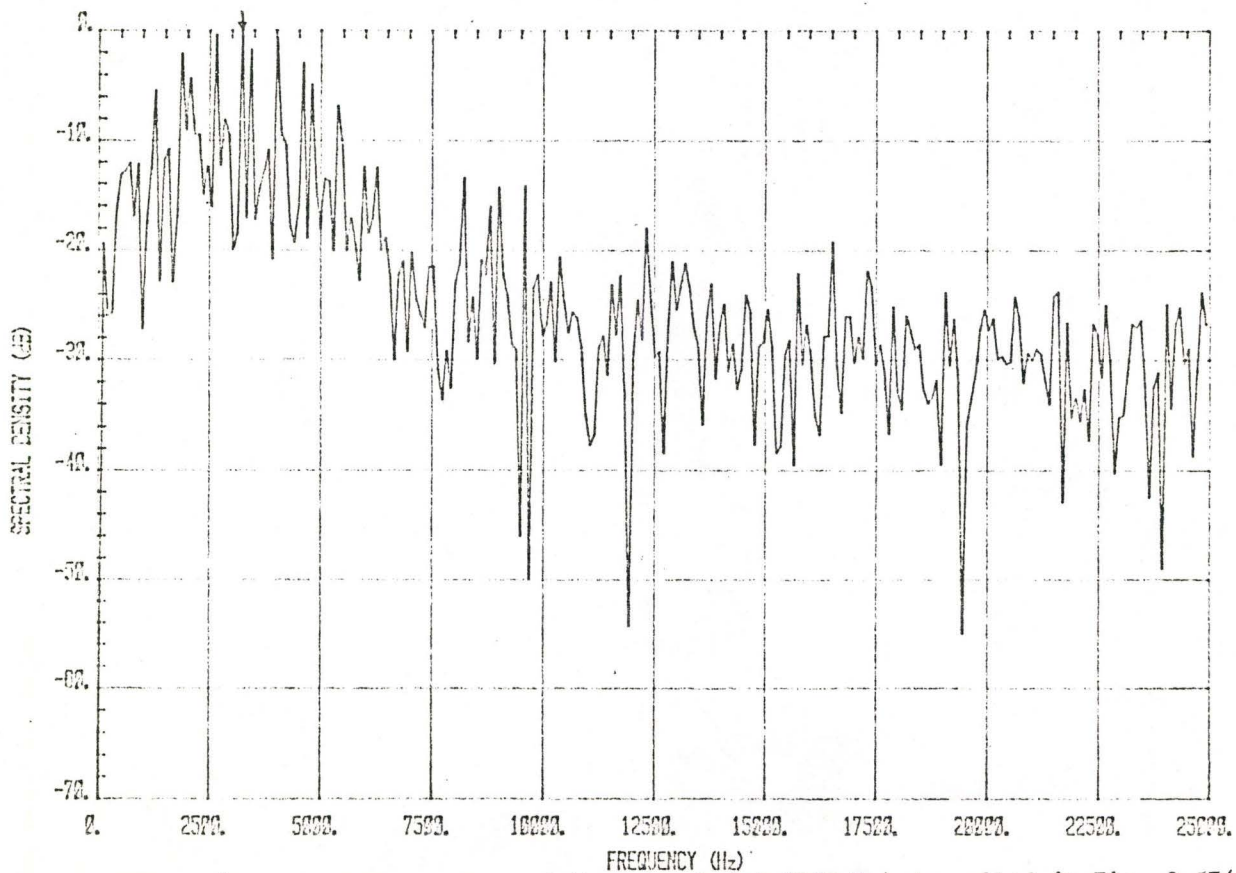


Fig. 3.62: The FFT spectrum of the signal (at 3250 Hz) described in Fig. 3.57(a).

### 3.4.3 Sinusoidal-Modulated

The absence of nulls between pulses of sinusoidal-modulated signals plays an important role in the processing techniques. This is evident by judging from the error curves included in Fig. 3.63 to Fig. 3.66. The ACFMEM yields an error of less than 50 Hz within the 5 KHz to 20 KHz band.

### 3.4.4 Overall Performance

A study of these sets of error curves provides an insight to the understanding of the spectral performances of the MEM and the ACFMEM on ELT signals. The most interesting phenomenon is that for the above cases there is no error detected at the 12.5 KHz frequency. Furthermore, the curves between 5 KHz to 20 KHz region reflect an odd function symmetry about the bandcenter frequency. The actual causes that give rise to these curves are not yet determined. We anticipate that by processing a complete duration (0.25 s) of the received ELT signals, the spectral performance is likely to be improved.

## 3.5 THE SPECTRAL PERFORMANCE WITH VARIATIONS IN CARRIER-TO-NOISE DENSITY RATIO

The ELT signals, which we have analysed so far, are assumed to have an infinite value of carrier-to-noise ratio. In this section we extend our discussion about the spectral performances of ELT signals (which have the same characteristics defined in Section 3.2) at various carrier-to-noise density ratio (CNDR) levels. The relationship of carrier-to-noise ratio (in dB unit) and carrier-to-noise density ratio

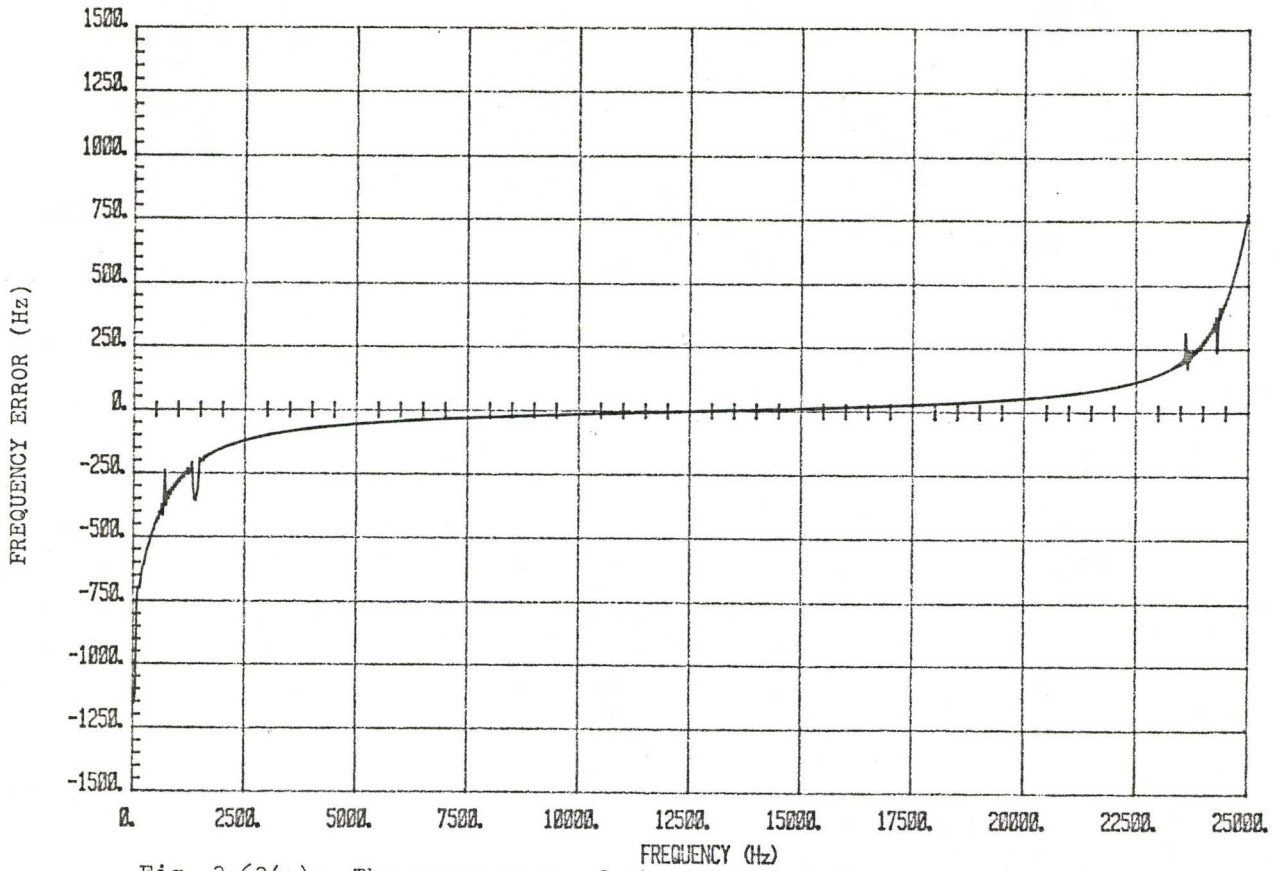


Fig. 3.63(a): The error curve of sinusoidal-modulated signal with linear frequency sweep and MEM at filter order 2.

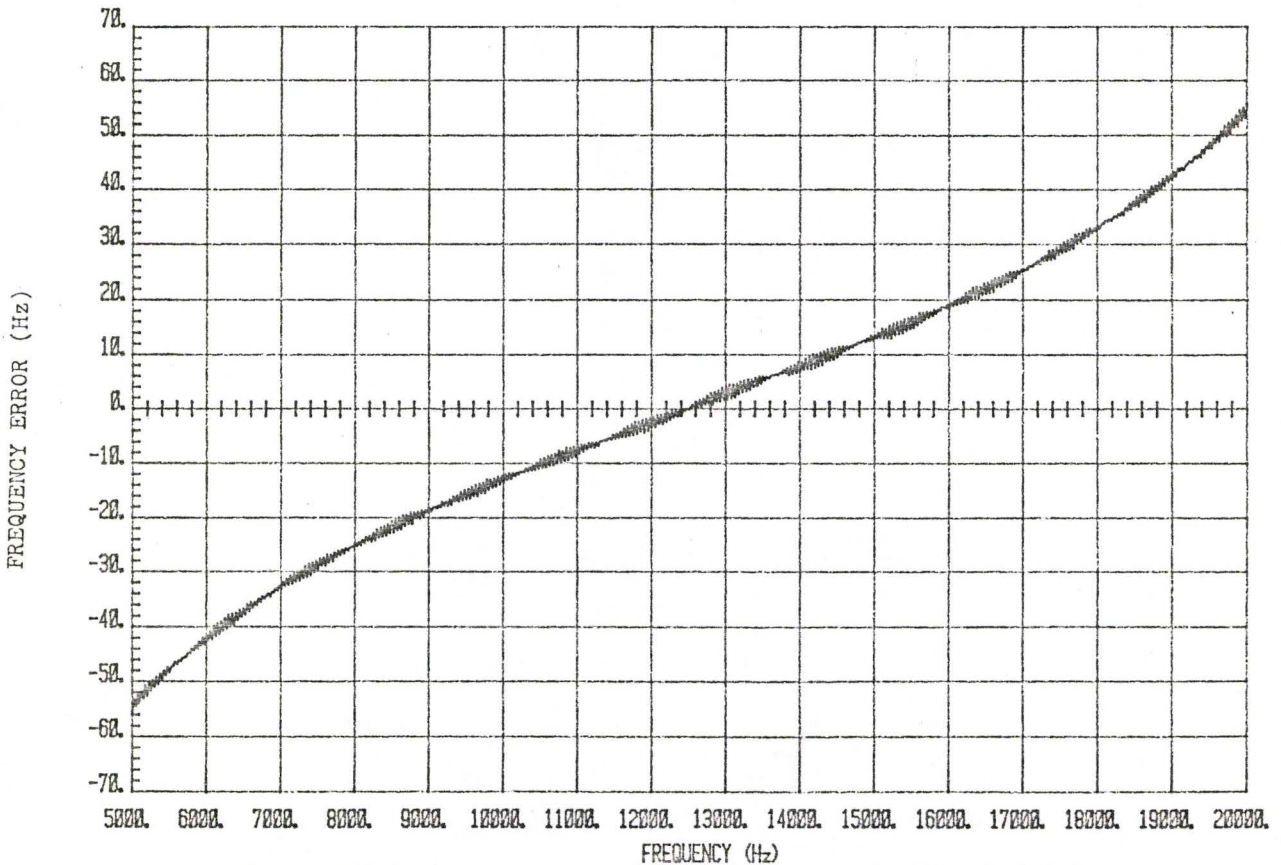


Fig. 3.63(b): An expanded view of the curve in Fig. 3.63(a).

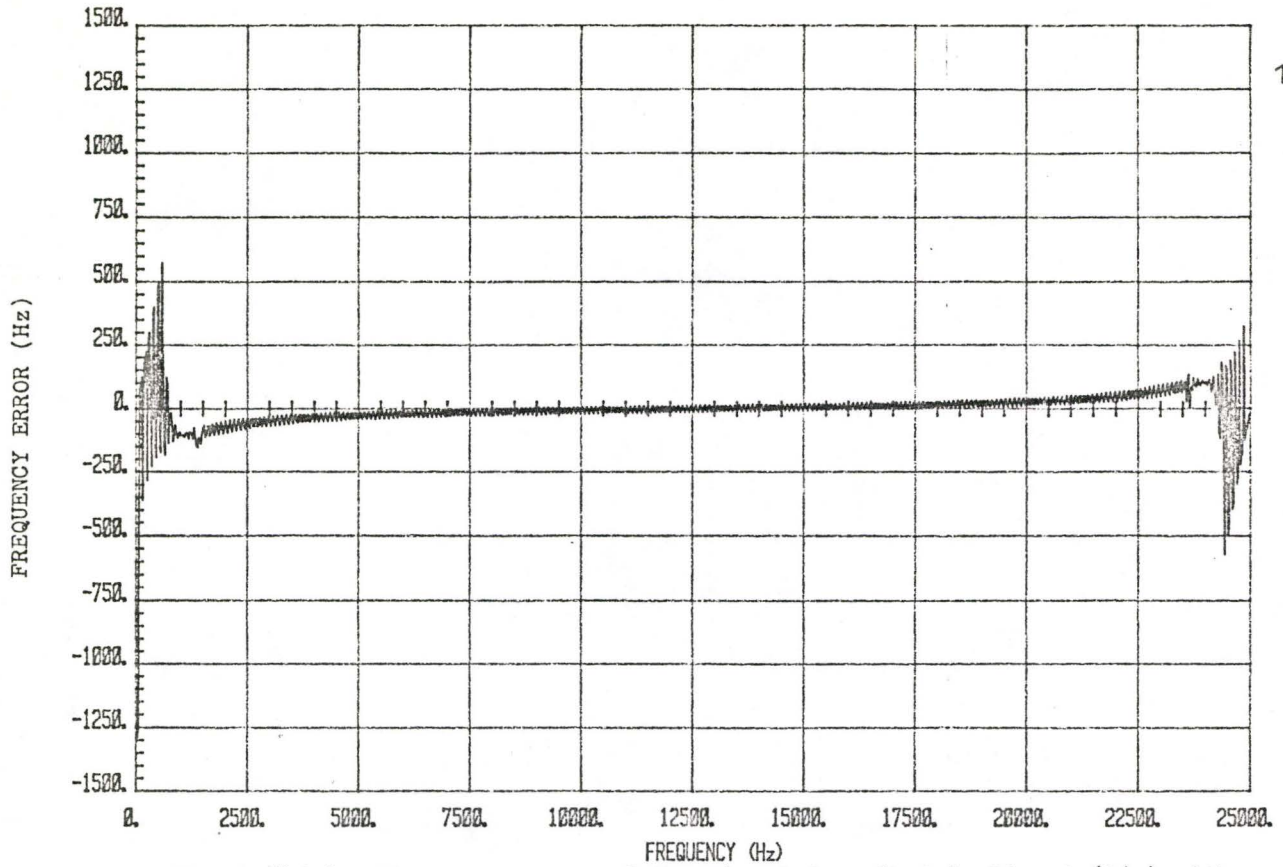


Fig. 3.64(a): The error curve of the signal described in Fig. 3.63(a) with the ACFMEM at filter order 2.

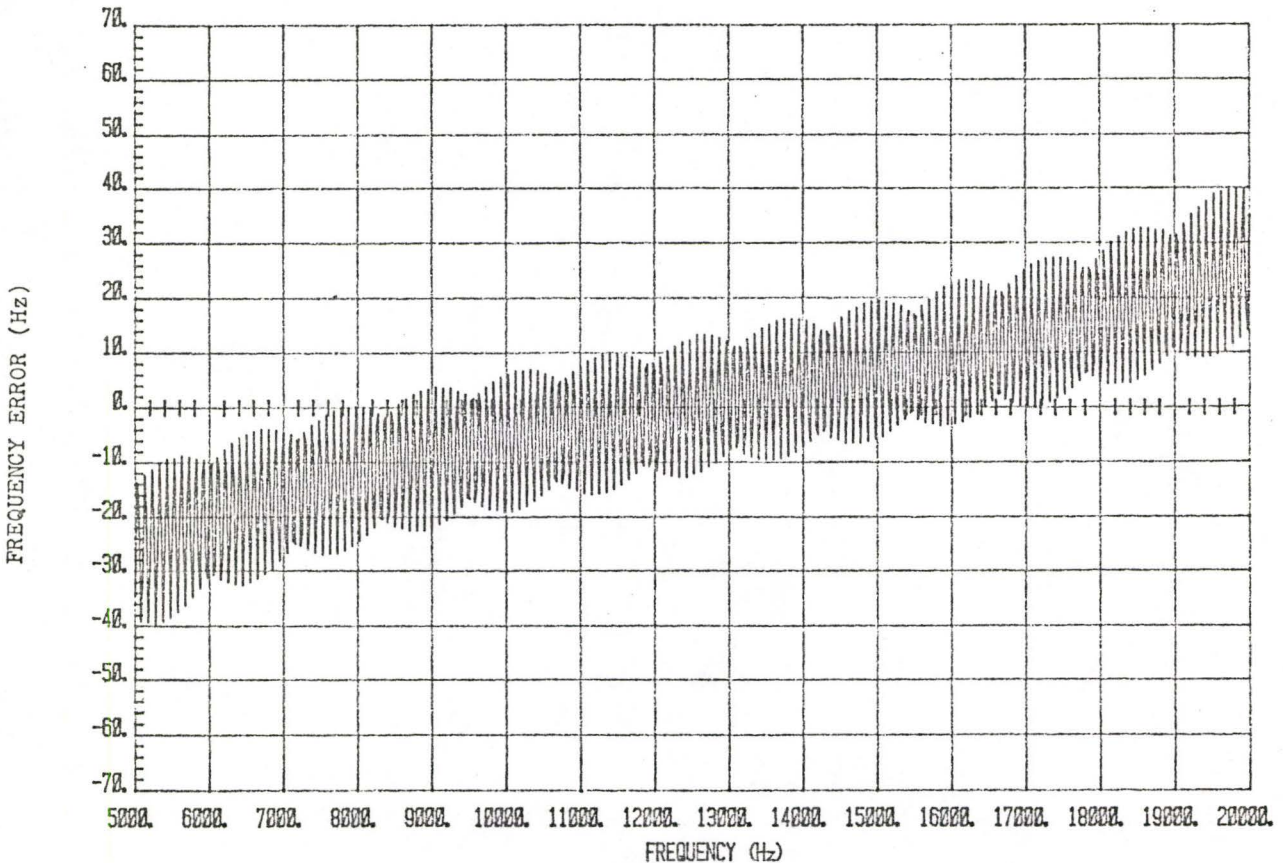


Fig. 3.64(b): An expanded view of the curve in Fig. 3.64(a).

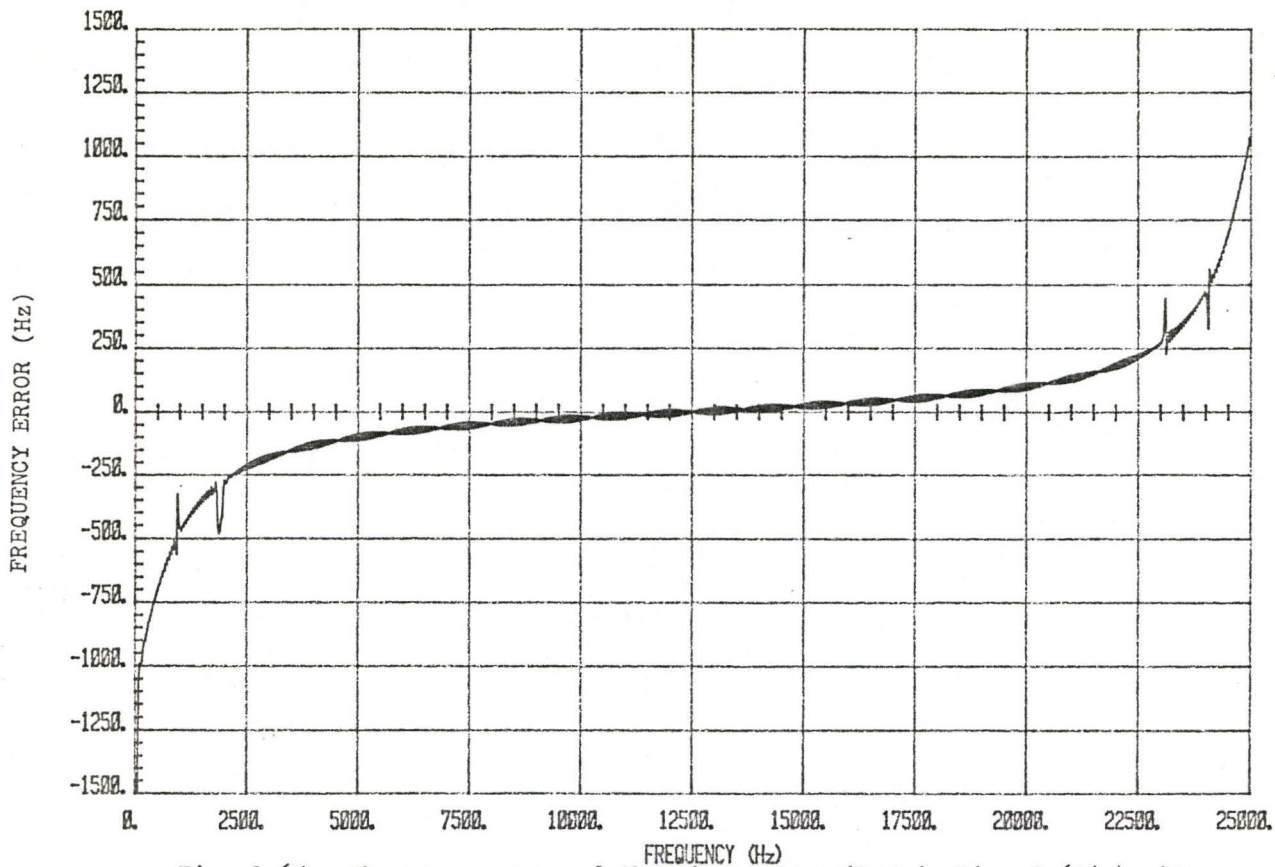


Fig. 3.65: The error curve of the signal described in Fig. 3.63(a) with quadratic frequency sweep and MEM at filter order 2.

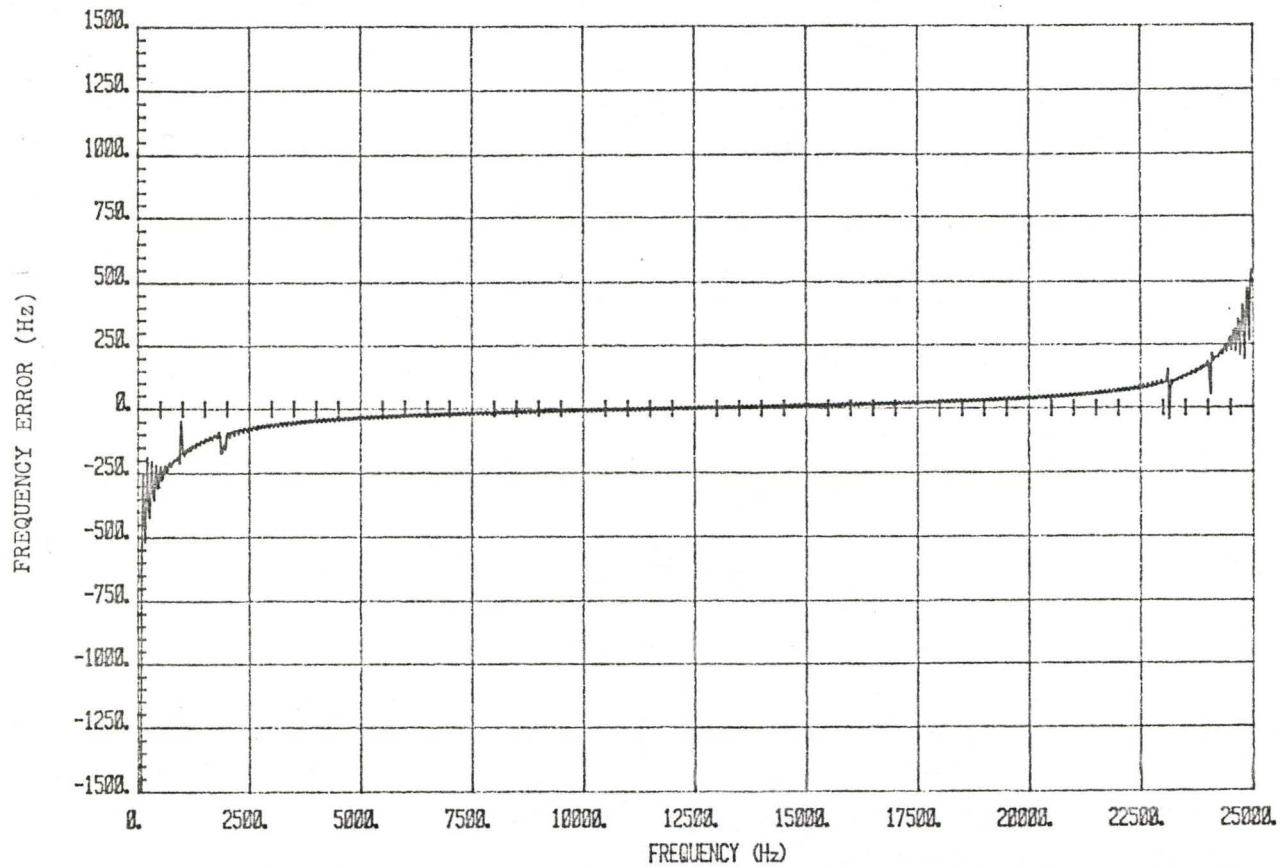


Fig. 3.66: The error curve of the signal described in Fig. 3.65 with the ACFMEM at filter order 2.

(in dB-Hz unit) is expressed by Eq. (2.34). We consider the values of 29 dB-Hz (-15 dB), 34 dB-Hz (-10 dB), 39 dB-Hz (-5 dB), 44 dB-Hz (0 dB) and 54 dB-Hz (10 dB) and two different carrier frequencies, namely 9237 Hz and 12832 Hz. Since the variation in spectral performance is insignificant between the linear and quadratic frequency sweeps, in the presentation we employ ELT signals with the former type only.

### 3.5.1 Pulse-Modulated, Continuous Phase

In order to provide a reference, Fig. 3.67 illustrates the spectrum obtained using the FFT when only noise is present. Fig. 3.68 to Fig. 3.71 show the FFT performance of a pulse-modulated signal (continuous phase) in the presence of different CNDR levels with carrier frequency 12832 Hz. At 34 dB-Hz, there are numerous sidelobes at above the -10 dB threshold level. The main peak, which is situated at 12793 Hz, is exceeded by the major sidelobes at 11426 Hz and 14260 Hz. The number of sidelobes decreases as the CNDR increases. However, the main peak is still dominated by the major sidelobes.

Changing the carrier frequency to 9237 Hz, the FFT spectrum produces a peak near the correct frequency as shown by Fig. 3.72, for 34 dB-Hz. Reducing the CNDR to a level of 29 dB-Hz causes severe degradation in signal detection, as shown in Fig. 3.73.

A Kaiser window ( $\beta=8.0$ ) is applied to the noisy signal having carrier frequency 12832 Hz. The spectra are given in Fig. 3.74 to Fig. 3.77. Windowing technique does not improve the frequency resolution at low value of CNDR.

To compare the MEM process with the FFT process, we first plot

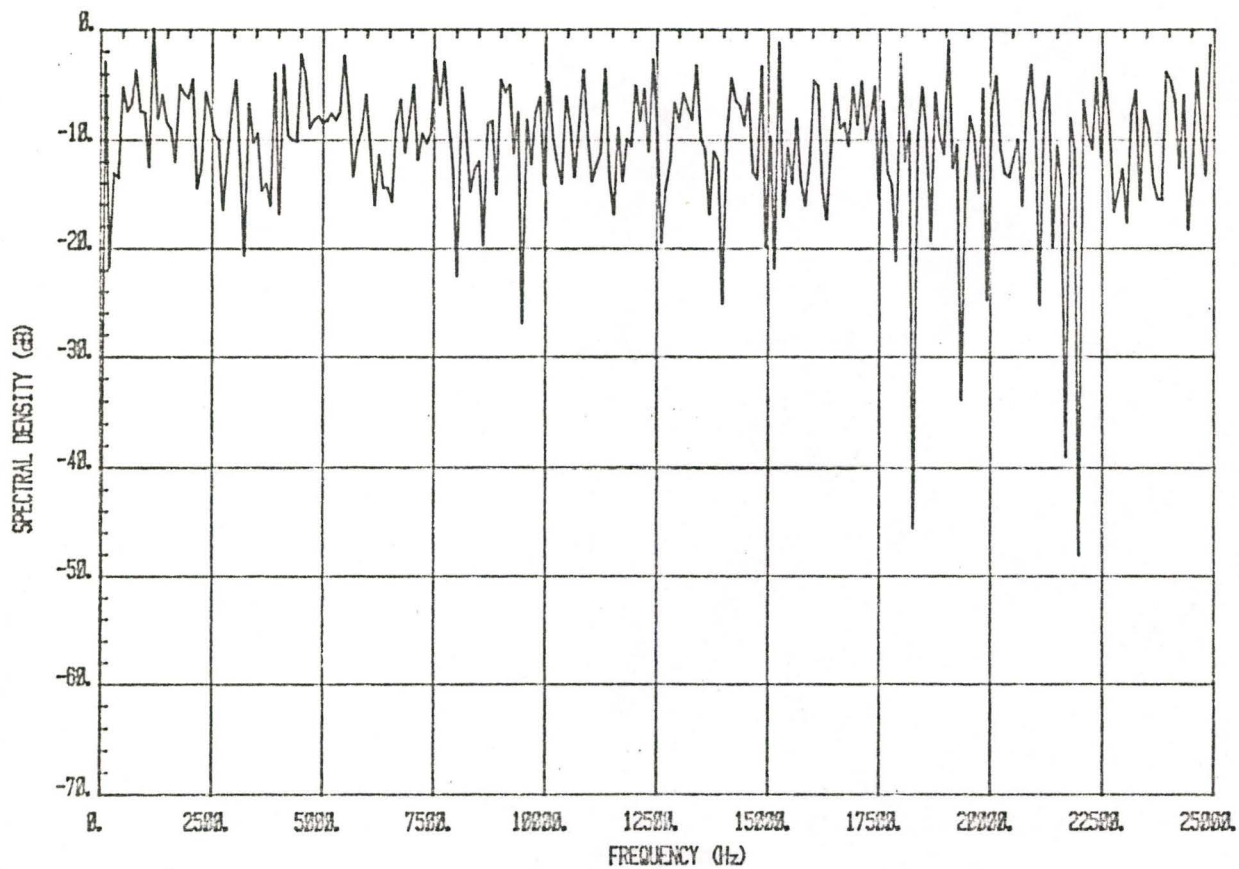


Fig. 3.67: The FFT spectrum when only noise is present.

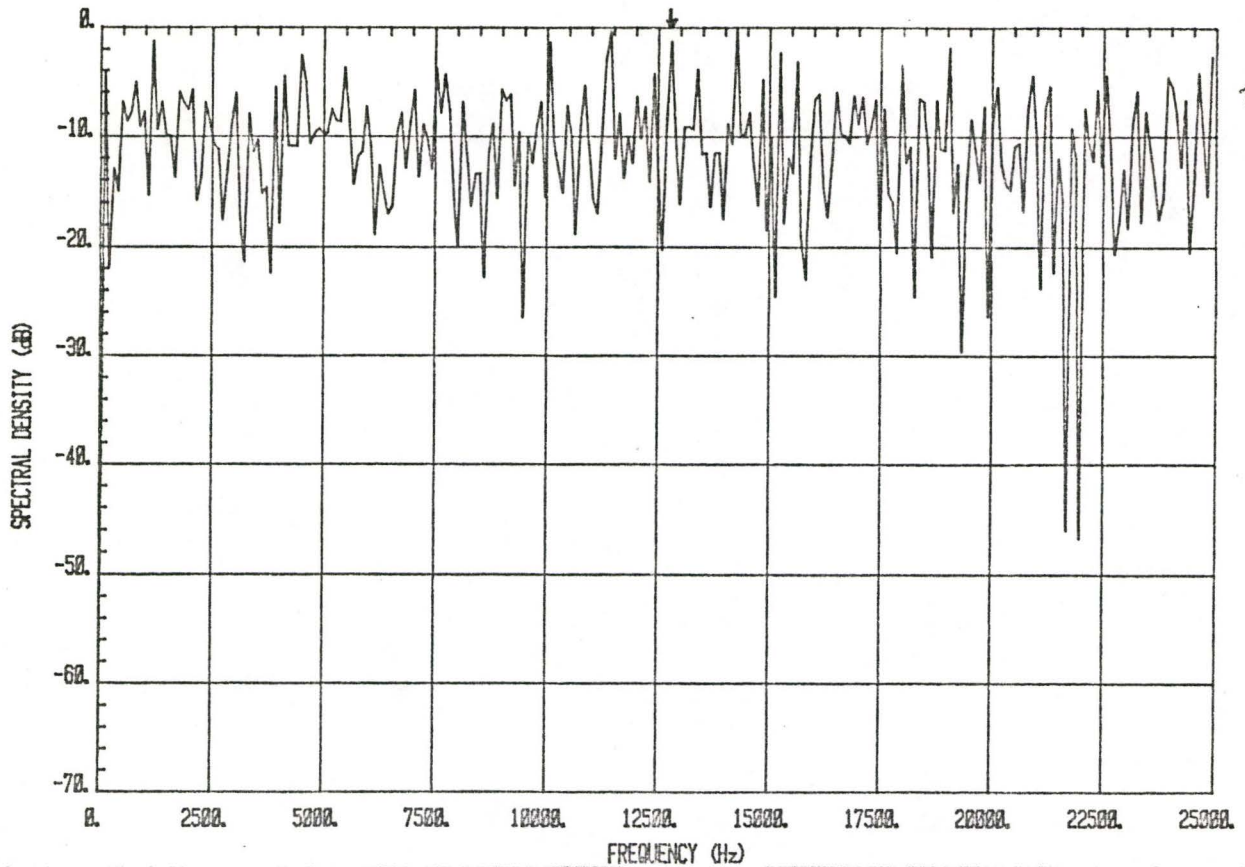


Fig. 3.68: The FFT spectrum of a continuous phase signal with carrier frequency=12832 Hz and CNDR=34 dB-Hz.

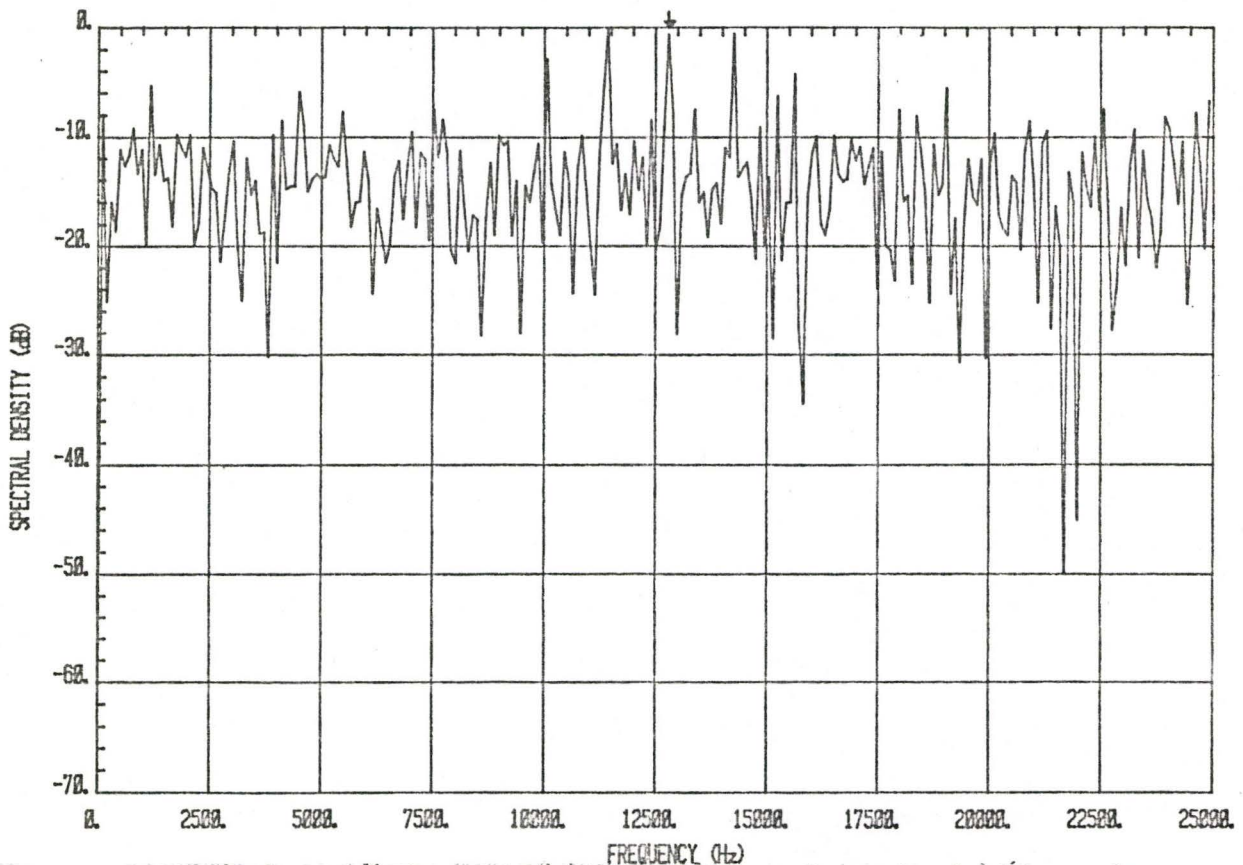


Fig. 3.69: The FFT spectrum of a continuous phase signal with carrier frequency=12832 Hz and CNDR=39 dB-Hz.

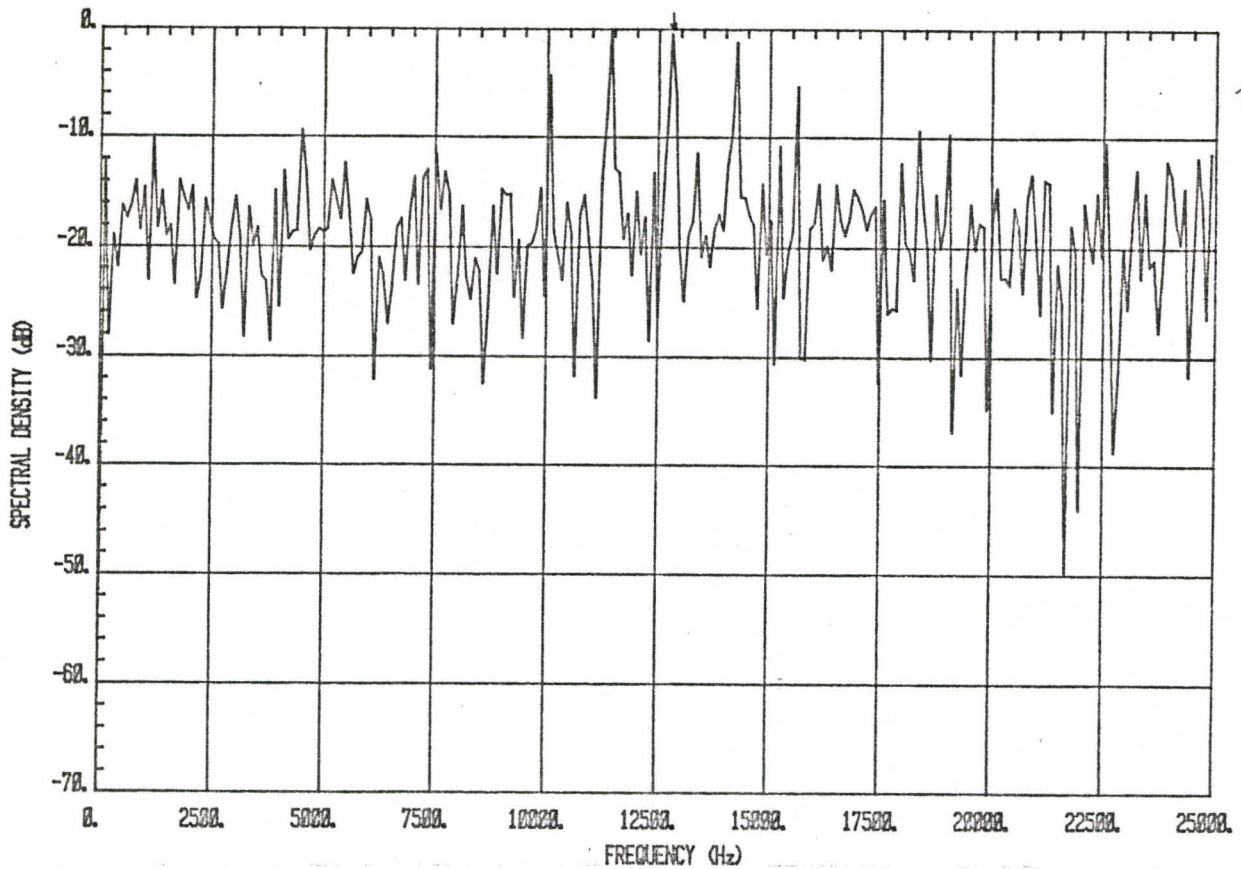


Fig. 3.70: The FFT spectrum of a continuous phase signal with carrier frequency=12832 Hz and CNDR=44 dB-Hz.

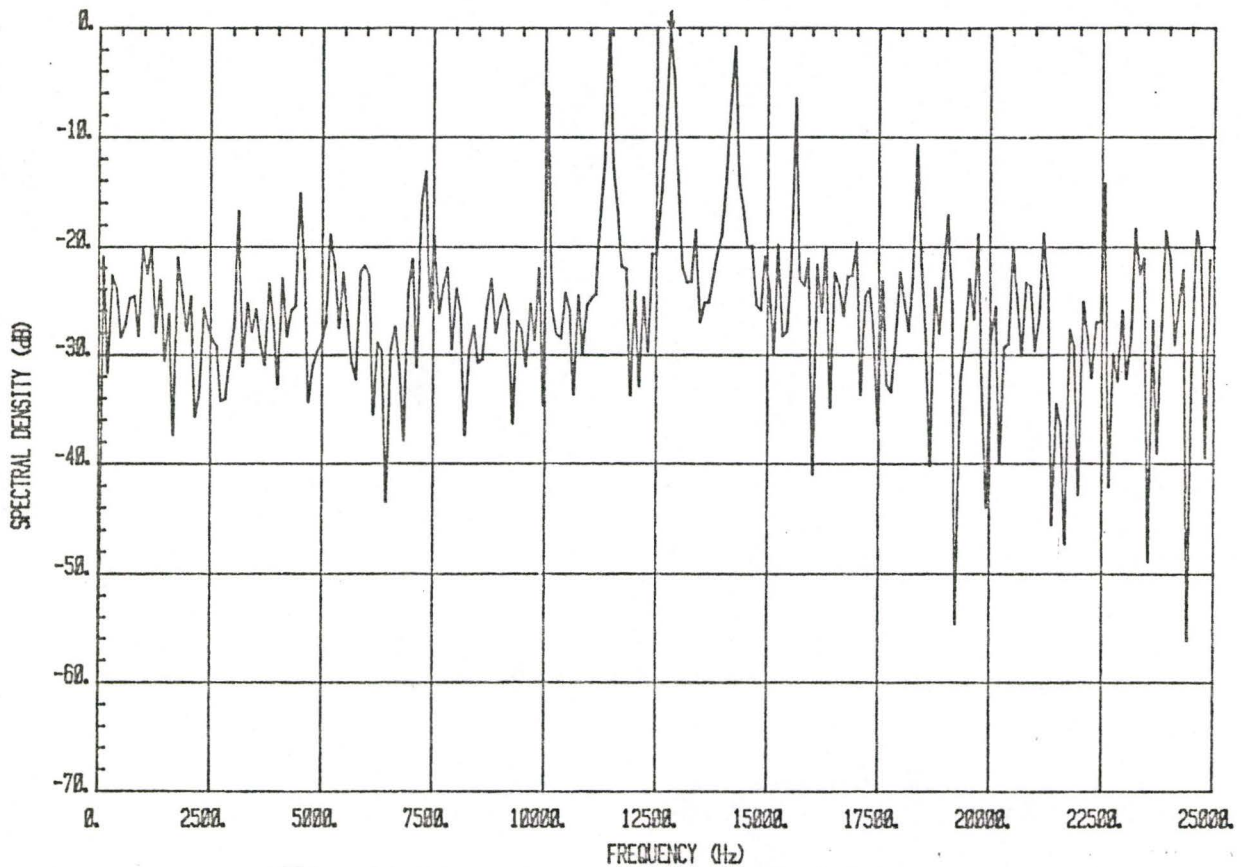


Fig. 3.71: The FFT spectrum of a continuous phase signal with carrier frequency=12832 Hz and CNDR=54 dB-Hz.

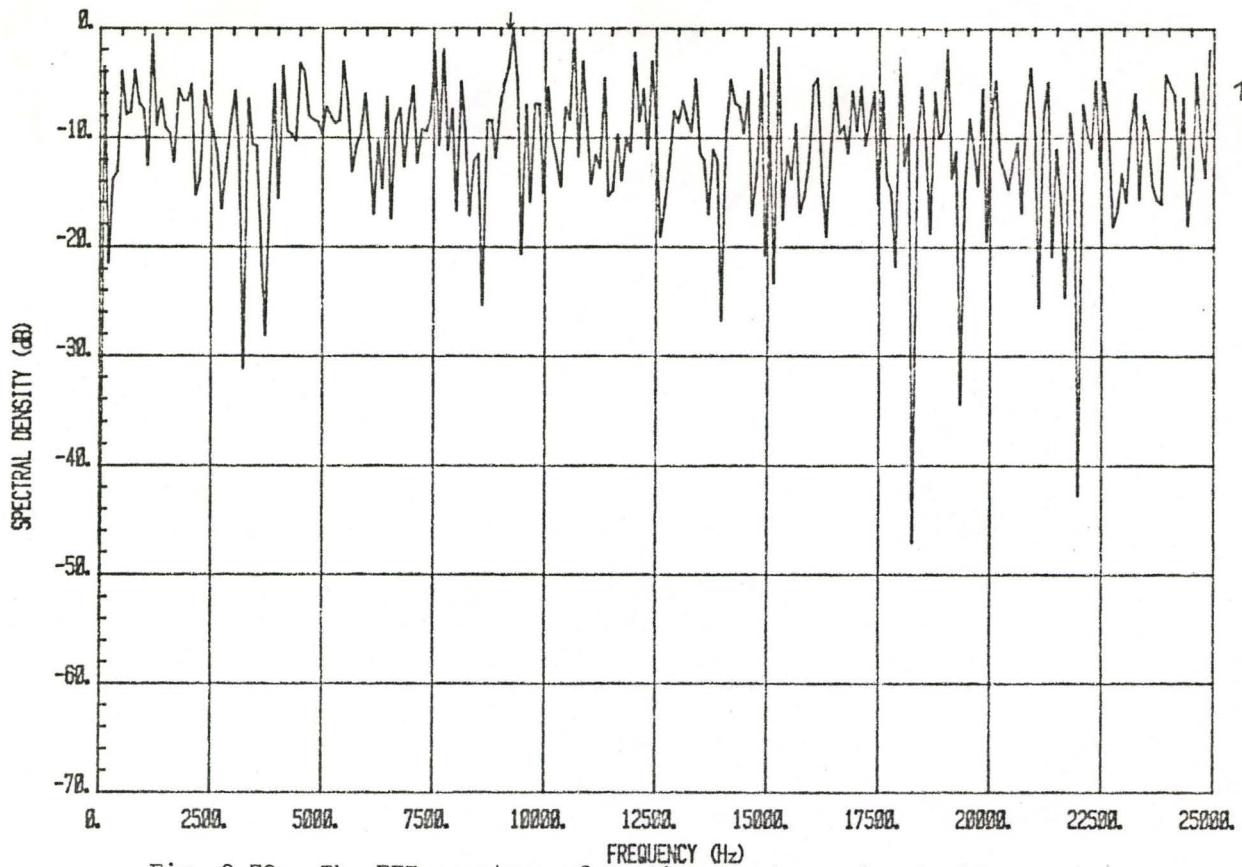


Fig. 3.72: The FFT spectrum of continuous phase signal with carrier frequency=9237 Hz and CNDR=34 dB-Hz.

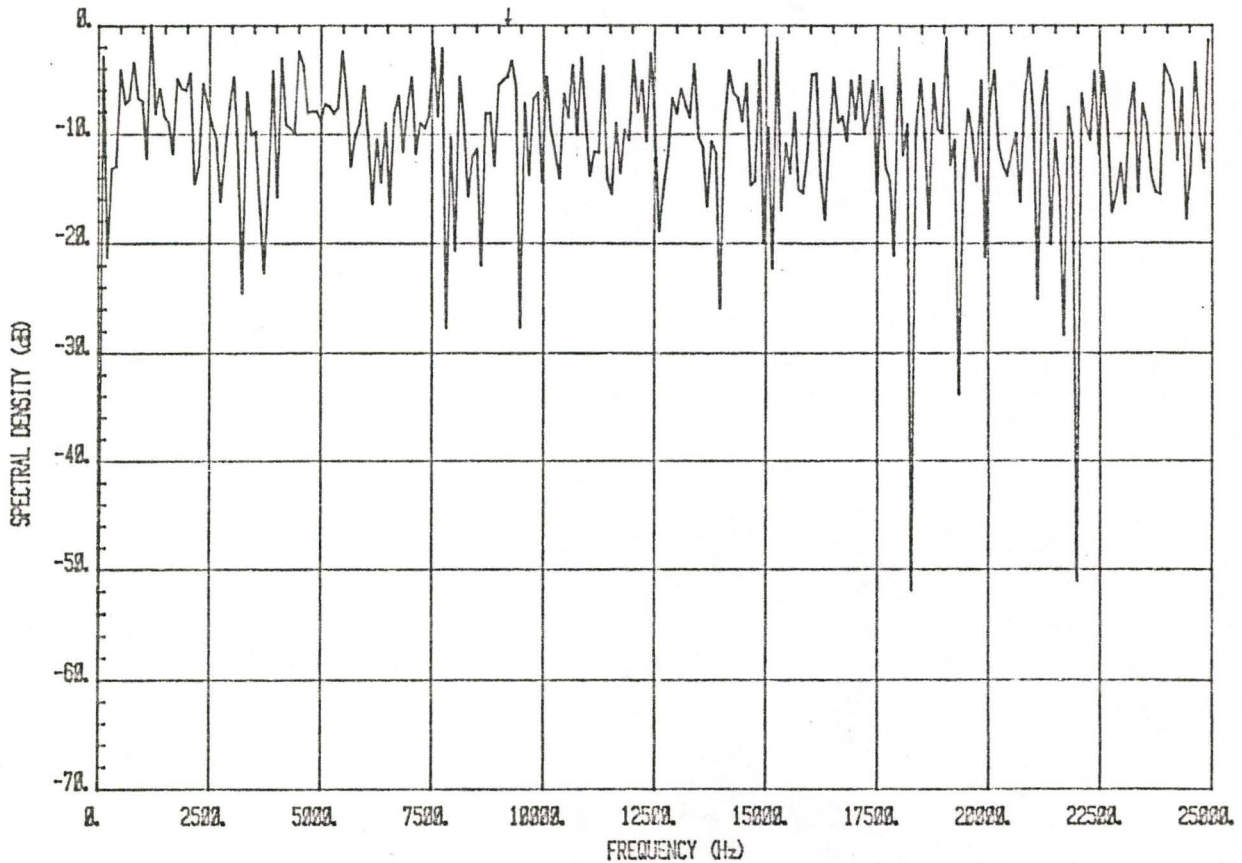


Fig. 3.73: The FFT spectrum of continuous phase signal with carrier frequency=9237 Hz and CNDR=29 dB-Hz.

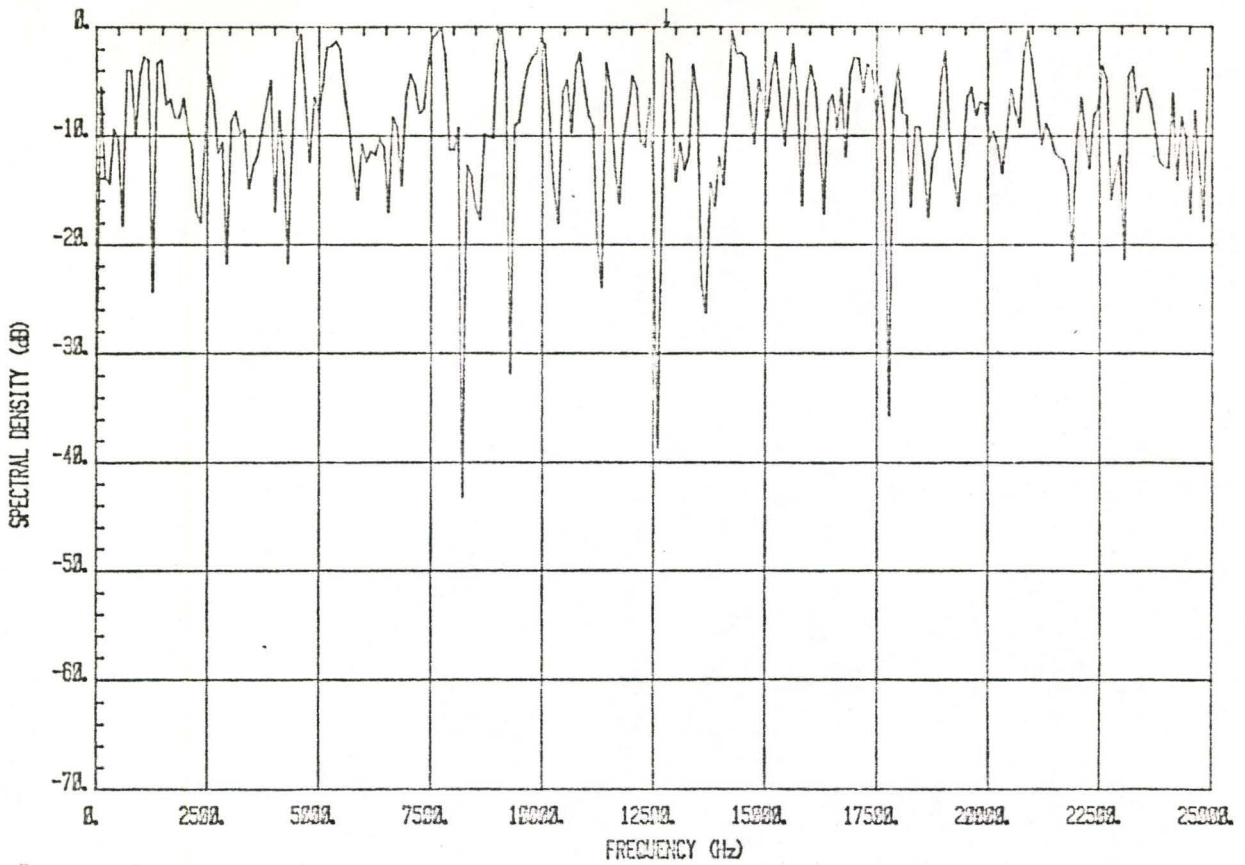


Fig. 3.74: The FFT spectrum of a windowed continuous phase signal with carrier frequency=12832 Hz and CNDR=34 dB-Hz.

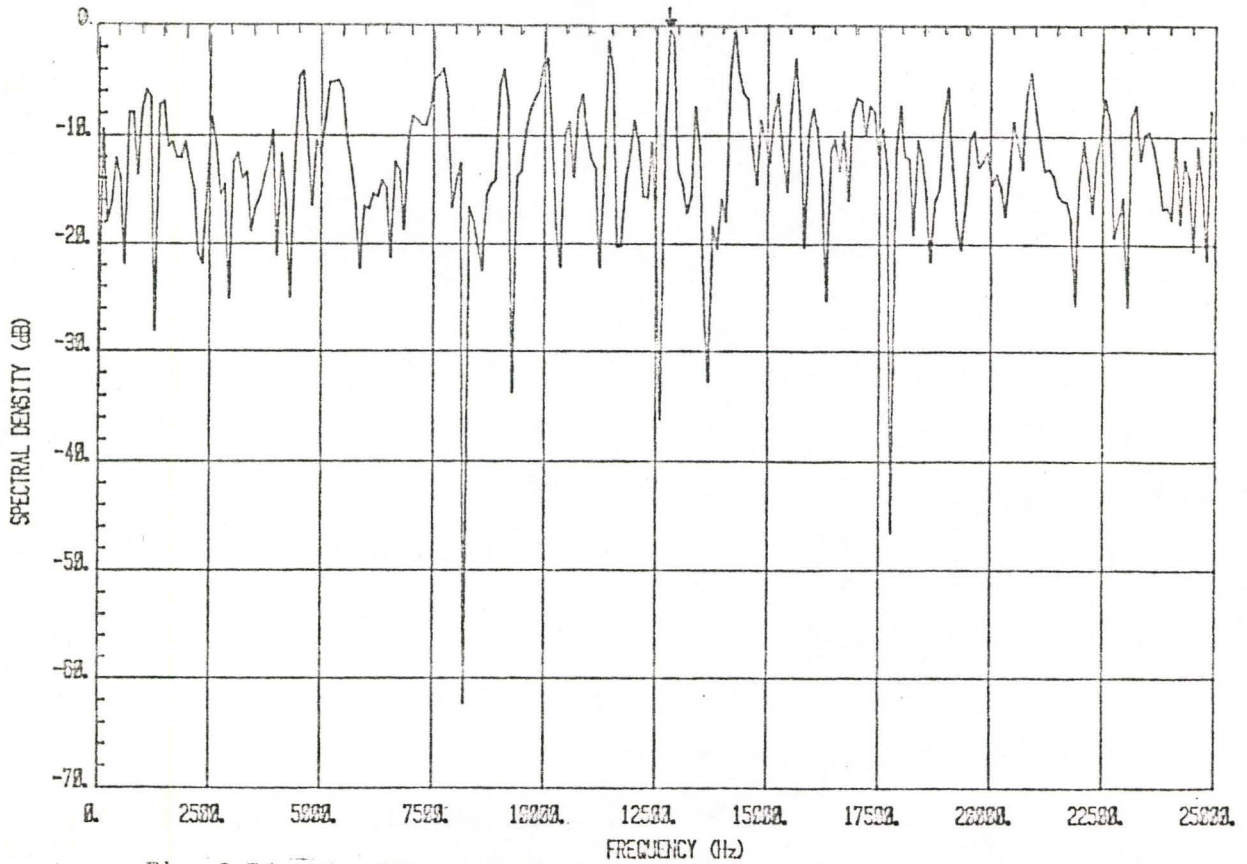


Fig. 3.75: The FFT spectrum of a windowed continuous phase signal with carrier frequency=12832 Hz and CNDR=39 dB-Hz.

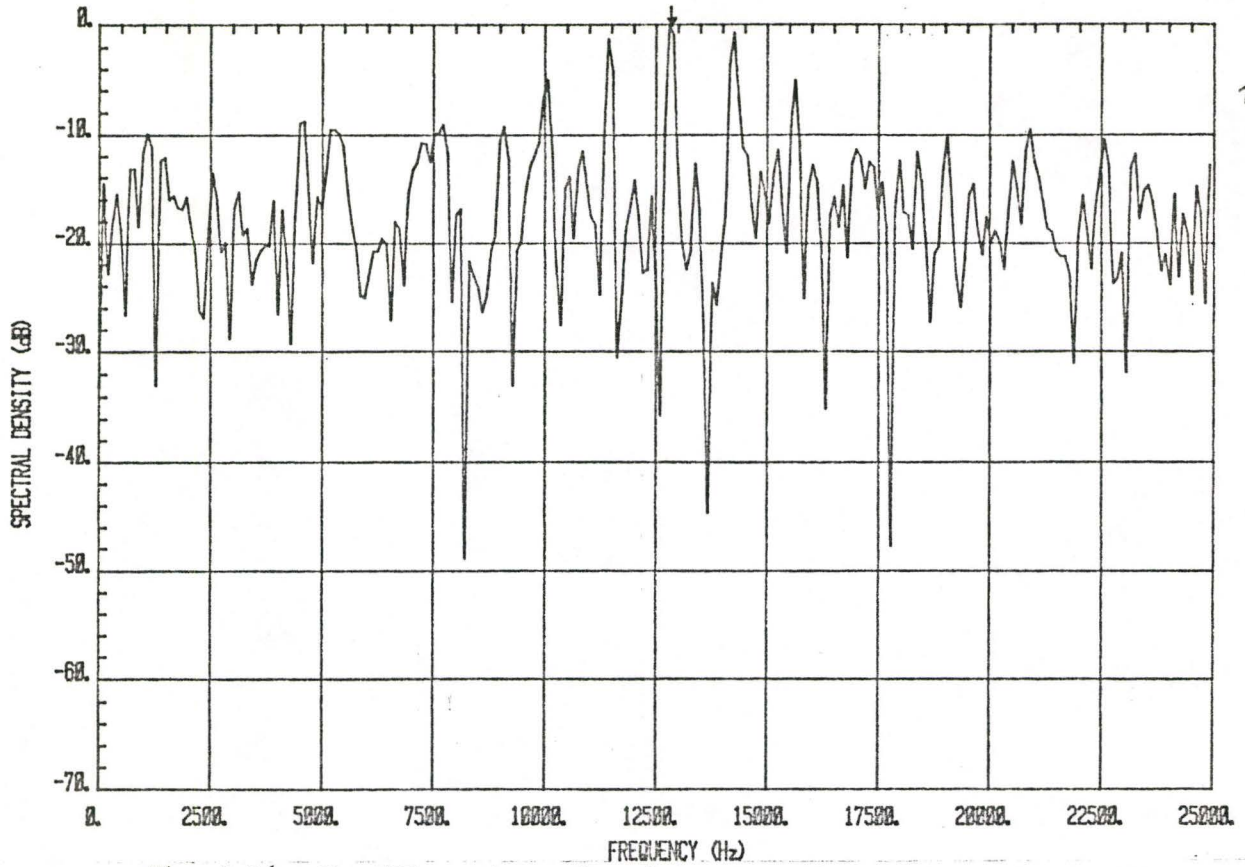


Fig. 3.76: The FFT spectrum of a windowed continuous phase signal with carrier frequency=12832 Hz and CNDR=44 dB-Hz.

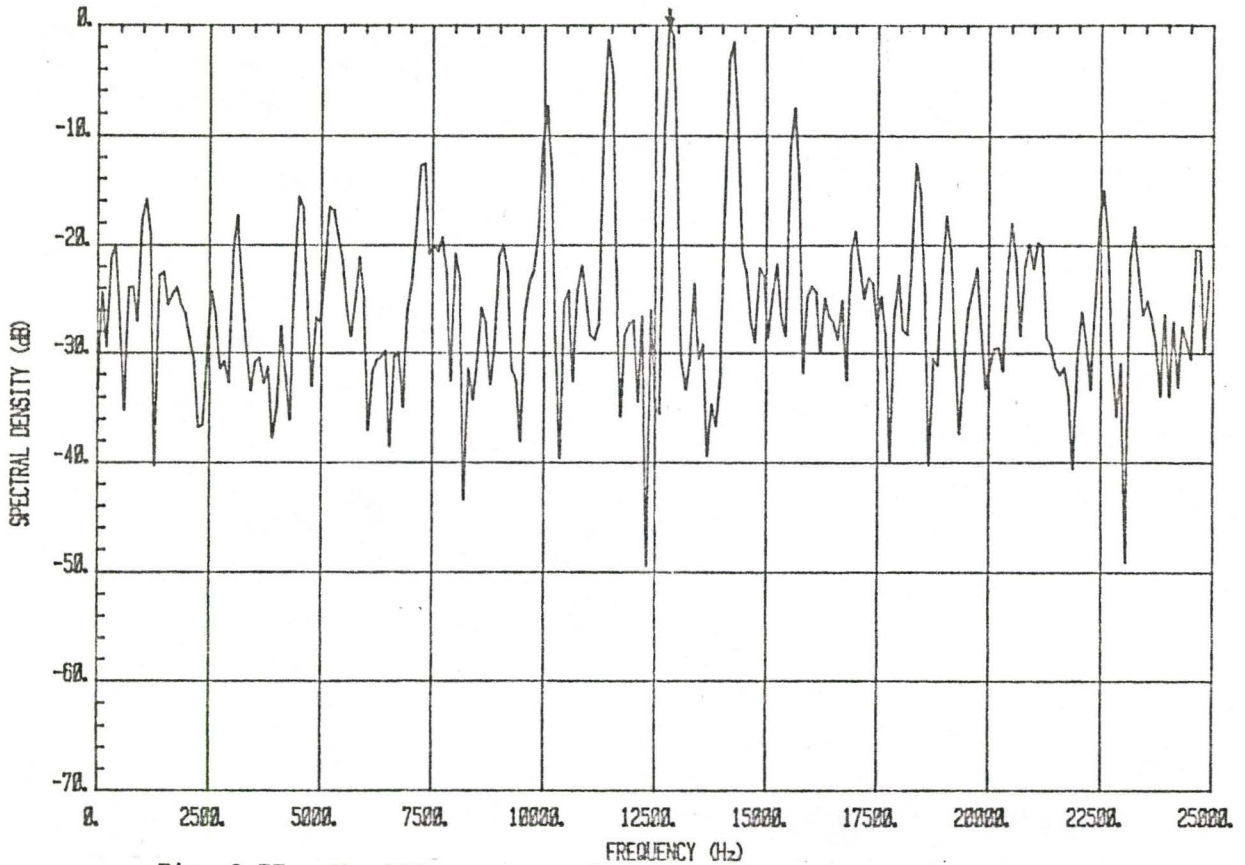


Fig. 3.77: The FFT spectrum of a windowed continuous phase signal with carrier frequency=12832 Hz and CNDR=54 dB-Hz.

the MEM spectra when only noise is present, as shown in Fig. 3.78. This can be compared to the FFT process of Fig. 3.67 without the bandpass filter and Fig. 3.79 with the bandpass filter. Using first a second order MEM, we plot the spectra for the four configurations described in Section 3.3, using CNDR increasing from 34 dB-Hz to 54 dB-Hz. Fig. 3.80 to Fig. 3.83 illustrate the curves for a signal frequency of 12832 Hz.

We now select a new carrier frequency of 9237 Hz and plot the spectra for CNDR varying from 29 dB-Hz to 54 dB-Hz with MEM filter order 2. The results seen in Fig. 3.84 to Fig. 3.88 demonstrate a serious problem at low CNDR since the frequency estimate is now affected by signal strength. This problem with the low order MEM processor may be resolved, however, by using a higher order MEM = 10 process, as shown in Fig. 3.89. Note that all four processes give an indication of carrier frequency with 34 dB-Hz CNDR. At 54 dB-Hz, the frequency estimate is further enhanced as illustrated in Fig. 3.90.

### 3.5.2 Pulse-Modulated, Random Phase

Fig. 3.91 to Fig. 3.94 illustrate the FFT spectral estimate as the CNDR is increased from 34 dB-Hz to 54 dB-Hz with frequency 12832 Hz. Note that measurement of the carrier frequency is difficult at all values of CNDR since there are many peaks to choose from.

Changing the frequency to 9237 produces a peak near the correct frequency, as shown in Fig. 3.95 for CNDR = 34 dB-Hz. However, decreasing the CNDR to 29 dB-Hz essentially eliminates detection (Fig. 3.96).

Results for the second order MEM process are again plotted at

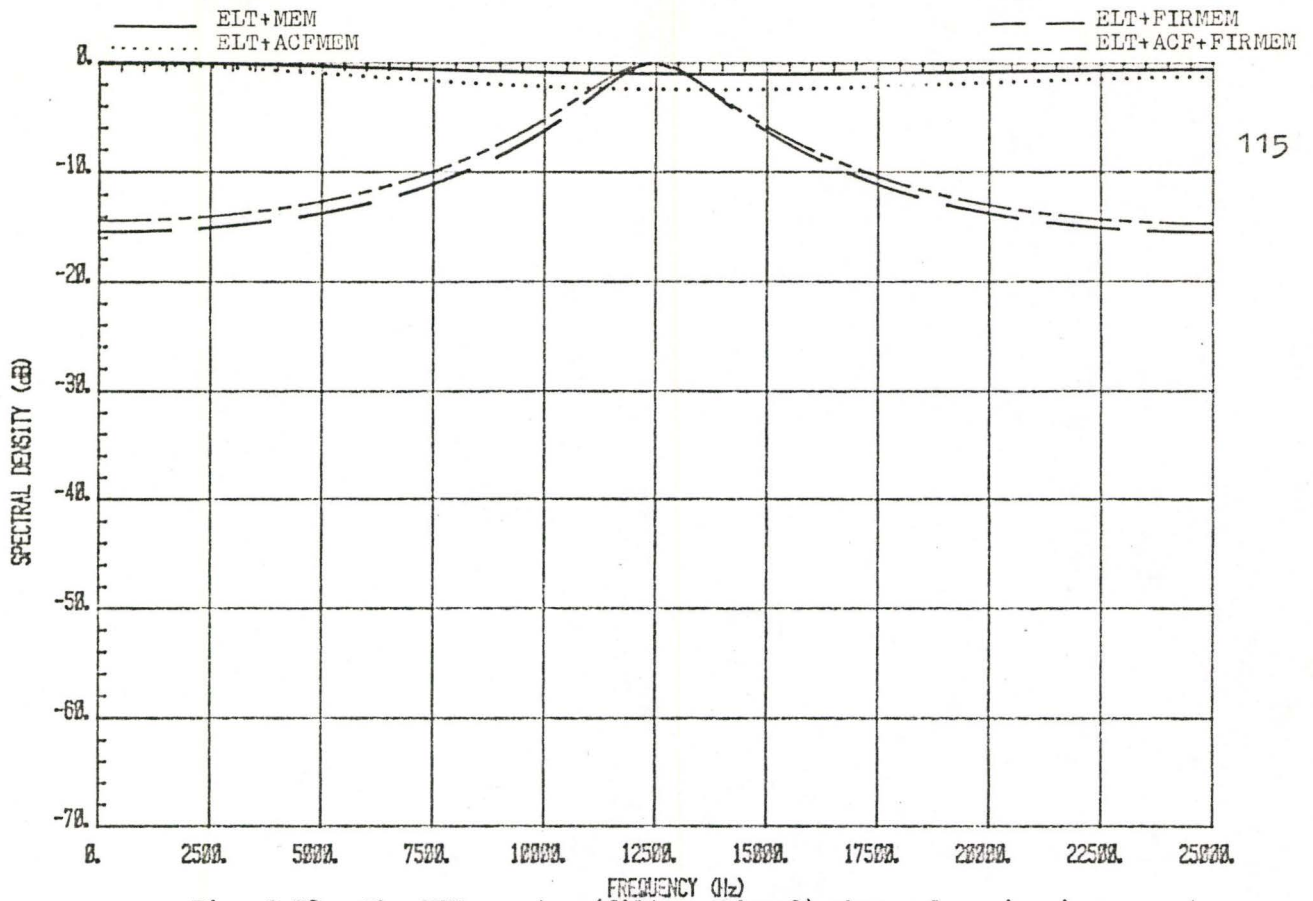


Fig. 3.78: The MEM spectra (filter order 2) when only noise is present.

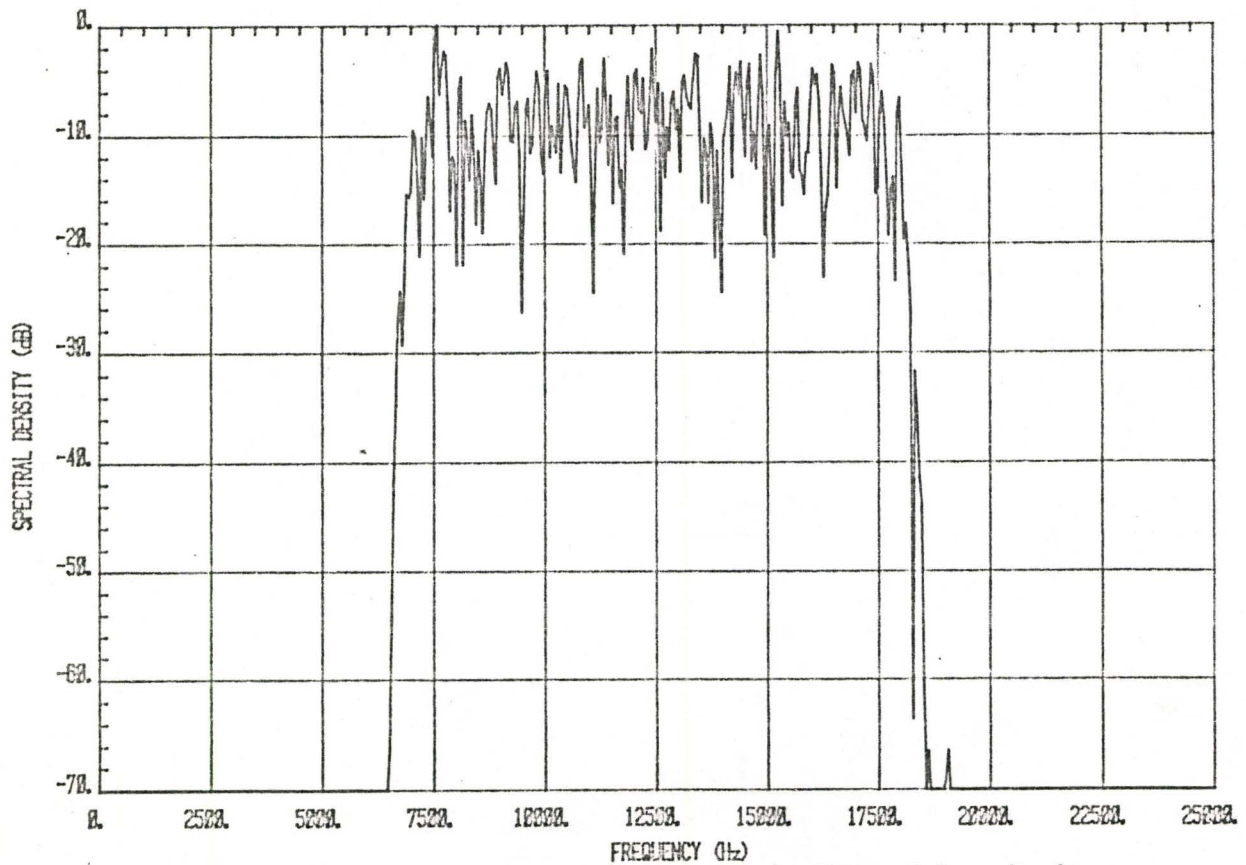


Fig. 3.79: The FFT spectrum when noise is filtered by a bandpass filter.

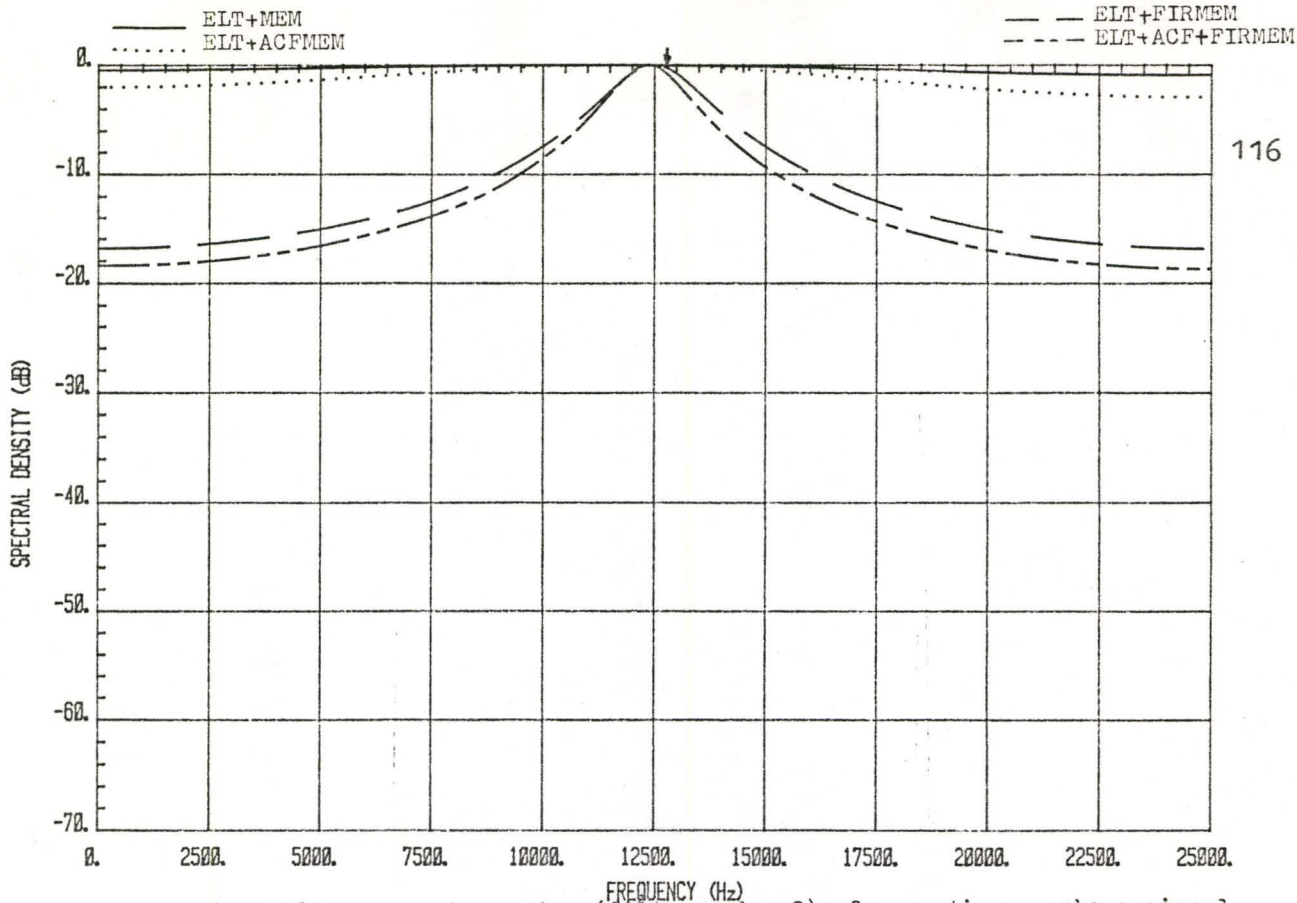


Fig. 3.80: The MEM spectra (filter order 2) of a continuous phase signal with carrier frequency=12832 Hz and CNDR=34 dB-Hz.

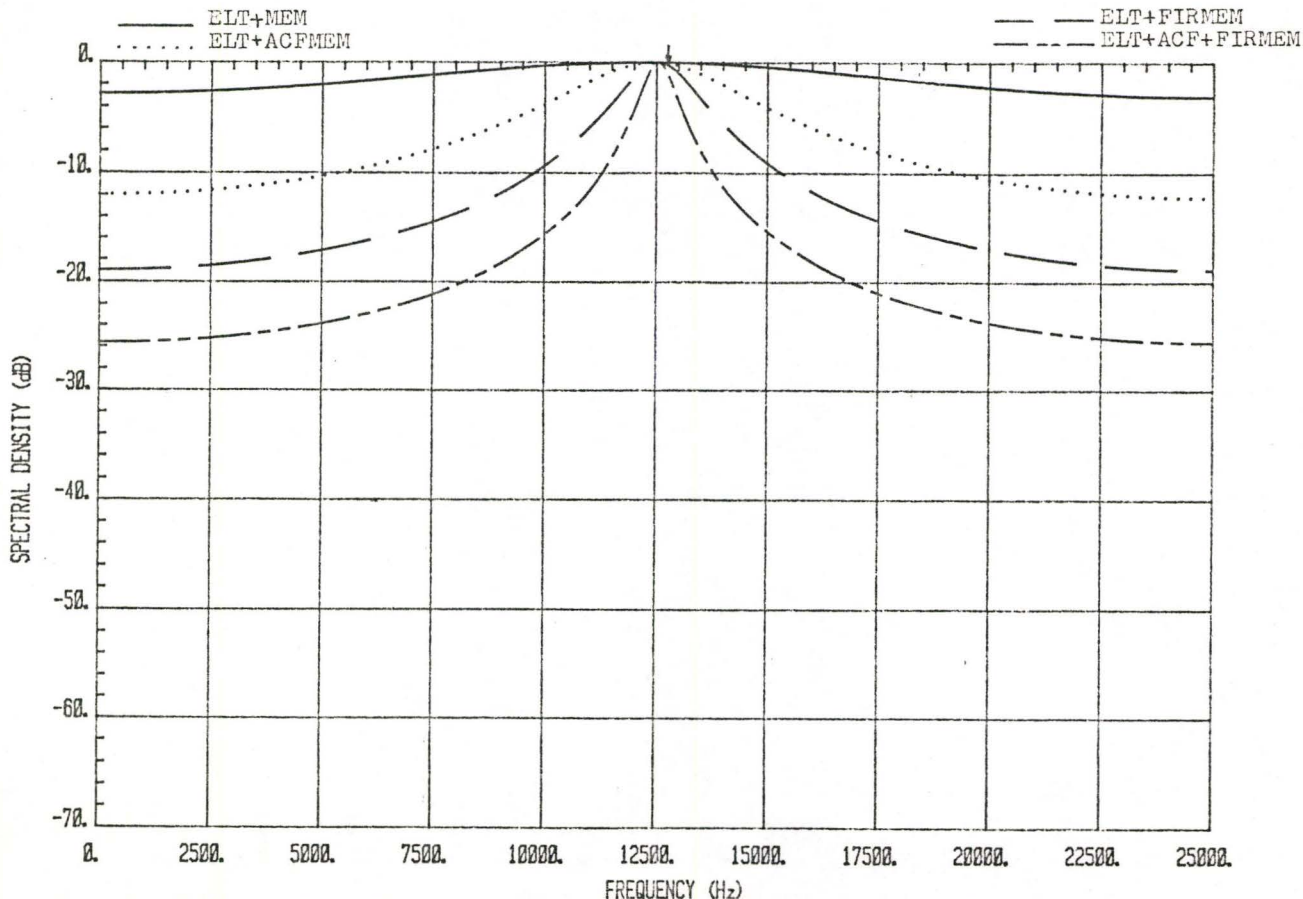


Fig. 3.81: The MEM spectra (filter order 2) of a continuous phase signal with carrier frequency=12832 Hz and CNDR=39 dB-Hz.

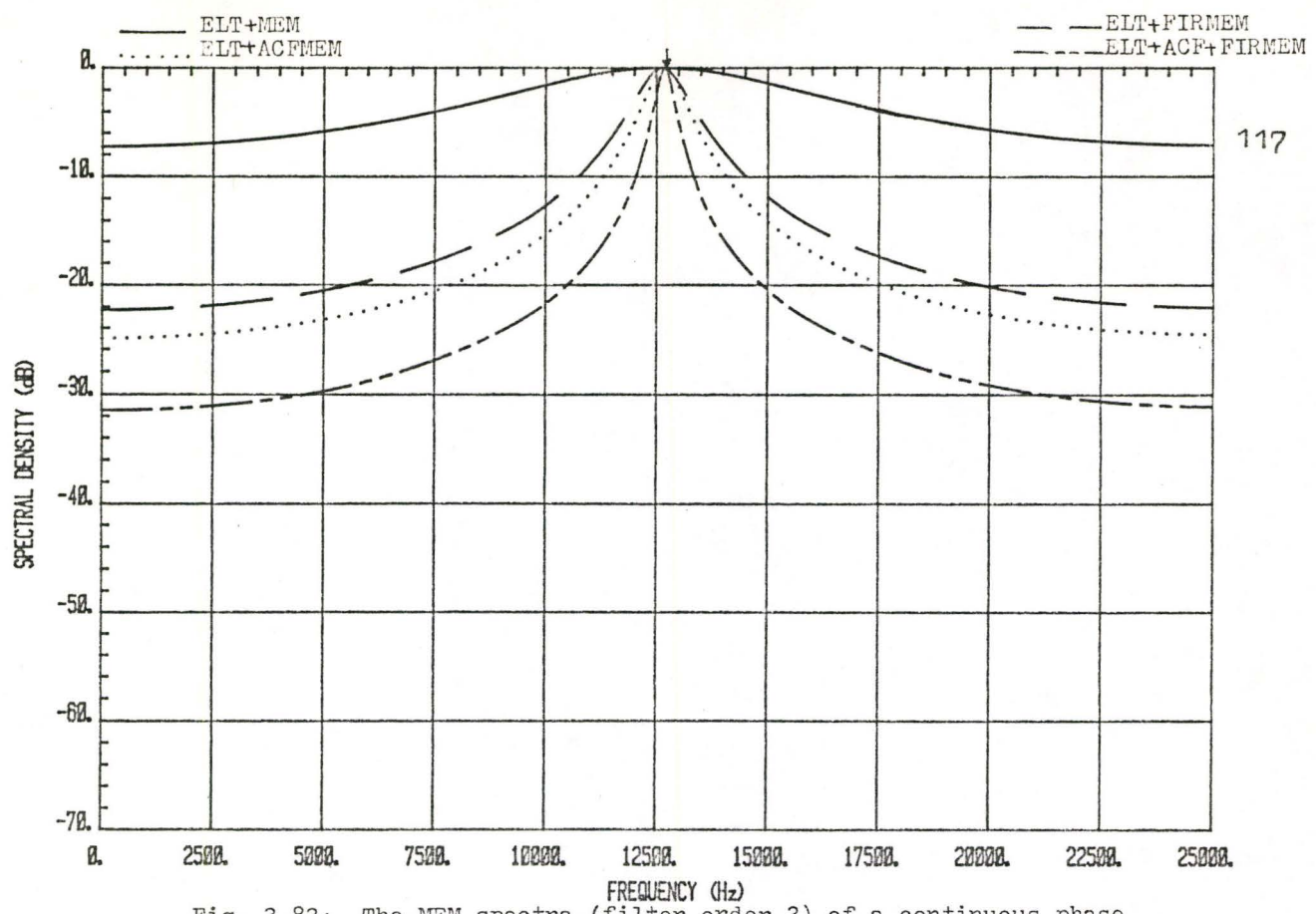


Fig. 3.82: The MEM spectra (filter order 2) of a continuous phase signal with carrier frequency=12832 Hz and CNDR=44 dB-Hz.

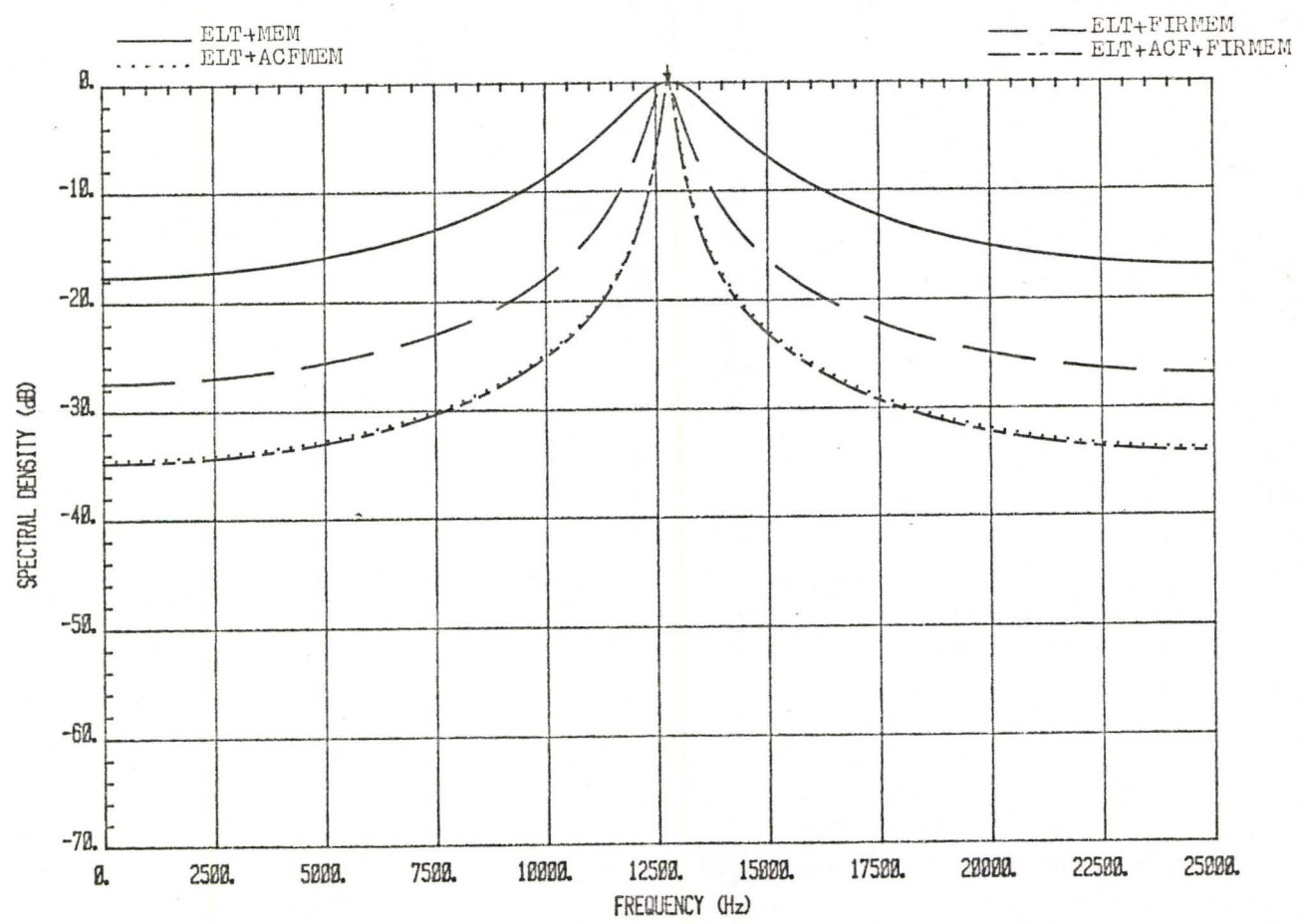


Fig. 3.83: The MEM spectra (filter order 2) of a continuous phase signal with carrier frequency=12832 Hz and CNDR=54 dB-Hz.

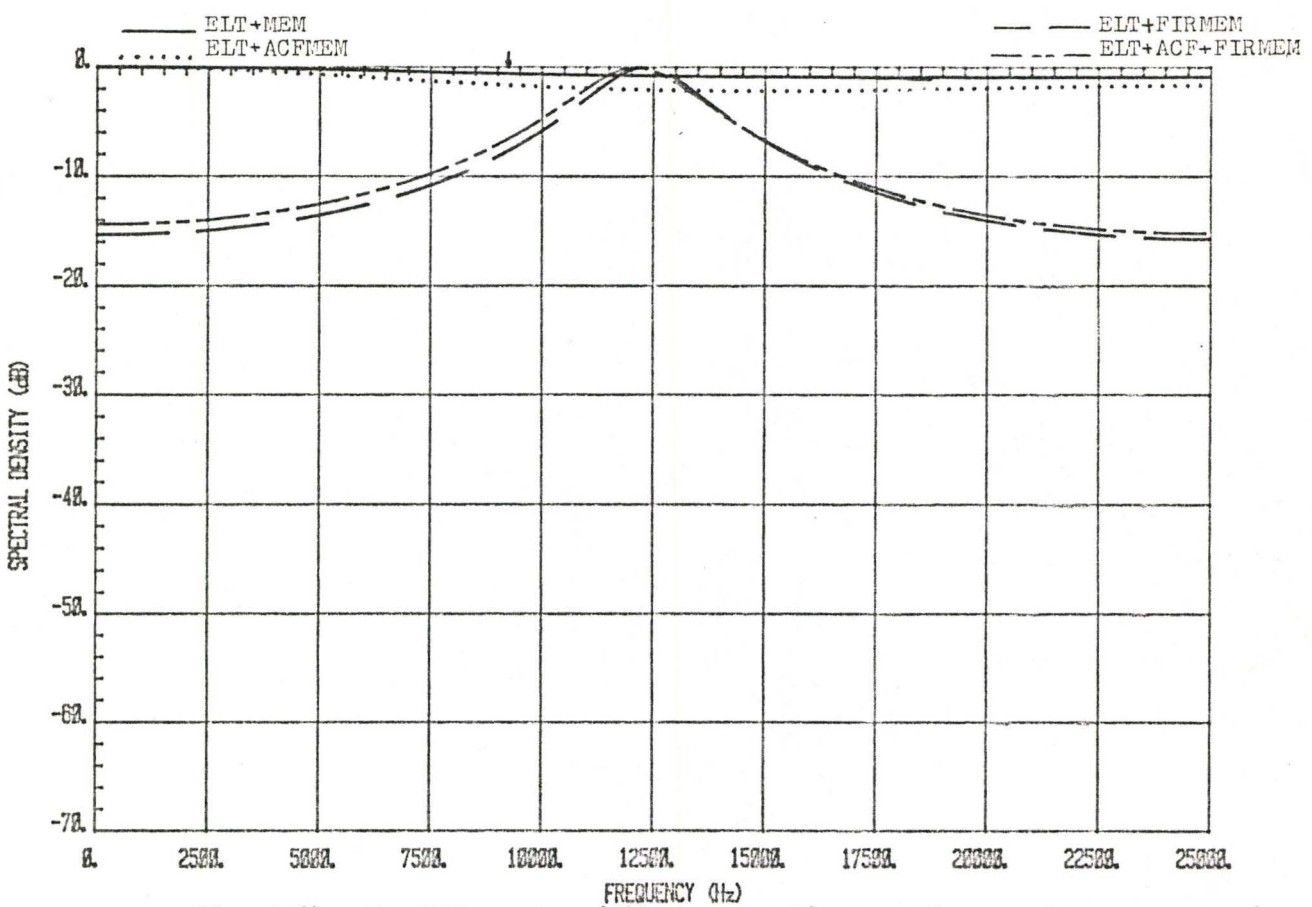


Fig. 3.84: The MEM spectra (filter order 2) of continuous phase signal with carrier frequency=9237 Hz and CNDR=29 dB-Hz.

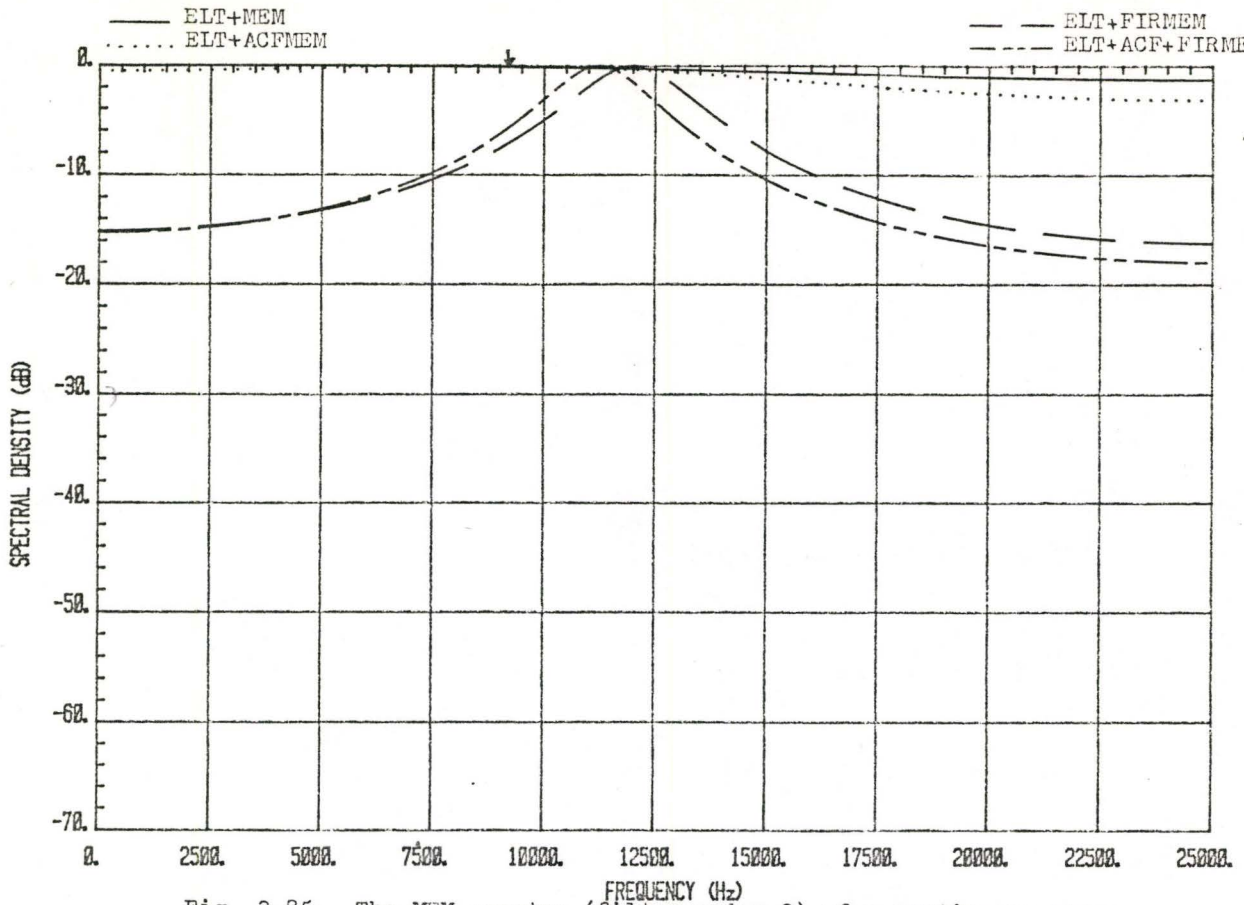


Fig. 3.85: The MEM spectra (filter order 2) of a continuous phase signal with carrier frequency=9237 Hz and CNDR=34 dB-Hz.

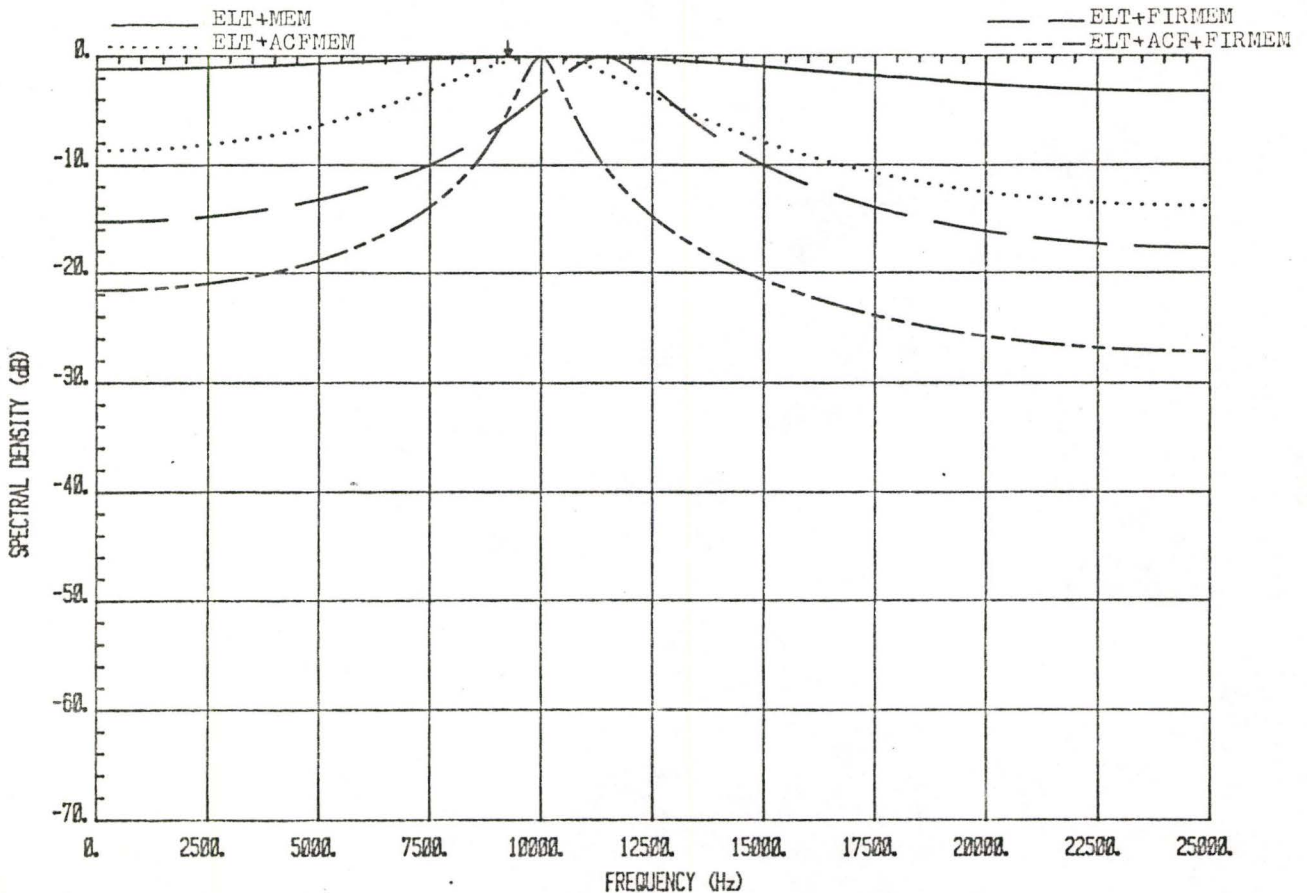


Fig. 3.86: The MEM spectra (filter order 2) of a continuous phase signal with carrier frequency=9237 Hz and CNDR=39 dB-Hz.

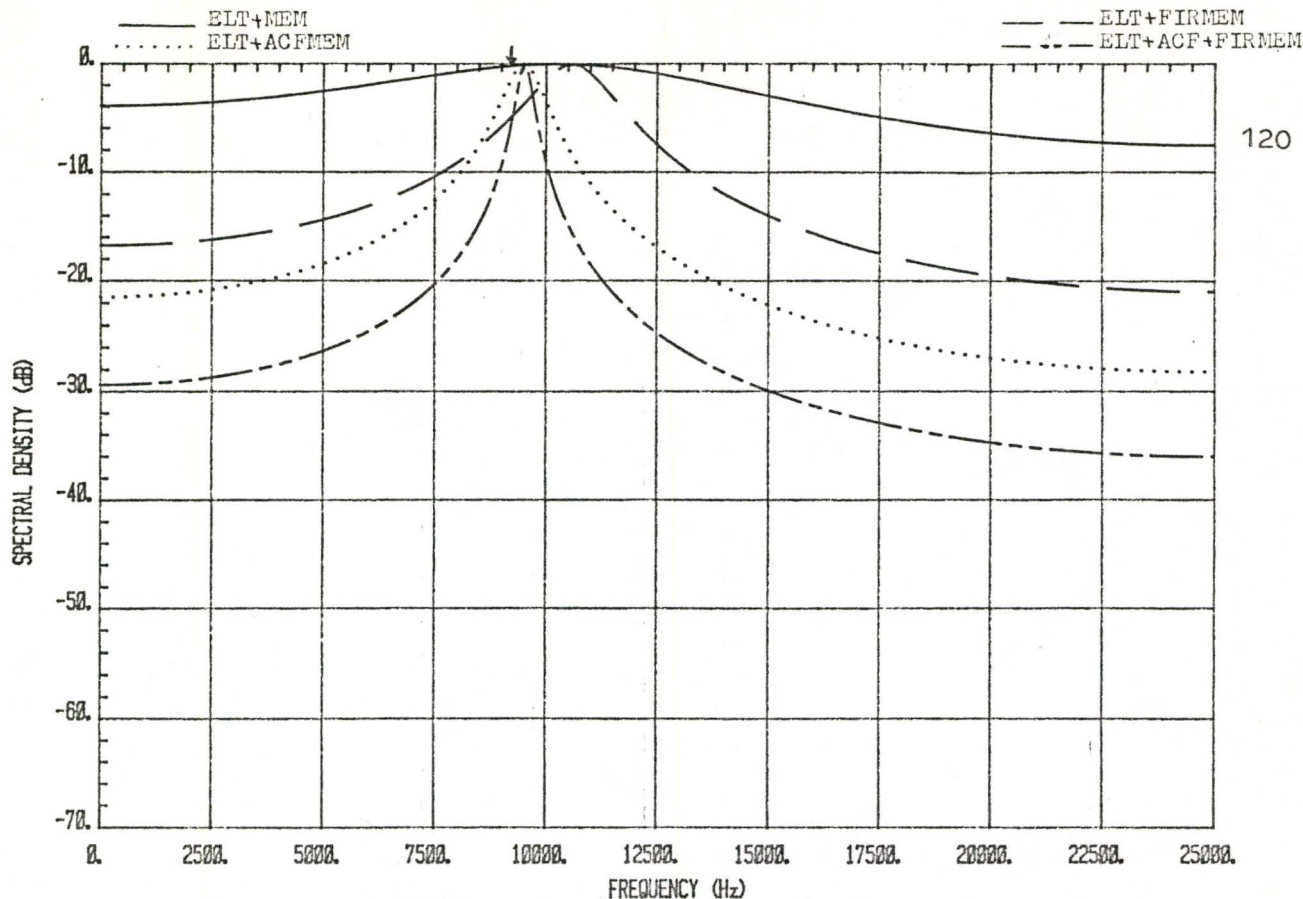


Fig. 3.87: The MEM spectra (filter order 2) of a continuous phase signal with carrier frequency=9237 Hz and CNDR=44 dB-Hz.

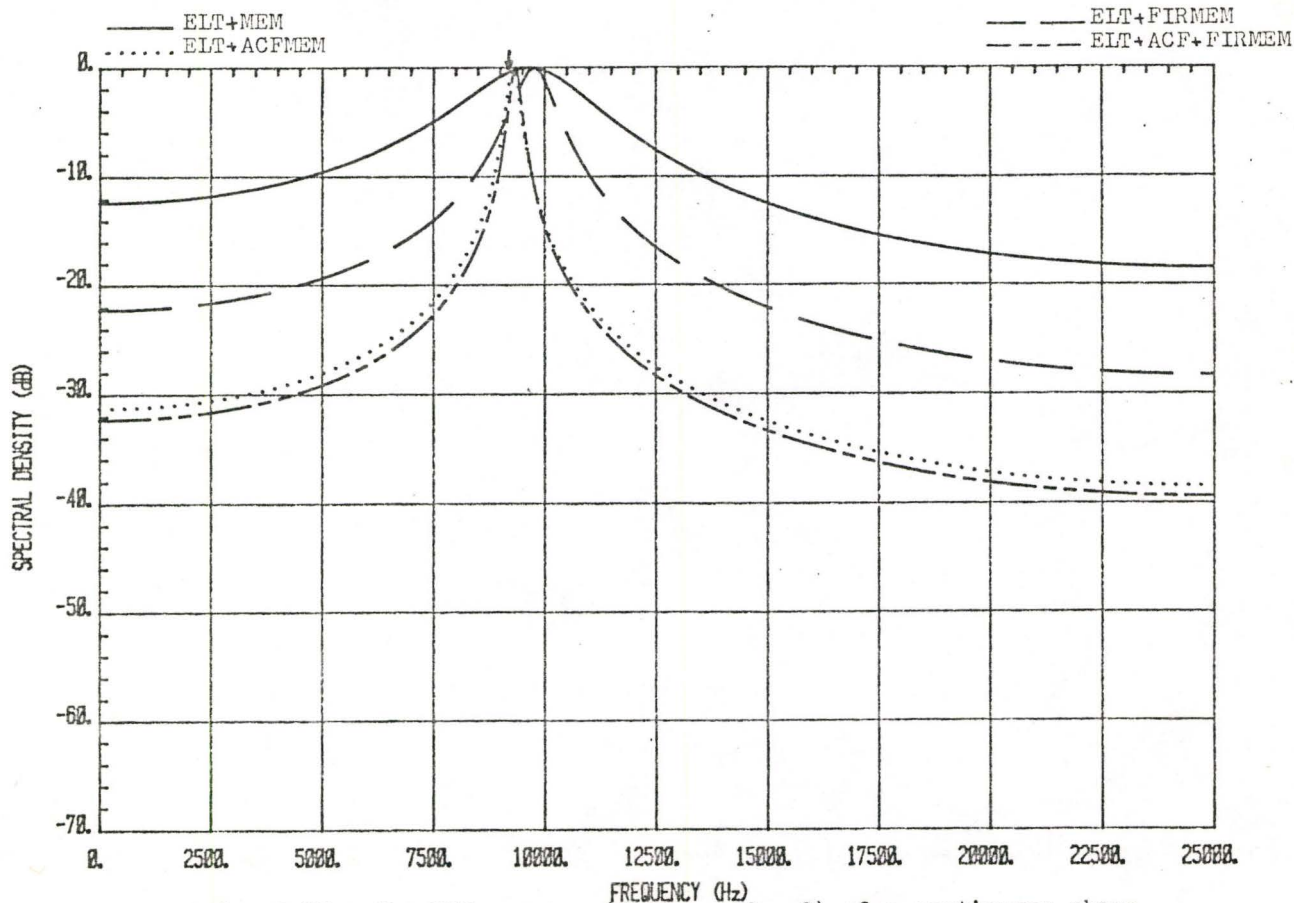


Fig. 3.88: The MEM spectra (filter order 2) of a continuous phase signal with carrier frequency=9237 Hz and CNDR=54 dB-Hz.

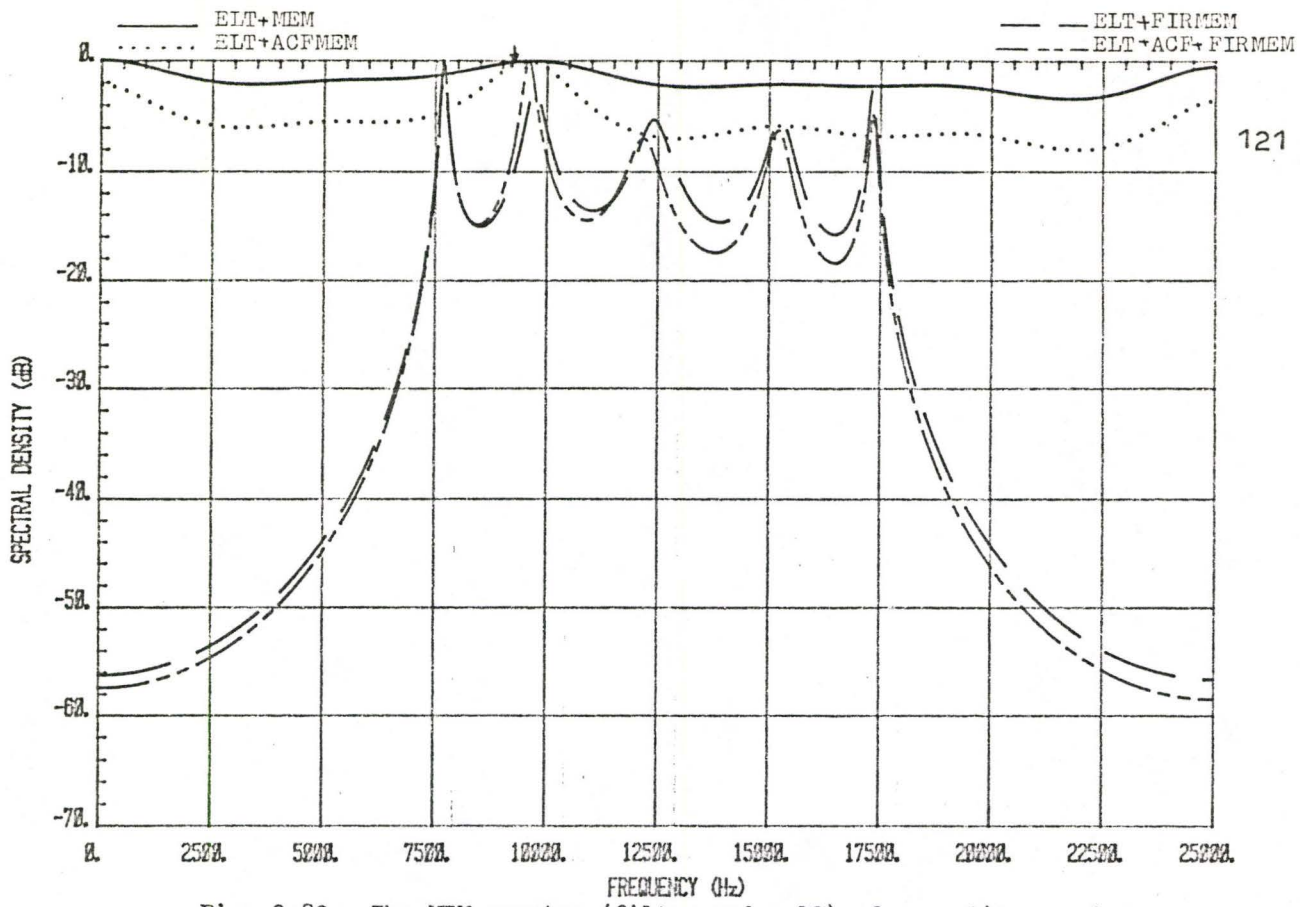


Fig. 3.89: The MEM spectra (filter order 10) of a continuous phase signal with carrier frequency=9237 Hz and 34 dB-Hz.

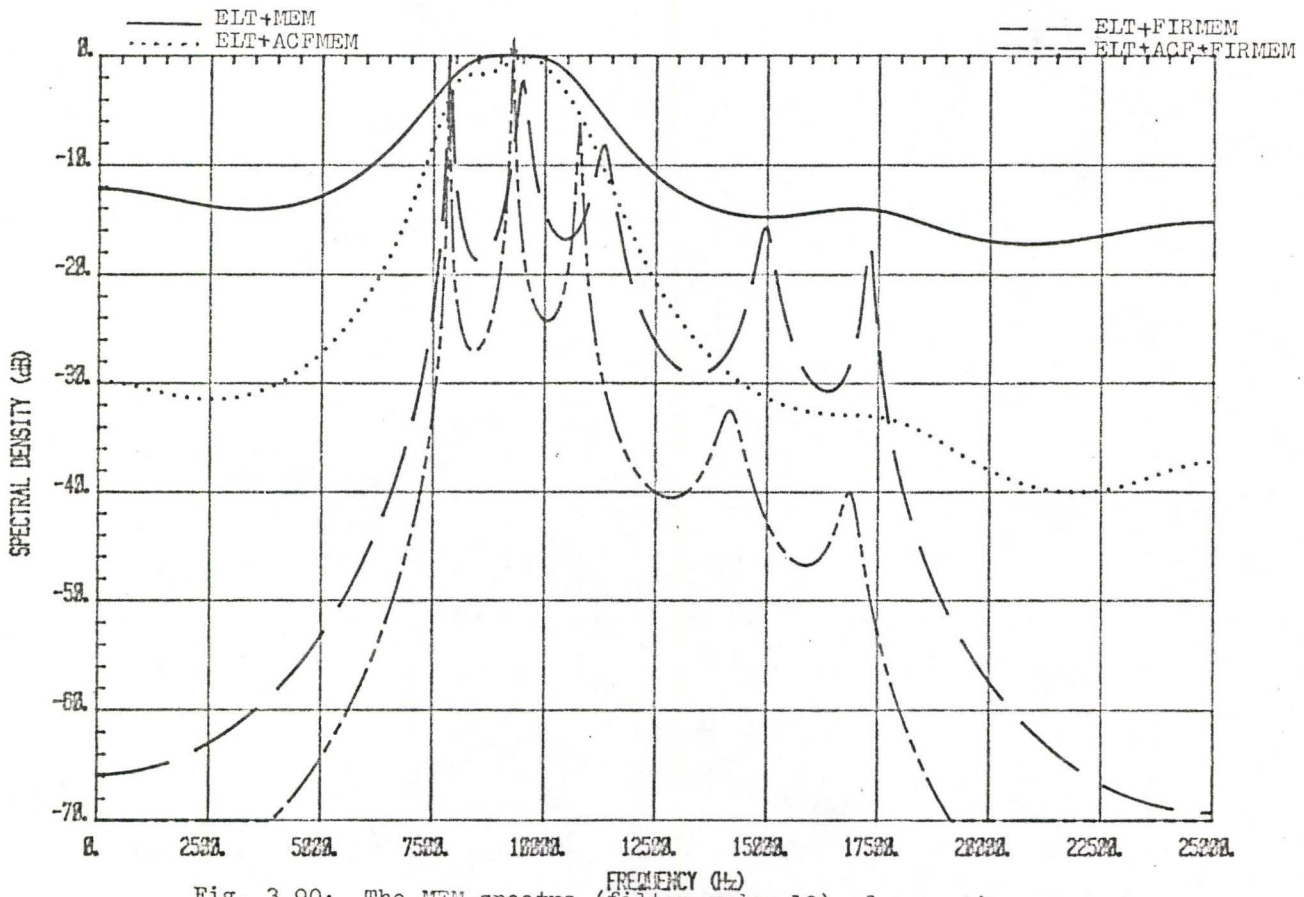


Fig. 3.90: The MEM spectra (filter order 10) of a continuous phase signal with carrier frequency=9237 Hz and CNDR=54 dB-Hz.

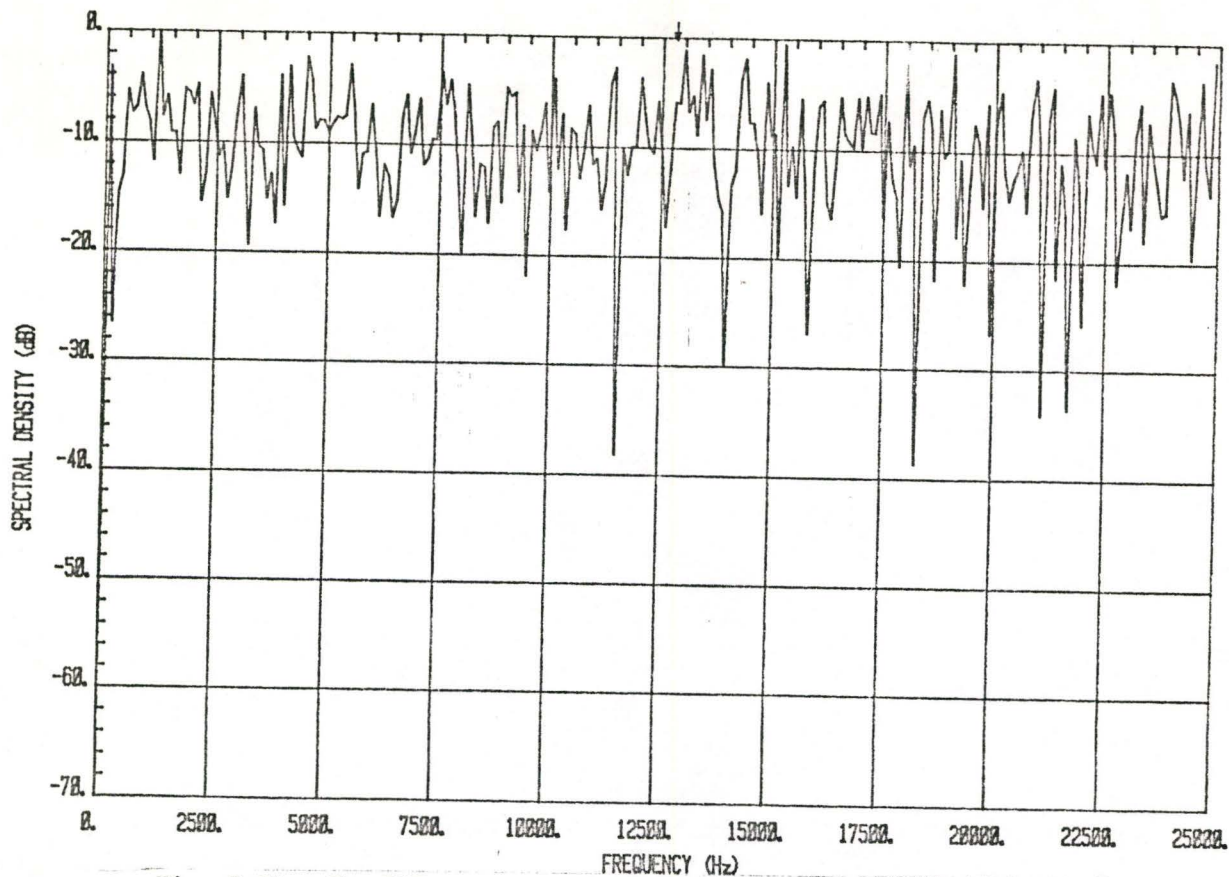


Fig. 3.91: The FFT spectrum of a random phase signal with carrier frequency=12832 Hz and CNDR=34 dB-Hz.

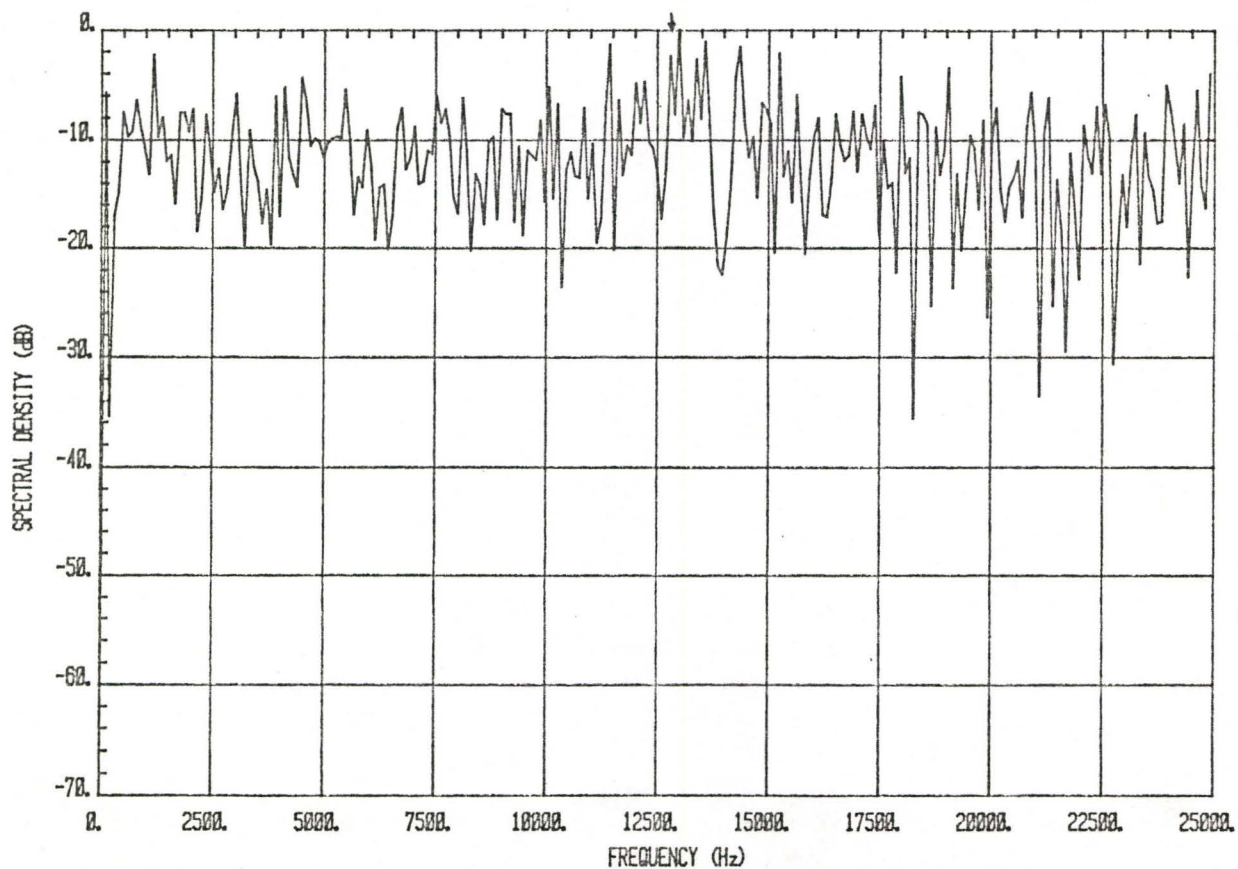


Fig. 3.92: The FFT spectrum of a random phase signal with carrier frequency=12832 Hz and CNDR=39 dB-Hz.

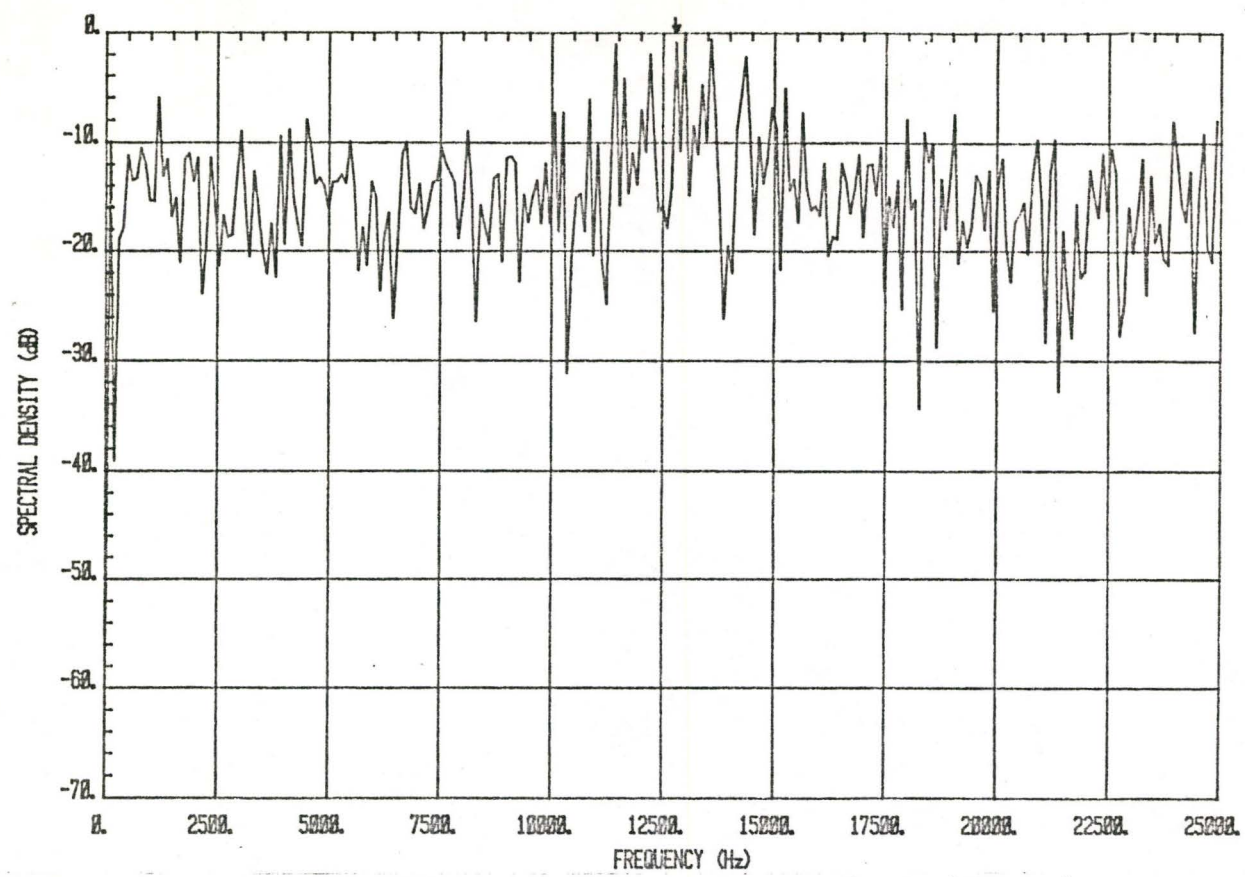


Fig. 3.93: The FFT spectrum of a random phase signal with carrier frequency=12832 Hz and CNDR=44 dB-Hz.

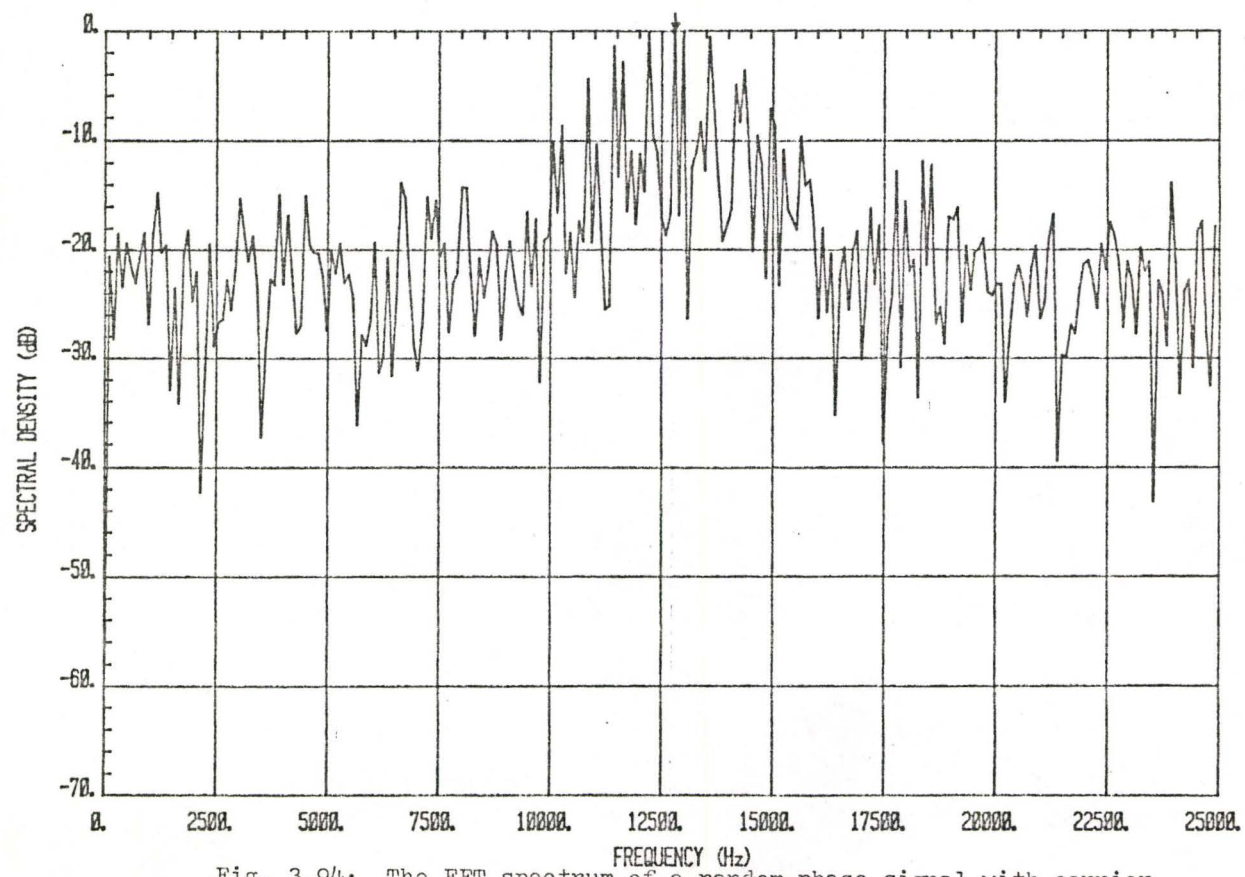


Fig. 3.94: The FFT spectrum of a random phase signal with carrier frequency=12832 Hz and CNDR=54 dB-Hz.

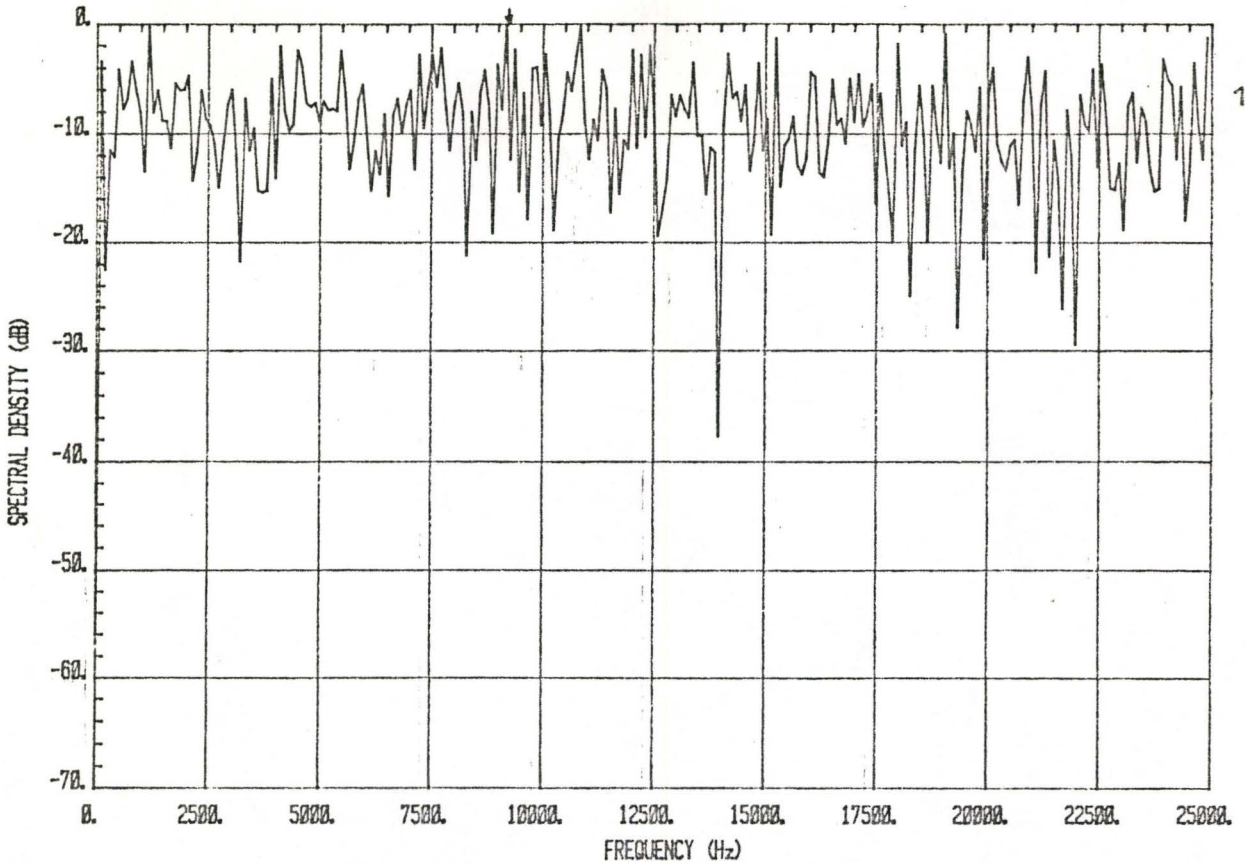


Fig. 3.95: The FFT spectrum of a random phase signal with carrier frequency=9237 Hz and CNDR=34 dB-Hz.

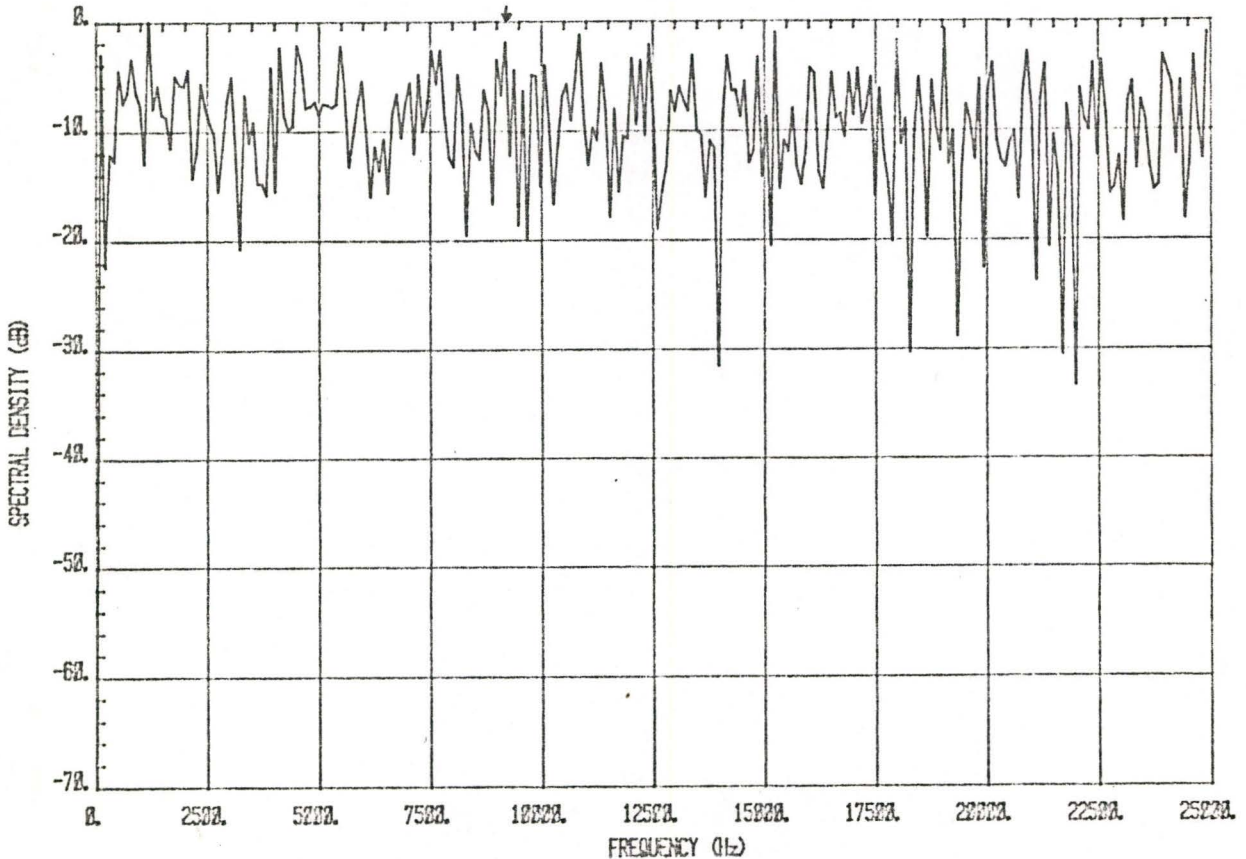


Fig. 3.96: The FFT spectrum of a random phase signal with carrier frequency=9237 Hz and CNDR=29 dB-Hz.

carrier frequencies of 12832 Hz and 9237 Hz for various CNDR values, as shown in Fig. 3.97 to Fig. 3.100, and Fig. 3.101 to Fig. 3.105, respectively. It is seen that once again the level of CNDR affects the estimate of carrier frequency.

### 3.5.3 Sinusoidal-Modulated

The FFT and MEM (with ACF and FIR) spectral estimations do not suffer large resolution error in evaluating the spectra of sinusoidal modulated signal at different values of CNDR. Detection is still feasible (for both techniques) even at 39 dB-Hz. Fig. 3.106 to Fig. 3.109 show the FFT spectral estimates as the CNDR increases from 34 dB-Hz to 54 dB-Hz, with signal frequency 12832 Hz. Fig. 3.110 illustrates the result at CNDR of 34 dB-Hz and signal frequency 9237 Hz. For all cases, detection appears to be straightforward.

For the second order MEM, the results are shown in Fig. 3.111 to Fig. 3.114 for different values of CNDR and signal frequency 12832 Hz. These results can be compared to those with signal frequency 9237, illustrated in Fig. 3.115 to Fig. 3.118. Again, the estimated carrier frequency is seen to be dependent on CNDR. In this case, it appears likely that use of a higher order MEM process will solve the problem.

## 3.6 SUMMARY

The FFT and the MEM spectral estimations, with preprocessing techniques provided by windowing, autocorrelation function and digital filtering (bandpass), are employed to process computer-generated ELT signals. In this chapter, we presented a detailed discussion about the

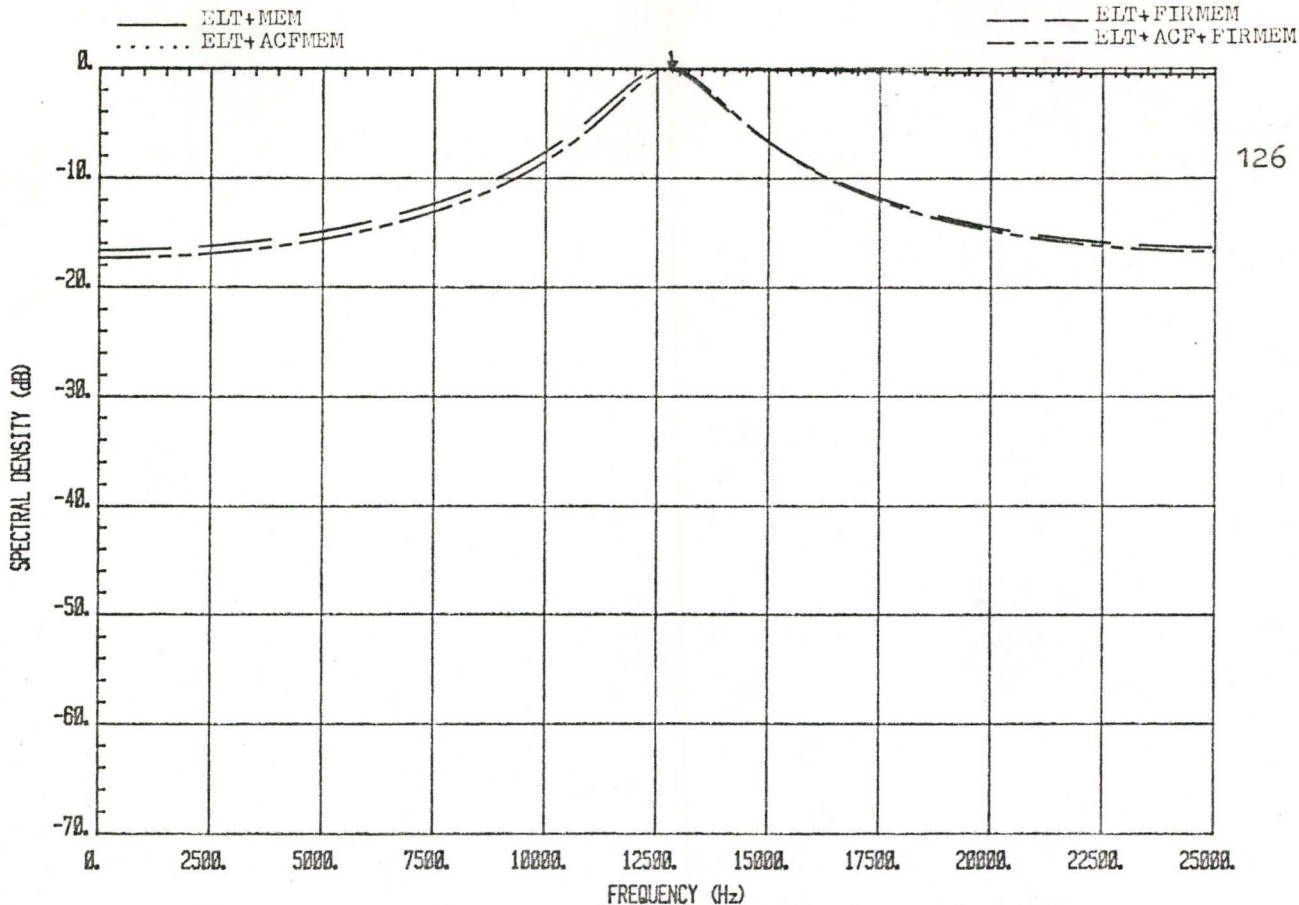


Fig. 3.97: The MEM spectra (filter order 2) of a random phase signal with carrier frequency=12832 Hz and CNDR=34 dB-Hz.

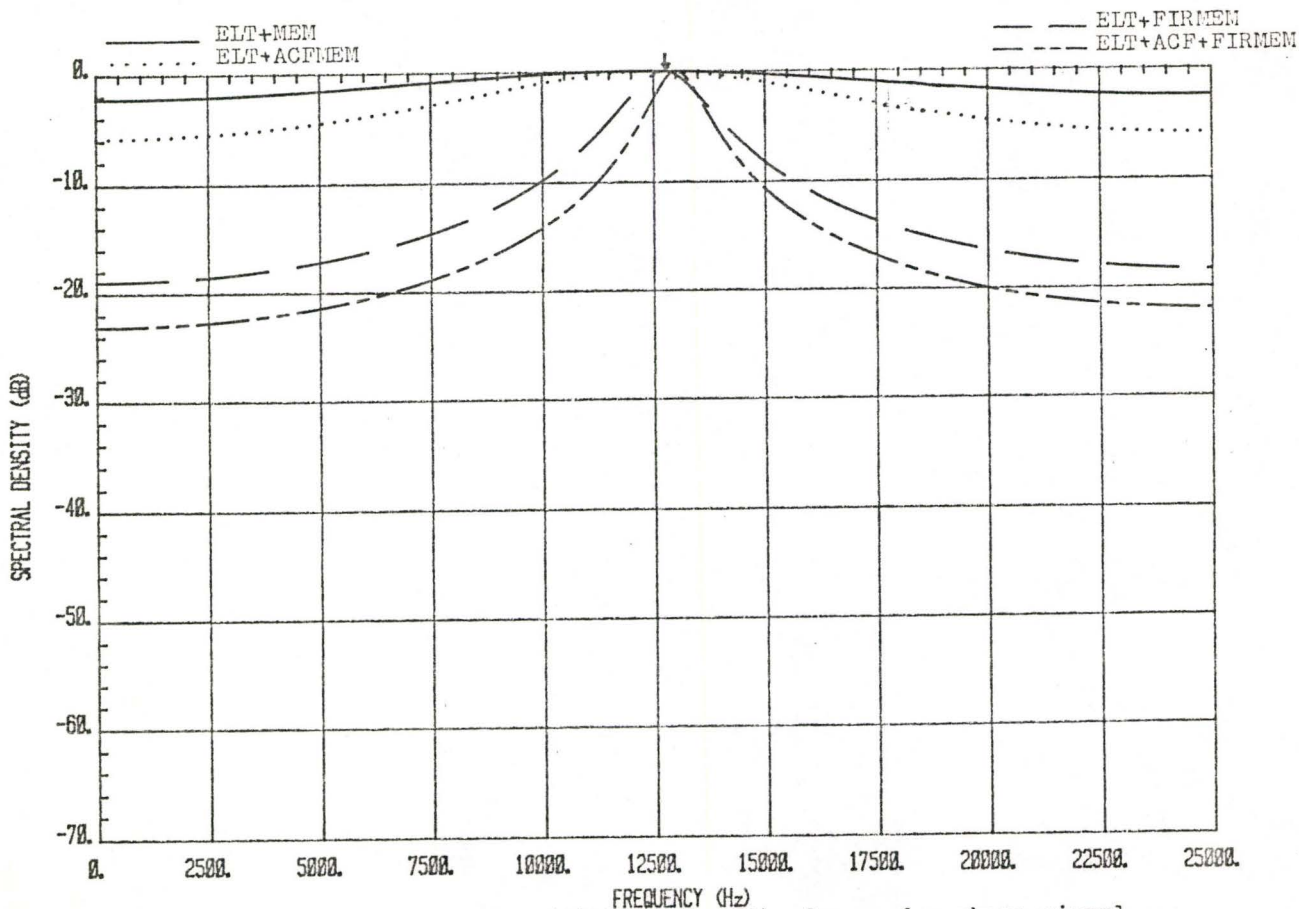
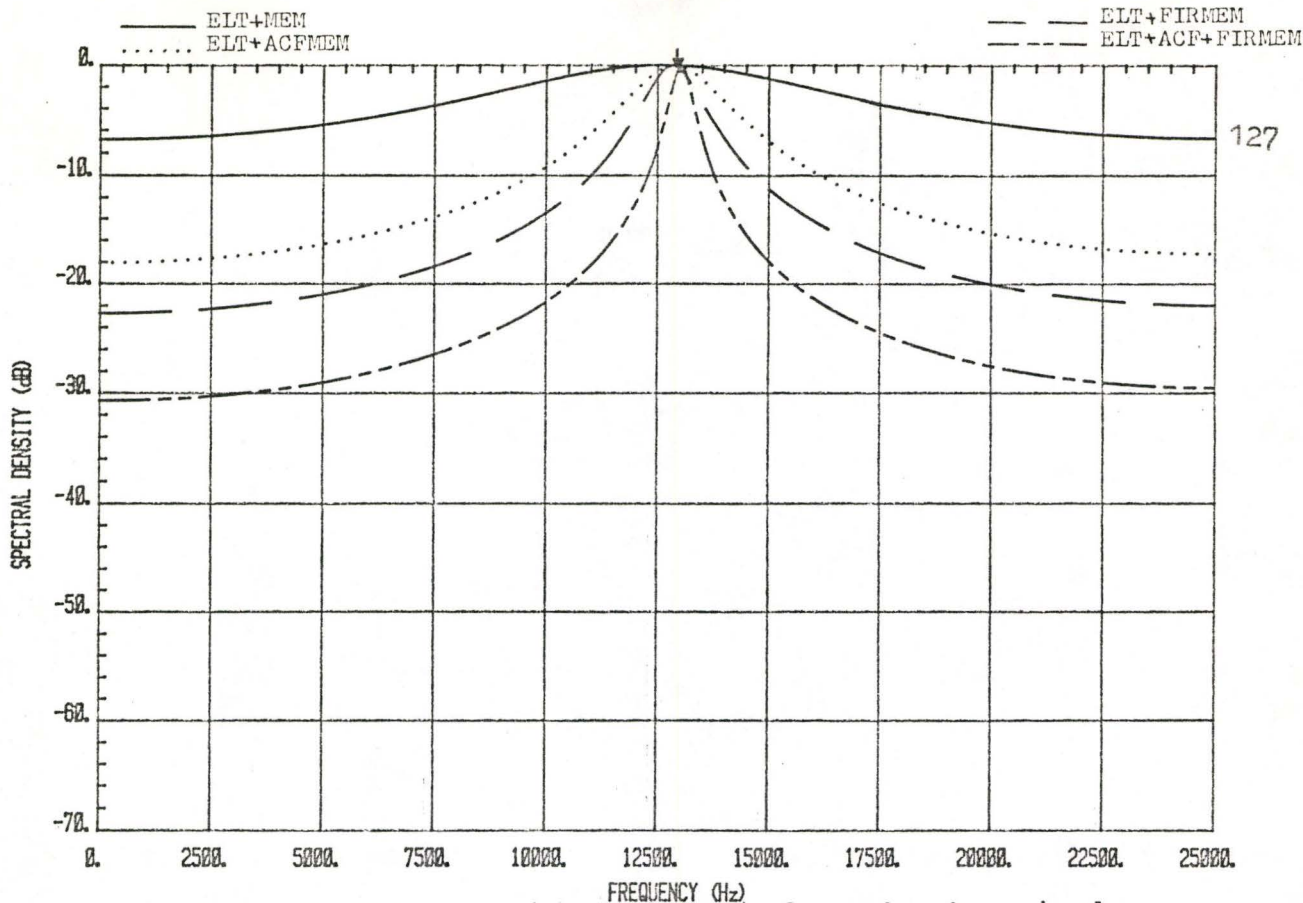


Fig. 3.98: The MEM spectra (filter order 2) of a random phase signal with carrier frequency=12832 Hz and CNDR=39 dB-Hz.



127

Fig. 3.99: The MEM spectra (filter order 2) of a random phase signal with carrier frequency=12832 Hz and CNDR=44 dB-Hz.

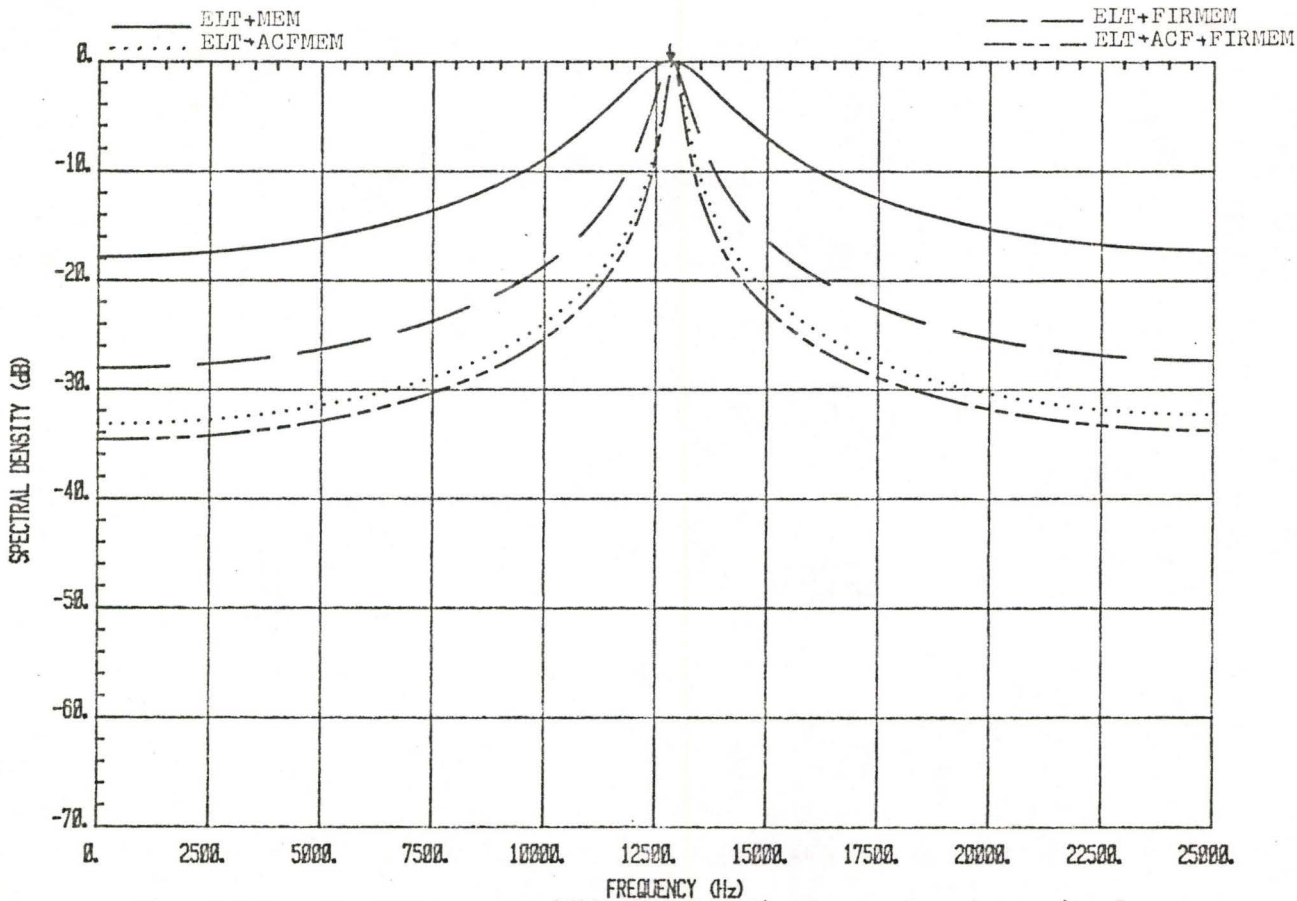


Fig. 3.100: The MEM spectra (filter order 2) of a random phase signal with carrier frequency=12832 Hz and CNDR=54 dB-Hz.

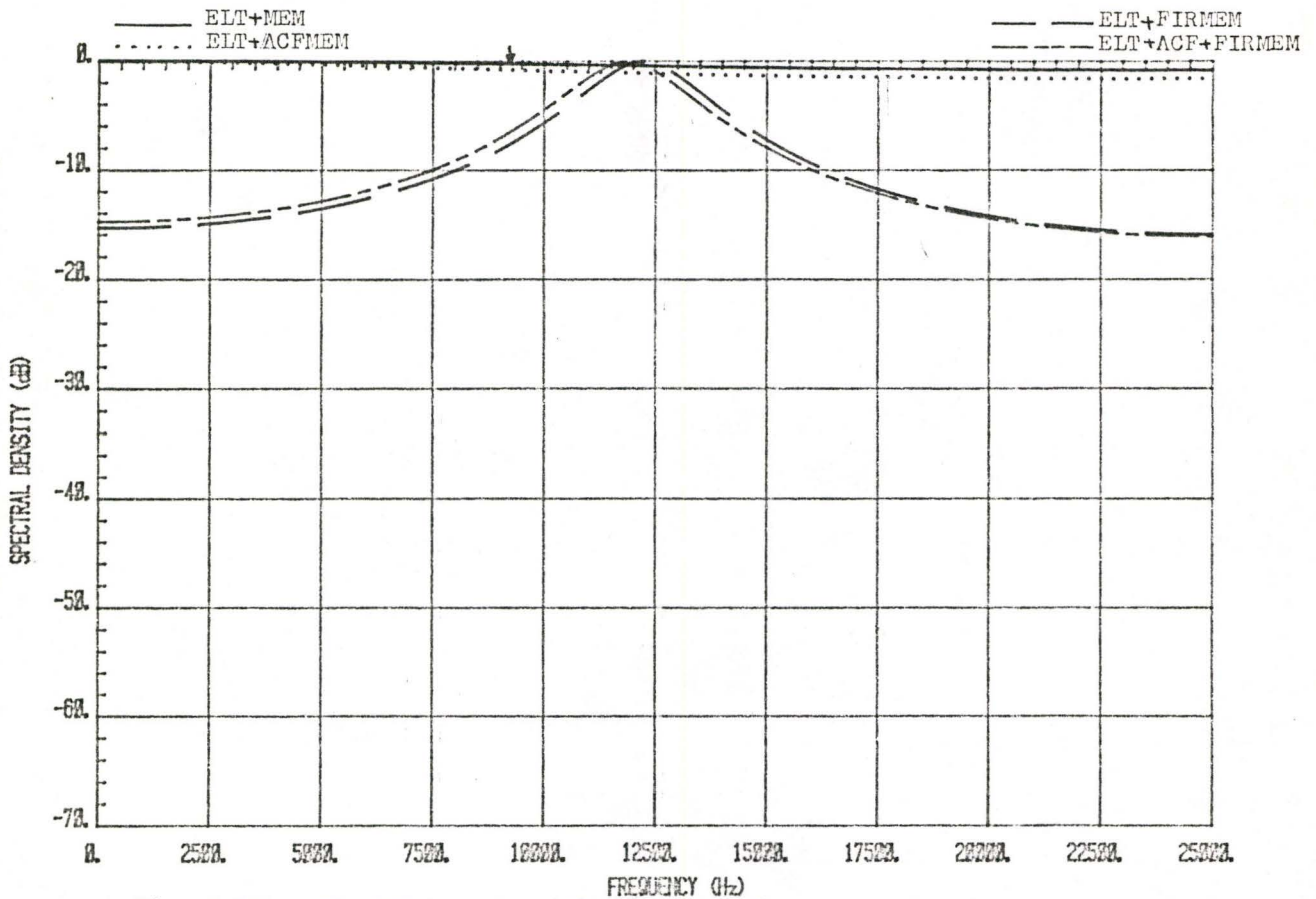


Fig. 3.101: The MEM spectra (filter order 2) of a random phase signal with carrier frequency=9237 Hz and CNDR=29 dB-Hz.

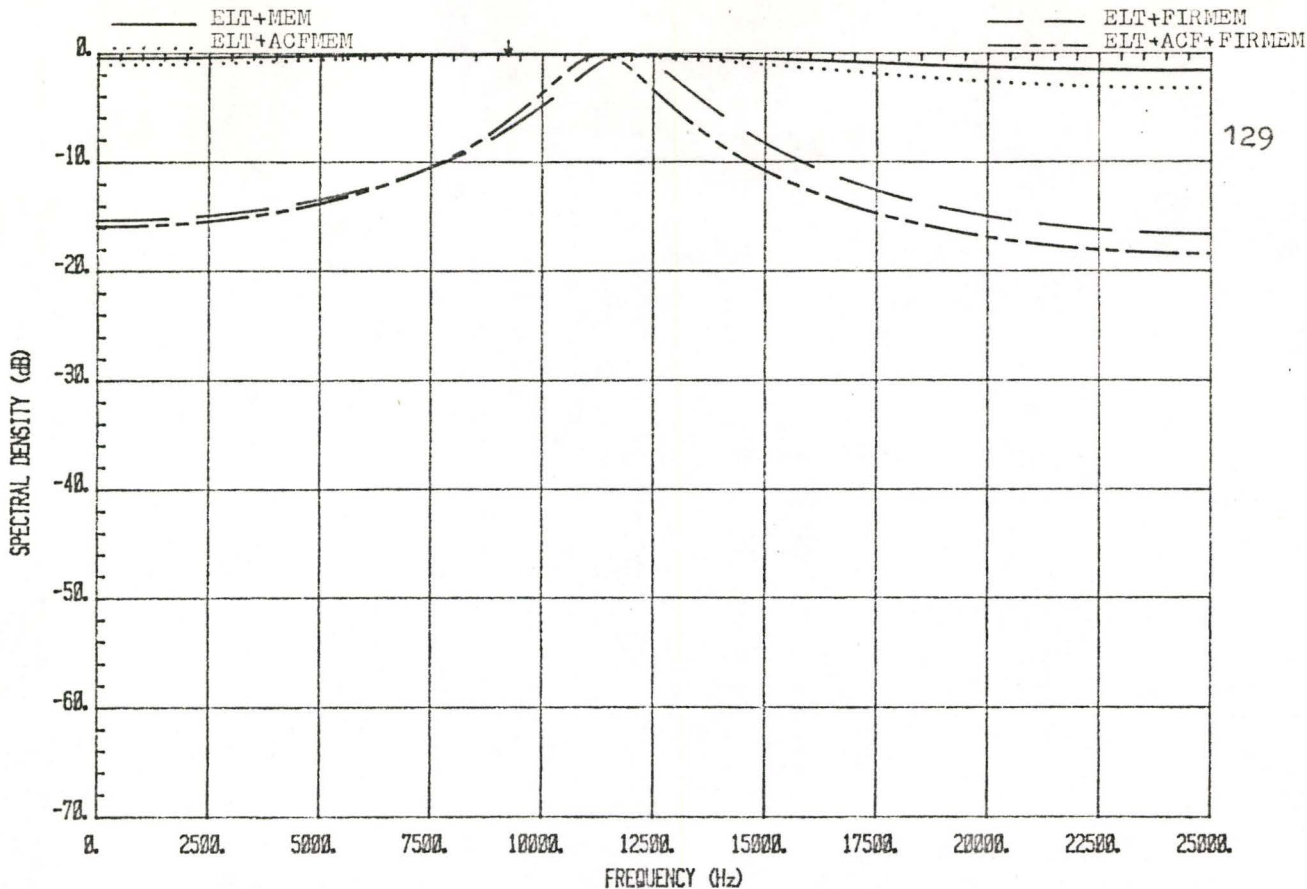


Fig. 3.102: The MEM spectra (filter order 2) of a random phase signal with carrier frequency=9237 Hz and CNDR=34 dB-Hz.

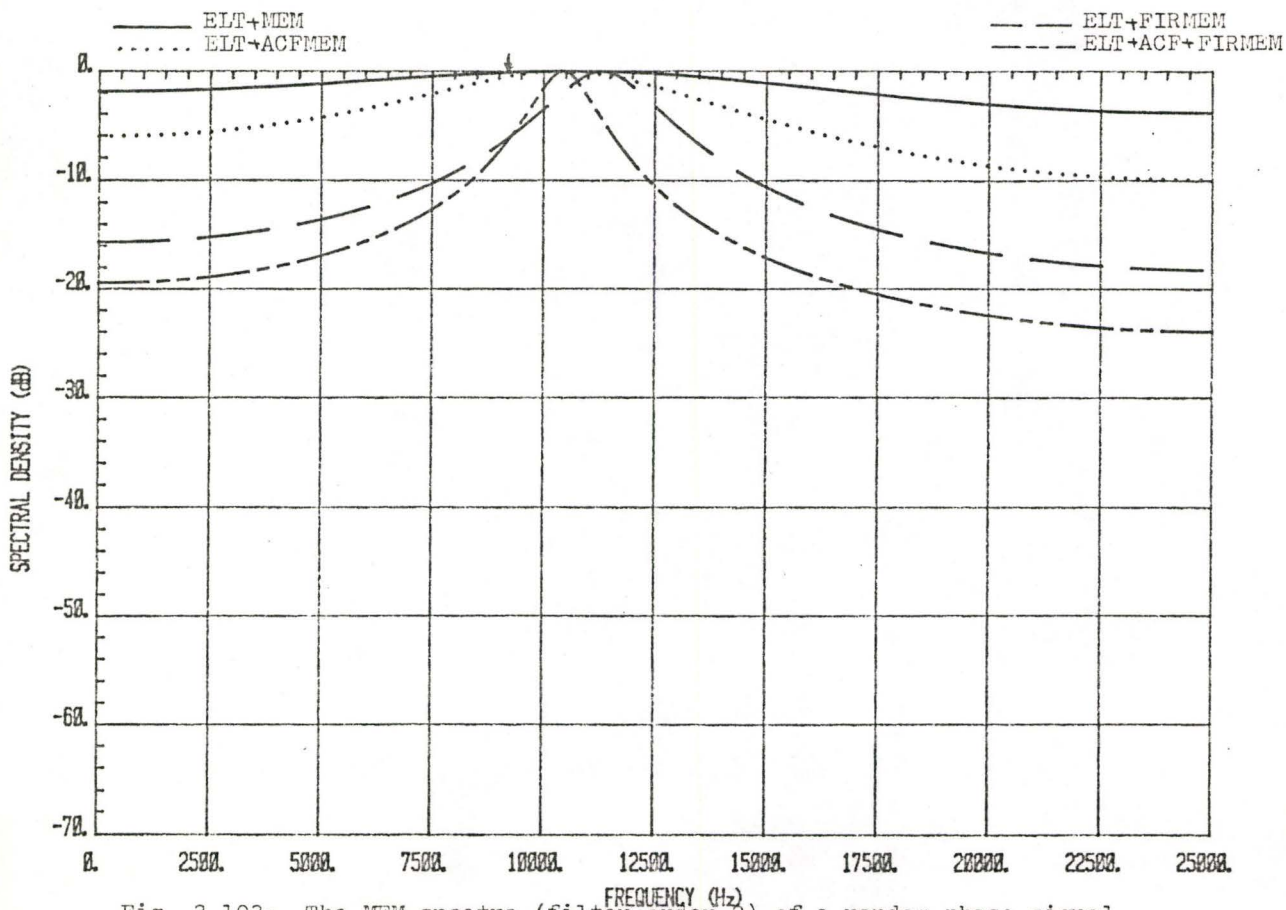


Fig. 3.103: The MEM spectra (filter order 2) of a random phase signal with carrier frequency=9237 Hz and CNDR=39 dB-Hz.

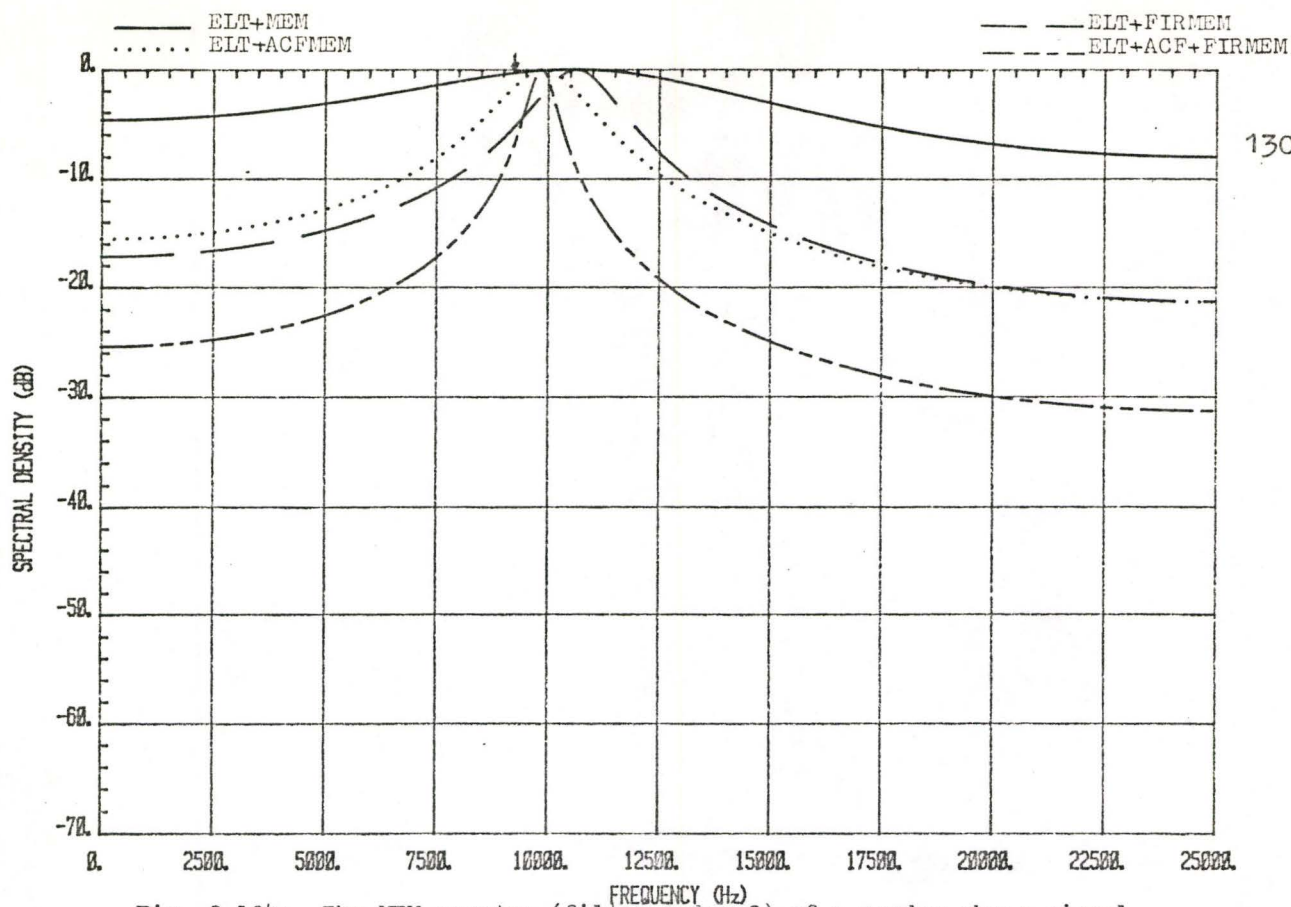


Fig. 3.104: The MEM spectra (filter order 2) of a random phase signal with carrier frequency=9237 Hz and CNDR=44 dB-Hz.

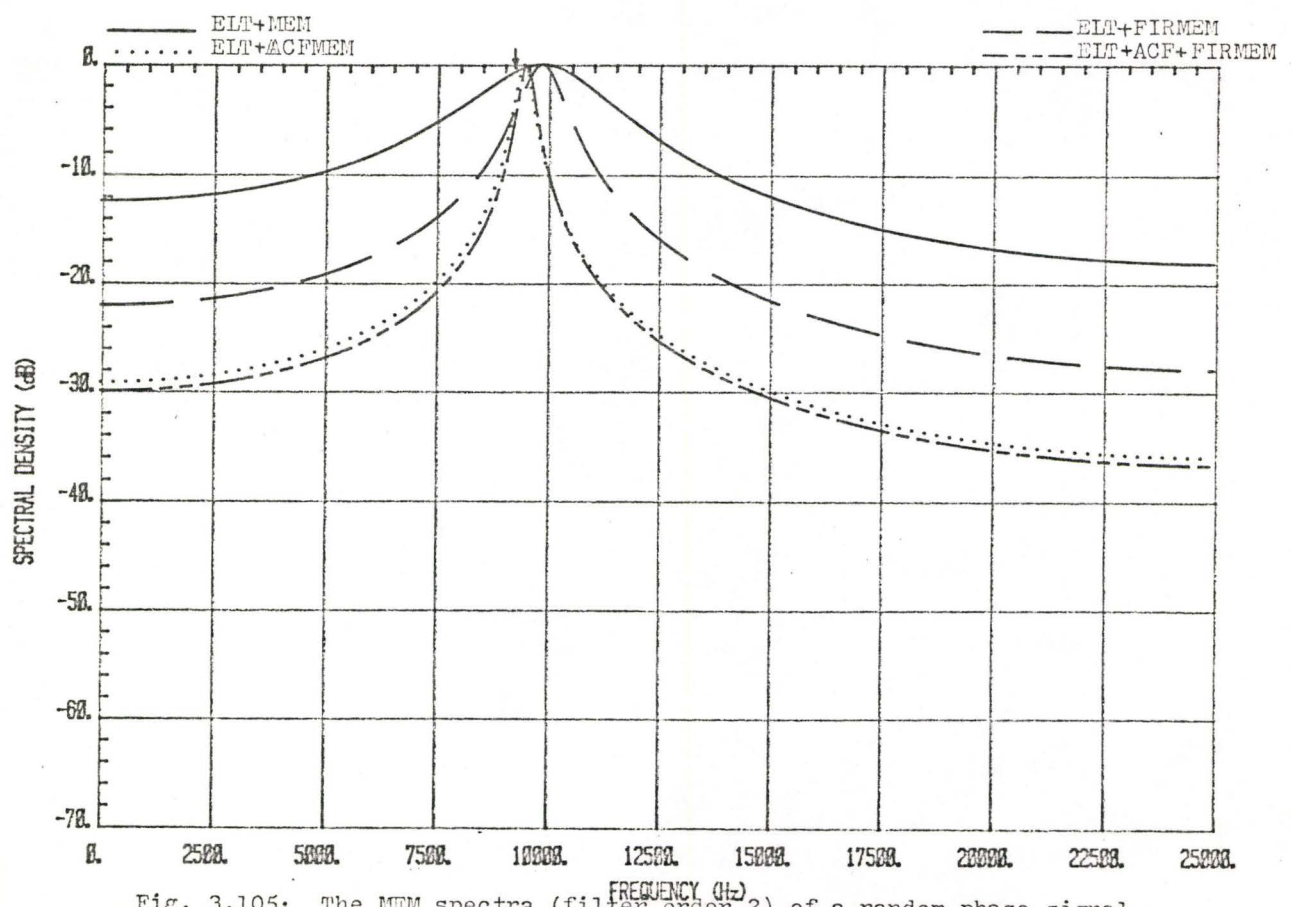


Fig. 3.105: The MEM spectra (filter order 2) of a random phase signal with carrier frequency=9237 Hz and CNDR=54 dB-Hz.

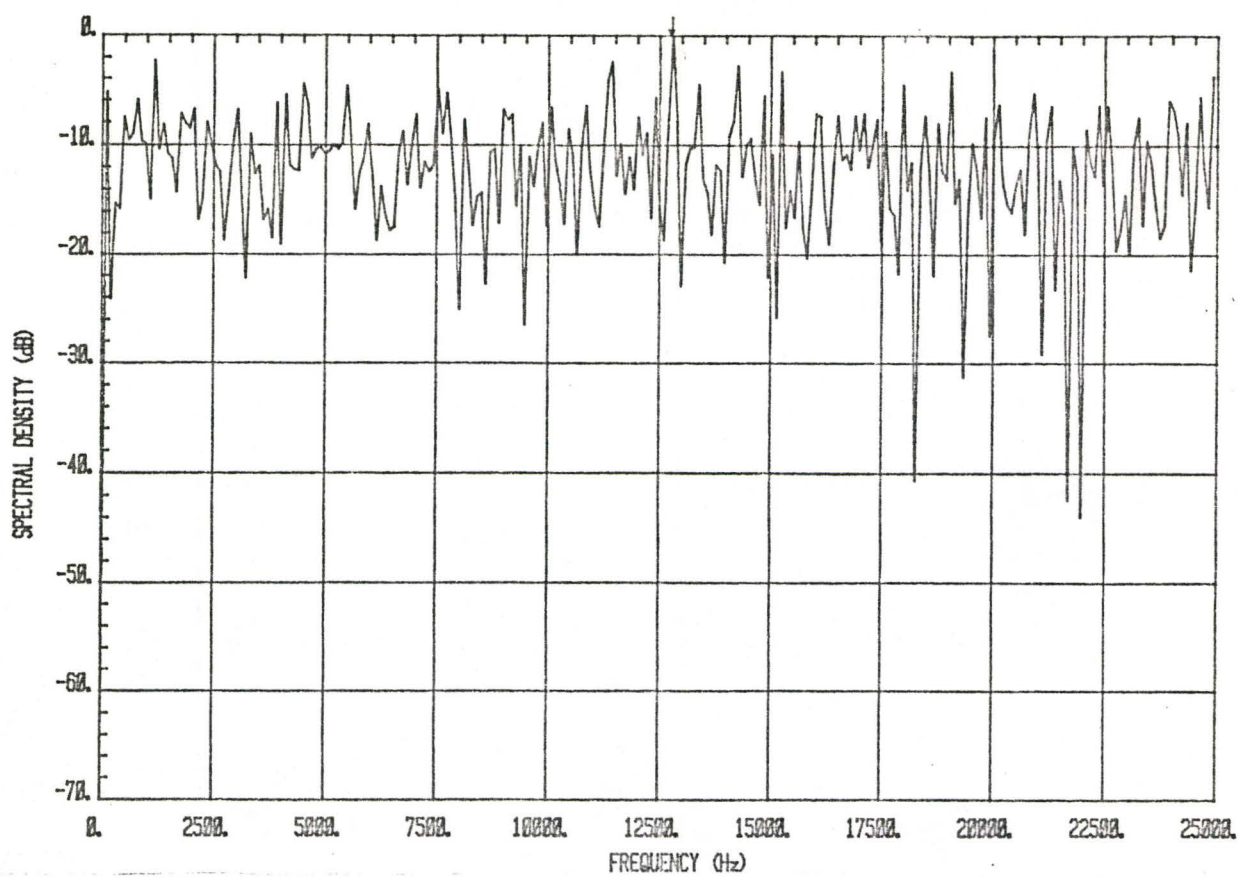


Fig. 3.106: The FFT spectrum of a sinusoidal-modulated signal with carrier frequency=12832 Hz and CNDR=34 dB-Hz.

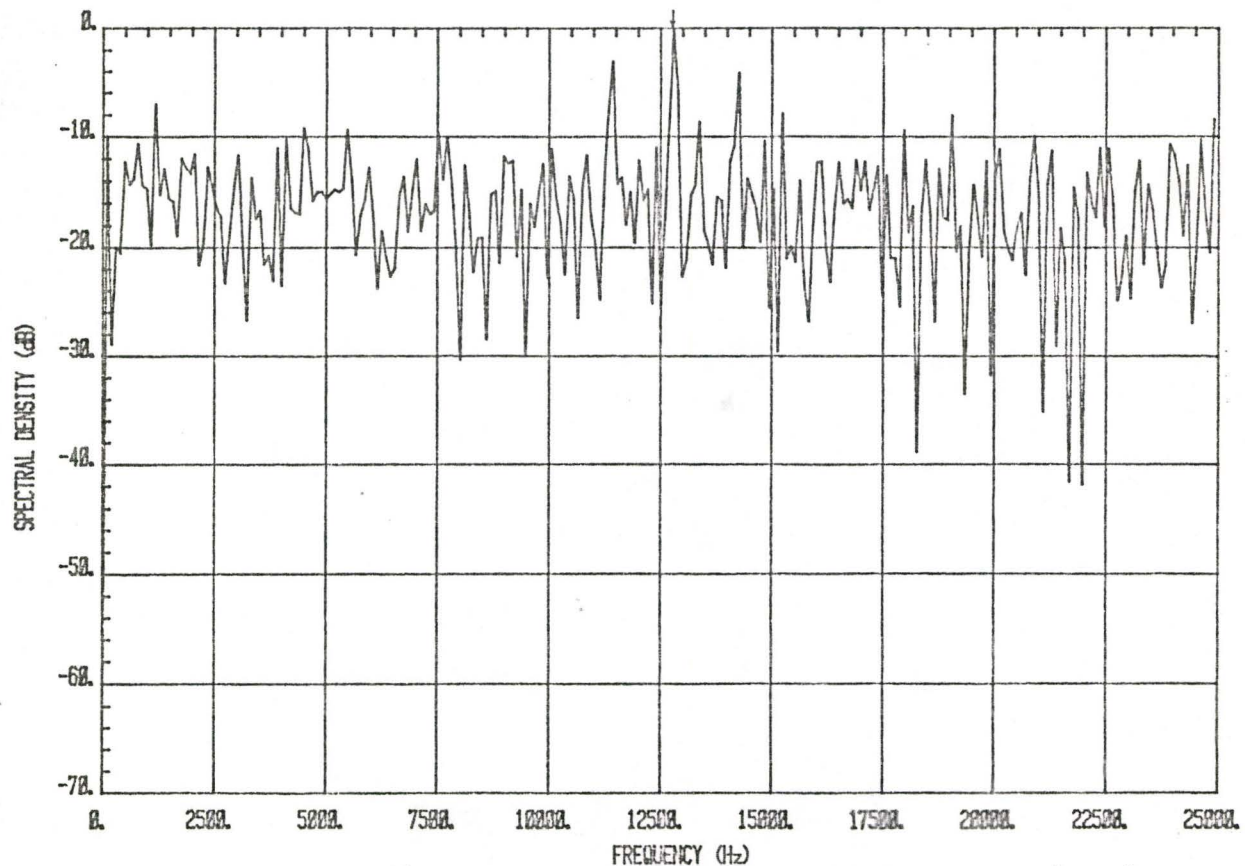


Fig. 3.107: The FFT spectrum of a sinusoidal-modulated signal with carrier frequency=12832 Hz and 39 dB-Hz.

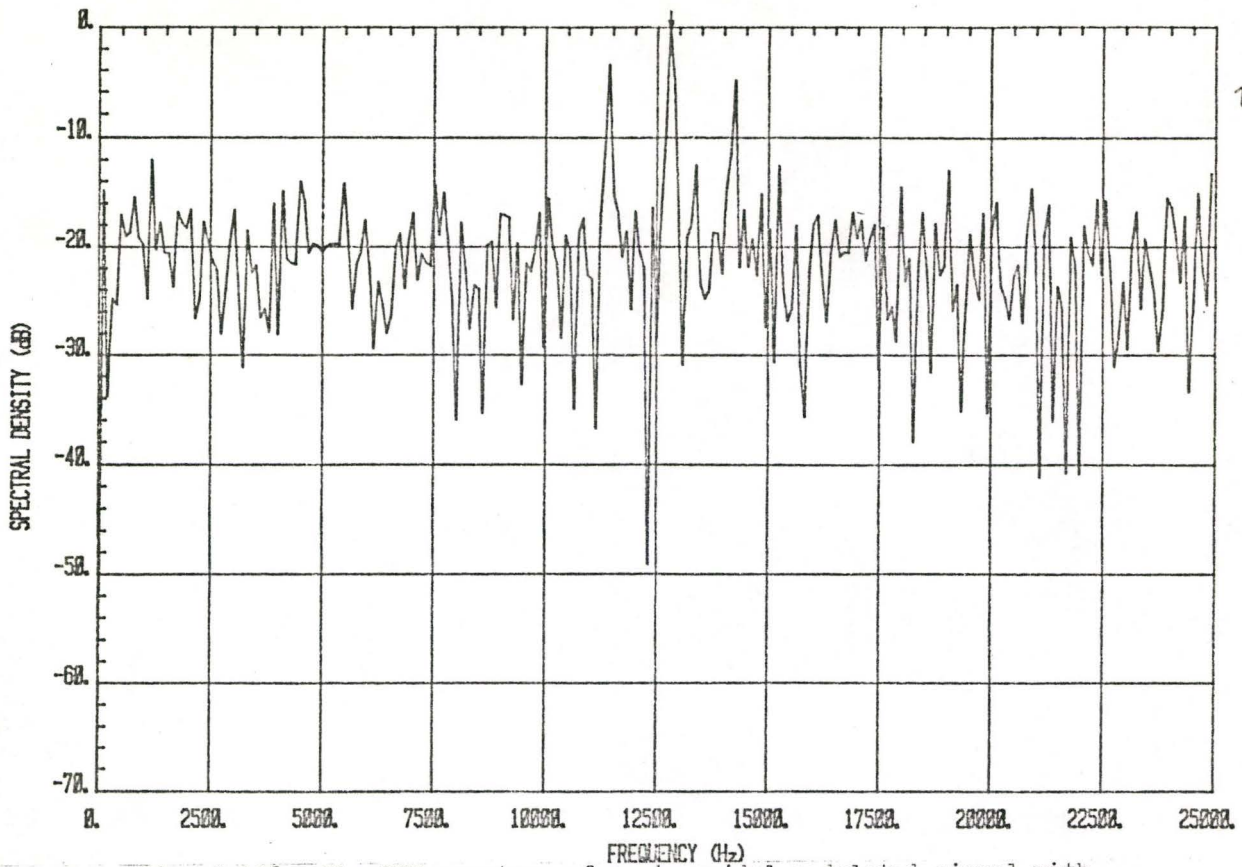


Fig. 3.108: The FFT spectrum of a sinusoidal-modulated signal with carrier frequency=12832 Hz and CNDR=44 dB-Hz.

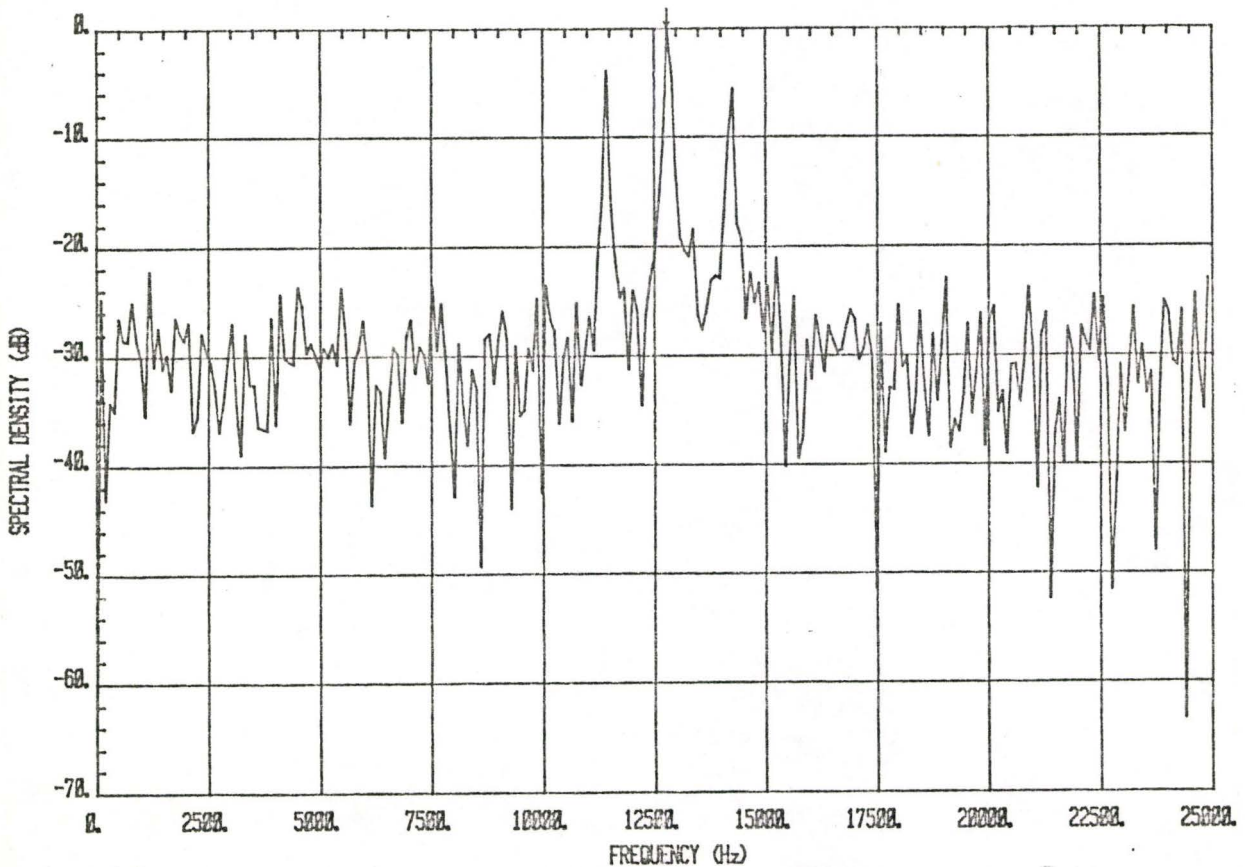


Fig. 3.109: The FFT spectrum of a sinusoidal-modulated signal with carrier frequency=12832 Hz and CNDR=54 dB-Hz.

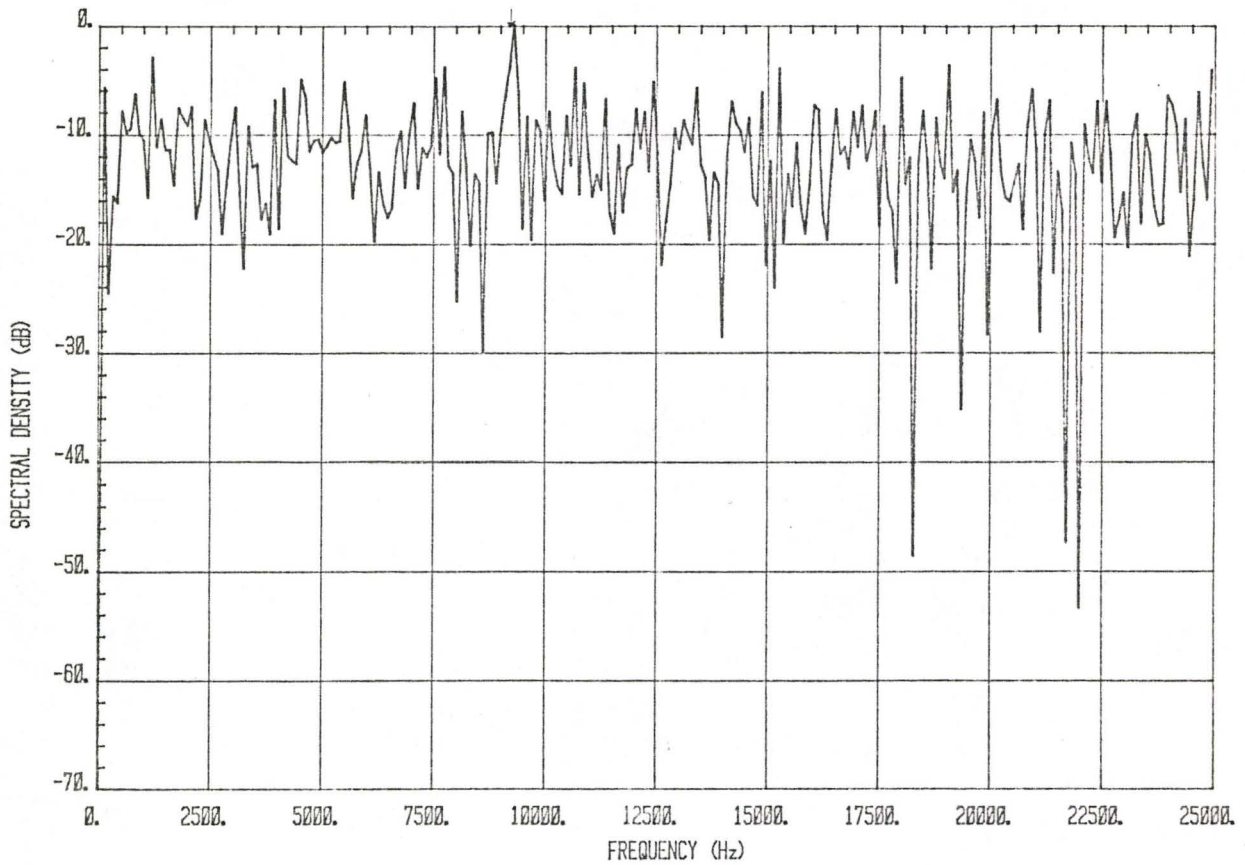


Fig. 3.110: The FFT spectrum of a sinusoidal-modulated signal with carrier frequency=9237 Hz and CNDR=34 dB-Hz.

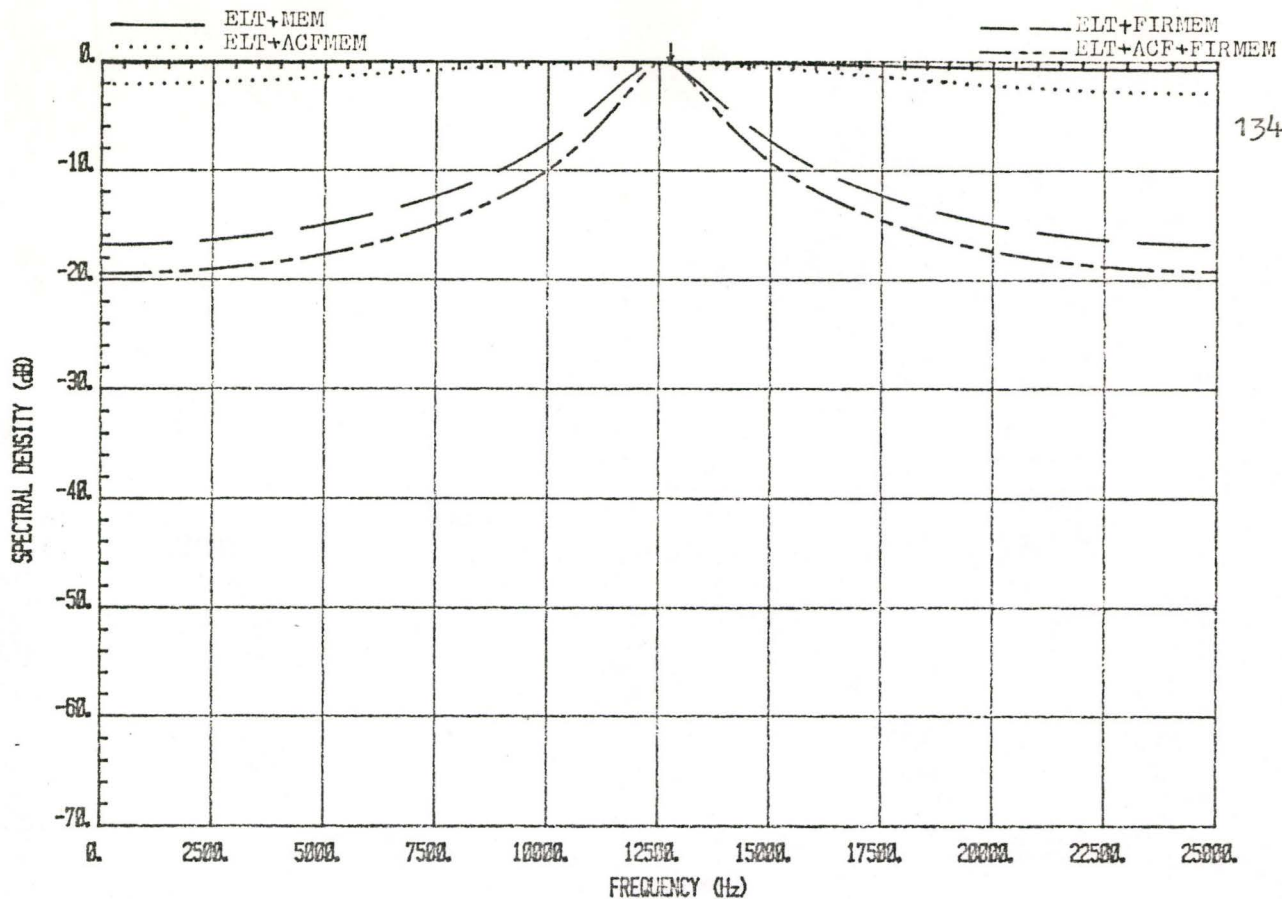


Fig. 3.111: The MEM spectra (filter order 2) of a sinusoidal-modulated signal with carrier frequency=12832 Hz and CNDR=34 dB-Hz.

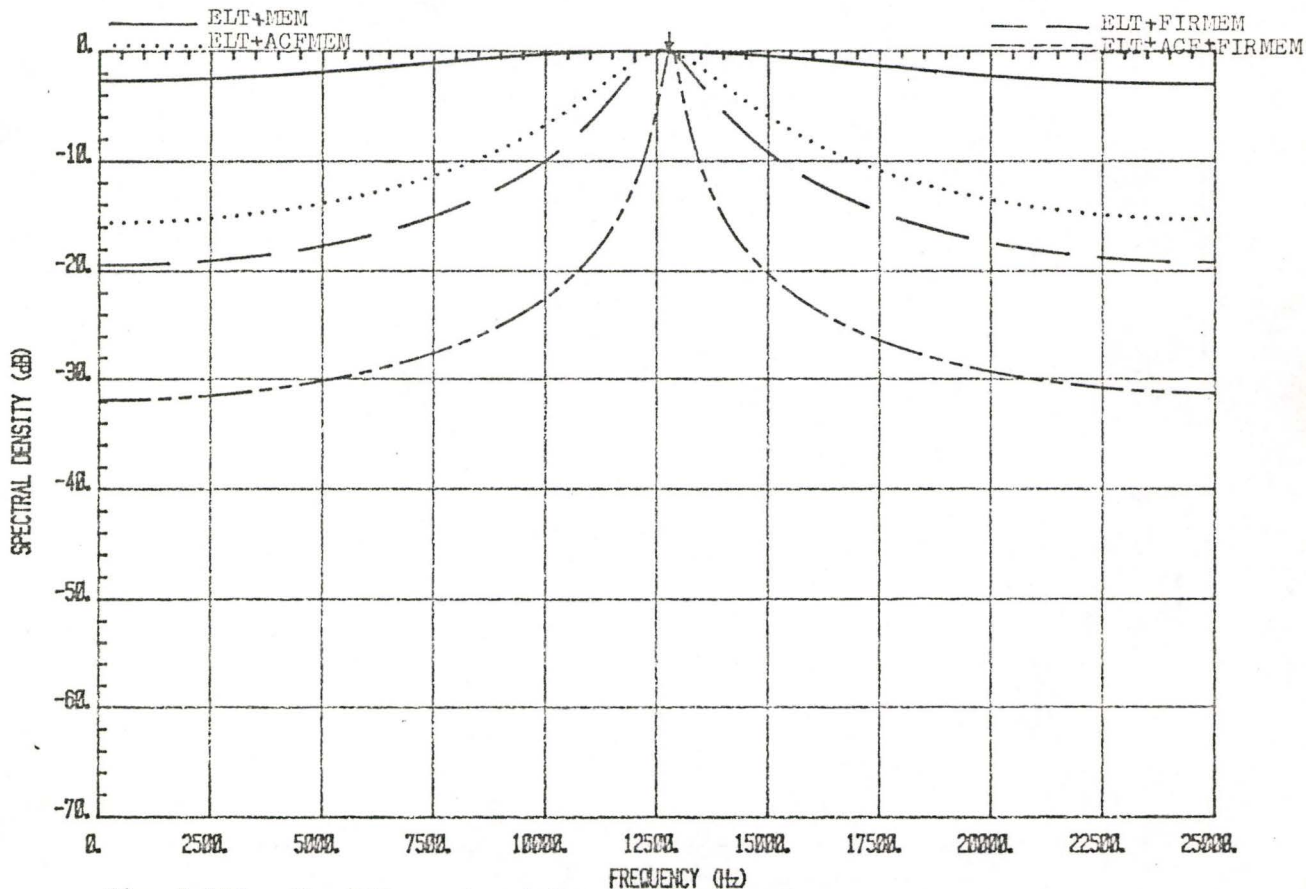


Fig. 3.112: The MEM spectra (filter order 2) of a sinusoidal-modulated signal with carrier frequency=12832 Hz and CNDR=39 dB-Hz.

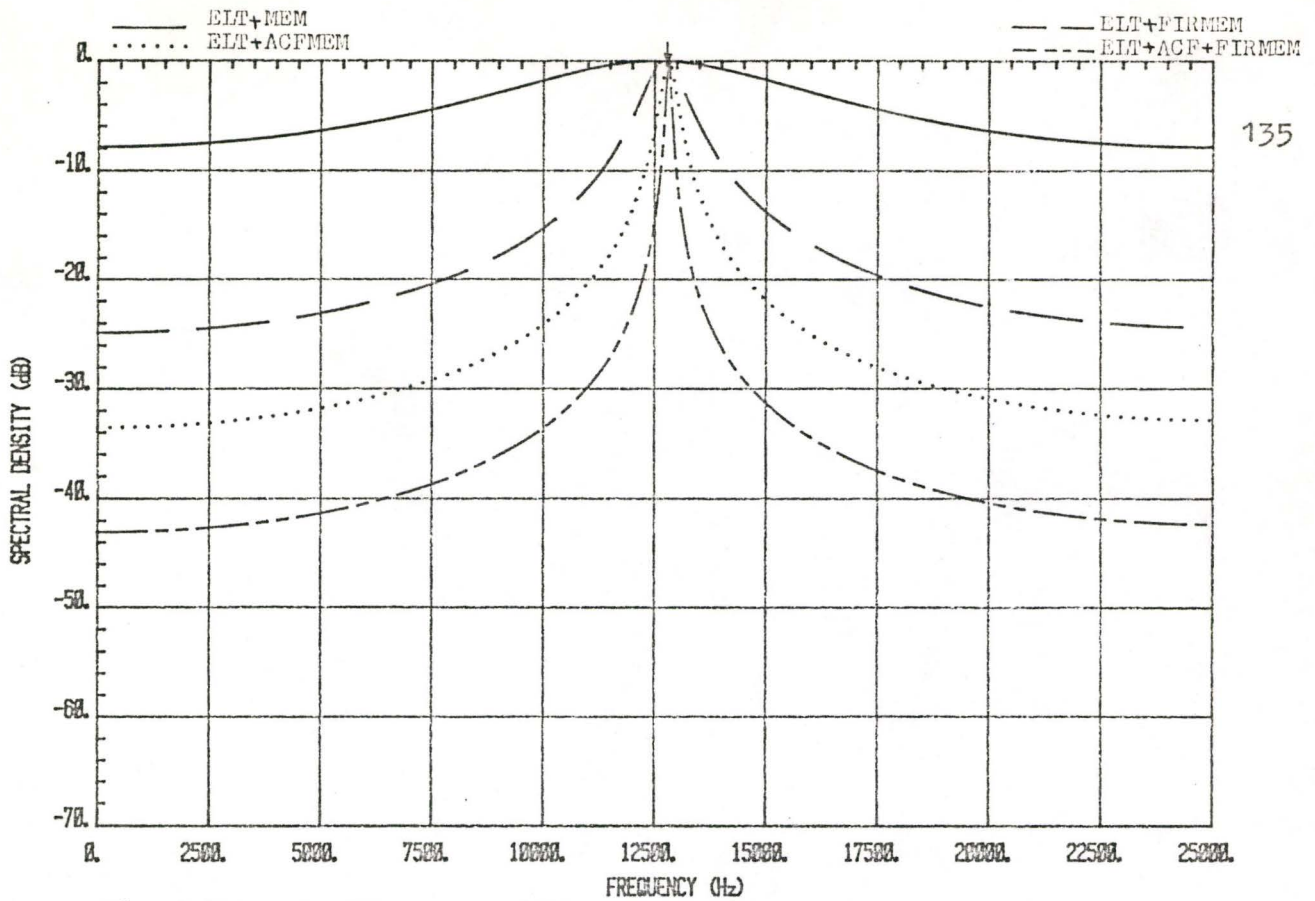


Fig. 3.113: The MEM spectra (filter order 2) of a sinusoidal-modulated signal with carrier frequency=12832 Hz and CNDR=44 dB-Hz.

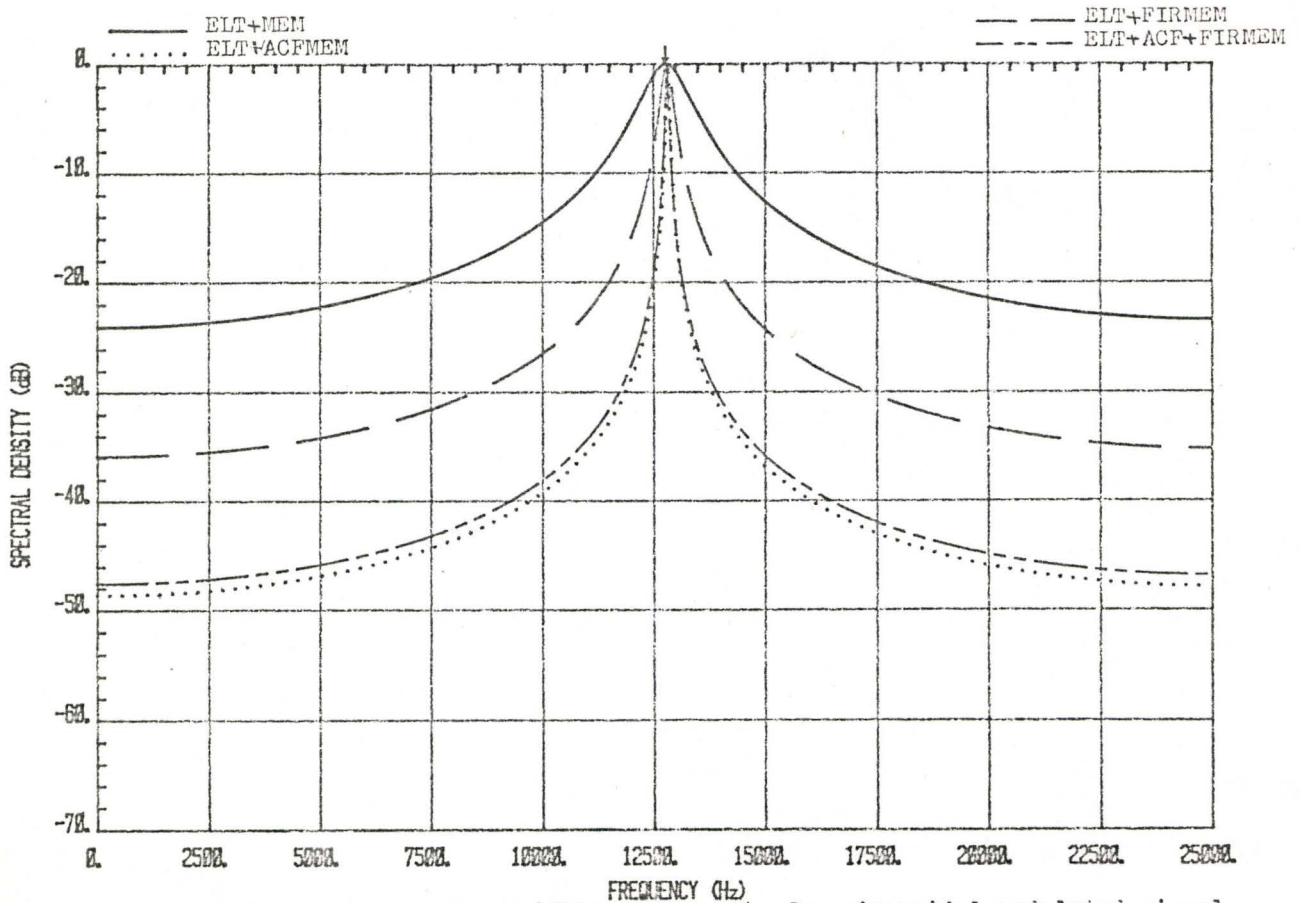


Fig. 3.114: The MEM spectra (filter order 2) of a sinusoidal-modulated signal with carrier frequency=12832 Hz and CNDR=54 dB-Hz.

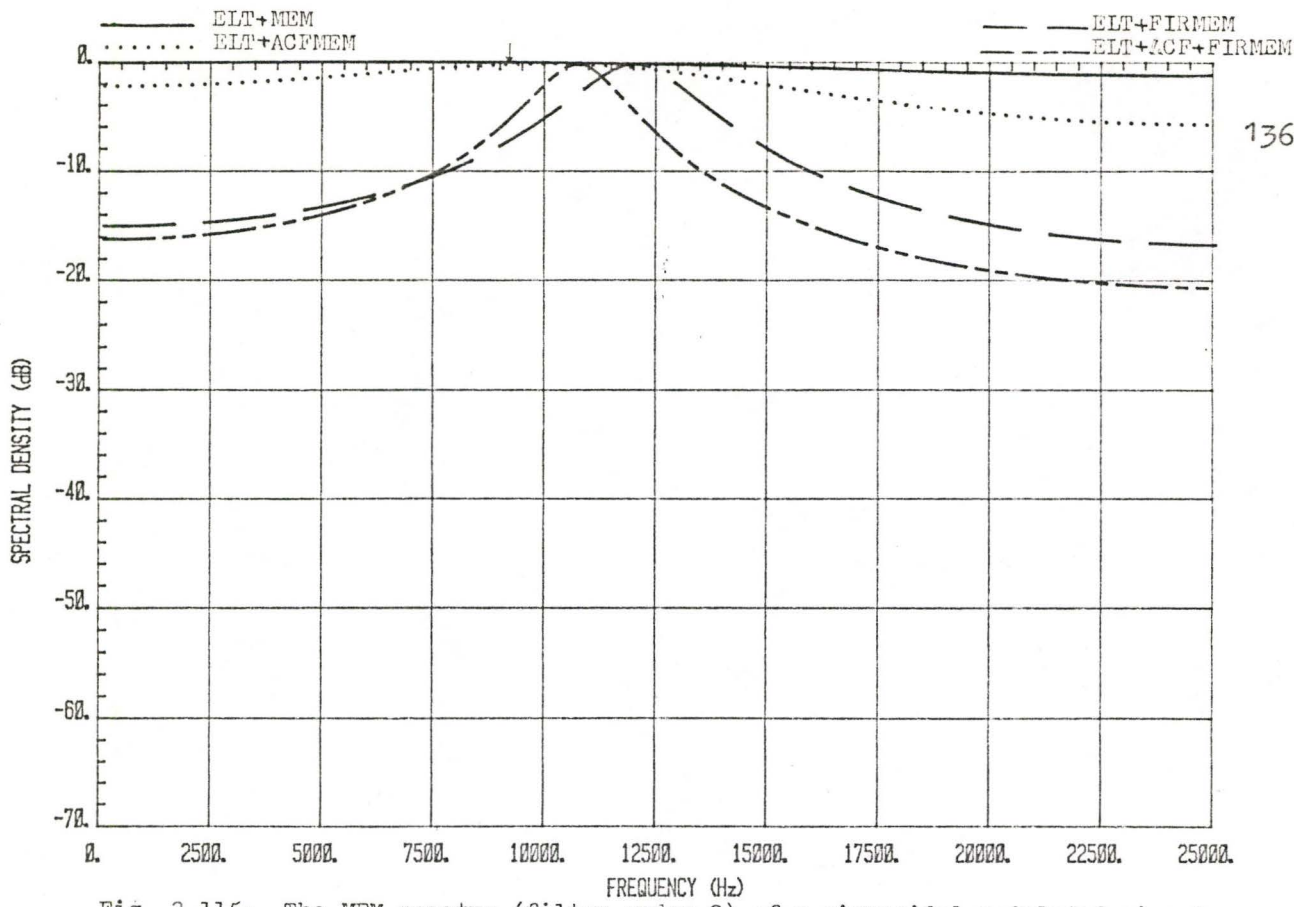


Fig. 3.115: The MEM spectra (filter order 2) of a sinusoidal-modulated signal with carrier frequency=9237 Hz and CNDR=34 dB-Hz.

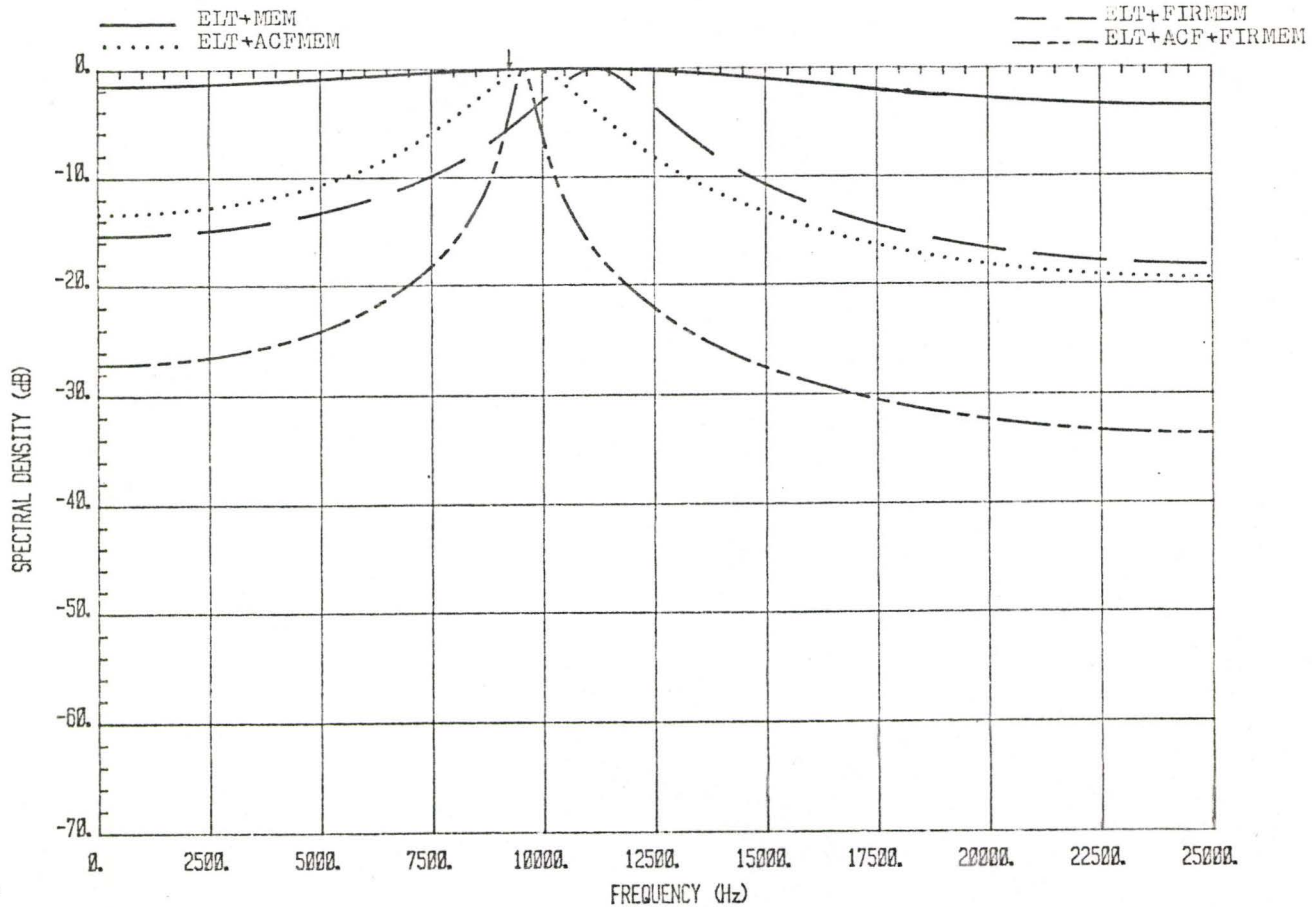


Fig. 3.116: The MEM spectra (filter order 2) of a sinusoidal-modulated signal with carrier frequency=9237 Hz and CNDR=39 dB-Hz.

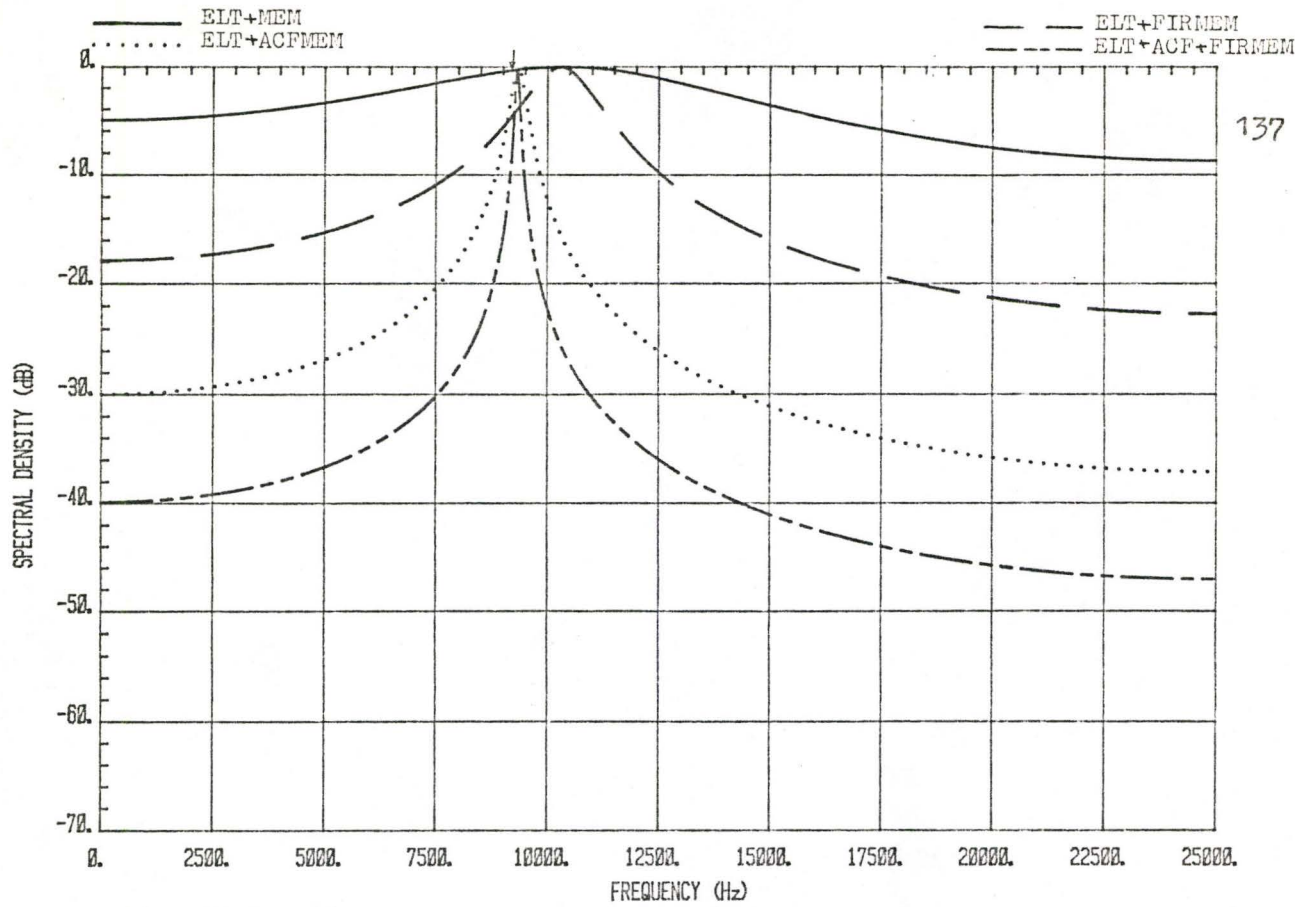


Fig. 3.117: The MEM spectra (filter order 2) of a sinusoidal-modulated signal with carrier frequency=9237 Hz and CNDR=44 dB-Hz.

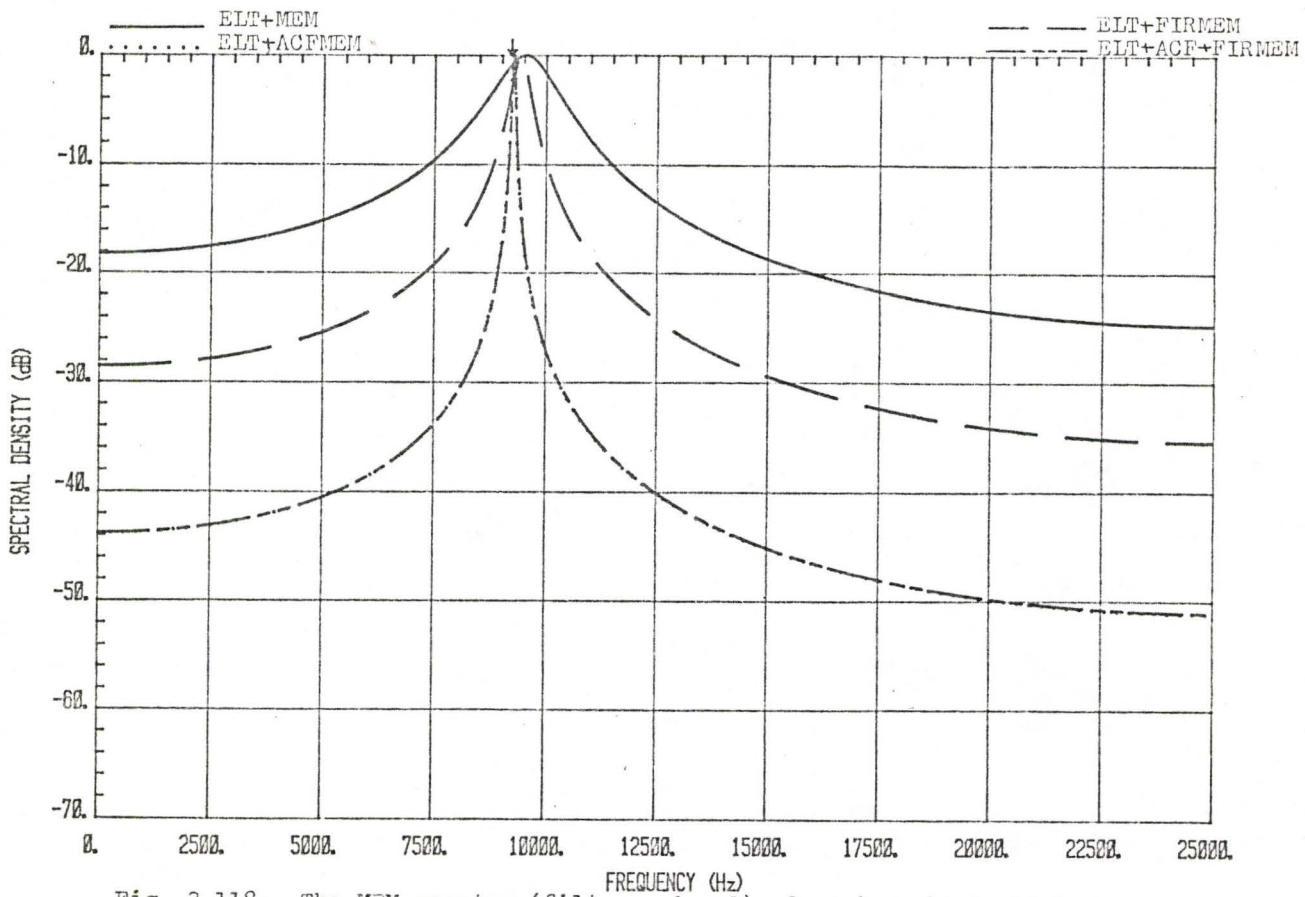


Fig. 3.118: The MEM spectra (filter order 2) of a sinusoidal-modulated signal with carrier frequency=9237 Hz and CNDR=54 dB-Hz.

simulation procedures of these signals and the mentioned digital signal processing methods. Processing results of one ELT signal (this includes various signal formats) were used to compare the effectiveness of the two spectral estimations.

The occurrence of sidelobes, as a result of processing pulse-modulated ELT signal, in the FFT spectra jeopardizes detection substantially. Windowing techniques have the ability to alleviate the light sidelobe problem. Random phase ELT signal, which suffers severe sidelobes problem in the FFT spectra, possesses limited detection capability. The advantage of using the MEM spectral analysis is that it can suppress sidelobes activities at a low order of prediction error filter. With the combination of utilizing the autocorrelation function and bandpass filter as a preprocessor, the MEM spectral performance is improved drastically.

We observe that there is a substantial improvement in the frequency resolution of the MEM analysis if one processes the autocorrelation function of a given ELT signal. In view of this, the resolution errors produced by the MEM and the ACFMEM (using a filter order of 2) processors across the entire frequency band were measured.

The spectral performance of the ELT signals embedded in different values of carrier-to-noise density ratio were investigated at the end of the chapter.

## CHAPTER 4

### PROCESSING OF MULTIPLE ELT SIGNALS

#### 4.1 INTRODUCTORY REMARKS

In the previous chapter, we presented various methods of detecting the presence of one ELT signal. Now, we proceed with the investigation testing the capabilities of these processing techniques assuming multiple signals. The program ELTAP (Appendix D) is designed to simulate any number of ELT signals up to a maximum of ten. These signals are modelled under the worst case conditions in which the distance between emergency sites and the time of occurrences are close enough such that the satellite, in receiving the signals, treats their time differences as negligible. Specifically, in this chapter, the analysis is presented for two, three, five and ten distress signals. The simulations are mainly limited to signals with identical modulation (for instance, two signals with sinusoidal modulation or five signals with continuous phase pulse-modulation) and at equal carrier-to-noise density ratio. However, one case is considered having two signals with continuous phase pulse-modulation and one signal with random phase pulse-modulation described in Appendix F.

As the number of ELT signals increases, the performance of spectral estimation degrades significantly. Results of the FFT analysis indicates that detection is severely restricted in the presence of numerous sidelobes. In order to tackle the problem, we apply a high

value of MEM filter order to the four configurations of the preprocessors. One of the shortcomings of this technique is that we are unable to assign an appropriate filter order which can process all the incoming ELT signals. However, an estimate of the number of signals is indicated by both the MEM and ACFMEM plots. This will be discussed later. An alternative approach, using a bank of bandpass filters, is suggested to combat the problem.

#### 4.2 PROCESSING MULTIPLE ELT SIGNALS EMPLOYING THE FFT ALGORITHM

One major disadvantage which dominates the spectral estimation of the Fast Fourier Transform analysis in processing ELT signals is the sidelobe problem. Although the windowing technique is used to alleviate the trouble of high sidelobes, the result is still unsatisfactory. We expect that in solving multiple signals, the sidelobe interference increases substantially. The spectra of two, five and ten ELT signals are examined individually in this section. These signals contain linear frequency sweep and have carrier frequencies which are randomly selected. Also, we assume that the signals are transmitted in the absence of additive noise.

##### 4.2.1 Two ELT Signals

A received emergency signal containing two pulse-modulated ELT signals (36% duty cycle and continuous phase) at frequencies 9448 Hz and 15039 Hz is examined. The FFT spectrum is plotted in Fig. 4.1. It is an easy task to identify that one signal is at 15039 Hz. However, at -5dB threshold level we need to determine the true peak of the other

signal. Using Kaiser window ( $\beta = 8.0$ ), both of the peaks at 9472 Hz and 15039 Hz emerge from the sidelobes, as shown in Fig. 4.2. A frequency error (according to Eq. (3.6)) of -24 Hz is measured for the ELT signal at 9448 Hz. Detection (even with windowing) is extremely difficult if the signals are pulse-modulated and random phase. Fig. 4.3 gives the FFT spectra of these signals and Fig. 4.4 illustrates the spectra with Kaiser window  $\beta = 8$ .

When a bandpass filter (Fig. 2.8) is employed in the analysis, there is a slight improvement in the spectral performance of the continuous phase signals (without windowing technique). The two desired peaks are situated at 9423 Hz and 15039 Hz. For the random phase signals, the true peak at 9448 Hz are masked by the sidelobes. The spectra are shown in Fig. 4.5 and Fig. 4.6 for continuous phase and random phase signals, respectively. If the signals have sinusoidal modulation, an uncluttered spectrum (Fig. 4.7) is obtained.

#### 4.2.2 Five ELT Signals

Five ELT signals at frequencies 7588 Hz, 9000 Hz, 11924 Hz, 13527 Hz and 15425 Hz are used to test the capability of the FFT analysis. The spectrum of the continuous phase signals provides four prominent peaks at frequencies 7617 Hz, 8984 Hz, 11914 Hz and 15429 Hz in Fig. 4.8. These correspond to frequency errors of -29 Hz, 16 Hz, 10 Hz and -4 Hz, respectively. However, the FFT fails to resolve the signal at 13527 Hz. The windowing technique loses its usefulness as more signals are involved. This can be proved by Fig. 4.9. Note that the signal at frequency 13527 Hz is still not resolved and the sidelobe at frequency

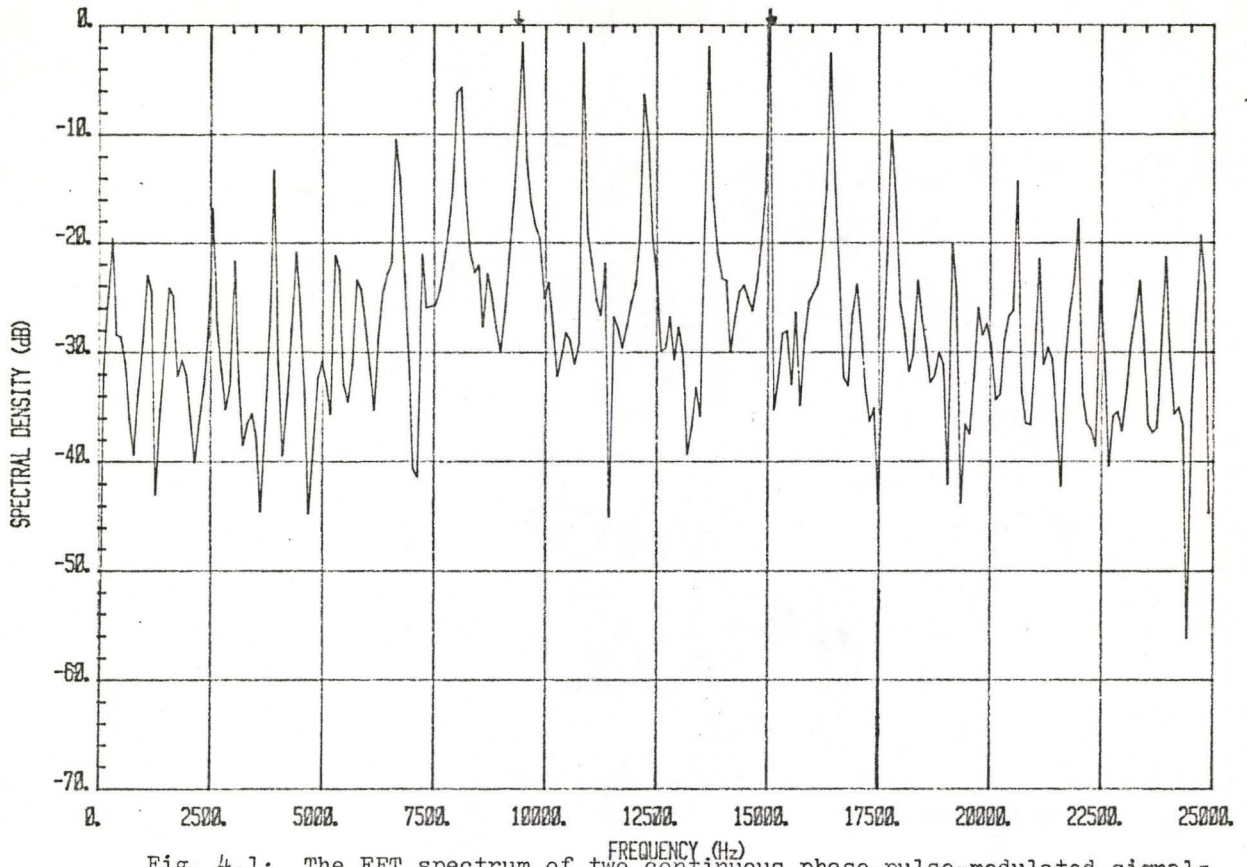


Fig. 4.1: The FFT spectrum of two continuous phase, pulse-modulated signals with carrier frequencies 9448 Hz and 15039 Hz.

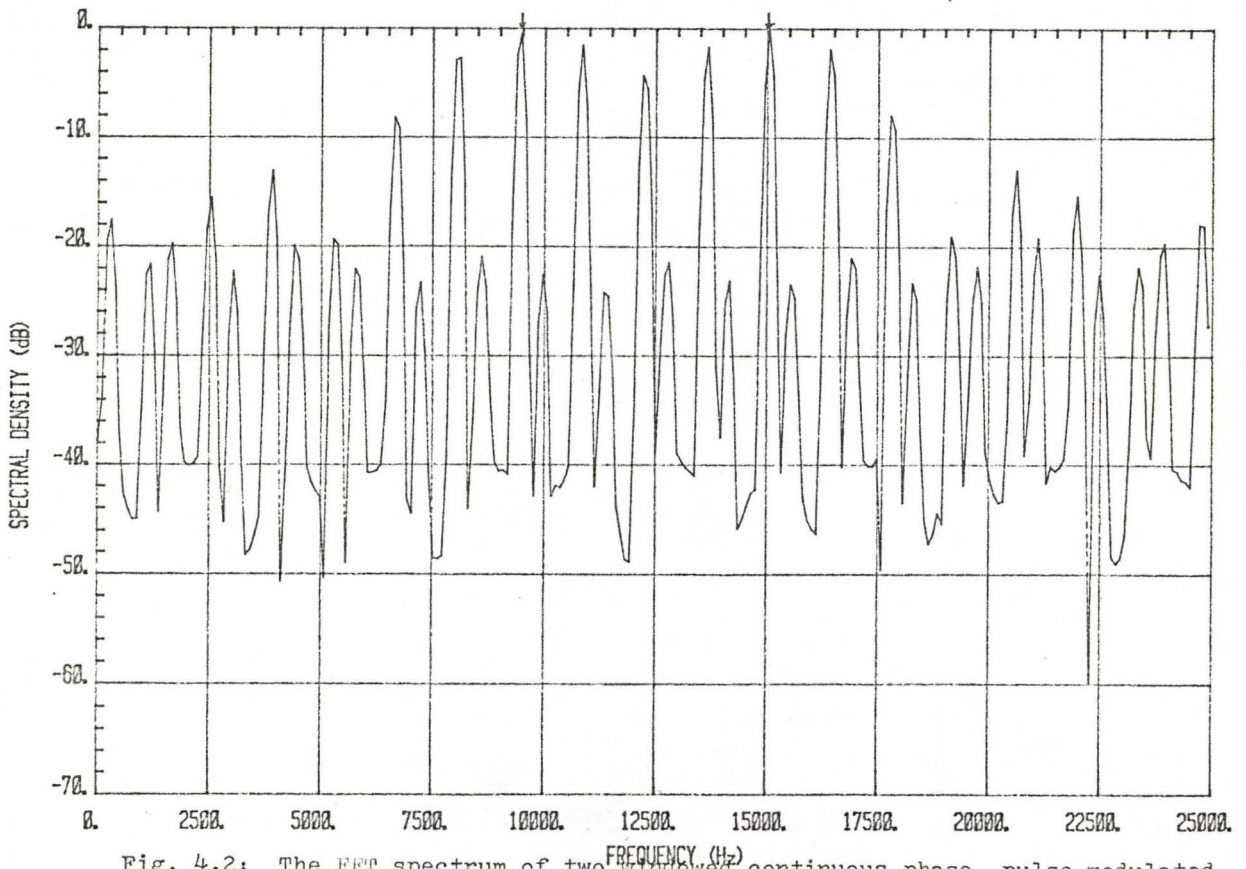


Fig. 4.2: The FFT spectrum of two windowed continuous phase, pulse-modulated signals with carrier frequencies 9448 Hz and 15039 Hz.

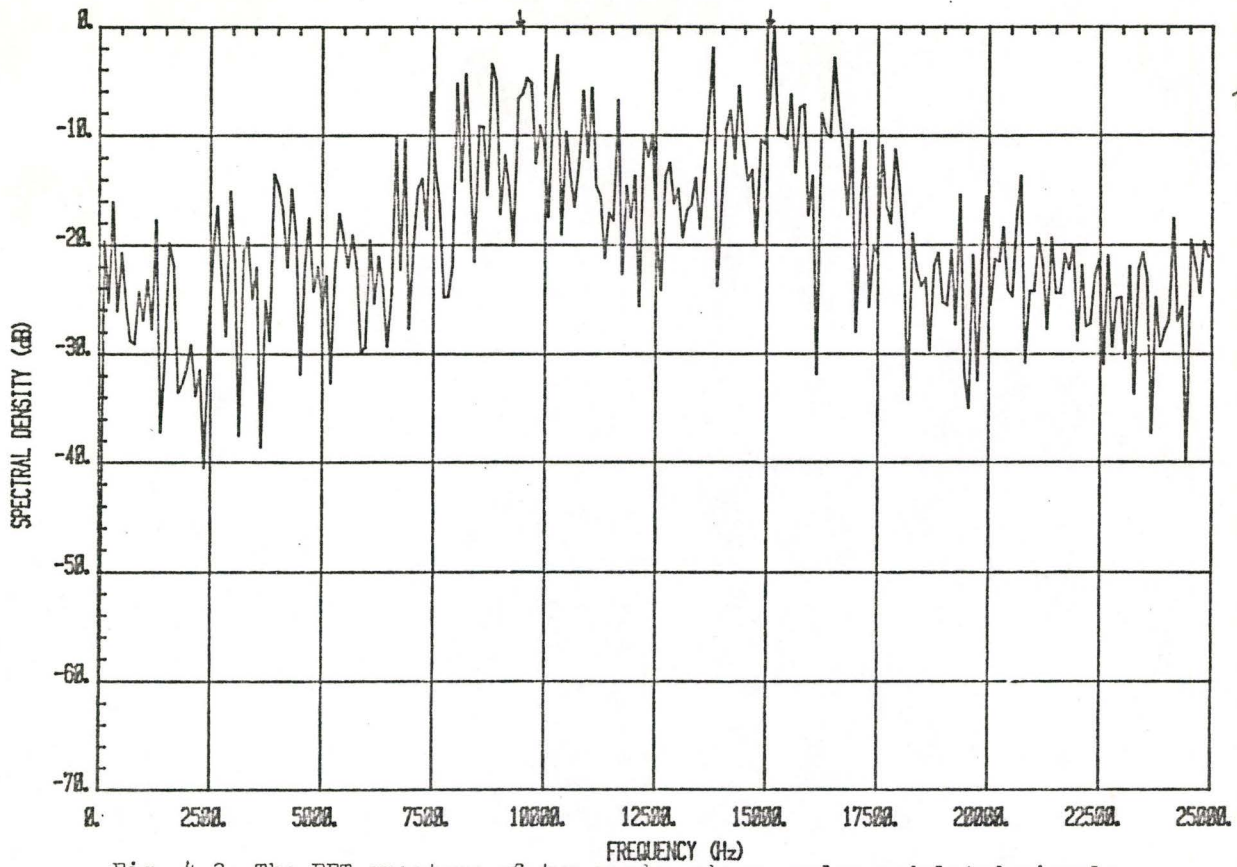


Fig. 4.3: The FFT spectrum of two random phase, pulse-modulated signals with carrier frequencies 9448 Hz and 15039 Hz.

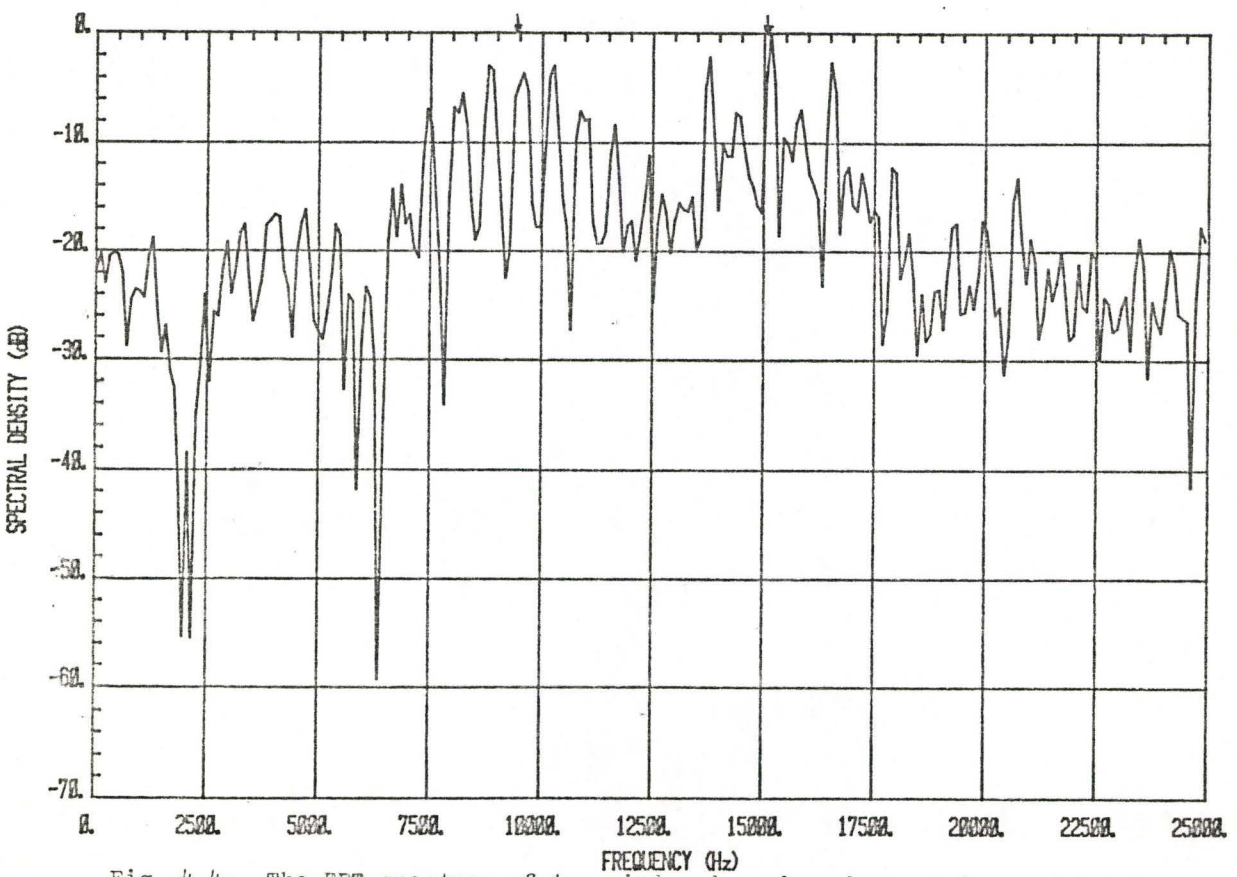


Fig. 4.4: The FFT spectrum of two windowed random phase, pulse-modulated signals with carrier 9448 Hz and 15039 Hz.

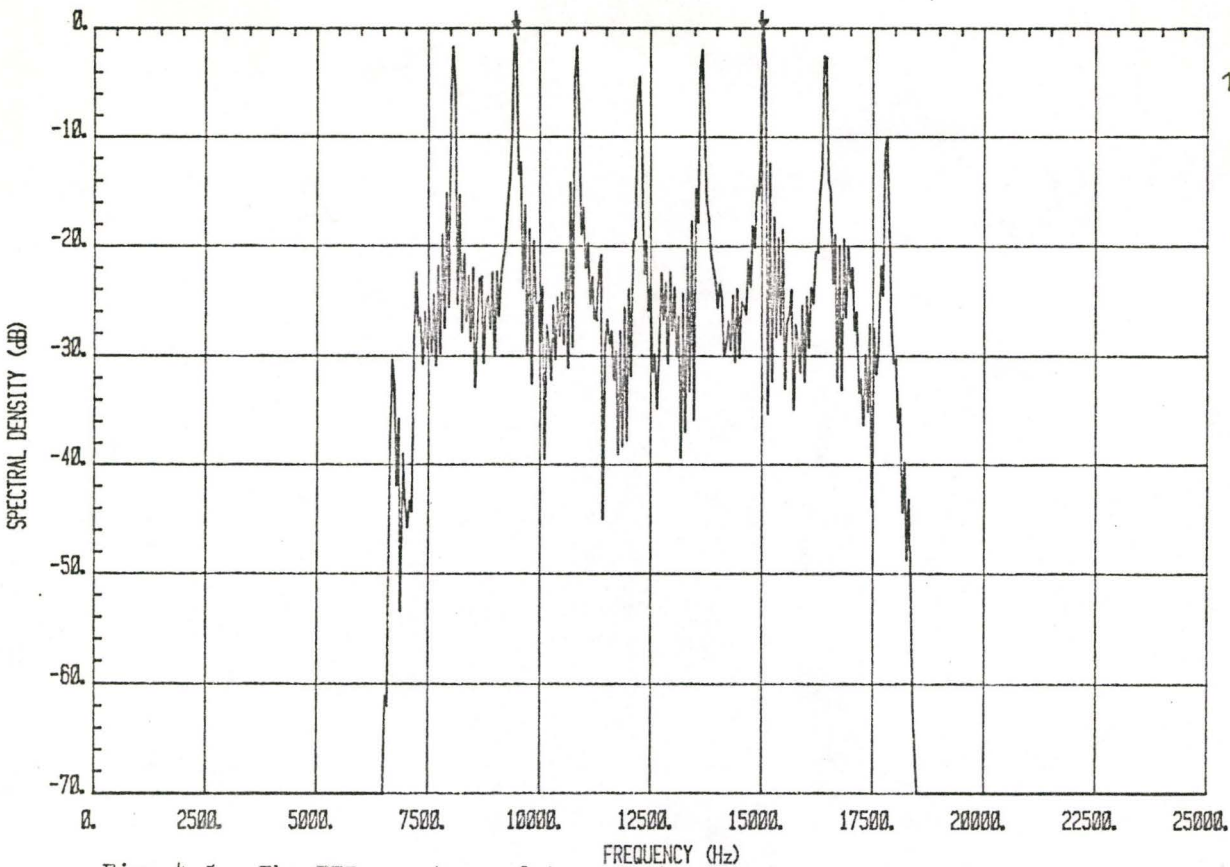


Fig. 4.5: The FFT spectrum of two continuous phase, pulse-modulated signals with carrier frequencies 9448 Hz and 15039 Hz filtered by a bandpass filter.

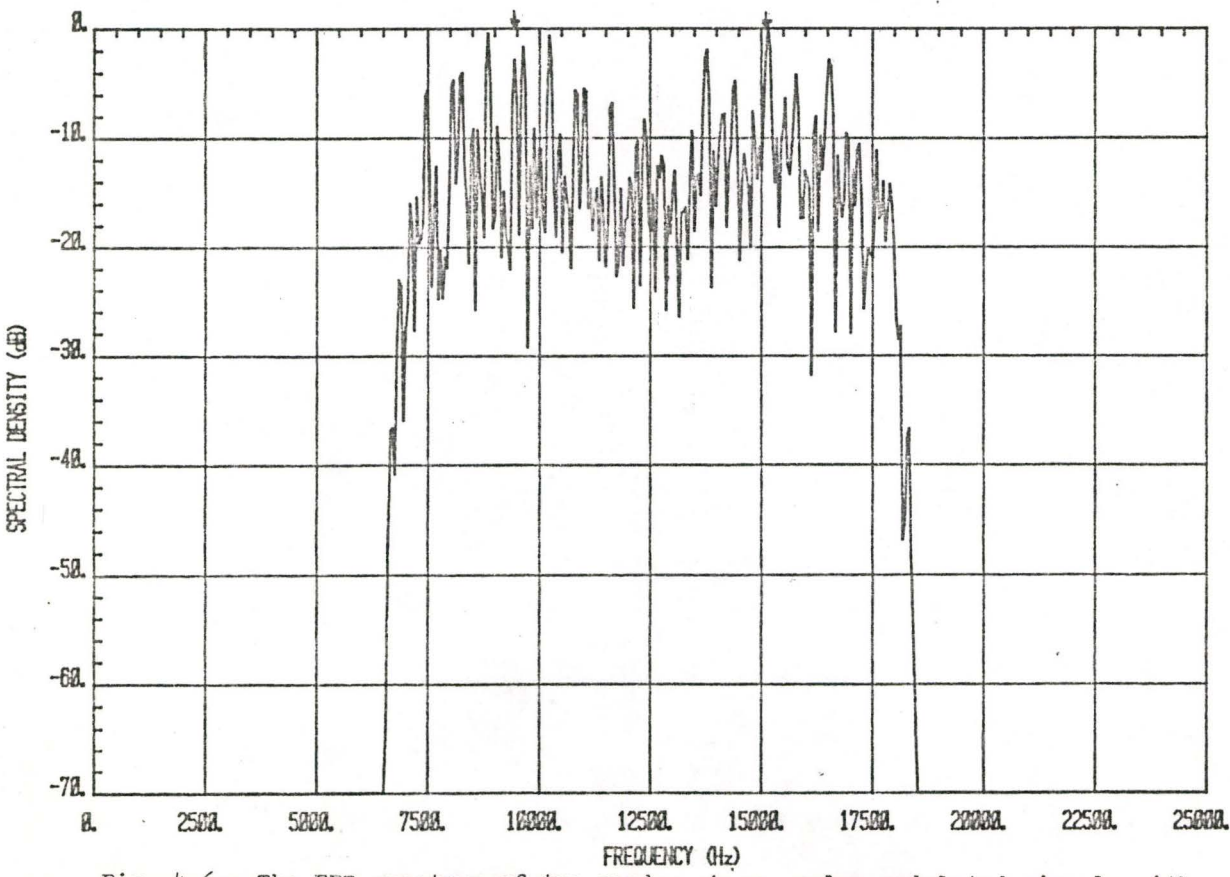


Fig. 4.6: The FFT spectrum of two random phase, pulse-modulated signals with carrier frequencies 9448 Hz and 15039 Hz filtered by a bandpass filter.

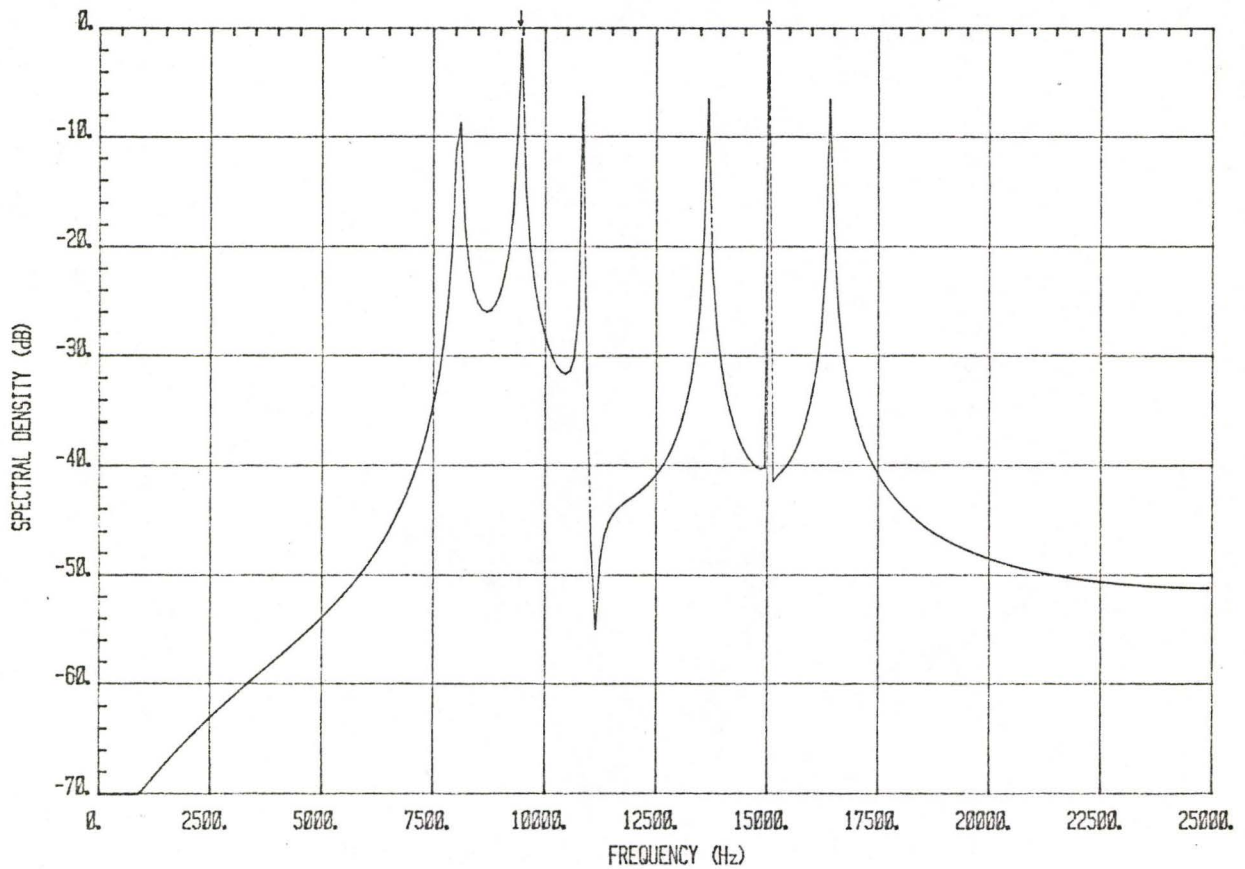


Fig. 4.7: The FFT spectrum of two sinusoidal-modulated signals with carrier frequencies 9448 Hz and 15039 Hz.

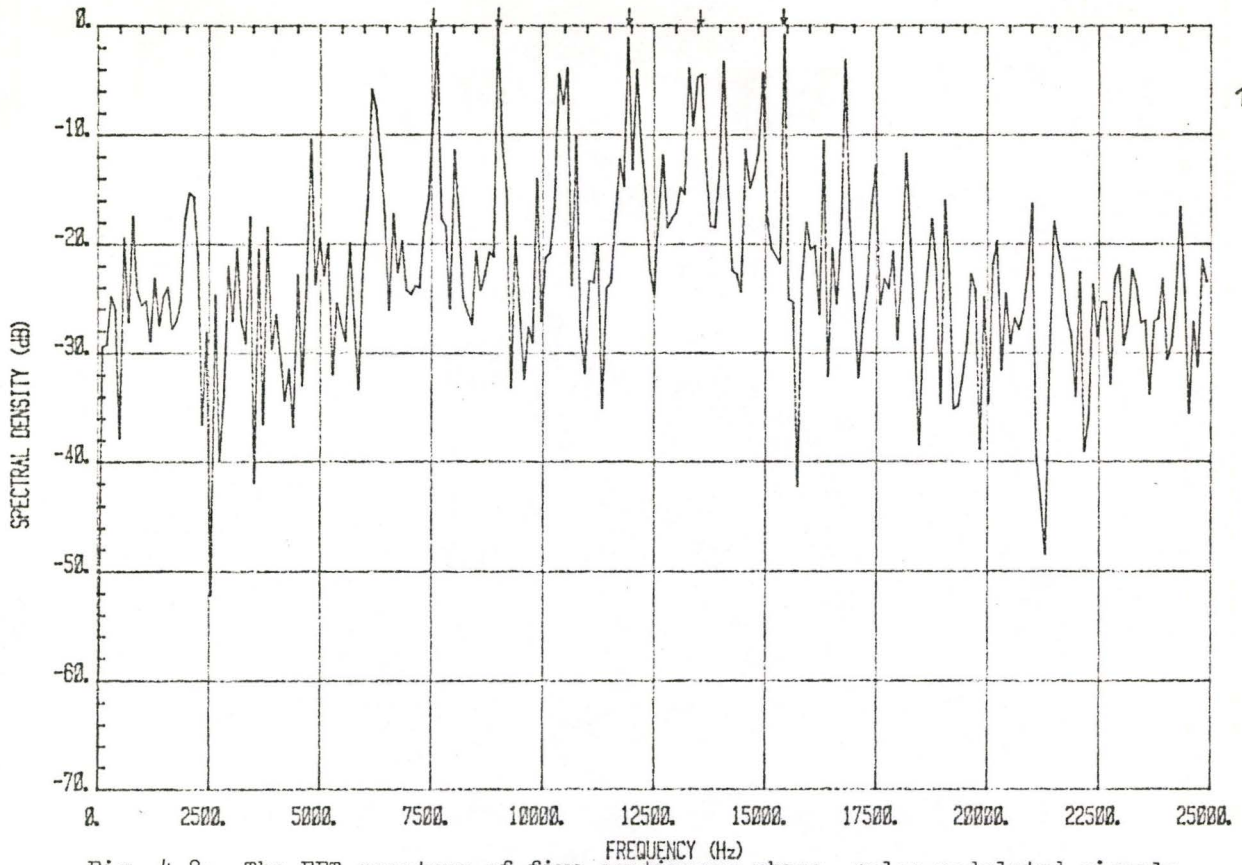


Fig. 4.8: The FFT spectrum of five continuous phase, pulse-modulated signals with carrier frequencies 7588 Hz, 9000 Hz, 11924 Hz, 13527 Hz and 15425 Hz.

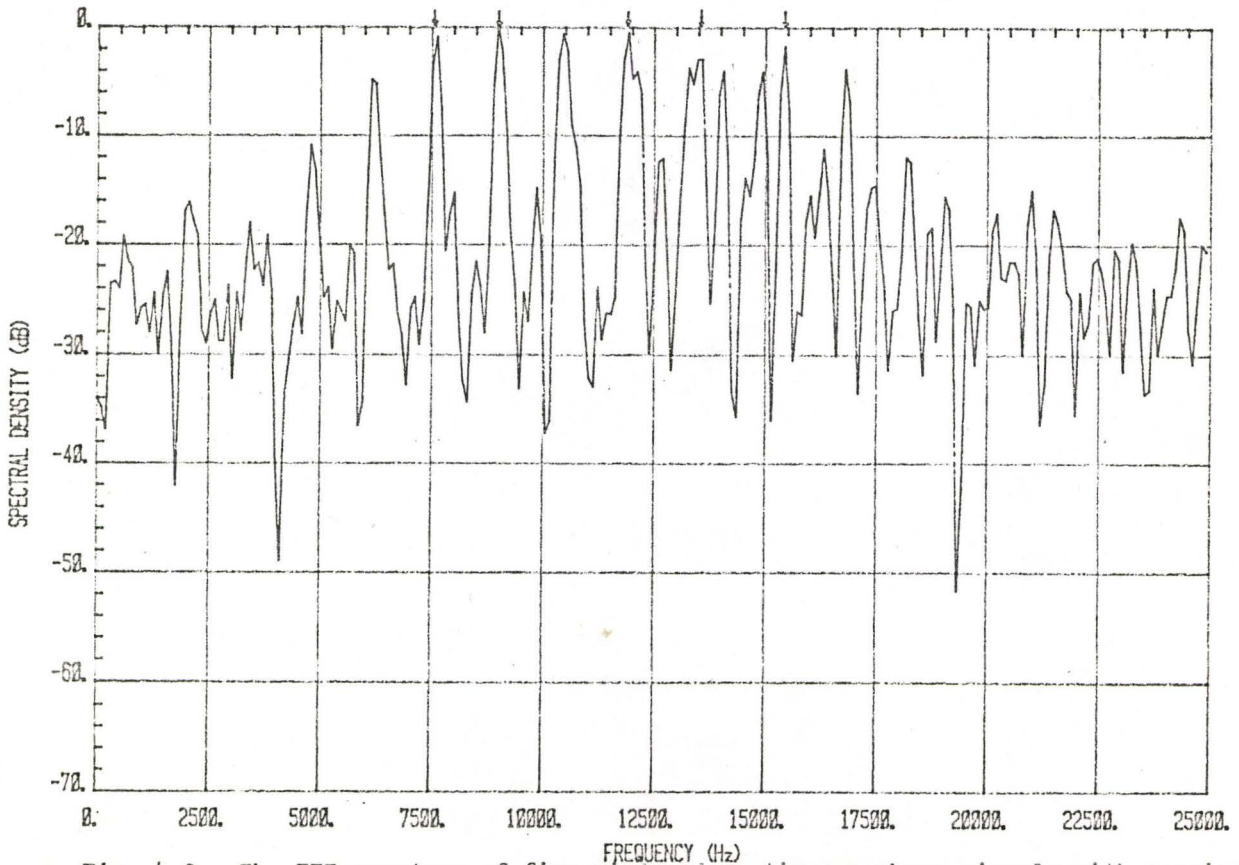


Fig. 4.9: The FFT spectrum of five windowed continuous phase signals with carrier frequencies 7588 Hz, 9000 Hz, 11924 Hz, 13527 Hz and 15425 Hz.

10500 Hz has risen by approximately 4 dB.

The spectrum of the random phase signals given in Fig. 4.10 discloses that detection is very difficult. Both continuous phase and random phase signals are then passed through the bandpass filter. Fig. 4.11 and Fig. 4.12 illustrate the spectra of the two cases. The peak which is missed in Fig. 4.8 can be recovered in Fig. 4.11 at frequency 13525 Hz. There is no improvement for the random phase signals. At -5 dB threshold level, the sinusoidal modulation signals yield reasonable frequency resolution which is presented in Fig. 4.13.

#### 4.2.3 Ten ELT Signals

The spectra of ten ELT signals, at carrier frequencies 7441 Hz, 8504 Hz, 9640 Hz, 10483 Hz, 11876 Hz, 12683 Hz, 13636 Hz, 14846 Hz, 16165 Hz and 17595 Hz, are depicted in Fig. 4.14 to Fig. 4.18. Detection fails completely for the pulse-modulated signals either with continuous phase or with random phase.

It has been verified that the FFT approach does not offer feasible resolution in the event of multiple ELT signals. In the next section, the same sets of signals are applied to explore the MEM spectral estimation.

### 4.3 PROCESSING MULTIPLE ELT SIGNALS EMPLOYING THE MEM

In spite of its ability to reduce the sidelobe problem, the MEM experiences the dilemma of choosing filter order for the prediction error filter. For a single ELT signal, filter orders 2, 3 or 10 favour the MEM analysis. Nevertheless, when an incident of multiple ELT

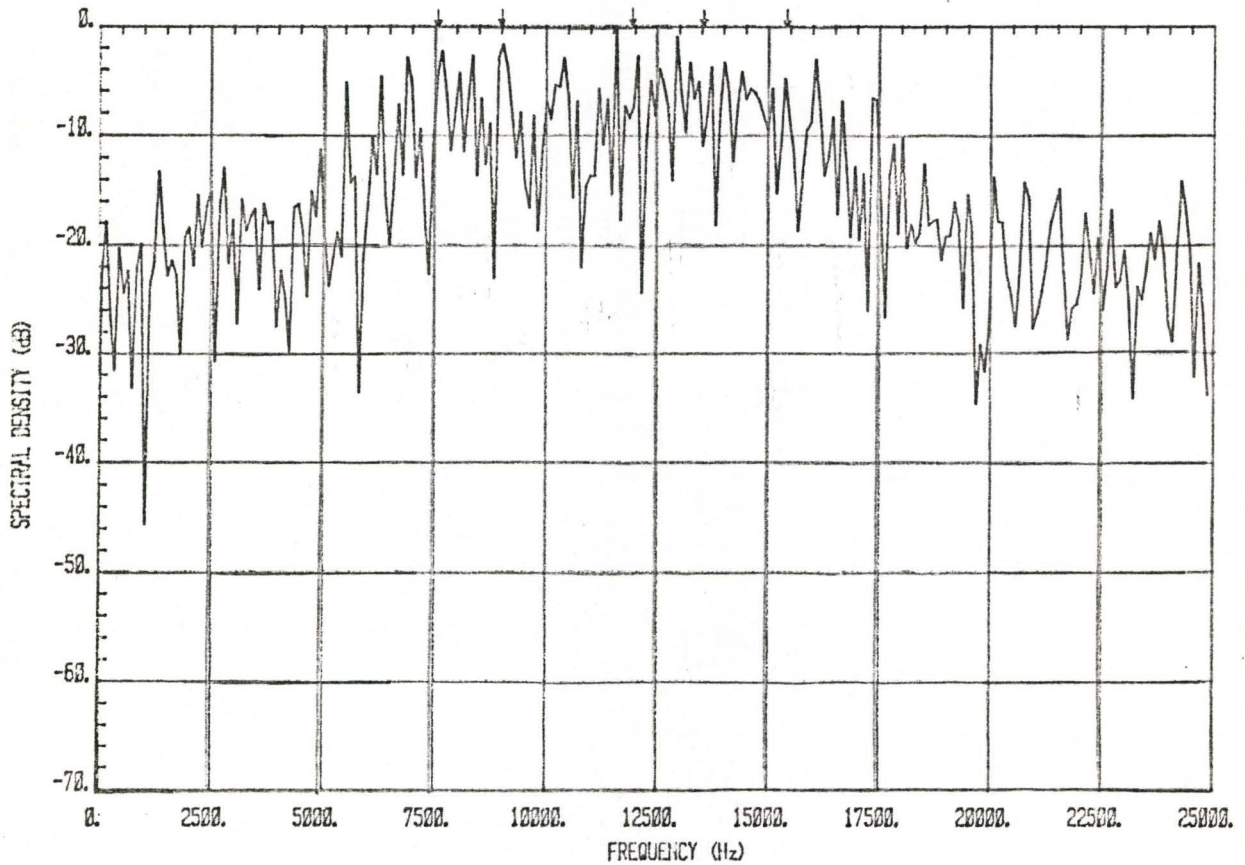


Fig. 4.10: The FFT spectrum of five random phase, pulse-modulated signals with carrier frequencies 7588 Hz, 9000 Hz, 11924 Hz, 13527 Hz and 15425 Hz.

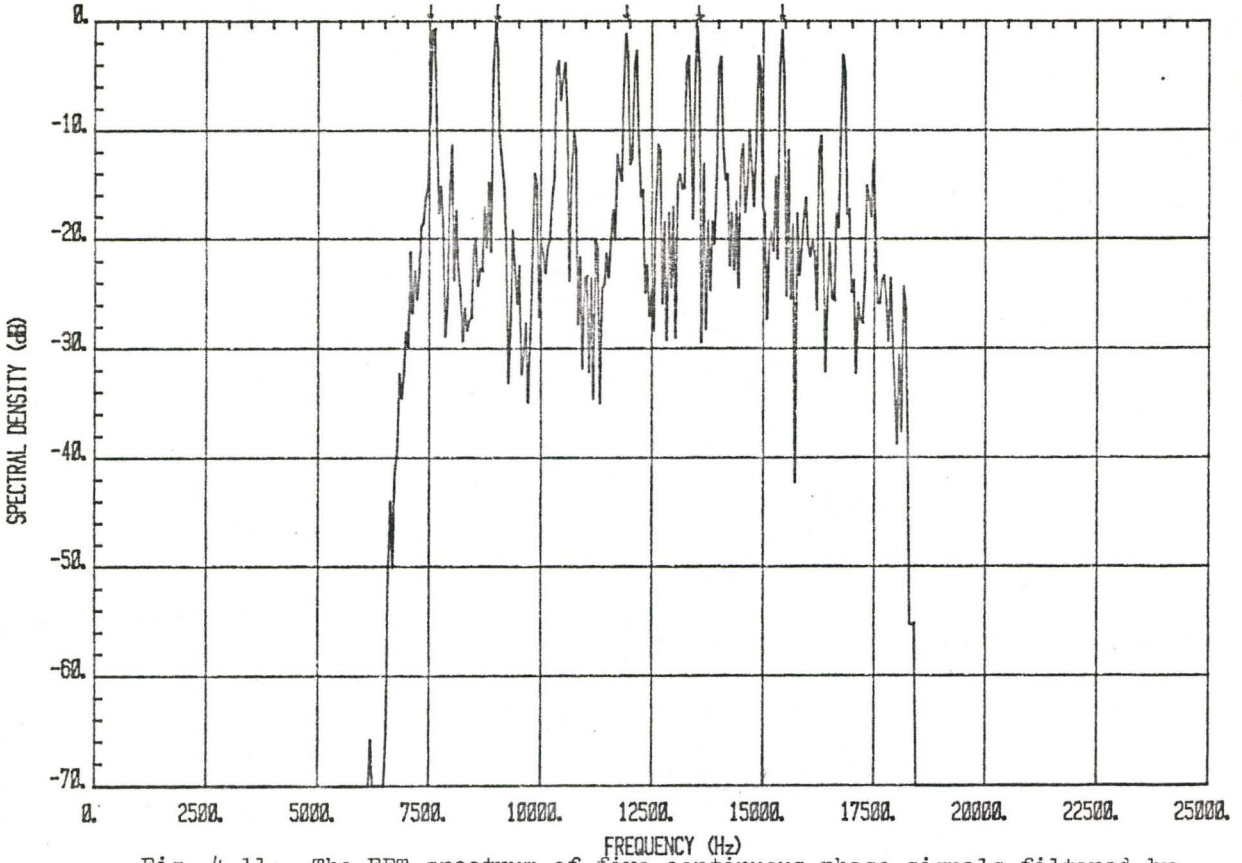


Fig. 4.11: The FFT spectrum of five continuous phase signals filtered by a bandpass filter.

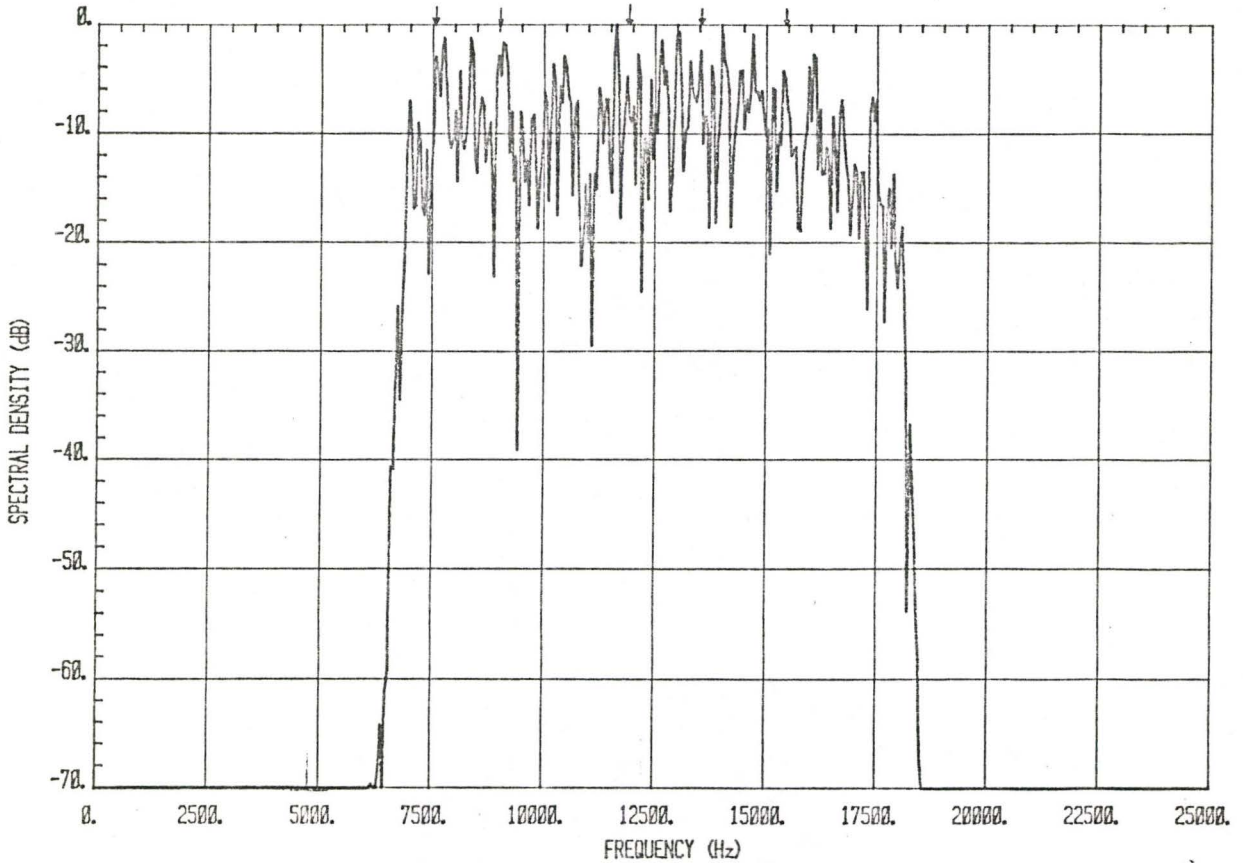


Fig. 4.12: The FFT spectrum of five random phase signals filtered by a bandpass filter.

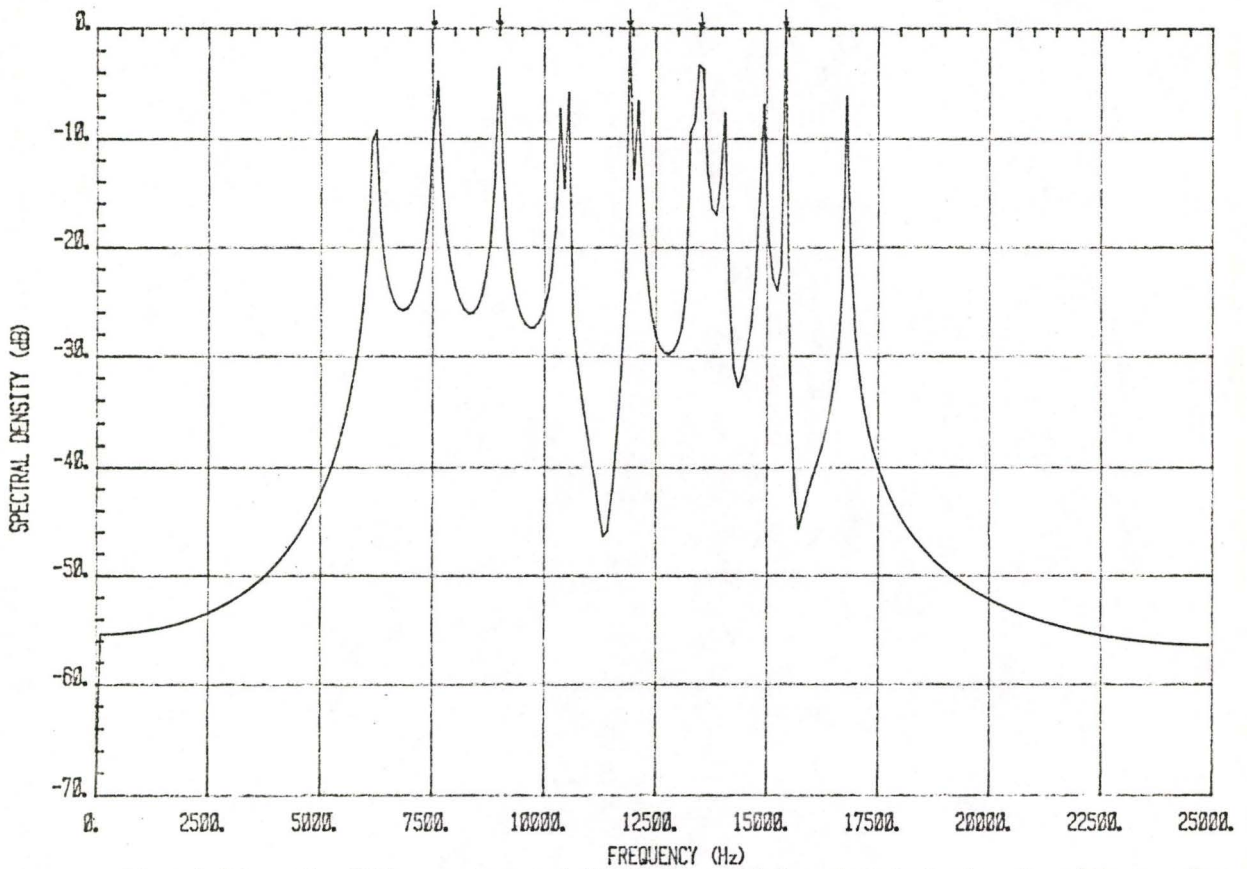


Fig. 4.13: The FFT spectrum of five sinusoidal-modulated signals with carrier frequencies 7588 Hz, 9000 Hz, 11924 Hz, 13527 Hz and 15425 Hz.

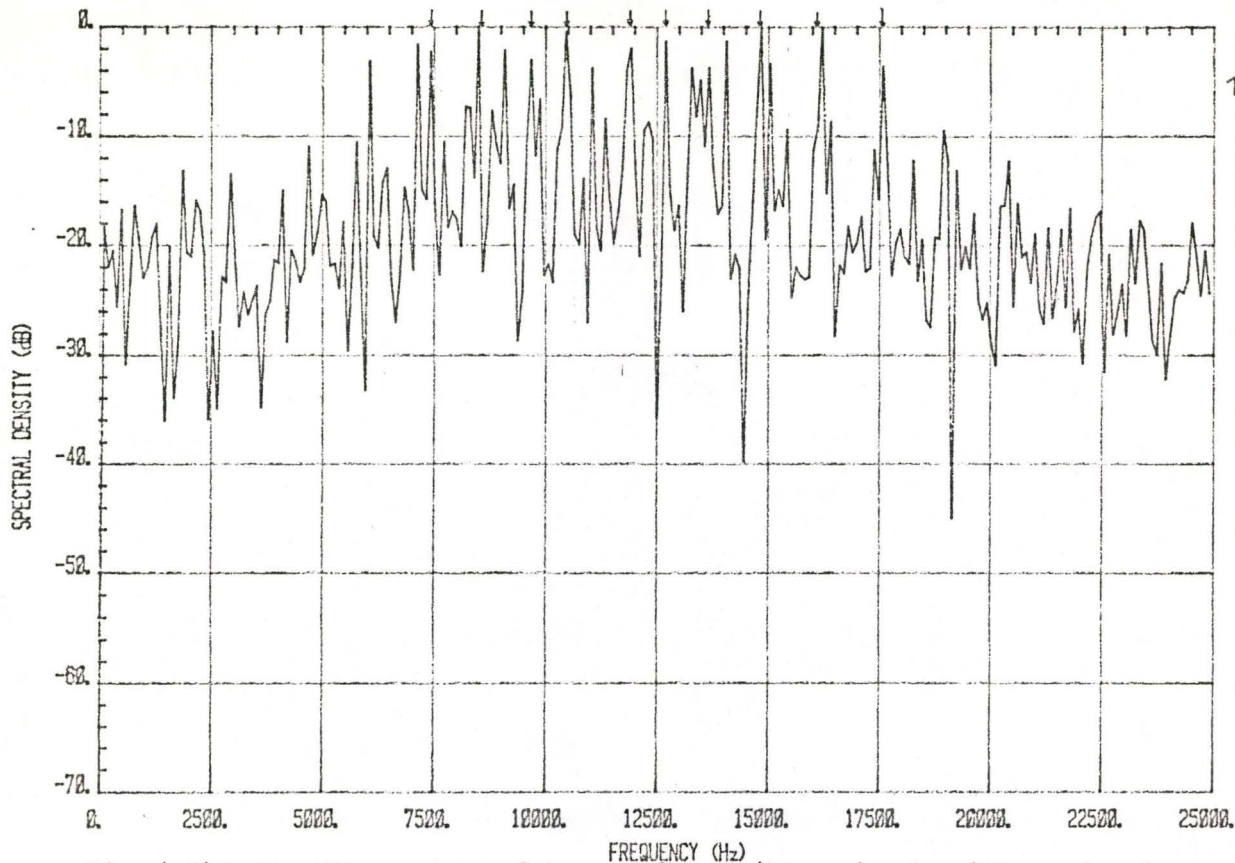


Fig. 4.14: The FFT spectrum of ten continuous phase signals with carrier frequencies 7441 Hz, 8504 Hz, 9640 Hz, 10483 Hz, 11876 Hz, 12683 Hz, 13636 Hz, 14846 Hz, 16165 Hz and 17595 Hz.

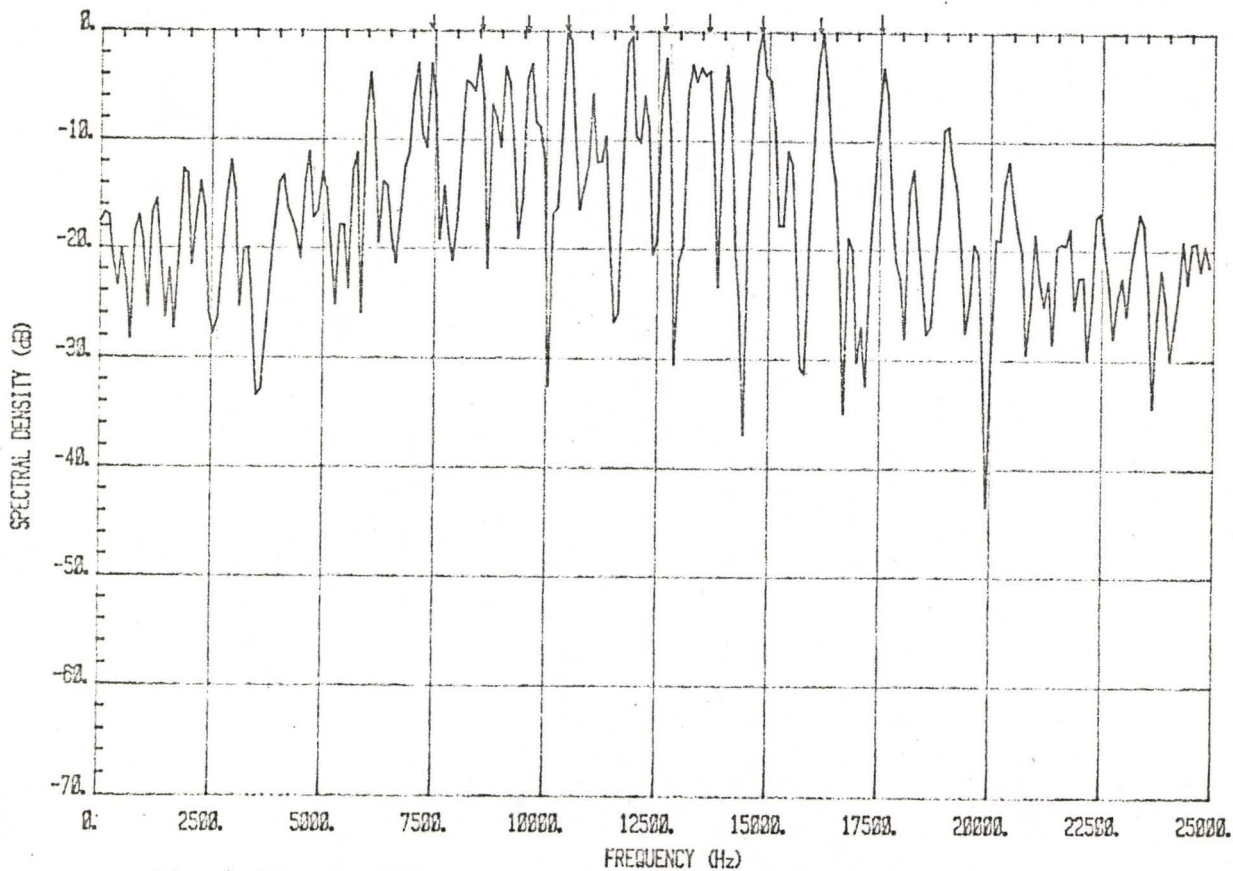


Fig. 4.15: The FFT spectrum of ten windowed continuous phase signals.

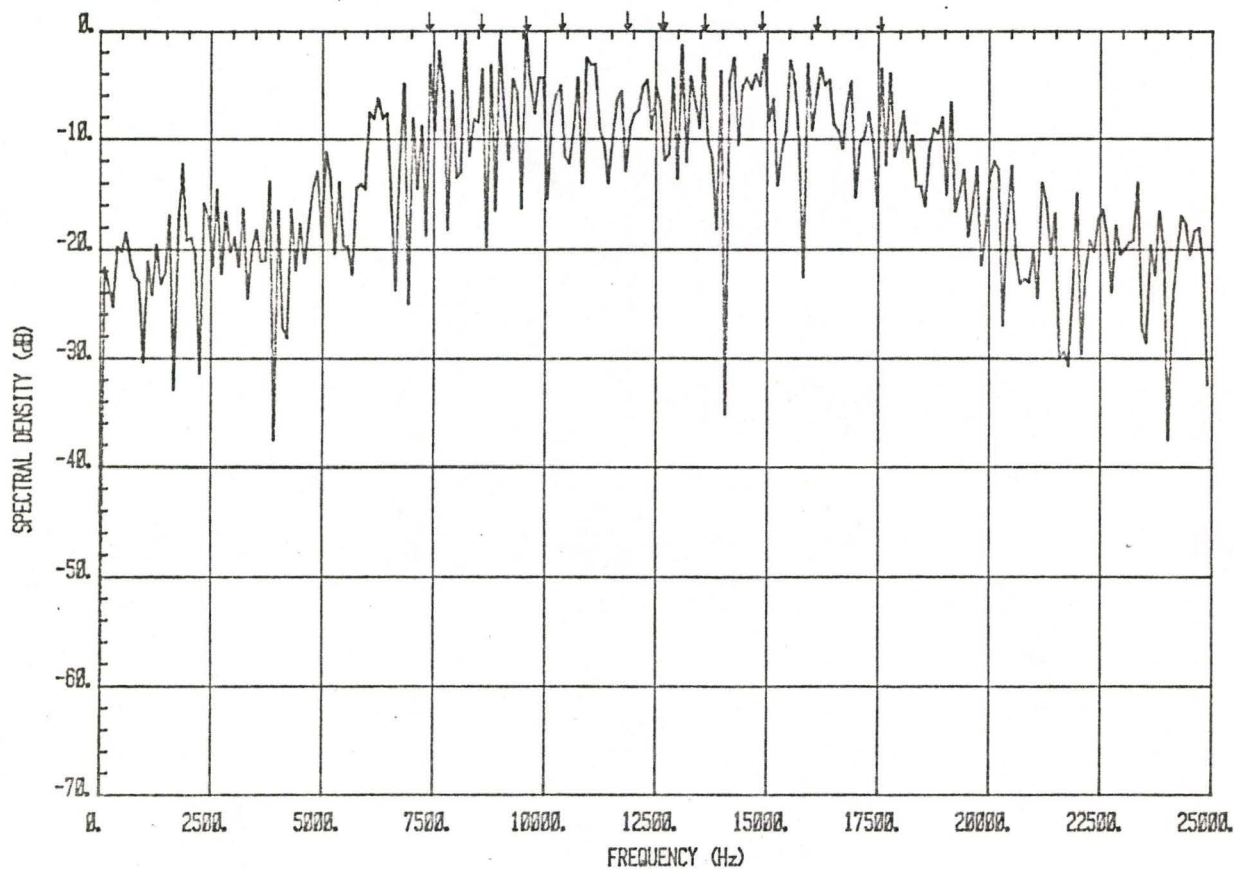


Fig. 4.16: The FFT spectrum of ten random phase signals with carrier frequencies 7441 Hz, 8504 Hz, 9640 Hz, 10483 Hz, 11876 Hz, 12683 Hz, 13636 Hz, 14846 Hz, 16165 Hz and 17595 Hz.

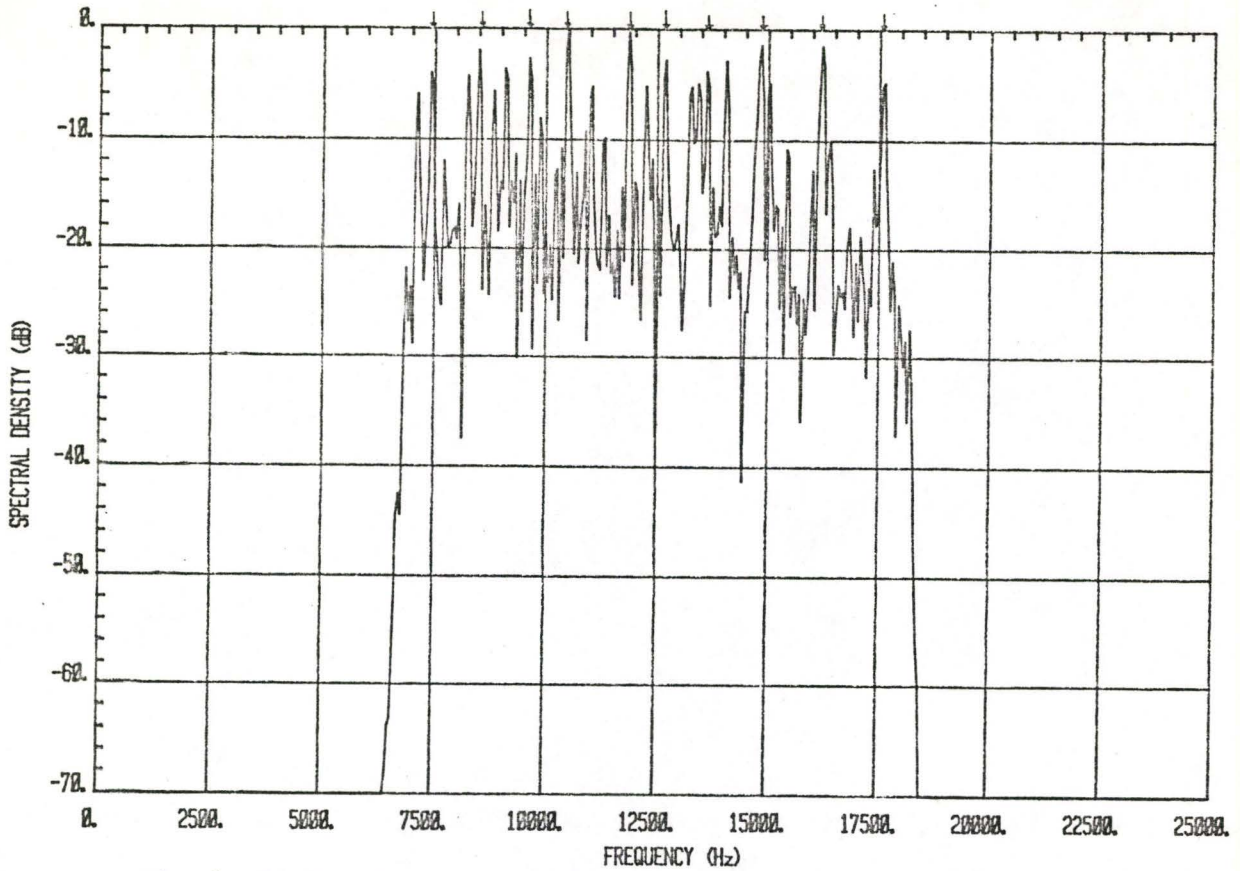


Fig. 4.17: The FFT spectrum of ten continuous phase signals filtered by a bandpass filter.

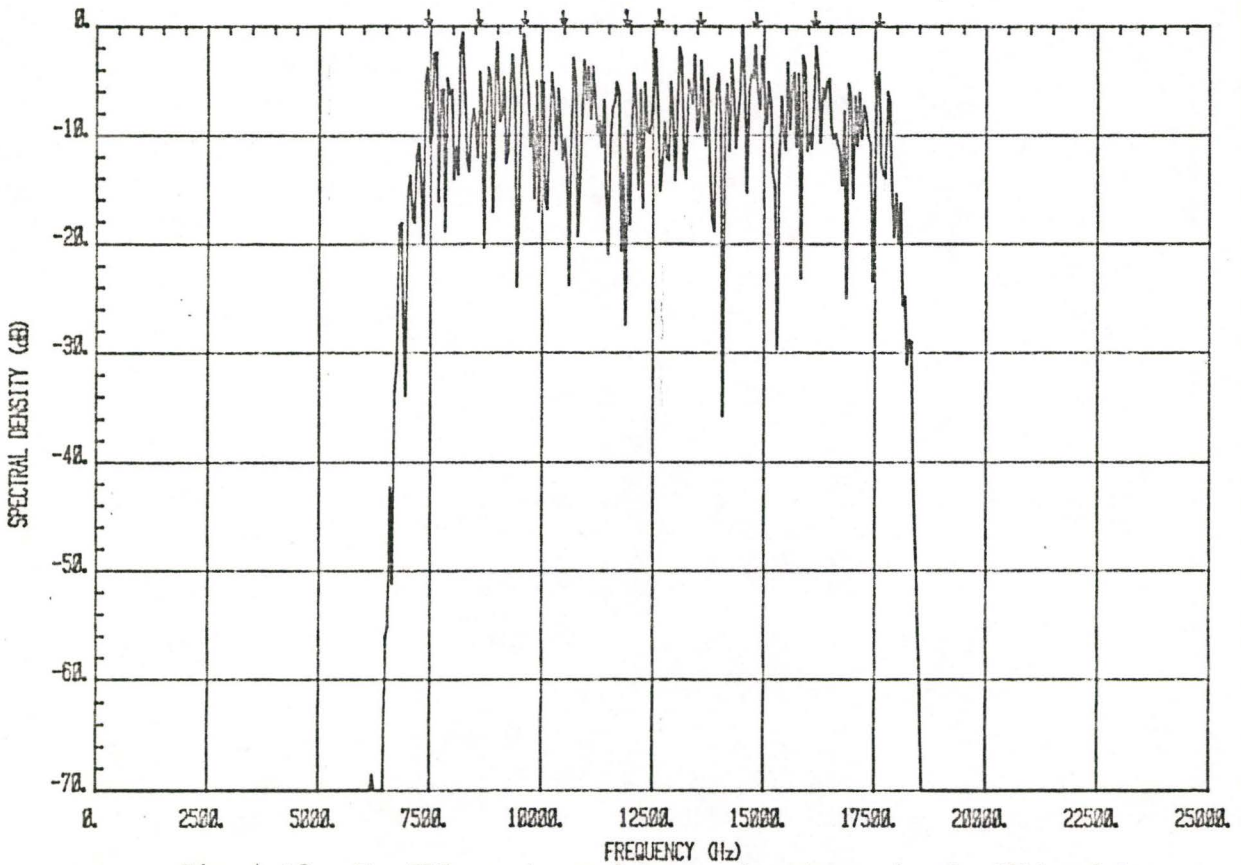


Fig. 4.18: The FFT spectrum of ten random phase signals filtered by a bandpass filter.

signals is encountered, it is a complex task to determine which filter order is eligible to produce a sound spectrum.

One possible method is to examine the number of peaks in the spectral curves for both MEM and ACFMEM as the filter order increases. We note that the number of peaks increases until the point is reached where the number of peaks equals the number of signals. Beyond this point, there is no increase in the number of peaks as filter order is increased. This test is most reliable with small numbers of signals.

#### 4.3.1 Two ELT Signals

The two pulse-modulated ELT signals with continuous phase structure at carrier frequencies 9448 Hz and 15039 Hz are processed by the four configurations ('ELT+MEM', 'ELT+ACFMEM', 'ELT+FIRMEM' and 'ELT+ACF+FIRMEM') using the MEM approach. Initially, the second order MEM is selected. The spectra which are shown in Fig. 4.19 generate a broad peak for each of the configurations. These peaks are approximately at the mid-point between the two given frequencies. From the information obtained, we might conclude that the received emergency signal is due to just one ELT. If a fourth order MEM is used, the situation becomes clearer. Although the 'ELT+MEM' gives very broad peaks, as in Fig. 4.20, these are close to the correct frequencies. Among the other three cases, only the 'ELT+ACF+FIRMEM' offers a good resolution. The two peaks are separately located at 9457 Hz and 15139 Hz which are equivalent to frequency errors of -9 Hz and -100 Hz. One point which is worthy of mention is that in processing a single ELT signal at the same MEM filter order (Fig. 3.26), the spectra are

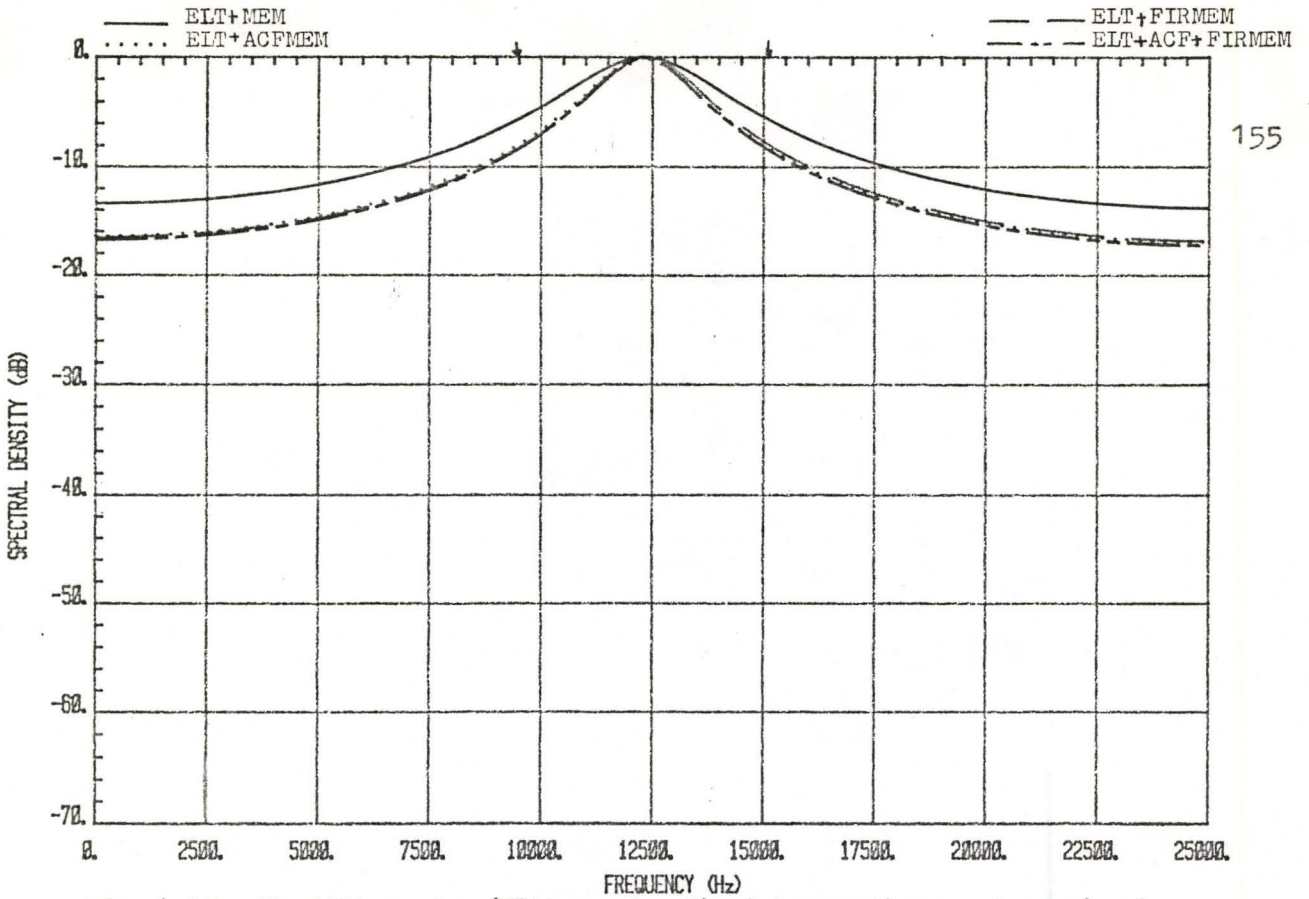


Fig. 4.19: The MEM spectra (filter order 2) of two continuous phase signals with carrier frequencies 9448 Hz and 15039 Hz.

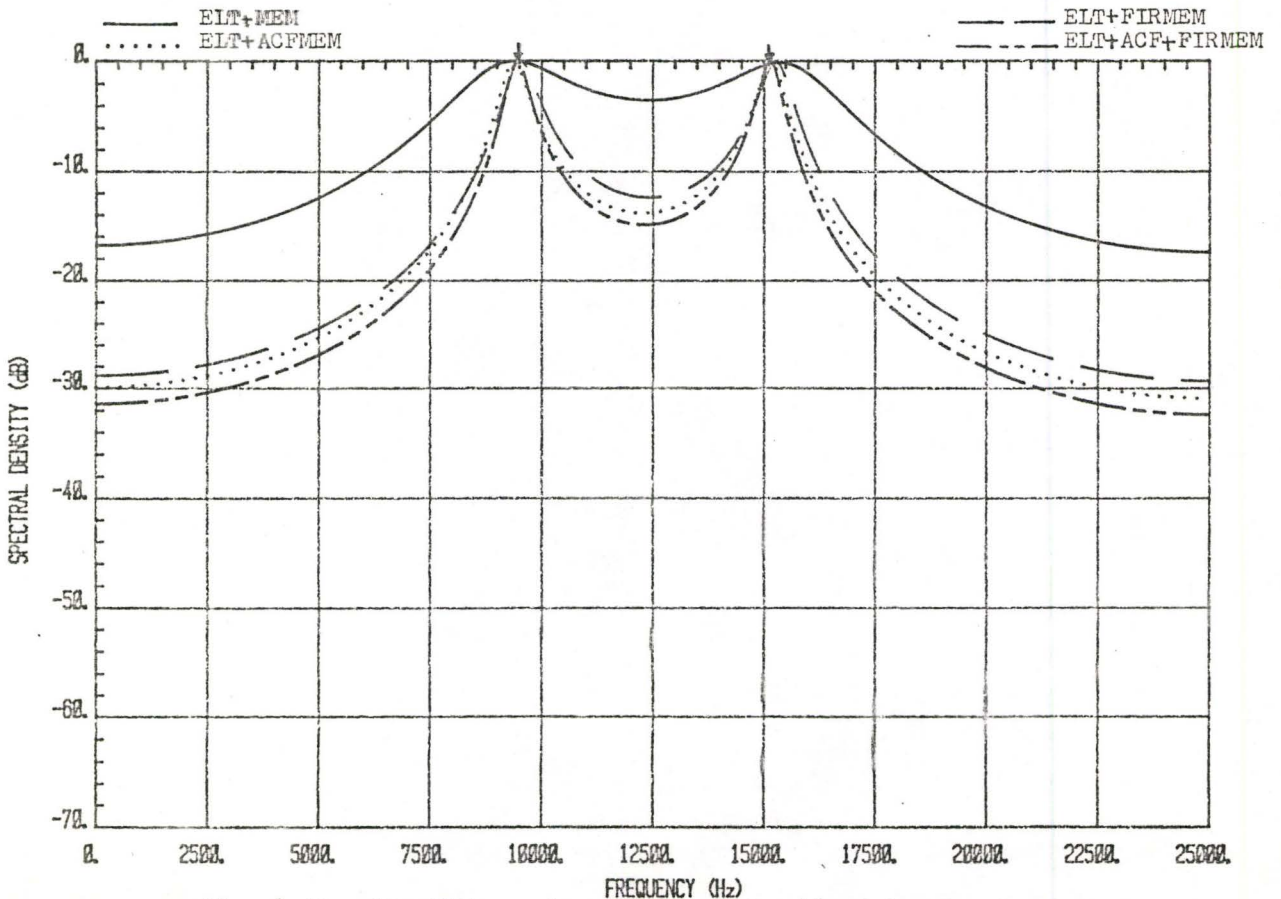


Fig. 4.20: The MEM spectra (filter order 4) of two continuous phase signals.

relatively ~~inconsistent~~ as compared with the current results.

Fig. 4.21 to Fig. 4.23 are the spectra at MEM filter orders 6, 8 and 10. The MEM and ACFMEM indicate that two signals are present. Note that these spectra are quite different to that obtained from one ELT signal (Fig. 3.27 to Fig. 3.29). With MEM filter order 20 (Fig. 4.24) the 'ELT+ACF+FIRMEM' yields excellent performance. Contrasting with the FFT spectrum given in Fig. 4.1, at -5 dB threshold level Fig. 4.24 shows that the two required peaks at frequencies 9420 Hz and 15065 Hz are given by the 'ELT+ACF+FIRMEM'. The frequency error is within 30 Hz for both measurements.

For random phase signals, the spectra are plotted in Fig. 4.25 through Fig. 4.30. Once again, we note that MEM and ACFMEM provide an indication of the number of signals present by simply observing the peak structure. Note that the lower order MEM estimates give the best estimates of carrier frequencies.

ELT signals which carry sinusoidal modulation achieve the best frequency resolution at both MEM filter orders 4 and 20, when the 'ELT+ACF+FIRMEM' is employed. The spectra are given in Fig. 4.31 and Fig. 4.32.

#### 4.3.2 Five ELT Signals

The spectral estimate for five ELT signals having frequencies 7588 Hz, 9000 Hz, 11924 Hz, 13527 Hz and 15425 Hz with continuous phase and pulse-modulation are examined in this section. The results are given in Fig. 4.33 through 4.38 for MEM orders varying from 4 to 50. Note that both the MEM and ACFMEM spectral estimates are quite flat as

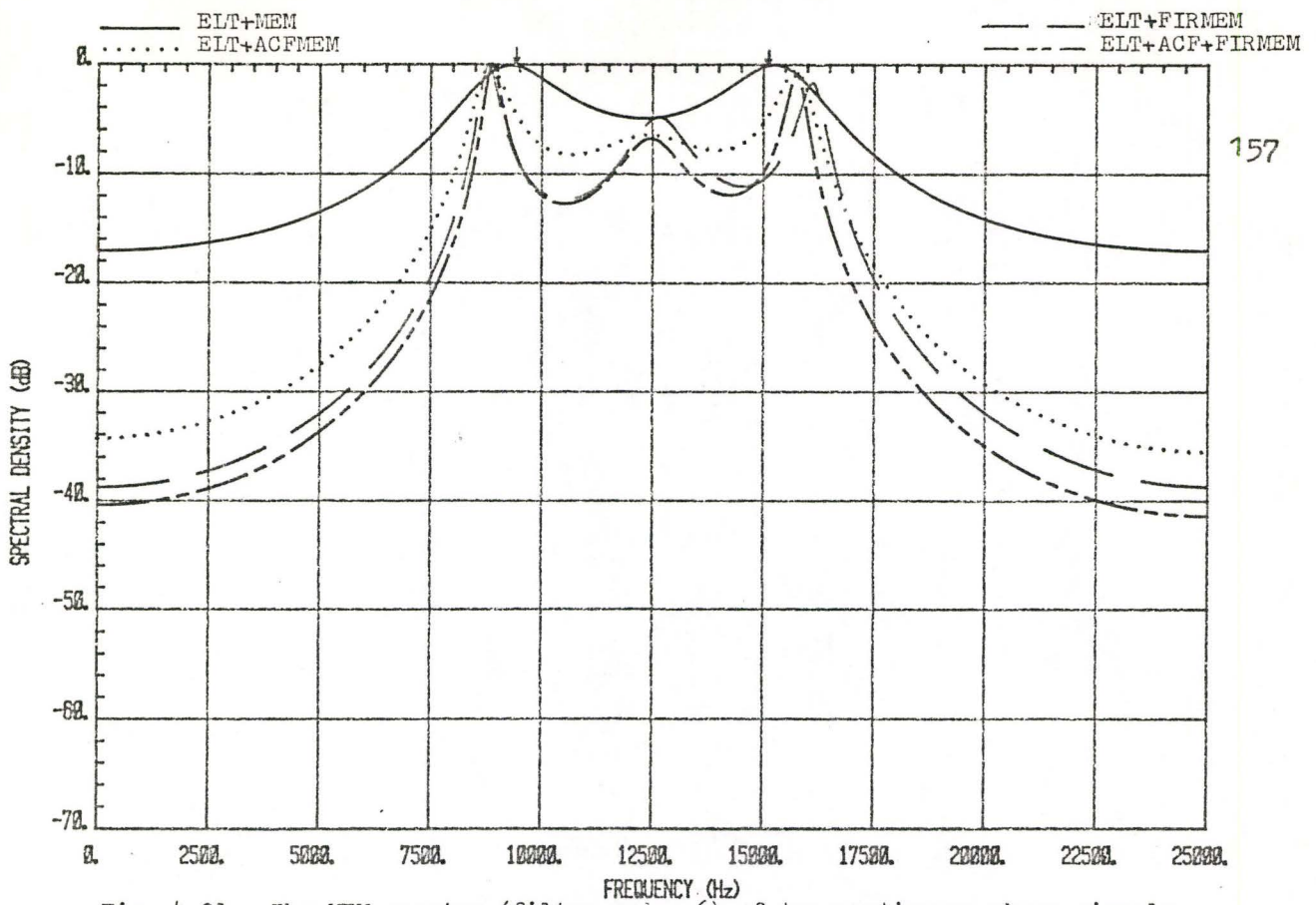


Fig. 4.21: The MEM spectra (filter order 6) of two continuous phase signals.

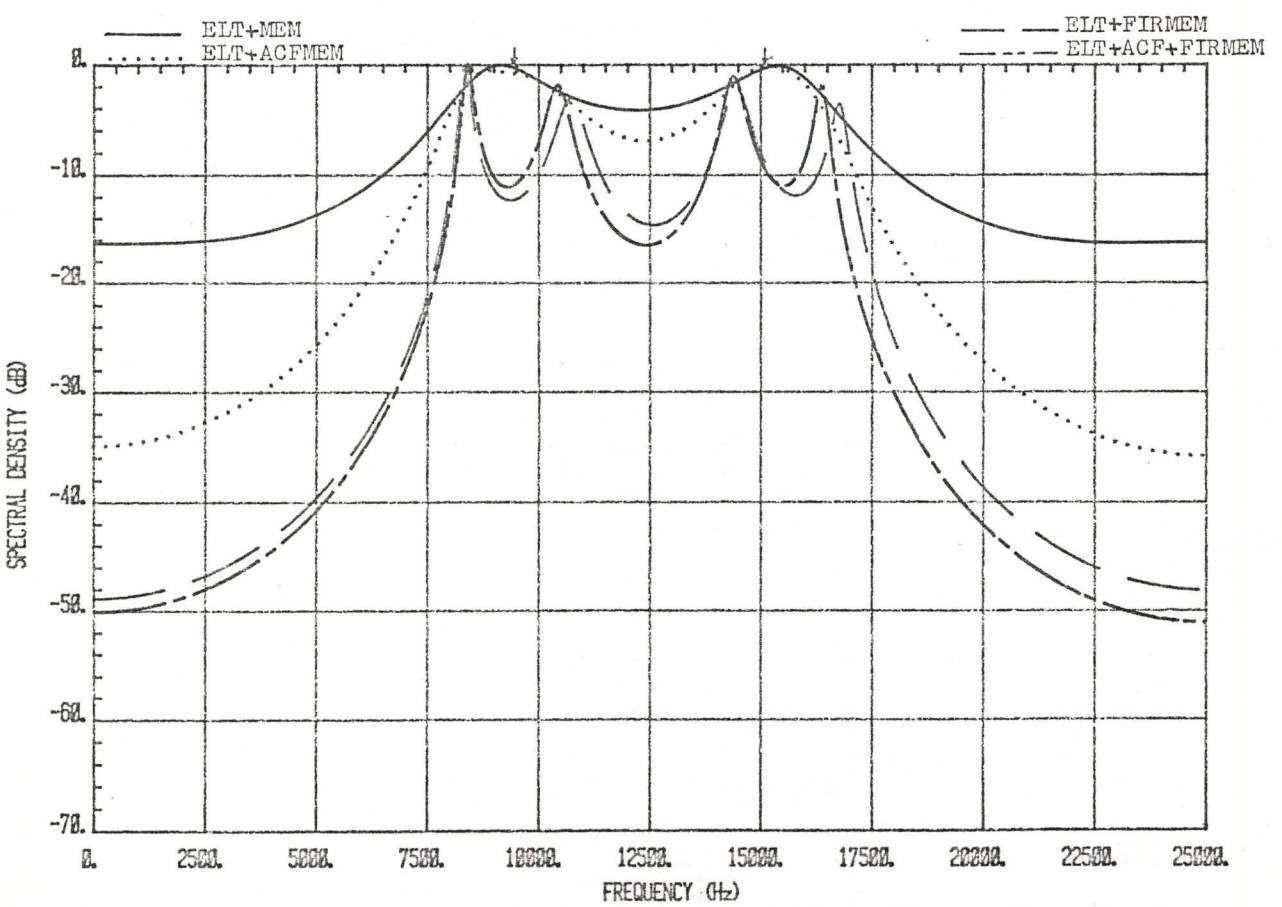


Fig. 4.22: The MEM spectra (filter order 8) of two continuous phase signals.

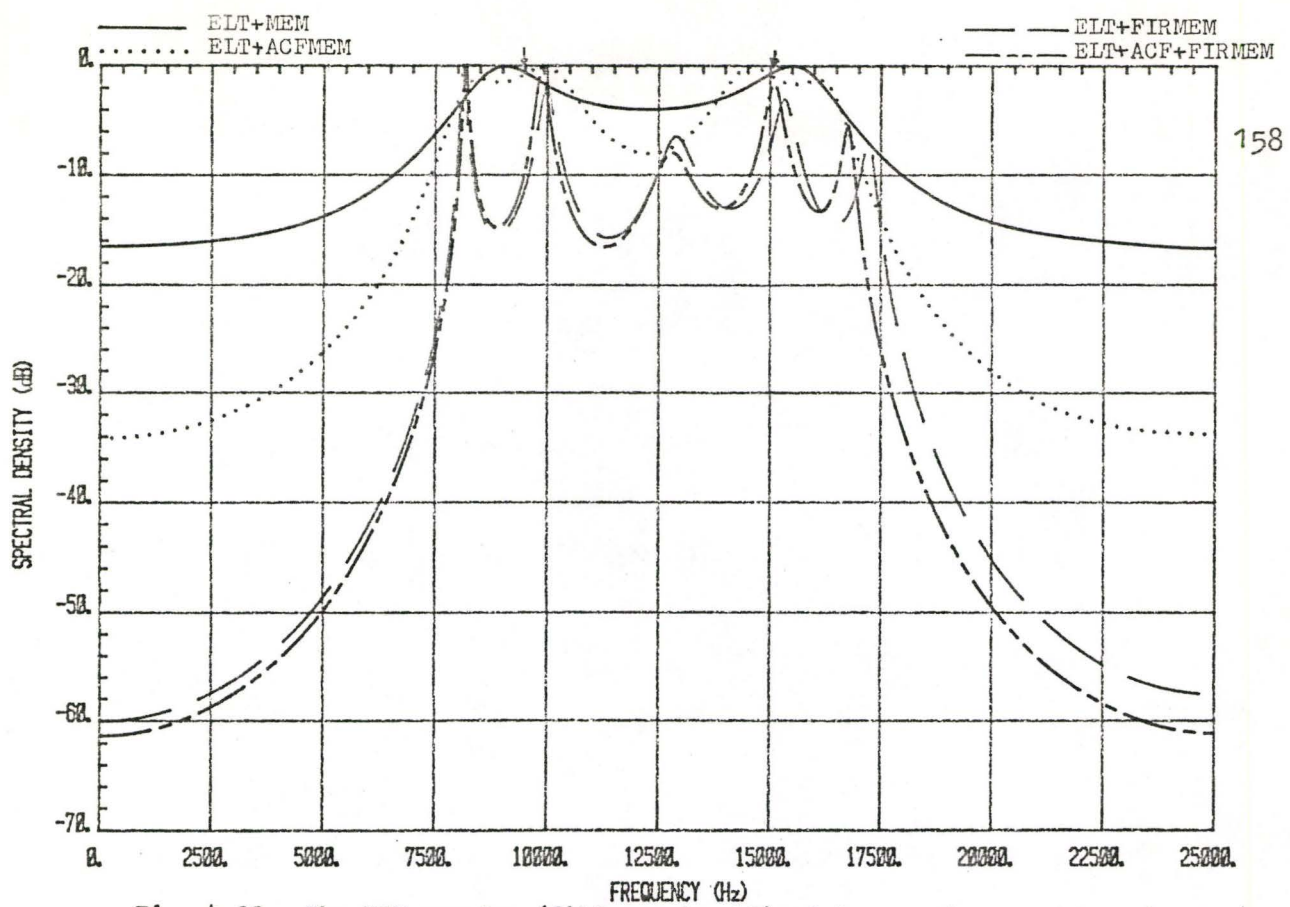


Fig. 4.23: The MEM spectra (filter order 10) of two continuous phase signals.

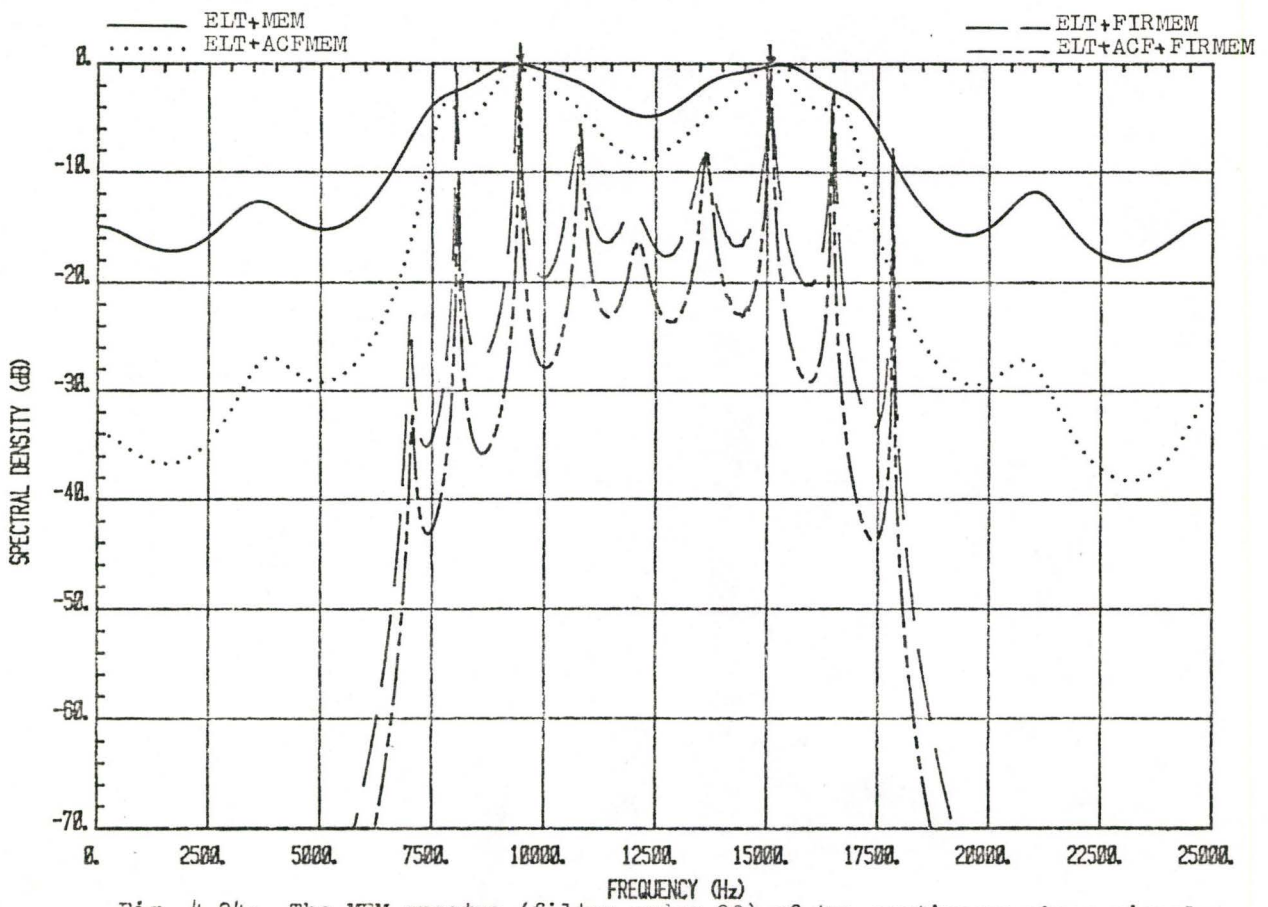


Fig. 4.24: The MEM spectra (filter order 20) of two continuous phase signals.

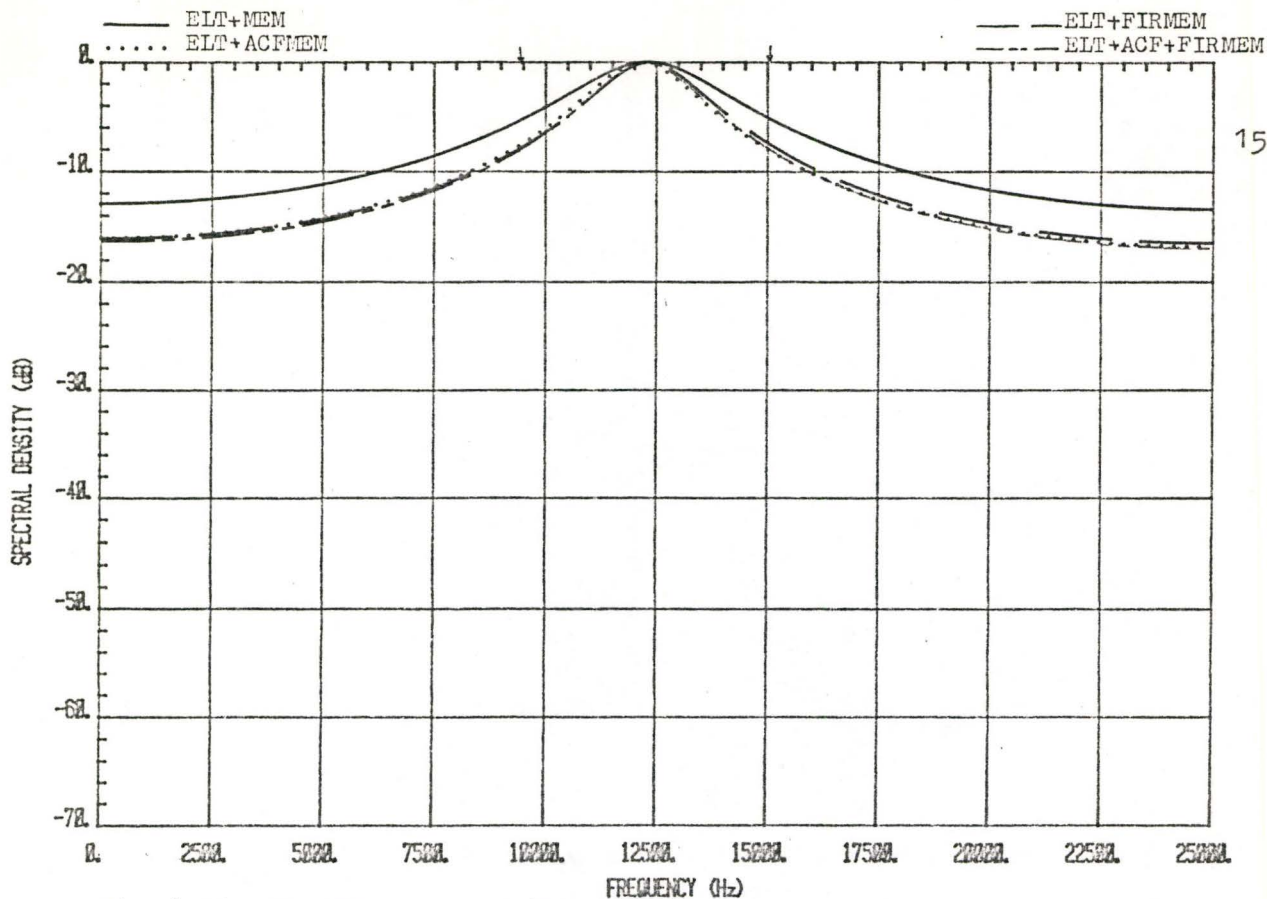


Fig. 4.25: The MEM spectra (filter order 2) of two random phase signals with carrier frequencies 9448 Hz and 15039 Hz.

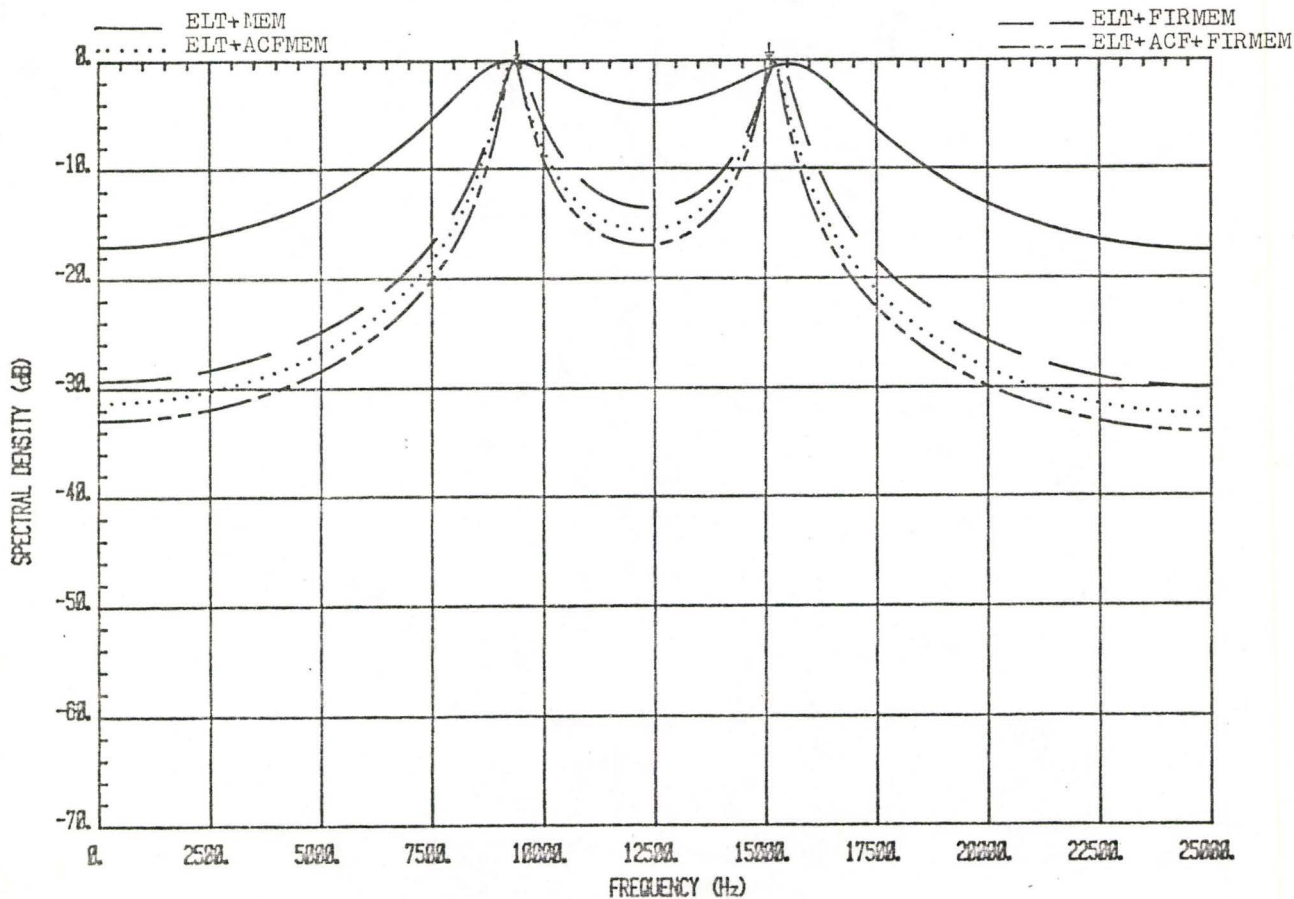


Fig. 4.26: The MEM spectra (filter order 4) of two random phase signals.

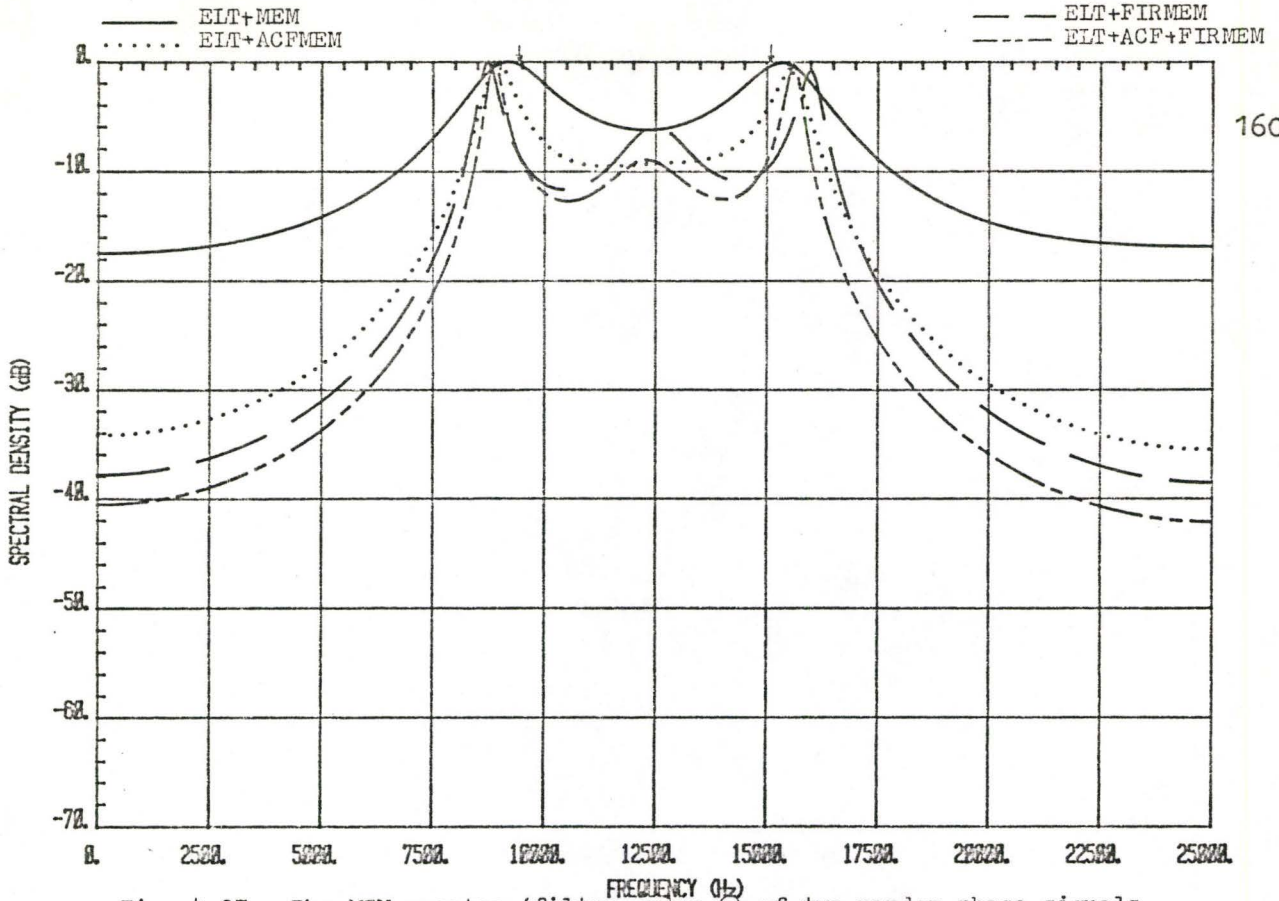


Fig. 4.27: The MEM spectra (filter order 6) of two random phase signals.

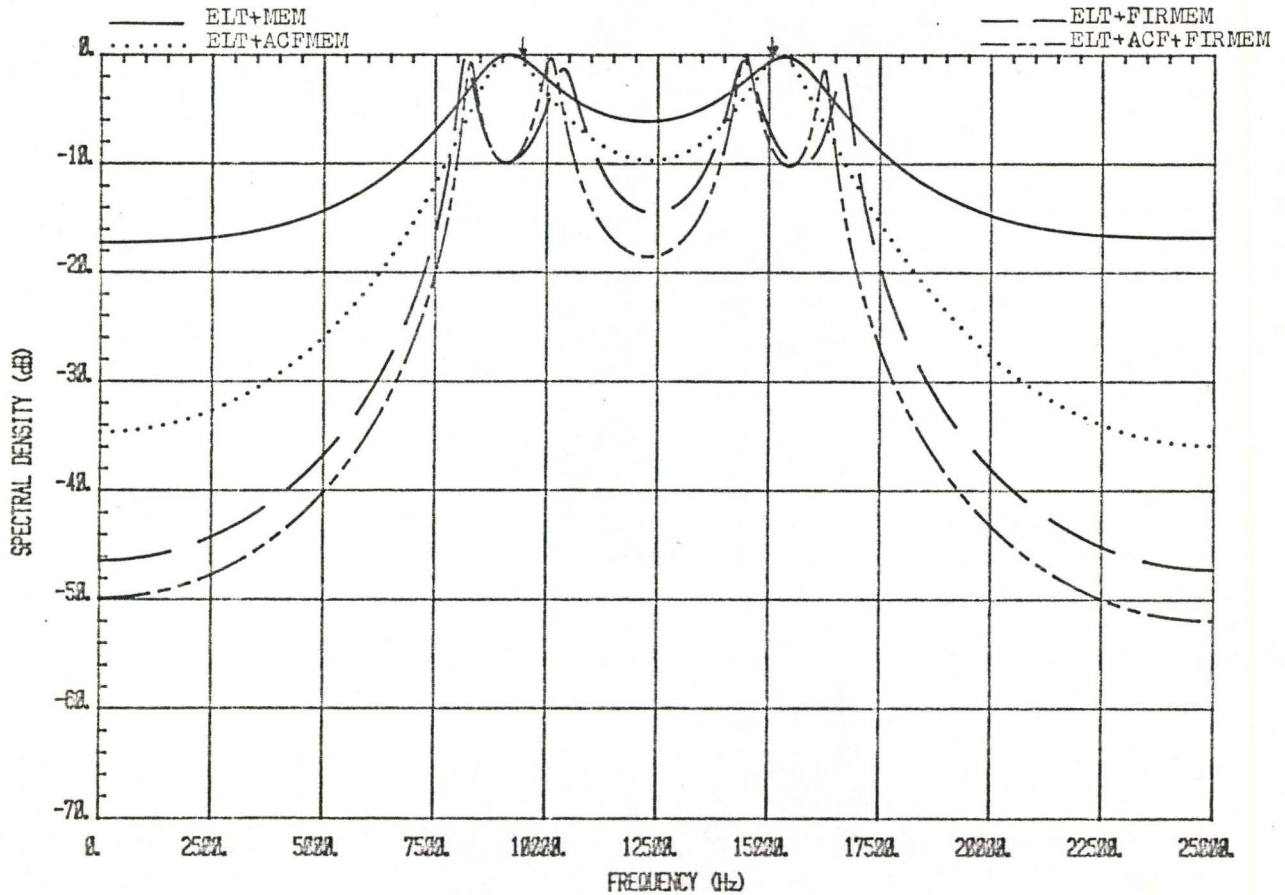


Fig. 4.28: The MEM spectra (filter order 8) of two random phase signals.

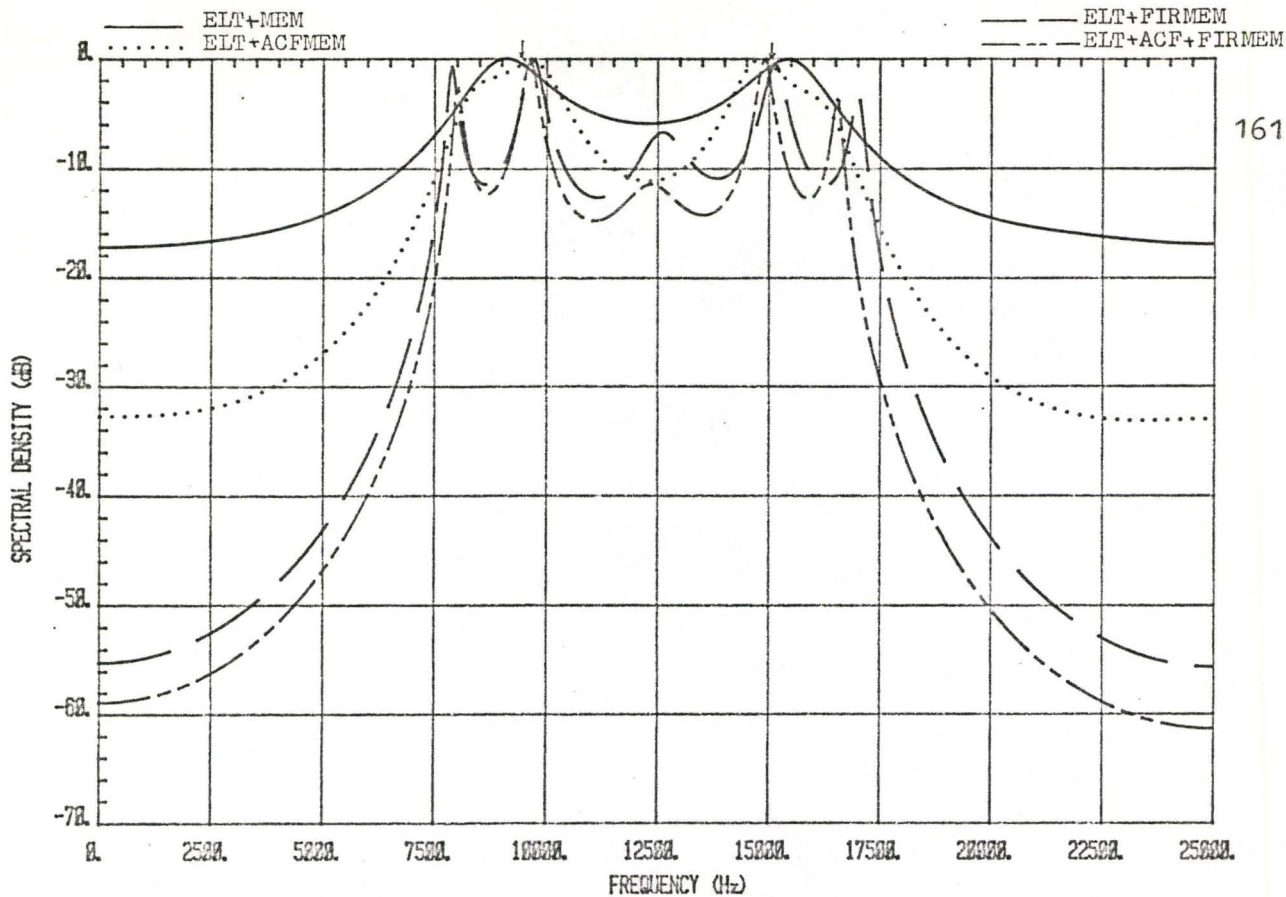


Fig. 4.29: The MEM spectra (filter order 10) of two random phase signals.

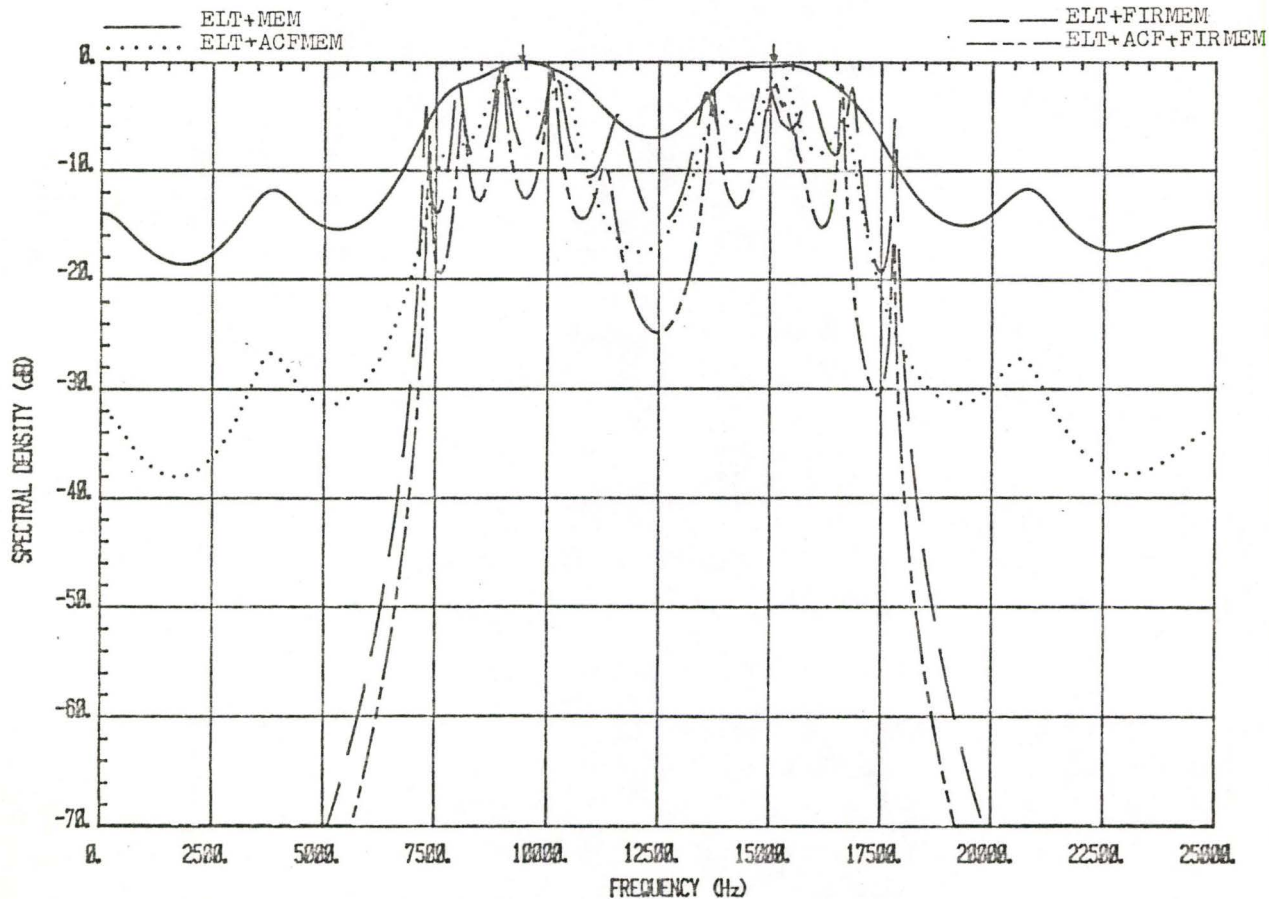


Fig. 4.30: The MEM spectra (filter order 20) of two random phase signals.



Fig. 4.31: The MEM spectra (filter order 4) of two sinusoidal-modulated signals with carrier frequencies 9448 Hz and 15039 Hz.

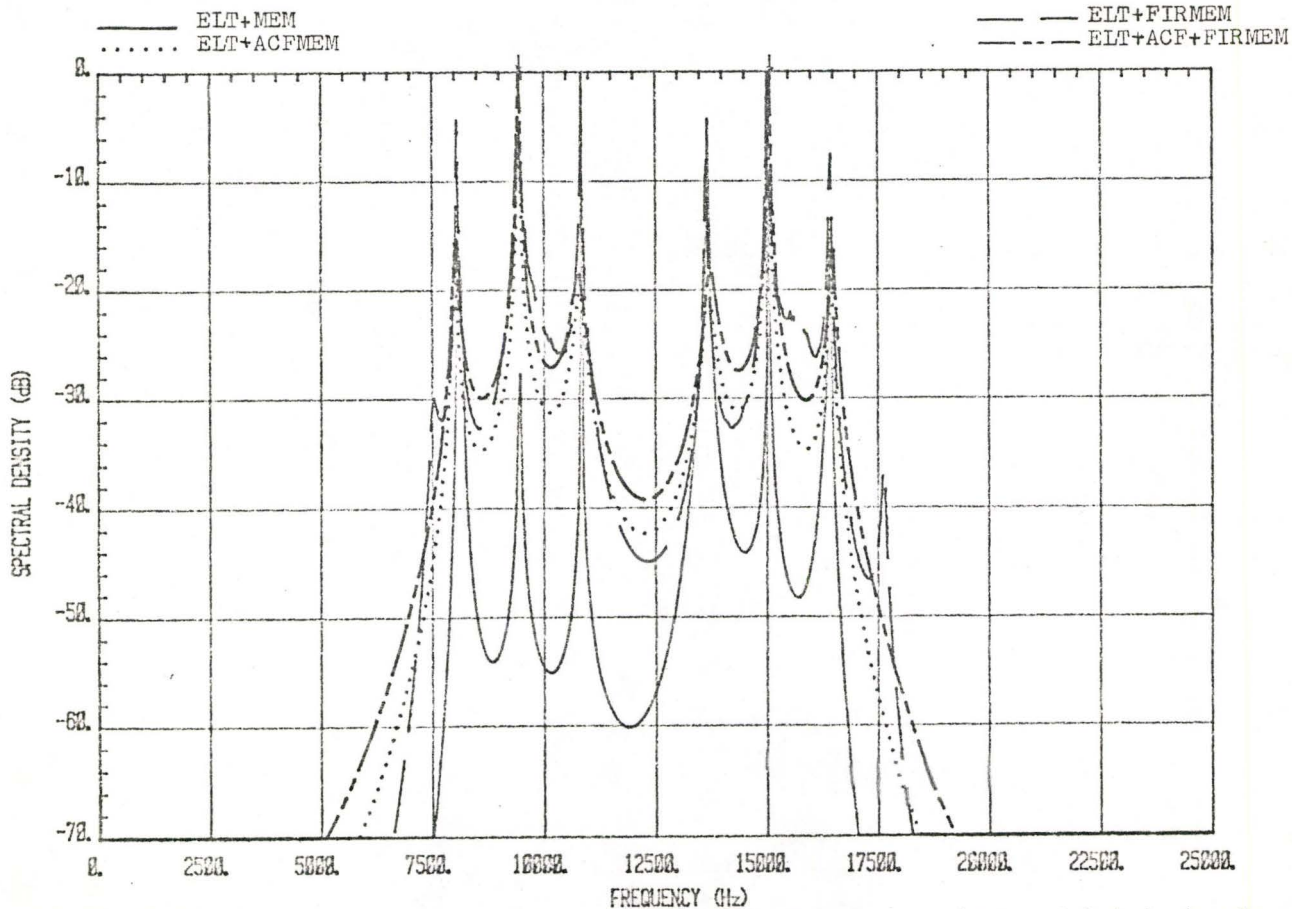


Fig. 4.32: The MEM spectra (filter order 20) of two sinusoidal-modulated signals.

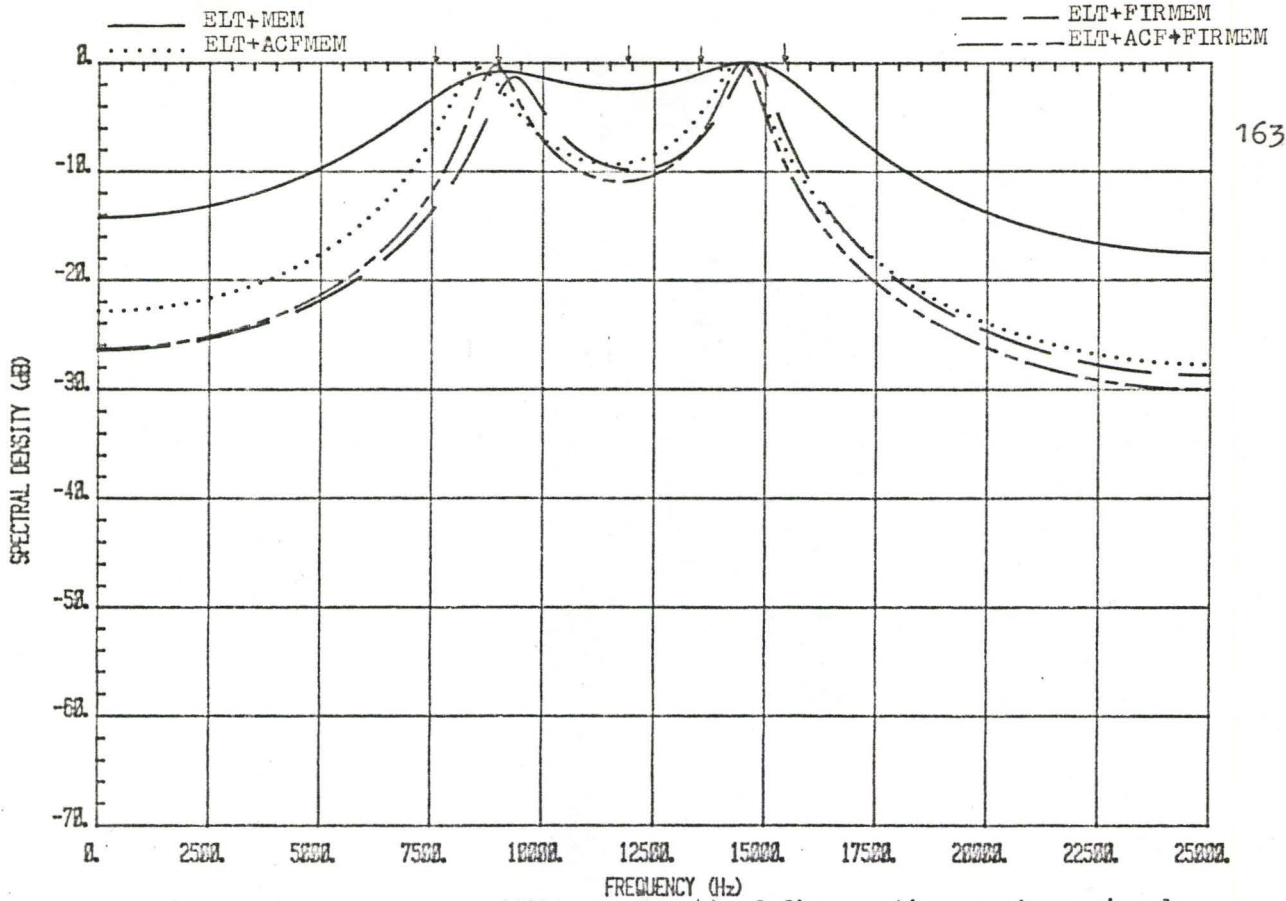


Fig. 4.33: The MEM spectra (filter order 4) of five continuous phase signals with carrier frequencies 7588 Hz, 9000 Hz, 11924 Hz, 13527 Hz and 15425 Hz.

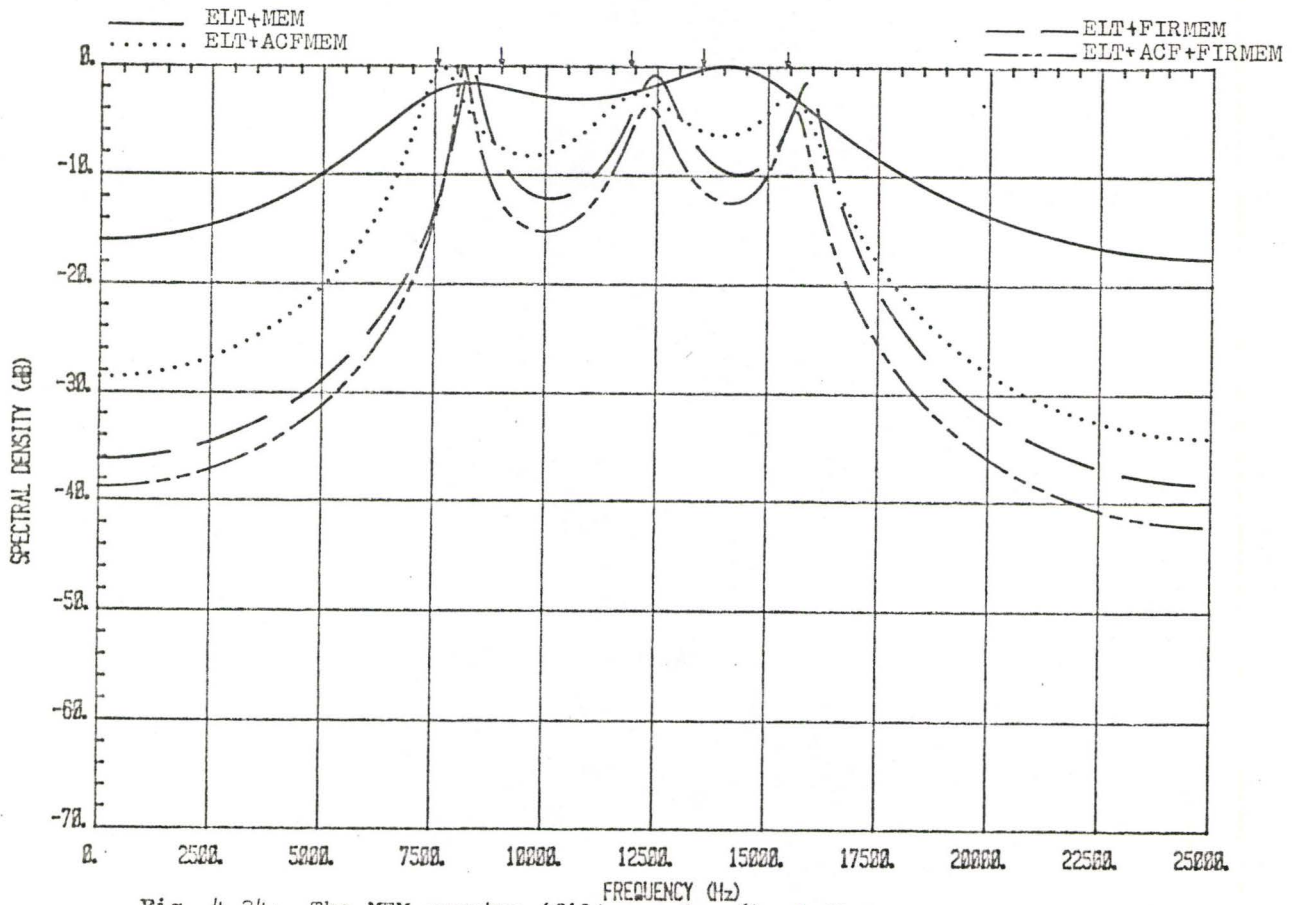


Fig. 4.34: The MEM spectra (filter order 6) of five continuous phase signals.

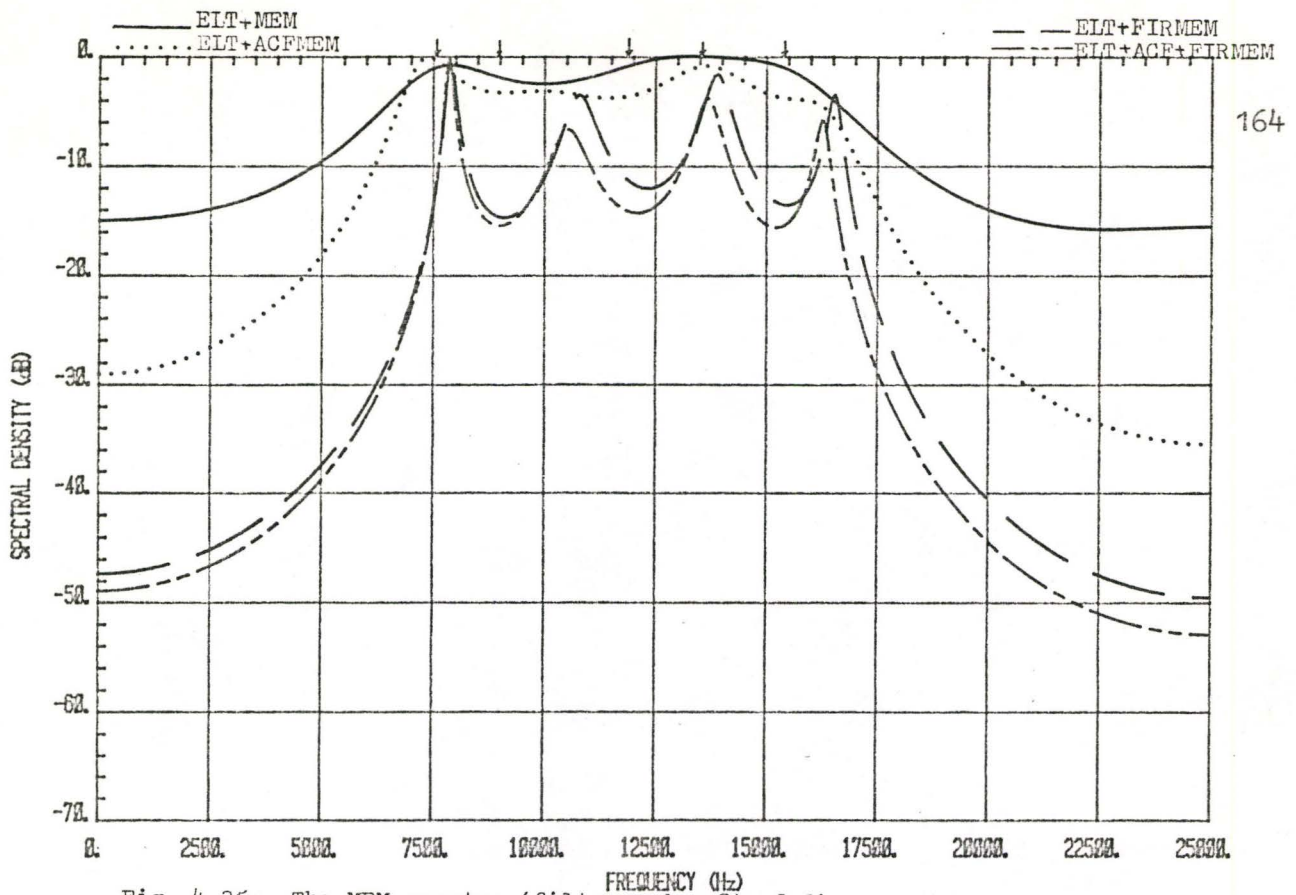


Fig. 4.35: The MEM spectra (filter order 8) of five continuous phase signals.

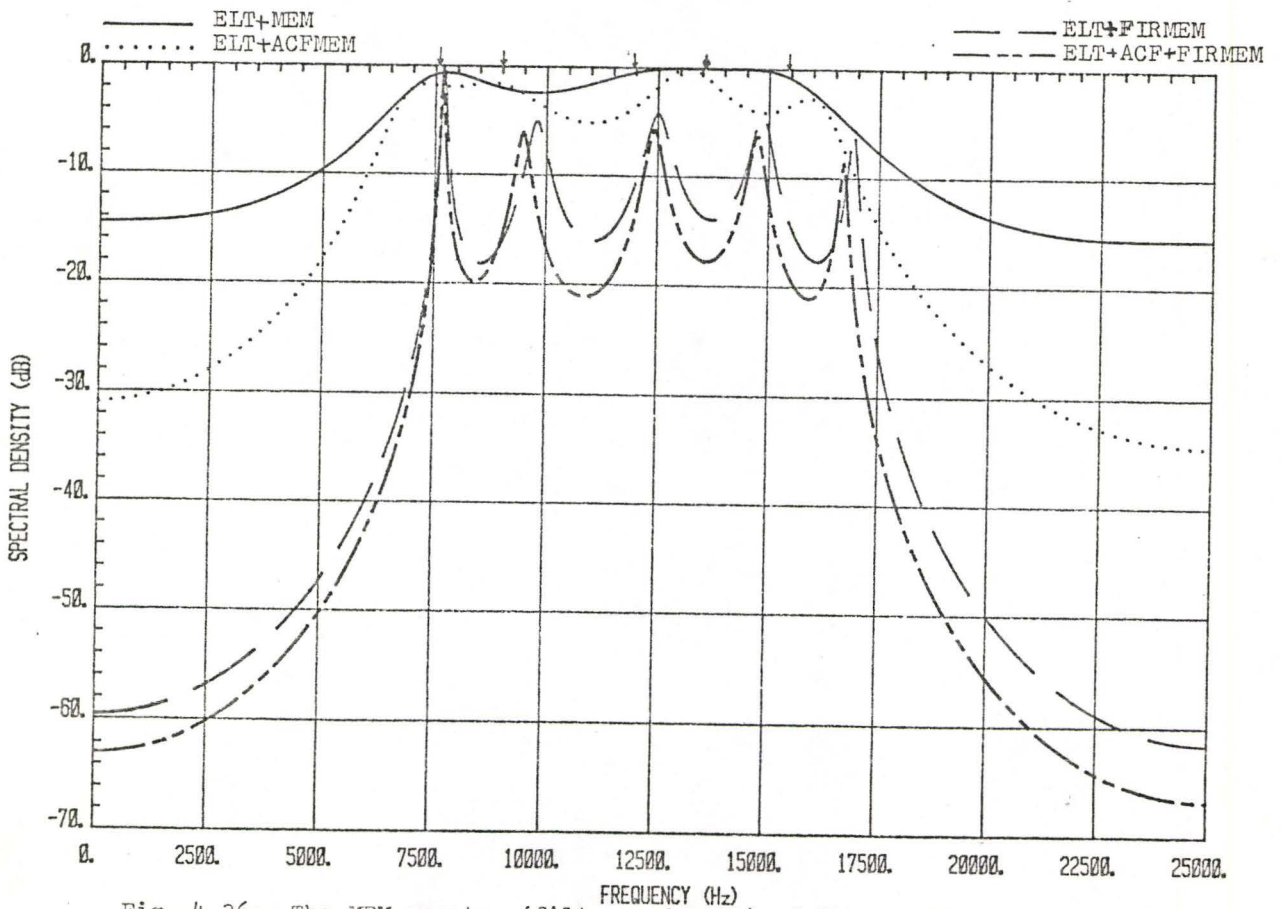


Fig. 4.36: The MEM spectra (filter order 10) of five continuous phase signals.

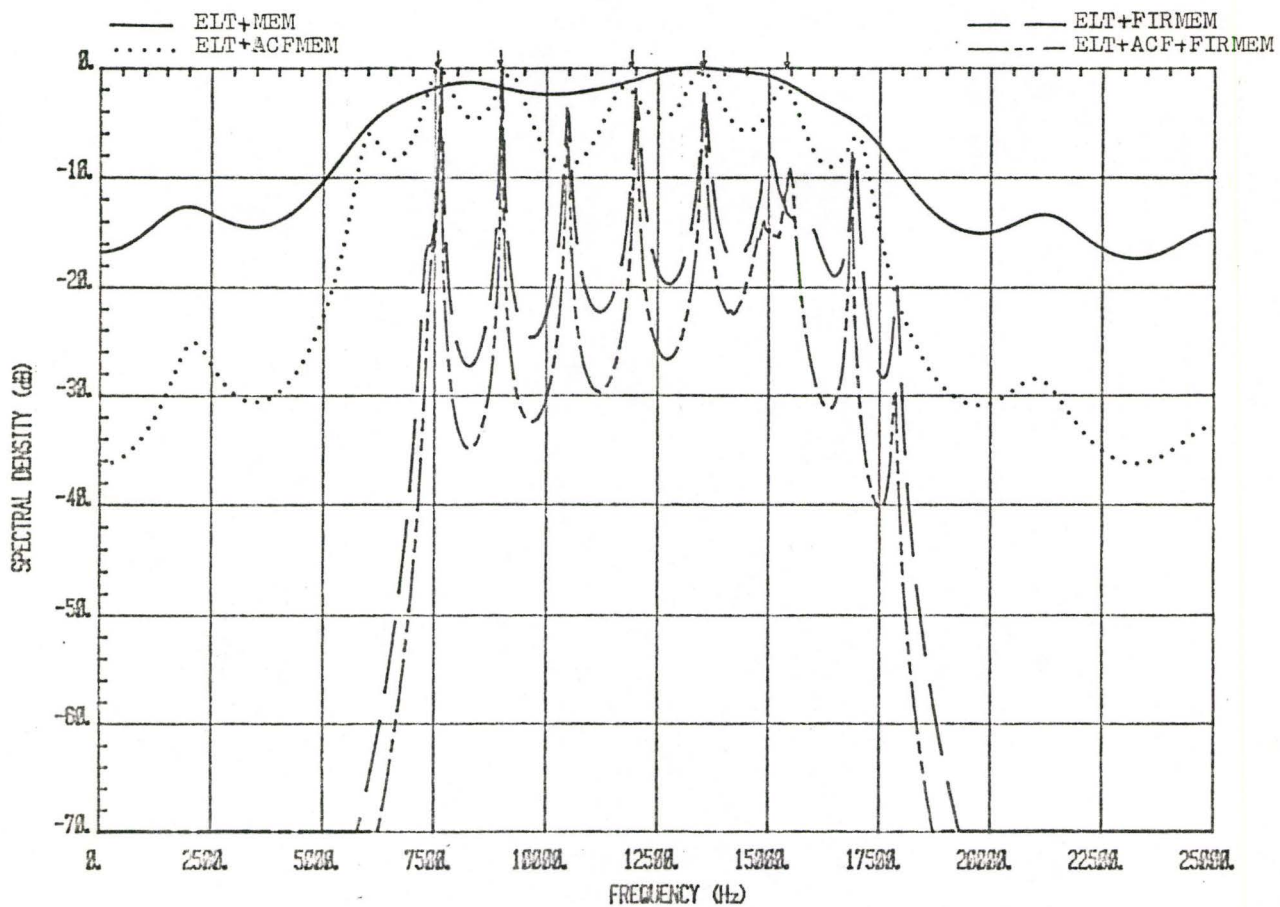


Fig. 4.37: The MEM spectra (filter order 20) of five continuous phase signals.

compared to those due to one or two signals. No clear indication of exactly how many signals are present can be made from these curves except to observe that for MEM = 20 (ACFMEM), there are 5 peaks and for MEM = 50 there are 8 peaks (at -10 dB spectral density). As we proceed to MEM filter order 50, the 'ELT+MEM' and 'ELT+ACFMEM' have peaks at the correct frequencies but they are shadowed by other undesirable side peaks. The spectra are plotted in Fig. 4.38(a). At -5 dB threshold level, both configurations with digital filtering are able to resolve the signals. The peaks shown in Fig. 4.38(b) are at 7587 Hz, 8980 Hz, 11950 Hz, 13453 Hz and 15432 Hz. An expanded plot of the 'ELT+ACF+FIRMEM' is given in Fig. 4.38(c). Comparing Fig. 4.8 with Fig. 4.38(c), the FFT spectral analysis appears to be inferior to the MEM spectral estimator in terms of performance.

The results obtained in Fig. 4.39, Fig. 4.40(a) and Fig. 4.40(b) are the spectra of the random phase signals which are processed by MEM filter order 20 and 50, respectively. We observe that phase randomization is a formidable barrier to spectral estimations.

For the sinusoidal modulation signals, both the 'ELT+ACFMEM' and 'ELT+ACF+FIRMEM' provide outstanding performances which are presented in Fig. 4.41(a) and Fig. 4.41(b).

### 4.3.3 Ten ELT Signals

To detect the presence of ten ELT signals (at carrier frequencies 7441 Hz, 8504 Hz, 9640 Hz, 10483 Hz, 11876 Hz, 12683 Hz, 13636 Hz, 14846 Hz, 16165 Hz and 17595 Hz) a MEM filter order 20 is applied to the continuous phase signals. None of the four configurations are effective

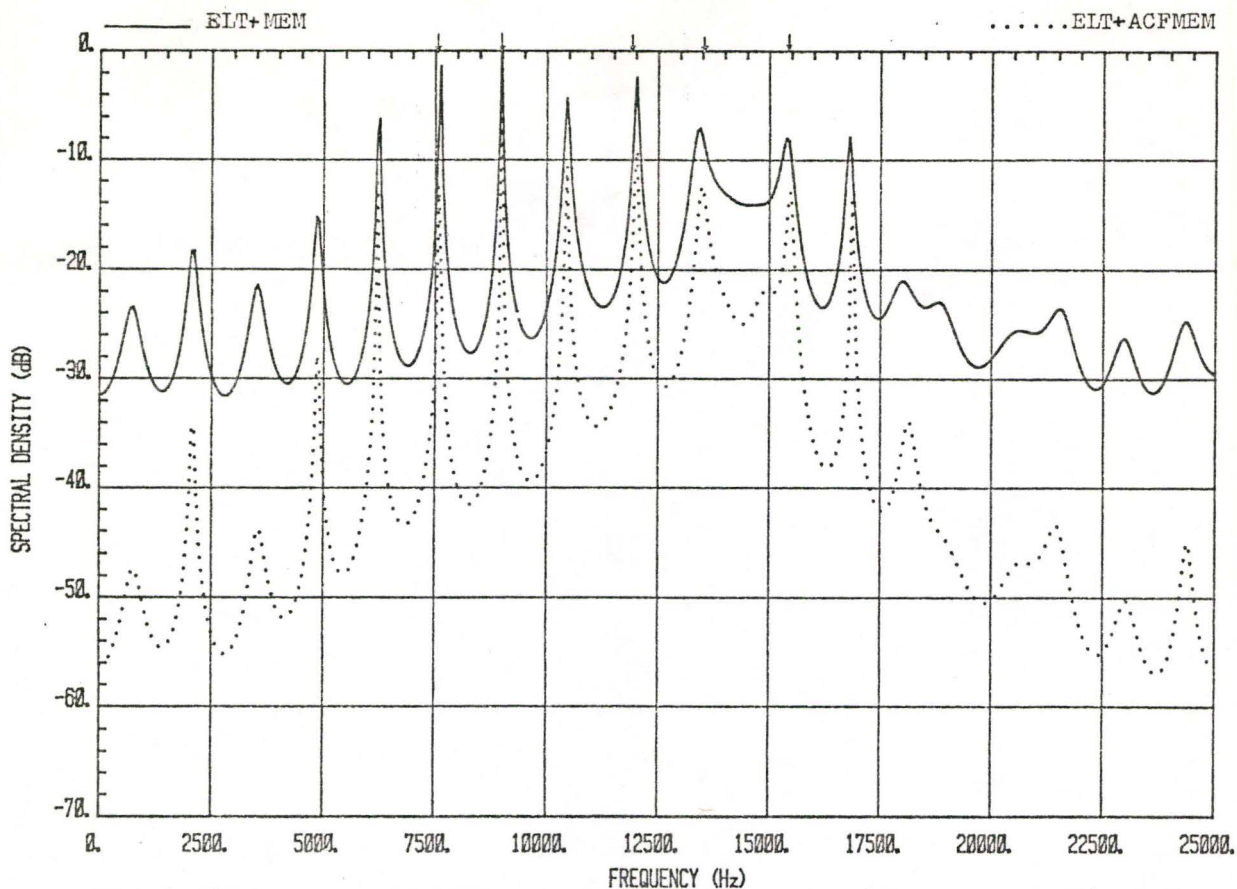


Fig. 4.38(a): The 'ELT+MEM' and 'ELT+ACFMEM' spectra (filter order 50) of five continuous phase signals.

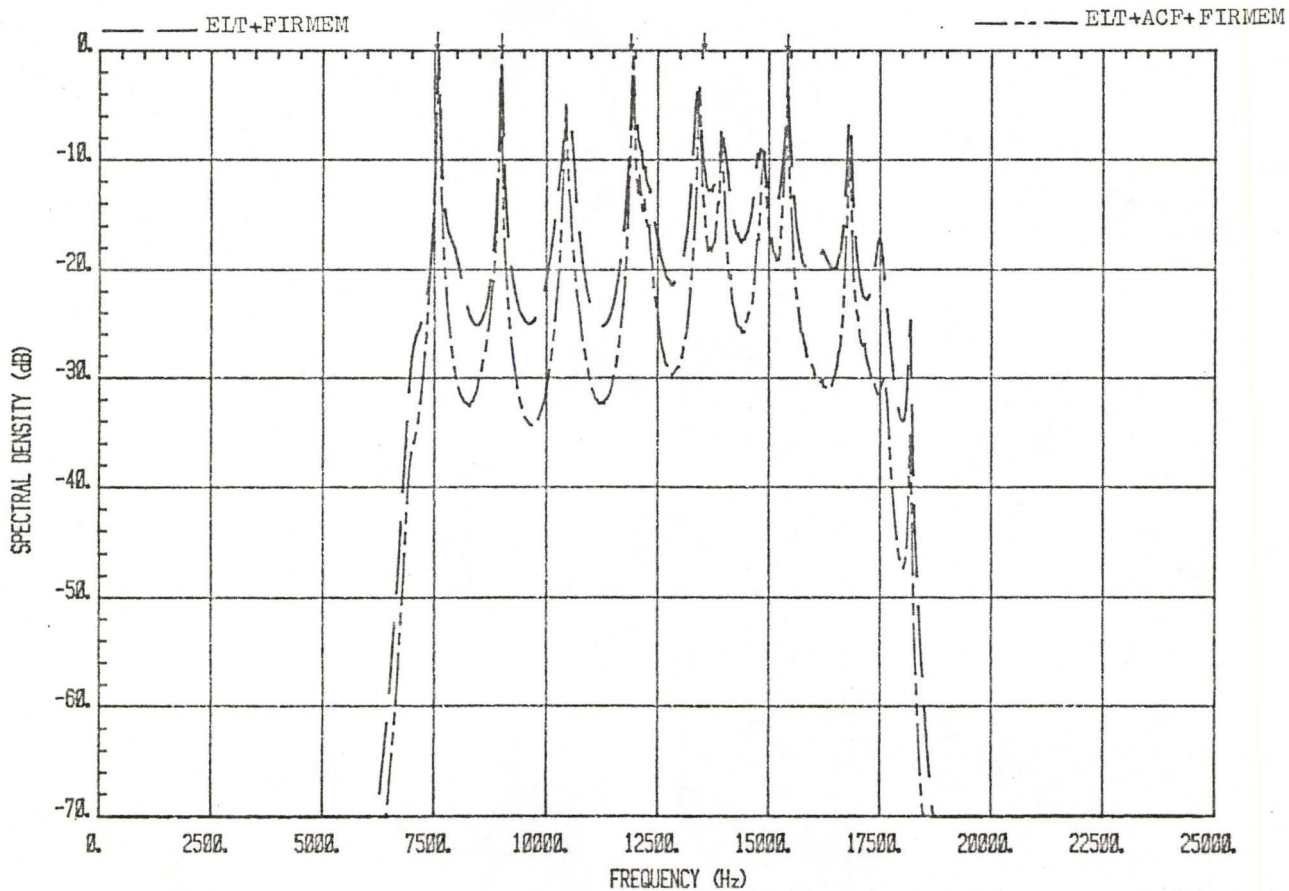


Fig. 4.38(b): The 'ELT+FIRMEM' and 'ELT+ACF+FIRMEM' spectra (filter order 50) of five continuous phase signals.

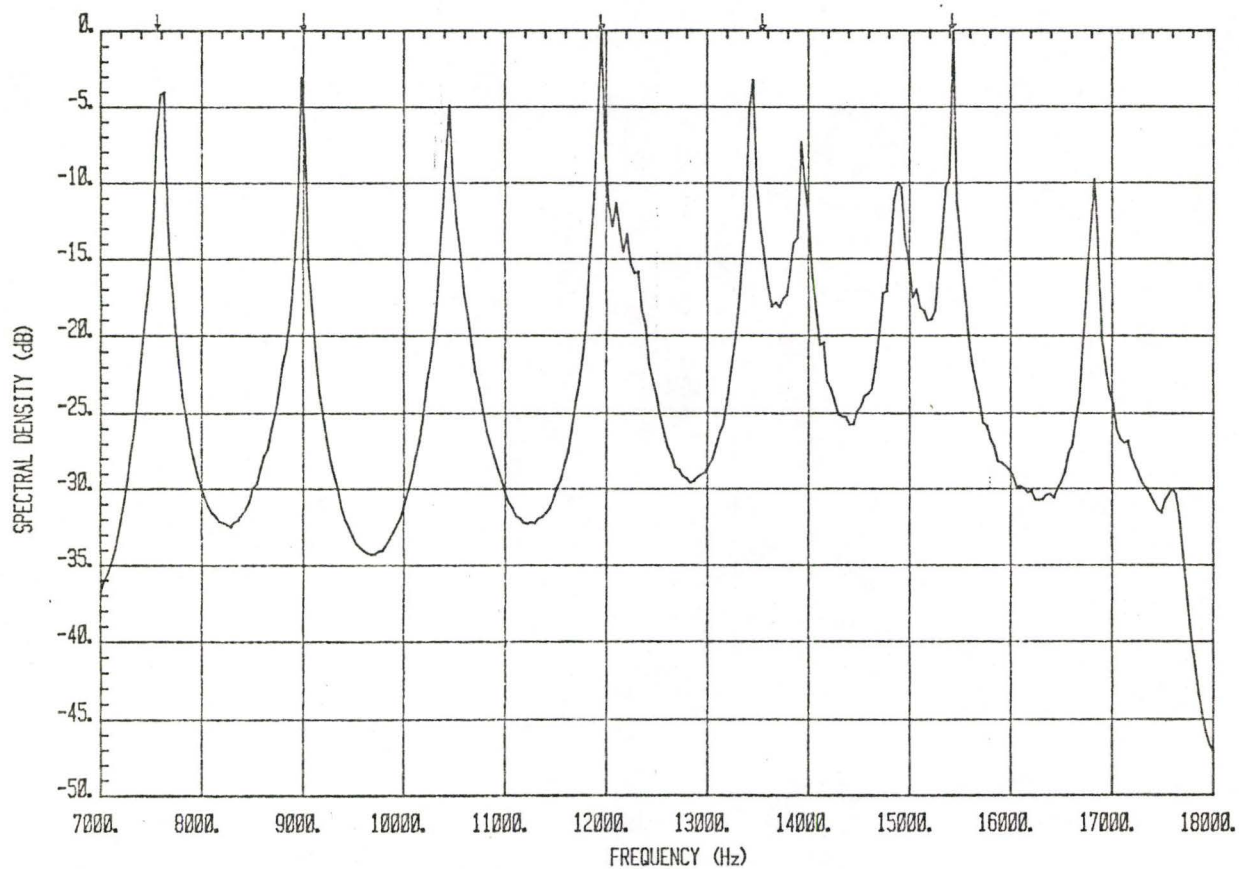


Fig. 4.38(c): An expanded view of the 'ELI+ACF+FIRMEM' spectrum in Fig. 4.38(b).

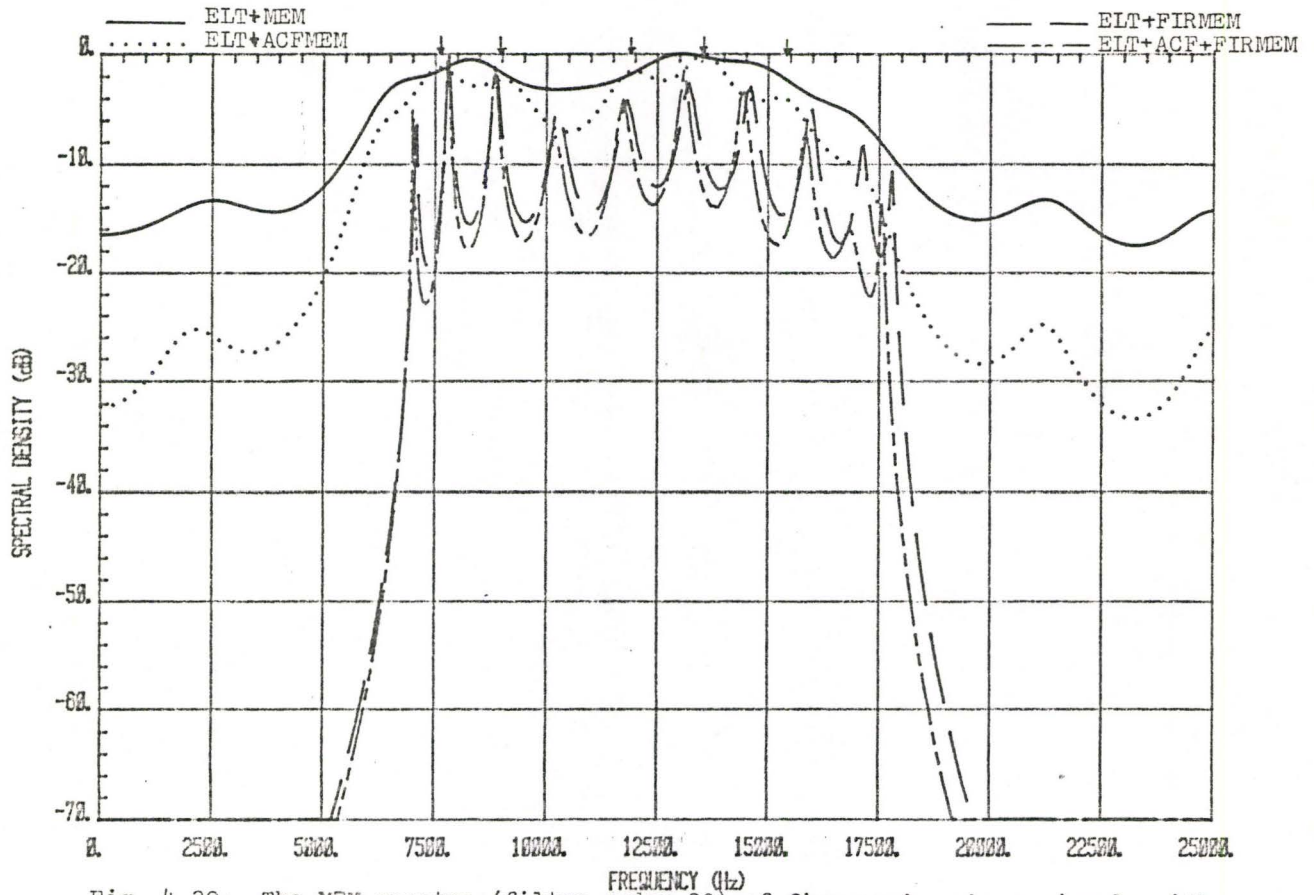


Fig. 4.39: The MEM spectra (filter order 20) of five random phase signals with carrier frequencies 7588 Hz, 9000 Hz, 11924 Hz, 13527 Hz and 15425 Hz.

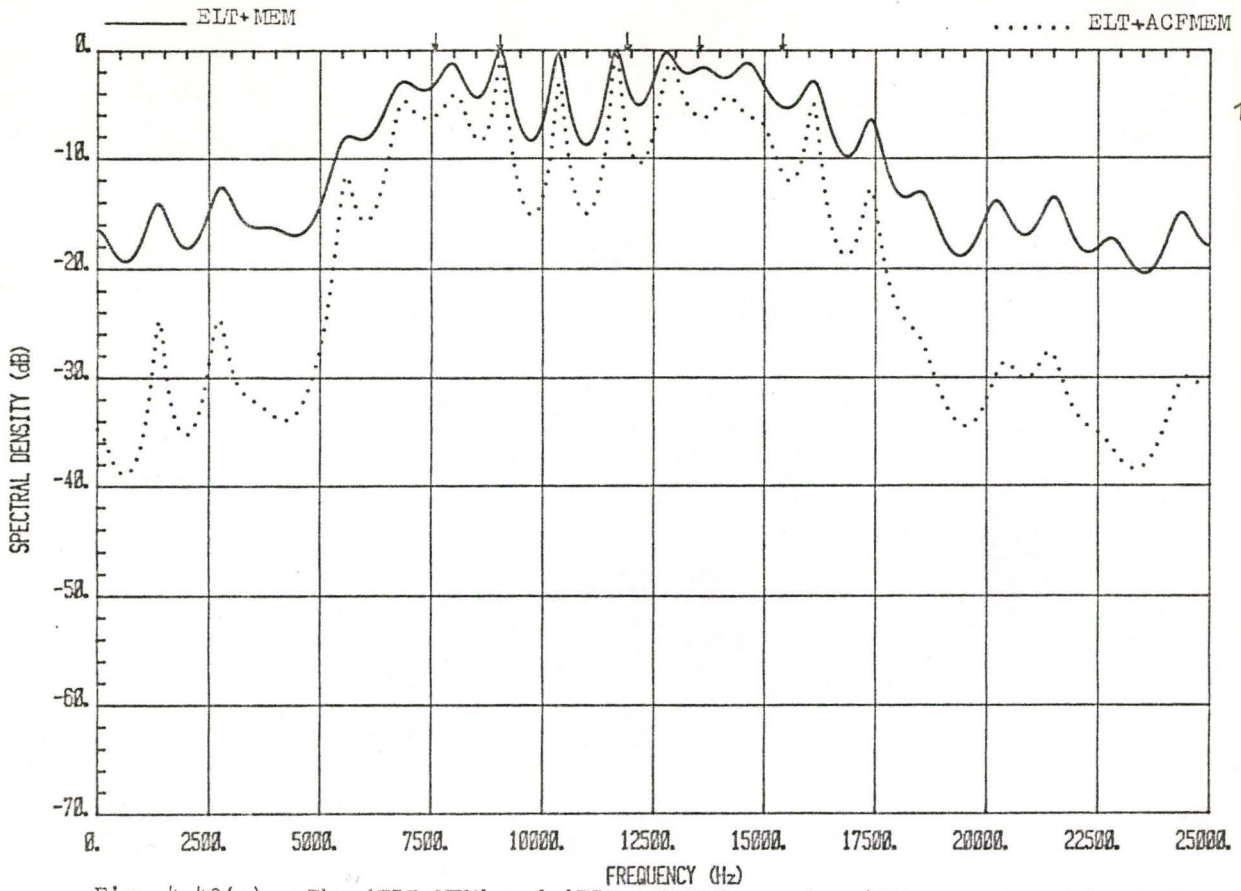


Fig. 4.40(a): The 'ELT+MEM' and 'ELT+ACFMEM' spectra (filter order 50) of five random phase signals.

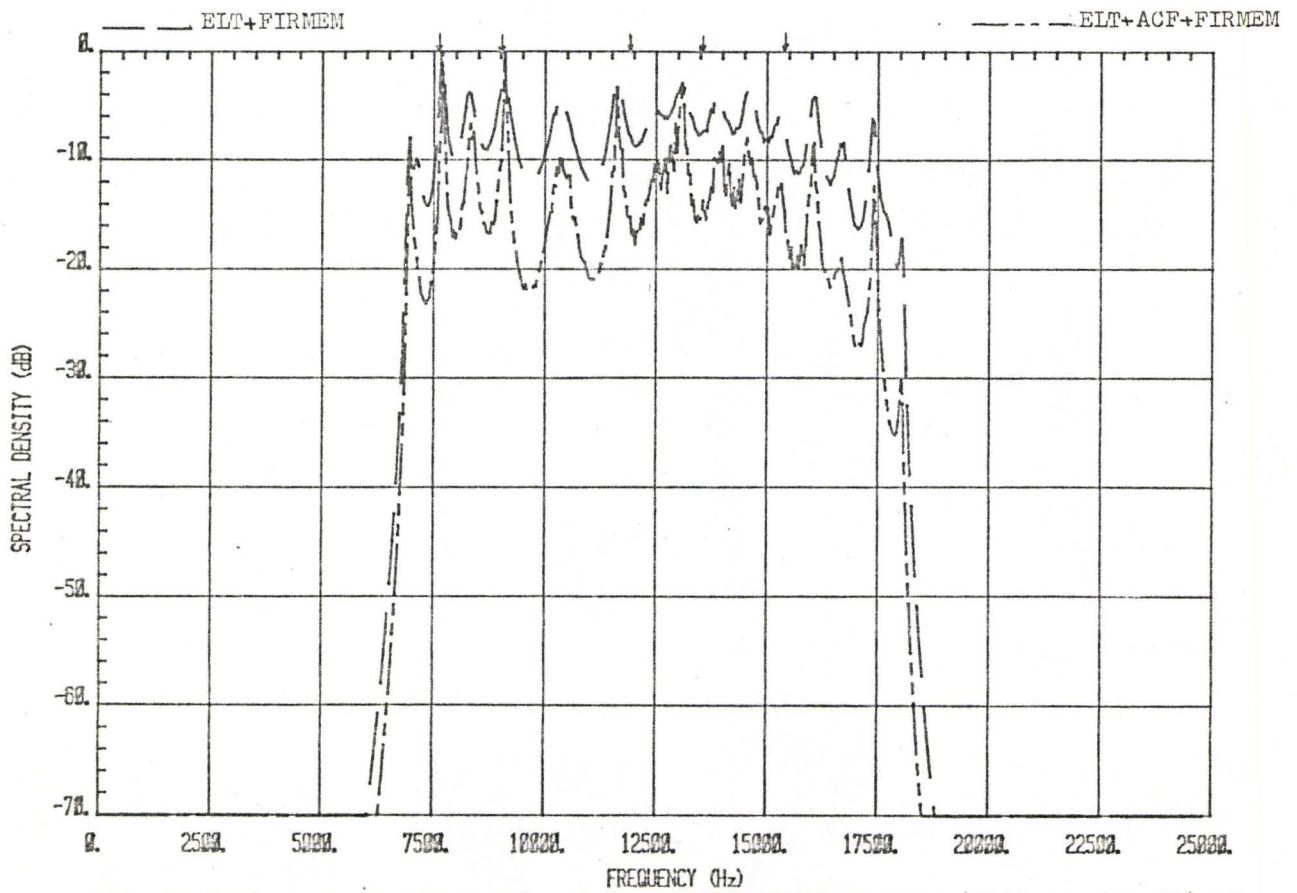


Fig. 4.40(b): The 'ELT+FIRMEM' and 'ELT+ACF+FIRMEM' spectra (filter order 50) of five random phase signals.

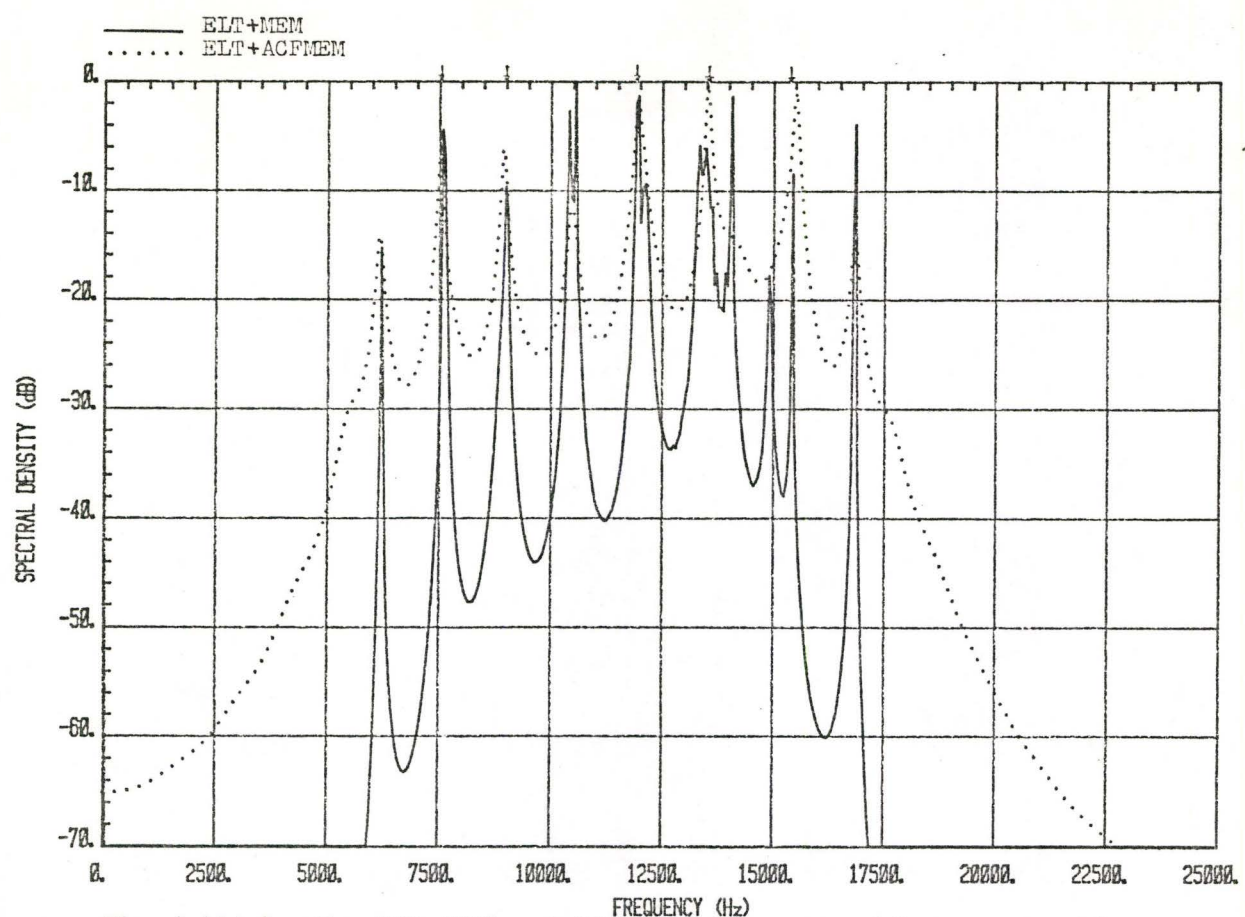


Fig. 4.41(a): The 'ELT+MEM' and 'ELT+ACFMEM' spectra (filter order 50) of five sinusoidal-modulated signals.

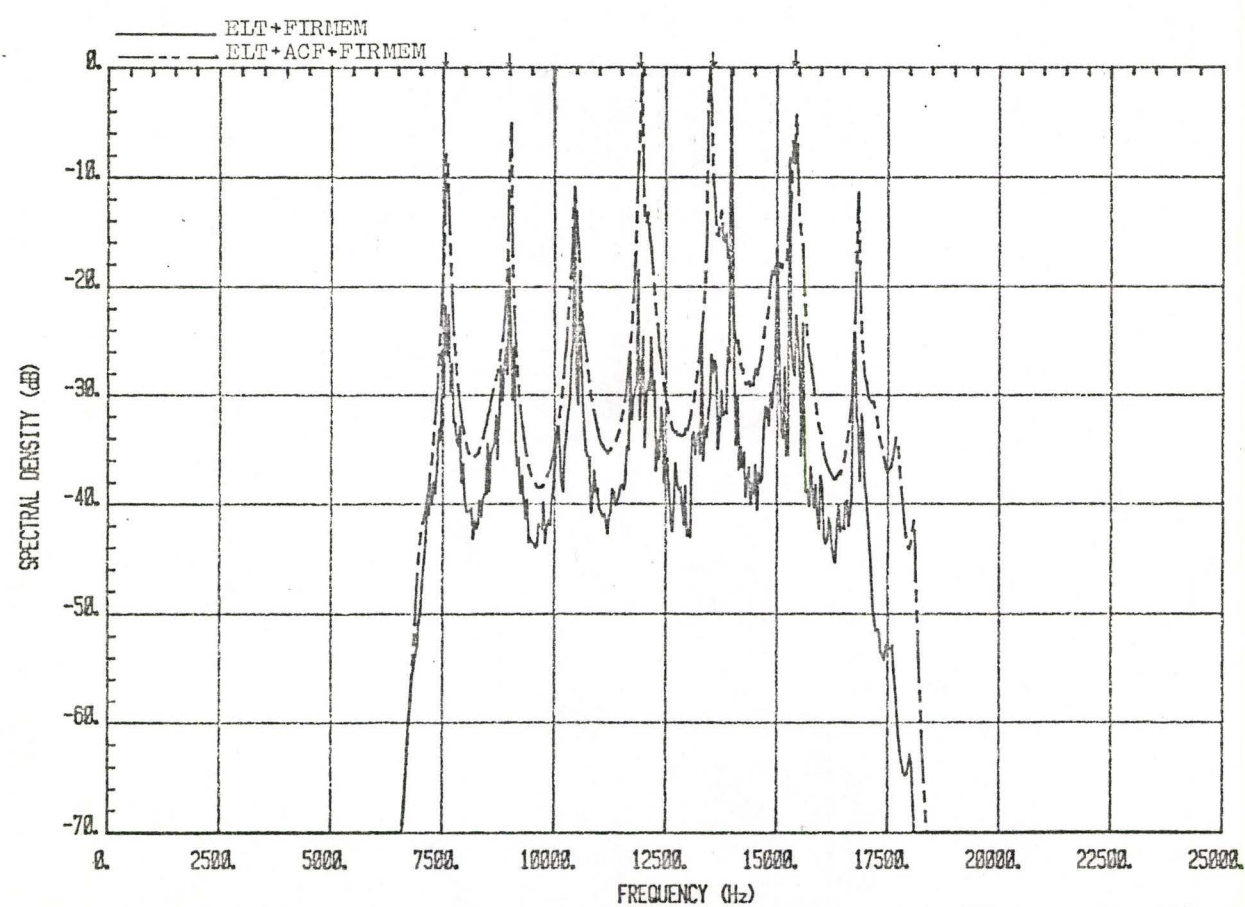


Fig. 4.41(b): The 'ELT+FIRMEM' and 'ELT+ACF+FIRMEM' spectra (filter order 50) of five sinusoidal-modulated signals.

at this MEM filter order. Fig. 4.42 shows the results. Note that in this case the MEM and ACFMEM are quite flat even at MEM = 20 indicating a large number of signals. The next MEM filter order which we attempt is 100. The spectra are given in Fig. 4.43(a) and Fig. 4.43(b). Only seven relevant peaks in Fig. 4.43(b) can be detected by the 'ELT+ACF+FIRMEM' at -10 dB threshold level. These are at frequencies 8541 Hz, 9677 Hz, 10483 Hz, 11865 Hz, 12683 Hz, 14843 Hz and 17596 Hz. The peaks at 7404 Hz and 13636 Hz are barely above -10 dB level and at 16165 Hz the peak is below the threshold value.

At MEM filter order 100 we examine the spectrum of the random phase signals using the 'ELT+ACF+FIRMEM' configuration only. The spectrum shown in Fig. 4.44 appear to be difficult to interpret.

#### 4.3.4 General Remarks

The order of the prediction error filter cannot be fixed if one intends to measure a good spectral estimator by the MEM for multiple emergency signals. This is chiefly due to the reason that it is impossible to anticipate the number of ELT signals embedded in the received signal. We have shown that a low order of MEM fails to resolve a moderately large number of distress signals and at a high MEM filter order it gives rise to spurious peaks which hamper detection. The situation becomes serious when random phase signals are involved. However, the MEM develops difficulties to a minor degree as compared with the FFT, when the number of ELT signals increases. In the next section, the possibility of implementing a bank of bandpass filters as a preprocessor is explored. Each of these digital filters has 5 KHz

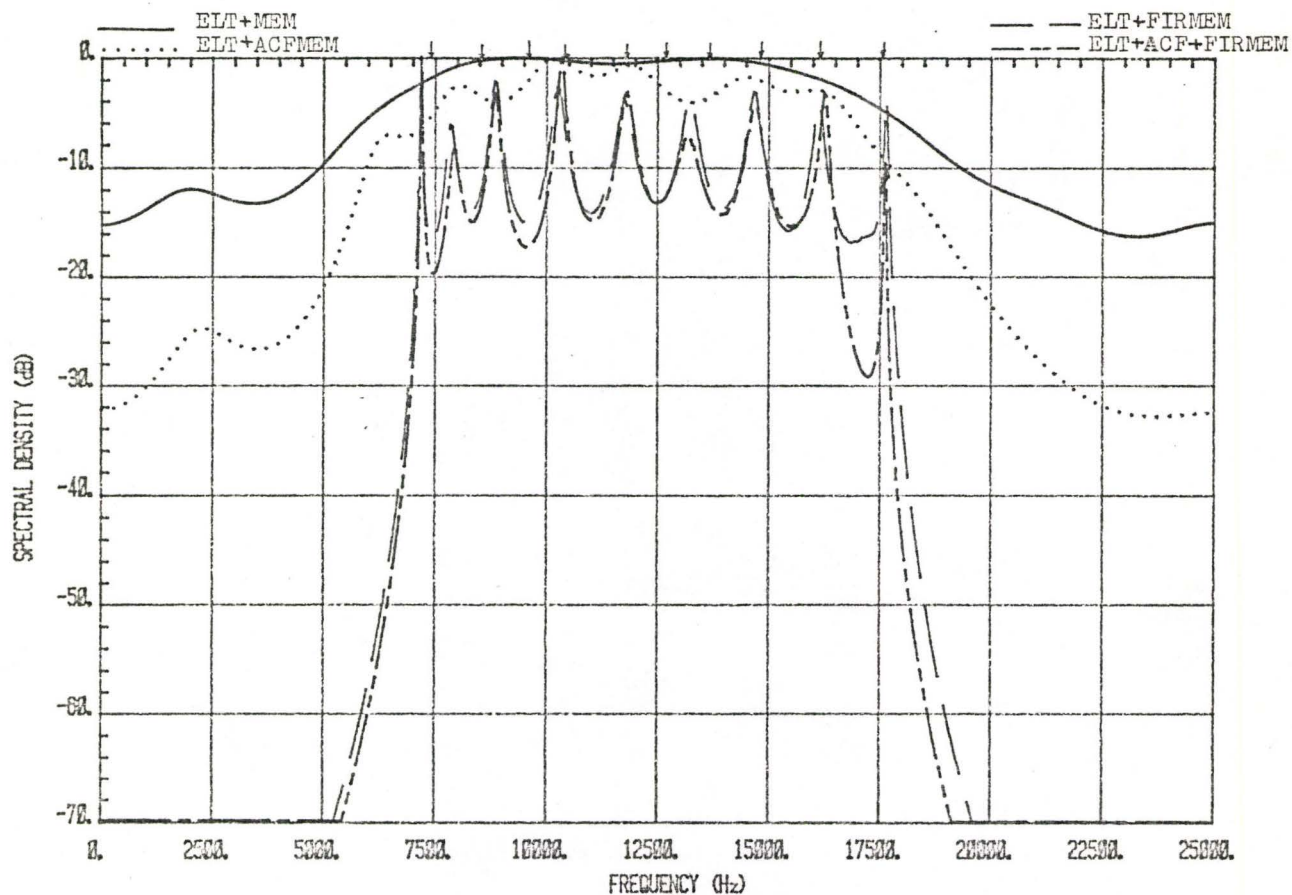


Fig. 4.42: The MEM spectra (filter order 20) of ten continuous phase signals with carrier frequencies 7441 Hz, 8504 Hz, 9640 Hz, 10483 Hz, 11876 Hz, 12683 Hz, 13636 Hz, 14846 Hz, 16165 Hz and 17595 Hz.

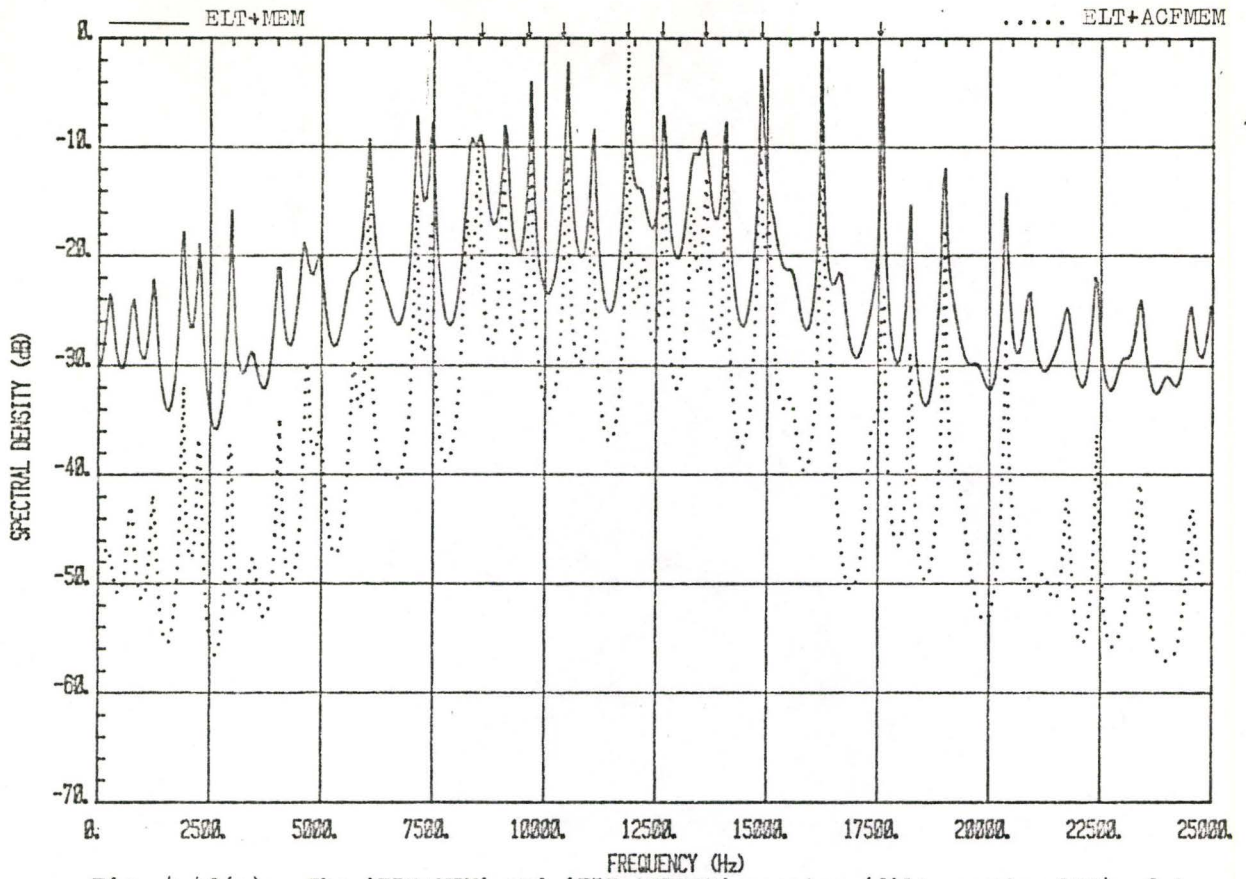


Fig. 4.43(a): The 'ELT+MEM' and 'ELT+ACFMEM' spectra (filter order 100) of ten continuous phase signals.

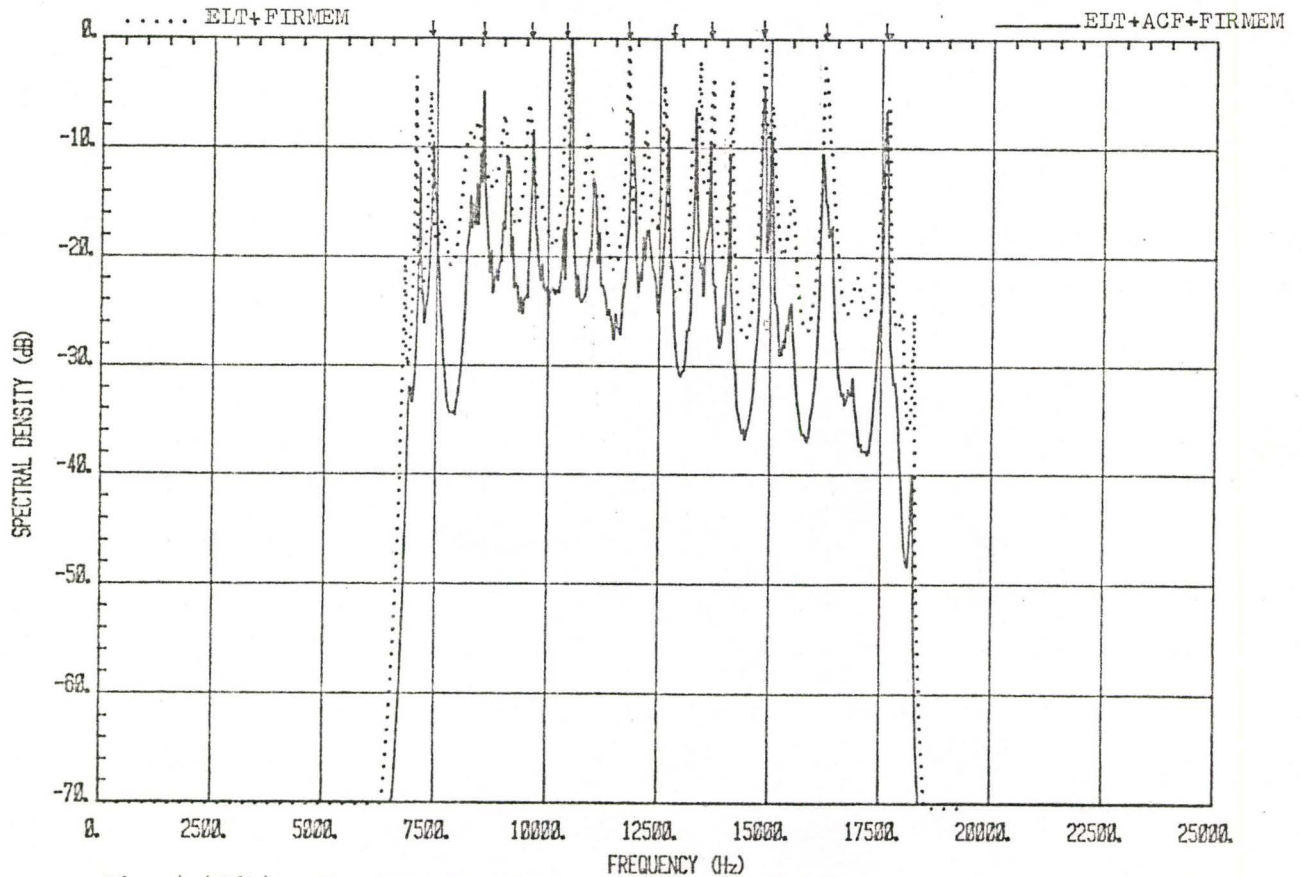


Fig. 4.43(b): The 'ELT+FIRMEM' and 'ELT+ACF+FIRMEM' spectra (filter order 100) of ten continuous phase signals.

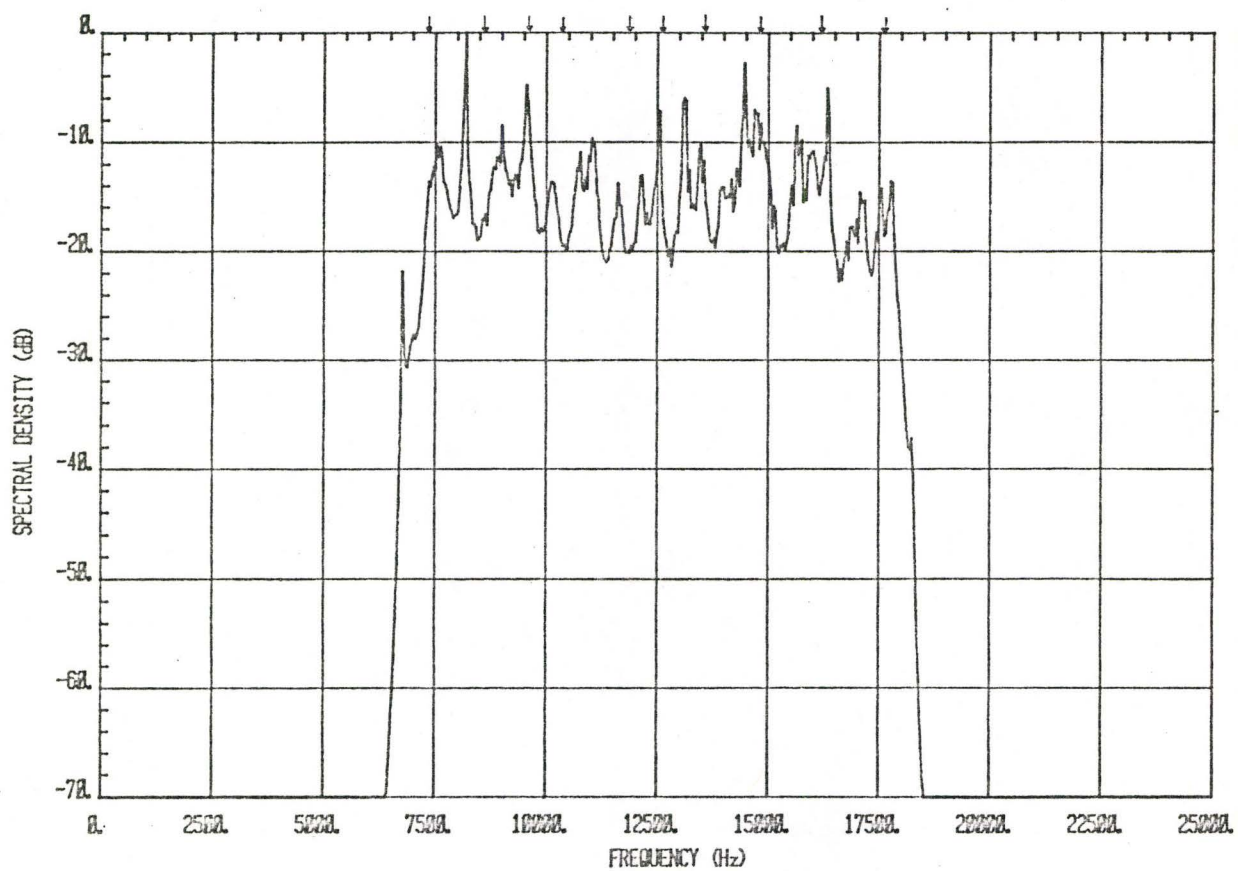


Fig. 4.44: The 'ELF+ACF+FIRMEM' spectrum (filter order 100) of ten random phase signals.

(instead of 11 KHz) bandwidth passband and is dedicated to accommodate two ELT signals only. A fixed order of the prediction error filter is chosen to carry out the MEM processing.

#### 4.4 PREPROCESSING WITH A BANK OF BANDPASS FILTERS

This section examines the possibility of processing using the 'ELT+ACF+FIRMEN' configuration with the modification of a bank of bandpass filters (BPF) as a preprocessor. Received ELT signals have frequencies within the range of 6.5 KHz to 18.5 KHz. The bandwidth of the bandpass filter is designed to operate in the frequency band from 7 KHz to 18 KHz. Instead of the 11 KHz bandwidth filter, we follow the specifications (except the cutoff frequencies) described in Section 2.7 and implement four bandpass filters with 5 KHz passband. These filters have 2 KHz overlapping bandwidth. The necessity of this action is explained later. Table 4.1 indicates the required cutoff frequencies of the four bandpass filters. In the subsequent discussion, we refer to these filters by this format: BPF 1 denotes the bandpass filter which has cutoff frequencies at 5 KHz and 10 KHz.

	cutoff frequency (KHz)
BPF 1	5 and 10
BPF 2	8 and 13
BPF 3	11 and 16
BPF 4	14 and 19

Table 4.1 The cutoff frequencies of the four bandpass filters

The principal aim of having a 5 KHz bandwidth is that at most two ELT signals will be processed by each filter. With this limitation, we expect that a fixed MEM filter order can be used to estimate the spectral characteristics of multiple ELT signals. Due to considerations of Section 3, a low order MEM filter order is preferred. Fig. 4.45 depicts the processor. The results of each filtering at a fixed MEM order are plotted on the same graph. We employ the same sets of multiple signals which were described in the preceding sections.

#### 4.4.1 Two ELT Signals

We have shown that MEM filter orders 2 and 3 generate only a single peak. In order to study the spectral performance of two ELT signals, it is adequate to begin with MEM filter order 4. At this filter order, the two pulse-modulated signals (linear frequency sweep and continuous phase) with carrier frequencies 9448 Hz and 15039 Hz are processed by the scheme outlined in Fig. 4.45. In this case, each bandpass filter involves only one ELT signal. Fig. 4.46 shows that, at locations around the two carrier frequencies, there are two peaks overlapping each other. The resolution of the peaks are at 9420 Hz, 9384 Hz, 14919 Hz and 15065 Hz. Comparing these spectra with Fig. 4.20, a significant improvement in sharpening the peaks is obtained. MEM filter orders 8 and 10 are also attempted to test the spectral performance. Although both orders provide peaks at 9457 Hz and 15029 Hz, MEM filter order 8 has superior resolution. These spectra are plotted in Fig. 4.47 and Fig. 4.48.

The same technique is applied to the random phase signals. Fig.

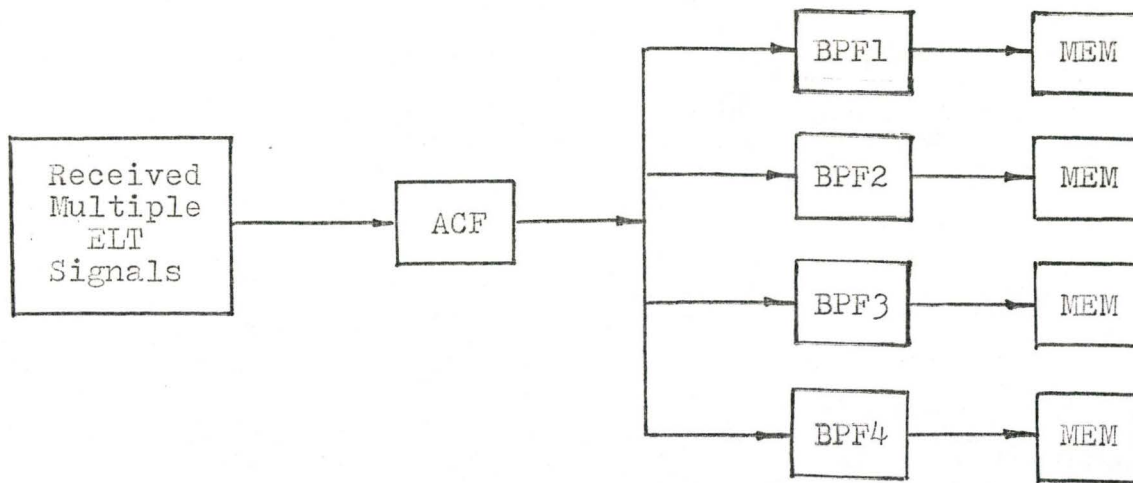


Fig. 4.45: The 'ELT+ACF+FIRMEM' configuration modified with a bank of bandpass filters as an alternate preprocessor.

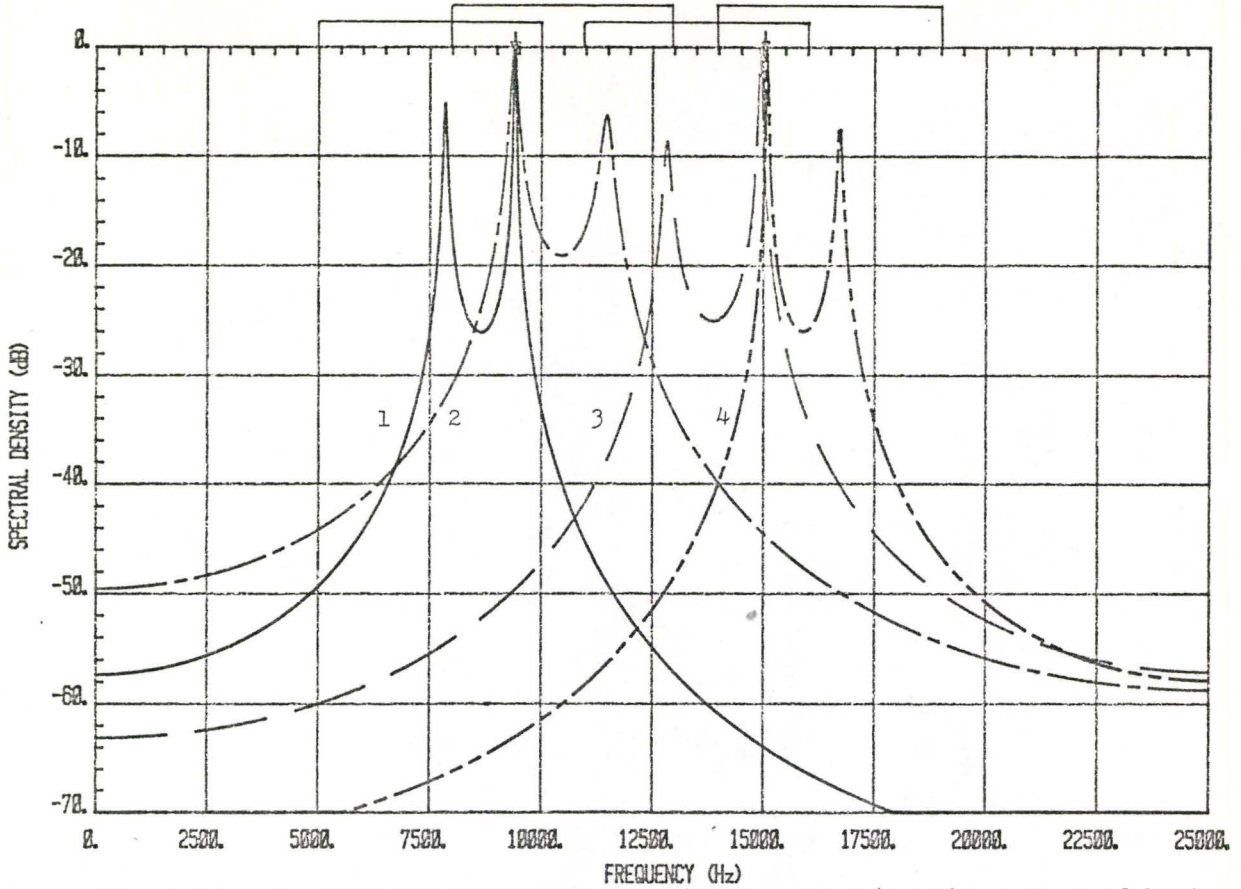


Fig. 4.46: The 'ELT+ACF+FIRMEM' spectra (filter order 4, using a bank of bandpass filters) of two continuous phase signals with carrier frequencies 9448 Hz and 15039 Hz. The bars at top of the graph indicate the frequency range of the filters and the numbers (1,2,3,4) represent the corresponding spectra produced by using BPF1, BPF2, BPF3 and BPF4, respectively.

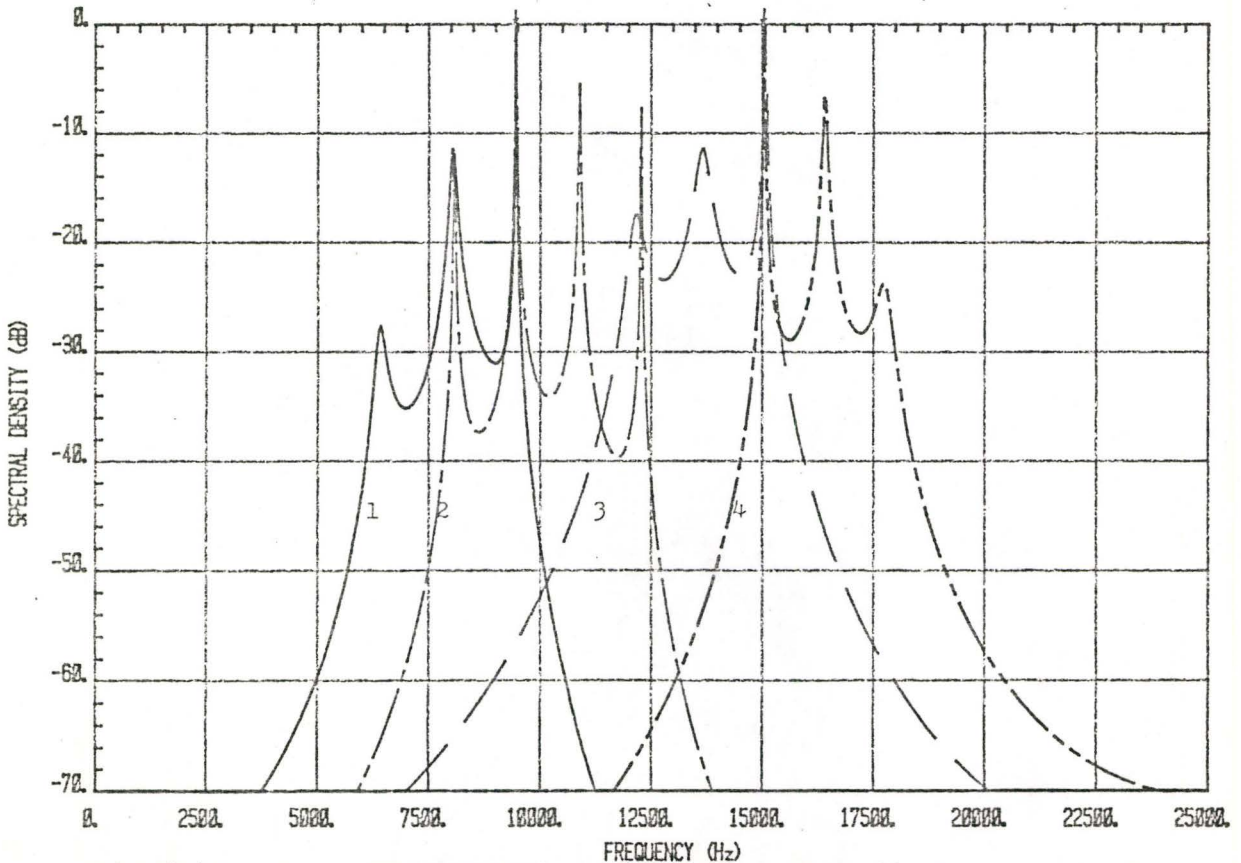


Fig. 4.47: The 'ELT+ACF+FIRMEM' spectra (filter order 8) of two continuous phase signals.

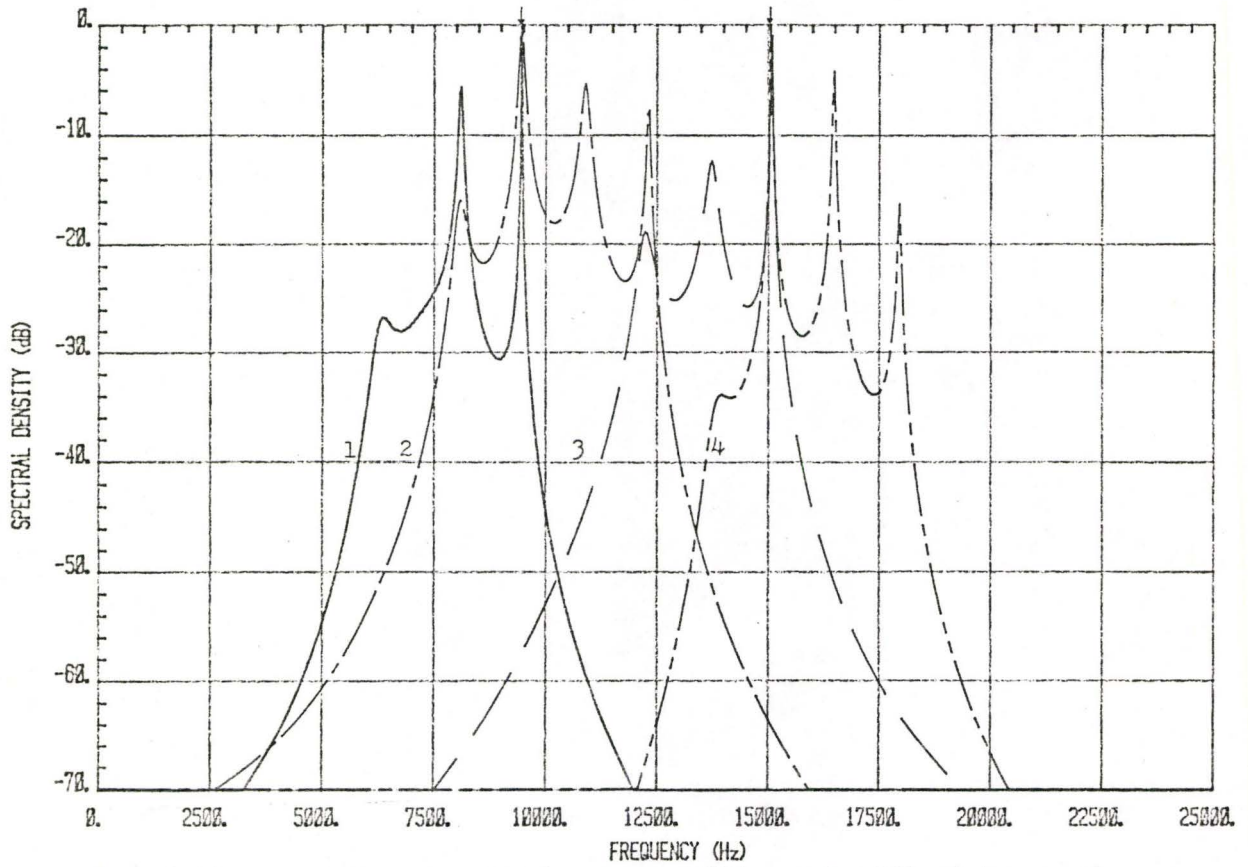


Fig. 4.48: The 'ELT+ACF+FIRMEM' spectra (filter order 10) of two continuous phase signals.

4.49, Fig. 4.50 and Fig. 4.51 are the spectra at MEM filter orders 4, 8 and 10, respectively. As expected, a low order MEM favours random phase structure.

For the sinusoidal-modulated signals, the spectra which are illustrated in Fig. 4.52, Fig. 4.53 and Fig. 4.54 are outstanding at the three MEM filter orders.

The merit of employing a bank of narrow band bandpass filters is evident immediately by the achievement of using MEM filter orders 4 or 8, rather than MEM filter order 20, in processing two ELT signals.

#### 4.4.2 Five ELT Signals

From the above results, we find that MEM filter order 8 is a suitable choice to carry out the analysis. The spectra of five continuous phase signals (7588 Hz, 9000 Hz, 11924 Hz, 13527 Hz and 15425 Hz) using the same filter order are presented in Fig. 4.55. With the exception of the peak at around 6120 Hz, the rest of the required peaks appear at the correct frequencies. The capability of resolving two signals is revealed by BPF 1 and BPF 2. In BPF 3, there are three signals but only two can be detected by the method. The missing signal (11924 Hz), which occurs in the overlapping area between BPF 2 and 3, is recognized by BPF 2. BPF 4 has one signal and the peak is shifted by 100 Hz. At MEM filter order 10, the processing results are included in Fig. 4.56. A false peak at 10500 Hz is produced by BPF 2, otherwise the spectral performance is good.

Both of the MEM filter orders fail to resolve the random phase signals. The spectra are given in Fig. 4.57 and Fig. 4.58. There is no

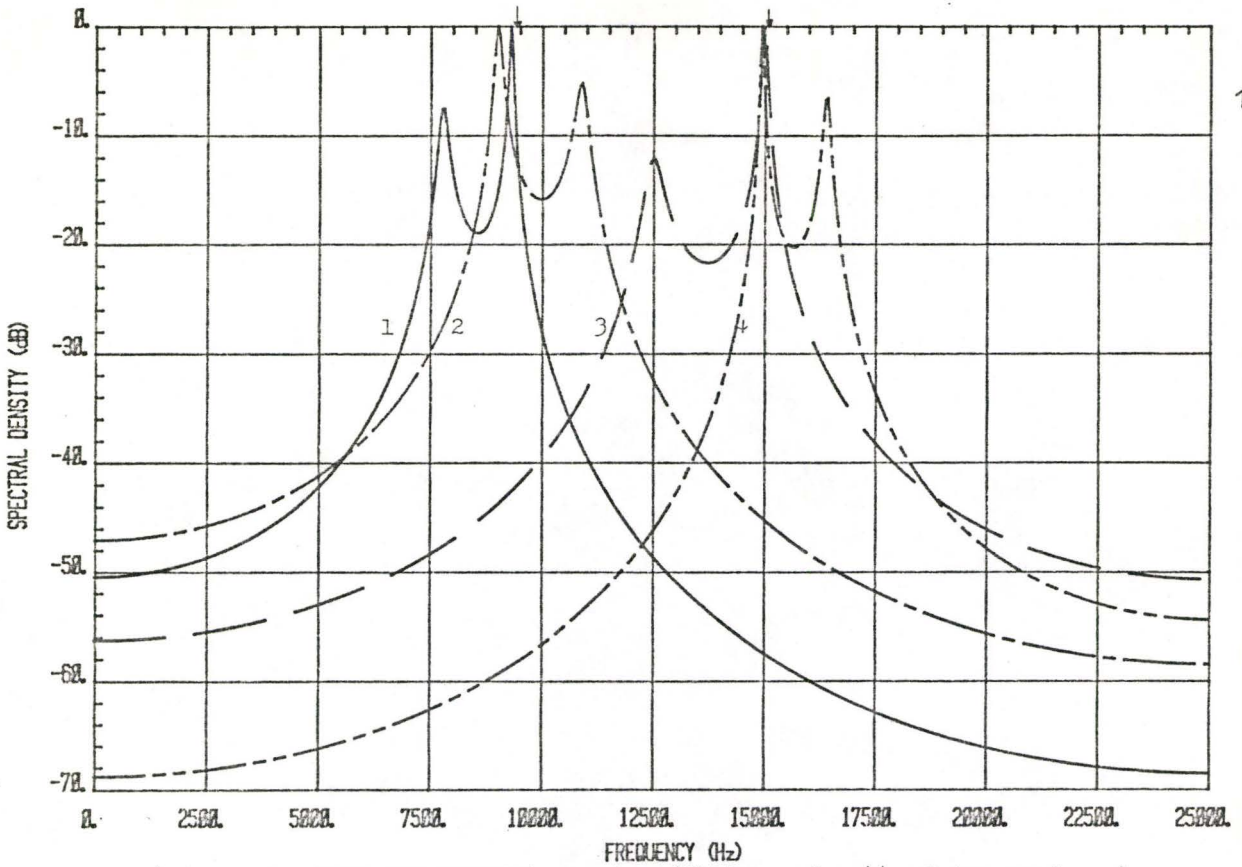


Fig. 4.49: The 'ELT+ACF+FIRMEM' spectra (filter order 4) of two random phase signals with carrier frequencies 9448 Hz and 15039 Hz.

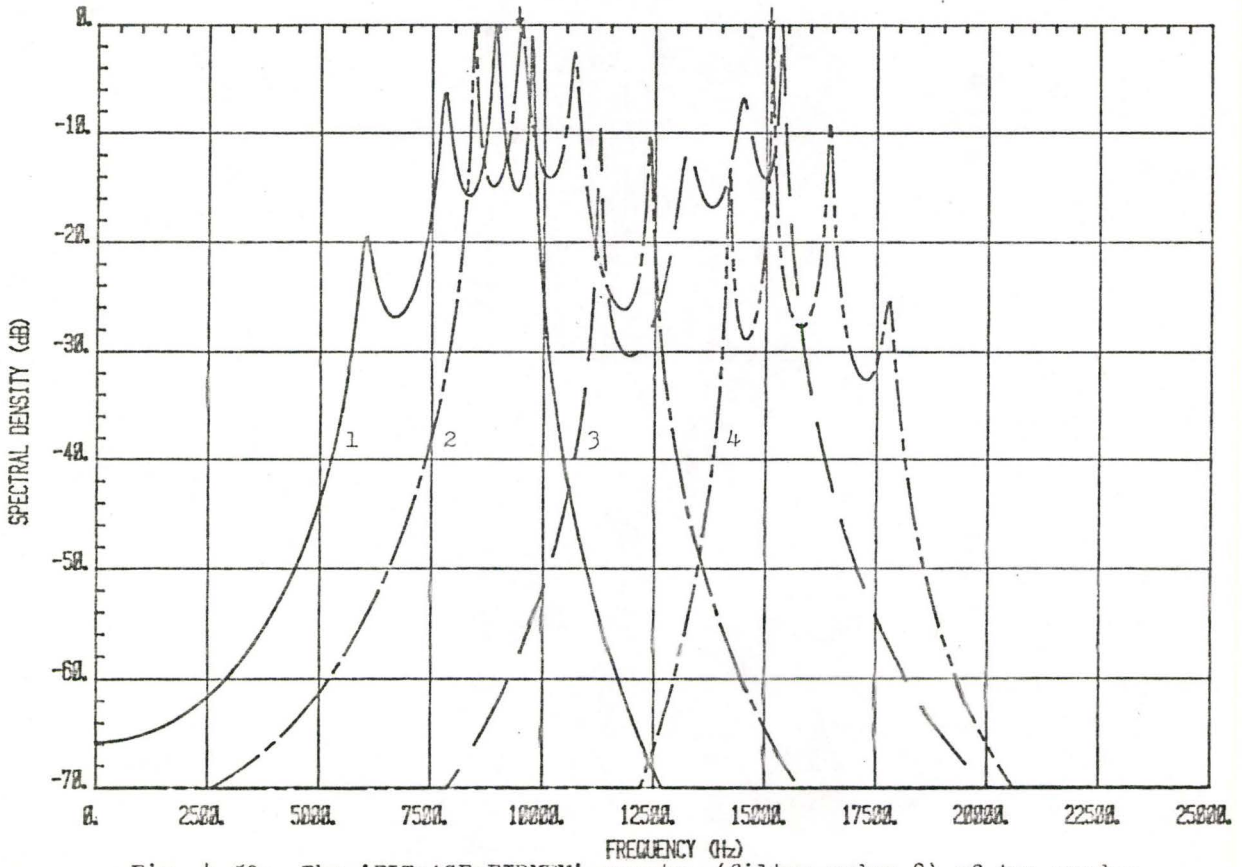


Fig. 4.50: The 'ELT+ACF+FIRMEM' spectra (filter order 8) of two random phase signals.

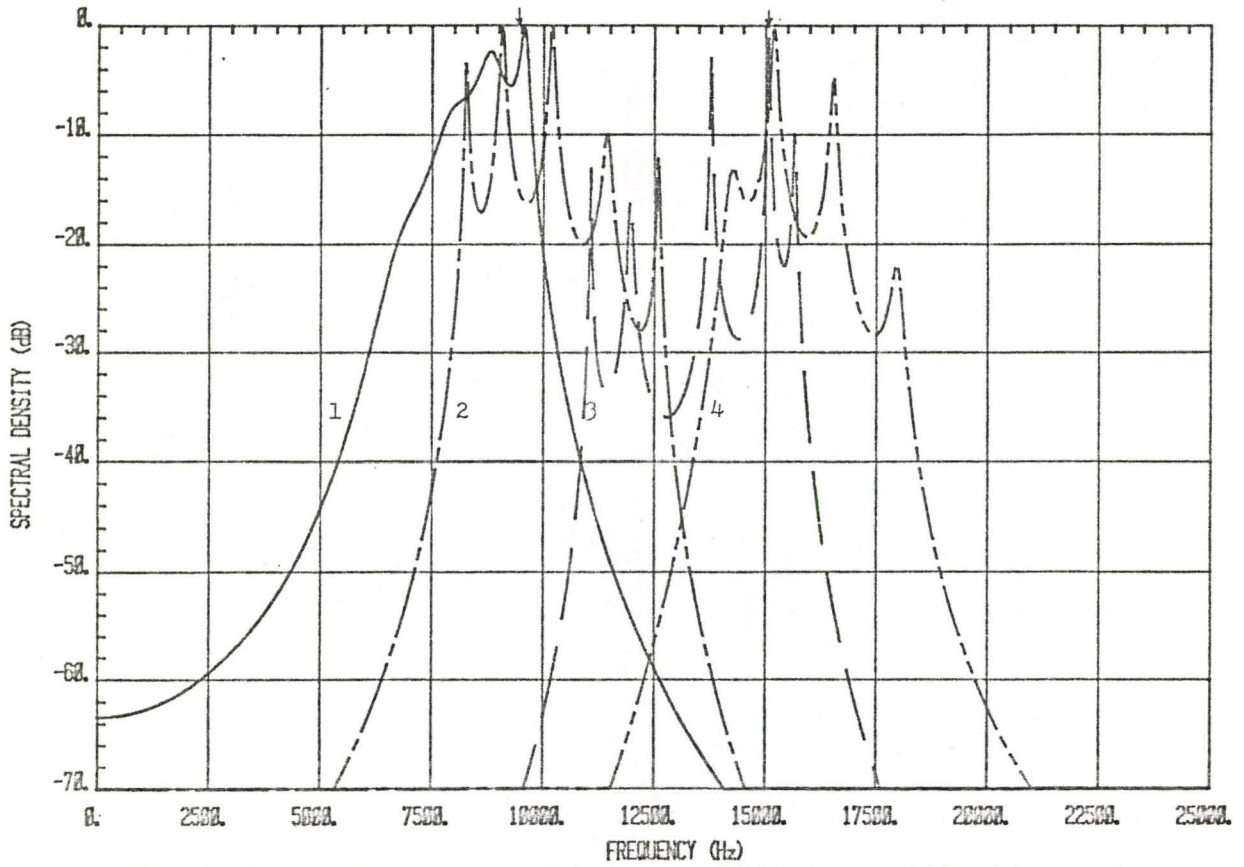


Fig. 4.51: The 'ELT+ACF+FIRMEM' spectra (filter order 10) of two random phase signals.

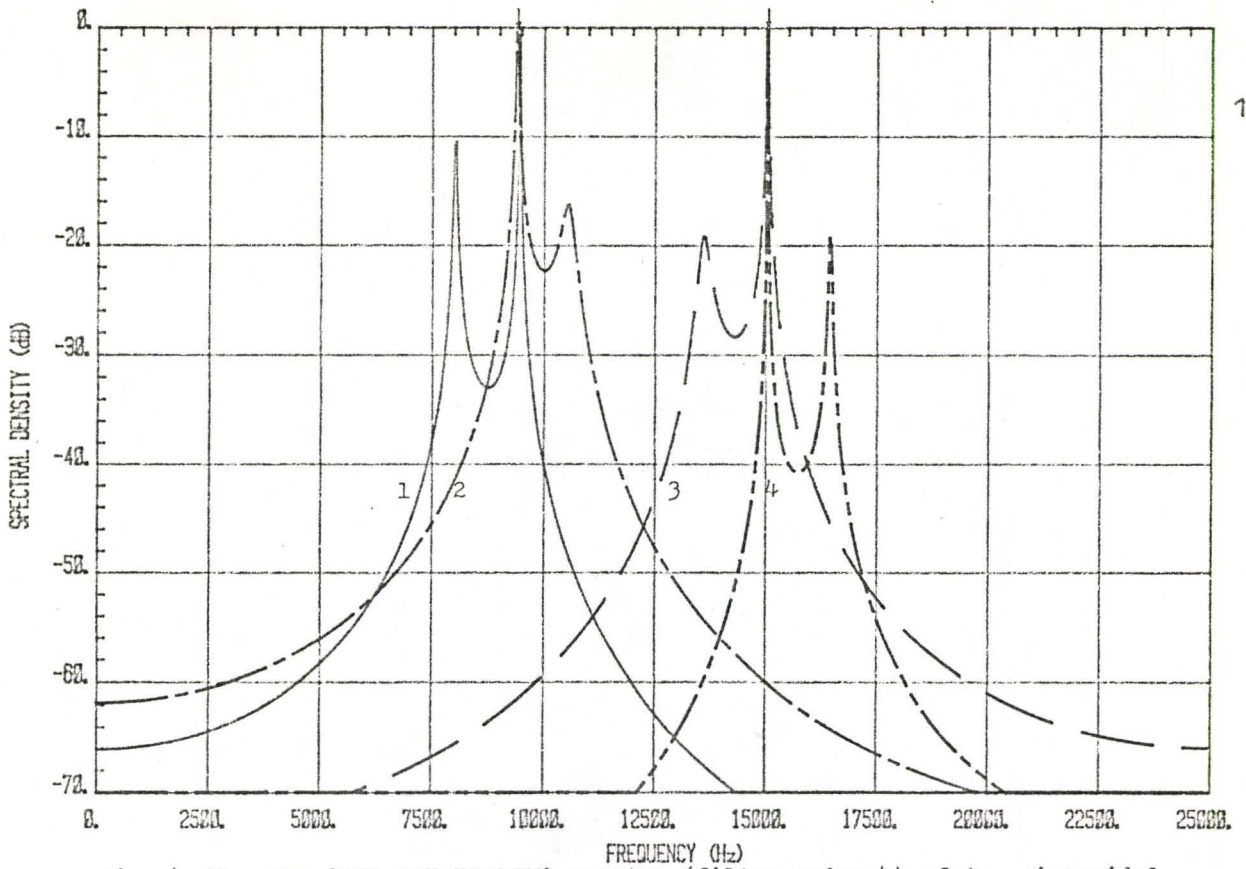


Fig. 4.52: The 'ELT+ACF+FIRMEM' spectra (filter order 4) of two sinusoidal-modulated signals with carrier frequencies 9448 Hz and 15039 Hz.

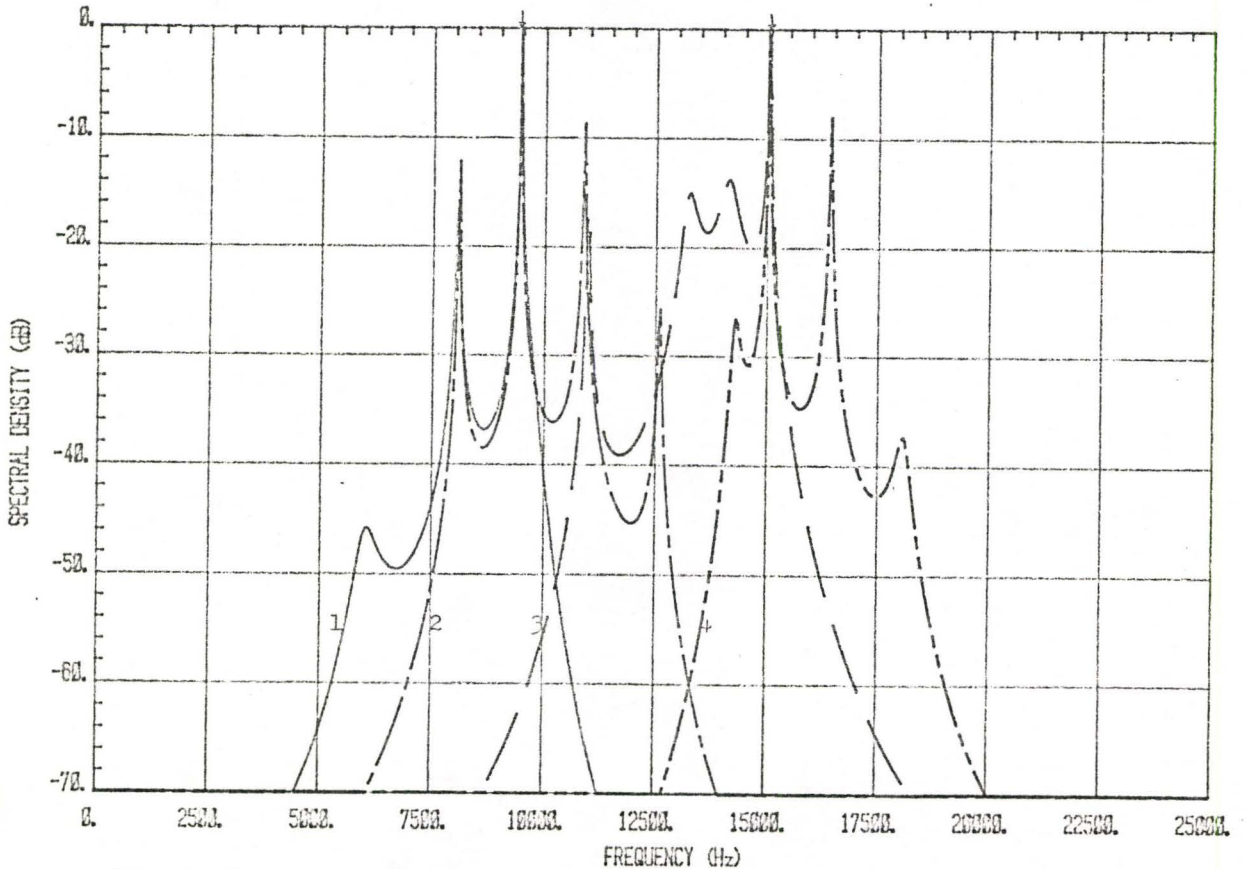


Fig. 4.53: The 'ELT+ACF+FIRMEM' spectra (filter order 8) of two sinusoidal-modulated signals.

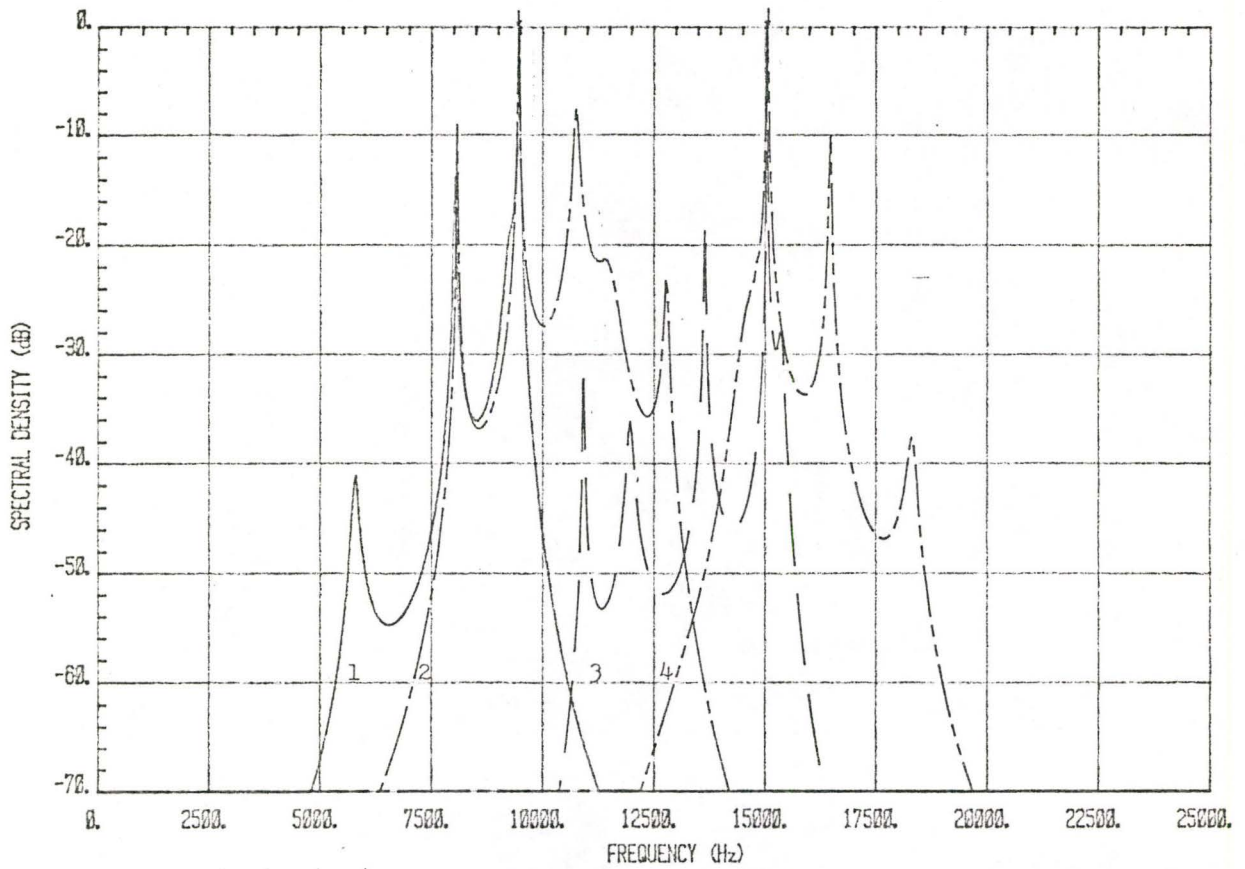


Fig. 4.54: The 'ELT+ACF+FIRMEM' spectra (filter order 10) of two sinusoidal-modulated signals.

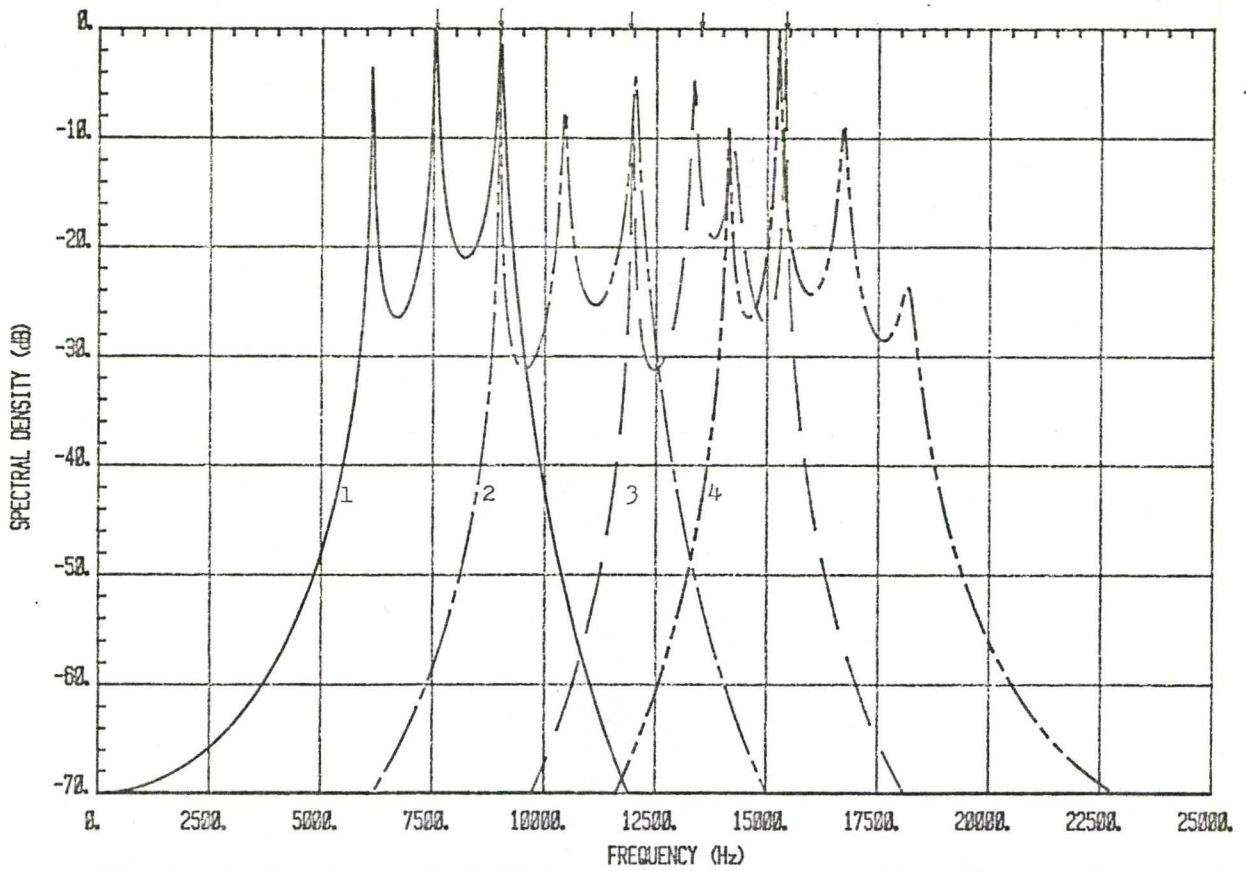


Fig. 4.55: The 'ELT+ACF+FIRMEM' spectra (filter order 8) of five continuous phase signals with carrier frequencies 7588 Hz, 9000 Hz, 11924 Hz, 13527 Hz and 15425 Hz.

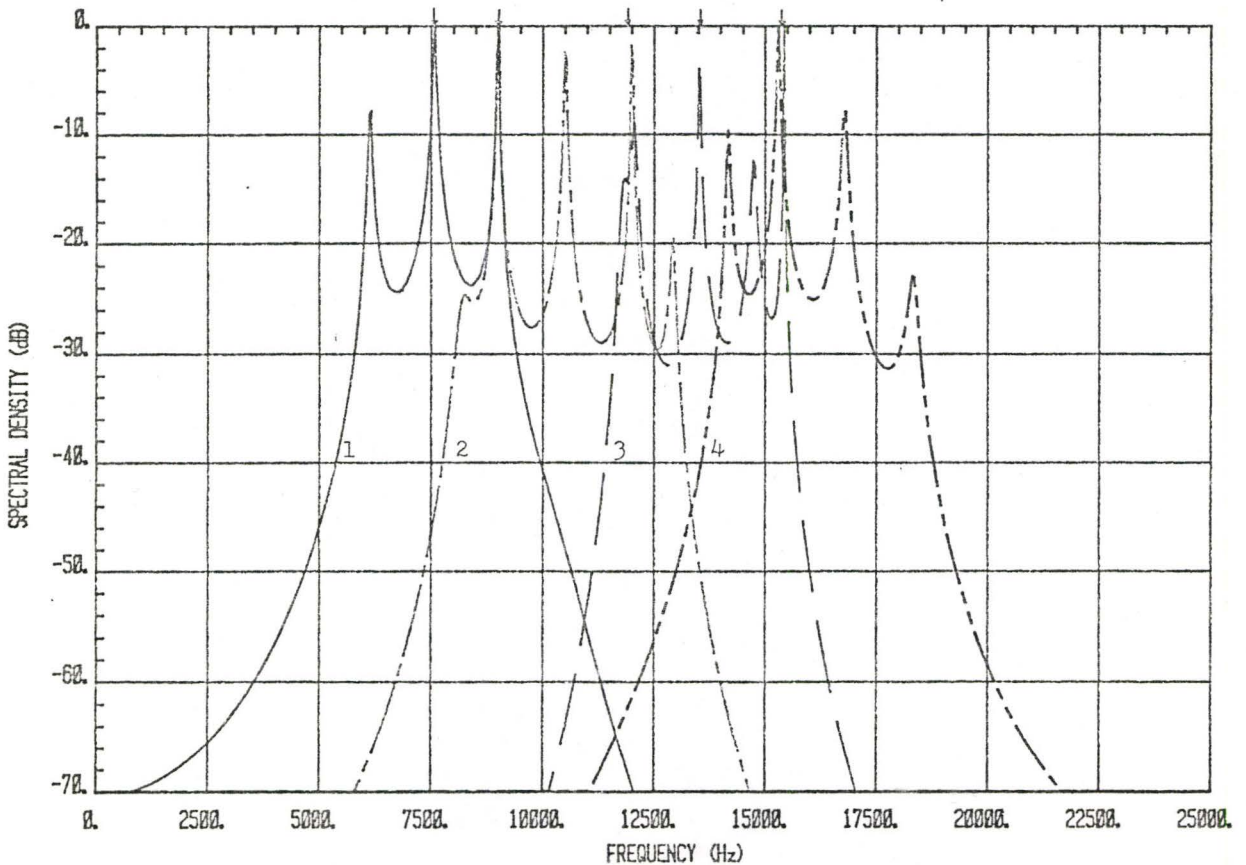


Fig. 4.56: The 'ELT+ACF+FIRMEM' spectra (filter order 10) of five continuous phase signals.

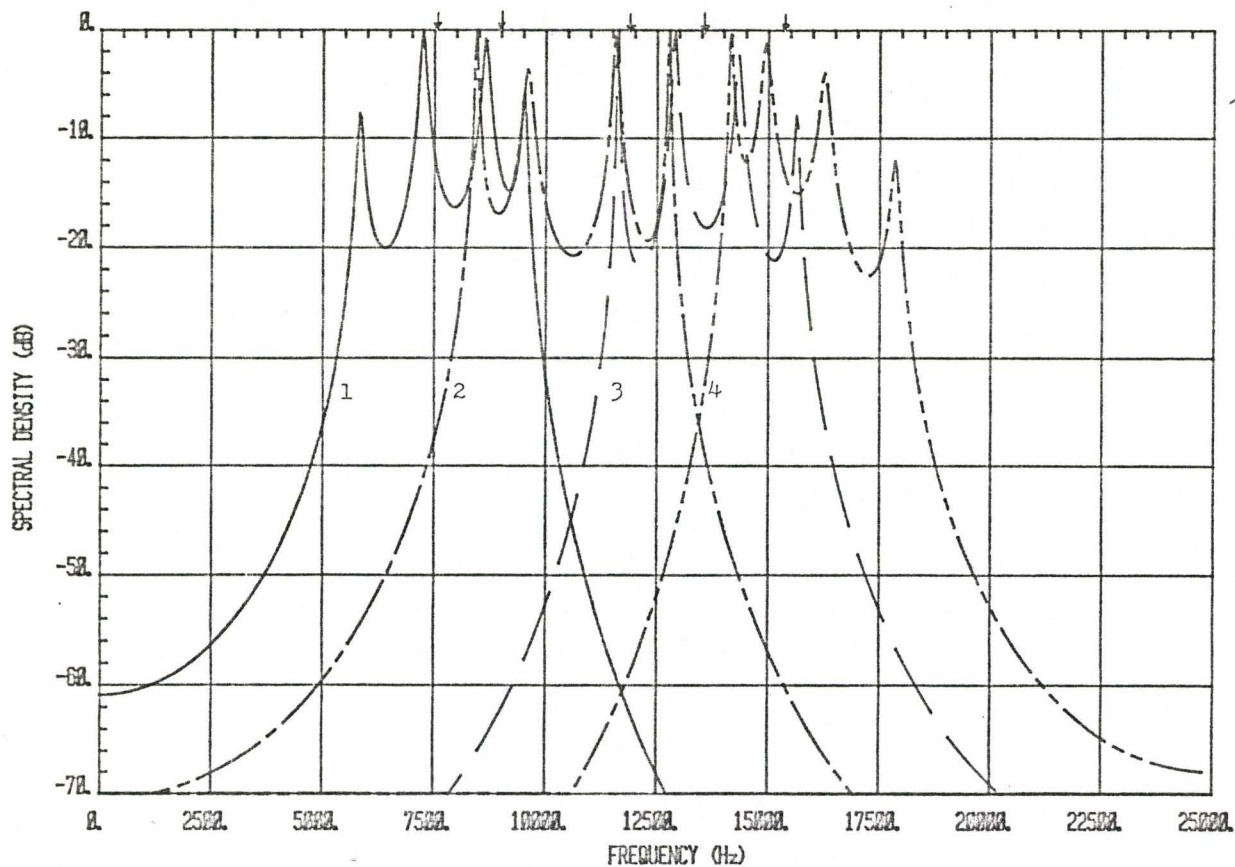


Fig. 4.57: The 'ELT+ACF+FIRMEM' spectra (filter order 8) of five random phase signals with carrier frequencies 7588 Hz, 9000 Hz, 11924 Hz, 13527 Hz and 15425 Hz.

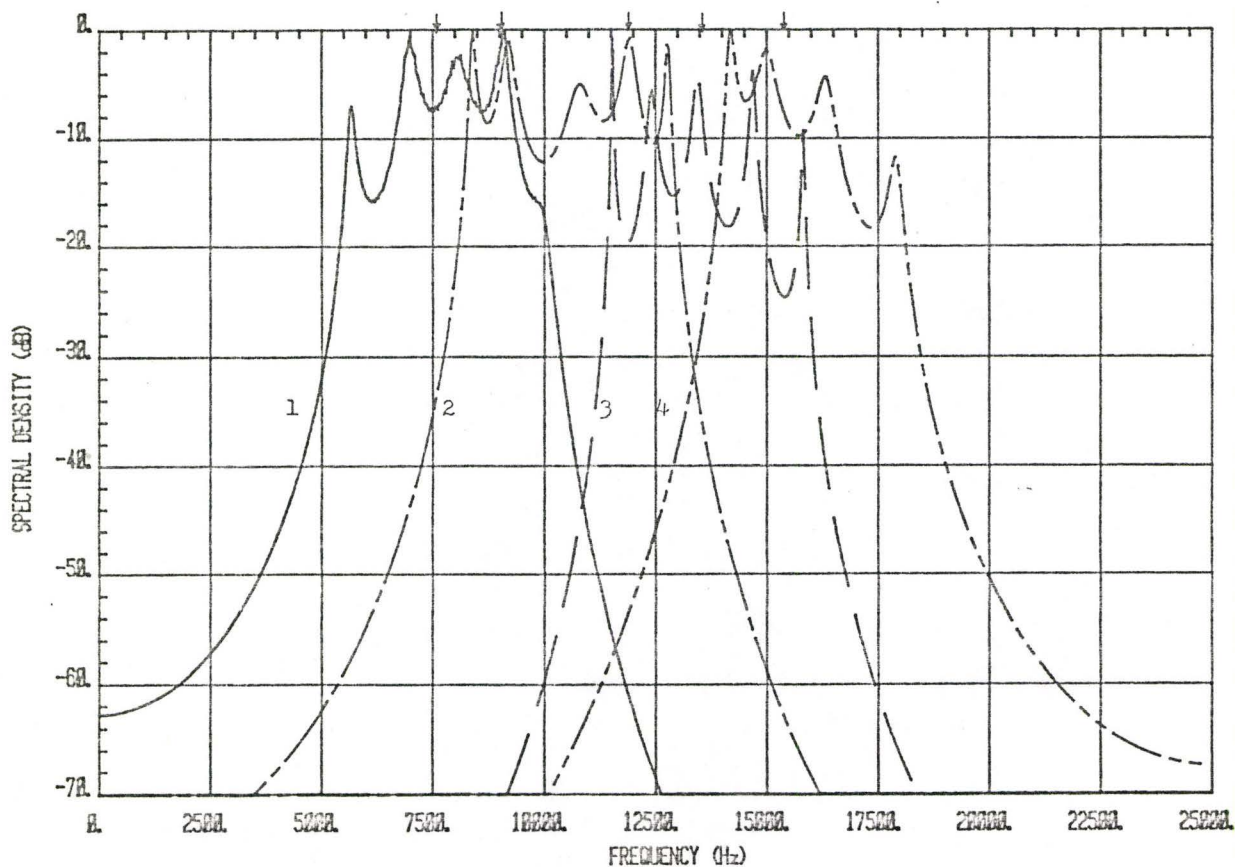


Fig. 4.58: The 'ELT+ACF+FIRMEM' spectra (filter order 10) of five random phase signals.

problem in dealing with the sinusoidal-modulated signals whose spectra at the two MEM filter orders are shown in Fig. 4.59 and Fig. 4.60.

One important accomplishment deserves attention. Selecting a fixed MEM filter order, two and five pulse-modulated (continuous phase) signals and sinusoidal-modulated signals can be resolved by the 'ELT+ACF+FIRMEM' configuration which is based on the technique of utilizing a bank of 5 KHz bandwidth bandpass filters. This method permits the use of a low order prediction error filter to resolve multiple ELT signals. High MEM filter orders such as 20 and 50 are avoided. The 2 KHz overlapping between filters guarantees that no signals are left undetected near the band edge of the filters.

#### 4.4.3 Ten ELT Signals

As the number of ELT signals increases, each of the four bandpass filters experiences more than two ELT signals. This inflicts substantial difficulties into the analysis. Fig. 4.61 shows the spectra of ten continuous phase emergency signals (7441 Hz, 8504 Hz, 9640 Hz, 10483 Hz, 11876 Hz, 12683 Hz, 13636 Hz, 14846 Hz, 16165 Hz and 17595 Hz) which are processed by MEM filter order 8. BPF 1 and 4 contain three signals. Five signals are present in BPF 2 and four signals are in BPF 3. Under the circumstances, it is necessary to employ higher MEM filter order. At -6 dB threshold level, Fig. 4.62 shows that nine signals are detected at MEM filter order 10. However, we are unable to achieve the same fruitful results in processing the random phase signals. The spectra are plotted in Fig. 4.63.

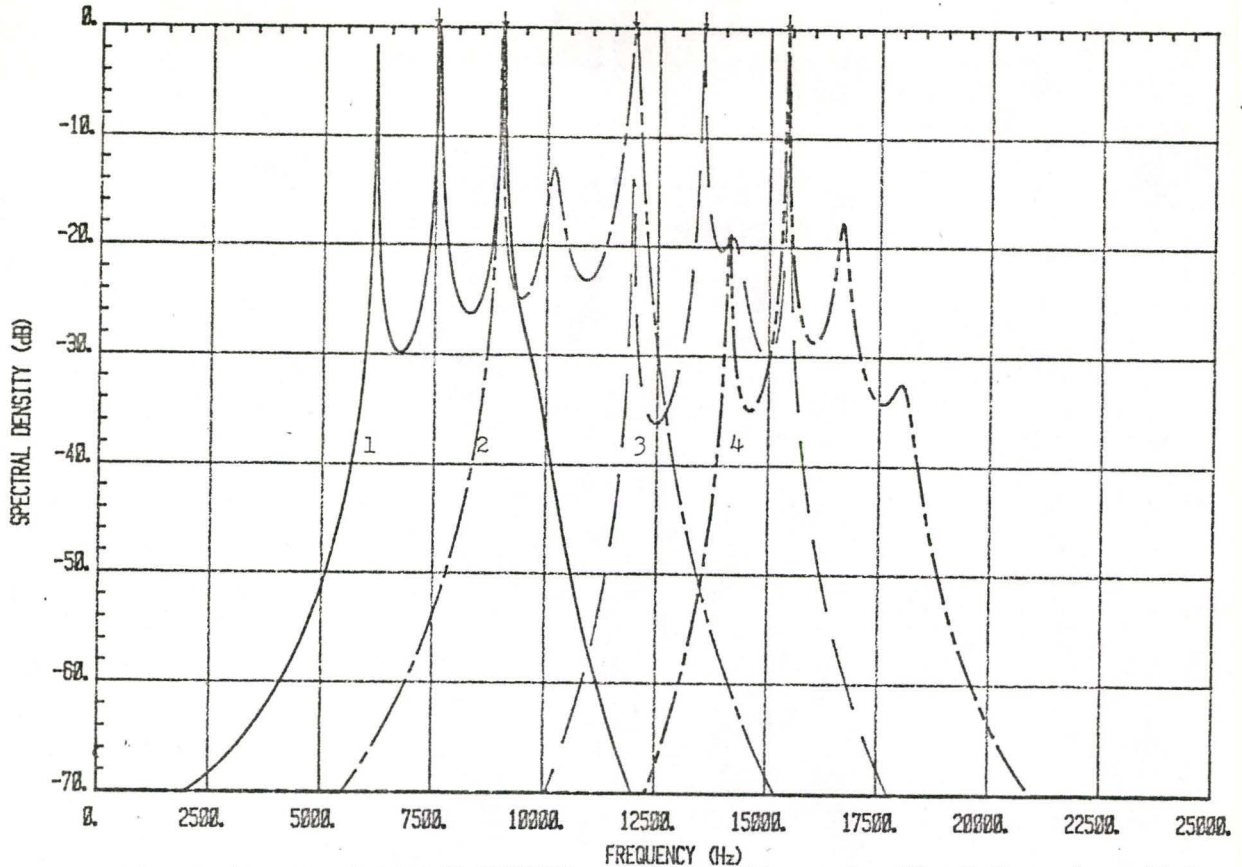


Fig. 4.59: The 'ELT+ACF+FIRMEM' spectra (filter order 8) of five sinusoidal-modulated signals with carrier frequencies 7588 Hz, 9000 Hz, 11924 Hz, 13527 Hz and 15425 Hz.

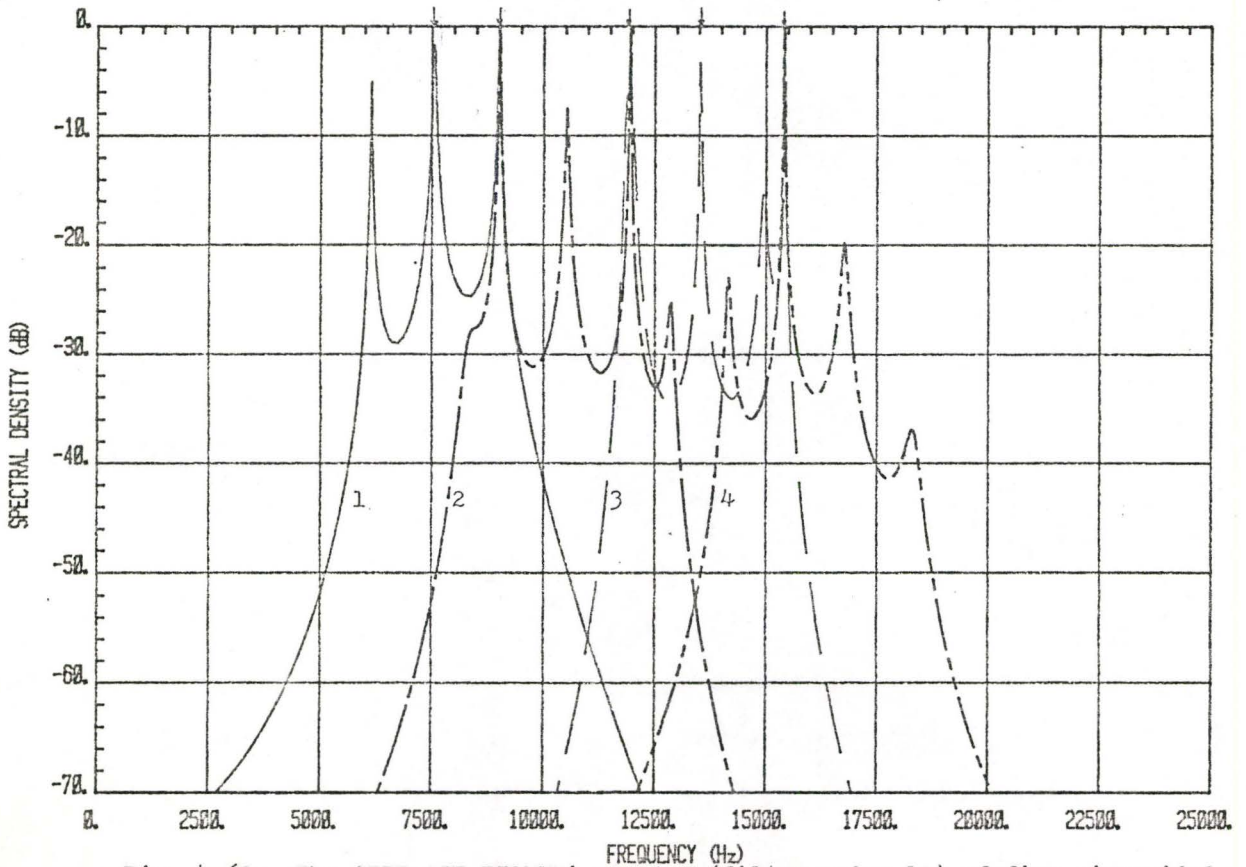


Fig. 4.60: The 'ELT+ACF+FIRMEM' spectra (filter order 10) of five sinusoidal-modulated signals.

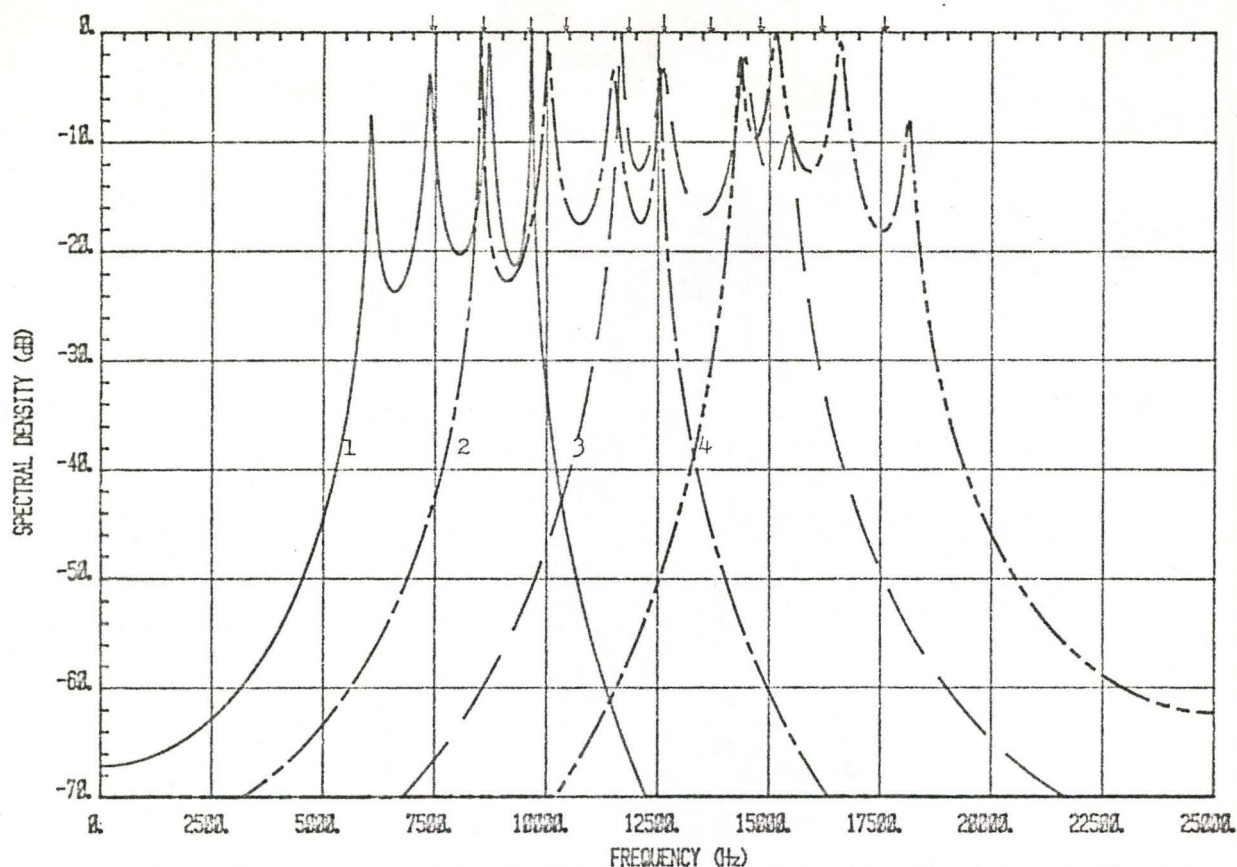


Fig. 4.61: The 'ELT+ACF+FIRMEM' spectra (filter order 8) of ten continuous phase signals with carrier frequencies 7441 Hz, 8504 Hz, 9640 Hz, 10483 Hz, 11876 Hz, 12683 Hz, 13636 Hz, 14846 Hz, 16165 Hz and 17595 Hz.

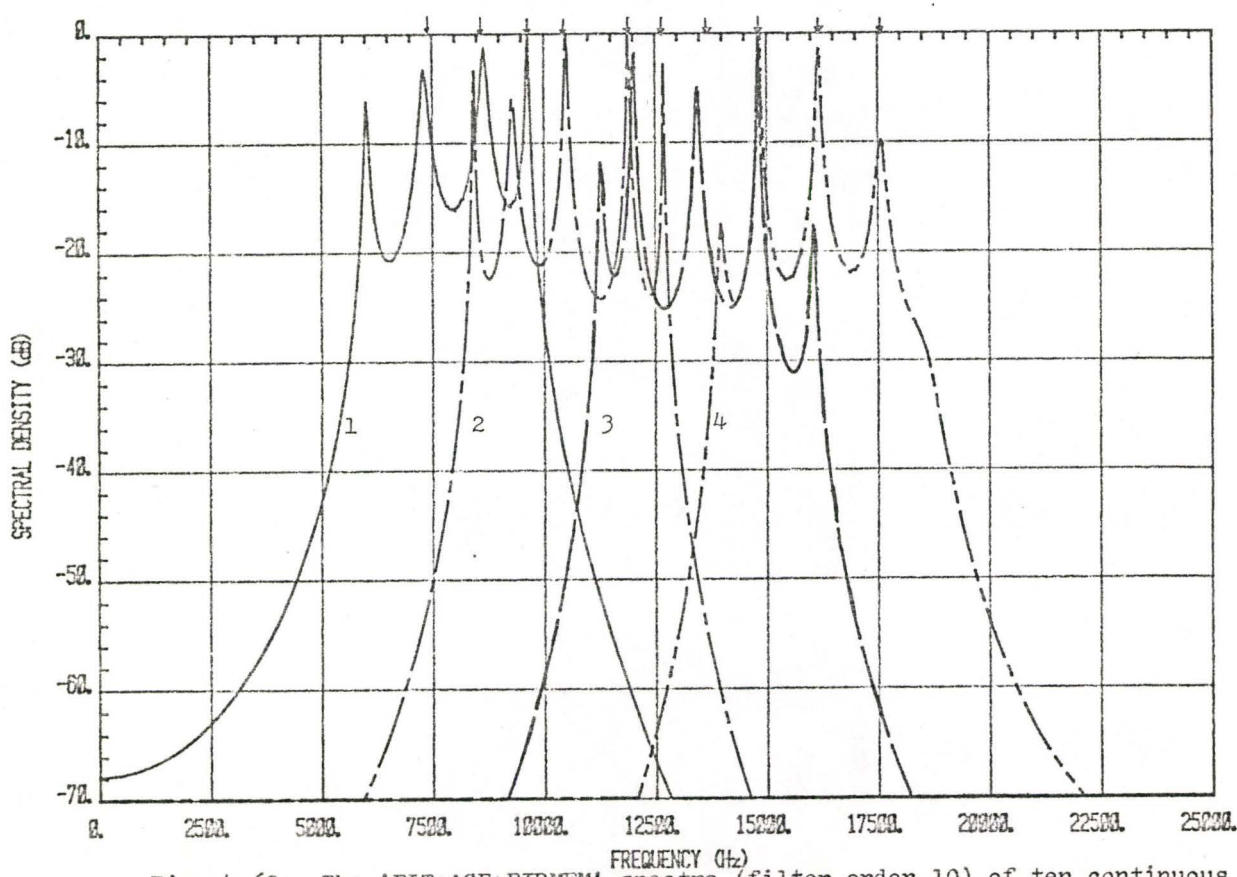


Fig. 4.62: The 'ELT+ACF+FIRMEM' spectra (filter order 10) of ten continuous phase signals.

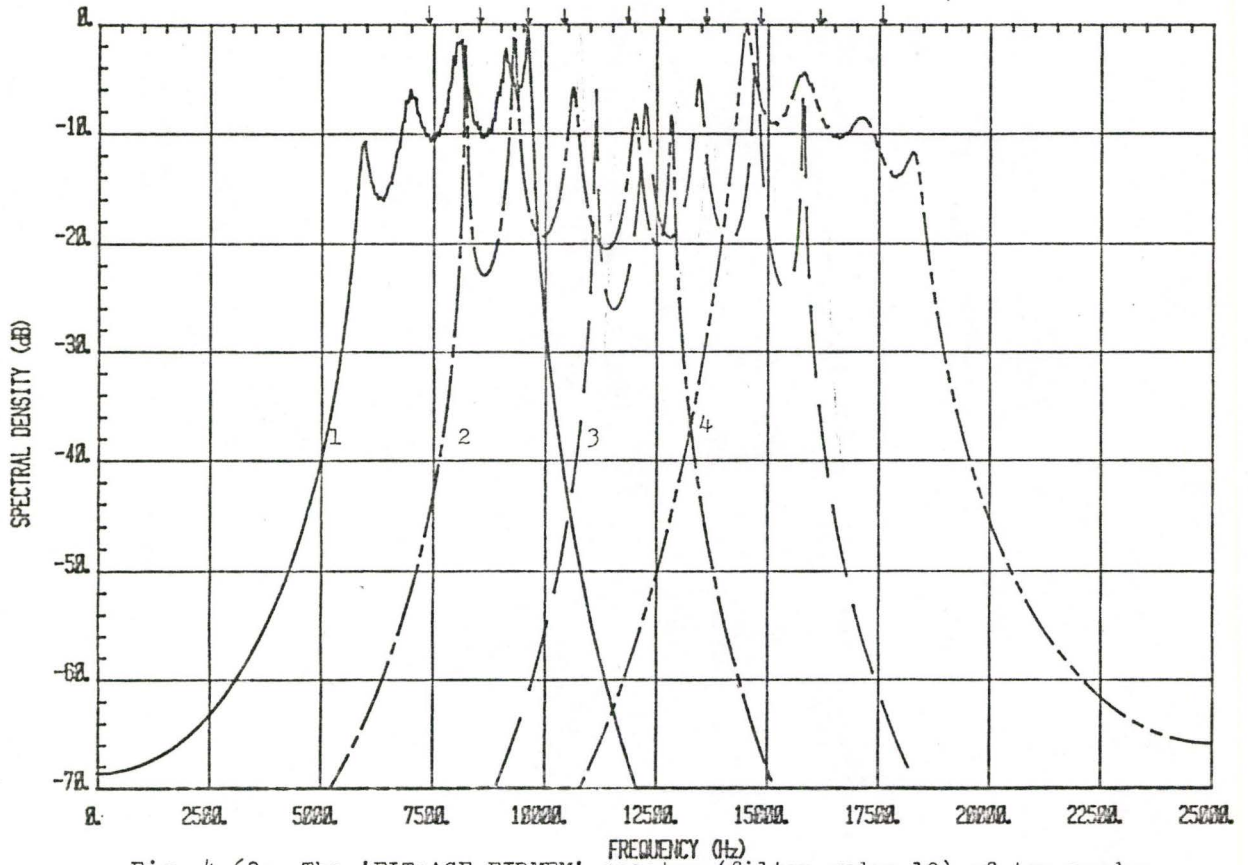


Fig. 4.63: The 'ELT+ACF+FIRMEM' spectra (filter order 10) of ten random phase signals with carrier frequencies 7441 Hz, 8504 Hz, 9640 Hz, 10483 Hz, 11876 Hz, 12683 Hz, 13636 Hz, 14846 Hz, 16165 Hz and 17595 Hz.

#### 4.4.4 General Remarks

A trade off between the number of bandpass filters and the MEM filter order has a significant influence on the MEM spectral estimation. If one desires to operate the MEM at a very low fixed filter order (for instance at filter orders, 2, 4 or 6), the penalty is to implement more bandpass filters with much narrower bandwidth. It is because each bandpass filter has to be restricted to accommodate just one ELT signal in order to satisfy the requirement.

#### 4.5 THE SPECTRAL PERFORMANCE OF MULTIPLE ELT SIGNALS WITH VARIATIONS IN CARRIER-TO-NOISE DENSITY RATIO

This section discusses the spectral performance of multiple ELT signals in a noisy environment assuming ELT units with pulse-modulated signals. Carrier-to-noise density ratio (CNR) at 34 dB-Hz (-10 dB), 39 dB-Hz (-5 dB), 44 dB-Hz (0 dB) and 54 dB-Hz (10 dB) are considered. All the multiple distress signals, in this study, are processed at equal CNR values.

The FFT spectra of the two continuous phase signals (9448 Hz and 15039 Hz) at the mentioned CNR are shown in Fig. 4.64 to Fig. 4.67. (Processing results with the windowing technique are not included.) The risk of having false alarm detection is imminent if the threshold level is placed at -5 dB amplitude. In comparing the FFT spectra with the MEM analysis from Fig. 4.68 to Fig. 4.71, at MEM filter order 20 the 'ELT+ACF+FIRMEM' configuration provides concrete detection ability even when the CNR is at 44 dB-Hz.

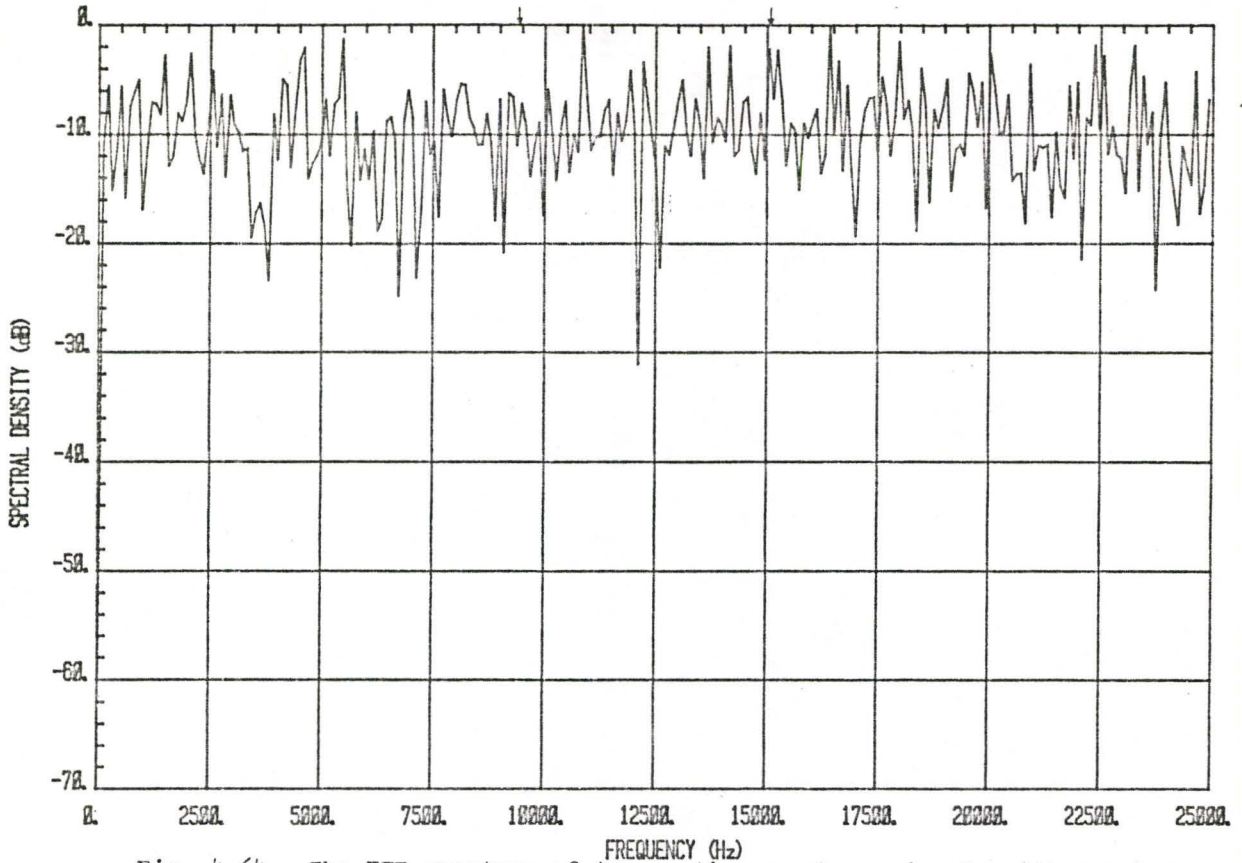


Fig. 4.64: The FFT spectrum of two continuous phase signals with carrier frequencies 9448 Hz and 15039 Hz. The CNDR is 34 dB-Hz.

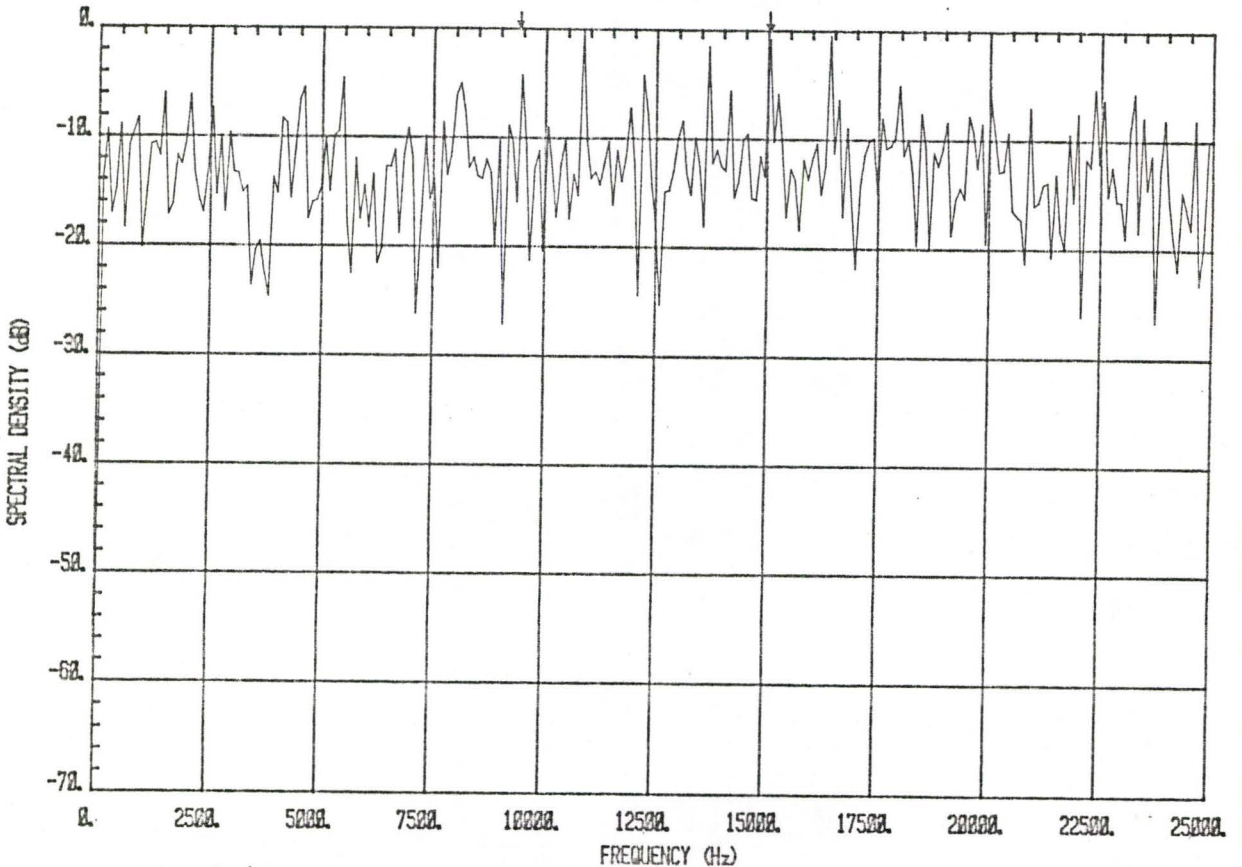


Fig. 4.65: The FFT spectrum of two continuous phase signals with CNDR=39 dB-Hz.

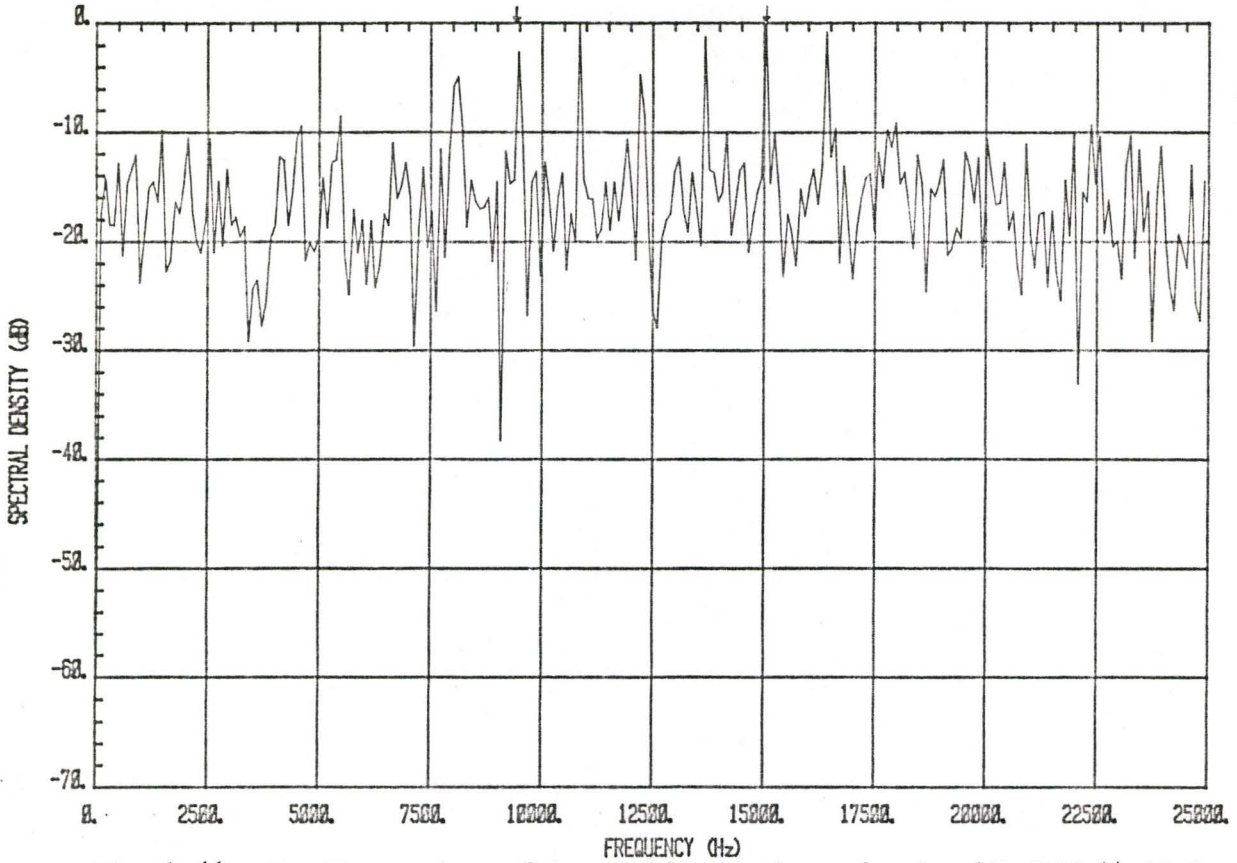


Fig. 4.66: The FFT spectrum of two continuous phase signals with CNDR=44 dB-Hz.

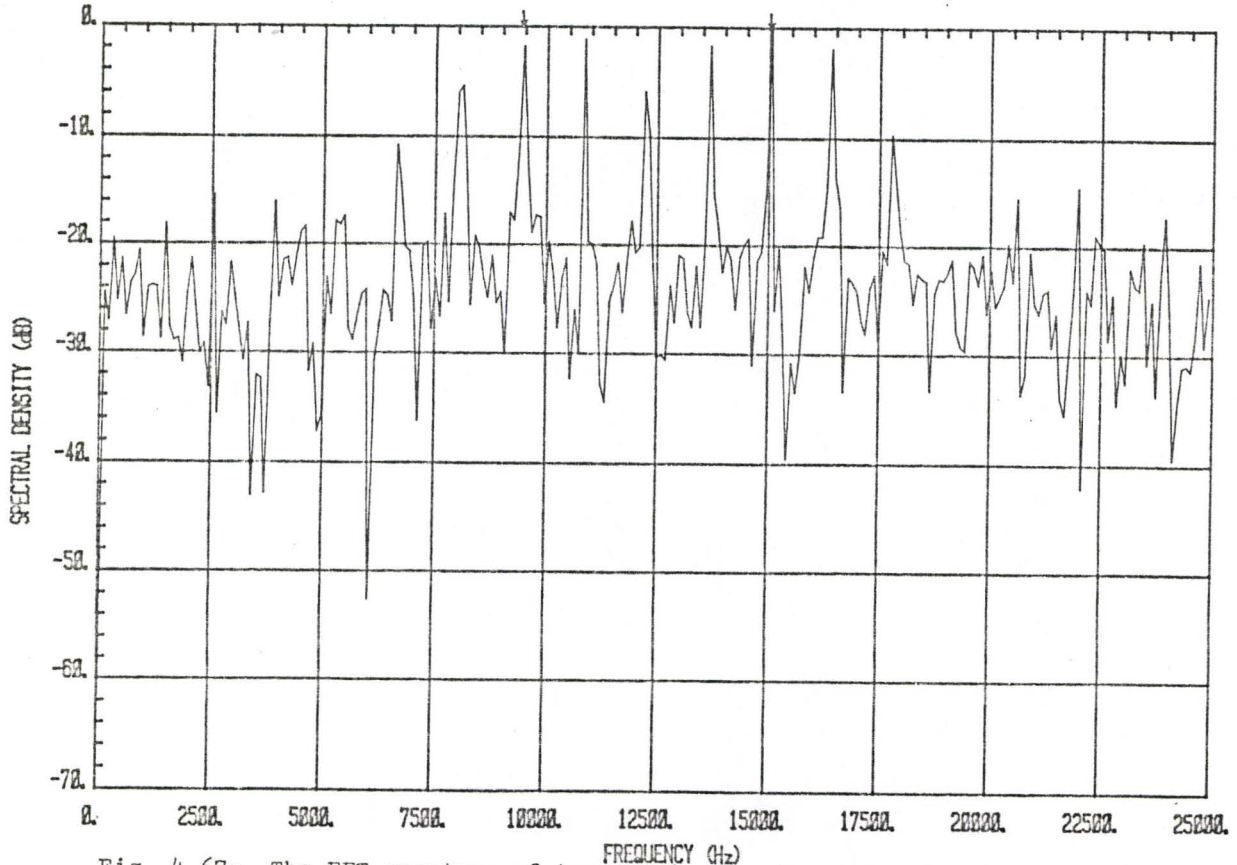


Fig. 4.67: The FFT spectrum of two continuous phase signals with CNDR=54 dB-Hz.

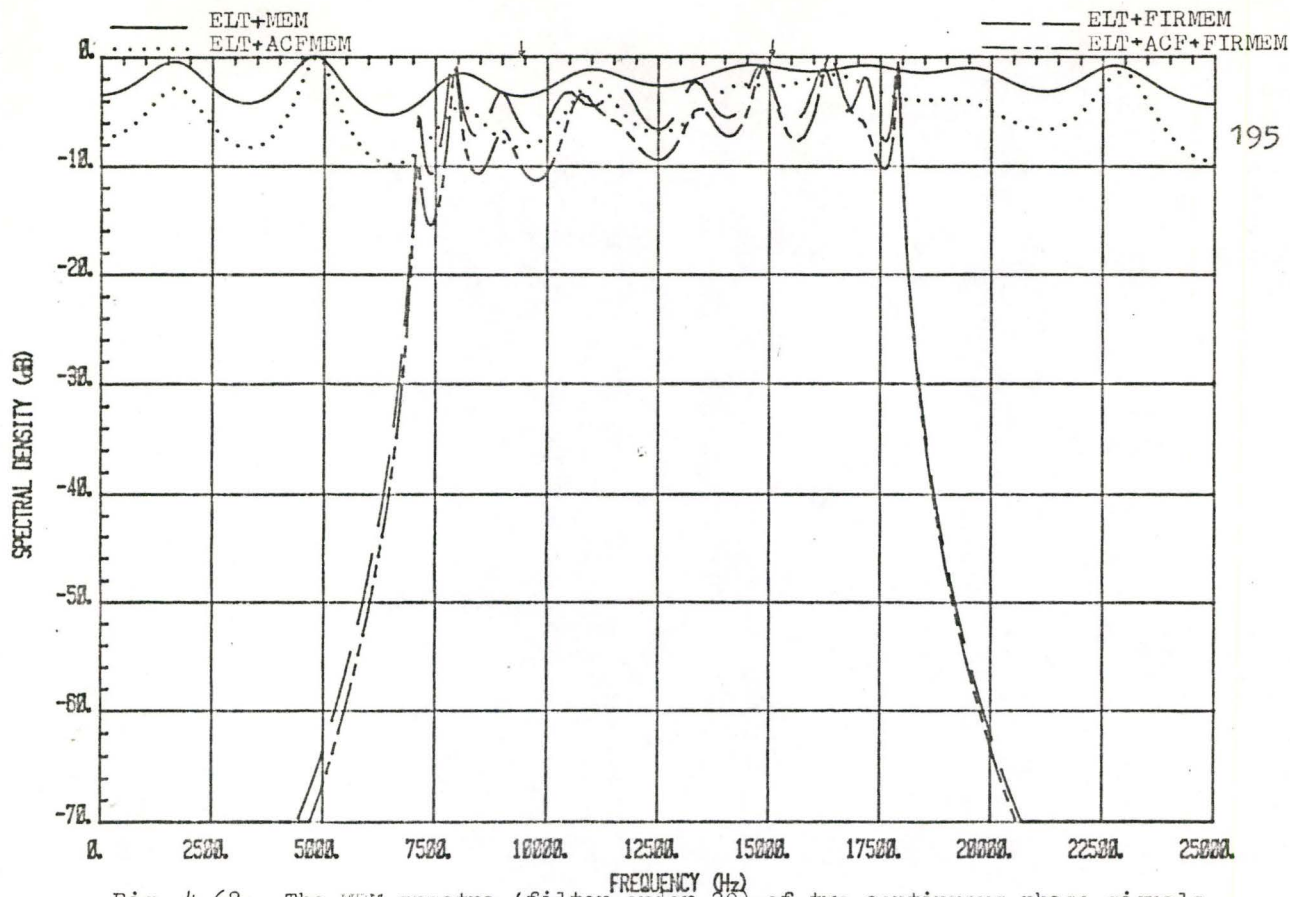


Fig. 4.68: The MEM spectra (filter order 20) of two continuous phase signals with CNDR=34 dB-Hz.

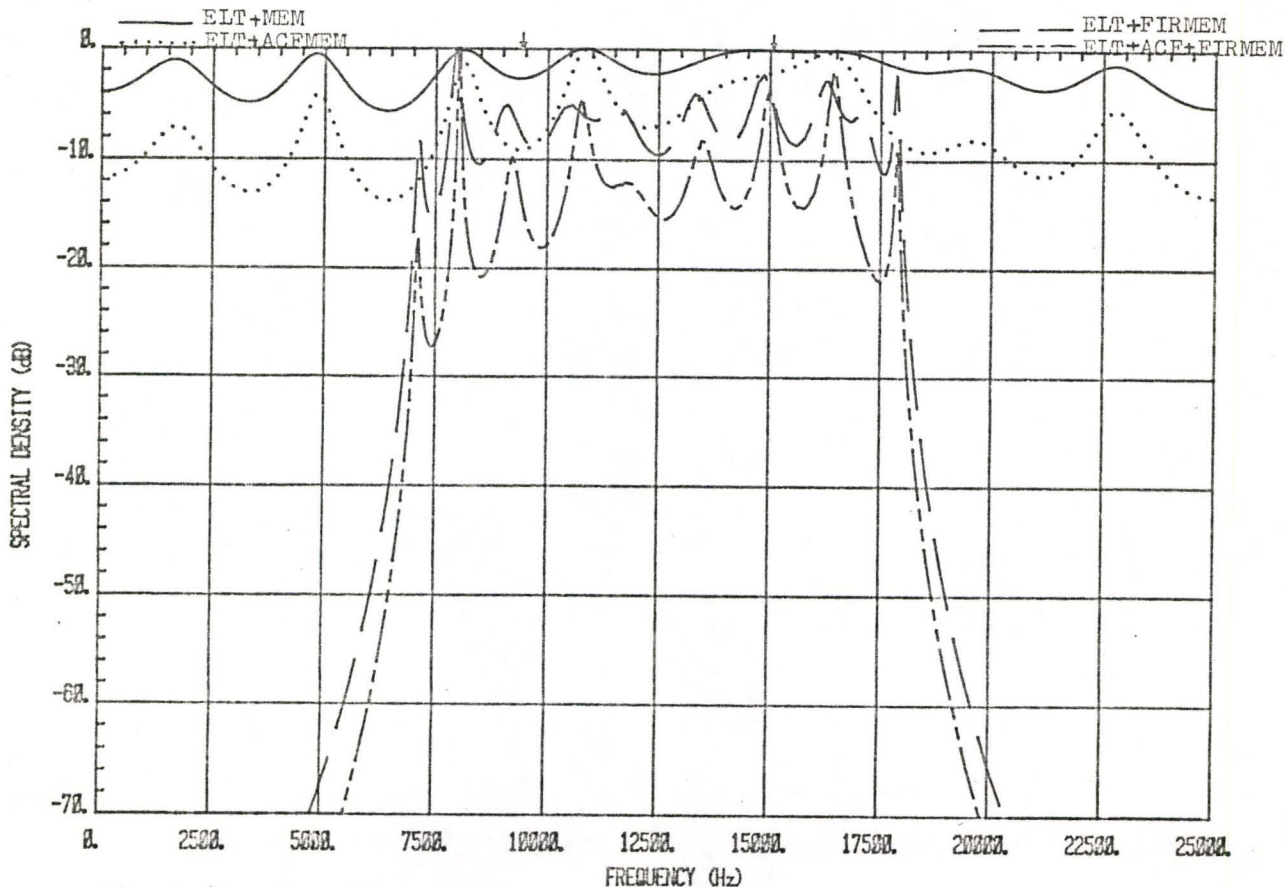


Fig. 4.69: The MEM spectra (filter order 20) of two continuous phase signals with CNDR=39 dB-Hz.

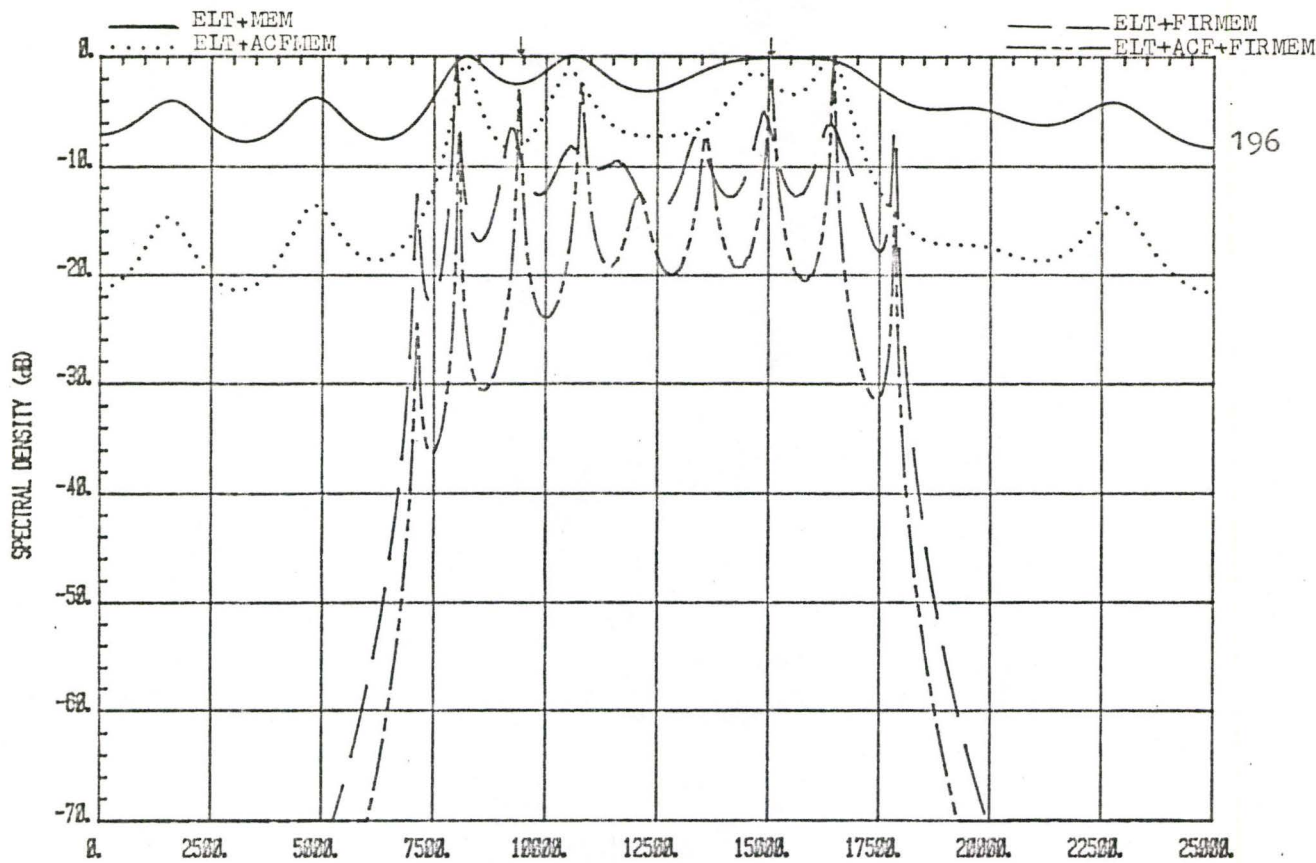


Fig. 4.70: The MEM spectra (filter order 20) of two continuous phase signals with CNDR=44 dB-Hz.

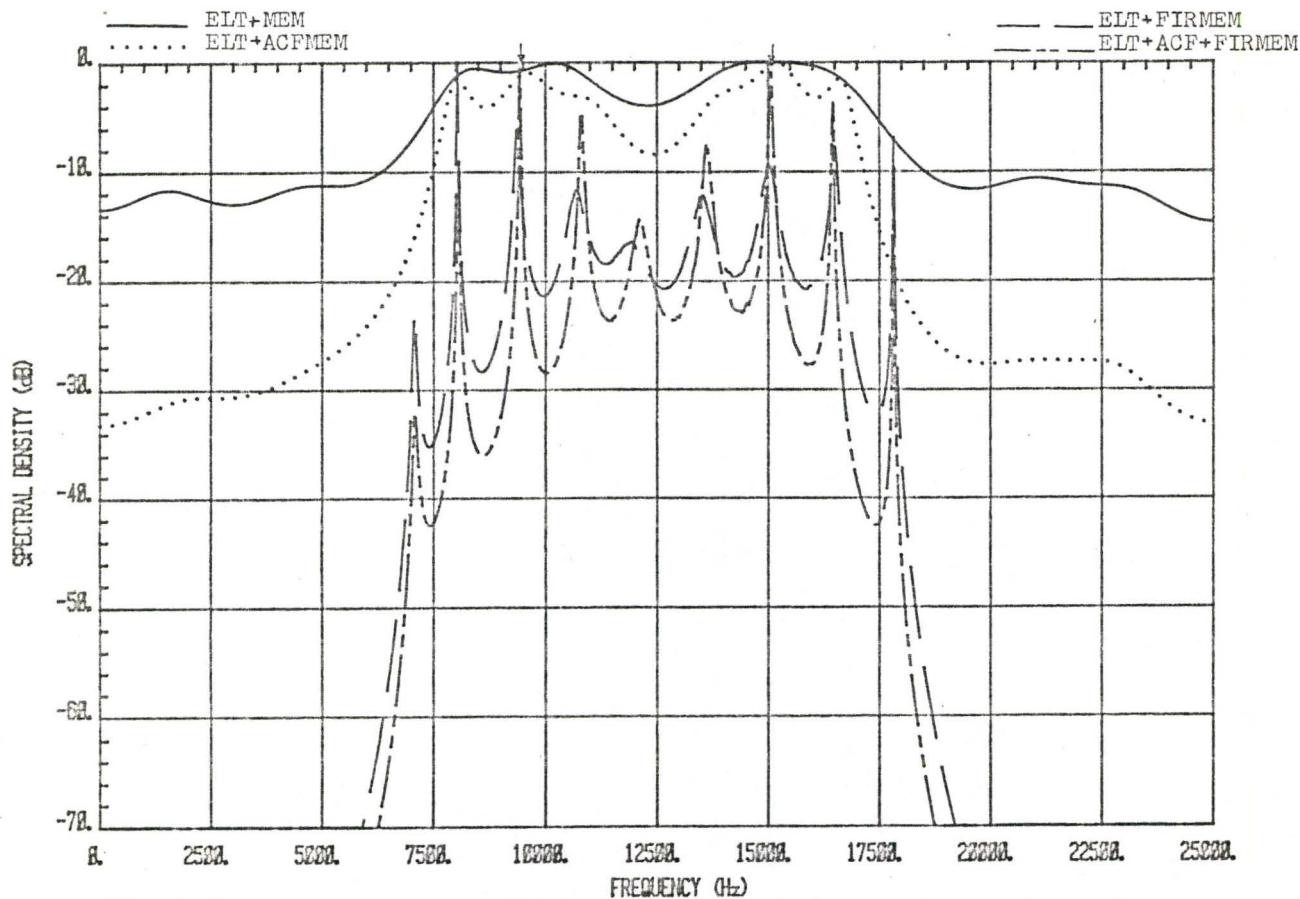


Fig. 4.71: The MEM spectra (filter order 20) of two continuous phase signals with CNDR=54 dB-Hz.

Using a bank of bandpass filters as described in Section 4.4, the spectral performance still maintains a promising feature in the presence of additive noise. Fig. 4.72 to Fig. 4.75 illustrate the situation where MEM filter order 8 is employed.

For the two random phase signals transmitted in noisy surroundings, the spectral estimation becomes much worse. The FFT method performs irrationally whereas the MEM approach cannot function efficiently. With variations in CNDR, the FFT spectral performance of the above signals with random phase structure is presented in Fig. 4.76 to Fig. 4.79. Since only the 'ELT+ACF+FIRMEM' configuration is able to operate at MEM filter order 20 (for two random phase signals), we examine its spectral performance at the different CNDR. The spectra are plotted in Fig. 4.80. At MEM filter order 8, the processing results which engage a bank of bandpass filter are depicted in Fig. 4.81 to Fig. 4.84.

Fig. 4.85 to Fig. 4.92 compare the FFT and MEM spectra of five continuous phase ELT signals (7588 Hz, 9000 Hz, 11924 Hz, 13527 Hz and 15425 Hz). The numerous sidelobes make the FFT approach difficult to use as compared with the MEM. From Fig. 4.93 to Fig. 4.96 the spectra with the bank of bandpass filters preprocessor technique using MEM filter order 8 are given.

#### 4.6 SUMMARY

This chapter focused on measuring the spectral characteristics of multiple ELT signals. Specifically, we examined the problem of two,

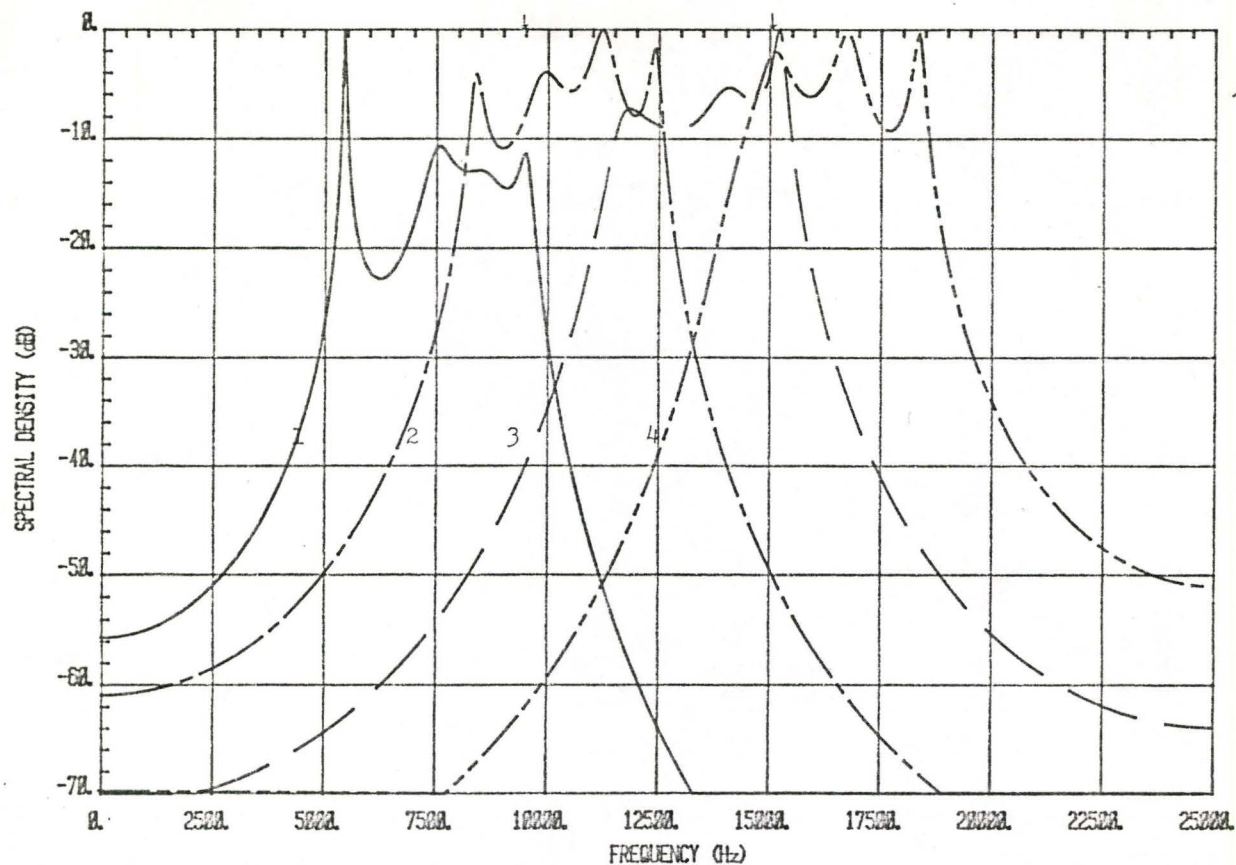


Fig. 4.72: The 'ELT+ACF+FIRMEM' spectra (filter order 8) of two continuous phase signals with CNDR=34 dB-Hz.

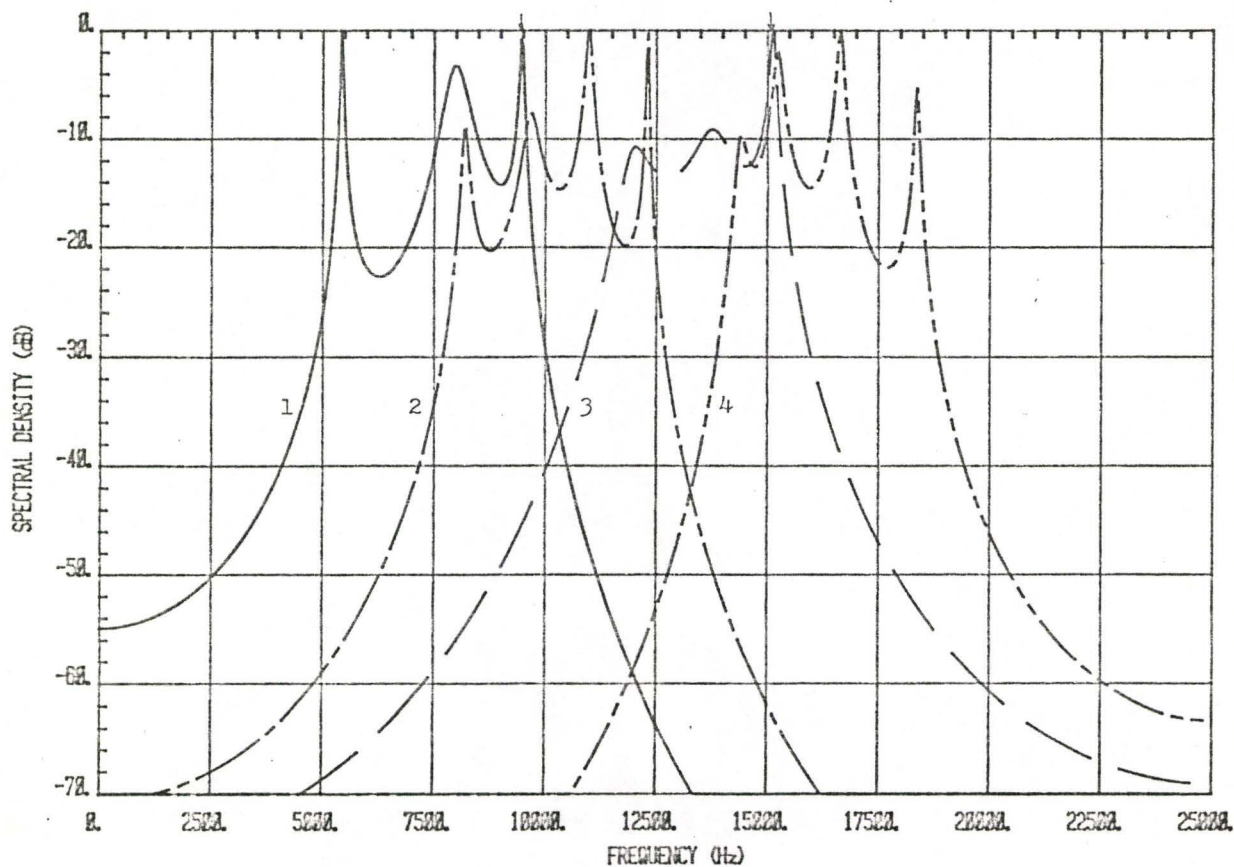


Fig. 4.73: The 'ELT+ACF+FIRMEM' spectra (filter order 8) of two continuous phase signals with CNDR=39 dB-Hz.

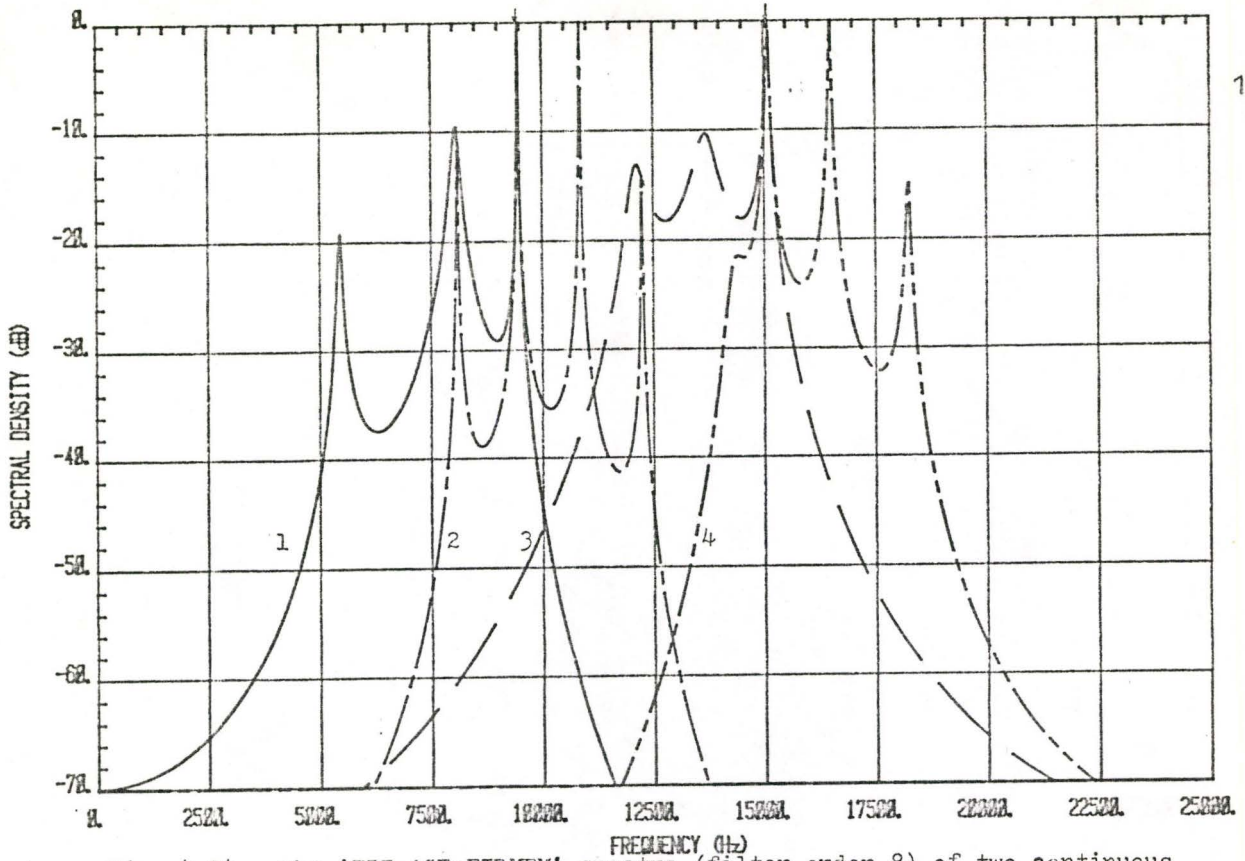


Fig. 4.74: The 'ELT+ACF+FIRMEM' spectra (filter order 8) of two continuous phase signals with CNDR=44 dB-Hz.

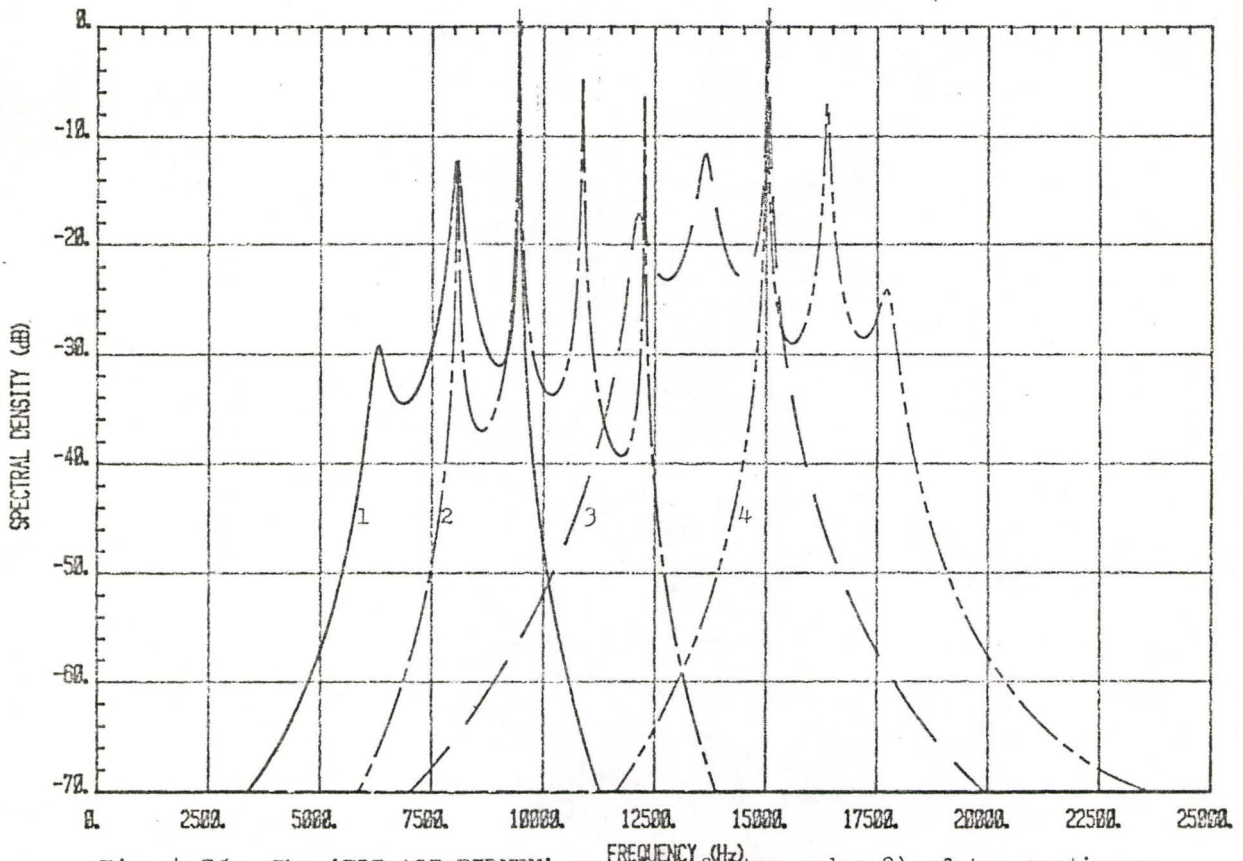


Fig. 4.75: The 'ELT+ACF+FIRMEM' spectra (filter order 8) of two continuous phase signals with CNDR=54 dB-Hz.

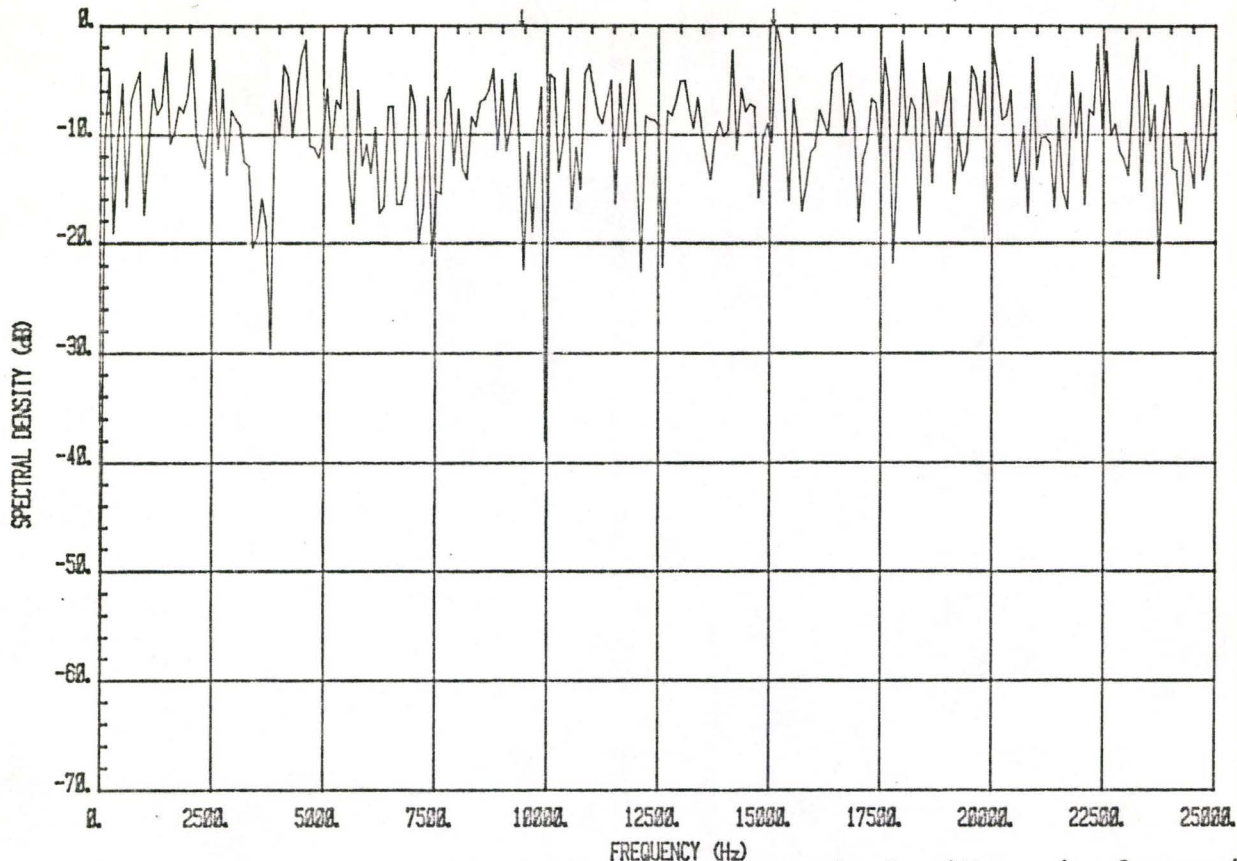


Fig. 4.76: The FFT spectrum of two random phase signals with carrier frequencies 9448 Hz and 15039 Hz. The CNDR is 34 dB-Hz.

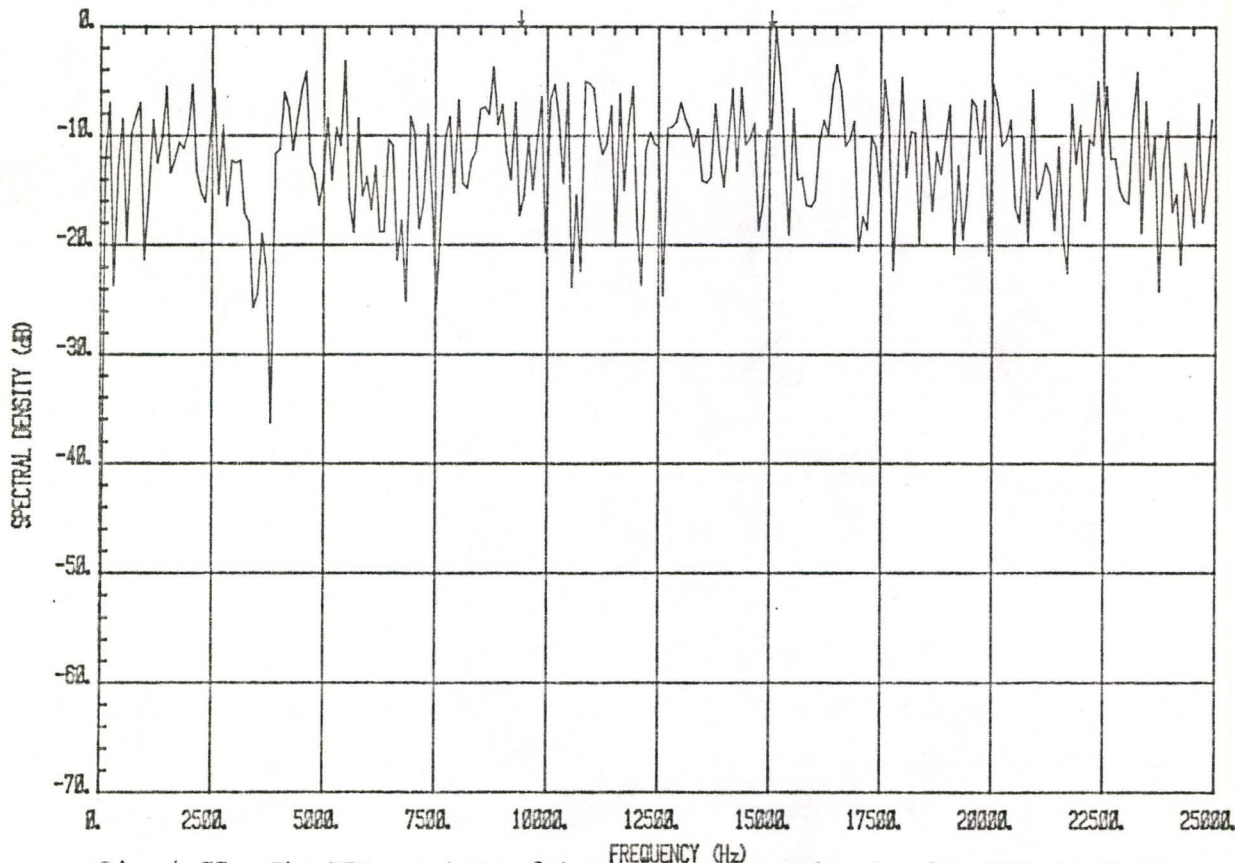


Fig. 4.77: The FFT spectrum of two random phase signals with CNDR=39 dB-Hz.

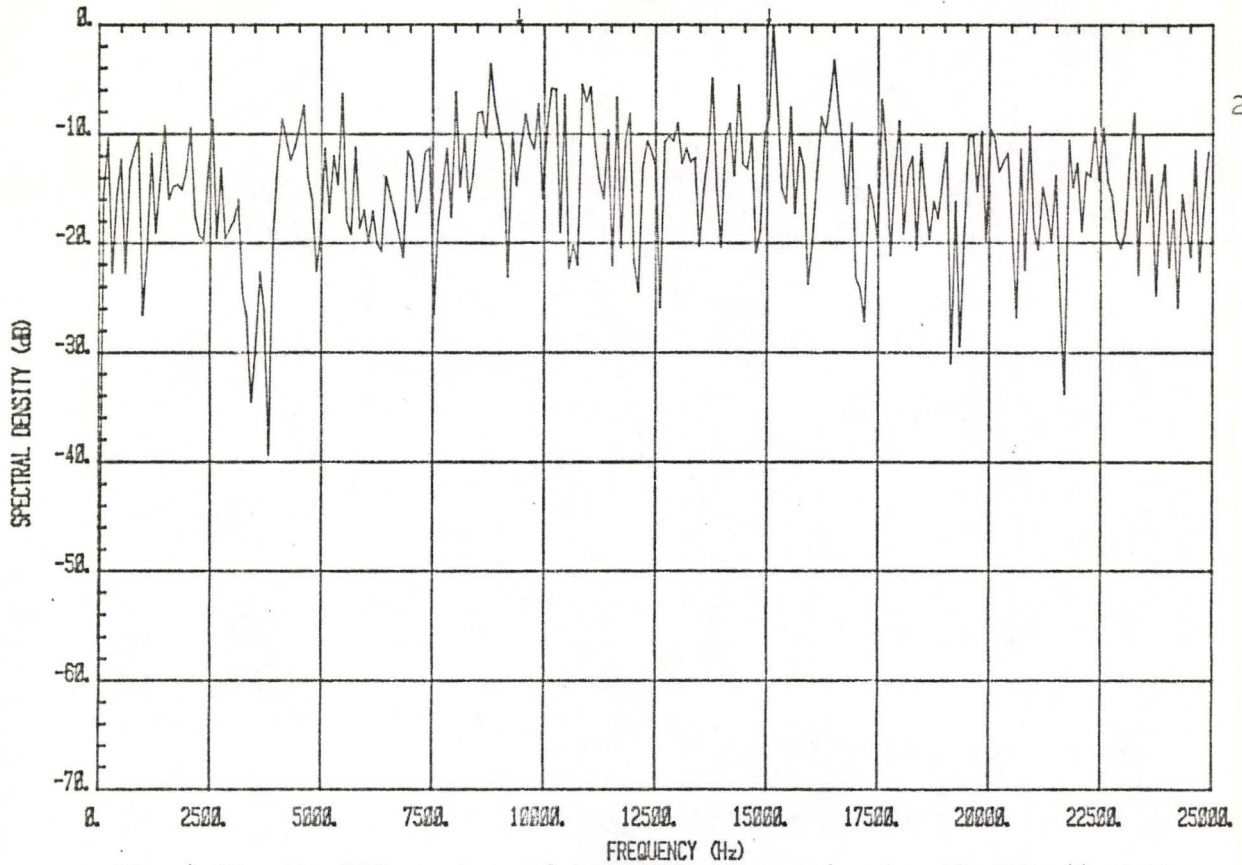


Fig. 4.78: The FFT spectrum of two random phase signals with CNDR=44 dB-Hz.

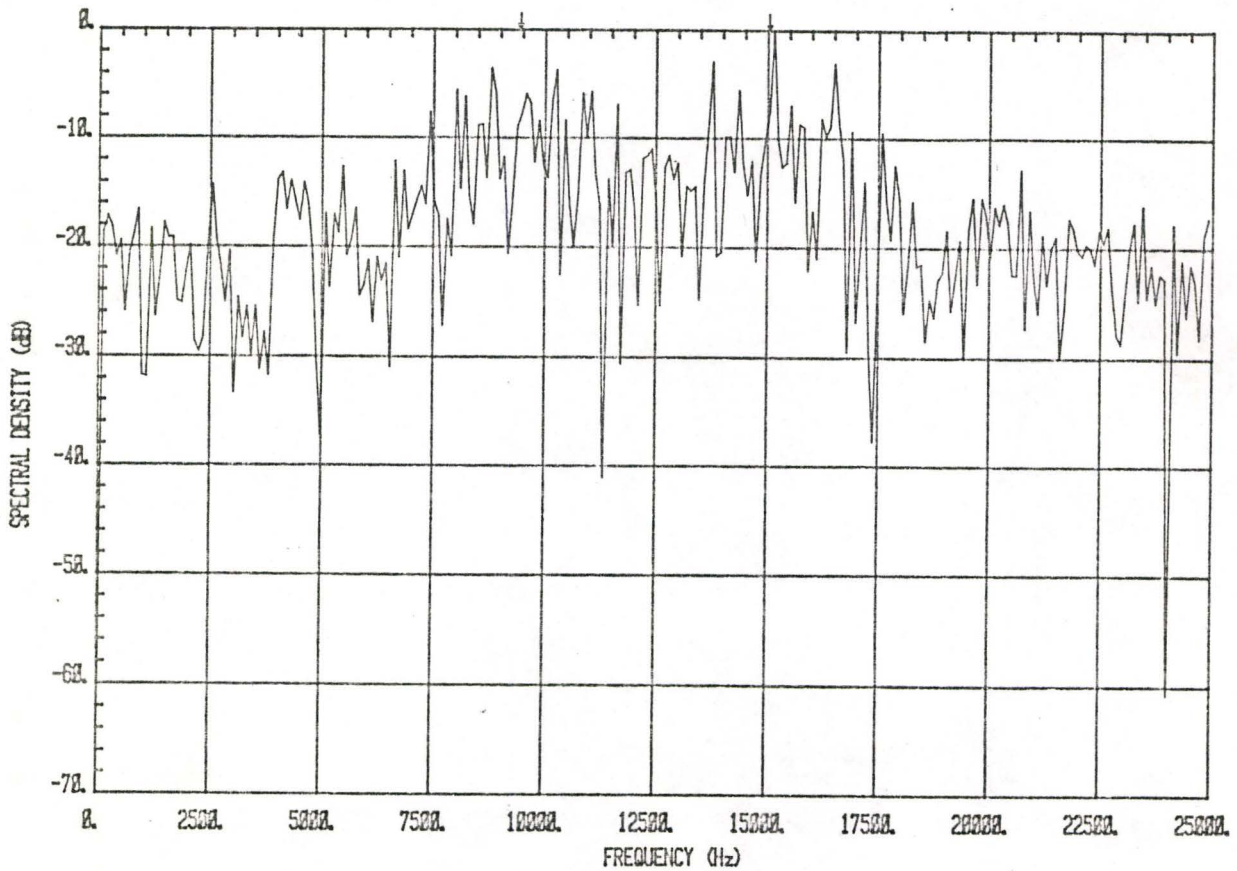


Fig. 4.79: The FFT spectrum of two random phase signals with CNDR=54 dB-Hz.

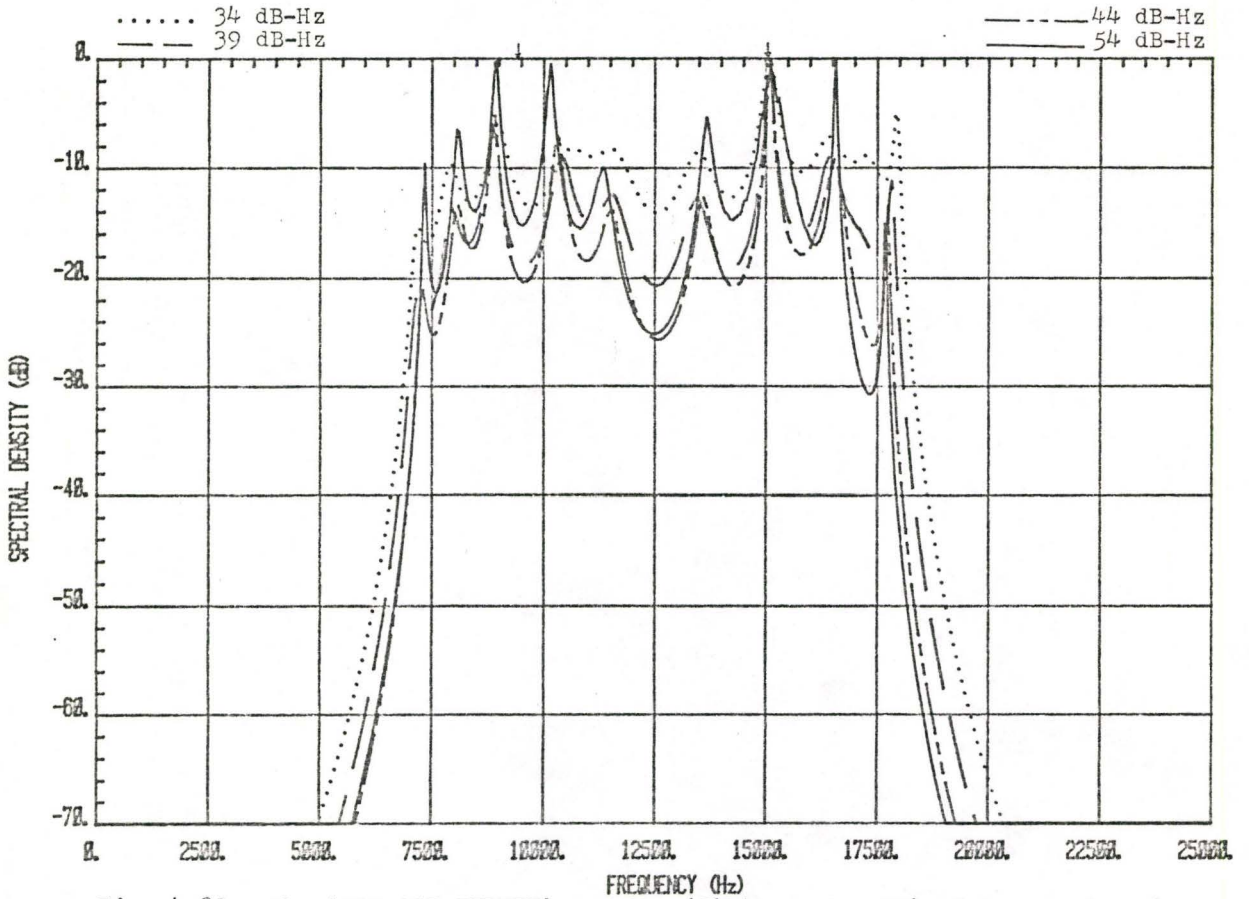


Fig. 4.80: The 'ELT ACF FIRMEM' spectra (filter order 20) of two random signals with CNDR equals to 34 dB-Hz, 39 dB-Hz, 44 dB-Hz and 54 dB-Hz.

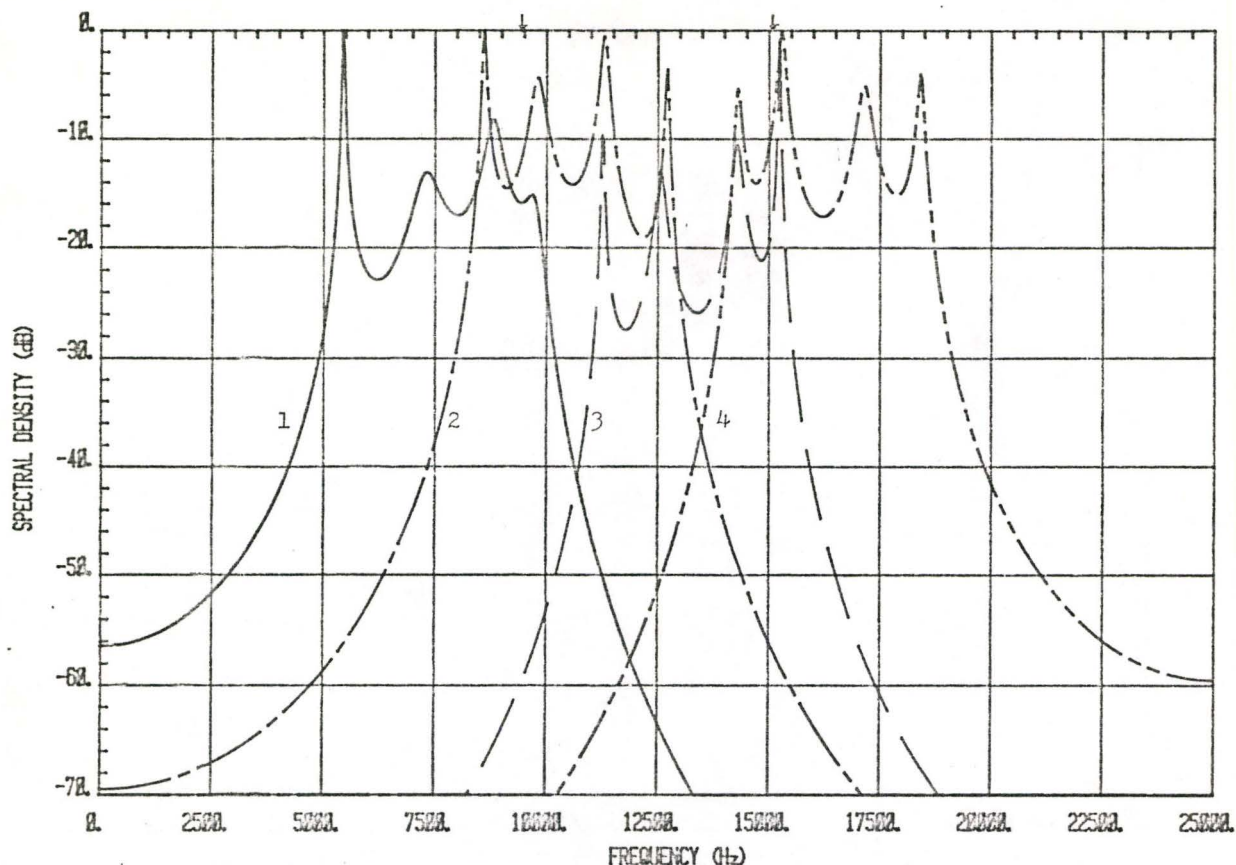


Fig. 4.81: The 'ELT+ACF+FIRMEM' spectra (filter order 8) of two random phase signals with CNDR=34 dB-Hz.

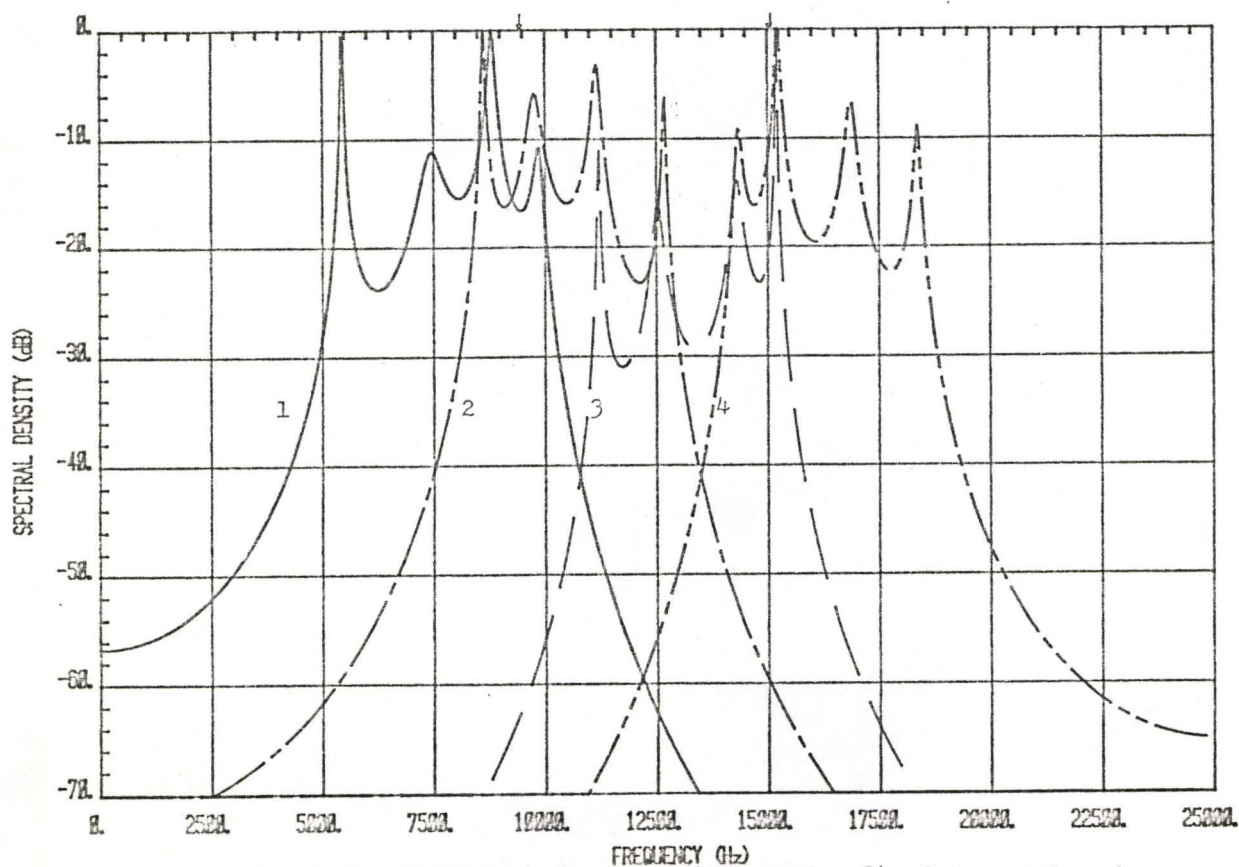


Fig. 4.82: The 'ELT+ACF+FIRMEM' spectra (filter order 8) of two random phase signals with CNDR=39 dB-Hz.

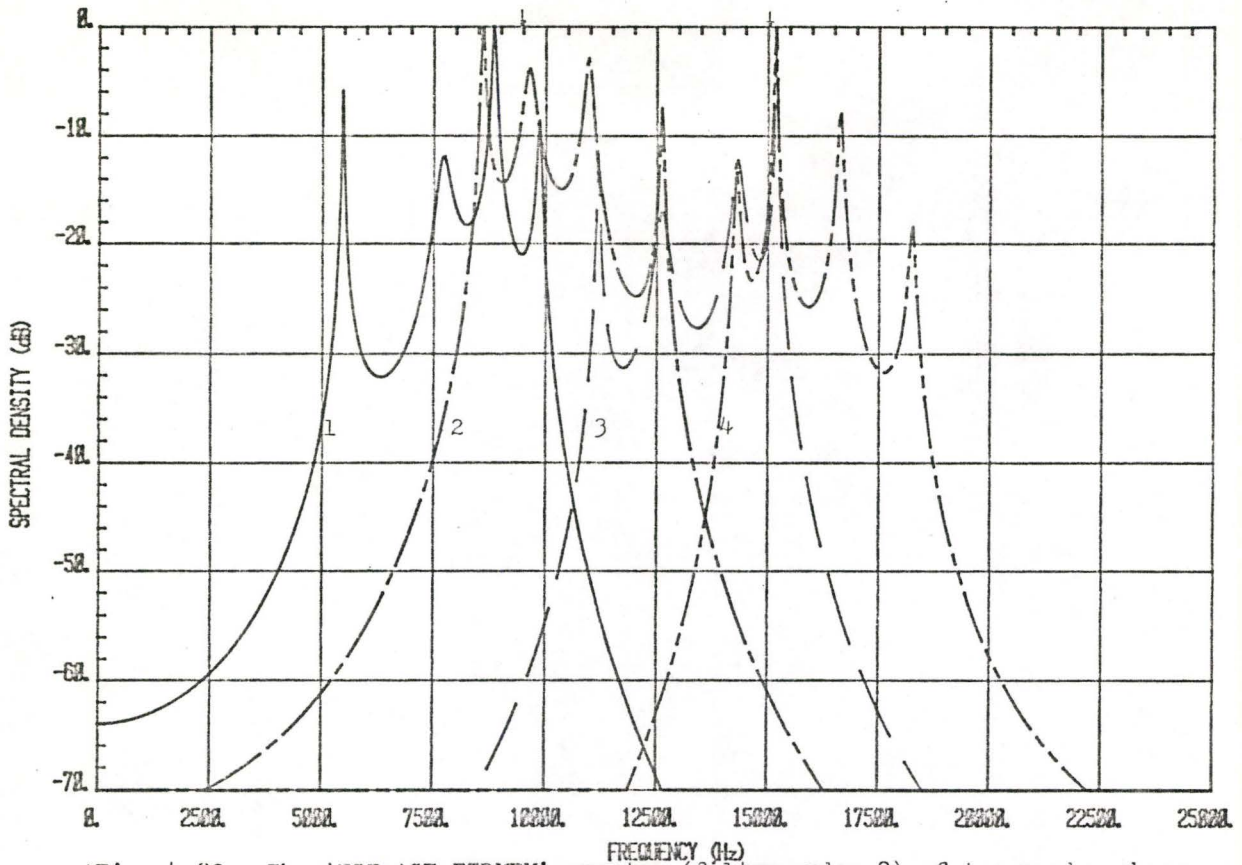


Fig. 4.83: The 'BLT+ACF+FIRMEM' spectra (filter order 8) of two random phase signals with CNDR=44 dB-Hz.

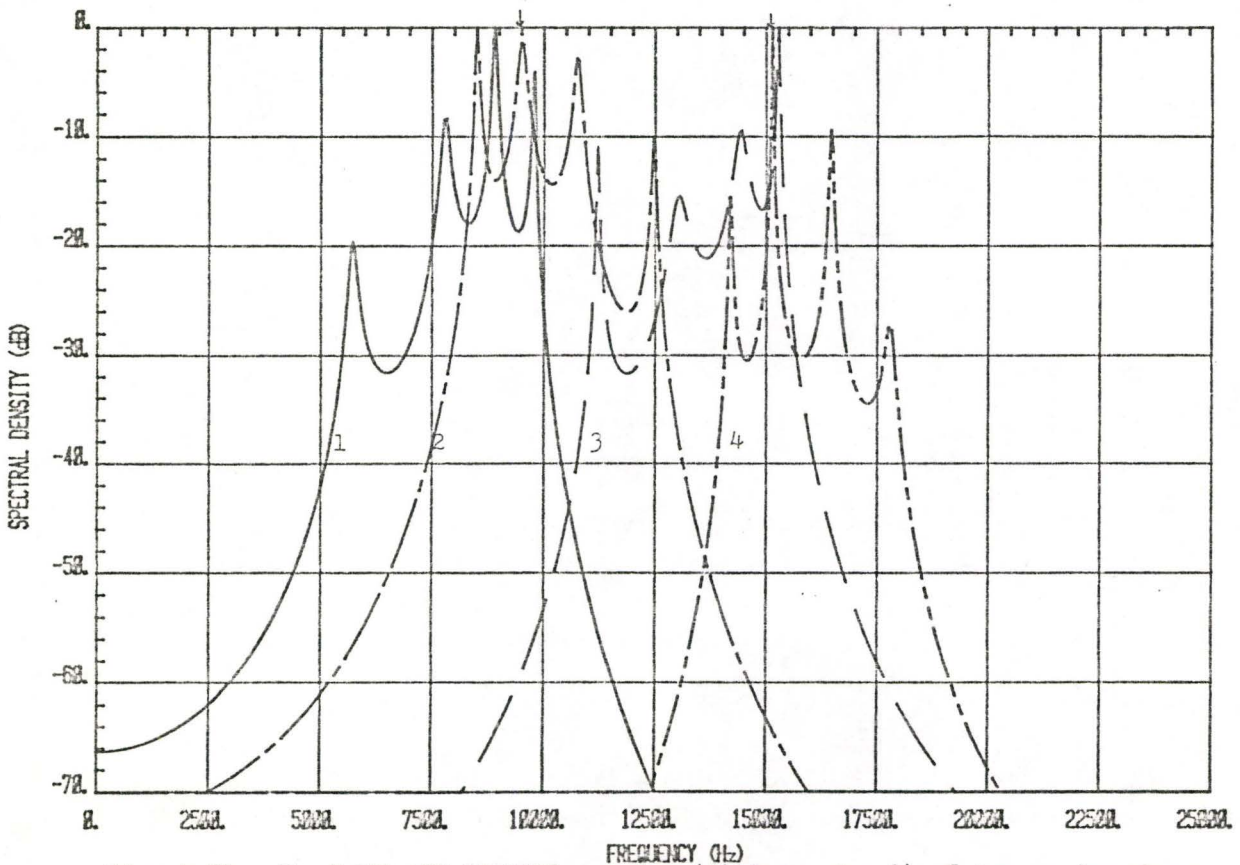


Fig. 4.84: The 'BLT+ACF+FIRMEM' spectra (filter order 8) of two random phase signals with CNDR=54 dB-Hz.

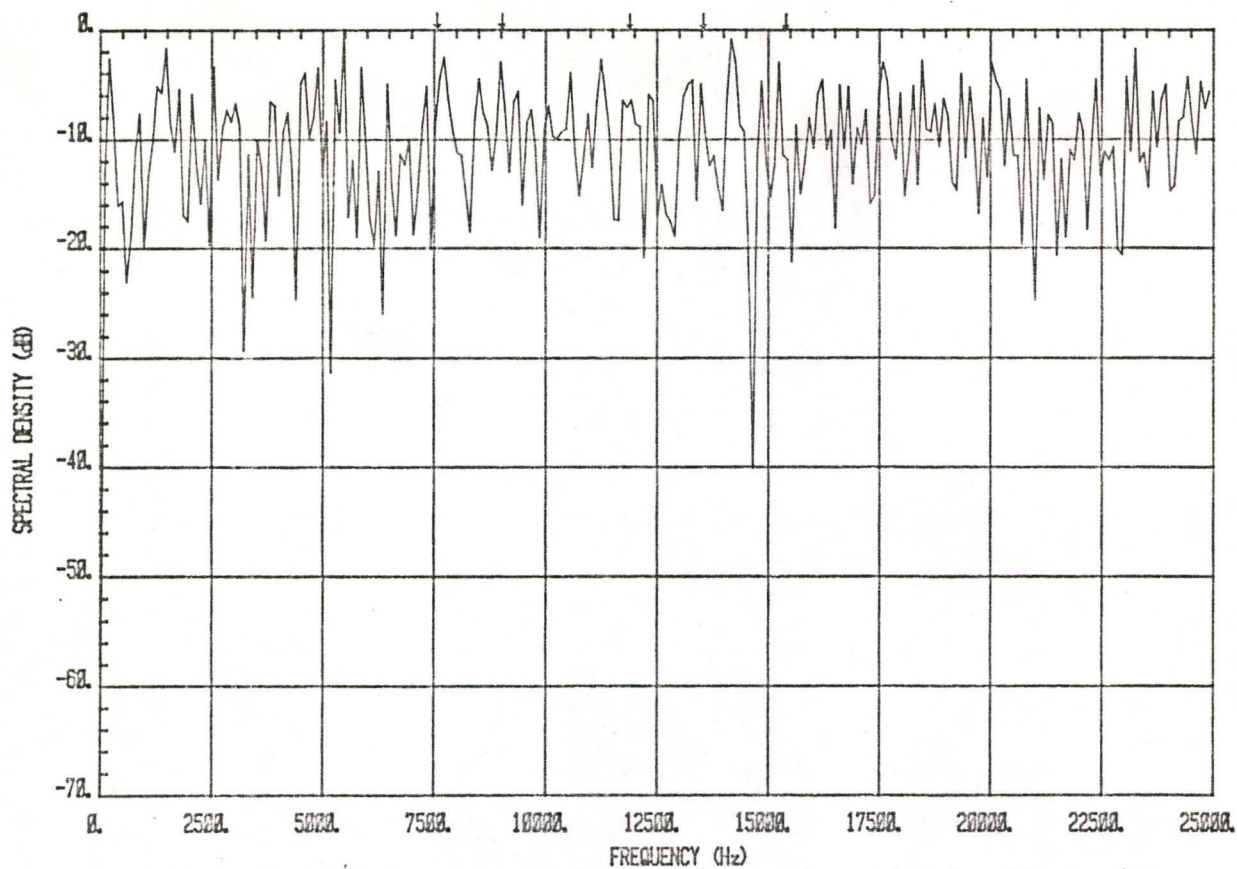


Fig. 4.85: The FFT spectrum of five continuous phase signals with carrier frequencies 7588 Hz, 9000 Hz, 11924 Hz, 13527 Hz and 15425 Hz. The CNDR is 34 dB-Hz.

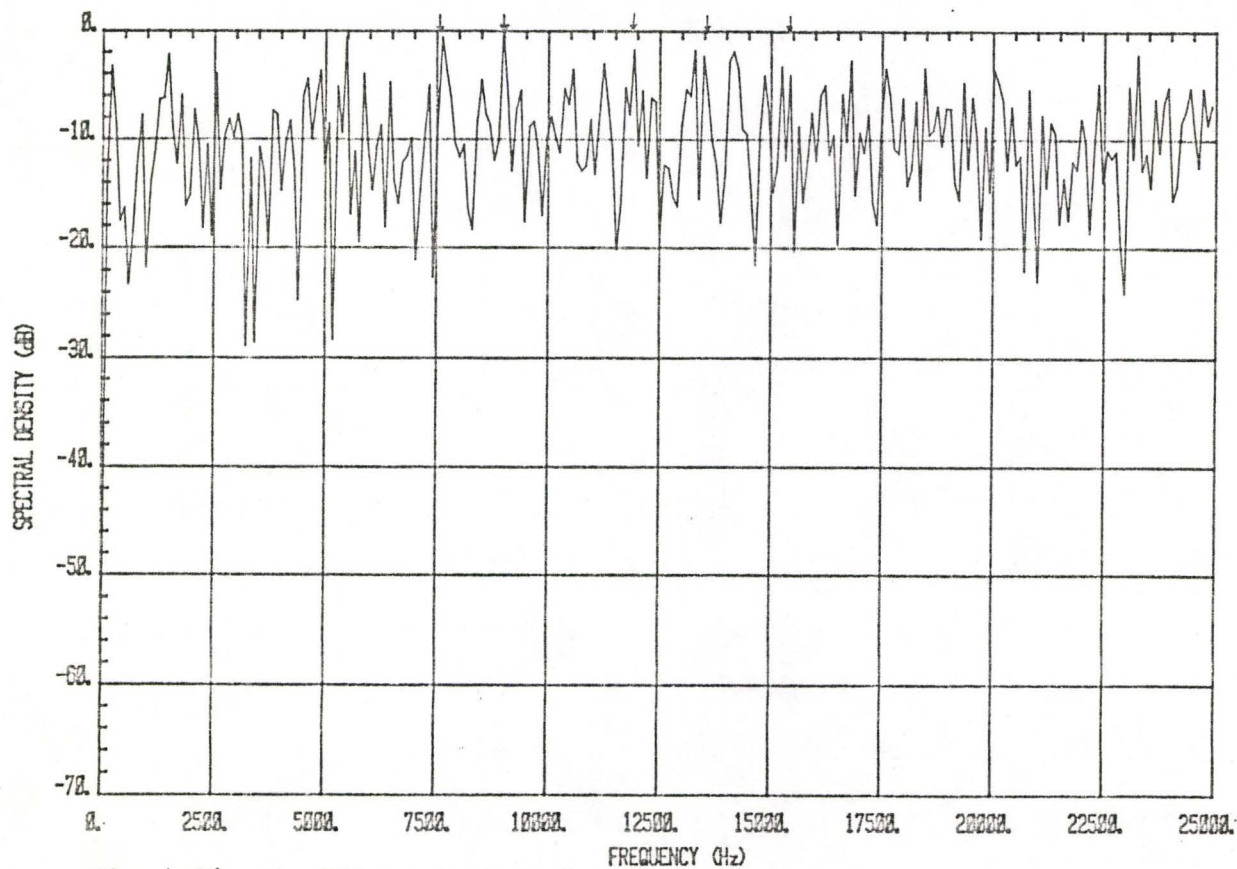


Fig. 4.86: The FFT spectrum of five continuous phase signals with CNDR=39 dB-Hz.

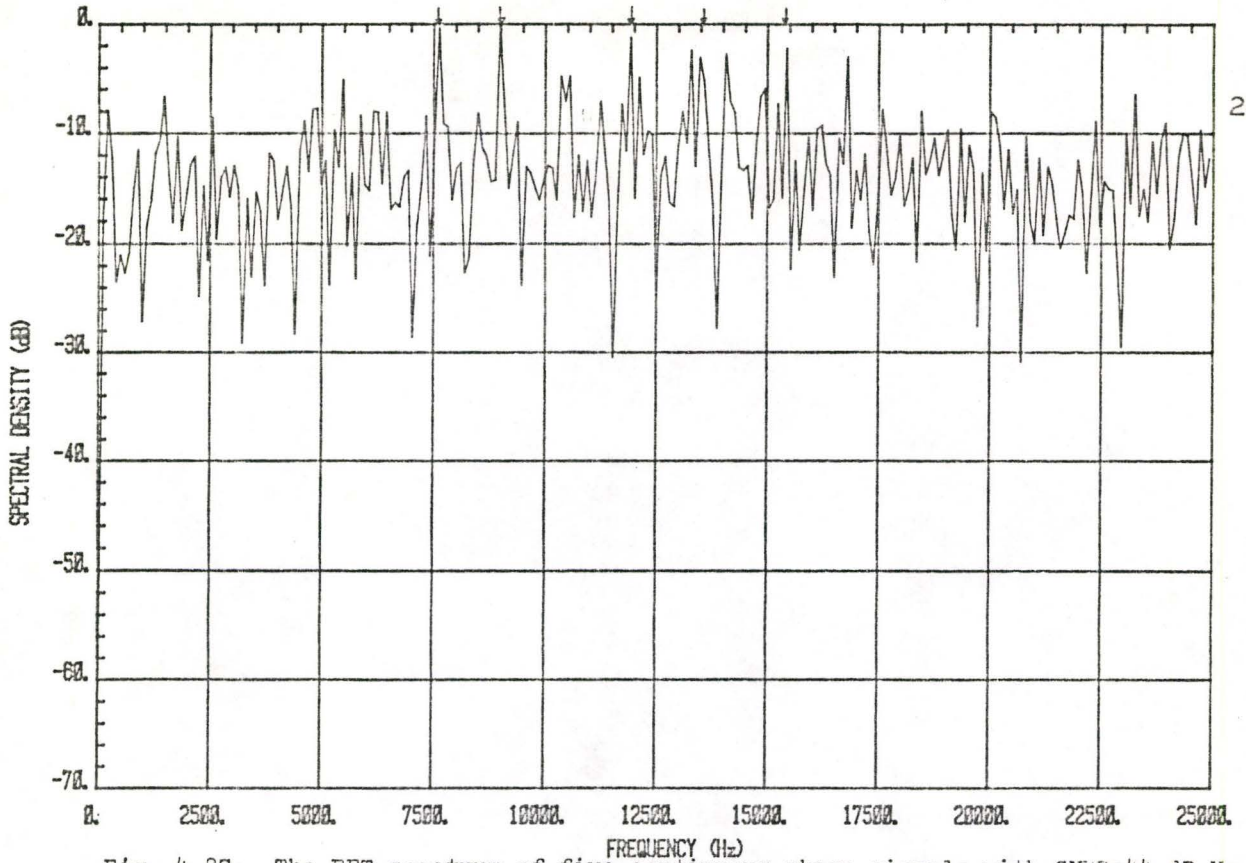


Fig. 4.87: The FFT spectrum of five continuous phase signals with CNLR=44 dB-Hz.

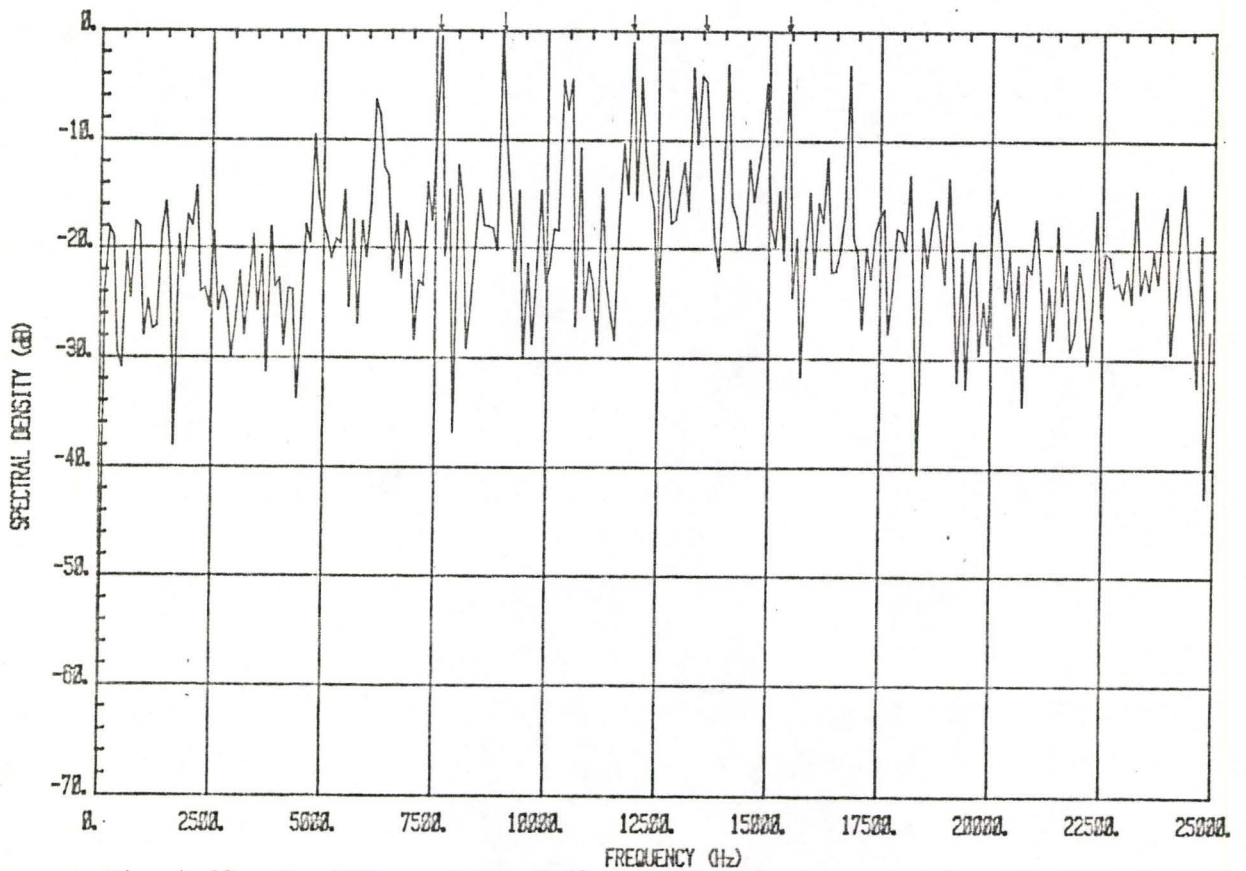


Fig. 4.88: The FFT spectrum of five continuous phase signals with CNLR=54 dB-Hz.

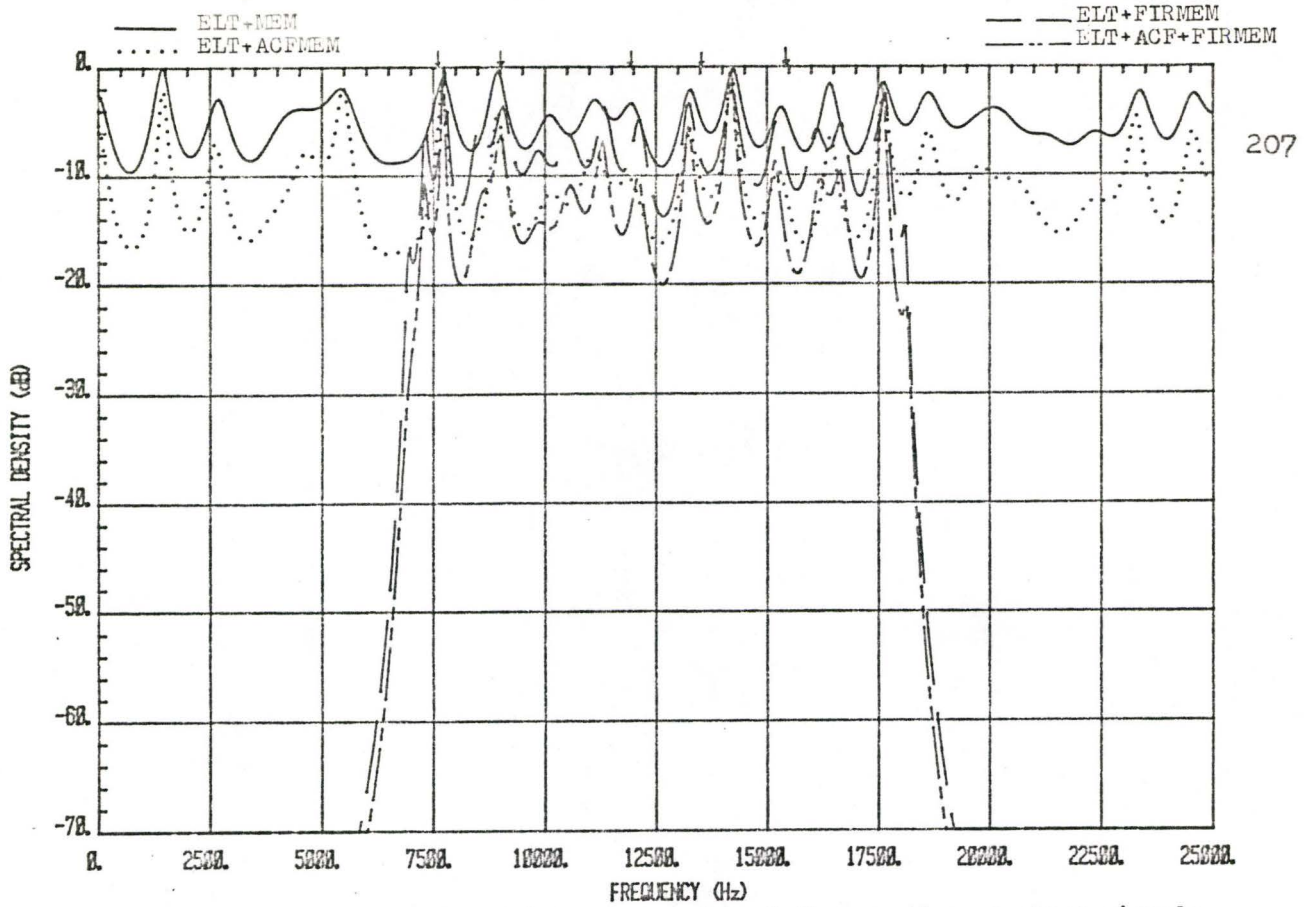


Fig. 4.89: The MEM spectra (filter order 50) of five continuous phase signals with CDR=34 dB-Hz.

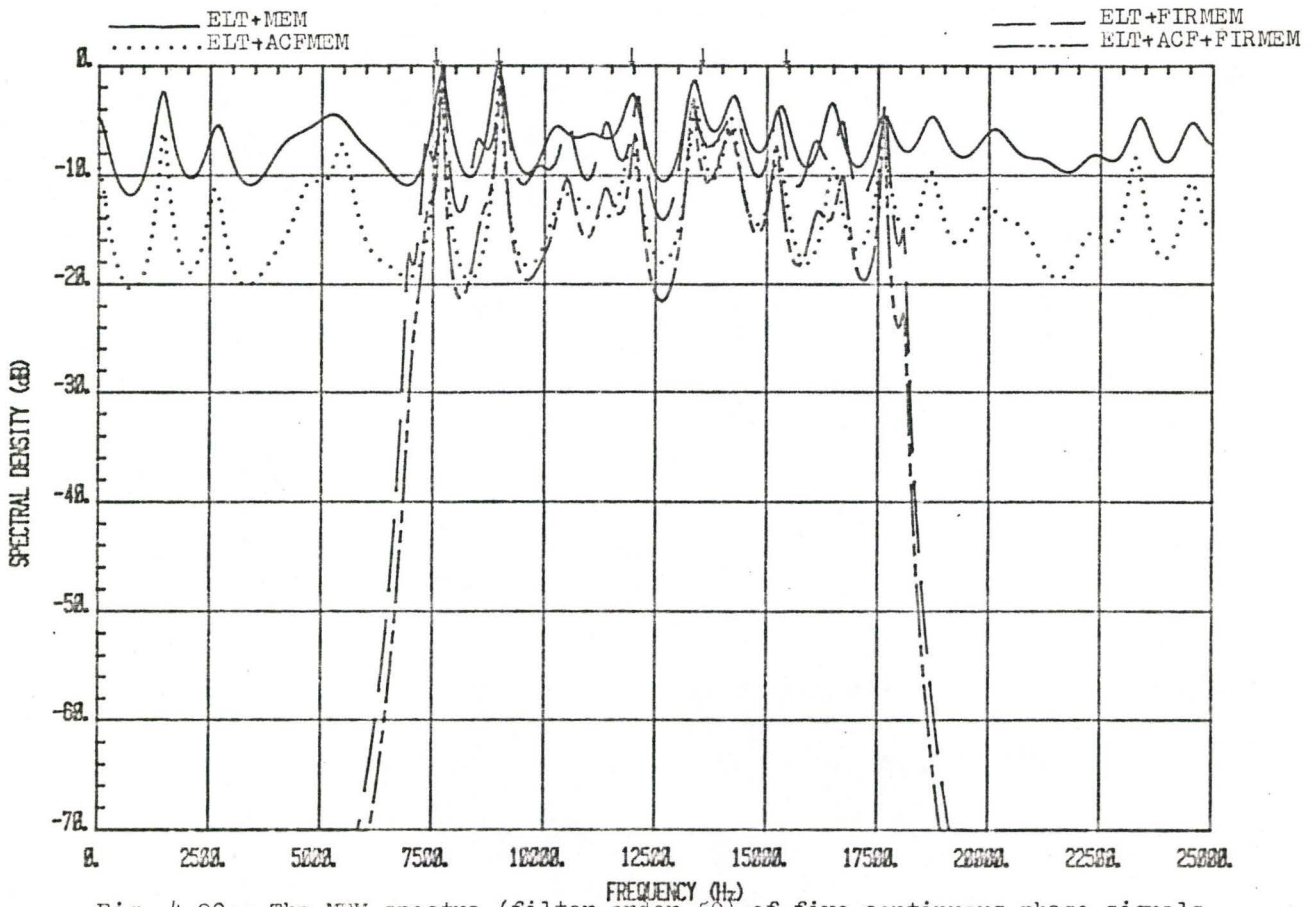


Fig. 4.90: The MEM spectra (filter order 50) of five continuous phase signals with CDR=39 dB-Hz.

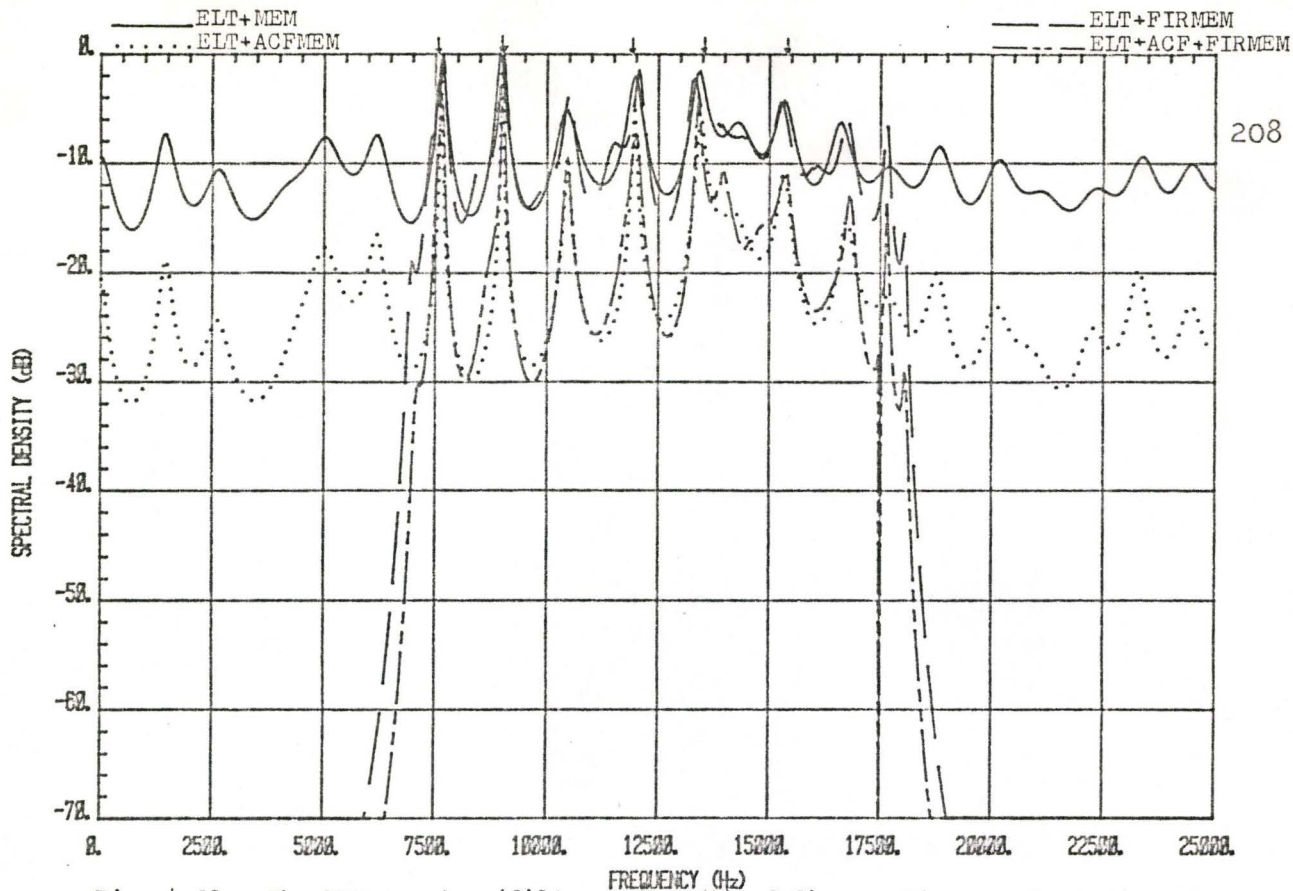


Fig. 4.91: The MEM spectra (filter order 50) of five continuous phase signals with CNDR=44 dB-Hz.

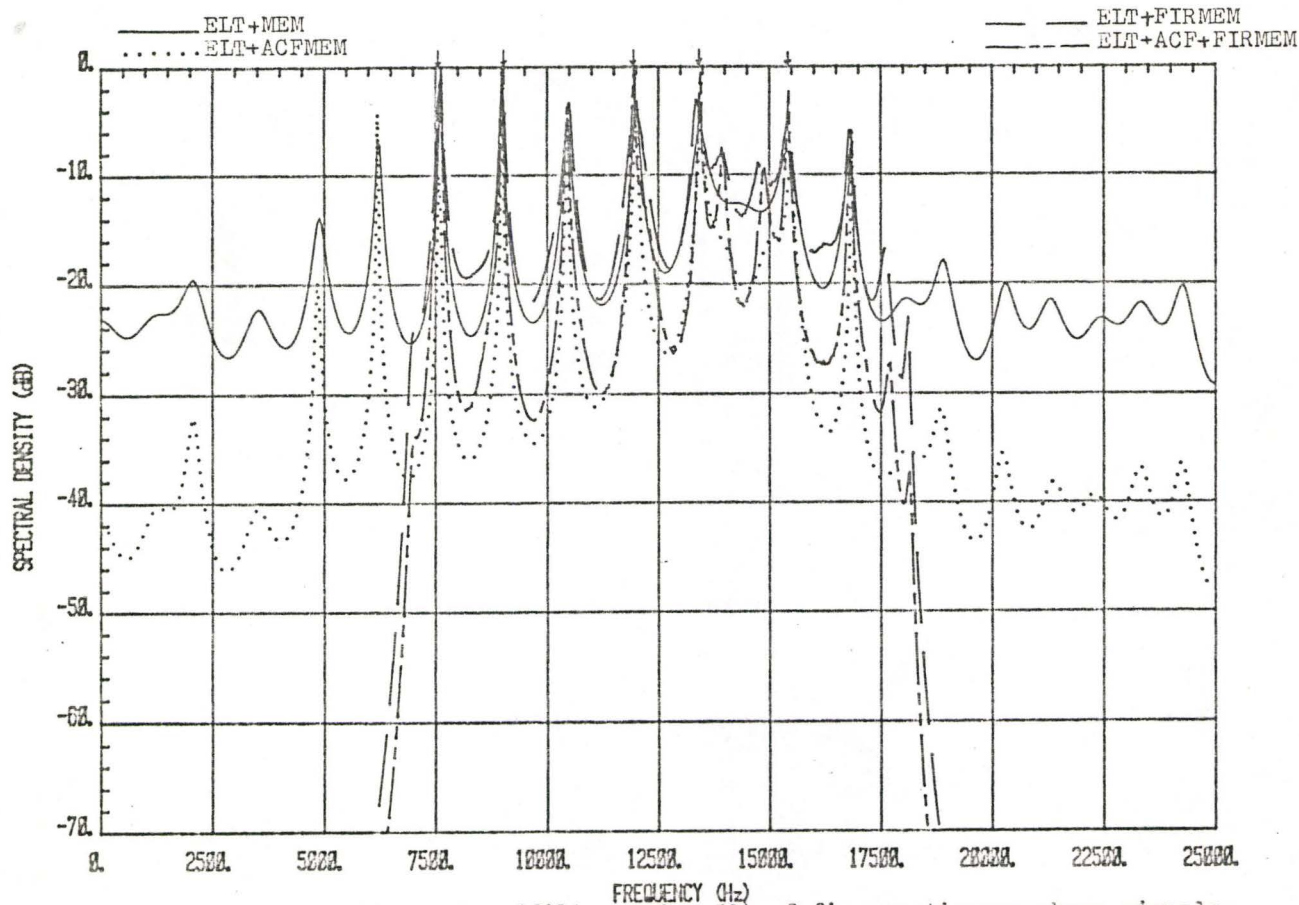


Fig. 4.92: The MEM spectra (filter order 50) of five continuous phase signals with CNDR=54 dB-Hz.

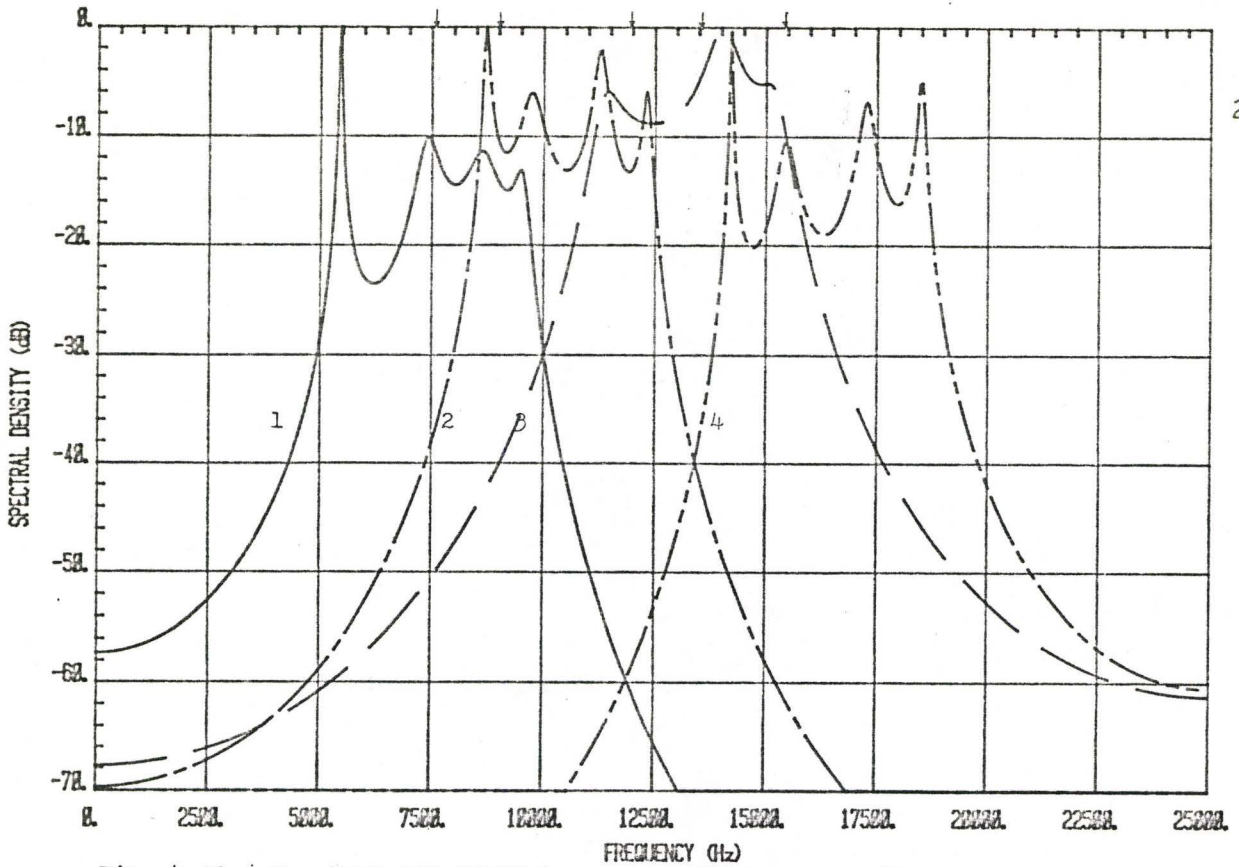


Fig. 4.93: The 'BLT+ACF+FIRMEM' spectra (filter order 8) of five continuous phase signals with CDR=34 dB-Hz.

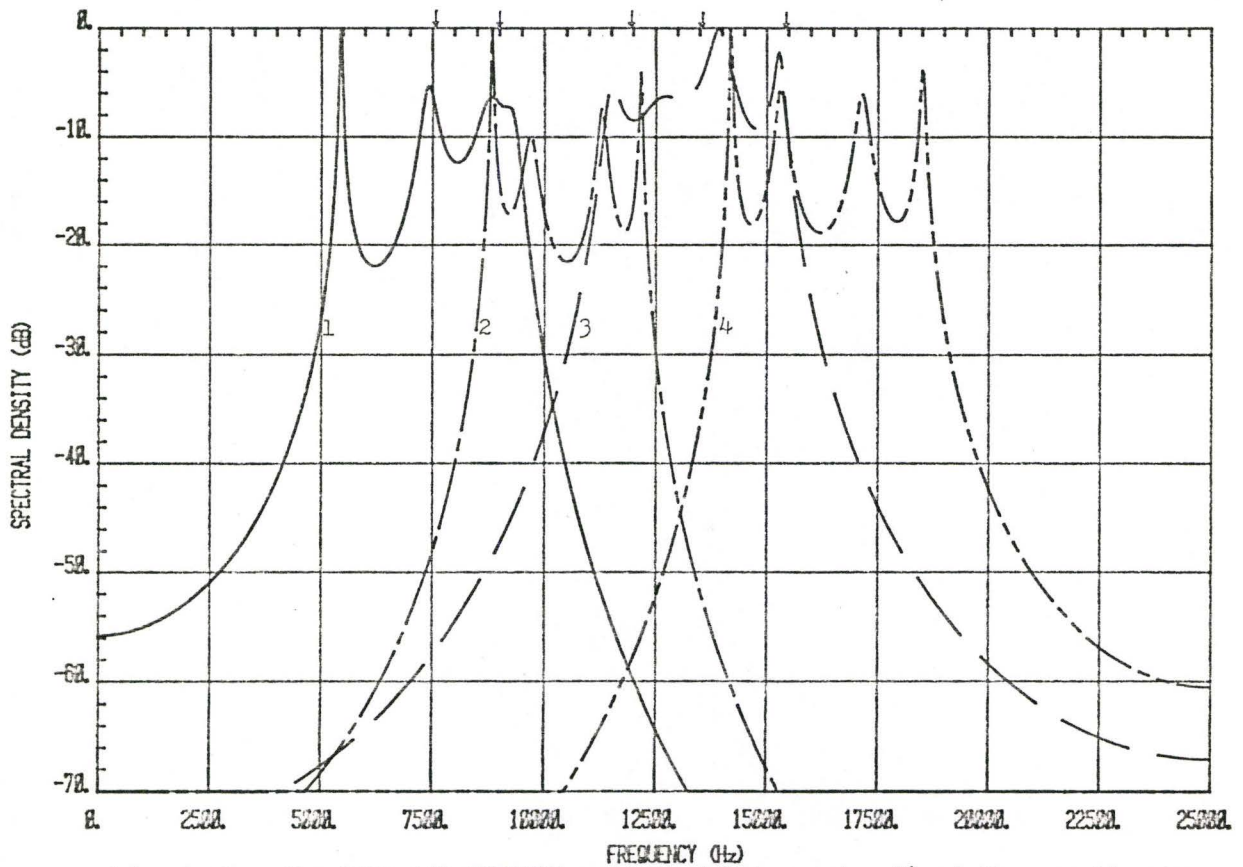


Fig. 4.94: The 'BLT+ACF+FIRMEM' spectra (filter order 8) of five continuous phase signals with CDR=39 dB-Hz.

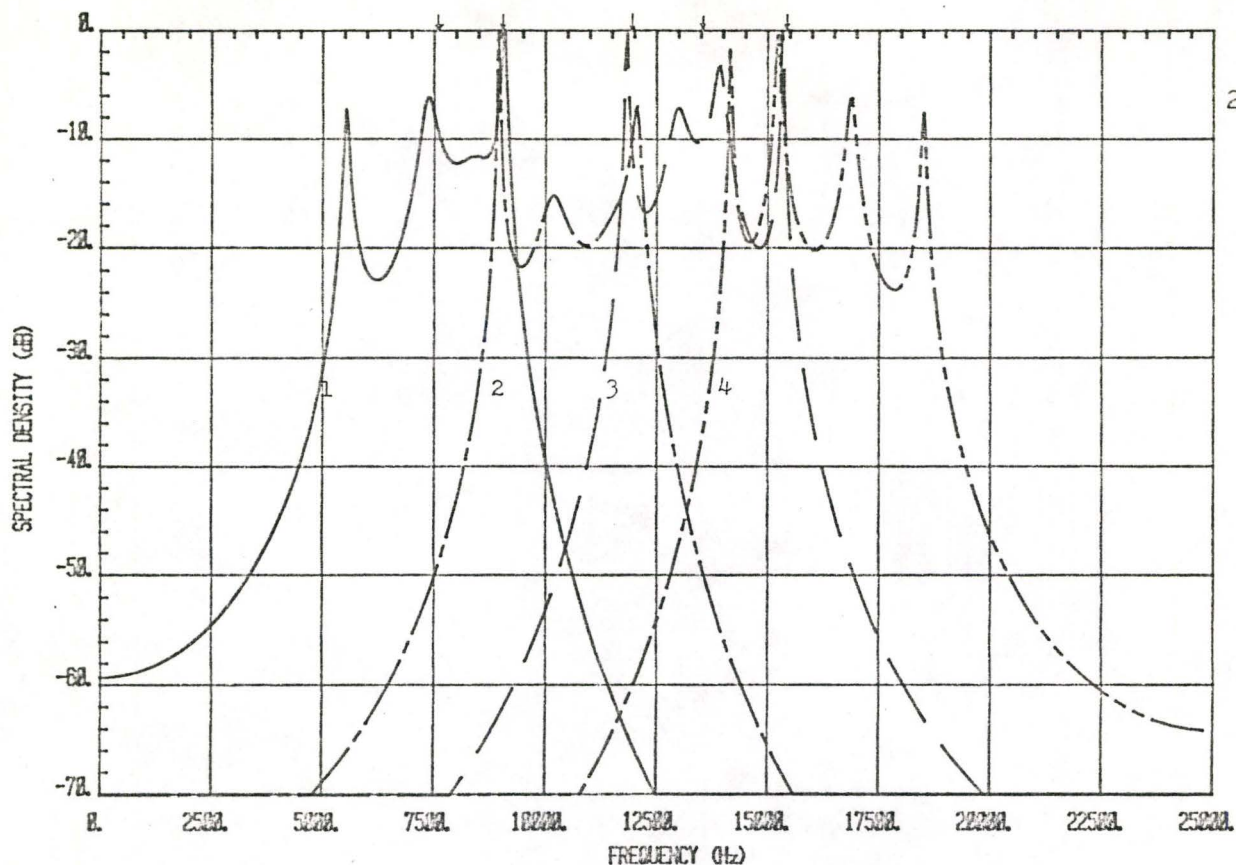


Fig. 4.95: The 'ELT+ACF+FIRMEM' spectra (filter order 8) of five continuous phase signals with CNDR=44 dB-Hz.

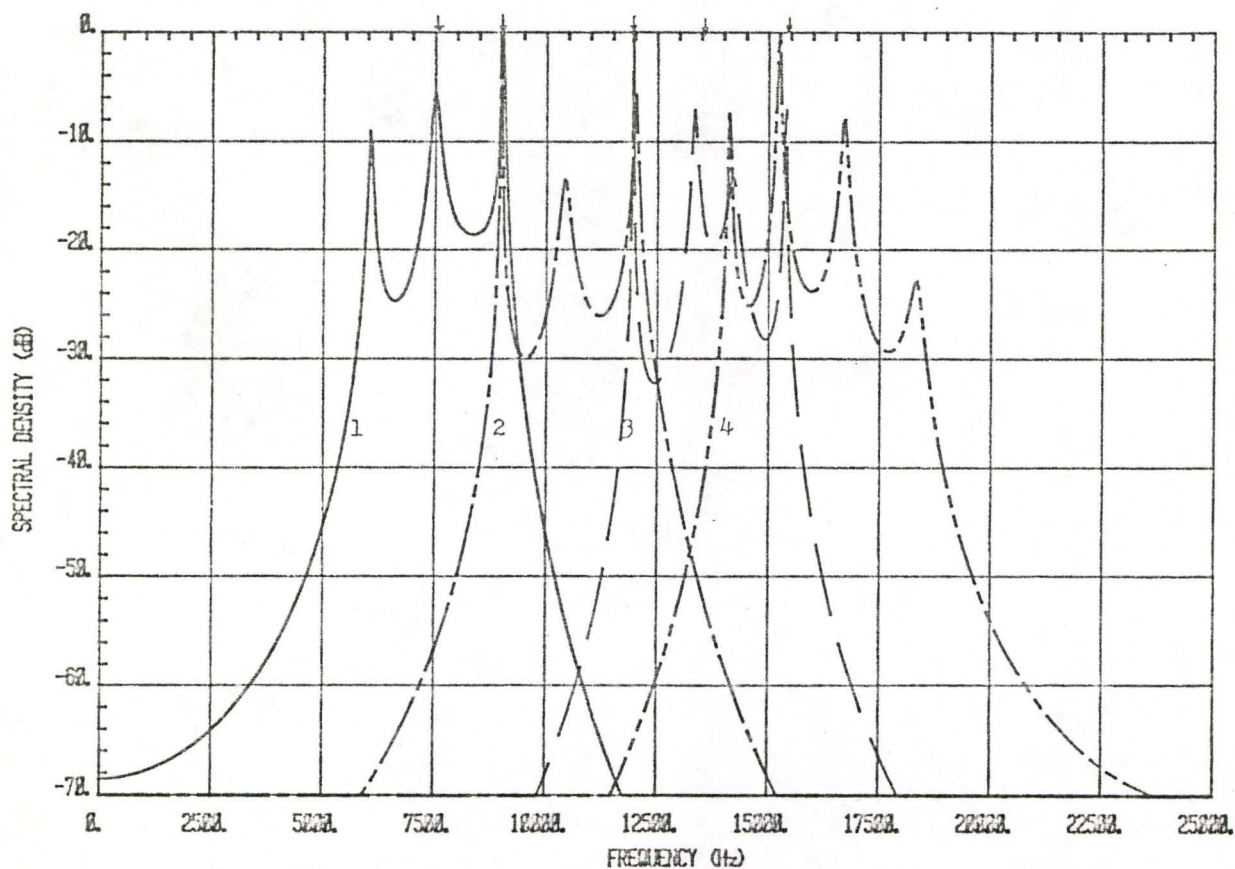


Fig. 4.96: The 'ELT+ACF+FIRMEM' spectra (filter order 8) of five continuous phase signals with CNDR=54 dB-Hz.

five and ten emergency signals which were assumed to be simultaneously visible to the satellite. Processing results showed that both the FFT and the MEM analyses undergo difficulties as the number of ELT signals increases. It is the sidelobes problem that overshadows the linear processing method. The MEM is handicapped by a lack of having an efficient way of determining an optimum order for the prediction error filter. Phase randomization creates further difficulties for the two spectral estimators.

A bank of 5 KHz bandpass filters was tested to determine the MEM performance. This method manages detection at a constant MEM filter order. One of the shortcomings of this modification is that it requires several narrow band bandpass filters in order to attain fine resolutions.

## CHAPTER 5

### CONCLUSIONS AND SUGGESTIONS FOR FURTHER RESEARCH

#### 5.1 CONCLUSIONS

A package of computer simulation programs has been developed to study the spectral characteristics of ELT signal. Both the HP-1000 computer and FPS-AP 120B array processor have been programmed to provide the following processes: 1) FFT, 2) MEM, 3) autocorrelation function (ACF), 4) digital bandpass filtering (FIR), 5) windowing.

These processes have been applied to three different modulations, namely, continuous phase, pulse-modulated; random phase, pulse-modulated; and sinusoidal-modulated. In addition, Gaussian noise was added to these signals in order to study the effects of different levels of carrier-to-noise density ratio (CNR).

For a single ELT signal it was found that:

- 1) The FFT performs satisfactorily when the signal is either continuous phase, i.e. pulse-modulated or sinusoidal-modulated. However the performance is poor when the signal is random phase, pulse-modulated (even at high values of CNR).
- 2) The MEM processor significantly reduces the sidelobe level as compared to the FFT processor when applied to all types of modulation. In addition, the MEM processor gives good performance when processing the random phase pulse-modulated signal at high values of CNR.

- 3) The effect of noise on the FFT is to produce multiple indications of carrier signal. At low values of CNDR, the amplitude of the false indications often exceeds the amplitude of the actual signal.
- 4) The effect of noise on the MEM is to produce an erroneous indication of carrier frequency. With low order MEM filters, there is only one peak in the spectrum but the frequency error is large at small values of CNDR. With high order MEM filters, there are multiple peaks in the spectrum but the frequency error is greatly reduced as compared to low order MEM filters.

For multiple ELT signals, it was found that:

- 1) The FFT performs well when two ELT units are present having either continuous phase, pulse-modulation or sinusoidal modulation. However, with random phase, pulse-modulation the results are poor even at high values of CNDR.
- 2) When five signals are present, the problem of spectral overlap begins to affect the performance of the FFT, even with continuous phase, pulse-modulation. With random phase, pulse-modulation ELT units, detection is extremely difficult even at high CNDR.
- 3) With ten ELT signals, the FFT processor of spurious responses makes detection difficult.
- 4) The MEM processor performs well when two ELT signals are present even if the modulation is random phase.
- 5) When five signals are present, the MEM processor provides good detection properties for continuous phase, pulse-modulation and

sinusoidal modulation. However, for random phase, pulse-modulation the performance is degraded.

- 6) With ten ELT signals, detection is difficult due to many spurious responses.
- 7) The MEM processor is capable of providing an estimate of the number of signals present at any time whereas the FFT processor is not.
- 8) A bank of bandpass filters may be useful in providing spectrum separation. In this case, it is possible to use a fixed order MEM process to measure multiple ELT carrier frequencies.
- 9) For two ELT units and noise, the MEM processor appears to offer some advantage over the FFT when random phase, pulse-modulation is encountered. However, for continuous phase, pulse-modulation, the results are comparable. The use of a bank of bandpass filters appears to enhance MEM performance at low CNDR.
- 10) For five continuous phase, pulse-modulated ELT signals and noise, the performance of the MEM and the FFT is comparable. The usefulness of a bank of bandpass filters is reduced when five signals are processed by the MEM.

## 5.2 Suggestions for Further Research

- 1) The problem of low carrier-to-noise ratio should be studied in greater detail.
- 2) The problems relating to the random phase structure should be examined.
- 3) Methods of averaging spectral estimates should be studied.

- 4) The possibility of a baseband processor should be investigated.
- 5) The possibility of an autoregressive moving average (ARMA) processor should be studied.
- 6) The use of real signals should be implemented as soon as possible in order to test the processors under actual conditions.

## REFERENCES

1. T.E. McGunigal, "COSPAS/SARSAT: An International Joint Venture in Satellite-aided Search and Rescue", Presented at the AGARD Symposium on Operational Modelling of the Aerospace Environment, Ottawa, Canada, 24-28, April 1978.
2. "SARSAT System Summary", Unpublished Report, available from any of the SARSAT parties.
3. H.L. Werstiuk and A.E. Winter, "The Search and Rescue Satellite (SARSAT) System Project", presented at the AGARD Symposium on Operational Modelling of the Aerospace Environment, Ottawa, Canada, 24-28, April 1978.
4. J.D. Lambert and A.E. Winter, "A Search and Rescue Satellite System (SARSAT) Experiment", presented at Communications 1976 Conference, 8-11 June 1976, Brighton, England, and published in IEE publication 139, p. 351-355.
5. "COSPAS-SARSAT: Implementation Plan (CSIP)", Unpublished report.
6. S. Haykin, Communications Systems, Wiley and Sons, N.Y., 1978.
7. "Fourier Analysis and Identification of ELT Signals", KMV Technical Report no. 76-2, KMV Associates, Inc. Baltimore, Maryland, unpublished.
8. A. Premji, "Processing of ELT Signals for Search and Rescue Satellite Aided Tracking (SARSAT) using the MEM and FFT", M.Eng. Thesis, McMaster University, March 1982.
9. S.M. Selby, Standard Mathematical Tables, CRC Press Inc., Ohio, 23rd edition, 1973, p. 103-104.
10. J.W. Cooley and J.W. Tukey, "An Algorithm for the Machine Computation of Complex Fourier Series", Math. Comp. vol. 19, no. 90, pp. 297-301, April 1965.
11. L.R. Rabiner and B. Gold, Theory and Application of Digital Signal Processing, Prentice-Hall Inc., Englewood Cliffs, N.J., 1975.
12. A.V. Oppenheim and R.W. Schaffer, Digital Signal Processing, Prentice-Hall Inc., Englewood Cliffs, N.J., 1975.

13. V. Cappellini, A.G. Constantinides and P. Emiliani, Digital Filters and Their Applications, Academic Press, London, 1978.
14. R. Coates, "Fourier Transform Methods", in Introduction to Digital Engineering, ed., R.E. Bogner and A.G. Constantinides, John Wiley and Sons, London, 1975, Ch. 7.
15. W.T. Cochran, et al., "What is the Fast Fourier Transform?", IEEE Trans. Audio and Electroacoustics, vol. AU-15, pp. 45-55, June 1967.
16. G.D. Bergland, "A Guided Tour of the Fast Fourier Transform", IEEE Spectrum, vol. 6, pp. 41-52, July 1969.
17. E.O. Brigham, The Fast Fourier Transform, Prentice-Hall, Inc., Englewood Cliffs, N.J., 1974.
18. J.F. Kaiser, "Digital Filters", in System Analysis by Digital Computer, ed., Kuo and Kaiser, John Wiley and Sons, N.Y., 1966, Ch. 7.
19. L.R. Rabiner, "Techniques for Designing Finite-Duration Impulse-Response Digital Filters", IEEE Trans. Commun. Technol. vol. COM-19, pp. 188-195, April 1971.
20. J.F. Kaiser, "Nonrecursive Digital Filter Design using the  $I_0$ -Sinh Window Function", IEEE Int., Symp. on Circuits and Syst., April 22-25, pp. 20-23.
21. R.W. Hamming, Digital Filters, Prentice-Hall, Inc., Englewood Cliffs, N.J., 1977.
22. A. Antoniou, Digital Filters: Analysis and Design, McGraw Hill, Inc., N.Y., 1979.
23. J.P. Burg, "Maximum Entropy Spectral Analysis", Ph.D. Thesis, Stanford University, Stanford, California, May 1975.
24. S. Haykin and S.B. Kesler, "Prediction-Error Filtering and Maximum-Entropy Spectral Estimation", in Non-linear Methods of Spectral Analysis, ed., S. Haykin, Springer Verlag, Berlin, 1979, Ch. 2.
25. D.G. Childers ed., Modern Spectrum Analysis, IEEE Press, N.Y., 1978.
26. T.J. Ulrych and M. Ooe, "Autoregressive and Mixed Autoregressive-Moving Average Models and Spectra", in Non-linear methods of Spectral Analysis, ed., S. Haykin, Springer-Verlag, Berlin, 1979, Ch. 3.

27. S.B. Kesler, "Non-linear Spectral Analysis", Ph.D. Thesis, McMaster University, Hamilton, Ontario, Dec. 1977.
28. H.C. Chan and S. Haykin, "Application of the Maximum Entropy Method in Radar Signal Processing", CRL-62, Communication Research Laboratory, Faculty of Engineering, McMaster University, Hamilton, Ontario, March 1979.
29. N. Anderson, "On the Calculation of Filter Coefficients for Maximum Entropy Method of Spectral Analysis", *Geophysics*, vol. 39, no. 1, pp. 69-72, Feb. 1974.
30. S. Haykin and S.B. Kesler, "The Complex Form of the Maximum Entropy Method of Spectral Estimation", *Proc. IEEE*, vol. 64, no. 5, pp. 822-823, May 1976.
31. S.B. Kesler and S. Haykin, "The Maximum Entropy Method Applied to the Spectral Analysis of Radar Clutter", *IEEE Trans. Information Theory*, vol. IT-24, no. 2, pp. 269-272, March 1978.
32. W.Y. Chen and G.R. Stegen, "Experiments with Maximum Entropy Power Spectra of Sinusoids", *J. Geophys. Res.*, vol. 79, no. 20, pp. 3019-3022, July 1974.
33. T.J. Ulrych, "Maximum Entropy Power Spectrum of Truncated Sinusoids", *J. Geophys. Res.*, vol. 77, no. 8, pp. 1396-1400, March 10, 1972.
34. H.R. Radoski, P.F. Fougere and E.J. Zawalick, "A Comparison of Power Spectral Estimates and Applications of the Maximum Entropy Method", *J. Geophys. Res.*, vol. 80, no. 4, pp. 619-625, Feb. 1, 1975.
35. A. Premji and C.R. Carter, "A Comparison of Spectral Estimation Techniques for Search and Rescue Satellites", *NAECON'80*, Dayton, Ohio, May 1980, pp. 1153-1158.
36. E. Kreyszig, Advanced Engineering Mathematics, 3rd ed., John Wiley and Sons, Inc., N.Y., 1972.
37. J.N. Franklin, Matrix Theory, Prentice-Hall, Englewood Cliffs, N.J., 1968.
38. D.G. Childers and A. Durling, Digital Filtering and Signal Processing, West Publishing Company, N.J., 1975.
39. A. Papoulis, Probability, Random Variables and Stochastic Processes, McGraw Hill, Inc., N.Y., 1965.

40. G.E.P. Box and G.M. Jenkins, Time Series Analysis: Forecasting and Control, revised edition, Holden-Day, San Francisco, Calif., 1976.
41. C. Chatfield, The Analysis of Time Series: Theory and Practice, Chapman and Hall Ltd., London, 1975.
42. L.R. Rabiner, B. Gold and C.A. McGonegal, "An Approach to the Approximation Problem for Nonrecursive Digital Filters", IEEE Trans. Audio Electroacoust., vol. AU-18, pp. 83-106, June 1970.

APPENDIX A

EQUATIONS FOR THE VALUES OF  $t_i$  AND  $p_i$   
OF A PULSE-MODULATED ELT SIGNAL

This appendix computes and formulates the equations which represent the values of  $t_i$  and  $p_i$  of the  $i$ -th pulse of a pulse-modulated emergency signal. The equations describing the linear and quadratic fit of instantaneous frequency which are defined in Chapter 1 are given by

$$f_{in}(t) = 1400.0 - 700.0 \frac{t}{T_r} \quad (A.1)$$

$$f_{in}(t) = 1930.8 - 1784.8 \frac{t}{T_r} + 870.82 \frac{t^2}{T_r} \quad (A.2)$$

In order to calculate the value of  $t_i$  of the  $i$ -th pulse of a linear sweep pulse-modulated signal, Eq. (A.1) is substituted into

$$\int_0^{t_i} f_{in}(t) dt = i-1 \quad (A.3)$$

For  $T_r=0.25$  s, this yields

$$1400 t_i^2 - 1400 t_i + (i-1) = 0 \quad (A.4)$$

Solving for  $t_i$ , we have

$$t_i = \frac{1400 \pm \sqrt{(1400)^2 - 4(1400)(i-1)}}{2(1400)}$$

But since the total signal length is 0.25 s, it is necessary to choose

the root yielding

$$t_i = \frac{1400 - \sqrt{(1400)^2 - 4(1400)(i-1)}}{2(1400)} . \quad (\text{A.5})$$

The value of  $p_i$  can be obtained by solving the integral of

$$\int_0^{p_i} f_{in}(t) dt = i-1+d \quad (\text{A.6})$$

which yields

$$1400p_i^2 - 1400p_i + (i-1+d) = 0 \quad (\text{A.7})$$

where  $d$  ( $0.3 \leq d \leq 0.5$ ) is the duty cycle. By completing the square in Eq. (A.7) and choosing the correct root, we obtain

$$p_i = \frac{1400 - \sqrt{(1400)^2 - 4(1400)(i-1+d)}}{2(1400)} . \quad (\text{A.8})$$

Using Eq. (A.2) and (A.3), the values of  $t_i$  of a quadratic sweep pulse-modulated signal can be calculated as

$$4644.3t_i^3 - 3569.6t_i^2 + 1930.8t_i = i-1$$

By rearranging the equation, we have

$$t_i^3 - 0.7685859t_i^2 + 0.4157289t_i + 2.153143 \times 10^{-4}(1-i) = 0 \quad (\text{A.9})$$

This cubic equation can be rewritten as

$$t_i^3 + pt_i^2 + qt_i + r = 0 \quad (\text{A.10})$$

where the coefficients  $p, q$  and  $r$  are related to the corresponding terms in Eq. (A.9). The solutions to this equation can be obtained by substituting  $t_i = x - p/3$  [9]. This immediately reduces Eq. (A.10) in the form

$$x^3 + ax + b = 0 \quad (\text{A.11})$$

$$\text{where } a = \frac{1}{3}(3q - p^2) \quad (\text{A.12})$$

$$b = \frac{1}{27}(2p^3 - 9pq + 27r) \quad (\text{A.13})$$

The roots to Eq. (A.11) are

$$A+B, -\frac{A+B}{2} + \frac{A-B}{2}\sqrt{-3}, -\frac{A+B}{2} - \frac{A-B}{2}\sqrt{-3}$$

where

$$A = \sqrt[3]{-\frac{b}{2} + \sqrt{\frac{b^2}{4} + \frac{a^3}{27}}} \quad (\text{A.14})$$

$$B = \sqrt[3]{-\frac{b}{2} - \sqrt{\frac{b^2}{4} + \frac{a^3}{27}}} \quad (\text{A.15})$$

Since we are only interested in a real root, the value of  $t_i$  is given by

$$t_i = A + B - \frac{p}{3} \quad (\text{A.16})$$

The value of  $p_i$  in this case, can be easily obtained by following the above procedures employing Eq. (A.2) and (A.6).

## APPENDIX B

### PREDICTION ERROR FILTER

By giving the present and past values of a weakly stationary zero mean time series  $\{x(n)\}$  ( $0 \leq n \leq N-1$ ), which can be complex in general, it is sometimes necessary to predict the sample value of the input signal one-step into the future. That is, we need our desired form of the output

$$d(n) = x(n+1) \quad (\text{B.1})$$

This is a classical study of one-step prediction problem [24].

Consider a linear digital filter whose impulse response is denoted by the sequence  $\{h(k)\}$  ( $k=1,2,\dots,M$ ). The time series  $\{y(n)\}$  represents the resulting output of the filter whose input is the sequence  $\{x(n)\}$ . The input-output relationship of this filter is

$$y(n) = \sum_{k=1}^M h(k) x(n-k+1) \quad 1 \leq n \leq N+M-1 \quad (\text{B.2})$$

The resulting error between the filter output and the desired output is defined by

$$e(n) = d(n) - y(n) \quad (\text{B.3})$$

Putting Eq. (B.1) and (B.2) into (B.3) we obtain

$$e(n) = x(n+1) - \sum_{k=1}^M h(k) x(n-k+1) \quad (\text{B.4})$$

The requirement of the one-step prediction problem is to make the mean square value of the error  $e(n)$  as small as possible. This is equivalent

to minimize the output error power of the filter with respect to the set of filter coefficients  $\{h(k)\}$  [24]. The mathematical representation of the mean square error is

$$P = E[|e(n)|^2] \quad (\text{B.5})$$

where  $P$  is the output error power which is a positive real scalar quantity. Using Eq. (B.4), we can express Eq. (B.5) in the form

$$\begin{aligned} P = & E[x(n+1) x^*(n+1)] - \sum_{k=1}^M h^*(k) E[x(n+1) x^*(n-k+1)] \\ & - \sum_{k=1}^M h(k) E[x(n-k+1) x^*(n+1)] \\ & + \sum_{\ell=1}^M \sum_{k=1}^M h(\ell) h^*(k) E[x(n-\ell+1) x^*(n-k+1)] \end{aligned} \quad (\text{B.6})$$

Note that:

$$\begin{aligned} E[x(n+1) x^*(n+1)] &= R_x(0) \\ E[x(n+1) x^*(n-k+1)] &= R_x(k) \\ E[x(n-k+1) x^*(n+1)] &= R_x(-k) \\ E[x(n-\ell+1) x^*(n-k+1)] &= R_x(k-\ell) \end{aligned}$$

We recall that  $R_x(-z) = R_x^*(z)$  [6]. Thus, Eq. (B.6) becomes

$$\begin{aligned} P = & R_x(0) - \sum_{k=1}^M h^*(k) R_x(k) - \sum_{k=1}^M h(k) R_x^*(k) \\ & + \sum_{\ell=1}^M \sum_{k=1}^M h(\ell) h^*(k) R_x(k-\ell) \end{aligned} \quad (\text{B.7})$$

Next, let

$$(1) \quad \underline{h} = \begin{bmatrix} h(1) \\ h(2) \\ \vdots \\ h(M) \end{bmatrix}, \quad \underline{h}^H = [h^*(1) \ h^*(2) \ \dots \ h^*(M)] \quad (\text{B.8a})$$

$$(2) \quad \underline{R}_x = \begin{bmatrix} R_x(1) \\ R_x(2) \\ \vdots \\ R_x(M) \end{bmatrix}, \quad \underline{R}_x^H = [R_x^*(1) \ R_x^*(2) \ \dots \ R_x^*(M)] \quad (\text{B.8b})$$

$$= [R_x(-1) \ R_x(-2) \ \dots \ R_x(-M)]$$

(3) Rewrite  $R_x(k-l) = R_{xx}(k-l)$ . The reason to do this is to differentiate the difference of a square matrix from a vector

$$\underline{R}_{xx} = \begin{bmatrix} R_x(0) & R_x(-1) & \dots & R_x(1-M) \\ R_x(1) & R_x(0) & \dots & R_x(2-M) \\ \vdots & \vdots & \ddots & \vdots \\ \vdots & \vdots & \ddots & \vdots \\ R_x(M-1) & R_x(M-2) & \dots & R_x(0) \end{bmatrix} = \underline{R}_{xx}^H \quad (\text{B.8c})$$

where the superscript H denotes the operation of Hermitian transposition [36], [37]. The  $M \times M$  autocorrelation matrix  $\underline{R}_{xx}$  is an equidiagonal matrix which is called a Toeplitz matrix [24]. The Hermitian transposition of  $\underline{R}_{xx}$ , in this case, is also itself. Eq. (B.7) can now be expressed in matrix form

$$P = R_x(0) - \underline{h}^H \underline{R}_x - \underline{R}_x^H \underline{h} + \underline{h}^H \underline{R}_{xx} \underline{h} \quad (\text{B.9})$$

Minimizing this equation with respect to the vector  $\underline{h}$  and set the derivative to zero, we obtain the optimum value of the filter

coefficient vector,  $\underline{h}_{opt}$

$$\underline{0} = -\underline{R}_x^H + \underline{h}_{opt}^H \underline{R}_{xx} \quad (\text{B.10})$$

so that

$$\underline{h}_{opt}^H \underline{R}_{xx} = \underline{R}_x^H \quad (\text{B.11})$$

Taking the Hermitian transpose of both sides of Eq. (B.11), we have

$$\underline{R}_{xx} \underline{h}_{opt} = \underline{R}_x \quad (\text{B.12})$$

Hence

$$\underline{h}_{opt} = \underline{R}_{xx}^{-1} \underline{R}_x \quad (\text{B.13})$$

The corresponding value of the error  $e(n)$ , which is given by Eq. (B.4), is in the form

$$e(n) = x(n+1) - \sum_{k=1}^M h_{opt}(k) x(n-k+1) \quad (\text{B.14})$$

$$= \sum_{k=0}^M a(k) x(n-k+1) \quad (\text{B.15})$$

where the coefficient  $a(k)$  is defined by the equation

$$a(k) = \begin{cases} 1 & k = 0 \\ -h_{opt}(k) & k = 1, 2, \dots, M \end{cases} \quad (\text{B.16})$$

We interpret Eq. (B.15) in the following way: the error  $e(n)$  is the output of a filter whose impulse response is characterized by the set of coefficients

$$\underline{a} = \begin{bmatrix} a(0) \\ a(1) \\ \vdots \\ \vdots \\ a(M) \end{bmatrix} = \begin{bmatrix} 1 \\ -h_{opt}(1) \\ \vdots \\ \vdots \\ -h_{opt}(M) \end{bmatrix} \quad (\text{B.17})$$

and the input time series is  $\{x(n)\}$ . A filter in this form is called

the prediction error filter (PEF) of order  $M$ . Fig. B.1 illustrates a prediction filtering model of Eq. (B.15).

The mean square value of the error is given by Eq. (B.9). Substituting Eq. (B.13) in Eq. (B.9), we find that the minimum value of the error power is

$$P_{\min} = R_x(0) - \tilde{R}_x^H h_{\text{opt}}$$

Since  $e(n)$  is the output of a PEF of order  $M$ , it follows that we can denote  $P(M)$  as the output power of this filter, that is

$$P(M) = P_{\min}$$

or

$$P(M) = R_x(0) - \sum_{k=1}^M h_{\text{opt}}(k) R_x(-k) \quad (\text{B.18})$$

$$= \sum_{k=0}^M a(k) R_x(-k) \quad (\text{B.19})$$

where  $a(k)$  is defined by Eq. (B.16).

By comparing Eq. (B.12) and (B.18), we can rewrite Eq. (B.12) in the following form

$$\tilde{0} = \tilde{R}_x - \tilde{R}_{xx} h_{\text{opt}}$$

or

$$0 = R_x(k) - \sum_{k=1}^M h_{\text{opt}}(k) R_x(k-l) \quad l = 1, 2, \dots, M \quad (\text{B.20})$$

If we use Eq. (B.18) to augment Eq. (B.20), we get

$$\sum_{k=0}^M a(k) R_x(m-k) = \begin{cases} P(M) & m = 0 \\ 0 & m = 1, 2, \dots, M \end{cases} \quad (\text{B.21})$$

which in expanded form is

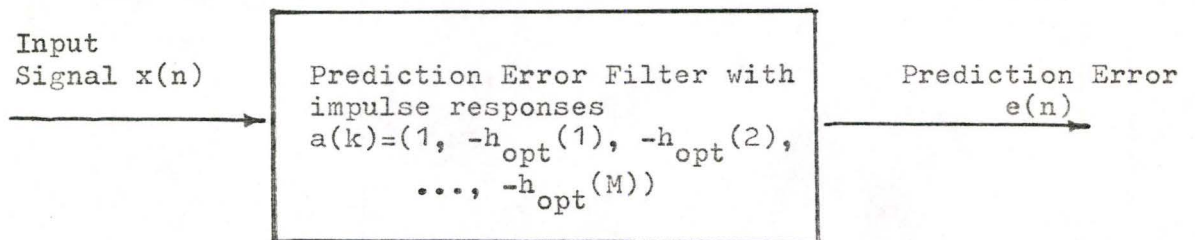


Fig. B.1: Prediction error filter.

$$\begin{bmatrix} R_x(0) & R_x(-1) & \dots & R_x(-M) \\ R_x(1) & R_x(0) & \dots & R_x(1-M) \\ \vdots & \vdots & \ddots & \vdots \\ \vdots & \vdots & \ddots & \vdots \\ R_x(M) & R_x(M-1) & \dots & R_x(0) \end{bmatrix} \begin{bmatrix} 1 \\ a(1) \\ \vdots \\ a(M) \end{bmatrix} = \begin{bmatrix} P(M) \\ 0 \\ \vdots \\ 0 \end{bmatrix} \quad (\text{B.22})$$

Eq. (B.22) is identical to Eq. (2.13). This system of  $M + 1$  linear simultaneous equations is called the prediction error filter equations.

## APPENDIX C

### DESIGN OF A BANDPASS FILTER

Suppose we are given a time series  $\{x(n)\}$  ( $0 \leq n \leq N-1$ ) which is applied to a linear filter of impulse response  $\{h(n)\}$  ( $0 \leq n \leq M-1$ ). The resulting response of this filter, which is denoted by  $\{y(n)\}$  ( $0 \leq n \leq N+M-2$ ), is given by the convolution sum

$$y(n) = \sum_{k=0}^{M-1} h(k) x(n-k) \quad (\text{C.1})$$

A direct form realization, according to Eq. (C.1) is depicted in Fig. C.1. A filter which has a finite length of impulse response and has the expression of Eq. (C.1) is usually called a finite impulse response (FIR) filter or nonrecursive digital filter [11], [12]. The second terminology is due to the structure given in Fig. C.1 in which the present filter output  $y(n)$  is obtained in terms of the past and current inputs. The previous filter outputs are not required in the system. FIR filters possess certain desirable properties which make them attractive for digital signal processing applications. One of the most important features of FIR systems is that they can be designed to have exactly linear phase [12]. For a casual FIR filter with impulse response which is symmetric about the midpoint, the linear phase condition is given by [11], [22],

$$h(n) = h(N-1-n) \quad (\text{C.2})$$

Furthermore, the stability condition is always guaranteed if the filter

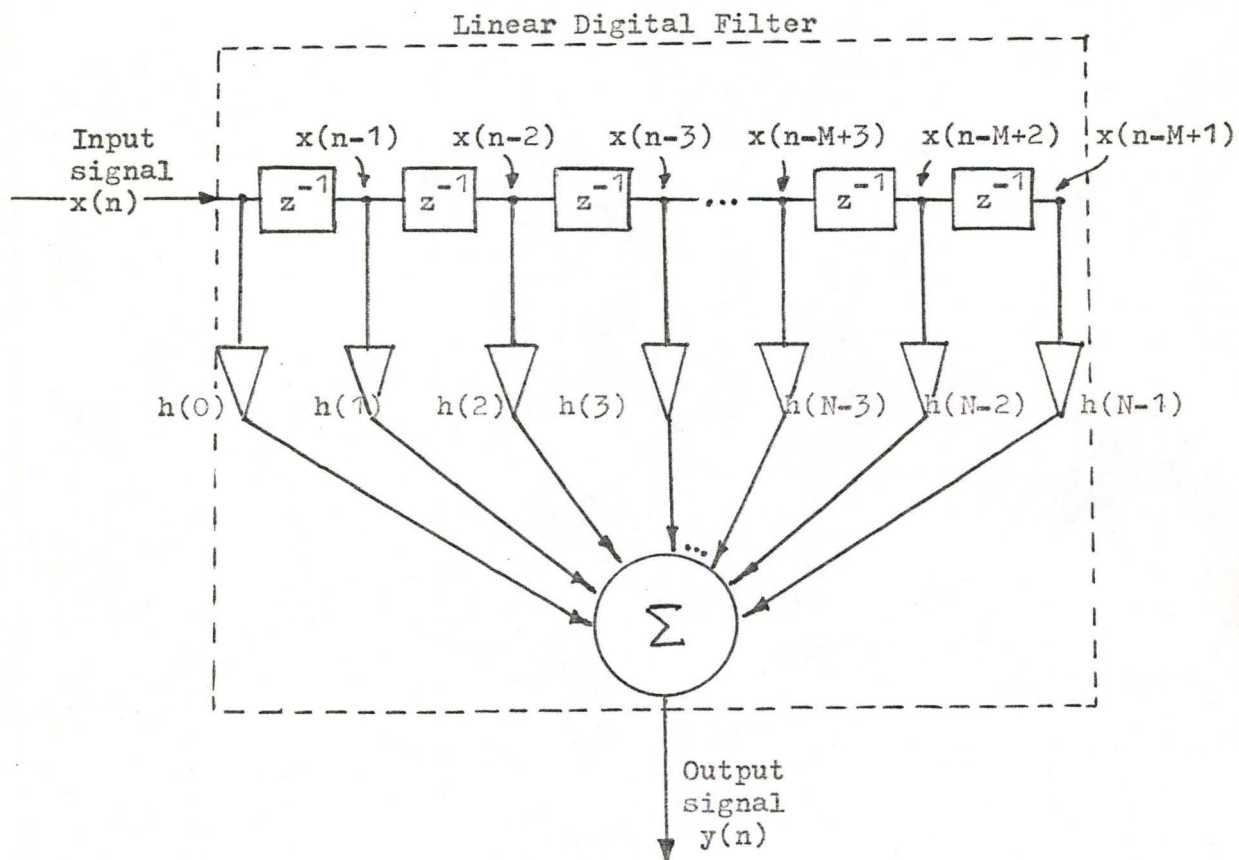


Fig. C.1: A direct form realization of an FIR system. The  $z^{-1}$  is a unit delay operator.

is realized nonrecursively. The transfer function for such a system is of the form

$$H(z) = \sum_{n=0}^{N-1} h(n) z^{-n} \quad (C.3)$$

It is obvious that the poles, of Eq. (2.3) are located at the origin of the  $z$ -plane. Thus, this type of filter is always stable. Although FIR filters have a variety of alternative forms of implementation, we restrict our discussion only to linear phase design.

The definitions in Eq. (C.2) and (C.3) can be utilized to formulate the frequency response of a linear phase FIR filter. If  $N$  is the length of a symmetrical impulse response and  $N$  is odd, then the sequence  $\{h(n)\}$  ( $0 \leq n \leq N-1$ ) is symmetric about the midpoint  $n=(N-1)/2$ . We write Eq. (C.3) as

$$H(z) = \sum_{n=0}^{\frac{N-1}{2}-1} h(n) z^{-n} + h\left(\frac{N-1}{2}\right) z^{-\left(\frac{N-1}{2}\right)} + \sum_{n=\frac{N+1}{2}}^{N-1} h(n) z^{-n} \quad (C.4)$$

Using the substitution  $m=N-1-n$  and  $m=n$  in the last summation in Eq. (C.4) gives [11]

$$H(z) = \sum_{n=0}^{\frac{N-1}{2}-1} h(n) z^{-n} + h\left(\frac{N-1}{2}\right) z^{-\left(\frac{N-1}{2}\right)} + \sum_{n=0}^{\frac{N-1}{2}-1} h(N-1-n) z^{-(N-1-n)} \quad (C.5)$$

We make use of Eq. (C.2) and factor out  $z^{-(N-1)/2}$ . Eq. (C.5) can be expressed as follows:

$$H(z) = z^{-\left(\frac{N-1}{2}\right)} \left[ h\left(\frac{N-1}{2}\right) + \sum_{n=0}^{\frac{N-1}{2}-1} h(n) \left( z^{\left(\frac{N-1}{2}-n\right)} + z^{-\left(\frac{N-1}{2}-n\right)} \right) \right] \quad (C.6)$$

If we evaluate Eq. (C.6) for  $z=\exp(j\omega)$ , we obtain

$$H[\exp(j\omega)] = \exp[-j\omega(\frac{N-1}{2})] [h(\frac{N-1}{2}) + 2 \sum_{n=0}^{\frac{N-1}{2}-1} h(n) \cos(\omega(\frac{N-1}{2}-n))] \quad (C.7)$$

For  $N$  even, the frequency response is

$$H[\exp(j\omega)] = \exp[-j\omega(\frac{N-1}{2})] [2 \sum_{n=0}^{\frac{N}{2}-1} h(n) \cos(\omega(\frac{N-1}{2}-n))] \quad (C.8)$$

A major implication of Eqs. (C.7) and (C.8) is that the network implementation requires only  $(N+1)/2$  ( $N$  odd) or  $N/2$  ( $N$  even) multiplications rather than the  $N$  multiplications needed for Eq. (C.1) [12].

The simplest method to design a nonrecursive linear phase filter is by means of Fourier series [21], [22]. It is evident that the frequency response of any digital filter is periodic in frequency with period  $2\pi$

$$H[\exp(j\omega)] = H[\exp(j(\omega+2n\pi))] \quad \text{for } n = 0, \pm 1, \pm 2, \dots$$

This periodic function can be written in terms of the Fourier series

$$H[\exp(j\omega)] = \sum_{n=-\infty}^{\infty} h(n) \exp(-j\omega n) \quad (C.9)$$

where the Fourier coefficients,  $h(n)$ , are the impulse responses of the filter. Eq. (C.9) indicates that the impulse response is infinite in duration ( $-\infty \leq n \leq \infty$ ). In order to achieve a finite representation, the infinite series of Eq. (C.9) can be truncated by assigning

$$h(n) = 0 \quad \text{for } |n| > \frac{N-1}{2} \quad (\text{C.10})$$

in which case the expanded form of the Fourier series is

$$H[\exp(j\omega)] = h(0) + 2 \sum_{n=1}^{\frac{N-1}{2}} h(n) \cos(n\omega) \quad (\text{C.11})$$

Here we use the fact that the amplitude of the frequency response is symmetrical (that is  $H[\exp(j\omega)]$  is an even function). The coefficients  $h(0)$  and  $h(n)$  can be determined according to [36]

$$h(0) = \frac{1}{\pi} \int_0^{\pi} H[\exp(j\omega)] d\omega \quad (\text{C.12})$$

$$h(n) = \frac{1}{\pi} \int_0^{\pi} H[\exp(j\omega)] \cos(n\omega) d\omega$$

The filter given in the form of Eq. (C.9) is unrealizable because the impulse response begins at  $-\infty$ . This, also, means that the filter is noncasual. It is suggested [22] that casuality can be brought about by multiplying Eq. (C.11) by  $\exp[-j\omega(N-1)/2]$

$$H'[\exp(j\omega)] = \exp[-j\omega(\frac{N-1}{2})] [h(0) + 2 \sum_{n=1}^{\frac{N-1}{2}} h(n) \cos(n\omega)] \quad (\text{C.13})$$

$$= \cos(\frac{N-1}{2} \omega) [h(0) + 2 \sum_{n=1}^{\frac{N-1}{2}} h(n) \cos(n\omega)] \quad (\text{C.14})$$

Comparing Eq. (C.13) with Eq. (C.7) both equations have the same representation except that the former has the impulse response symmetrical about the origin ( $n=0$ ) and the latter is symmetrical about the  $n = (N-1)/2$ .

As we recall (Section 2.3), direct truncation of a very long sequence results in sharp transition at both ends of the data length. A window function is utilized in Eq. (C.10) to reduce the Gibbs' phenomenon. This window must also have the ability to manipulate the passband ripple and the stopband attenuation of the frequency response of the filter. Thus, the choice of window function is a critical decision in the design of FIR filter. The Kaiser window described by Eq. (2.9) is reproduced here for convenience

$$w(n) = \frac{I_0(\beta \sqrt{1 - (\frac{2n}{N-1})^2})}{I_0(\beta)} \quad |n| \leq \frac{N-1}{2} \quad (C.15)$$

where the parameter  $\beta$  is a constant which can be adjusted so as to trade off the main-lobe width for the sidelobe amplitude.  $I_0(\cdot)$  is the modified Bessel Function of the first kind and order zero. In order to show how the value of  $\beta$  can be determined, we go through the steps of the design of a bandpass filter.

We begin the example by making a sketch (Fig. C.2) of the ideal bandpass filter. This figure includes the specified lower cutoff frequency ( $f_a$ ), the upper cutoff frequency ( $f_b$ ) and the parameter  $\delta$  which denotes the maximum allowable tolerance for the stopband attenuation and the passband ripple. The ideal frequency response of such filter can be written in the form

$$|H(f)| = \begin{cases} 0 & 0 \leq |f| < f_a \\ 1 & f_a \leq |f| \leq f_b \\ 0 & f_b < |f| \leq 0.5 \end{cases} \quad (C.16)$$

The impulse response ( $N$  odd) of the bandpass filter can be obtained

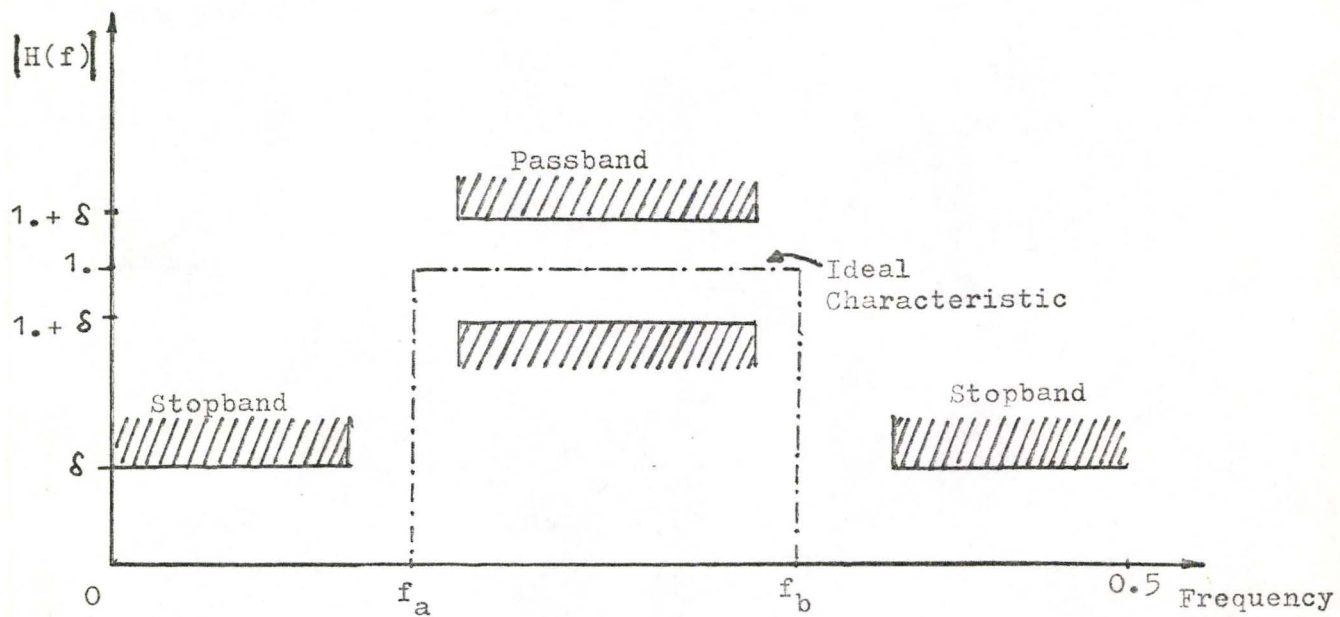


Fig. C.2: Bandpass filter specifications.

readily from Eq. (C.16) and (C.12)

$$\begin{aligned} h(0) &= 2 (f_b - f_a) \\ h(n) &= \frac{1}{n\pi} [\sin(2n\pi f_b) - \sin(2n\pi f_a)] \end{aligned} \quad (C.17)$$

Suppose in our design specification, we want the passband ripple to have a value of  $A_p$  decibel (dB) and the minimum stopband attenuation has  $A_a$  dB. According to Kaiser [22], we calculate a suitable value of the tolerance  $\delta$  such that

$$\delta = \min(\delta_1, \delta_2) \quad (C.18)$$

where

$$\begin{aligned} \delta_1 &= 10^{-0.05 A_a} \\ \delta_2 &= \frac{10^{0.05 A_p} - 1}{10^{0.05 A_p} + 1} \end{aligned}$$

A set of empirical formula is given by Kaiser [20], [21], [22] to calculate the window parameter  $\beta$

$$\beta = \begin{cases} 0 & \text{ATN} \leq 21 \\ .5842(\text{ATN} - 21)^{0.4} + .07886 (\text{ATN} - 21) & 21 < \text{ATN} \leq 50 \\ .1102(\text{ATN} - 8.7) & \text{ATN} > 50 \end{cases} \quad (C.19)$$

where  $\text{ATN} = -20 \log_{10} \delta$  and  $\delta$  is determined by Eq. (C.18). Using Eq. (C.15) and (C.19) we obtain a desired window function. The actual filter coefficients ( $h'(n)$ ) are given by

$$h'(n) = h(n) \frac{I_0(\beta \sqrt{1 - (\frac{2n}{N-1})^2})}{I_0(\beta)} \quad n = 0, 1, 2, \dots, \frac{N-1}{2} \quad (C.20)$$

The frequency response can be calculated by employing Eq. (C.14) and (C.20). This concludes our discussion on the design of an FIR bandpass filter.

0001 FTN4,L  
0002 C.....  
0003 C.....  
0004 C.....  
0005 D..... APPENDIX D .....  
0006 C.....  
0007 C..... LISTINGS OF THE PROGRAM ELTAP, WFIR .....  
0008 C..... PROAP, SPMAP AND CURVE .....  
0009 C.....  
0010 C.....  
0011 C.....  
0012 C  
0013 C\*\*\*\*\* .MESSAGE TO USERS. \*\*\*\*\*  
0014 C  
0015 C THE OBJECTIVE OF THIS SIMULATION IS A STUDY OF SIGNAL PROCESSING  
0016 C METHODS FOR EMERGENCY LOCATOR TRANSMITTER (ELT) SIGNALS. THESE  
0017 C SIGNALS ARE BEING USED IN THE SEARCH AND RESCUE SATELLITE-AIDED  
0018 C TRACKING (SARSAT) OPERATION AS RELATED TO AIR TRAFFIC CONTROL SYSTEM.  
0019 C  
0020 C SEVERAL SIGNAL PROCESSING METHODS ARE EMPLOYED TO EXAMINE THE  
0021 C SPECTRAL CHARACTERISTICS OF ELT SIGNALS, AS THESE CHARACTERISTICS  
0022 C ARE OF PARAMOUNT IMPORTANCE IN THE DESIGN OF SATELLITE-AIDED  
0023 C SEARCH AND RESCUE SYSTEM.  
0024 C  
0025 C SPECTRAL ESTIMATIONS BY MEANS OF THE FAST FOURIER TRANSFORM  
0026 C (FFT) ALGORITHM AND THE MAXIMUM ENTROPY METHOD (MEM) SPECTRAL  
0027 C ANALYSIS WITH PRE-PROCESSING PROVIDED BY THE AUTOCORRELATION  
0028 C FUNCTION (ACF) AND FINITE IMPULSE RESPONSE (FIR) FILTERING RESPECTIVELY  
0029 C (OR A COMBINATION OF BOTH), ARE EMPLOYED IN THE INVESTIGATION.  
0030 C  
0031 C THE ENTIRE SIMULATION IS A PACKAGE OF FIVE SEPARATE COMPUTER PROGRAMS:  
0032 C  
0033 C 1) ELTAP - SIMULATE A SINGLE OR A MULTIPLE ELT SIGNAL.  
0034 C  
0035 C 2) WFIR - DESIGN FINITE IMPULSE RESPONSE BANDPASS FILTER.  
0036 C  
0037 C 3) PROAP - PERFORM PRE-PROCESSING TECHNIQUES SUCH AS THE  
0038 C AUTOCORRELATION FUNCTION, WINDOWING AND FILTERING.  
0039 C  
0040 C 4) SPMAP - TO ESTIMATE THE SPECTRAL DENSITY OF ELT SIGNALS  
0041 C BY THE FFT AND MEM SPECTRAL ANALYSIS.  
0042 C  
0043 C 5) CURVE - TO PLOT THE ELT SIGNALS AND SPECTRUMS.  
0044 C  
0045 C THESE FIVE PROGRAMS HAVE TO BE EXECUTED BY FOLLOWING THE ABOVE ORDER.  
0046 C THE SECOND PROGRAM (WFIR) CAN BE IGNORED IF FILTERING IS NOT NEEDED.  
0047 C 512 SAMPLE POINTS ARE USED TO SIMULATE ELT SIGNALS.  
0048 C THE SAMPLING TIME IS AT TWICE THE NYQUIST RATE.  
0049 C THE FREQUENCY SPECTRUM HAS A BANDWIDTH OF 25 KHZ.  
0050 C  
0051 C ALL SIMULATIONS ARE DONE ON THE HP1000 COMPUTER SYSTEM IN CONJUNCTION  
0052 C WITH THE FPS-AP120B ARRAY PROCESSOR.  
0053 C  
0054 C EACH PROGRAMS HAS BEEN GIVEN A DETAILED DOCUMENTATION, USERS ARE ADVISED  
0055 C TO CONSULT THE NECESSARY PROGRAM WHENEVER PROBLEMS ARISE.  
0056 C  
0057 C  
0058 C

```

0059 C
0060 C*****
0061 C*****
0062 C***** PROGRAM ELTAP *****
0063 C*****
0064 C***** OCTOBER 1981 *****
0065 C*****
0066 C*****
0067 $EMA(XYZ,0)
0068 PROGRAM ELTAP
0069 COMMON /XYZ/ S(512),GN(512),ELT(1024)
0070 C***** NOTES *****
0071 C THIS PROGRAM (ELTAP) PERFORMS THE FOLLOWING TASKS:
0072 C 1) GENERATE GAUSSIAN NOISE (USING ARRAY PROCESSOR) IN SUBROUTINE
0073 C GAUSS.
0074 C 2) GENERATE PULSE-MODULATION ELT SIGNAL IN SUBROUTINE SPSIG.
0075 C 3) GENERATE SINUSOIDAL MODULATION ELT SIGNAL IN SUBROUTINE
0076 C SNSIG.
0077 C FOR THE CASE OF MULTIPLE ELT SIGNALS, DIFFERENT FORMATS OF ELT SIGNALS
0078 C CAN BE GENERATED SIMULTANEOUSLY IN THIS PROGRAM.
0079 C DETAILED DESCRIPTION IS DOCUMENTED AT THE BEGINNING OF EACH SUBROUTINES.
0080 C
0081 C BEFORE EXECUTING THIS PROGRAM (i.e. ;RU,ELTAP), USERS ARE ADVISED
0082 C TO MAKE SURE THAT THE SPOOL FILE FORMAT (i.e. ;SL COMMAND)
0083 C ;SL,12,DSIG,WR
0084 C IS TYPED. THIS INSTRUCTS THE LOGICAL UNIT LU=12 TO WRITE RESULTS,
0085 C FROM ELTAP, INTO DATA FILE DSIG.
0086 C
0087 C DEFINITION OF VARIABLES:
0088 C IFLAG= : 1-SET ERROR MESSAGE FLAG, 0-RELEASE FLAG.
0089 C N= : NUMBER OF SAMPLES FOR ELT SIGNALS (512 POINTS).
0090 C MODU= : SELECT MODULATION, 1-FOR SINUSOIDAL AND 0-FOR PULSE-
0091 C MODULATION ELT SIGNALS.
0092 C ISW= : SELECT SWEEP, 0-FOR LINEAR SWEEP AND 1-FOR QUADRATIC SWEEP.
0093 C SFREQ= : MINIMUM FREQUENCY (0.0 Hz) OF THE SPECTRUM BANDWIDTH.
0094 C FFREQ= : MAXIMUM FREQUENCY (25 KHz) OF THE SPECTRUM BANDWIDTH.
0095 C INS= : NUMBER OF ELT SIGNALS WANTED (MAXIMUM IS 10 SIGNALS).
0096 C NOISE= : 1-INDICATES NEED GAUSSIAN NOISE. OTHERWISE INPUT 0.
0097 C TSTEP= : SAMPLING TIME AT TWICE THE NYQUIST RATE.
0098 C CFREQ= : IS THE CARRIER FREQUENCY OF A PARTICULAR ELT SIGNAL.
0099 C ELT(,)= : IS THE ARRAY WHICH STORES THE RESULT OF ELT SIGNAL(S).
0100 C GN(,)= : IS THE ARRAY WHICH STORES THE RESULT OF NOISE SAMPLES.
0101 C S(,)= : IS A SERVICE VECTOR.
0102 C
0103 C***** INPUT SECTION *****
0104 WRITE(1,100)
0105 WRITE(1,102)
0106 WRITE(1,104)
0107 100 FORMAT("..... DID YOU TYPE IN .....")
0108 102 FORMAT(";SL,12,DSIG,WR")
0109 104 FORMAT("IF YES TYPE 1, OTHERWISE TYPE 0")
0110 READ(1,*)IC
0111 IF(IC.EQ.0)GO TO 1
0112 WRITE(1,106)
0113 106 FORMAT("INPUT: NUMBER OF ELT SIGNALS ")
0114 READ(1,*)INS
0115 IF(INS.LE.0,OR,INS.GT.10)GO TO 1
0116 DO 50 I=1,1024
0117 50 ELT(I)=0.0
0118 NRP=1

```

```

0119      DO 52 NS=1,INS
0120      WRITE(1,108)
0121 108   FORMAT(".....")
0122      WRITE(1,110)NS
0123 110   FORMAT("..... GENERATE ELT SIGNAL #",I2,".....")
0124      WRITE(1,112)
0125 112   FORMAT(".....")
0126      WRITE(1,114)NS
0127 114   FORMAT("INPUT: THE CARRIER FREQUENCY (IN Hz) OF SIGNAL #",I2)
0128      READ(1,*)CFREQ
0129      IF(CFREQ.LT.0.OR,CFREQ.GT.25000.)GO TO 1
0130      WRITE(1,116)
0131 116   FORMAT("SELECT MODULATION: PULSE/SINUSOIDAL (0/1)")
0132      READ(1,*)MODU
0133      WRITE(1,118)
0134 118   FORMAT("SELECT FREQUENCY SWEEP: LINEAR/QUADRATIC (0/1)")
0135      READ(1,*)ISW
0136      WRITE(1,120)
0137 120   FORMAT("WANT NOISE (0/1) ?")
0138      READ(1,*)NOISE
0139  C INITIALIZATION.
0140      SFREQ=0.0
0141      FFREQ=25000.0
0142      TSTEP=1.0/(2.0*FFREQ)
0143      N=512
0144      IFLAG=0
0145      DO 54 I=1,N
0146      GN(I)=0.0
0147 54    S(I)=0.0
0148  C***** CALL SUBROUTINES *****
0149      IF(NOISE.EQ.1)CALL GAUSS(N,MODU,ISW,DCYLE,IFLAG,SEED,NS)
0150      IF(IFLAG.EQ.1)GO TO 1
0151      IF(MODU.EQ.0)CALL SQSIG(N,TSTEP,ISW,NOISE,CFREQ,NRP,DCYLE,
0152      +IFLAG,XSEED)
0153      IF(IFLAG.EQ.1)GO TO 1
0154      IF(MODU.EQ.1)CALL SNSIG(N,TSTEP,ISW,CFREQ)
0155  C ADD MULTIPLE ELT SIGNALS TOGETHER IF INS IS GREATER THAN ONE.
0156      DO 56 J=1,INS
0157 56    ELT(J)=ELT(J)+S(J)
0158 52    CONTINUE
0159  C WRITE DATA FILE DSIG, WHICH STORES THE DATA OF ELT SIGNALS.
0160  C :SL,12,DSIG,WR
0161      WRITE(12)ELT
0162      GO TO 2
0163 1    DO 58 I=1,3
0164      WRITE(1,122)
0165 122   FORMAT(".....WARNING !!! EXECUTE THE PROGRAM AGAIN .....")
0166 58    CONTINUE
0167 2    STOP
0168      END
0169  C***** ADDITIVE NOISE *****
0170  $EMA(XYZ,0)
0171      SUBROUTINE GAUSS(N,MODU,ISW,DCYLE,IFLAG,SEED,NS)
0172      COMMON /XYZ/ S(512),GN(512),ELT(1024)
0173      DIMENSION SS(512)
0174      DATA RI1,RI2/4.3056801E-7,5.8011508E-8/
0175  C*****
0176  C ARRAY PROCESSOR IS USED TO GENERATE GAUSSIAN RANDOM NUMBERS W(.) WITH
0177  C ZERO MEAN AND UNIT VARIANCE, ACCORDING TO
0178  C      W(I)=SQRT[-2*LN(X(I))]*COS[2*PI*X(I+1)]

```

```

0179 C      W(I+1)=SQRT[-2*LN(X(I))]*SIN[2*PI*X(I+1)]
0180 C WHERE X(.) ARE UNIFORM DISTRIBUTED RANDOM NUMBERS.
0181 C THE REQUIRED STANDARD DEVIATION (i.e.SIGMA) OF NOISE SAMPLES TO ATTAIN
0182 C GIVEN NOISE DENSITY RATIO (i.e.dB-Hz) SUBJECTS TO DUTY CYCLE (DCYLE) IS
0183 C      SIGMA=SQRT(SIGNAL POWER/SNR)
0184 C WHERE SIGNAL POWER (PS) CAN BE CALCULATED ACCORDING TO THE SPECIFIC
0185 C KINDS OF ELT SIGNAL, AND SNR (IN dB) IS DEFINED AS
0186 C      SNR=[dBHz]-[10.0*ALOG10(SPECTRUM BANDWIDTH)]
0187 C ADDITIVE WHITE GAUSSIAN NOISE COMPONENTS ARE STORED IN GN(.).
0188 C THE ARRAY SS(.) IS A SERVICE VECTOR.
0189 C
0190      WRITE(1,100)
0191 100  FORMAT("..... ADDITIVE NOISE .....")
0192 C FOR DUTY RATIO, THE RANGE IS 0.3 TO 0.5 FOR PULSE-MODULATION ELT
0193 C SIGNALS (THIS VALUE HAS TO BE IDENTICAL TO THE DUTY RATIO GIVEN FOR
0194 C PULSE-MODULATION IN THE SUBROUTINE SCSIG), AND IT IS EQUAL TO ONE
0195 C FOR SINUSOIDAL MODULATION SIGNAL.
0196      WRITE(1,102)
0197 102  FORMAT("INPUT; DUTY RATIO AND NOISE DENSITY RATIO")
0198      READ(1,*)DCYLE,DBHZ
0199      IF(DCYLE.NE.1.AND.MODU.EQ.1)GO TO 1
0200 C INITIALIZE RANDOM NUMBER SEED.
0201      IF(NS.EQ.1)SEED=0.251063794879
0202      CSEED=SEED
0203      IF(MODU.EQ.0)GO TO 2
0204      IF(MODU.EQ.1)GO TO 3
0205 C
0206 C CALCULATE THE REQUIRED SIGNAL POWER AND STANDARD DEVIATION.
0207 C
0208 2     PS=0.5*DCYLE
0209      GO TO 4
0210 3     SQ=DCYLE*DCYLE
0211      PS=0.5+4.0*DCYLE*RI1+SQ*(0.25+RI2)
0212      IF(ISW.EQ.1)PS=0.5+0.25*SQ
0213 4     BW=10.0*ALOGT(25000.0)
0214      SHR=DBHZ-BW
0215      DENOM=0.1*SNR
0216      DENOM=10.0**DENOM
0217      SIGMA=PS/DENOM
0218      SIGMA=SIGMA**0.5
0219      WRITE(1,104)DBHZ,SNR
0220 104  FORMAT(1X,"dB-Hz=",F12.9,2X,"SNR (dB)=",F12.9)
0221 C
0222 C CALCULATE GAUSSIAN RANDOM NUMBERS, AND GAUSSIAN NOISE SAMPLES.
0223 C
0224      CALL APINT(0,0,ISTAT)
0225      CALL APCLR
0226      CALL APPUT(CSEED,0,1,2)
0227      CALL APPUT(SIGMA,1,1,2)
0228      CALL APWD
0229      CALL VRAND(0,101,1,512)
0230      CALL VLN(101,2,101,2,256)
0231      CALL VNEG(101,2,101,2,256)
0232      CALL VTSML(101,2,4002B,101,2,256)
0233      CALL VSQRT(101,2,101,2,256)
0234      CALL VTSML(102,2,4415B,102,2,256)
0235      CALL RECT(101,2,101,2,256)
0236      CALL VSNUL(101,1,1,101,1,512)
0237      CALL APWR
0238      CALL APGET(SS,101,512,2)

```

```

0239 CALL APGET(CSEED,0,1,2)
0240 CALL APWD
0241 CALL APRLE
0242 SEED=CSEED
0243 C ARRAY GN(.) STORES THE ADDITIVE NOISE SAMPLES.
0244 DO 50 I=1,N
0245 50 GN(I)=SS(I)
0246 RETURN
0247 1 IFLAG=1
0248 RETURN
0249 END
0250 C***** PULSE-MODULATION *****
0251 $EMA(XYZ,0)
0252 SUBROUTINE SPSIG(N,TSTEP,ISW,NOISE,CFREQ,NRP,DCYLE,IFLAG,XSEED)
0253 COMMON /XYZ/ S(512),GN(512),ELT(1024)
0254 DIMENSION RISE(25),FALL(25),SS(512)
0255 DATA AQ,BQ,CQ/4644.3733,3569.6,1930.8/
0256 DATA AL,BL,CL,DL/1400.0,5600.0,2800.0,1960000.0/
0257 DATA A,B,C,RR/3.8806252E-4,7.2876493E-2,2.5619531E-1,2.153153E-4/
0258 C*****
0259 C PULSE-MODULATION ELT SIGNAL WITH CHOICES OF HAVING EITHER LINEAR OR
0260 C QUADRATIC SWEEP IS SIMULATED IN THIS SUBROUTINE.
0261 C LINEAR SWEEP; F(T)=1400.-700.*(T/TR)
0262 C QUADRATIC SWEEP; F(T)=1980.8-1784.8*(T/TR)+870.82*(T**2/TR**2)
0263 C WHERE TR=0.25 SEC. IS THE REPETITION TIME.
0264 C THE RISE AND FALL TIME OF EACH PULSES ARE CALCULATED BY INTEGRATING
0265 C THE ABOVE EQUATIONS WITH RESPECT TO T. THE INTEGRATION LIMITS ARE
0266 C FROM 0 TO K. FOR CALCULATING RISE TIME, THE INTEGRATION RESULT IS
0267 C SET EQUAL TO I-1 AND EXPRESSED K AS A FUNCTION OF I. THE SAME
0268 C PROCEDURE IS APPLIED IN FINDING THE FALL TIME, BUT THE INTEGRATION
0269 C RESULT IS EQUAL TO I-1+D AND K IS EXPRESSED AS A FUNCTION OF I AND D.
0270 C WHERE I INDICATES PULSE INDEXES OF THE PULSE TRAIN AND D IS THE
0271 C DUTY RATIO OF PULSES.
0272 C THESE SIGNALS ARE ASSUMED TO HAVE UNIT AMPLITUDE.
0273 C ALSO THESE SIGNALS CAN EITHER HAVE CONSTANT OR RANDOM PHASE.
0274 C THE ARRAY SS(.) IS A SERVICE VECTOR.
0275 C
0276 WRITE(1,100)
0277 100 FORMAT("..... PULSE-MODULATION SIGNAL .....")
0278 WRITE(1,102)
0279 102 FORMAT(" INPUT: DUTY RATIO (0.3<DUTY RATIO<0.5)")
0280 READ(1,*)DUTY
0281 IF(DUTY.NE.DCYLE.AND.NOISE.EQ.1)GO TO 1
0282 T=0.0
0283 PI=8.0*ATAN(1.0)
0284 C THE ARRAYS RISE(.) AND FALL(.) STORE THE RISE TIME AND FALL TIME OF
0285 C EACH PULSES.
0286 C IST INDICATES THE STARTING INDEX OF PULSES.
0287 C IFIN INDICATES THE FINAL INDEX OF PULSES.
0288 C
0289 C LINEAR SWEEP.
0290 C
0291 IF(ISW.EQ.1)GO TO 2
0292 IST=IFIX(T*(AL-AL*T)+1.0)
0293 TMOD=T+FLOAT(N)*TSTEP
0294 IFIN=IFIX(TMOD*(AL-AL*TMOD)+1.0)
0295 IMOD=IFIN+1
0296 L=IST
0297 K=1
0298 DO 50 I=IST,IFIN

```

```

0299      IF(I.EQ.IMOD)L=1
0300      RISE(K)=0.5-((DL-BL*FLOAT(L-1))*0.5)/CL
0301      FALL(K)=0.5-((DL-BL*(FLOAT(L-1)+DUTY))*0.5)/CL
0302      K=K+1
0303  50    L=L+1
0304      GO TO 3
0305  C
0306  C QUADRATIC SWEEP.
0307  C
0308  2    IST=IFIX(T*(CQ-T*(BQ-T*AQ))+1.0)
0309      TMOD=T+FLOAT(N)*TSTEP
0310      IFIN=IFIX(TMOD*(CQ-TMOD*(BQ-TMOD*AQ))+1.0)
0311      IMOD=IFIN+1
0312      L=IST
0313      K=1
0314      THIRD=1.0/3.0
0315      DO 52 I=IST,IFIN
0316      IF(I.EQ.IMOD)L=1
0317      BS=(B+RR*(1.0-FLOAT(L)))*0.5
0318      BSS=((BS**2)+A)**0.5
0319      AS=(-BS+BSS)**THIRD
0320      BS=- (BS+BSS)**THIRD
0321      RISE(K)=AS+BS+C
0322      BS=(B+RR*(1.0-FLOAT(L)-DUTY))*0.5
0323      BSS=((BS**2)+A)**0.5
0324      AS=(-BS+BSS)**THIRD
0325      BS=- (BS+BSS)**THIRD
0326      FALL(K)=AS+BS+C
0327      K=K+1
0328  52    L=L+1
0329  C
0330  3    WRITE(1,104)
0331  104  FORMAT(" WANT RANDOM PHASE (0/1) ?")
0332      READ(1,*)IRP
0333      IF(IRP.EQ.0)GO TO 4
0334      DO 54 I=1,N
0335  54    SS(I)=0.0
0336      IF(NRP.EQ.1)XSEED=0.251063794879
0337      NRP=0
0338      SSEED=XSEED
0339  C
0340  C GENERATE RANDOM PHASE BY USING ARRAY PROCESSOR.
0341  C
0342      CALL APINT(0,0,ISTAT)
0343      CALL APCLR
0344      CALL APPUT(SSEED,0,1,2)
0345      CALL APWD
0346      CALL VRAND(0,2000,1,512)
0347      CALL YTSML(2000,1,4415B,2000,1,512)
0348      CALL APWR
0349      CALL APGET(SS,2000,512,2)
0350      CALL APGET(SSEED,0,1,2)
0351      CALL APWD
0352      CALL APRLE
0353      XSEED=SSEED
0354  C
0355  C MODULATE THE CARRIER FREQUENCY ON THE PULSE TRAIN.
0356  C
0357  4    RISE(K)=0.25
0358      FALL(K)=0.25

```

```

0359      TMOD=T
0360      RNOW=RISE(1)
0361      FNOW=FALL(1)
0362      K=2
0363      PH=0.0
0364      DO 56 I=1,N
0365      IF(TMOD.GT.FNOW)GO TO 5
0366      S(I)=SIN(CFREQ*PI*T+PH)
0367 5      T=T+TSTEP
0368      TMOD=TMOD+TSTEP
0369      IF(TMOD.LT.RISE(K))GO TO 56
0370      RNOW=RISE(K)
0371      FNOW=FALL(K)
0372      IF(IRP.EQ.1)PH=SS(K)
0373      K=K+1
0374      IF(TMOD.GE.0.25)TMOD=TMOD-0.25
0375 56     CONTINUE
0376  C FIND THE MEAN VALUE OF THE SIGNAL. THE RESULTANT SIGNAL IS OF THE
0377  C FORM: S(.)=S(.)-MEAN VALUE.
0378      EMS=0.0
0379      DO 58 I=1,N
0380      S(I)=S(I)+GN(I)
0381 58     EMS=EMS+S(I)
0382      EMS=EMS/FLOAT(N)
0383  C THE SIGNAL SAMPLES ARE STORED IN THE ARRAY S(.).
0384      DO 60 I=1,N
0385 60     S(I)=S(I)-EMS
0386      RETURN
0387 1      IFLAG=1
0388      RETURN
0389      END
0390  C***** SINUSOIDAL MODULATION *****
0391  $EMA(XYZ,0)
0392      SUBROUTINE SNSIG(N,TSTEP,ISM,CFREQ)
0393      COMMON /XYZ/ S(512),GN(512),ELT(1024)
0394      DATA AQ,BQ,CQ/4644.3733,3569.6,1930.8/
0395      DATA ALS,BLS/8796.4594,4.712389/
0396  C*****
0397  C THIS SUBROUTINE GENERATES SINUSOIDAL MODULATION ELT SIGNAL HAVING
0398  C EITHER LINEAR OR QUADRATIC SWEEP.
0399  C THE SIGNAL IS IN THE FORM OF AMPLITUDE MODULATION:
0400  C      S(I)=A*[1.0+U*SIN(ARG)]*SIN[2*PI*FRQ*T]
0401  C WHERE FRQ IS THE CARRIER FREQUENCY OF ELT SIGNAL.
0402  C FOR LINEAR SWEEP, ARG IS THE INTEGRATION OF
0403  C      1400.0-700.0*(T/TR)
0404  C WITH RESPECT TO T, AND
0405  C FOR QUADRATIC SWEEP, ARG IS THE INTEGRATION OF
0406  C      1930.8-1784.8*(T/TR)+870.82*(T**2/TR**2)
0407  C WITH RESPECT TO T. THE INTEGRATION CONSTANT FOR BOTH SWEEPS CAN BE
0408  C SOLVED BY SETTING [1.0+U*SIN(ARG)]=0 AT T=0. IN BOTH SWEEPS TR=0.25 SEC.
0409  C ALSO A: IS THE AMPLITUDE OF SIGNAL.
0410  C      U: IS THE DUTY CYCLE.
0411  C FOR SIMPLICITY BOTH A AND U ARE ASSUMED TO HAVE UNIT VALUE IN THE
0412  C SIMULATION.
0413  C
0414      WRITE(1,100)
0415 100     FORMAT("..... SINUSOIDAL MODULATION SIGNAL .....")
0416      PI=8.0*ATAN(1.0)
0417      T=0.
0418      TMOD=0.

```

```
0419      AQ=PI*AQ
0420      BQ=PI*BQ
0421      CQ=PI*CQ
0422      DQ=PI*0.75
0423      U=1.0
0424      DO 50 I=1,N
0425      IF(1SW.EQ.1)GO TO 1
0426      C
0427      C LINEAR SWEEP.
0428      C
0429      EMS=SIN(TM0D*(ALS-ALS*TM0D)+CLS)
0430      GO TO 2
0431      C
0432      C QUADRATIC SWEEP.
0433      C
0434      1   EMS=SIN(TM0D*(CQ-TM0D*(BQ-TM0D*AQ))+DQ)
0435      2   EMS=1.0+U*EMS
0436      SS=EMS*SIN(CFREQ*PI*T)
0437      T=T+TSTEP
0438      TM0D=TM0D+TSTEP
0439      IF(TM0D.GT.0.25)TM0D=0.
0440      50  S(I)=SS+GN(I)
0441      C FIND THE MEAN VALUE OF THE SIGNAL. THE RESULTANT SIGNAL IS OF THE
0442      C FORM: S(.)=S(.)-MEAN VALUE.
0443      EMS=0.0
0444      DO 52 I=1,N
0445      52  EMS=EMS+S(I)
0446      EMS=EMS/FLOAT(N)
0447      C ARRAY S(.) STORES THE SIGNAL SAMPLES.
0448      DO 54 I=1,N
0449      54  S(I)=S(I)-EMS
0450      C
0451      C***** .THOMAS CHUNG, REVISED; 30 JUNE, 1982. *****
0452      C
0453      RETURN
0454      END
```

FTN4,L

```

C*****
C*****
C*****          PROGRAM WFIR          *****
C*****          OCTOBER 1981          *****
C*****

```

\$EMA(XYZ,0)

PROGRAM WFIR

COMMON /XYZ/ G(512),X(1024),XX(1024)

```

C***** NOTES *****

```

```

C THIS PROGRAM USES KAISER WINDOW TO DESIGN A FINITE IMPULSE RESPONSE
C BANDPASS FILTER.

```

```

C THE BANDPASS FILTER HAS AN IDEAL TRANSFER FUNCTION IN THE FOURIER
C SERIES:

```

```

C  $H(F) = C(0) + 2 * C(K) * \cos[2 * \pi * K * F]$ 

```

```

C WHERE K=1,2,...,N.

```

```

C AND C(K) ARE THE COEFFICIENTS IN THE DIGITAL FILTER DESIGN, WE GET
C FOR THE C(K):

```

```

C  $C(0) = 2 * (FH - FL)$ 

```

```

C  $C(K) = [1 / (K * \pi)] * [\sin(2 * \pi * K * FH) - \sin(2 * \pi * K * FL)]$ 

```

```

C WHERE FH IS THE UPPER IDEAL CUTOFF FREQUENCY

```

```

C FL IS THE LOWER IDEAL CUTOFF FREQUENCY.

```

```

C THE SIMULATION PROCEDURES ARE DONE IN THE FOLLOWING ORDER :

```

```

C 1) CALCULATE BANDPASS FILTER IMPULSE RESPONSE.

```

```

C 2) CALCULATE KAISER WINDOW FUNCTION.

```

```

C 3) WINDOW THE IMPULSE RESPONSE.

```

```

C 4) PERFORM DISCRETE FOURIER TRANSFORM TO OBTAIN FILTER
C SPECTRUM.

```

```

C 5) PLOT FILTER IMPULSE RESPONSE OR SPECTRUM.

```

```

C BEFORE EXECUTING THIS PROGRAM USERS HAVE TO TYPE THE SPOOL

```

```

C FILE FORMAT:

```

```

C :SL,10,DWFIR,WR

```

```

C THIS INSTRUCTS THE LOGICAL UNIT LU=10 TO STORE THE IMPULSE RESPONSES.

```

```

C VALUE INTO THE DATA FILE DWFIR.

```

```

C DEFINITION OF VARIABLES:

```

```

C IFL=          : DESIRE FILTER LENGTH (MAXIMUM IS 511 POINTS).

```

```

C FMAX=        : MAXIMUM FREQUENCY (SPECTRUM BANDWIDTH), WHICH IS
C              25000.0 Hz.

```

```

C ATT=         : MINIMUM ATTENUATION (IN dB) OF FILTER RESPONSE.

```

```

C PRIP=        : PASSBAND RIPPLE (IN dB) WHICH CAN BE TOLERATED.

```

```

C***** INPUT SECTION *****

```

```

WRITE(1,100)

```

```

WRITE(1,102)

```

```

WRITE(1,104)

```

```

100 FORMAT("..... DID YOU TYPE IN .....")

```

```

102 FORMAT(":SL,10,DWFIR,WR")

```

```

104 FORMAT("IF YES TYPE 1, OTHERWISE TYPE 0")

```

```

READ(1,*)IC

```

```

IF(IC.EQ.0)GO TO 1

```

```

WRITE(1,106)

```

```

106 FORMAT("INPUT: FILTER LENGTH ")

```

```

READ(1,*)IFL

```

```

59 IF(IFL.GT.511)GO TO 1
60 WRITE(1,108)
61 108 FORMAT("INPUT: LOWER AND UPPER IDEAL CUTOFF FREQUENCIES (IN Hz)")
62 READ(1,*)FL,FH
63 IF(FH.LE.FL.OR.FL.LT.0.OR.FH.GT.25000.)GO TO 1
64 WRITE(1,110)
65 110 FORMAT("INPUT: MINIMUM ATTENUATION (IN X dB)")
66 READ(1,*)ATT
67 WRITE(1,112)
68 112 FORMAT("INPUT: PASSBAND RIPPLE (IN X dB)")
69 READ(1,*)PRIP
70 C***** CALCULATE FILTER PARAMETERS *****
71 C NORMALIZE BANDWIDTH TO 0.5.
72 FMAX=25000.
73 FL=FL/(2.0*FMAX)
74 FH=FH/(2.0*FMAX)
75 FMAX=FMAX/(2.0*FMAX)
76 C
77 C ATTENUATION.
78 C
79 DEL1=-0.05*ATT
80 DEL1=10.0**DEL1
81 DEL2=0.05*PRIP
82 DEL2=((10.0**DEL2)-1.0)/((10.0**DEL2)+1.0)
83 IF(DEL1.LE.DEL2)DEL=DEL1
84 IF(DEL2.LE.DEL1)DEL=DEL2
85 ATT=-20.0*ALOGT(DEL)
86 C
87 C CALCULATE PARAMETER (BETA) FOR KAISER WINDOW.
88 C
89 IF(ATT.GT.50.)BETA=0.1102*(ATT-8.7)
90 IF(ATT.GE.20.96.AND.ATT.LE.50.)BETA=0.58417*(ATT-20.96)**0.4+
91 + 0.07886*(ATT-20.96)
92 IF(ATT.LT.20.96)BETA=0.0
93 N=(IFL+1)/2
94 C CHECK FOR EVEN (IEO=0) OR ODD (IEO=1) NUMBER OF SAMPLE.
95 IEO=IFL-(IFL/2)*2
96 CALL KAISR(IFL,N,IEO,BETA)
97 C ***** IMPULSE RESPONSE *****
98 C1=FH-FL
99 IF(IEO.EQ.1)G(1)=2.*C1
100 I1=IEO+1
101 PI=4.0*ATAN(1.0)
102 DO 50 I=I1,N
103 XN=I-1
104 IF(IEO.EQ.0)XN=XN+0.5
105 C=PI*XN
106 C3=C*C1
107 C STORE IMPULSES IN THE ARRAY G(.).
108 G(I)=SIN(C3)/C
109 50 G(I)=G(I)*2.0*COS(C*(FL+FH))
110 C
111 C CALCULATE THE WINDOWED IMPULSE RESPONSES.
112 C
113 DO 52 I=1,N
114 G(I)=G(I)*X(I)
115 52 X(I)=0.0
116 C WINDOWED IMPULSE RESPONSE VALUES ARE STORED IN THE ARRAY X(.).
117 DO 54 I=1,N
118 X(I)=G(N+1-I)

```

```

19 54 X(IFL+1-I)=X(I)
20 C STORE IMPULSE RESPONSES INTO THE DATA FILE DWFIR.
21 C :SL,10,DWFIR,WR.
22 WRITE(10)X
23 WRITE(1,114)
24 114 FORMAT("WANT PLOT IMPULSE RESPONSE (0/1) ?")
25 READ(1,*)IR
26 IF(IR.EQ.0)GO TO 2
27 CALL GRAPH(IFL,NR,IR)
28 IR=0
29 2 CALL FLCHR(IFL,FL,FH,N,IEO,NR)
30 WRITE(1,116)
31 116 FORMAT("WANT PLOT ENERGY SPECTRUM (0/1) ?")
32 READ(1,*)IP
33 IF(IP.EQ.0)GO TO 3
34 CALL GRAPH(IFL,NR,IR)
35 GO TO 3
36 1 DO 56 I=1,3
37 WRITE(1,118)
38 118 FORMAT("..... WARNING !!! EXECUTE THE PROGRAM AGAIN .....")
39 56 CONTINUE
40 3 STOP
41 END
42 C ***** KAISER WINDOW *****
43 $EMA(XYZ,0)
44 SUBROUTINE KAISR(IFL,N,IEO,BETA)
45 COMMON /XYZ/ G(512),X(1024),XX(1024)
46 REAL INO
47 C*****
48 C THIS SUBROUTINE GENERATES KAISER WINDOW FUNCTION.
49 C THE WINDOW VALUES ARE STORED IN THE ARRAY X(.).
50 C
51 BES=INO(BETA)
52 XIND=FLOAT(IFL-1)*FLOAT(IFL-1)
53 DO 50 I=1,N
54 XI=I-1
55 IF(IEO.EQ.0)XI=XI+0.5
56 XI=4.*XI*XI
57 X(I)=INO(BETA*SQRT(1.-XI/XIND))
58 50 X(I)=X(I)/BES
59 RETURN
60 END
61 C
62 C BESSEL FUNCTION FOR 25 TERMS.
63 C
64 REAL FUNCTION INO(Q)
65 Y=Q/2.
66 T=1.E-08
67 E=1.
68 DE=1.
69 DO 50 I=1,25
70 XI=I
71 DE=DE*Y/XI
72 SDE=DE*DE
73 E=E+SDE
74 IF(E*T-SDE)50,50,1
75 50 CONTINUE
76 1 INO=E
77 RETURN
78 END

```

```

79 C ***** ENERGY SPECTRUM *****
80 $EMA(XYZ,0)
81     SUBROUTINE FLCHR(IFL,FL,PH,N,IEO,NR)
82     COMMON /XYZ/ G(512),X(1024),XX(1024)
83 C*****
84 C THIS SUBROUTINE USES DISCRETE FOURIER TRANSFORM TO CALCULATE
85 C THE POWER SPECTRUM OF THE BANDPASS FILTER.
86 C INTRAPOLATION IS USED TO CALCULATE FINER FREQUENCY RESOLUTION.
87 C 1024 POINTS ARE USED.
88 C
89     PI=4.0*ATAN(1.0)
90     NR=1024
91     DO 50 I=1,NR
92 50     X(I)=0.0
93 C
94 C PERFORM DISCRETE FOURIER TRANSFORM, RESULTS ARE STORED IN THE
95 C ARRAY X(.).
96 C
97     XNR=NR
98     TWN=PI/XNR
99     SUMI=-G(1)/2.
100    IF(IEO.EQ.0)SUMI=0.
101    DO 52 I=1,NR
102    XI=I-1
103    TWNI=TWN*XI
104    SUM=SUMI
105    DO 54 J=1,N
106    XJ=J-1
107    IF(IEO.EQ.0)XJ=XJ+0.5
108 54    SUM=SUM+G(J)*COS(XJ*TWNI)
109 52    X(I)=2.*SUM
110    RETURN
111    END
112 C***** GRAPHIC *****
113 $EMA(XYZ,0)
114     SUBROUTINE GRAPH(IFL,NR,IR)
115     COMMON /XYZ/ G(512),X(1024),XX(1024)
116     DIMENSION IGCB(192)
117 C*****
118 C THE IMPULSE RESPONSE OR FILTER RESPONSE IS PLOTTED IN THIS
119 C SUBROUTINE. THE PLOT CAN BE DONE ON PLOTTER, GRAPHIC TERMINAL,
120 C OR LINE PRINTER IF
121 C     LU=40, ID=2 ; ON PLOTTER.
122 C     LU=1, ID=1 ; ON GRAPHIC TERMINAL.
123 C     LU=58, ID=4 ; ON LINE PRINTER.
124 C
125     IF(IR.EQ.0)GO TO 1
126 C
127 C PLOT IMPULSE RESPONSE.
128 C
129     TSTEP=1.0/(50000.0)
130 C XX(.) IS THE VALUE OF TIME AXIS IN MILLISECOND.
131     XX(1)=0.0
132     DO 50 I=2,IFL
133 50     XX(I)=FLOAT(I-1)*TSTEP*1000.
134 C INITIALIZE PARAMETERS FOR PLOTTING IMPULSE RESPONSE.
135     XMIN=0.0
136     XMAX=XX(IFL)
137     XDIV=-XMAX/20.
138     YDIV=0.10

```

```

39     YMIN=-0.001
40     YMAX=0.001
41     XD=2.
42     YD=1.
43     IFIX=2
44 C SEARCH FOR THE MAXIMUM AND MINIMUM VALUE IN Y-AXIS.
45     DO 52 I=1,IFL
46     IF(X(I).GT.YMAX)YMAX=X(I)
47 52   IF(X(I).LT.YMIN)YMIN=X(I)
48     WRITE(1,100)YMAX,YMIN,YDIV,YD
49 100  FORMAT("YMAX=",F12.9," YMIN=",F12.9," YDIV=",F3.2," YD=",F2.1)
50     WRITE(1,102)
51 102  FORMAT("INPUT: THE UPPER AND LOWER LIMITS FOR Y-AXIS.")
52     READ(1,*)YMAX,YMIN
53     NR=IFL
54     GO TO 2
55 C
56 C PLOT POWER SPECTRUM.
57 C
58 1   FSTEP=1.0/(2.*FLOAT(NR))
59 C XX(,) IS THE VALUE OF FREQUENCY RESOLUTION.
60     XX(1)=0.0
61     DO 54 I=2,NR
62     XX(I)=FLOAT(I-1)*FSTEP
63 54   XX(I)=XX(I)*50000.0
64 C USE dB UNIT FOR SPECTRUM PLOT.
65     DO 56 I=1,NR
66 56   X(I)=20.0*ALOGT(ABS(X(I)))
67 C INITIALIZE PARAMETERS FOR SPECTRUM PLOT.
68     XMIN=0.0
69     XMAX=25000.0
70     YMIN=-140.0
71     YMAX=0.0
72     XDIV=-500.0
73     YDIV=2.0
74     YD=5.
75     XD=5.
76     IFIX=0
77 C
78 2   WRITE(1,104)
79 104  FORMAT(" SELECT PLOTTING DEVICES: LU,ID")
80     READ(1,*)LU,ID
81 C***** GRAPHIC SUBROUTINES *****
82     CALL PLOTX(IGCB,ID,1,LU)
83     CALL PEN(IGCB,1)
84     WRITE(LU,106)
85 106  FORMAT("VSS")
86     CALL SETAR(IGCB,1.5)
87     CALL VIEWP(IGCB,25.,105.,25.,80.)
88     CALL WINDW(IGCB,XMIN,XMAX,YMIN,YMAX)
89     CALL FXD(IGCB,IFIX)
90     CALL CSIZE(IGCB,2.5,0.3,0.)
91     CALL LGRID(IGCB,XDIV,YDIV,XMIN,0.,XD,YD,1.)
92     XA=XX(1)
93     YA=X(1)
94     CALL MOVE(IGCB,XA,YA)
95     CALL LINE(IGCB,0)
96     CALL PEN(IGCB,2)
97     DO 58 I=2,NR
98     XA=XX(I)

```

```
99 YA=X(I)
00 CALL DRAW(IGCB,XA,YA)
01 58 CONTINUE
02 CALL VIEWP(IGCB,0.,150.,0.,100.)
03 CALL WINDW(IGCB,0.,150.,0.,100.)
04 CALL MOVE(IGCB,70.,20.)
05 CALL CPLOT(IGCB,-11.,0.,0)
06 IF(IR.EQ.1)CALL CPLOT(IGCB,+1.,0.,0)
07 CALL PEN(IGCB,1)
08 CALL LABEL(IGCB)
09 IF(IR.EQ.1)GO TO 3
10 WRITE(LU,108)
11 108 FORMAT("FREQUENCY (Hz)")
12 GO TO 4
13 3 WRITE(LU,110)
14 110 FORMAT("TIME (MSEC.)")
15 4 CALL MOVE(IGCB,20.,49.)
16 CALL CPLOT(IGCB,0.,-2.,0)
17 IF(IR.EQ.1)CALL CPLOT(IGCB,0.,+1.,0)
18 CALL LDIR(IGCB,1.57)
19 CALL LABEL(IGCB)
20 IF(IR.EQ.1)GO TO 5
21 WRITE(LU,112)
22 112 FORMAT("FREQUENCY SPECTRUM (dB)")
23 GO TO 6
24 5 WRITE(LU,114)
25 114 FORMAT("AMPLITUDE (VOLT.)")
26 6 CALL PEN(IGCB,0)
27 WRITE(LU,116)
28 116 FORMAT("VS")
29 CALL PLOT(IGCB,ID,0)
30 C
31 C***** .THOMAS CHUNG. REVISED: 4 JUNE, 1982. *****
32 C
33 RETURN
34 END
```

```

01 FTN4,L
02 C*****
03 C*****
04 C*****          PROGRAM PROAP          *****
05 C*****          *****
06 C*****          OCTOBER 1981          *****
07 C*****          *****
08 C*****
09 $EMA(XYZ,0)
10     PROGRAM PROAP
11     COMMON /XYZ/ S(1024)
12 C***** NOTES *****
13 C THE AIM OF THIS PROGRAM IS TO CARRY OUT THE PRE-PROCESSING TECHNIQUES
14 C FOR ELT SIGNALS.
15 C THESE TECHNIQUES INCLUDE:
16 C     1) AN N/2-LAG (NORMALIZED) AUTOCORRELATION FUNCTION
17 C        OF THE ELT SIGNALS (GENERATED USING THE ARRAY
18 C        PROCESSOR).
19 C     2) WINDOW THE SIGNALS.
20 C     3) BANDPASS FILTERING (FAST CONVOLUTION USING ARRAY
21 C        PROCESSOR).
22 C THE ELT SIGNAL WAS SIMULATED IN THE PROGRAM ELTAP.
23 C THE SPOOL FILE FORMATS
24 C     :SL,11,DWFIR,RE
25 C     :SL,22,DSIG,RE
26 C     :SL,12,DPRO,WR
27 C HAVE TO BE TYPED PRIOR TO EXECUTING THE PROGRAM.
28 C THE FIRST COMMAND ALLOWS TO READ IN THE BANDPASS FILTER IMPULSE
29 C RESPONSE VALUES IF FILTERING IS NEEDED.
30 C THE SECOND COMMAND ALLOWS ELT SIGNAL DATA TO BE READ FROM
31 C THE DATA FILE DSIG INTO THIS PROGRAM. THE THIRD COMMAND INSTRUCTS
32 C THE PRE-PROCESSING VALUES TO BE STORED INTO THE DATA FILE DPRO.
33 C
34 C DEFINITION OF VARIABLES:
35 C IFLAG=      : 1-SET ERROR MESSAGE FLAG. 0-RELEASE FLAG.
36 C IACF=       : 0-FOR DON'T WANT ACF, 1-FOR PERFORMING N/2-LAG ACF.
37 C IWIND=      : 0-FOR DON'T WANT WINDOWING, 1-FOR WINDOWING ELT SIGNAL.
38 C IFIR=       : 0-FOR DON'T WANT FILTERING, 1-FOR PERFORMING FAST
39 C              CONVOLUTION.
40 C***** INPUT SECTION *****
41     WRITE(1,100)
42     WRITE(1,102)
43     WRITE(1,104)
44     WRITE(1,106)
45     WRITE(1,108)
46 100  FORMAT("..... DID YOU TYPE IN .....")
47 102  FORMAT(":SL,11,DWFIR,RE (IF FILTERING IS NEEDED)")
48 104  FORMAT(":SL,22,DSIG,RE (TO READ ELT SIGNAL VALUES)")
49 106  FORMAT(":SL,12,DPRO,WR (TO STORE PRE-PROCESSING VALUES)")
50 108  FORMAT("IF YES TYPE 1, OTHERWISE TYPE 0")
51     READ(1,*)IC
52     IF(IC.EQ.0)GO TO 1
53     WRITE(1,110)
54 110  FORMAT("WANT AUTOCORRELATION FUNCTION (0/1) ?")
55     READ(1,*)IACF
56     WRITE(1,112)
57 112  FORMAT("WANT WINDOWING (0/1) ?")
58     READ(1,*)IWIND

```

```

09      WRITE(1,114)
10  114  FORMAT("WANT FILTERING (0/1) ?")
11      READ(1,*)IFIR
12  C :SL,22,DSIG,RE. (GET ELT SIGNAL FROM THE DATA FILE DSIG).
13      READ(22)S
14  C SIMULATED ELT SIGNAL IS 512-DATA SAMPLE.
15      N=512
16      IFLAG=0
17  C***** CALL SUBROUTINES *****
18      IF(IACF.EQ.1)CALL ACF(N)
19      IF(IWIND.EQ.1)CALL WINDW(N,IFLAG)
20      IF(IFLAG.EQ.1)GO TO 1
21      IF(IFIR.EQ.1)CALL FIR(N)
22  C :SL,12,DPRO,WR (WRITE DATA FILE, THE PRE-PROCESSING VALUES ARE
23  C      STORED IN DPRO).
24      WRITE(12)S
25      GO TO 2
26  1     DO 50 I=1,3
27      WRITE(1,116)
28  116  FORMAT("..... WARNING !!! EXECUTE THE PROGRAM AGAIN .....")
29  50   CONTINUE
30  2     STOP
31      END
32  C***** AUTOCORRELATION FUNCTION *****
33  $EMA(XYZ,0)
34      SUBROUTINE ACF(N)
35      COMMON /XYZ/ S(1024)
36      DIMENSION SS(1024)
37  C*****
38  C AN N/2-LAG (NORMALIZED) AUTOCORRELATION FUNCTION IS PERFORMED, ON THE
39  C ELT SIGNAL, USING THE ARRAY PROCESSOR.
40  C THE VECTOR SS(.) IS A SERVICE VECTOR.
41  C
42      WRITE(1,100)
43  100  FORMAT("..... AUTOCORRELATION FUNCTION .....")
44      N1=N/2
45      NL=N+1
46      DO 50 I=1,N
47  50   SS(I)=S(I)
48      CALL APINT(0,0,ISTAT)
49      CALL APCLR
50      CALL APPUT(SS,1,N,2)
51      CALL APWD
52      CALL ACORT(1,NL,N1,N)
53      CALL APWR
54      CALL APGET(SS,NL,N1,2)
55      CALL APWD
56      CALL APRLE
57  C STORE THE NORMALIZED ACF VALUES IN THE ARRAY S(.).
58      DO 52 I=1,N1
59      S(N1+1-I)=SS(I)/FLOAT(N)
60  52   S(N1+I-1)=SS(I)/FLOAT(N)
61      S(N)=0.0
62      RETURN
63      END
64  C***** WINDOWING *****
65  $EMA(XYZ,0)
66      SUBROUTINE WINDW(N,IFLAG)
67      COMMON /XYZ/ S(1024)
68      DIMENSION W(512),WW(1024)

```

```

19 C*****
20 C THE ELT SIGNAL CAN BE WINDOWED BY ANY OF THE FOLLOWING WINDOW FUNCTIONS.
21 C TYPES ARE: RECTANGULAR, HAMMING, HANNING, BLACKMAN,
22 C     GENERALIZED HAMMING, TRIANGULAR AND KAISER.
23 C THE ARRAY WK(.) STORES THE WINDOW SAMPLES. WW(.) IS A SERVICE VECTOR.
24 C
25     WRITE(1,100)
26 100  FORMAT("..... WINDOWING .....")
27     WRITE(1,102)
28 102  FORMAT("SELECT WINDOW TYPES:")
29     WRITE(1,104)
30     WRITE(1,106)
31 104  FORMAT("1-KAISER, 2-RECTANGULAR, 3-HAMMING, 4-HANNING")
32 106  FORMAT("5-GENERALIZE HAMMING, 6-BLACKMAN, 7-TRIANGULAR")
33     READ(1,*)IW
34     IF(IW.GT.7)GO TO 10
35     PI=9.0*ATAN(1.0)
36     N1=(N+1)/2
37 C CHECK FOR EVEN (IEO=0) OR ODD (IEO=1) NUMBER OF SAMPLE.
38     IEO=N-(N/2)*2
39     GO TO(1,2,3,4,5,6,7), IEO
40 C
41 C KAISER WINDOW:
42 C
43 1     WRITE(1,108)
44 108  FORMAT("INPUT: BETA (4.0<BETA<10.0)")
45     READ(1,*)BETA
46     IF(BETA.LE.0.OR.BETA.GT.10.)GO TO 10
47     CALL KAISR(N,N1,IEO,BETA,W)
48     GO TO 9
49 C
50 C RECTANGULAR WINDOW:
51 C
52 2     DO 50 I=1,N1
53 50    WK(I)=1.0
54     GO TO 9
55 C
56 C HAMMING WINDOW:
57 C
58 3     ALPHA=0.54
59     GO TO 8
60 C
61 C HANNING WINDOW:
62 C
63 4     ALPHA=0.5
64     GO TO 8
65 C
66 C GENERALIZE HAMMING WINDOW:
67 C
68 5     WRITE(1,110)
69 110  FORMAT("INPUT: ALPHA (0.0<ALPHA<1.0)")
70     READ(1,*)ALPHA
71     IF(ALPHA.LE.0.OR.ALPHA.GT.1.)GO TO 10
72 8     FN=N-1
73     DO 52 I=1,N1
74     FI=I-1
75     IF(IEO.EQ.0)FI=FI+0.5
76     WK(I)=ALPHA+(1.0-ALPHA)*COS((PI*FI)/FN)
77 52    CONTINUE
78     GO TO 9

```

```

79 C
80 C BLACKMAN WINDOW:
81 C
82 6      FN=N-1
83      DO 54 I=1,N1
84      FI=I-1
85      IF<IEO.EQ.0>FI=FI+0.5
86      ARG1=PI*FI/FN
87      ARG2=PI*2.0*FI/FN
88      W<I>=0.42+0.5*COS<ARG1>+0.08*COS<ARG2>
89 54    CONTINUE
90      GO TO 9
91 C
92 C TRIANGULAR WINDOW:
93 C
94 7      FN=N1
95      DO 56 I=1,N1
96      XI=I-1
97      IF<IEO.EQ.0>XI=XI+0.5
98      W<I>=1.0-XI/FN
99 56    CONTINUE
100 C
101 C WINDOWS THE ELT SIGNAL.
102 C
103 9      DO 58 I=1,N1
104      WW<I>=W<N1+1-I>
105 58    WW<N+1-I>=WW<I>
106 C STORE THE WINDOWED SIGNAL IN THE ARRAY S(.),
107      DO 60 I=1,N
108 60    S<I>=S<I>*WW<I>
109      RETURN
110 10    IFLAG=1
111      RETURN
112      END
113 C
114 C KAISER WINDOW SUBROUTINE.
115 C
116      SUBROUTINE KAISR<N,N1,IEO,BETA,W>
117      DIMENSION W<1>
118      REAL INO
119      BES=INO<BETA>
120      XIND=FLOAT<N-1>*FLOAT<N-1>
121      DO 50 I=1,N1
122      XI=I-1
123      IF<IEO.EQ.0>XI=XI+0.5
124      XI=4.0*XI*XI
125      W<I>=INO<BETA*SQRT<1.-XI/XIND>>
126      W<I>=W<I>/BES
127 50    CONTINUE
128      RETURN
129      END
130 C
131 C BESSEL FUNCTION <UP TO 25 TERMS>
132 C
133      REAL FUNCTION INO<Q>
134      Y=Q/2.
135      T=1.E-08
136      E=1.
137      DE=1.
138      DO 50 I=1,25

```

```

39      XI=I
40      DE=DE*Y/XI
41      SDE=DE*DE
42      E=E+SDE
43      IF(E*T-SDE)50,50,1
44  50   CONTINUE
45      INO=E
46      RETURN
47      END
48  C***** FILTERING *****
49  $EMA(XYZ,0)
50      SUBROUTINE FIR(N)
51      COMMON /XYZ/ S(1024)
52      DIMENSION SS(1024),Z(1024)
53  C*****
54  C FAST CONVOLUTION IS PERFORMED USING ARRAY PROCESSOR IN THIS SUBROUTINE.
55  C THE IMPULSE RESPONSE OF THE BANDPASS FILTER IS IN THE DATA FILE DWFIR.
56  C THE ARRAYS SS(.) AND Z(.) ARE THE SERVICE VECTORS.
57  C IFL IS THE SAME FILTER LENGTH WHICH HAS BEEN USED IN THE PROGRAM WFIR.
58  C
59      WRITE(1,100)
60  100  FORMAT("..... FILTERING .....")
61      WRITE(1,102)
62  102  FORMAT("INPUT: THE FILTER LENGTH USED IN THE PROGRAM WFIR")
63      READ(1,*)IFL
64  C READ THE BANDPASS FILTER IMPULSE RESPONSES.
65  C:SL,11,DWFIR,RE
66      READ(11)SS
67      DO 50 I=1,N
68  50   Z(I)=S(I)
69      NFFT=1024
70      ITRACE=0
71      IFILT=ITRACE+NFFT
72      CALL APINT(0,0,ISTAT)
73      CALL APCLR
74      CALL APPUT(Z,ITRACE,N,2)
75      CALL APPUT(SS,IFILT,IFL,2)
76      CALL APWD
77      CALL VCLR(ITRACE+N,1,NFFT-N)
78      CALL VCLR(IFILT+IFL,1,NFFT-IFL)
79      CALL RFFT(ITRACE,NFFT,1)
80      CALL RFFT(IFILT,NFFT,1)
81      CALL VMUL(ITRACE,1,IFILT,1,ITRACE,1,2)
82      CALL CYMUL(ITRACE+2,2,IFILT+2,2,ITRACE+2,2,N-1,1)
83      CALL RFFTC(ITRACE,NFFT,0,-1)
84      CALL RFFT(ITRACE,NFFT,-1)
85      CALL APWR
86      CALL APGET(SS,ITRACE,NFFT,2)
87      CALL APWD
88      CALL APRLE
89  C STORE THE FILTERED SIGNAL IN THE ARRAY S(.).
90      DO 52 I=1,NFFT
91  52   S(I)=SS(I)
92  C
93  C***** .THOMAS CHUNG. REVISED: 24 JUNE, 1982. *****
94  C
95      RETURN
96      END

```

```

01 FTN4,L
02 C*****
03 C*****
04 C***** PROGRAM SPMAP *****
05 C*****
06 C***** OCTOBER 1981 *****
07 C*****
08 C*****
09 $EMA(XYZ,0)
10 PROGRAM SPMAP
11 COMMON /XYZ/ S(1024)
12 C***** NOTES *****
13 C THIS PROGRAM USES ARRAY PROCESSOR TO CALCULATE THE FAST FOURIER
14 C TRANSFORM AND MAXIMUM ENTROPY METHOD SPECTRUM OF THE ELT SIGNAL.
15 C THE ELT SIGNAL WAS SIMULATED IN THE PROGRAM ELTAP, AND HAVE PRE-
16 C PROCESSED IN THE PROGRAM PROAP.
17 C THE SPOOL FILE FORMATS
18 C :SL,22,DSIG,RE
19 C OR(:SL,22,DPRO,RE)
20 C :SL,16,DSPEC,WR
21 C HAVE TO BE TYPED PRIOR TO EXECUTING THE PROGRAM.
22 C THE FIRST COMMAND ALLOWS ELT SIGNAL DATA TO BE READ FROM THE
23 C THE DATA FILE DSIG INTO THIS PROGRAM. THE SECOND COMMAND GETS THE
24 C PRE-PROCESSED SIGNAL FROM DPRO IF PRE-PROCESSED SIGNAL IS REQUIRED.
25 C THE SPECTRUM VALUES ARE STORED INTO THE DATA FILE DSPEC.
26 C
27 C DEFINITION OF VARIABLES:
28 C IFLAG= : 1-SET ERROR MESSAGE FLAG, 0-RELEASE FLAG.
29 C IFM= : 0-FOR CALCULATE FFT SPECTRUM, 1-FOR CALCULATE MEM
30 C SPECTRUM.
31 C THL= : IS THE THRESHOLD LEVEL (-dB) AT WHICH THE FREQUENCIES
32 C ARE DETECTED.
33 C
34 C***** INPUT SECTION *****
35 WRITE(1,100)
36 WRITE(1,102)
37 WRITE(1,104)
38 WRITE(1,106)
39 WRITE(1,108)
40 100 FORMAT("..... DID YOU TYPE IN .....")
41 102 FORMAT(":SL,22,DSIG,RE (TO READ ELT SIGNAL VALUE)")
42 104 FORMAT(" OR ( :SL,22,DPRO,RE (IF PRE-PROCESSING IS NEEDED) )")
43 106 FORMAT(":SL,16,DSPEC,WR (TO STORE SPECTRUM VALUE)")
44 108 FORMAT("IF YES TYPE 1, OTHERWISE TYPE 0")
45 READ(1,*)IC
46 IF(IC.EQ.0)GO TO 1
47 WRITE(1,110)
48 110 FORMAT("WANT FFT OR MEM (0/1) ?")
49 READ(1,*)IFM
50 WRITE(1,112)
51 112 FORMAT("INPUT: THRESHOLD LEVEL (IN -X dB)")
52 READ(1,*)THL
53 IF(THL.GT.0.)GO TO 1
54 C READ DATA FILE DSIG OR DPRO
55 C :SL,22,DSIG,RE (TO READ ELT SIGNALS)
56 C :SL,22,DPRO,RE (TO READ PRE-PROCESSED ELT SIGNALS)
57 READ(22)S
58 N=512

```

```

59      IFLAG=0
60 C***** CALL SUBROUTINES *****
61      IF<IFM.EQ.0>CALL FFT<N,THL>
62      IF<IFM.EQ.1>CALL MEM<N,THL,IFLAG>
63      IF<IFLAG.EQ.1>GO TO 1
64 C :SL,16 DSPEC,WR <WRITE DATA FILE, THE SPECTRUM VALUES ARE STORED
65 C           IN DSPEC>.
66      WRITE<16>S
67      GO TO 2
68 1     DO 50 I=1,3
69      WRITE<1,114>
70 114   FORMAT<"..... WARNING !!!           EXECUTE THE PROGRAM AGAIN .....>
71 50    CONTINUE
72 2     STOP
73      END
74 C***** FFT SPECTRUM *****
75 $EMA<XYZ,0>
76      SUBROUTINE FFT<N,THL>
77      COMMON /XYZ/ S<1024>
78      DIMENSION SS<1024>
79 C*****
80 C NFFT-POINT IN PLACE FAST FOURIER TRANSFORM IS PERFORMED BY MEANS
81 C OF ARRAY PROCESSOR.
82 C THE POWER SPECTRUM IS IN TERM OF dB UNIT.
83 C
84 C DEFINITION OF VARIABLES:
85 C TSTEP=           : TIME SAMPLING OF ELT SIGNAL, AT TWICE THE NYQUIST RATE.
86 C FSTEP=           : FREQUENCY RESOLUTION STEP OF SPECTRUM.
87 C ZRO=             : IS THE LOWER LIMIT OF POWER SPECTRUM VALUE.
88 C
89      WRITE<1,100>
90 100   FORMAT<"..... FFT SPECTRUM .....>
91      WRITE<1,102>
92 102   FORMAT<"WAS ACF <0/1> OR FIR <0/1> NEEDED IN PROGRAM PROAP ?>
93      READ<1,*>IACF,IFIR
94      NFFT=N
95 C AFTER FILTERING, THE OUTPUT HAS Y=N+IFL-1 POINTS, WHERE N IS THE
96 C INPUT SAMPLES AND IFL IS THE FILTER LENGTH.
97 C IN ORDER TO PERFORM FFT, THE Y-POINT HAS TO BE EQUAL TO THE
98 C NEAREST NFFT=X**2.
99      IF<IFIR.EQ.1>NFFT=1024
100     DO 50 I=1,NFFT
101 50    SS<I>=S<I>
102     TSTEP=1.0/50000.0
103     ZRO=1.0E-7
104     ONE=1.0
105     IL=NFFT+2
106     FSTEP=1.0/<TSTEP*FLOAT<NFFT>>
107 C
108 C PERFORM NFFT-POINT IN PLACE FFT.
109 C
110     CALL APINT<0,0,ISTAT>
111     CALL APCLR
112     CALL APPUT<ZRO,0,1,2>
113     CALL APPUT<ONE,1,1,2>
114     CALL APPUT<SS,2,NFFT,2>
115     CALL APWD
116     CALL CVREL<2,1,IL,2,NFFT>
117     CALL CFFT<IL,NFFT,1>
118     CALL CFFT<IL,NFFT>

```

```

19 CALL CVMASK(IL,2,2,1,NFFT)
20 CALL APWR
21 IF(IACF.EQ.0)GO TO 1
22 CALL VSQRT(2,1,2,1,NFFT)
23 CALL APWR
24 1 CONTINUE
25 CALL MAXV(2,1,IL,NFFT)
26 CALL VFILL(IL,IL,1,NFFT)
27 CALL QVDIV(IL,1,2,1,2,1,NFFT)
28 CALL VCLIP(2,1,0,1,2,1,NFFT)
29 CALL VDBPR(2,1,1,2,1,NFFT)
30 CALL APWR
31 CALL APGET(SS,2,NFFT,2)
32 CALL APWD
33 CALL APRLE
34 C THE FFT SPECTRUM VALUES ARE STORED IN THE VECTOR S(.), AND
35 C THE ARRAY SS(.) STORES THE FREQUENCY RESOLUTION.
36 N1=NFFT/2
37 DO 52 I=1,N1
38 S(I)=SS(I)
39 SS(I)=FLOAT(I-1)*FSTEP
40 C SEARCH FOR THE FREQUENCY RESOLUTIONS WHICH HAVE SPECTRAL VALUES
41 C GREATER THAN THE THRESHOLD VALUE.
42 IF(S(I).LT.THL)GO TO 52
43 WRITE(1,104)SS(I),S(I)
44 104 FORMAT(1X,"FREQUENCY RESOLUTION=",F12.9," Hz",3X,
45 + "SPECTRUM AMPLITUDE=",F5.2," dB")
46 52 CONTINUE
47 RETURN
48 END
49 C***** MEM SPECTRUM *****
50 $ENAC(XYZ,0)
51 SUBROUTINE MEM(N,THL,IFLAG)
52 COMMON /XYZ/ S(1024)
53 DIMENSION SS(1024),A(101)
54 C*****
55 C ARRAY PROCESSOR IS EMPLOYED TO CALCULATE THE MAXIMUM ENTROPY METHOD
56 C FILTER COEFFICIENTS. THESE ARE STORED IN THE ARRAY A(.).
57 C THE MEM FILTER ORDER CANNOT BE MORE THAN 100.
58 C THE MEM SPECTRUM IS CALCULATED IN TERM OF DECIBEL UNIT.
59 C
60 C DEFINITION OF VARIABLES:
61 C IORDER= : MEM FILTER ORDER, MAXIMUM IS 100.
62 C PTEST= : LOWER LIMIT OF OUTPUT POWER OF PREDICTION ERROR FILTER.
63 C RLIM= : LOWER LIMIT OF DENOMINATOR IN CALCULATING THE
64 C MEM COEFFICIENTS.
65 C ZRO= : LOWER LIMIT OF POWER SPECTRUM VALUES.
66 C TSTEP= : TIME SAMPLING OF SIGNAL AT TWICE THE NYQUIST RATE.
67 C FSTEP= : FREQUENCY RESOLUTION STEP OF SPECTRUM.
68 C SFREQ= : LOWER FREQUENCY OF THE SPECTRUM BANDWIDTH.
69 C FFREQ= : UPPER FREQUENCY OF THE SPECTRUM BANDWIDTH.
70 C P= : OUTPUT POWER OF PREDICTION ERROR FILTER.
71 C
72 WRITE(1,100)
73 100 FORMAT("..... MEM SPECTRUM .....")
74 WRITE(1,102)
75 102 FORMAT("INPUT: MEM FILTER ORDER ( 1 < ORDER < 101 )")
76 READ(1,*)IORDER
77 IF(IORDER.GT.100.OR.IORDER.LT.2)GO TO 1
78 WRITE(1,104)

```

```

79 104  FORMAT("WAS FILTERING NEEDED IN PRE-PROCESSING PROGRAM (0/1)?")
80      READ(1,*)IFIR
81      IF(IFIR.EQ.0)GO TO 2
82      WRITE(1,106)
83 106  FORMAT("INPUT: THE FILTER LENGTH USED IN THE PROGRAM WFIR")
84      READ(1,*)IFL
85  C FILTER OUTPUT HAS Y=N+IFL-1 POINTS.
86      N=N+IFL-1
87      IF(N.GT.1024)GO TO 1
88  2    DO 50 I=1,N
89  50    SS(I)=S(I)
90  C INITIALIZE PARAMETERS FOR CALCULATING MEM SPECTRUM.
91      PTEST=1.0E-15
92      RLIM=1.0E-10
93      ONE=1.0
94      TSTEP=1.0/50000.
95      SFREQ=0.0
96      FFREQ=25000.
97      FSTEP=(FFREQ-SFREQ)/FLOAT(N)
98      FSTP=FSTEP*TSTEP
99      F=SFREQ*TSTEP
00      ISTEP1=1001
01      ISTEP2=ISTEP1+N
02      ISTEP3=ISTEP2+N
03      ISTEP4=ISTEP3+N
04  C
05  C CALCULATE MEM COEFFICIENTS.
06  C
07      CALL APINT(0,0,ISTAT)
08      CALL APCLR
09      CALL APPUT(ONE,1,1,2)
10      CALL APPUT(SS,ISTEP1,N,2)
11      CALL APWD
12      CALL MEASV(ISTEP1,1,0,N)
13      CALL APWR
14      DO 52 I=1,IORDER
15      IP1=I+1
16      NLM=N-I
17      CALL VCLR(IP1,1,IORDER+1-I)
18      CALL VRVRS(1,1,IP1)
19      CALL CONV(ISTEP1,1,1,1,ISTEP2,1,NLM,IP1)
20      CALL CONV(ISTEP1,1,1+I,-1,ISTEP3,1,NLM,IP1)
21      CALL DOTPR(ISTEP2,1,ISTEP3,1,103,NLM)
22      CALL VMMA(ISTEP2,1,ISTEP2,1,ISTEP3,1,ISTEP3,1,ISTEP4,1,NLM)
23      CALL SYE(ISTEP4,1,102,NLM)
24      CALL VRVRS(1,1,IP1)
25      CALL QVDIV(102,1,103,1,103,1,1)
26      CALL VTSML(103,1,4002B,103,1,1)
27      CALL VNEG(103,1,103,1,1)
28      CALL VSQ(103,1,104,1,1)
29      CALL VNEG(104,1,104,1,1)
30      CALL VTSAD(104,1,4001B,104,1,1)
31      CALL VMUL(104,1,0,1,0,1,1)
32      CALL VSMUL(IP1,-1,103,500,1,IP1)
33      CALL QVADD(1,1,500,1,500,1,IP1)
34      CALL QVMOV(500,1,1,1,IP1)
35      CALL APWR
36  52   CONTINUE
37      CALL APGET(A,1,IP1,2)
38      CALL APGET(P,0,1,2)

```

```

39 CALL APGET(DENOM,102,1,2)
40 CALL APWD
41 CALL APRLE
42 C
43 MMAX=IP1
44 IF(P.LT.PTEST)GO TO 3
45 IF(DENOM.LT.RLIM)GO TO 4
46 GO TO 5
47 3 WRITE(1,108)P,PTEST
48 108 FORMAT("WARNING: P=",E12.9," IS LESS THAN PTEST=",E12.9)
49 GO TO 5
50 4 WRITE(1,110)DENOM,RLIM
51 110 FORMAT("WARNING: DENOM=",E12.9," IS LESS THAN RLIM=",E12.9)
52 MMAX=I
53 5 WRITE(1,112)P,IORDER
54 112 FORMAT("OUTPUT POWER OF PREDICTION ERROR FILTER IS: ",
55 + E12.9," , OF ORDER: ",I3)
56 C
57 C CALCULATE MEM SPECTRUM IN dB, THE RESULTS ARE STORED IN THE
58 C ARRAY S(.).
59 C
60 ZRO=1.0E-7
61 AMAX=0.0
62 DO 54 I=1,N
63 ARG=8.0*ATAN(1.0)*F
64 DEN1=1.0
65 DEN2=0.0
66 DO 56 J=2,MMAX
67 PHI=ARG*FLOAT(J-1)
68 DEN1=DEN1+A(J)*COS(PHI)
69 56 DEN2=DEN2+A(J)*SIN(PHI)
70 S(I)=P/(DEN1*DEN1+DEN2*DEN2)
71 IF(S(I).GT.AMAX)AMAX=S(I)
72 54 F=F+FSTEP
73 DO 58 I=1,N
74 S(I)=S(I)/AMAX
75 IF(S(I).LT.ZRO)S(I)=ZRO
76 S(I)=10.0*ALOGT(S(I))
77 SS(I)=FLOAT(I-1)*FSTEP
78 C SEARCH FOR THE FREQUENCY RESOLUTIONS WHICH HAVE SPECTRAL VALUES
79 C GREATER THAN THE THRESHOLD VALUE.
80 IF(S(I).LT.THL)GO TO 58
81 WRITE(1,114)SS(I),S(I)
82 114 FORMAT(1X,"FREQUENCY RESOLUTION=",F12.9," Hz",3X,
83 + "SPECTRUM AMPLITUDE=",F5.2," dB")
84 58 CONTINUE
85 RETURN
86 I IFLAG=1
87 C
88 C***** .THOMAS CHUNG. REVISED: 22 JUNE, 1982. *****
89 C
90 RETURN
91 END

```

```

01 FTN4,L
02 C*****
03 C*****
04 C***** PROGRAM CURVE *****
05 C*****
06 C***** OCTOBER 1981 *****
07 C*****
08 C*****
09 $EMA(XYZ,0)
10 PROGRAM CURVE
11 COMMON /XYZ/ X(1024),S(1024)
12 DIMENSION IGC(192)
13 C***** NOTES *****
14 C THIS PROGRAM USES HP1000 GRAPHIC PACKAGE TO PLOT THE ELT SIGNAL OR
15 C PRE-PROCESSED SIGNAL, AND THE FAST FOURIER TRANSFORM SPECTRUM OR
16 C MAXIMUM ENTROPY METHOD SPECTRUM. THESE VALUES ARE STORED IN THE
17 C DATA FILES DSIG, DPRO AND DSPEC RESPECTIVELY.
18 C IF PLOT ELT SIGNAL, THE SPOOL FILE FORMAT IS
19 C :SL,22,DSIG,RE
20 C OR <IF PLOT PRE-PROCESSED SIGNAL, THE SPOOL FILE FORMAT IS
21 C :SL,22,DPRO,RE>
22 C IF PLOT SPECTRUM, THE SPOOL FILE FORMAT IS
23 C :SL,17,DSPEC,RE
24 C THE SIGNAL AND SPECTRUM CAN BE PLOTTED BY INPUTTING
25 C LU=40, ID=2 : ON PLOTTER
26 C LU=58, ID=4 : ON LINE PRINTER
27 C LU=1, ID=1 : ON GRAPHIC TERMINAL
28 C
29 WRITE(1,100)
30 WRITE(1,102)
31 WRITE(1,104)
32 WRITE(1,106)
33 WRITE(1,108)
34 100 FORMAT("..... DID YOU TYPE IN .....")
35 102 FORMAT(":SL,22,DSIG,RE (IF PLOT SIGNAL)")
36 104 FORMAT(" OR (:SL,22,DPRO,RE (IF PLOT PRE-PROCESSED SIGNALS) )")
37 106 FORMAT(":SL,17,DSPEC,RE (IF PLOT SPECTRUM)")
38 108 FORMAT("IF YES TYPE 1, OTHERWISE TYPE 0")
39 READ(1,*)IC
40 IF(IC.EQ.0)GO TO 1
41 WRITE(1,110)
42 110 FORMAT("SELECT PLOTTING DEVICE: LU,ID")
43 READ(1,*)LU,ID
44 WRITE(1,112)
45 112 FORMAT("PRE-PROCESSED ? 0-NO, 1-ACF OR WINDOWING, 2-FIR")
46 READ(1,*)IPP
47 WRITE(1,114)
48 114 FORMAT("PLOT ? 1-SIGNAL OR PRE-PROCESSED SIGNAL, 2-FFT, 3-MEM")
49 READ(1,*)ISS
50 N=512
51 IF(IPP.LT.2.OR.ISS.LT.3)GO TO 2
52 WRITE(1,116)
53 116 FORMAT("INPUT: THE FILTER LENGTH USED IN THE PROGRAM WFIR")
54 READ(1,*)IFL
55 2 XMIN=0.0
56 IF(ISS.GT.1)GO TO 3
57 C
58 C PLOT ELT SIGNAL OR PRE-PROCESSED SIGNAL.

```

```

59 C
60 C :SL,22,DSIG,RE (READ DATA FOR PLOTTING SIGNAL),
61 C :SL,22,DPRO,RE (READ DATA FOR PLOTTING PRE-PROCESSED SIGNAL),
62 READ(22)S
63 TSTEP=1.0/50000.0
64 IF(IPP.EQ.2)N=N+IFL-1
65 IF(N.GT.1024)GO TO 1
66 C X(.) IS THE ARRAY OF TIME AXIS IN MILLISECONDS.
67 C S(.) IS THE SIGNAL DATA.
68 DO 50 I=1,N
69 50 X(I)=FLOAT(I-1)*TSTEP*1000.0
70 C INITIALIZE PARAMETERS FOR PLOTTING SIGNAL.
71 XMAX=X(N)
72 XDIV=-(XMAX/20.0)
73 YDIV=0.25
74 YMIN=-0.05
75 YMAX=0.05
76 XD=2.
77 YD=1.
78 IFIX=3
79 DO 52 I=1,N
80 IF(S(I).GT.YMAX)YMAX=S(I)
81 52 IF(S(I).LT.YMIN)YMIN=S(I)
82 WRITE(1,118)YMAX,YMIN,YDIV,YD
83 118 FORMAT("YMAX=",F12.9," YMIN=",F12.9," YDIV=",F3.2," YD=",F2.1)
84 GO TO 4
85 C
86 C PLOT SPECTRUM
87 C
88 C :SL,17,DSPEC,RE (READ DATA FOR PLOTTING SPECTRUM)
89 3 READ(17)S
90 IF(IPP.EQ.2.AND.ISS.EQ.2)N=1024
91 IF(IPP.EQ.2.AND.ISS.EQ.3)N=N+IFL-1
92 IF(N.GT.1024)GO TO 1
93 FSTEP=25000.0/FLOAT(N)
94 IF(ISS.EQ.2)FSTEP=50000.0/FLOAT(N)
95 IF(ISS.EQ.2)N=N/2
96 C X(.) IS THE ARRAY OF FREQUENCY AXIS, S(.) IS THE SPECTRUM DATA.
97 DO 54 I=1,N
98 54 X(I)=FLOAT(I-1)*FSTEP
99 C INITIALIZE PARAMETERS FOR PLOTTING SPECTRUM.
100 XMAX=25000.
101 XDIV=-500.
102 YDIV=2.0
103 XD=5.
104 YD=5.
105 IFIX=0
106 4 WRITE(1,120)
107 120 FORMAT("INPUT: THE UPPER AND LOWER BOUNDS FOR Y-AXIS")
108 READ(1,*)YMAX,YMIN
109 IF(YMAX.LE.YMIN.OR.YMIN.LT.-70.)GO TO 1
110 WRITE(1,122)
111 122 FORMAT("WANT FRAME (0/1) ?")
112 READ(1,*)MP
113 WRITE(1,124)
114 124 FORMAT("SELECT LINE STYLE: 0,1,2,3,4,5,6")
115 READ(1,*)ICASE
116 IF(ICASE.GT.6)ICASE=0
117 C***** GRAPHIC SUBROUTINES *****
118 CALL PLOTX(IGCB,ID,1,LU)

```

```
19 IF(MP.EQ.1)CALL PEN(IGCB,1)
20 WRITE(LU,126)
21 126 FORMAT("VS")
22 CALL SETAR(IGCB,1,5)
23 CALL VIEWP(IGCB,25.,105.,25.,80.)
24 CALL WINDW(IGCB,XMIN,XMAX,YMIN,YMAX)
25 CALL FXD(IGCB,IFIX)
26 CALL CSIZE(IGCB,2.50,0.3,0.)
27 IF(MP.EQ.1)CALL LGRID(IGCB,XDIV,YDIV,XMIN,0.,XD,YD,1.)
28 WRITE(1,128)
29 128 FORMAT("SELECT PEN NUMBER: 1,2,3,4")
30 READ(1,*)IPN
31 IF(IPN.GT.4)IPN=1
32 CALL PEN(IGCB,IPN)
33 XA=X(1)
34 YA=S(1)
35 CALL LINE(IGCB,ICASE)
36 CALL MOVE(IGCB,XA,YA)
37 DO 56 I=2,N
38 XA=X(I)
39 YA=S(I)
40 CALL DRAW(IGCB,XA,YA)
41 56 CONTINUE
42 IF(MP.EQ.0)GO TO 5
43 CALL VIEWP(IGCB,0.,150.,0.,100.)
44 CALL WINDW(IGCB,0.,150.,0.,100.)
45 CALL MOVE(IGCB,70.,20.)
46 CALL CPLOT(IGCB,-11.,0.,0)
47 IF(ISS.EQ.1)CALL CPLOT(IGCB,+1.,0.,0)
48 CALL PEN(IGCB,1)
49 CALL LABEL(IGCB)
50 IF(ISS.EQ.1)GO TO 6
51 WRITE(LU,130)
52 130 FORMAT("FREQUENCY (Hz)")
53 GO TO 7
54 6 WRITE(LU,132)
55 132 FORMAT("TIME (MSEC.)")
56 7 CALL MOVE(IGCB,20.,49.)
57 CALL CPLOT(IGCB,0.,-2.,0)
58 IF(ISS.EQ.1)CALL CPLOT(IGCB,0.,+1.,0)
59 CALL LDIR(IGCB,1.57)
60 CALL LABEL(IGCB)
61 IF(ISS.EQ.1)GO TO 8
62 WRITE(LU,134)
63 134 FORMAT("SPECTRAL DENSITY (dB)")
64 GO TO 5
65 8 WRITE(LU,136)
66 136 FORMAT("AMPLITUDE")
67 5 CALL PEN(IGCB,0)
68 WRITE(LU,138)
69 138 FORMAT("VS")
70 CALL PLOT(IGCB,ID,0)
71 IF(ISS.EQ.1)GO TO 9
72 WRITE(1,140)
73 140 FORMAT("WANT BLOW UP PLOT (0/1) ?")
74 READ(1,*)IBU
75 IF(IBU.EQ.0)GO TO 9
76 11 WRITE(1,142)
77 142 FORMAT("INPUT: XMIN,XMAX,XDIV")
78 READ(1,*)XMIN,XMAX,XDIV
```

79 IF(XMIN.GE.XMAX.OR.XMIN.LT.0.OR.XMAX.GT.25000.)GO TO 10  
80 XDIV=XDIV\*(-1.0)  
81 XD=5. 265  
82 YDIV=1.  
83 YD=5.  
84 GO TO 4  
85 10 WRITE(1,146)  
86 146 FORMAT("..... WARNING !!! ENTER VALUES AGAIN .....")  
87 GO TO 11  
88 1 DO 58 I=1,3  
89 WRITE(1,144)  
90 144 FORMAT("..... WARNING !!! EXECUTE THE PROGRAM AGAIN .....")  
91 58 CONTINUE  
92 C  
93 C\*\*\*\*\* .THOMAS CHUNG, REVISED: 14 JUNE, 1982. \*\*\*\*\*  
94 C  
95 9 STOP  
96 END

## APPENDIX E

### CALCULATING THE MEM SPECTRA OF A PULSE-MODULATED RANDOM PHASE SIGNAL

#### BASED ON THE AVERAGING TECHNIQUE

One of the properties of the ELT signal is that the duration of pulses varies with time. The increase in duration implies the nulls between pulses decrease. We have mentioned in Section 3.2 that the spectral performance of the distress signal is likely to benefit by this consequence since the ELT signal has a period of a quarter of a second. We section the received signal into blocks of 512-samples each. The first eight blocks of the signal (81.89 ms) are processed, in this analysis, using the 'ELT+MEM<sub>ave</sub>', 'ELT+ACFMEM<sub>ave</sub>' and 'ELT+ACF+FIRMEM<sub>ave</sub>'. The subscript 'ave' differentiates itself from the configurations discussed in Section 3.3. For each block of the signal, the prediction error power and a set of prediction error coefficients at filter order 2 and 10 are determined. By taking the average of these parameters, over the required number of blocks, the MEM spectral estimate is evaluated according to Eq. (2.11). The processing results are compared with those obtained from the first block of the signal (which is 10.22 ms in length).

Fig. E.1 to Fig. E.3 show the MEM spectra of the three configurations at filter order 2. The processed ELT signal (at carrier frequency 12832 Hz) is pulse-modulated random phase and linear frequency sweep. The averaging technique has the effect of sharpening the MEM

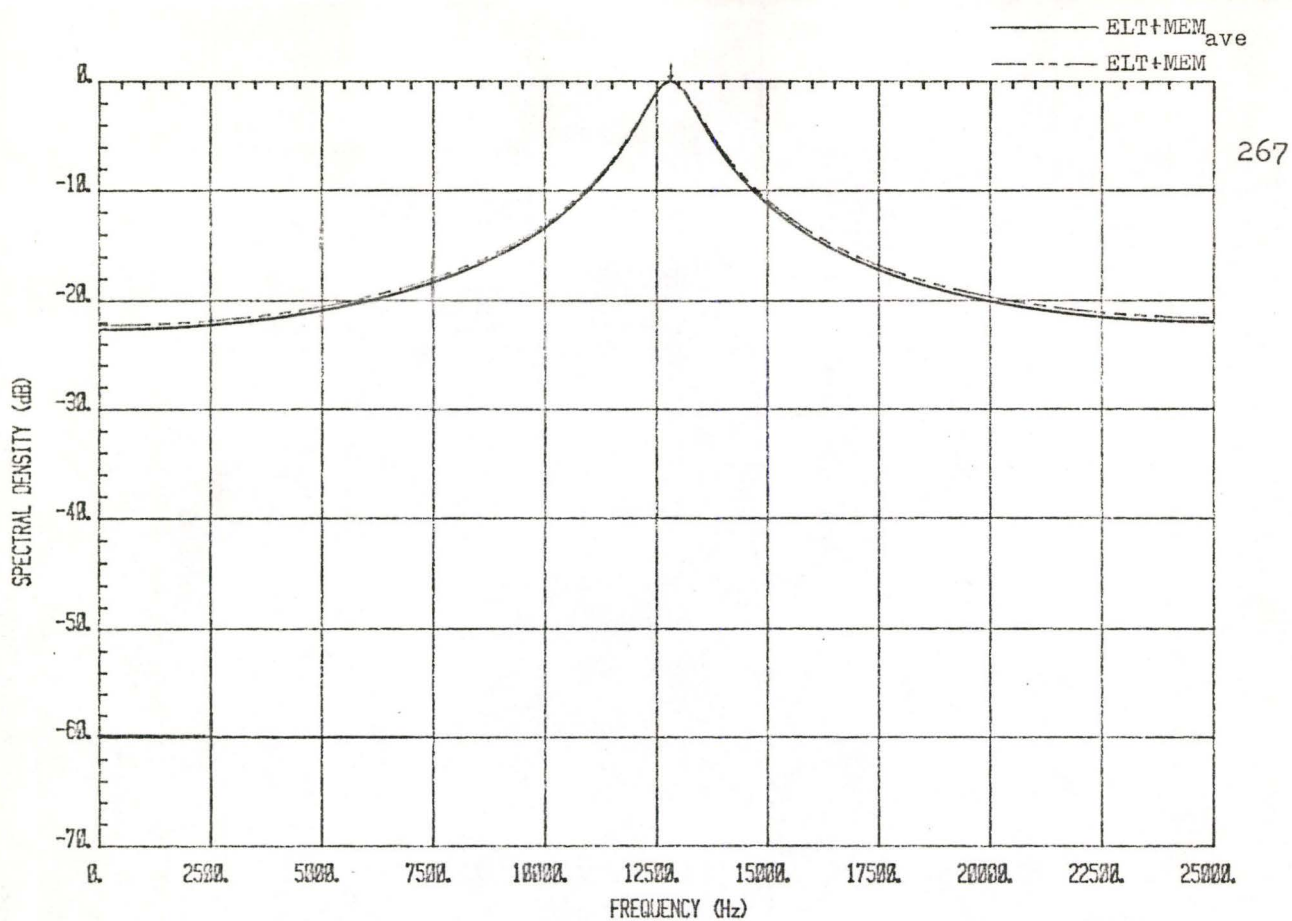


Fig. E.1: The MEM spectra (filter order 2) of random phase, pulse-modulated signal using averaging technique. Carrier frequency is 12832 Hz.

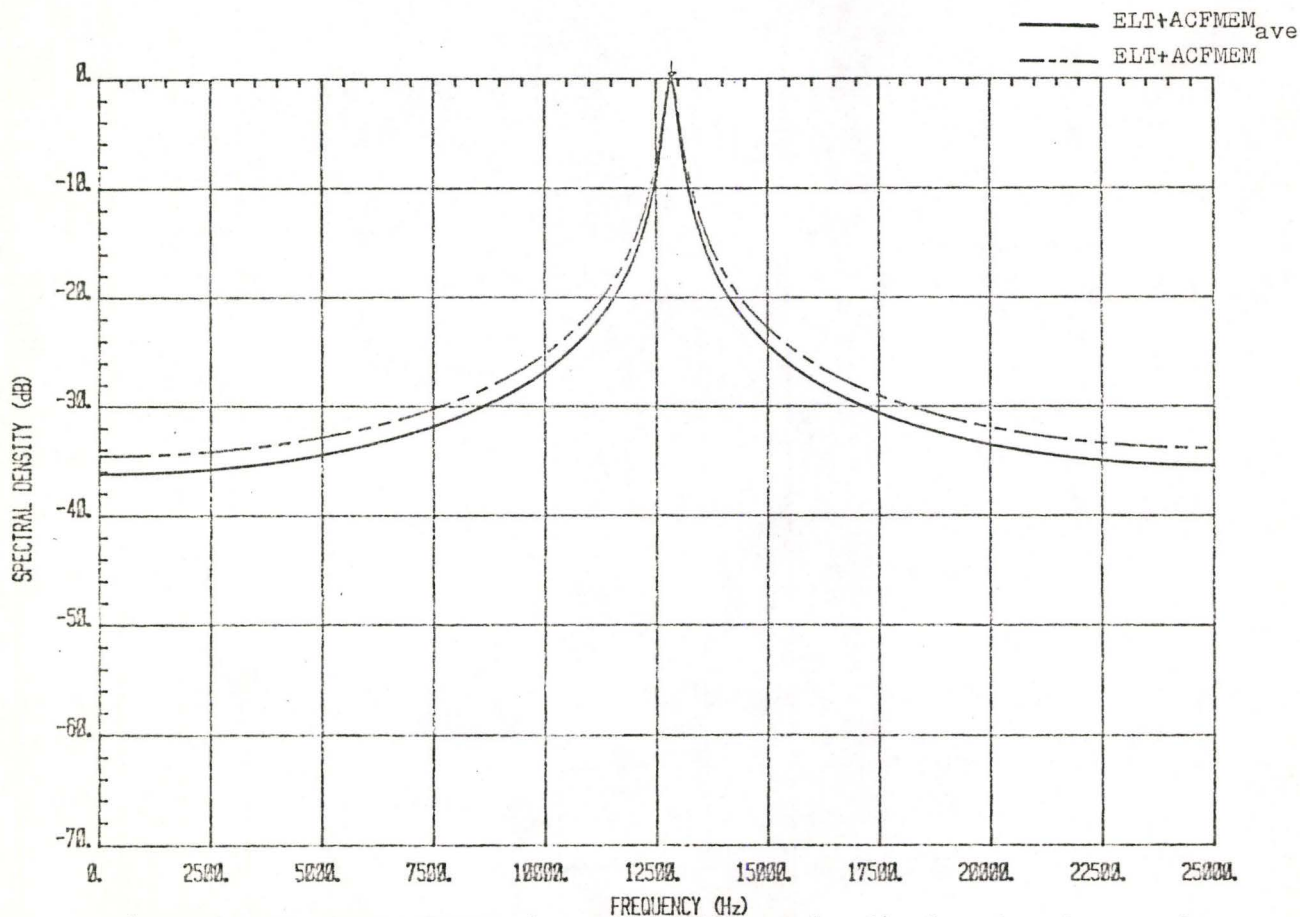
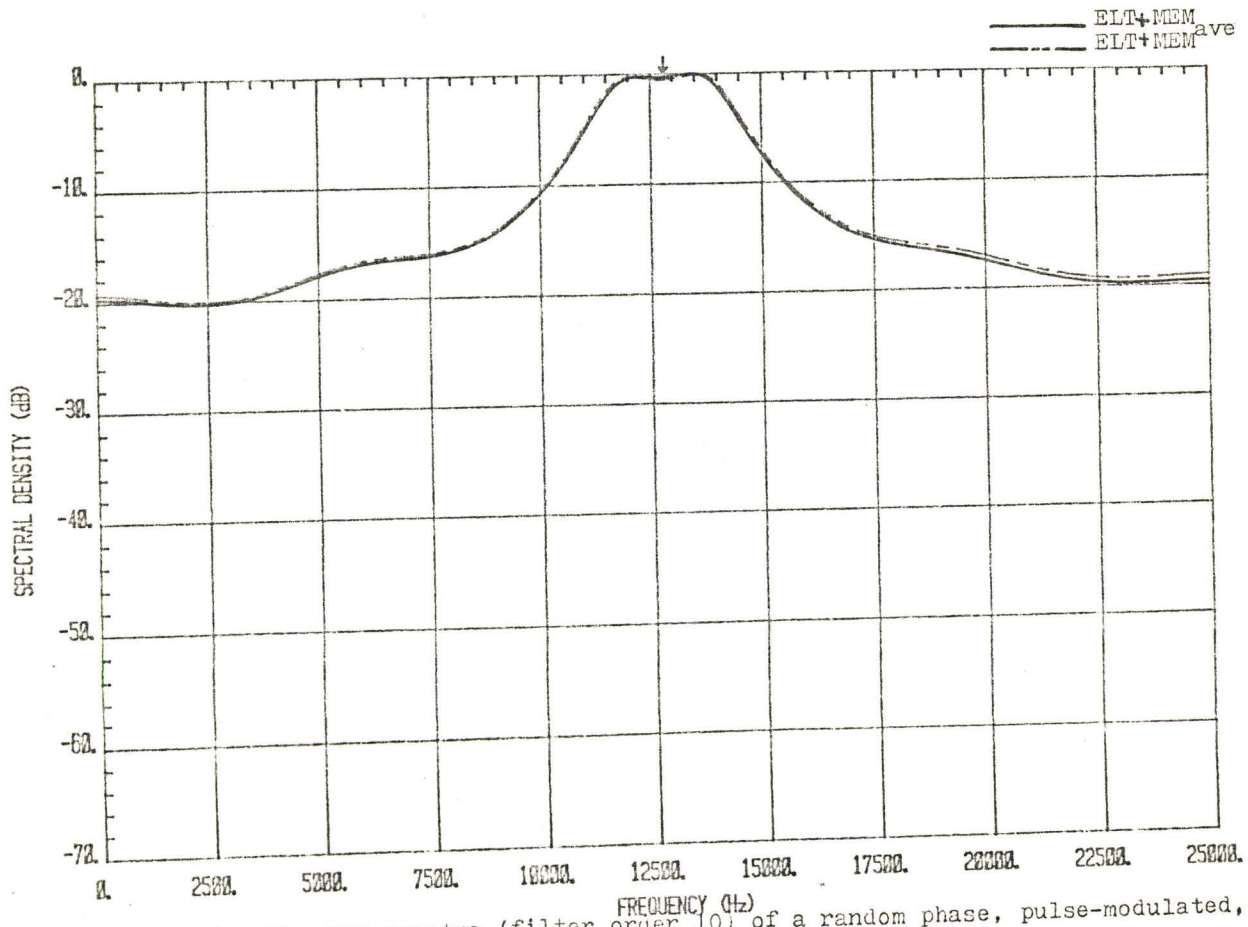
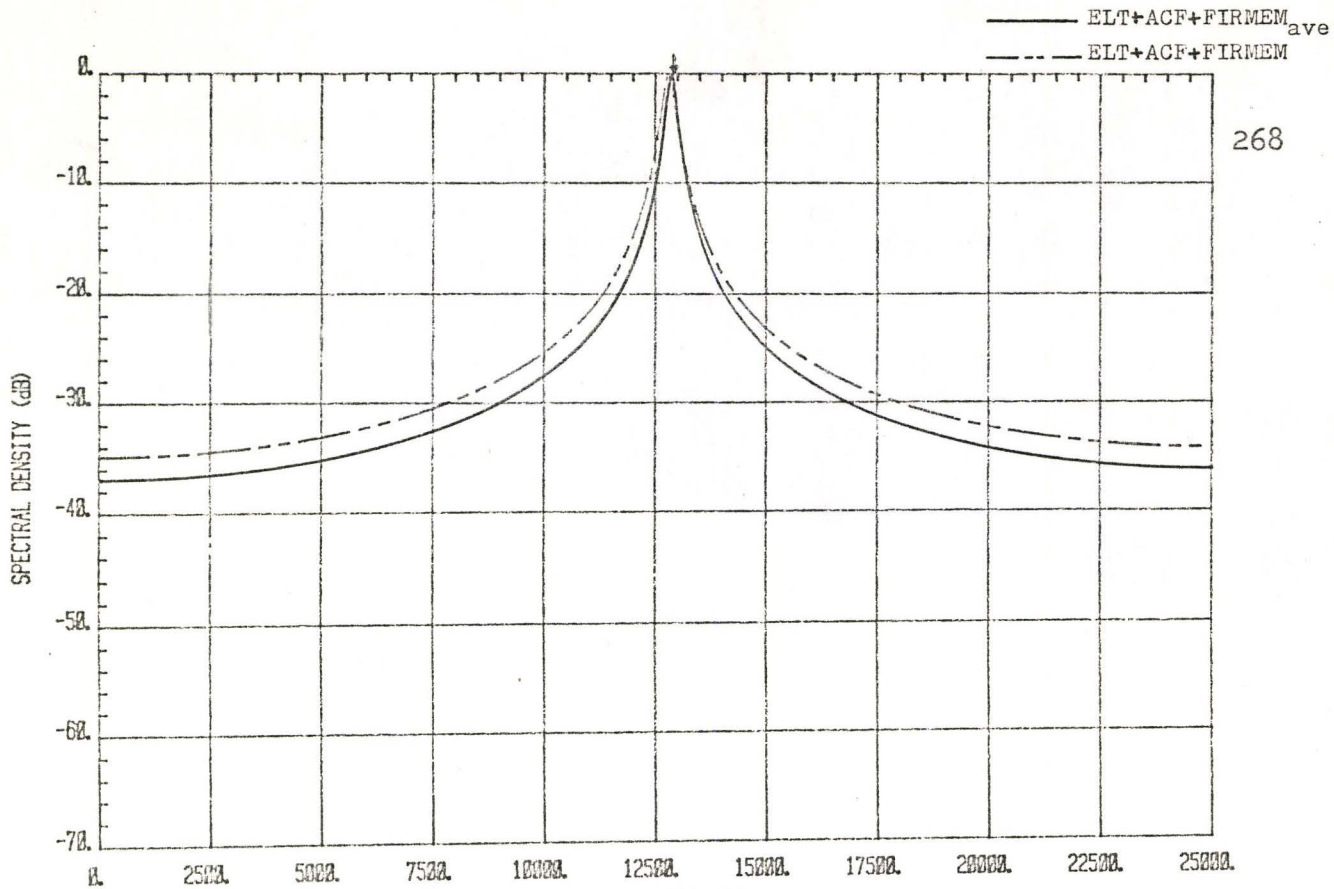


Fig. E.2: The 'ELT+ACFMEM' spectra (filter order 2) of random phase, pulse-modulated signal.



spectra. The peaks of both the 'ELT+MEM<sub>ave</sub>' and 'ELT+ACFMEM<sub>ave</sub>' are situated at 12842 Hz (this is the same frequency for the peak of 'ELT+MEM' and 'ELT+ACFMEM'). In the case of 'ELT+ACF+FIRMEM<sub>ave</sub>', the peak is measured to be 12830 Hz which is an improvement of 37 Hz from the spectral estimate (12793 Hz) obtained by the 'ELT+ACF+FIRMEM'. At filter order 10, the MEM spectra calculated by the 'ELT+MEM<sub>ave</sub>' and 'ELT+ACFMEM<sub>ave</sub>', in Fig. E.4 and Fig. E.5, do not offer valuable information. However, the same magnitude of improvement (37 Hz) is achieved by the 'ELT+ACF+FIRMEM<sub>ave</sub>' which has a main peak at 12757 Hz. This is plotted in Fig. E.6.

The averaging operation, with the aid of digital filtering, does provide an alternate possible solution in studying the spectral performance of random phase ELT signal.

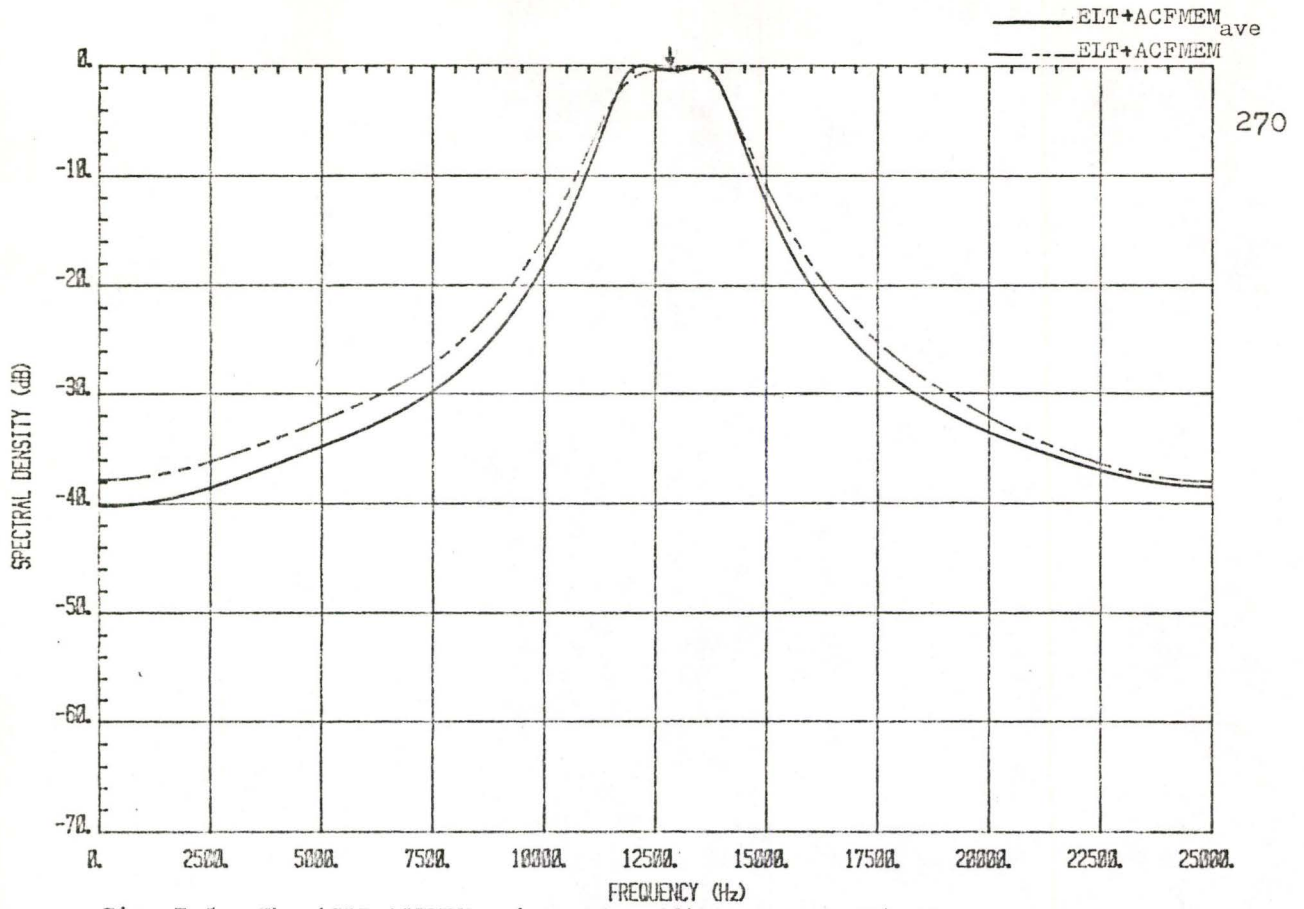


Fig. E.5: The 'ELT+ACFMEM' spectra (filter order 10) of a random phase, pulse-modulated signal.

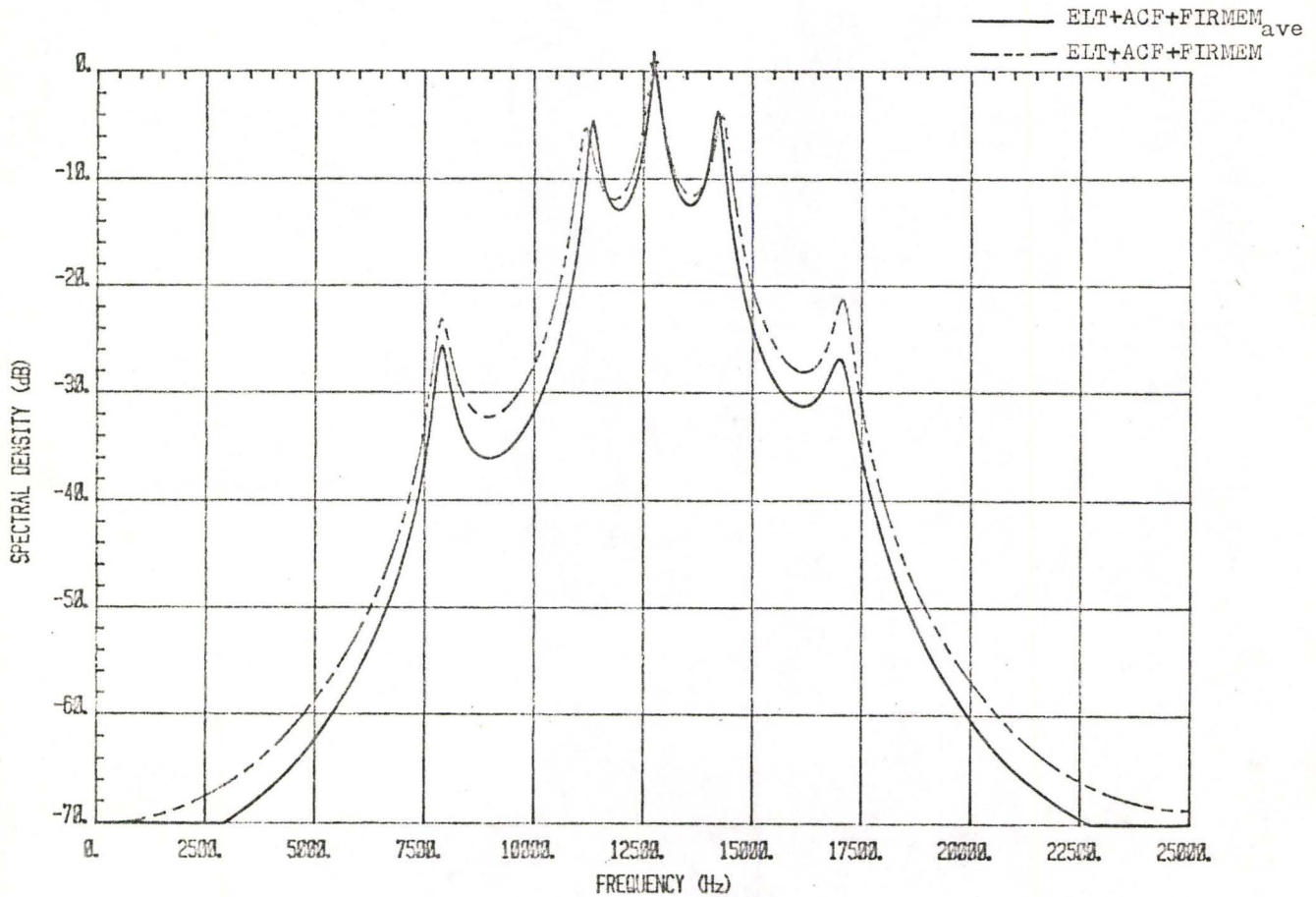


Fig. E.6: The 'ELT+ACF+FIRMEM' spectra (filter order 10) of a random phase, pulse-modulated signal.

## APPENDIX F

### PROCESSING RESULTS FOR ELT SIGNALS WITH MIXED MODULATION

In this appendix, we present the processing results for ELT signals with mixed modulation. Specifically, we examine three ELT signals at carrier frequencies 8504 Hz (pulse-modulated, continuous phase), 12683 Hz (pulse-modulated, continuous phase) and 13796 Hz (pulse-modulated, random phase).

Figure F.1 to Fig. F.8 compares the performances of the FFT processor and the MEM processor (filter order 30) at various carrier-to-noise density ratio (CNR). At all values of CNR (34 dB-Hz, 39 dB-Hz, 44 dB-Hz and 54 dB-Hz), both processors give a prominent peak for the signal at carrier frequency 8504 Hz. As the value of CNR increases, the signal at frequency 12683 Hz can be detected by the two processors; whereas, the resolution for the signal at 13796 Hz is displaced by an amount of approximately 300 Hz. This resolution error may be caused by the two ELT signals which have carrier frequencies that are so close to each other. (The frequency separation for 12683 Hz and 13796 Hz is about 1 KHz.) Furthermore, mixed modulation may also be one of the factor that gives rise to this error.

By using a bank of bandpass filters, the 'ELT + ACF + FIRMEM' configuration (at MEM filter order 8) is able to provide feasible detection at a CNR value above 44 dB-Hz. These results are shown in Fig. F.9 to Fig. F.12.

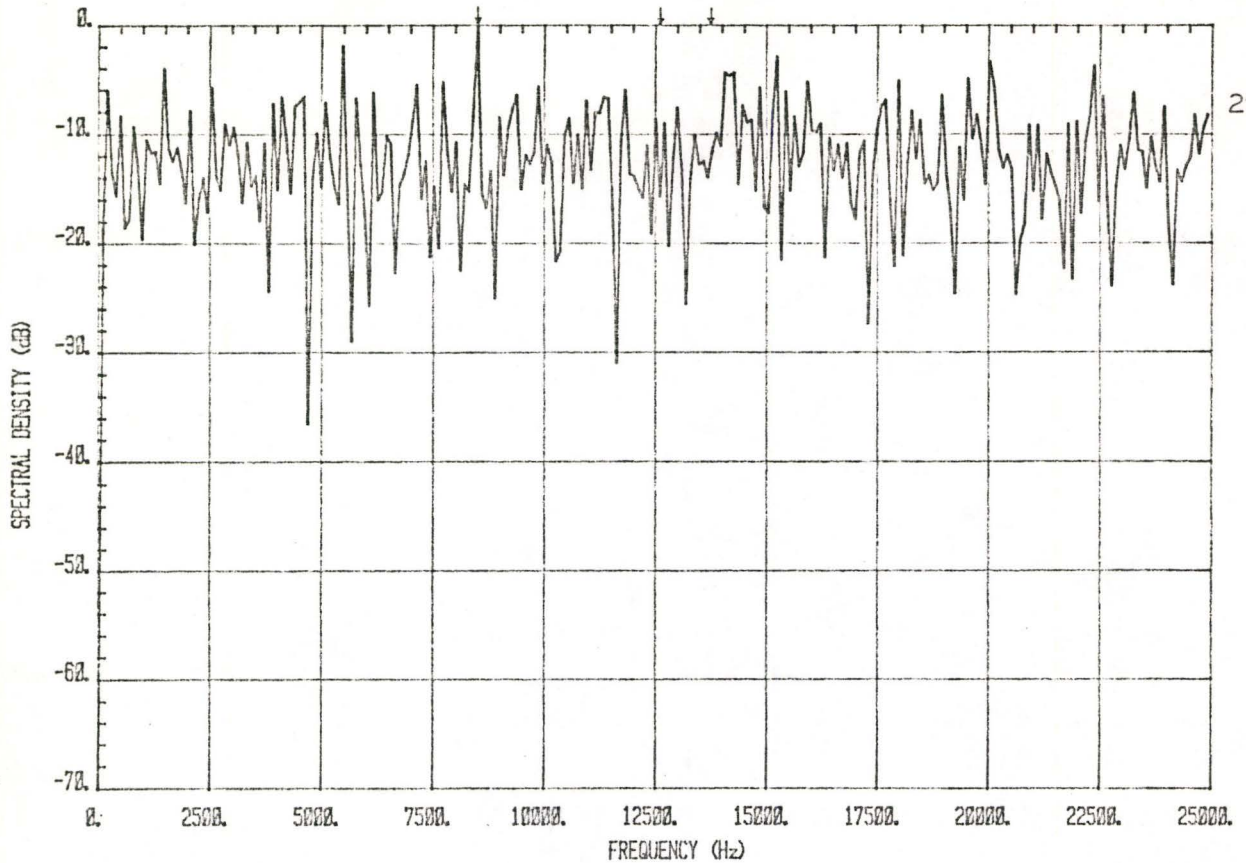


Fig. F.1: The FFT spectrum of three pulse-modulated ELT signals with carrier frequencies 8504 Hz (continuous phase), 12683 Hz (continuous phase) and 13796 Hz (random phase). The CNDR is 34 dB-Hz.

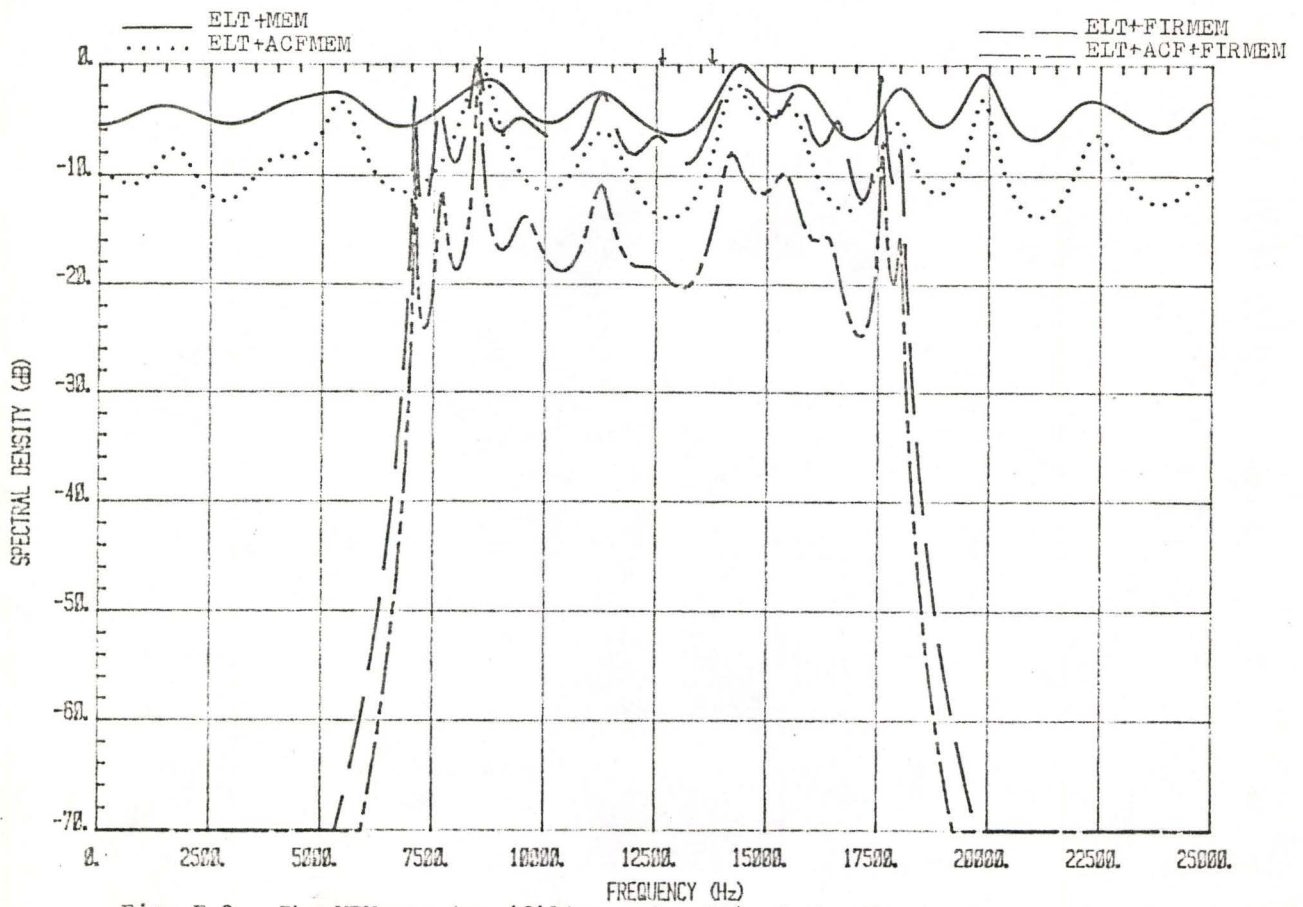


Fig. F.2: The MEM spectra (filter order 30) of the three pulse-modulated signals with 34 dB-Hz CNDR.

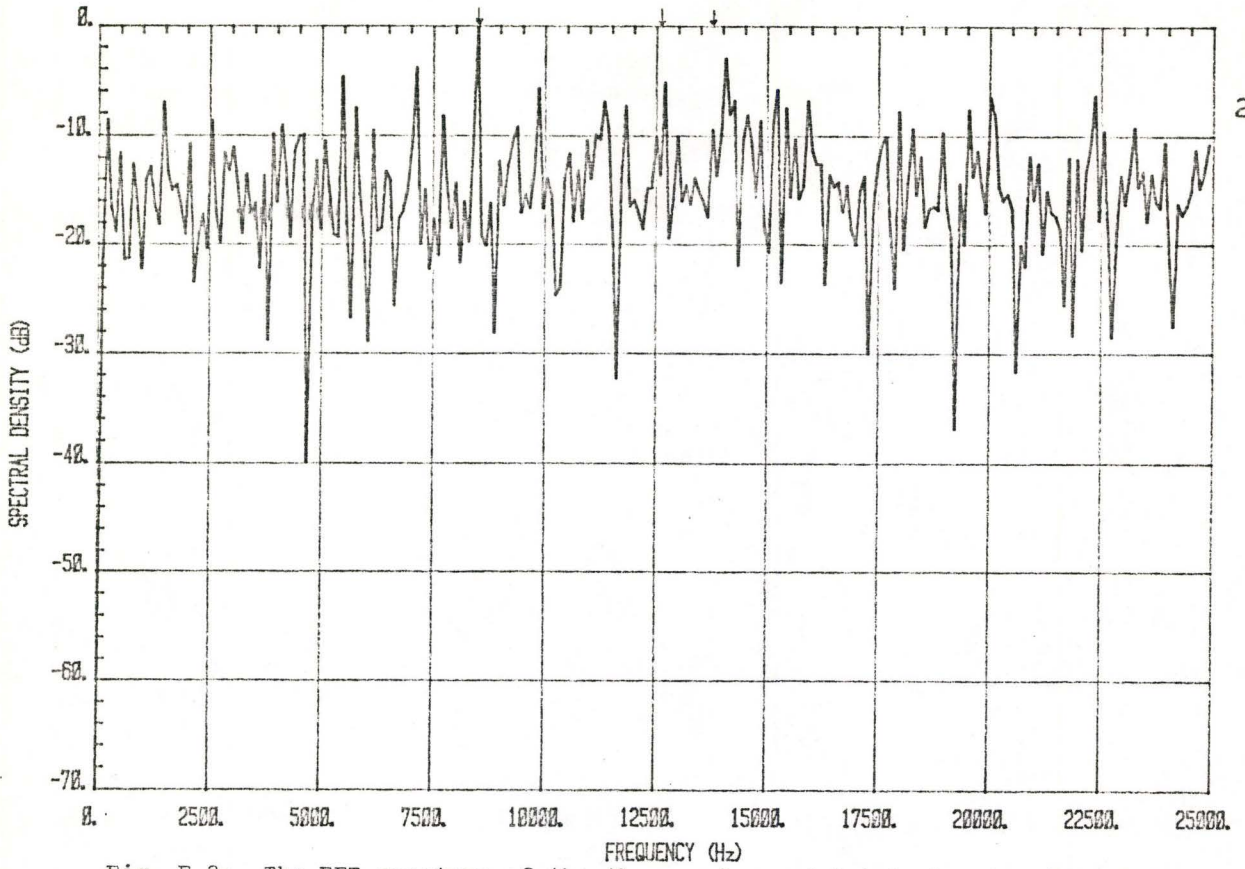


Fig. F.3: The FFT spectrum of the three pulse-modulated signals with 39 dB-Hz CNDR.

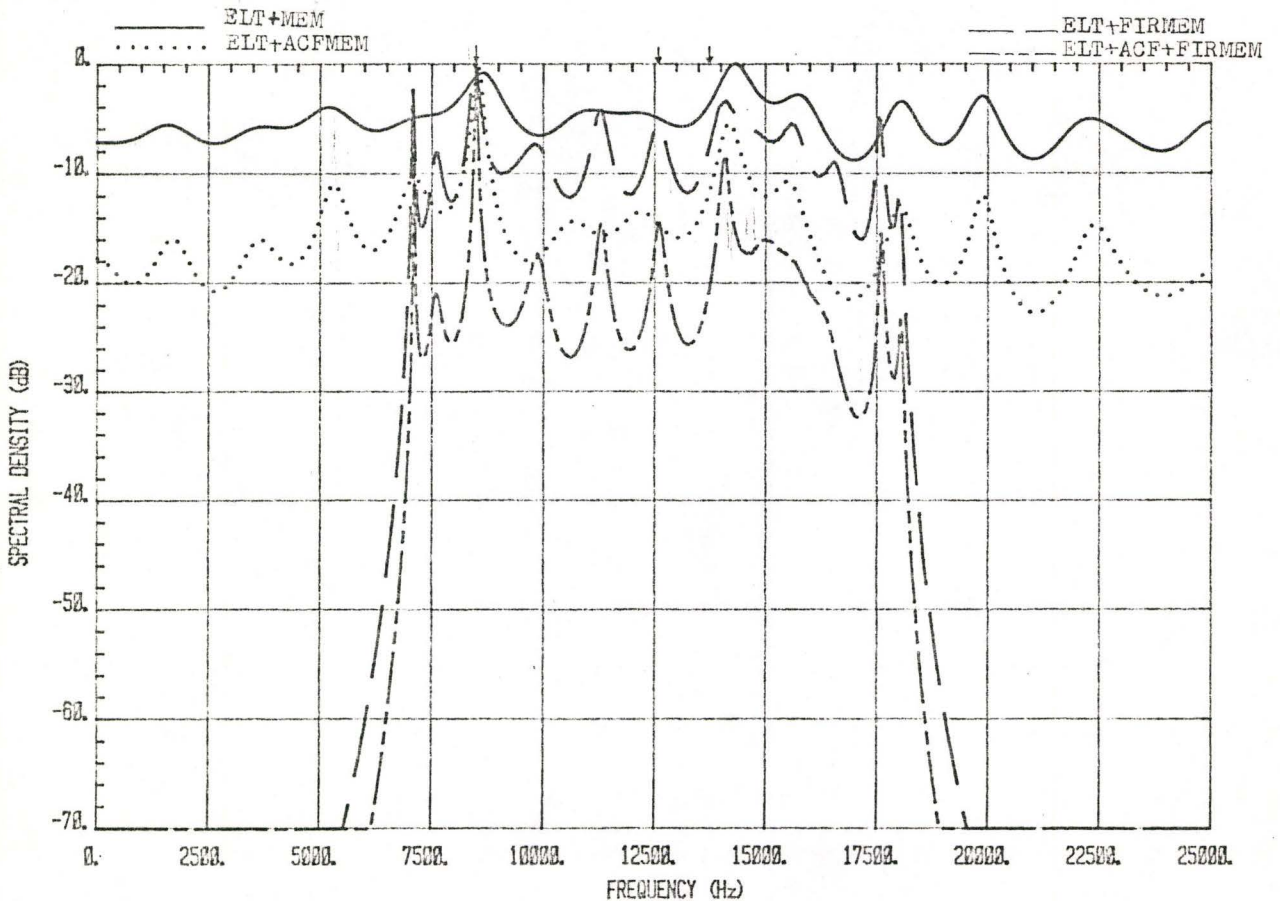


Fig. F.4: The MEM spectra (filter order 30) of the three pulse-modulated signals with 39 dB-Hz CNDR.

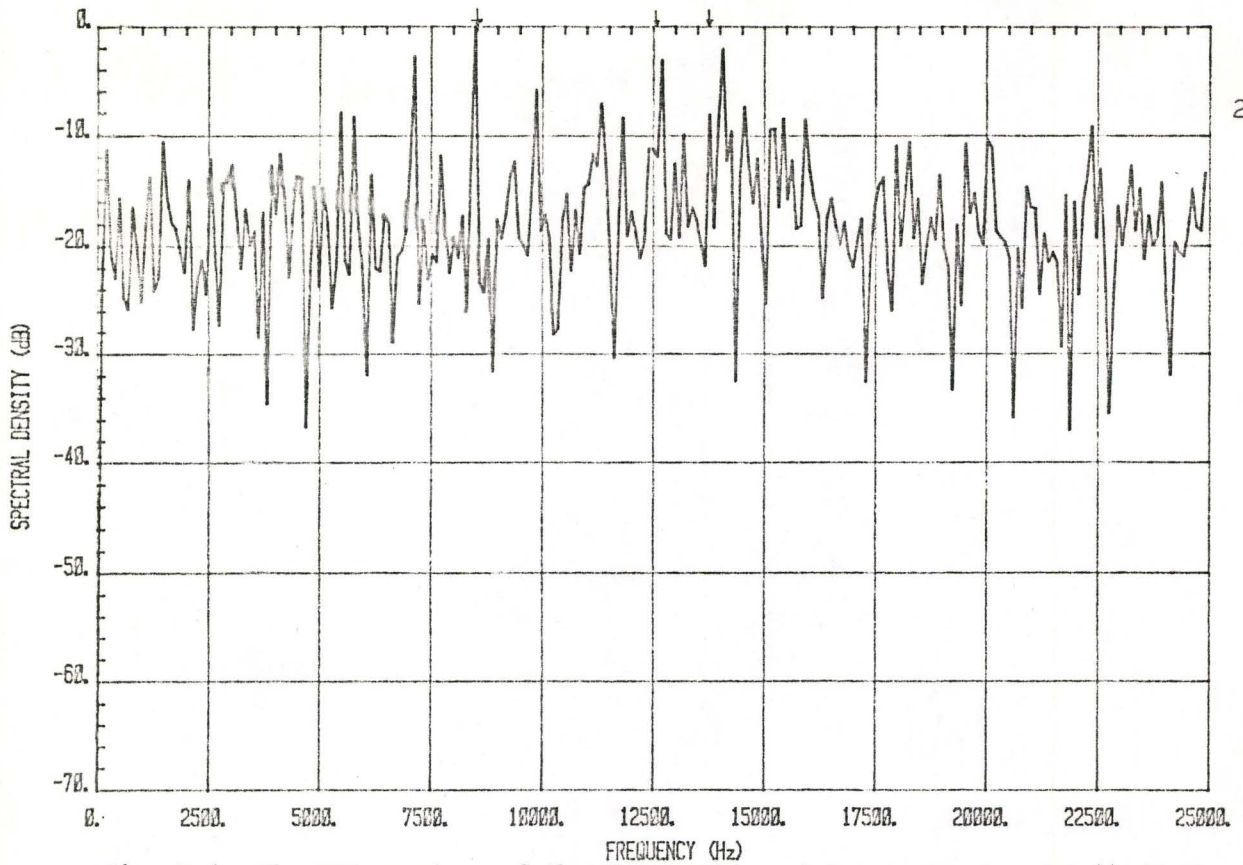


Fig. F.5: The FFT spectrum of the three pulse-modulated signals with 44 dB-Hz CNDR.

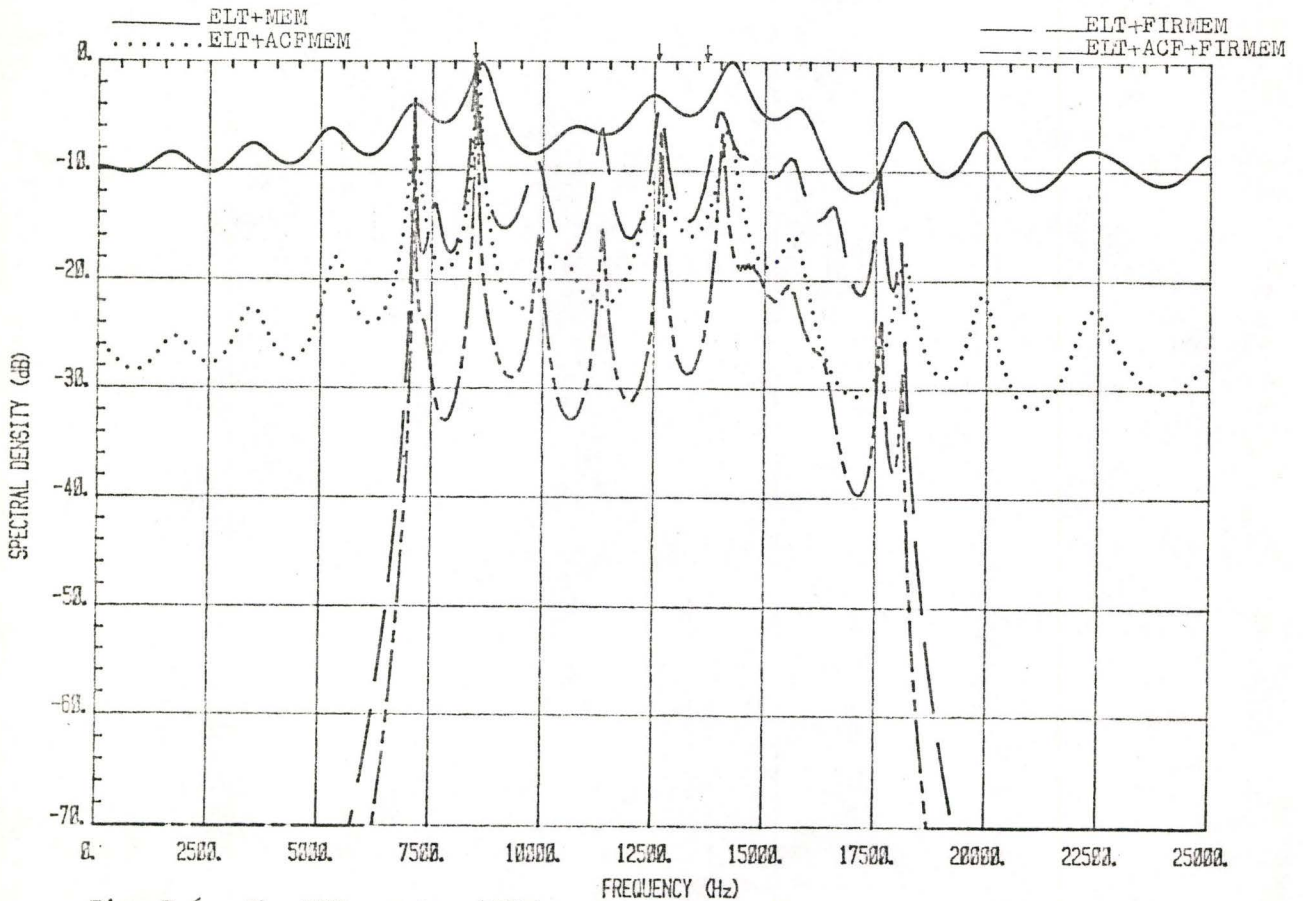


Fig. F.6: The MEM spectra (filter order 30) of the three pulse-modulated signals with 44 dB-Hz CNDR.

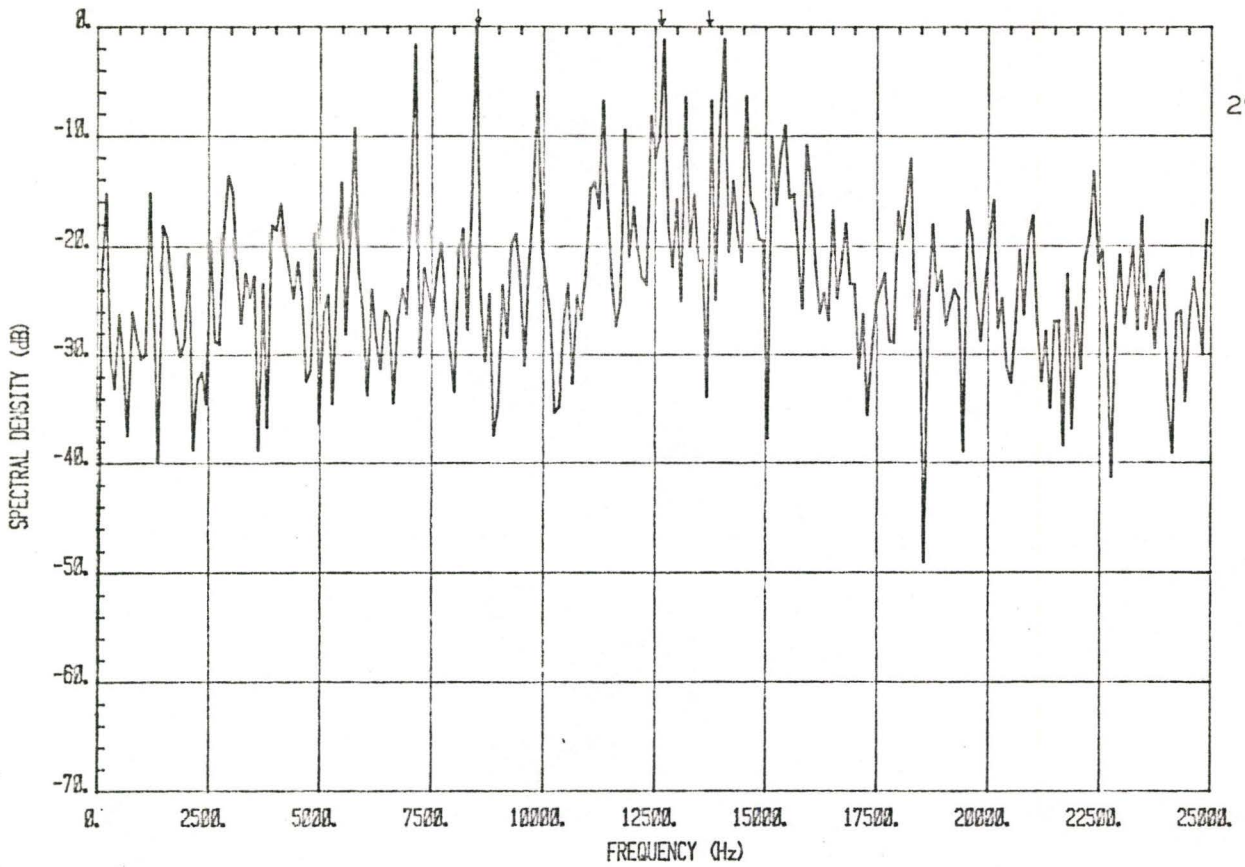


Fig. F.7: The FFT spectrum of the three pulse-modulated signals with 54 dB-Hz CNDR.

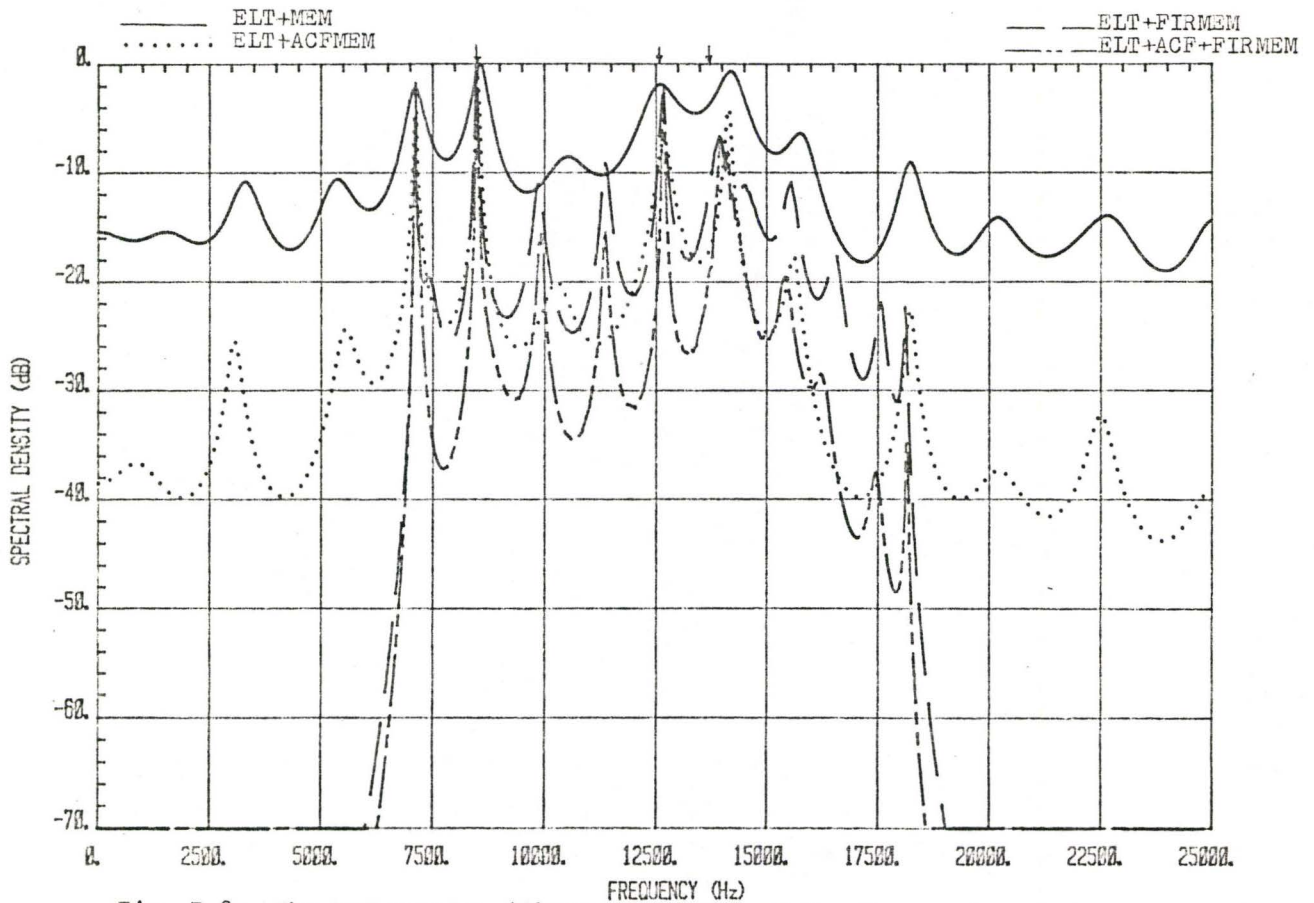


Fig. F.8: The MEM spectra (filter order 30) of the three pulse-modulated signals with 54 dB-Hz CNDR.

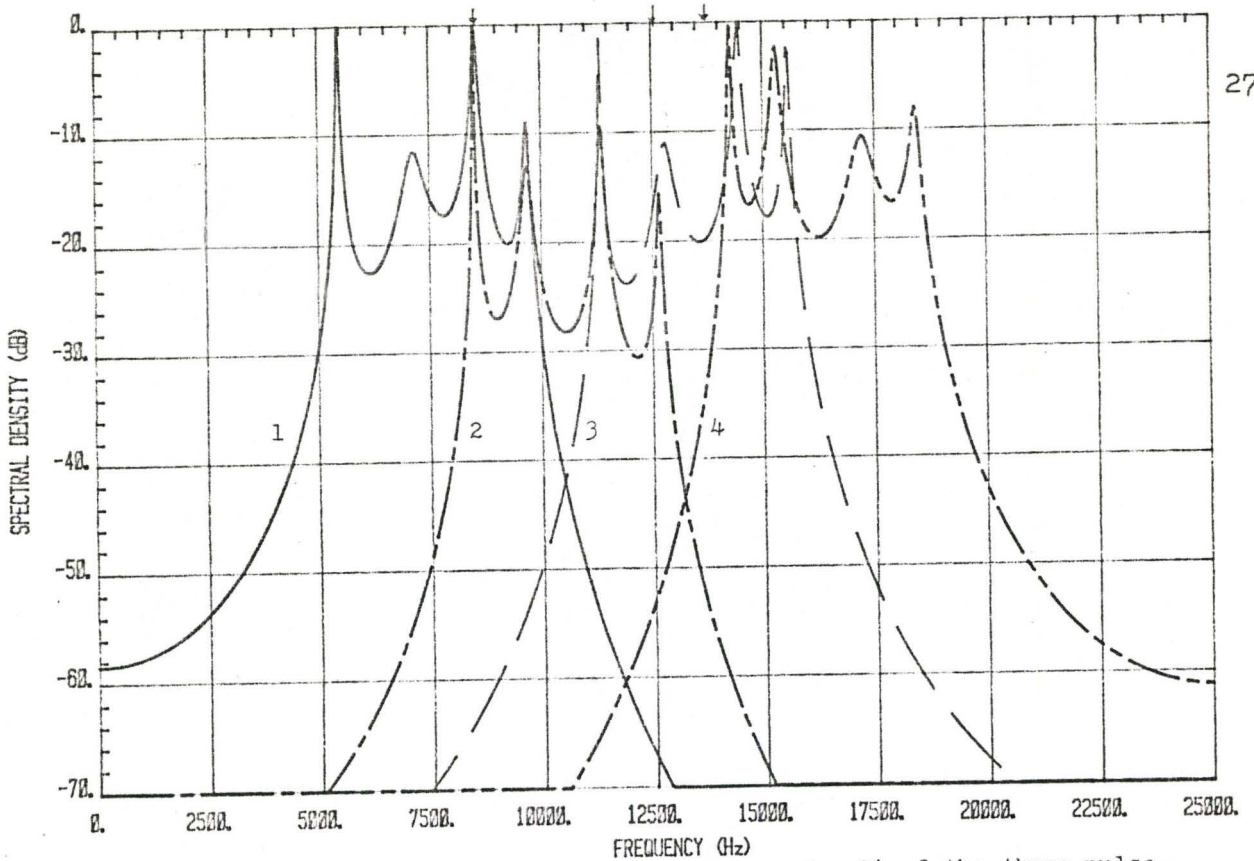


Fig. F.9: The 'ELT+ACF+FIRMEM' spectra (filter order 8) of the three pulse-modulated signals with 34 dB-Hz CNDR.

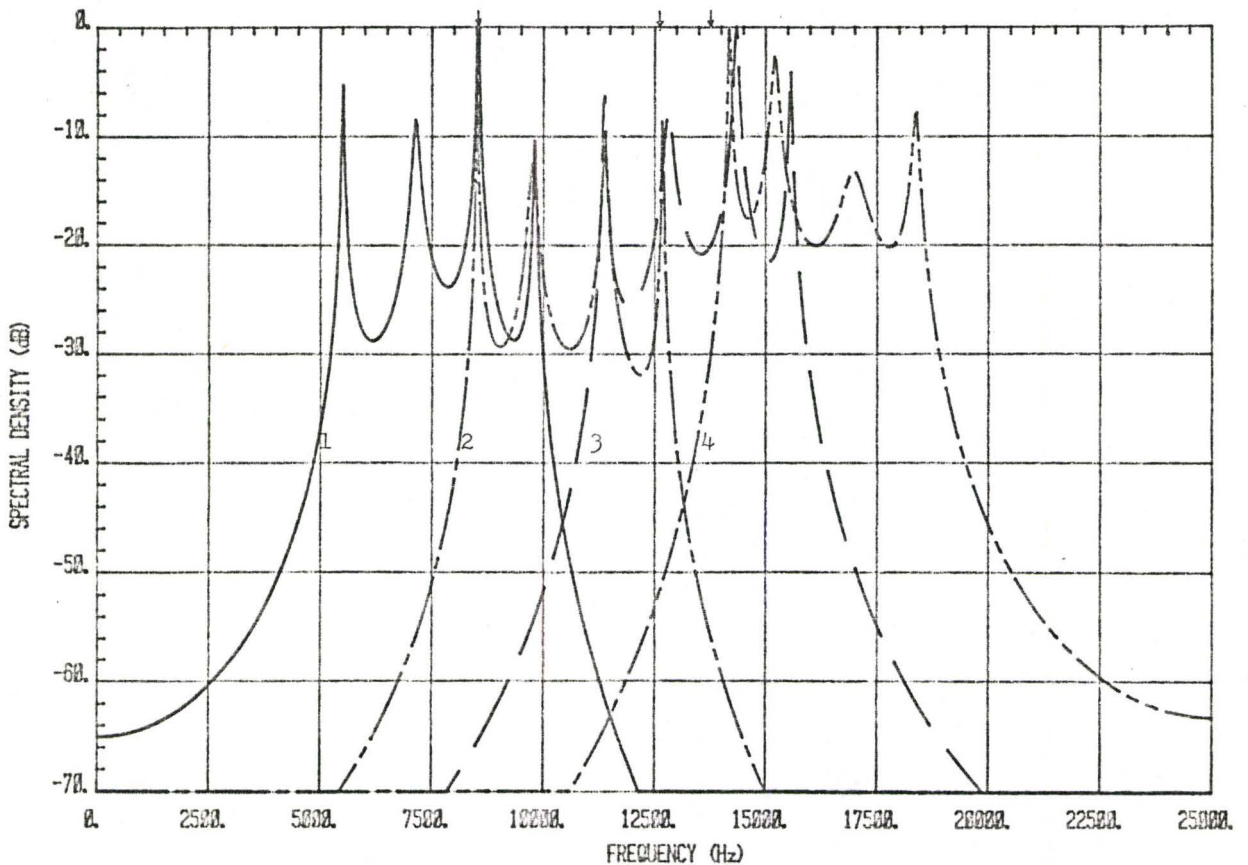


Fig. F.10: The 'ELT+ACF+FIRMEM' spectra (filter order 8) of the three pulse-modulated signals with 39 dB-Hz CNDR.

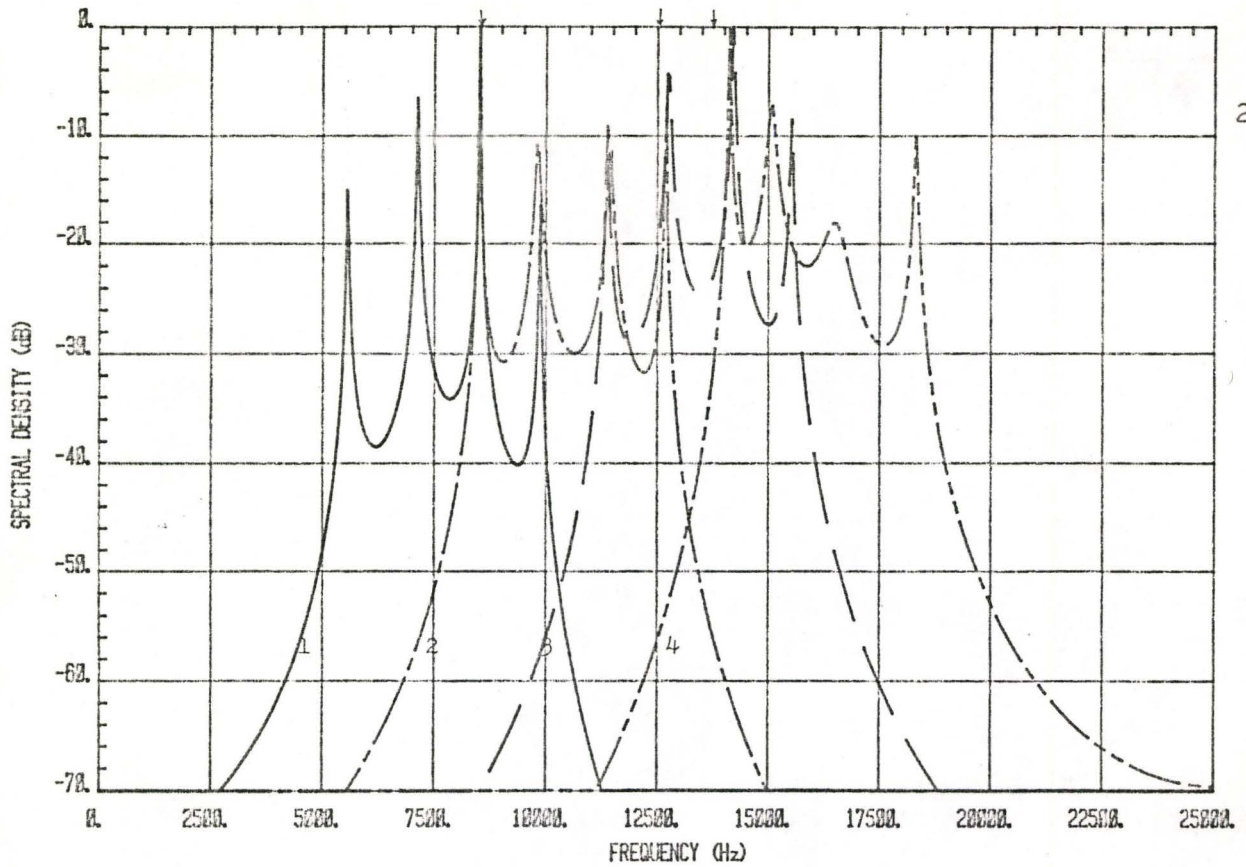


Fig. F.11: The 'ELT+ACF+FIRMEM' spectra (filter order 8) of the three pulse-modulated signals with 44 dB-Hz CNDR.

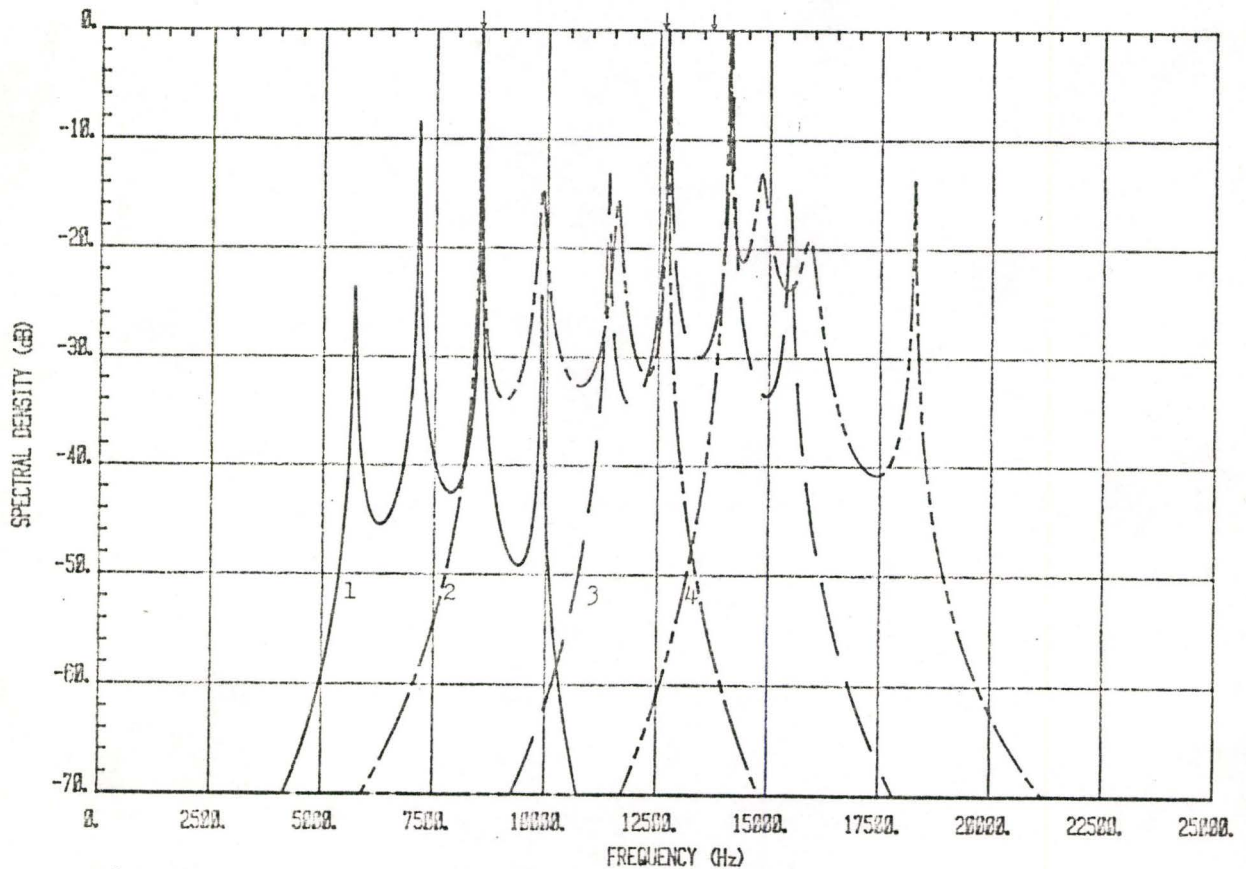


Fig. F.12: The 'ELT+ACF+FIRMEM' spectra (filter order 8) of the three pulse-modulated signals with 54 dB-Hz CNDR.